

1127 - 2 / 1521

JOURNAL OF COLLOID SCIENCE

Editor-in-Chief

VICTOR K. LA MER, Columbia University, New York

Advisory Board

C. O. BECKMANN
KATHARINE B. BLODGETT
K. F. BONHOEFFER
M. L. CORRIN
P. J. W. DEBYE
JOHN L. EDSALL
I. FANKUCHEN
JOHN D. FERRY
A. R. GORDON
WILFRIED HELLER
ERIC HUTCHINSON
GEORGE JURA
JOHN G. KIRKWOOD
E. C. LINGAFELTER
L. G. LONGSWORTH

J. W. MCBAIN
J. TH. G. OVERBEEK
R. RUYSSSEN
E. K. RIDEAL
WILLIAM SEIFRIZ
LEO SHEDLOVSKY
THEODORE SHEDLOVSKY
ROBERT SIMHA
JACINTO STEINHARDT
THE SVEDBERG
HUGH S. TAYLOR
ARNE TISELIUS
ROBERT D. VOLD
BERNARD VONNEGUT
RALPH W. G. WYCKOFF
BRUNO H. ZIMM

VOLUME 6

1951

ACADEMIC PRESS INC., PUBLISHERS
NEW YORK, N. Y.

Copyright 1951, by Academic Press Inc.
Made in United States of America

THE INTERACTION OF COLLOIDAL PARTICLES. VI. APPLICATION OF THE STERN THEORY OF THE DOUBLE LAYER

S. Levine

*Birkbeck College Research Laboratory, London, England **

Received July 27, 1949; revised July 12, 1950

1. INTRODUCTION

In the first paper (Part I) of this series (1), the author proposed a theory of interaction of colloidal particles which is a development of the work of Verwey and Overbeek, published in their recent book (2). A characteristic feature of our theory is that it provides a method of determining simultaneously the adsorption isotherm for ions on the particle surface and the mutual free energy of the particles. In a comprehensive theory of the interaction of particles, no special assumption concerning the variation of surface density of ions with interparticle distance should be made. In the present paper, this objective is partially achieved by applying the Stern theory of the double layer (3), since the latter does involve a number of assumptions. It should be remarked that in treating the surface layer of counter ions, which is introduced in the Stern theory, we have applied the standard method of determining the adsorption isotherm, which is based on statistical mechanics and which has been used in many adsorption problems. Although we have limited ourselves to developing a theory of interaction which includes the fundamental assumptions of the Stern theory, in principle it should not be difficult to modify our physical conditions to cover other cases.

Verwey and Overbeek also discuss the Stern theory of the double layer and comment [Ref. (2), p. 133]: "In our opinion, however, further progress in our understanding of the stability of hydrophobic colloids can only be expected from a further development, experimental as well as theoretical, of the principle underlying Stern's theory." By incorporating the latter theory into their method of calculating the interaction of particles, these authors account for the adsorption of ions on the surfaces of the particles. In this paper we shall examine this application more critically, and indeed shall introduce new terms in the mutual free-energy expression which are associated with the formation of the Stern layer of counter ions and which do not occur explicitly in the theory of Verwey and Overbeek.

* Present address: Dept. Mathematics, University of Manchester, Manchester, England.

2. FREE ENERGY OF DISCHARGED SYSTEM

We shall consider two parallel plates each of area A , at separation R and immersed in an electrolyte solution of volume V . It is assumed that the inner faces of these plates become charged by the adsorption of ions from the solution. (The outer faces can be ignored.) Prior to this adsorption process the total number of ions of type i in the solution is N_i , there being s types in all; N_0 is the total number of solvent (water) molecules. Suppose that ν_1 potential-determining ions of type 1 (positive) charge e_1 , are adsorbed per unit area of the inner sides of the plates, and then ν_2 counter ions of type 2 (negative) charge e_2 , are also adsorbed to form the Stern layer. The surface charge density $\nu_1 e_1$ on the particles can also originate from a desorption process, but this does not change the argument presented in this paper.

We shall adopt the method described in Parts I and II (1, 4) to determine the free energy of our system. All the ions, including the adsorbed ones, are assumed to be completely discharged, and then the familiar fictitious Debye—Hückel process of charging the ions at the same rate is used. The densities of adsorbed ions ν_1 and ν_2 will be kept fixed during this charging process. If the number of adsorbed counter ions is small compared with the total number of available sites, then we can write this energy in the convenient form

$$F_0(\nu_1, \nu_2) = \sum_{i=0}^s N_i \chi_i^0 - 2AB_1\nu_1 + 2A\nu_2(-B_2 + kT \ln \nu_2). \quad [1]$$

The three terms in [1] can be interpreted physically as follows. We first suppose that no ions are adsorbed on the plates, so that $\nu_1 = \nu_2 = 0$. Then χ_i^0 is the chemical potential of a discharged i ion and χ_0^0 is the corresponding potential of a solvent molecule. Thus, the first term is the usual expression for the free energy of the dispersion medium (for the hypothetical case of discharged ions). The second term represents the change in the free energy accompanying the adsorption of $2A\nu_1$ ions of type 1; the third term is the corresponding change when $2A\nu_2$ ions of type 2 are adsorbed; k is Boltzmann's constant, T is the temperature, and the quantities B_1 and B_2 are functions of N_0, N_1, \dots, N_s, V , and T .

The formula [1] can be derived by the methods of statistical mechanics in the following way. We regard our system as consisting essentially of two phases, the surface phase containing $2A\nu_1$ and $2A\nu_2$ adsorbed ions of types 1 and 2, respectively, and the solution phase; the phases are treated separately. Let μ_0 and μ_i be the chemical potentials of a solvent molecule and discharged i ions, respectively, in the dispersion medium. Then the free energy of the solution phase only in the discharged state can be expressed as

$$F_0^s(\nu_1, \nu_2) = N_0\mu_0 + N_1'\mu_1 + N_2'\mu_2 + \sum_{i=3}^s N_i\mu_i, \quad [2]$$

noting that the number of species 1 and 2 in the solution are $N_1' = N_1 - 2A\nu_1$ and $N_2' = N_2 - 2A\nu_2$, respectively. The standard formulas for the chemical potentials are written as

$$\begin{aligned}\mu_i &= \xi_i + kT \ln \left(N_i / \sum_{i=0}^s N_i \right), i \neq 1, 2, \\ \mu_i &= \xi_i + kT \ln \left(N_i' / \sum_{i=0}^s N_i \right), i = 1, 2,\end{aligned}\quad [3]$$

where $\sum_{i=0}^s N_i = N_0 + N_1' + N_2' + \sum_{i=3}^s N_i$ and ξ_i depends only on T and

V (or the pressure). If the two plates are immersed in a large volume of dispersion medium, then we can express these chemical potentials as powers of ν_1 and ν_2 and retain only linear terms. We find that $\mu_i = \chi_i^0$ very nearly and thus [2] becomes

$$F_0^s(\nu_1, \nu_2) = \sum_{i=0}^s N_i \chi_i^0 - 2A(\nu_1 \chi_1^0 + \nu_2 \chi_2^0). \quad [4]$$

It will be assumed that the part of the free energy to be associated with the $2A\nu_1$ adsorbed 1-type ions has the form $2A\nu_1\mu_1^p$, where μ_1^p is the chemical potential of a (discharged) 1 ion on the colloidal particle. (This form is found to be consistent with the Stern theory.) The free energy of the layer of counter ions is obtained by applying the usual statistical theory of a monolayer of molecules on a surface. Let N_s be the total number of adsorption sites on each plate and U_0 the energy of adsorption on one of these sites of a completely discharged ion of type 2. Then the free energy to be associated with $A\nu_2$ discharged ions on each plate is given by

$$\begin{aligned}F_0^p(\nu_2)/kT &= -N_s \ln N_s + A\nu_2 \ln(A\nu_2) \\ &+ (N_s - A\nu_2) \ln(N_s - A\nu_2) + A\nu_2 U_0/kT.\end{aligned}\quad [5]$$

Here the first three terms are obtained by applying Stirling's formula¹ to the number of configurations available to the $A\nu_2$ adsorbed ions, namely, $N_s! / [(N_s - A\nu_2)!(A\nu_2)!]$. We have omitted a factor which allows for a set of excited states for each adsorbed ion. The energy of our discharged system is therefore

$$F_0(\nu_1, \nu_2) = F_0^s(\nu_1, \nu_2) + 2F_0^p(\nu_2) + 2A\nu_1\mu_1^p. \quad [6]$$

¹ It is assumed that $A\nu_2 \gg 1$, so that the plates cannot be too small. In the numerical example in Sec. 5, $\nu_2 = 2.8 \times 10^{12}$, which is quite low, and thus the linear dimensions of each plate must be appreciably greater than 10^{-6} cm.

If we expand

$$\ln\left(1 - \frac{A\nu_2}{N_s}\right) = -\frac{A\nu_2}{N_s} - \frac{1}{2}\left(\frac{A\nu_2}{N_s}\right)^2 - \dots,$$

and retain only the first term, then [6] reduces to [1], and

$$B_2 = \chi_2^0 + kT \ln(N_s/A) + kT - U_0, \text{ and } B_1 = \chi_1^0 - \mu_1^p. \quad [7]$$

The analysis in this paper will be restricted to the case where $A\nu_2 \ll N_s$. It is possible to treat the more general case where the number of adsorbed ions $A\nu_2$ is comparable with (although less than) the number of available sites N_s , but we shall return to this in a later publication.

3. FREE ENERGY OF CHARGING THE IONS

We now charge all the ions, subject to constant density of adsorbed ions ν_1 and ν_2 , and introduce the fraction λ to represent the stage in this charging process. The electric potential at an adsorbed ion of type 1 (*i.e.*, at the wall of the particles) is written as $\psi_0(\lambda, R)$. The adsorbed layer of counter ions is assumed to be concentrated at a distance δ from the particle wall and the potential at this layer is denoted by $\psi_\delta(\lambda, R)$. Both these potential functions depend on ν_1 and ν_2 as well as on λ and R , but, to keep the notation simple, we shall not indicate this dependence explicitly.² The Stern condition reads

$$\lambda\nu_1e_1/K = \psi_0(\lambda, R) - \psi_\delta(\lambda, R), \quad K = D'/4\pi\delta, \quad [8]$$

where D' is the "dielectric constant" of the medium of the layer of counter ions. The manner in which the quantity K (presumably) varies with λ is not known. In view of the approximate character of the basic relation [8] we shall make the simplest choice, namely, consider K to be independent of λ . This assumption is partly justified in Sec. 4 where we derive the same expression for the free energy by an alternative method which avoids the hypothetical charging process.

The layers of potential-determining and counter ions yield the following two terms to the free energy of the double layers

$$\begin{aligned} 2A \left[\nu_1e_1 \int_0^1 \psi_0(\lambda, R) d\lambda + \nu_2e_2 \int_0^1 \psi_\delta(\lambda, R) d\lambda \right] \\ = 2A \left[\frac{\nu_1^2e_1^2}{2K} + (\nu_1e_1 + \nu_2e_2) \int_0^1 \psi_\delta(\lambda, R) d\lambda \right], \quad [9] \end{aligned}$$

² We shall neglect the correction arising from the mutual Debye—Hückel energy of the ions themselves in the dispersion medium. This implies that the separation R of the particles cannot be too large. In Part V of this series (5) we calculate that κR should be less than about 5 when the electrolyte concentration is 10^{-2} M of a 1-1 type, where κ is the characteristic parameter in the Debye—Hückel theory of electrolytes, defined in Sec. 5.

substituting [8]. Now the second term on the right of [9] represents the contribution to the free energy from a surface charge $2A\lambda(\nu_1 e_1 + \nu_2 e_2)$, which is the resultant charge on the two particles, at potential $\psi_\delta(\lambda, R)$. The diffuse outer layers carry an equal and opposite charge $-2A\lambda(\nu_1 e_1 + \nu_2 e_2)$. If we combine this second term in [9] with the corresponding expression for the work done in charging the outer layers, then the analysis in Parts II (4) and III (6) of this series shows that we obtain the quantity

$$2Ae_1 \int_0^\nu \psi_\delta(1, R) d\nu = 2A \int_0^\sigma \psi_\delta(1, R) d\sigma, \quad [10]$$

where we find it convenient to introduce the number ν and surface charge density σ , defined by

$$\sigma = \nu e_1 = \nu_1 e_1 + \nu_2 e_2. \quad [11]$$

Thus ν is the "effective" or "reduced" surface density of potential-determining ions, screened by the layer of counter ions. The formula [10] is the usual expression from electrostatics for the work done in bringing the charge $2A\sigma$ by infinitesimal amounts from the solution to the surface of the plates, through a potential difference of $\psi_\delta(1, R)$.

In Part III (6) we have proven quite generally by a method used by Casimir in the book by Verwey and Overbeek [Ref. (2), p. 63], that [10] is the correct result provided $\lambda\psi_\delta(\lambda, R)$ vanishes as λ tends to zero. Although we have been considering a model of finite plates, in the applications in Secs. 5 and 6, the formula used for $\psi_\delta(1, R)$ refers to infinitely large plates; *i.e.*, we regard our plates as being parts of infinitely large ones. However, in this case the above condition, which is necessary if [10] is to be valid, is violated since $\psi_\delta(\lambda, R)$ become infinite as $1/\lambda$ when λ goes to zero. This has been a source of difficulty in the earlier papers (1, 4, 6), and since it might appear to be a weak point in our theory, we shall proceed to clear it up and indicate how it only involves a small correction to our results. For finite plates, the surface potential would not be uniform over the inner faces of the parallel plates because of the edge effects, and thus we need to introduce an average. This average potential, which we may denote by $\psi_{av}(\lambda, R)$, must be substituted for $\psi_\delta(\lambda, R)$ in the integral with respect to λ in Eq. [9]. The essential point is that since the (discharged) ions are uniformly distributed throughout the whole dispersion medium at the start of the charging process, it immediately follows from the Boltzmann distribution law that $\lambda\psi_{av}(\lambda, R)$ vanishes as λ tends to zero. Correspondingly, the average potential $\psi_{av}(1, R)$ must replace the function $\psi_\delta(1, R)$ in Eq. [10]. But in the latter case, we are dealing with the fully charged system when λ is unity. Suppose now that the linear size of each plate, namely, \sqrt{A} , is large compared with both the separation R and the thickness $(1/\kappa)$ of the diffuse outer layers. Then the edge effects can be ignored and in practice we can identify the average

potential $\psi_{av}(1, R)$ with $\psi_s(1, R)$ which is derived from the model of two parallel infinite plates. It should be remarked that the two assumptions $\sqrt{A} \gg R$ and $\sqrt{A} \gg 1/\kappa$ are implicit in any theory which neglects the edge effects for two parallel plates.

Let the changes in electrical self-energy associated with the transfer of ions of types 1 and 2, from the solution to the surface, be denoted by $-\Delta\chi_1(1)$ and $-\Delta\chi_2(1)$, respectively, at stage $\lambda = 1$ (completion of the charging process). Then, making use of Eqs. [1], [9], and [10], the free energy of our actual system (*i.e.*, at $\lambda = 1$) is

$$F(\nu_1, \nu_2, R) = \sum_{i=0}^s N_i \chi_i^0 + 2A \left\{ -\nu_1 [\Delta\chi_1(1) + B_1] - \nu_2 [\Delta\chi_2(1) + B_2 - kT \ln \nu_2] + \frac{\nu_1^2 e_1^2}{2K} + e_1 \int_0^\nu \psi_s(1, R) d\nu \right\}. \quad [12]$$

The free energy $F(\nu_1, \nu_2, R)$ must be a minimum with respect to the numbers of adsorbed ions ν_1 and ν_2 . This yields the two equations

$$\Delta\chi_1(1) + B_1 = \frac{\nu_1^2 e_1^2}{K} + e_1 \psi_s(1, R) = e_1 \psi_0(1, R), \quad [13]$$

$$\Delta\chi_2(1) + B_2 = kT(1 + \ln \nu_2) + e_2 \psi_s(1, R), \quad [14]$$

which state that the work done in transferring either type of ion from solution to plate is zero. The equilibrium values of the surface densities of ions $\nu_1 = \bar{\nu}_1(R)$ and $\nu_2 = \bar{\nu}_2(R)$, for example (at stage $\lambda = 1$), can be determined as functions of R from the relations [13] and [14]. When we substitute the latter densities into the functions $\psi_0(1, R)$ and $\psi_s(1, R)$, we obtain the corresponding equilibrium values of the potential which we shall write simply as $\bar{\psi}_0$ and $\bar{\psi}_s(R)$, respectively. It follows from [13] that $\bar{\psi}_0$ is independent of R .

The equilibrium conditions [13] and [14] can be transformed into forms which are readily recognized. First, when there are no adsorbed ions, the chemical potential of a discharged i ion is the usual expression

$$\chi_i^0 = \xi_i + kT \ln \left(N_i / \sum_{i=0}^s N_i \right).$$

If we substitute this into the formula in [7] for B_0 , then Eq. [13] can be written as

$$e_1 \bar{\psi}_0 = \text{constant} + kT \ln \left(N_1 / \sum_{i=0}^s N_i \right), \quad [15]$$

which is the familiar relation giving the variation of electrode potential with ion concentration in the solution. In a similar fashion, introducing the

expression in [7] for B_2 , [14] can be expressed as

$$\frac{A\bar{\nu}_2(R)}{(N_2/V)} = \frac{N_s}{(N_0/V)} \exp\{[\varphi_2 - e_2\bar{\psi}_\delta(R)]/kT\}, \quad [16]$$

where $\varphi_2 = \Delta\chi_2(1) + \xi_2 - U_0$, a constant independent of R . In deriving [16], we assume that the electrolyte concentration in the dispersion

medium is not too large (*ca.* $< 1 M$) so that $\sum_{i=0}^s N_i$ is replaced by N_0 .

Equation [16] is identical with that given in the book of Verwey and Overbeek [Ref. (2), Eq. 21, p. 44], if φ_2 is equated to the specific adsorption potential of the counter ion adsorbed on the wall of a particle. Thus, [16] or its alternative form [14], is equivalent to the adsorption isotherm of Stern in the case where the number of adsorbed counter ions is small compared with the total number of available adsorption sites. The more general form of the Stern isotherm is obtained if we retain the first *two* terms in the expansion of $\ln(1 - A\nu_2/N_s)$. In this way, our theory of interaction of colloidal particles incorporates the Stern theory of the double layer.

Substituting the equilibrium conditions [13] and [14] into [12], we derive the mutual free energy as a function of separation

$$F(\bar{\nu}_1(R), \bar{\nu}_2(R), R) = \sum_{i=0}^s N\chi_i^0 + 2A \left[-\frac{kT}{e_2} \bar{\sigma}_2(R) - \frac{\bar{\sigma}_1^2(R)}{2K} - \int_0^{\bar{\psi}_\delta(R)} \sigma d\psi_\delta \right], \quad [17]$$

where $\bar{\sigma}_1(R)$, $\bar{\sigma}_2(R)$, and $\bar{\sigma}(R)$ are the equilibrium values of the surface charge densities σ_1 , σ_2 , and σ , respectively. The last term on the right of [17] is that used by Verwey and Overbeek, but in the theory of these authors the preceding two terms do not appear explicitly. In the following section we shall discuss at some length the physical significance of the three terms in Eq. [17].

The change in the mutual free energy when the particles are brought to position R from infinite separation can also be determined in principle by integrating the force between the particles with respect to the distance. This force is given by

$$\begin{aligned} -\frac{dF(\bar{\nu}_1(R), \bar{\nu}_2(R), R)}{dR} &= - \left[\frac{\partial F(\nu_1, \nu_2, R)}{\partial R} \right]_{\nu_1=\bar{\nu}_1(R), \nu_2=\bar{\nu}_2(R)} \\ &= -2Ae_1 \left[\int_0^{\bar{\nu}} \frac{\partial \psi_\delta(1, R)}{\partial R} d\nu \right]_{\nu=\bar{\nu}(R)} \\ &= 2A \left[\int_0^{\bar{\sigma}} \frac{\partial \psi_\delta(1, R)}{\partial R} d\sigma \right]_{\sigma=\bar{\sigma}(R)}, \quad [18] \end{aligned}$$

where $\bar{\nu}(R)$ is the equilibrium value of ν , and we keep ν_1 , and ν_2 (and hence ν) fixed when differentiating with respect to R . This follows from the conditions of minimum free energy [13] and [15], and the last expression in [18] is given by Verwey and Overbeek [Ref. (2), p. 62]. These authors also show that it is quite easy to obtain an alternative form for Eq. [18], namely,

$$2A \left[\frac{\partial}{\partial R} \int_0^{\psi_\delta} \sigma d\psi_\delta \right]_{\psi_\delta = \bar{\psi}_\delta(R)}, \quad [18a]$$

where we differentiate with respect to R under the condition of constant surface potential ψ_δ and then substitute $\psi_\delta = \bar{\psi}_\delta(R)$. By integrating [18a] with respect to R to obtain the energy, we see that it becomes possible to combine the method of Verwey and Overbeek (based on keeping the potential constant at the surface) with the theory of Stern. However, we believe that such an integration is unnecessary, since it is sufficient to work with Eq. [17].

4. ALTERNATIVE DERIVATION OF FREE ENERGY

In the preceding section the free energy was determined by carrying through the charging process under the conditions of constant densities of surface ions ν_1 and ν_2 . A different charging process has been employed by Verwey and Overbeek and its relation to our approach has been discussed in the earlier papers of this series (1, 4, 5, 6). Essentially, in the method of these authors, it is assumed that the surface phases of adsorbed ions and the solution phase can coexist in thermodynamic equilibrium for all values of λ and that the surface densities of ions ν_1 and ν_2 take on their equilibrium values at each stage λ during the charging. However, we shall proceed to demonstrate that it is quite possible that we cannot have equilibrium between the particle phase and solution phase over the whole range of λ . It can be shown that the two methods of charging described above are equivalent, but in the proof we assume a value $\nu_1 = \bar{\nu}_1^0$, say, can be found such that $\partial F_0(\nu_1, \nu_2)/\partial \nu_1 = 0$. Application of this condition to Eq. [1] means that $B_1 = 0$. However, it now follows from [13] that $e_1\psi_0 = \Delta\chi_1(1)$, a constant independent of the concentration of type 1 ions in the dispersion medium, whereas experimentally Eq. [15] seems to hold. We conclude that $B_1 \neq 0$ and hence $\nu_1 = \bar{\nu}_1^0$ does not exist, *i.e.*, equilibrium between the two phases with respect to the hypothetical discharged ions of type 1 has no meaning.

This raises the question of the physical meaning of the charging process employed by Verwey and Overbeek. These authors introduce yet another condition, namely, that the charging be carried out at constant surface potential. Now it has already been pointed out in Part IV (7) that it is quite permissible to charge at constant surface potential provided the density of adsorbed ions remains finite. However, for a particle of finite

extent, the considerations in Part III (6) show that if we assume the surface potential is constant during the charging, the surface density of ions becomes infinite as $\lambda \rightarrow 0$, which is physically impossible. In the cases where charging at constant potential yields the correct result (*e.g.*, infinite plate or cylindrical particle of infinite length), Verwey and Overbeek, in effect, assume that the condition of thermodynamic equilibrium at each stage λ is identical with the condition of constant surface potential. This assumption is probably not valid in the general case.

Now Casimir [Ref. (2), p. 63] has proved that the method of charging at constant surface potential is equivalent to the use of a Lippmann equation, and there is essentially no objection to the latter. However in Part III (6) we have derived the Casimir equivalence theorem by starting with a charging process in which the surface density of ions is kept fixed (the method adopted in the preceding sections). The assumption that $F_0(\nu_1, \nu_2)$ has a minimum at $\nu_1 = \bar{\nu}_1^0$ is not introduced in the latter method. In the opinion of the author, the equivalence theorem should be regarded as a convenient mathematical relation, but its physical meaning is unclear. Indeed, as shown in Part III, for a spherical particle (and presumably for particles which are not highly anisometric in shape), the Casimir theorem is not valid and a "correction" term must be introduced.

We conclude that the physical basis of the charging process of Verwey and Overbeek is obscure.* In the present series of papers, the author has developed in great detail the method of charging at constant density of adsorbed ions. We are able to derive the results of Verwey and Overbeek and avoid the doubtful assumptions which have been discussed above. In addition, our method has greater scope; for example, one cannot arrive at the results in this paper by charging at constant potential, except by integrating the force equation [18a], which presumably would have to be done numerically.

It might be claimed that the physical interpretation of the charging process employed by the author is also obscure in one respect. Onsager (7) has pointed out that λ , which appears in the potential energy expression of the ions, has essentially the same status as the parameter of an external force and can therefore be treated as a thermodynamic variable. This is precisely the approach adopted in this series of papers. If, however, the potential-determining type 1 ions form part of the crystal lattice of the

* *Note Added to Proof:* In a private communication, Professor Overbeek states that in the charging method of Verwey and Overbeek, thermodynamic equilibrium is conserved during the entire charging process by suitable (external) manipulation with their difference in chemical potential $\Delta\mu$. The criticisms in Sec. 4 of this paper refer to the text of the book by these authors (Ref. 2, pp. 57-60) in which the real meaning of manipulating their quantity $\Delta\mu$ is left unexplained. In a later paper, a detailed analysis of the charging method of Verwey and Overbeek will be given, and the various difficulties mentioned in Sec. 4 will be resolved.

particles, then we are dealing with the solid state and the usefulness of the charging process for such a system remains to be shown. Our theory apparently meets with no difficulty provided the adsorbed ions can be distinguished from the lattice ions of the particles. For we can regard the solution ions and the adsorbed ions as essentially belonging to one phase, and the walls of the particles as behaving like an external field. When we do differentiate between the adsorbed ions and the lattice ions, then presumably one should discharge all the lattice ions (or at least the first layer of lattice ions on the surface). Further investigation of this problem is desirable, but will not be attempted here.

In view of this last difficulty, we shall briefly indicate an alternative method of deriving Eq. [11], which avoids the charging process. This approach, originally proposed by Derjaguin (9), has been used by Verwey and Overbeek (2). We imagine that the potential-determining ions are transported by infinitesimal amounts from the interior of the solution to the particles, and then the counter ions are brought to the surface in a similar fashion. The change in the "chemical" (nonelectrical) and electrical self-energies are given by the second and third terms on the right of Eq. [12]. The work done against the electrical potential in the double layer is

$$2A \left[e_1 \int_0^{\nu_1} \psi_0(1, R) d\nu_1 + e_2 \int_0^{\nu_2} \psi_\delta(1, R) d\nu_2 \right] \\ = 2A \left[\frac{\nu_1^2 e_1^2}{2K} + e_1 \int_0^{\nu_1} \psi_\delta(1, R) d\nu \right], \quad [19]$$

applying the relation [8]. We therefore obtain again formula [12]. Strictly, we should assume that thermodynamic equilibrium can be achieved during this transfer process, which is an isothermal, reversible one, by postulating an appropriate external electrical potential acting at the surfaces. This does not contribute to the free-energy expression since the external potential vanishes at the end of the process. The preceding method suggests an explanation of the physical origin of the three terms (within brackets) in the free-energy expression [17]. The following picture is an extension of that given by Verwey and Overbeek (*loc. cit.*, p. 53), when they consider the case where the surface charge is due to potential-determining ions only. For simplicity, we assume unit area for the plates.

Let us transport the charge $\sigma = \nu_1 e_1 + \nu_2 e_2$, consisting of ν_1 ions of type 1 and ν_2 ions of type 2 by infinitesimal amounts through a potential difference $\psi_\delta(1, R)$, *i.e.*, under isothermal, reversible conditions. The electrical work done (per plate) is $\int_0^\sigma \psi_\delta(1, R) d\sigma$. Now when ν_2 ions of type 2 are brought from the solution to a plate, there is also a "chemical" free-energy change. (We adopt the terminology of Verwey and Overbeek al-

though their use of "chemical" is not the best of choices since the change in the electrical self-energy of the ion is included.) We shall denote this chemical energy by $\nu_2(\Delta\mu_2 + kT \ln \nu_2)$, where, in our notation $\Delta\mu_2 = -B_2 - \Delta\chi_2(1)$. Verwey and Overbeek did not consider the contribution $\nu_2 kT \ln \nu_2$ and this type of term has been discussed in some detail in Part I (1). It represents an entropy effect which is attributed to the various configurations available to the ν_2 counter ions on the N_s/A sites. The significance of this entropy term is that it is responsible for the variation of the potential $\bar{\psi}_\delta(R)$ with R . This follows from the equilibrium condition [14], since $\nu_2 = \bar{\nu}_2(R)$ varies with R .

Let us first suppose that there is no such entropy term, as would occur, for example, if the ions of type 2 were identical with one of the lattice ions constituting the colloidal particle. If, under this hypothetical condition, $\Delta\mu_2'$ is the chemical free-energy difference with respect to the type 2 ion between the solution and particle phases, then the equilibrium condition [14] would be replaced by

$$\Delta\mu_2' + e_2\psi_\delta(1, R) = 0. \quad [20]$$

This suggests that we imagine the chemical energy $\Delta\mu_2$ to be separated into two (fictitious) parts, $\Delta\mu_2 = \Delta\mu_2' + \Delta\mu_2''$, say. There is a corresponding energy term due to the chemical work done when ν_1 ions of type 1 are brought to the plate, namely, $\nu_1\Delta\mu_1$, where $\Delta\mu_1 = -\Delta\chi_1(1) - B_1$. We shall also divide $\Delta\mu_1$ in such a way that a simple interpretation can be given to the last two terms in [17], namely, we put $\Delta\mu_1 = (e_1/e_2)\Delta\mu_2' + \Delta\mu_1'$. (In the particular case where both types of adsorbed ions are univalent, $\Delta\mu_1 = -\Delta\mu_2' + \Delta\mu_1'$). It is now convenient to consider the part

$$\int_0^\sigma \psi_\delta(1, R) d\sigma + \nu_2\Delta\mu_2' + \nu_1 \frac{e_1}{e_2} \Delta\mu_2' \quad [21]$$

of the work done in bringing ν_1 type 1 ions and ν_2 type 2 ions to each plate. At equilibrium, it follows immediately from [20] that the sum of the three terms in [21] is precisely the integral $-\int_0^{\bar{\psi}_\delta(R)} \sigma d\psi_\delta$, which is derived from the Lippmann equation. Physically, if both types of ions formed part of the crystal lattice of the ions and the potential difference between the crystal phase and solution phase were $\bar{\psi}_\delta(R)$, then we would obtain this intergral for the free-energy difference. Since Verwey and Overbeek worked with this form, we shall refer to it as the "*V. and O.*" term.

In the case of the ions of type 2, there still remains the chemical contribution

$$\nu_2(\Delta\mu_2'' + kT \ln \nu_2), \quad [22]$$

which can be considered to be due to the entropy term. If we write the

equilibrium condition [14] in the form

$$\Delta\mu_2' + \Delta\mu_2'' + kT(1 + \ln\nu_2) + e_2\psi_\delta(1, R) = 0, \quad [14a]$$

and make use of [20], then we readily obtain that at equilibrium the quantity [22] becomes the first term $-kT\bar{\sigma}_2(R)/e_2$ in the brackets in Eq. [17]. We shall, therefore, describe the latter as the "entropy" term.

Finally, the ν_1 potential-determining ions are transported by infinitesimal amounts across the Stern layer. Since this layer has a capacity K , the potential change is $\nu_1 e_1/K = \sigma_1/K$ and the electric work done is

$$\frac{1}{K} \int_0^{\sigma_1} \sigma d\sigma = \frac{\sigma_1^2}{2K}. \quad [23a]$$

We need to add on the change in the chemical energy $\nu_1 \Delta\mu_1'$ since this contribution has not been included so far. If we use [20] and the equilibrium condition [13], which can be expressed as

$$\Delta\mu_1' + \frac{e_1}{e_2} \Delta\mu_2' + e_1\psi_\delta(1, R) + \frac{\nu_1 e_1^2}{K} = 0, \quad [13a]$$

then the above chemical energy becomes

$$\nu_1 \Delta\mu_1' = -\frac{\nu_1^2 e_1^2}{K} = -\frac{\sigma_1^2}{K}, \quad [23b]$$

at equilibrium. Adding the contributions [23a] and [23b], the second term in the brackets in the energy formula [17] is derived. We shall designate this as the "Stern condenser" or simply "condenser" term, since it can be regarded as arising from the introduction of the "atomic condenser" of thickness δ in the Stern theory.

The results [17], which must be examined in conjunction with the equilibrium conditions [13] and [14], is fairly complicated, particularly when the Poisson-Boltzmann equation is applied to find the form of $\bar{\psi}_\delta(R)$. Let us anticipate the general nature of the solution of the latter equation and make use of the result that the (positive) potential $\bar{\psi}_\delta(R)$ increases as R decreases. Then it is possible to gain some knowledge of a qualitative character concerning the behavior of the three terms in Eq. [17] in the following way. Verwey and Overbeek have calculated that when R is large, the potential at the Stern layer $\bar{\psi}_\delta(R)$ varies very little with R . As a consequence, it is convenient to work in terms of the change in this potential when the two plates are brought together from infinite separation. This change will be designated by

$$\Delta\bar{\psi}_\delta(R) = \bar{\psi}_\delta(R) - \bar{\psi}_\delta(\infty). \quad [24]$$

From [13], we derive

$$\bar{\sigma}_1(R) = K(\bar{\psi}_0 - \bar{\psi}_\delta(R)), \quad [25a]$$

and hence the corresponding change in the charge density of the layer of

potential-determining ions is

$$\Delta\bar{\sigma}_1(R) = \bar{\sigma}_1(R) - \bar{\sigma}_1(\infty) = -K\Delta\bar{\psi}_\delta(R). \quad [25b]$$

When computing numerical examples, it is particularly convenient to introduce the dimensionless (positive) quantities

$$\eta(R) = -e_2\bar{\psi}_\delta(R)/kT, \quad \Delta\eta(R) = -e_2\Delta\bar{\psi}_\delta(R)/kT. \quad [26]$$

If $T = 18^\circ\text{C}$. and $-e_2$ is the electronic charge, $\eta(R) = 1$, when $\bar{\psi}_\delta(R) = 25$ millivolts (mv). Thus, in a typical sol, $\eta(R)$ will be of the order of a small integer and at large separations $\Delta\eta(R) \ll 1$. From [16] we immediately derive the relations

$$\bar{\sigma}_2(R) = \bar{\sigma}_2(\infty) \exp[\Delta\eta(R)], \quad [27a]$$

$$\Delta\bar{\sigma}_2(R) = \bar{\sigma}_2(R) - \bar{\sigma}_2(\infty) = \bar{\sigma}_2(\infty)\Delta\eta(R)\{1 + g[\Delta\eta(R)]\}, \quad [27b]$$

where

$$g(x) = (e^x + x - 1)/x = \frac{x}{2} + \frac{x^2}{6} + \frac{x^3}{24} + \dots$$

When the separation R decreases, the positive potential change $\Delta\bar{\psi}_\delta(R)$ increases and, therefore, according to Eq. [25b], the positive charge density $\bar{\sigma}_1(R)$ of potential-determining ions decreases, whereas, according to [27a], the negative charge density $\bar{\sigma}_2(R)$ of counter ions increases in magnitude. These properties have already been observed by Verwey and Overbeek (*loc. cit.*, p. 128). It follows that the "entropy" term in [17] yields a repulsive contribution to the interaction energy; the "condenser" term yields an attraction. Now for large R , $\Delta\eta(R) \ll 1$ and hence both $\Delta\bar{\sigma}_1(R)$ and $\Delta\bar{\sigma}_2(R)$ are proportional to $\Delta\eta(R)$ [or to $\Delta\bar{\psi}_\delta(R)$]. The corresponding change in the net surface charge density is

$$\Delta\bar{\sigma}(R) = \Delta\bar{\sigma}_1(R) + \Delta\bar{\sigma}_2(R) = -\left(K + \frac{e_2\bar{\sigma}_2(\infty)}{kT}\right)\Delta\bar{\psi}_\delta(R). \quad [28]$$

Since $e_2\bar{\sigma}_2(\infty)$ is positive, we derive from [28] that when R is large, the resultant charge density on the plates $\bar{\sigma}(R)$ diminishes with R ; it has already been shown by Verwey and Overbeek that this property applies to all distances. However, these general considerations are not sufficient to determine whether the "V. and O." term in [17] contributes a repulsion or attraction, since its behavior is rather complicated. Let us first assume that $\bar{\psi}_\delta(R)$ is a constant, independent of R . In this case, Verwey and Overbeek have explained that $\bar{\sigma}(R)$ decreases with R and hence the integral in [17] represents a negative quantity which diminishes in magnitude as R is diminished; *i.e.*, its change is positive and thus it represents a repulsion. We find, however, that the upper limit of integration $\bar{\psi}_\delta(R)$ is not constant, but increases as R is decreased. Then it is possible that the magnitude of the "V. and O." term will increase, *i.e.*, the repulsion is

changed into an attraction. Indeed, it will be seen in Sec. 5 that this term may behave either as a repulsion or an attraction, depending on the density of counter ions, the electrolyte concentration, *etc.* Finally, our calculations at small potentials show that the repulsive effect due to the "condenser" term in Eq. [17] *always outweighs* the attractive contributions from the "entropy" and "V. and O." terms, and the net result is a repulsion between the plates.

5. SOLUTION OF APPROXIMATE DEBYE—HÜCKEL EQUATION

Since we are mainly concerned with conditions of coagulation, the potential $\psi_\delta(1, R)$ will be assumed small and proportional to ν (or σ). Then the integral term in [17] becomes

$$-A\bar{\sigma}(R)\bar{\psi}_\delta(R) = -A[\bar{\sigma}_1(R) + \bar{\sigma}_2(R)]\bar{\psi}_\delta(R). \quad [29]$$

This means that we are using the approximate Debye—Hückel equation which yields the formula

$$\psi_\delta(1, R) = \frac{4\pi\sigma}{D\kappa} \coth \frac{1}{2}\kappa R, \quad [30]$$

where $\kappa^2 = (4\pi/DkTV) \sum_{i=1}^s N_i e_i^2$. If we consider the special case where

$\bar{\psi}_\delta(R) = \bar{\psi}_\delta(\infty)$ is independent of R , then it follows from Eqs. [29] and [30] that the change in the energy term [29], when the plates are brought to a distance R from infinity, is

$$\Delta F_0(R) = \frac{AD\kappa}{4\pi} \left(\frac{kT}{e_2} \right)^2 \eta^2(\infty) (1 - \tanh \frac{1}{2}\kappa R), \quad [31]$$

where we substitute

$$\eta(\infty) = -e_2 \bar{\psi}_\delta(\infty)/kT. \quad [26a]$$

This is the expression for the free energy at small potentials used by Verwey and Overbeek and is chosen here as a standard.

If we equate the form

$$\bar{\sigma}(R) = \frac{D\kappa}{4\pi} \bar{\psi}_\delta(R) \tanh \frac{1}{2}\kappa R, \quad [30a]$$

which follows from [30], to the alternative expression $\bar{\sigma}(R) = \bar{\sigma}_1(R) + \bar{\sigma}_2(R)$, where $\bar{\sigma}_1(R)$ and $\bar{\sigma}_2(R)$ are given by [25a] and [27a], respectively, then we derive a relation which yields the variation of $\bar{\psi}_\delta(R)$ with R . Working in terms of $\Delta\eta(R)$, as defined in [26], this relation is

$$\begin{aligned} \Delta\eta(R) \left(1 + \frac{4\pi K}{D\kappa} \right) + l \{ \exp[\Delta\eta(R)] - 1 \} \\ = [\eta(\infty) + \Delta\eta(R)] (1 - \tanh \frac{1}{2}\kappa R), \quad [32] \end{aligned}$$

where we introduced the dimensionless positive quantity

$$l = \frac{4\pi e_2 \bar{\sigma}_2(\infty)}{D\kappa kT} = \frac{4\pi K}{D\kappa} [\eta_0 - \eta(\infty)] - \eta(\infty), \quad [33]$$

where $\eta_0 = -e_2\psi_0/kT > 0$. The second relation in [33] follows from Eqs. [25a], [26], and [30a] at $R = \infty$. A simple interpretation can be given to l . If only the charge density $\bar{\sigma}_2(\infty)$ were present on the wall of a single plate and the linear Debye—Hückel equation is used, then $l = e_2\bar{\psi}_2(\infty)/kT$, where $\bar{\psi}_2(\infty)$ would be the potential at the wall. In the numerical work it is most convenient to determine $\frac{1}{2}\kappa R$ as a function of $\Delta\eta(R)$ [or of $\Delta\bar{\psi}_s(R)$] from Eq. [32]. The change with R in the expression [17] for the free energy can be written as

$$\begin{aligned} \Delta F(R) &= F[\bar{\nu}_1(R), \bar{\nu}_2(R), R] - F[\bar{\nu}_1(\infty), \bar{\nu}_2(\infty), \infty] \\ &= \frac{AD\kappa}{4\pi} \left(\frac{kT}{e_2} \right)^2 \eta(\infty) \Delta\eta(R) \\ &\quad \times \left[h - \frac{l}{\eta(\infty)} \{ [2 - \eta(\infty) - \Delta\eta(R)] g[\Delta\eta(R)] - \Delta\eta(R) \} \right], \quad [34] \end{aligned}$$

where

$$h = \frac{4\pi K}{D\kappa} + l + 1.$$

This result is readily obtained on making use of the previous equations in Sec. 3 and 5.

For large values of R , $\Delta\eta(R) \ll 1$, and then Eq. [32] becomes

$$\Delta\eta(R) \approx \eta(\infty)(1 - \tanh \frac{1}{2}\kappa R)/(h - 1 + \tanh \frac{1}{2}\kappa R). \quad [32a]$$

An examination of Eqs. [32] and [32a] shows that $\Delta\eta(R)$ [and hence $\Delta\bar{\psi}_s(R)$] increases as R decreases, as already mentioned in Sec. 3. The free-energy quantity [34] simplifies to

$$\begin{aligned} \Delta F(R) &\approx \frac{AD\kappa}{4\pi} \left(\frac{kT}{e_2} \right)^2 \eta(\infty) \Delta\eta(R) h \\ &= \frac{AD\kappa}{4\pi} \left(\frac{kT}{e_2} \right)^2 \eta^2(\infty) (1 - \tanh \frac{1}{2}\kappa R) / \left[1 - \frac{1}{h} (1 - \tanh \frac{1}{2}\kappa R) \right] \quad [34a] \end{aligned}$$

for large R . Comparing [31] with [34a] we find that the ratio $\Delta F(R)/\Delta F_0(R)$ is greater than unity, but tends to unity as R increases.

An examination of the above equations shows that, when we use the linear Debye—Hückel equation, the force between the plates is always repulsive. Thus, if we expand the left-hand member of [32] in powers of $\Delta\eta(R)$, it is readily seen that $\Delta\eta(R)$ is a monotonic decreasing function of R and, in addition, that the approximation [32a] is an upper bound. The

expansion of [34] in powers of $\Delta\eta(R)$ yields

$$\Delta F(R) = \frac{AD\kappa}{4\pi} \left(\frac{kT}{e_2} \right)^2 \eta(\infty) \Delta\eta(R) \\ \times \left[h + \frac{l}{2} \Delta\eta(R) + \frac{l}{2} \left(1 + \frac{1}{\eta(\infty)} \right) \Delta\eta^2(R) + \frac{l}{24} \Delta\eta^3(R) + \dots \right] \quad [34b]$$

which is positive and is a monotonic decreasing function of R ; i.e., $\Delta F(R)$ decreases as R increases.

In calculating numerical examples, we have four quantities to choose: the electrolyte concentration (γM say, where $\kappa = \sqrt{\gamma}/3.04 \times 10^{-8}$ at $T = 18^\circ\text{C}$.), the "capacity" K and the potentials $\bar{\psi}_0$ and $\bar{\psi}_\delta$ [or equivalently η_0 and $\eta(\infty)$]. Now we can write [16] as $\bar{\sigma}_2(\infty) = C_1 \kappa^2 \exp[\eta(\infty)]$, where C_1 is a constant which involves the number of adsorption sites and the specific adsorption potential φ_2 . Also Eq. [15] can be expressed as $\eta_0 = C_2 + 2kT \ln \kappa$, where C_2 is another constant. By making use of these relations and of [29], it is possible to determine $\eta(\infty)$ as a function of κ for given C_1 , C_2 , and K . We shall not examine this dependence here but only show how the interaction energy varies with κR in a particular case. Choosing a 1-1 valency type of electrolyte, $T = 18^\circ\text{C}$., $\bar{\psi}_0 = 150$ mv., $\bar{\psi}_\delta(\infty) = 25$ mv. and $4\pi K/D\kappa = 0.3$, then $l = \frac{1}{2}$ and $h = 1.8$. (If $K = 10^7$ then $\kappa = \frac{1}{2} \times 10^7$, yielding an electrolyte concentration of $\gamma = 0.023 M$.) We have plotted the ratio $\Delta F(R)/\Delta F_0(R)$ as a function of $\frac{1}{2}\kappa R$. At contact of the two plates ($R = 0$) this ratio is 2.00 and $\Delta\eta(R)$ reaches its maximum value of 0.90.

The formulas developed in this paper can be considered valid provided $A\nu_2 < N_s/10$, for example. If we choose the number of adsorption sites per cm^2 as $N_s/A = 5 \times 10^{14}$ and $\kappa = \frac{1}{2} \times 10^7$, then it is readily seen that application of the linear Debye—Hückel equation yields $\bar{\nu}_2(\infty) = D\kappa kTl/4\pi e_2^2 = 2.8 \times 10^{12}$ at $T = 18^\circ\text{C}$. ($D = 81$), and hence $A\nu_2/N_s = 0.0056$. Since $l = \frac{1}{2}$ in the example chosen above, the potential $\bar{\psi}_2(\infty)$ associated with the layer of counter ions is only 12.5 mv. If we put $\bar{\psi}_2(\infty) = 100$ mv. and apply the Poisson—Boltzmann equation, then $\bar{\nu}_2(\infty)$ is multiplied by a factor $4 \sinh 2 = 14.5$ and thus $A\nu_2(\infty)/N_s = 0.081$ which is still within the range of validity of the formulas derived in Sec. 3. For higher potentials $\bar{\psi}_2(\infty)$, or appreciably greater electrolyte concentrations $\gamma[\bar{\nu}_2(\infty)]$ being proportional to $\sqrt{\gamma}$, we need to retain the first two terms in the expansion of $\ln(1 - A\nu_2/N_s)$.

Verwey and Overbeek (*loc. cit.*, p. 129) have stressed that for $\kappa R \geq 2$, the potential change $\Delta\bar{\psi}_\delta(R)$ is so small that, as a first approximation, we can assume $\bar{\psi}_\delta(R)$ is independent of R and equate it to its value $\bar{\psi}_\delta(\infty)$ at $R = \infty$. They conclude that at large separations, $\Delta F(R)$ differs only slightly from $\Delta F_0(R)$ and hence that one can use their formula for the free energy, namely, the integral term only, in Eq. [17], with the upper limit

of integration $\bar{\psi}_s(R)$ replaced by $\bar{\psi}_s(\infty)$. Now it can be seen from Fig. 1 that the ratio $\Delta F(R)/\Delta F_0(R)$ is not far from unity when $\kappa R \geq 2$. However the following considerations reveal that this does not mean that our two additional terms in the expression for the free energy, namely the "entropy" and "condenser" terms, are second-order effects at large distances between the plates.

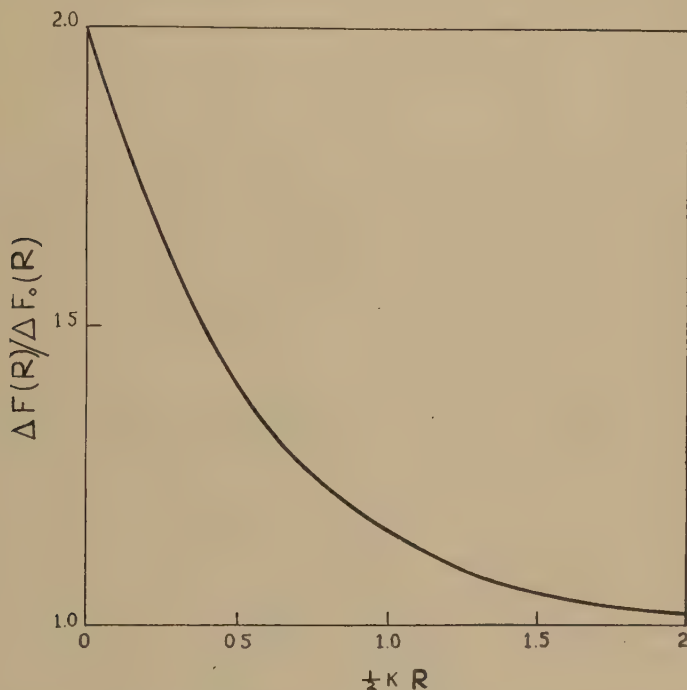


FIG. 1. Variation of the ratio $\Delta F(R)/\Delta F_0(R)$ for different values of κR .

We can express formula [34] for the mutual free energy as the sum of three terms which correspond to the three contributions in the brackets in Eq. [17]. Thus

$$\Delta F(R) = \frac{AD\kappa}{4\pi} \left(\frac{kT}{e_2} \right)^2 \eta(\infty) \Delta\eta(R) (f_1 + f_2 + f_3), \quad [34c]$$

where

$$f_1 = - \frac{2l}{\eta(\infty)} \{1 + g[\Delta\eta(R)]\}, \quad [35a]$$

$$f_2 = 1 + \frac{2l}{\eta(\infty)} + \left(1 + \frac{\Delta\eta(R)}{\eta(\infty)} \right) \tanh \frac{1}{2} \kappa R + \frac{\Delta\eta(R)}{\eta(\infty)} \{1 + g[\Delta\eta(R)]\} \quad [35b]$$

and

$$f_3 = h - 1 - \left(1 + \frac{\Delta\eta(R)}{\eta(\infty)}\right) \tanh \frac{1}{2} \kappa R + l g[\Delta\eta(R)]. \quad [35c]$$

Here f_1 represents the "entropy" term and yields an attraction; f_2 comes from the "condenser" term and gives a repulsion; f_3 represents the integral term of Verwey and Overbeek and is either an attraction or a repulsion. Thus, for large R ,

$$f_1 = -\frac{2l}{\eta(\infty)}, f_2 = 2 \left[1 + \frac{l}{\eta(\infty)}\right], f_3 = h - 2,$$

very nearly and f_3 is positive or negative according as $h \gtrless 2$ or $4\pi K/D\kappa + l \gtrless 1$. We find that at large separations R the "V. and O." term is negative and therefore attractive if the adsorption of counter ions is slight (l is small) and the electrolyte concentration is sufficiently large to make the quantity $4\pi K/D\kappa$ small. For the numerical example above $f_1 \approx -1$, $f_2 \approx 3$, and $f_3 \approx -0.2$ when $\kappa R \gg 1$. Whereas, at $R = 0$, $f_1 = -3.62$, $f_2 = 3.63$, and $f_3 = 2.11$. Thus the behavior of f_3 as a function of κR is rather complex.

Verwey and Overbeek have evaluated the integral term in Eq. [17] by applying the solution of the Poisson—Boltzmann equation and have expressed the free energy of the double layers in terms of elliptic integrals. However, in a forthcoming paper (10), the author, in collaboration with A. Suddaby, has obtained three types of series expansions for the free energy, which are more suitable for numerical work. These results are now being applied to extend the theory in the present paper outside the range of small potentials. It is often assumed that Eq. [30] is applicable only when $|e_2\psi_s(1, R)| \ll kT$ [$\psi_s(1, R) \ll 25$ mv. if $-e_2$ is the electronic charge]. However, this condition is too stringent when we are dealing with the interaction of colloidal particles. As an illustration, by using one of the series just referred to, it is possible to show that the use of the Poisson—Boltzmann equation leads to the values $\Delta\eta^*(0) = 0.971$ and $\Delta F^*(0)/\Delta F_0(0) = 2.15$ at contact of the plates. [The asterisk denotes that we are dealing with the exact (Poisson-Boltzmann) solution, and we assume $\eta^*(\infty) = 1$ and $\eta_0^* = 6$.] Although the potential of the plates at contact is $\bar{\psi}_s^*(0) = 49.3$ mv., the error in the free energy change is only 7% when the Debye-Hückel approximation is applied. Physically it is perhaps possible to understand the reason for this behavior from the following considerations.

First, in the integral [10] for the so-called electrical free energy we see that ψ_s increases from zero to its final value and thus we are dealing with an "effective" potential which is half of its full value. Secondly, the potential in the diffuse layers drops from its maximum value at the particle surface to zero in the bulk of the solution. The assumption which is im-

plicit in the formula [30] is that $|e_2\psi_{av}| \ll kT$, where ψ_{av} is some kind of average of the potential over the whole region of the diffuse layers.

The treatment of the layer of potential-determining ions and the use of the Stern relation (8) are perhaps the most unsatisfactory features of the Stern theory. Recently Grimley and Mott (11) have proposed a different theory in the case where the particle is an ionic crystal, in which these ions do not actually reside on the surface. It should be of considerable interest to investigate how their mechanism can be incorporated into the theory of the interaction of colloidal particles.

SUMMARY

A method is proposed that combines the Stern theory of the double layer with the theory of interaction of colloidal particles developed by the author in earlier papers. Our theory avoids the difficult problem of integrating the force between the particles with respect to the distances. As an illustration, the case of two parallel plates and small surface potentials is treated. In the final formula for the mutual free energy of two plates, there are three terms, one of which has the same form as that obtained by Verwey and Overbeek and can be derived from the Lippmann equation. The two additional terms, which are examined in some detail, are by no means small compared with the expression of these authors.

REFERENCES

1. LEVINE, (Part I), *Trans. Faraday Soc.* **42B**, 102 (1946).
2. VERWEY AND OVERBEEK, *Theory of the Stability of Lyophobic Colloids*. Elsevier, 1948.
3. STERN, *Z. Elektrochem.* **30**, 508 (1924).
4. LEVINE, (Part II), *Trans. Faraday Soc.* **44**, 833 (1948).
5. LEVINE, (Part V), *Proc. Cambridge Phil. Soc.*, in press.
6. LEVINE, (Part III), *Phil. Mag.* **51**, 53 (1950).
7. LEVINE, (Part IV), *Proc. Cambridge Phil. Soc.*, in press.
8. ONSAGER, *Chem. Revs.* **13**, 73 (1933).
9. DERJAGUIN, *Trans. Faraday Soc.* **36**, 203 (1940).
10. LEVINE AND SUDDABY, *Proc. Phys. Soc. (London)*, in press.
11. GRIMLEY AND MOTT, *Faraday Soc. Discussion* **1**, 3 (1947); GRIMLEY, *Proc. Roy. Soc. (London)* **A201**, 40 (1950).

STUDIES ON ION-EXCHANGE RESINS. CAPACITY OF SULFONIC ACID CATION-EXCHANGE RESINS¹

Harry P. Gregor, J. I. Bregman,² Fradelle Guttoff, Robert D. Broadley,
David E. Baldwin³ and C. G. Overberger

Department of Chemistry, Polytechnic Institute of Brooklyn, Brooklyn, N. Y.

Received October 10, 1950

INTRODUCTION

Most studies on ion-exchange resin systems assume that the capacity is based entirely on considerations of chemical equivalence. In most cases, the capacity is determined for a particular ion by using it to displace another ion (usually hydrogen) from the resin phase, followed by analysis for the displaced ion. This method does not consider complex-ion formation within the resin phase. It has also been reported (7,10) that the capacity of some resins for large organic ions is somewhat less than for small inorganic ions.

This paper describes the preparation of sulfonated polystyrene cation-exchange resins, and a study of their capacities for various inorganic and organic ions, as determined by direct analysis. The solution phase was always dilute ($< 0.1 M$), and all experiments were carried out at room temperatures (24–26°C.).

EXPERIMENTAL METHODS

A. Preparation of Resins

Since resins having a high degree of purity and uniformity in a series of varying degrees of cross-linking are not available, their preparation is described in some detail. The sulfonated polystyrene-divinylbenzene resins were prepared as follows (6):

Styrene was distilled under vacuum and stored at 0°C. under nitrogen. The divinylbenzene (Koppers Co.) used was a mixture containing approximately 40% of the divinylbenzene isomers, 45% of the ethylvinylbenzene isomers, 15% diethylbenzene and other nonpolymerizable material, with *tert*-butylcatechol as inhibitor. The crude divinylbenzene was washed three times with equal volumes of 5% sodium hydroxide and three times

¹ The authors wish to thank the Office of Naval Research for the support rendered to this work.

² Present address: National Aluminate Corp., Chicago, Illinois.

³ Present address: Westinghouse Research Laboratories, East Pittsburgh, Pennsylvania.

with distilled water, then dried over anhydrous potassium carbonate and stored at 0°C. under nitrogen. Before each polymerization mixture was made up, a sample of each monomer was added to methanol and used only if no precipitate or cloudiness formed.

Monomer mixtures totaling 100 g. each were made up. Each polymer, and the resin prepared from it, is named according to the percentage by weight of pure divinylbenzene (DVB) used. For example, DVB 8 was prepared from 80 g. styrene and 20 g. crude DVB (8 g. pure DVB). In each of these was dissolved 1.00 g. of benzoyl peroxide. Each monomer mixture was added to 800 ml. water in a 1-l., three-necked flask fitted with a reflux condenser and a sealed V-type glass stirrer, and immersed in a constant-temperature bath at 90°C. The speed of the stirrer was adjusted to give what appeared to be the desired size of beads (0.3–0.5 mm.). The greater the speed of stirring, the smaller the droplets. After 10 min., 10 g. of soluble starch powder was added. Stirring was continued for at least 3 hr. and heating for 20–24 hr., at the end of which time the beads of copolymer were collected, washed with water, and dried. From 92 to 99 g. of dried beads was obtained from each run.

The sulfonation procedure was patterned after that of Topp and Pepper (9). In a 1-l., three-necked flask immersed in a constant-temperature bath at 90°C. and fitted with a sealed glass stirrer were placed 75 g. (approximately 0.74 base moles) of a copolymer of styrene and divinylbenzene and 0.75 g. (1% by weight) of silver sulfate. To this was added 600 ml. (1080 g., 11 moles) of concentrated sulfuric acid, and the stirrer was started. Heating and stirring were continued 20–24 hr. for all copolymers DVB 17 or lower, 48 hr. for DVB 23, 72 hr. for DVB 26, and 1 week for DVB 36.

The sulfonation mixture was poured onto 3 l. of cracked ice with stirring, and the sulfonated beads were collected and washed. The beads were transferred to a large graduated cylinder which was filled with a 50% (by weight) solution of sulfuric acid, stirred well, and allowed to stand for several hours. The beads which floated were separated from those which sank and the procedure was repeated with each fraction at least once. The fraction which floated was incompletely sulfonated, as was shown by capacity determinations, and was not used.

Each DVB fraction was transferred to a column and washed free of electrolyte. Resin DVB 0.4 swelled strongly in distilled water, finally reaching a volume of about 7 l. This resin when wet was white in air but almost transparent in water. The colors of the other resins deepened from amber to black as the divinylbenzene content increased. All resins were dark-brown or black when dry.

The percentage of divinylbenzene in the polymer determines the degree of cross-linking. Since the molecular weights of styrene and divinyl-

benzene are not too different, the DVB number roughly corresponds to the degree of cross-linking.

B. Conditioning of Resins

The sulfonated polystyrene resins and a commercial resin prepared by the same general procedure, Dowex 50 (Dow Chemical Co.), which contains approximately 8% divinylbenzene, were then conditioned. The resin was wet-screened to $-20 + 30$ mesh size, with the exception of some of the highly cross-linked material, which was somewhat smaller. The resin was placed in a column. Then each resin was treated first with an excess of 1 *M* sodium chloride for several hours, then with an excess of 1 *M* hydrochloric acid for several hours. This alternate treatment with salt and with acid was repeated daily for a period of 2 weeks. The resin was then regenerated with a large excess of 1 *M* hydrochloric acid, until the effluent and influent concentrations were the same, and then rinsed with distilled water to an effluent pH of at least 4.5.

The wet resin was then air-dried until it was just free-flowing, following which it was bottled and weighed out as such. The resin decrepitates on rewetting if allowed to become too dry. This extensive conditioning process is necessary to remove low-molecular-weight material and foreign matter from the resin.

The moisture content was determined by vacuum drying at 40°C. The values obtained were the same as those determined by drying over P_2O_5 , although this latter procedure may require many weeks in a desiccator. Oven-drying at 105°C. for 10 hr. gives the same moisture-content values; however, this method results in minor, irreversible changes in the structure of the resin (4).

All of the experimental results described hereafter are given in terms of 1 g. of dry resin in the hydrogen state.

The resins were put into the various inorganic cation states by shaking a 0.5-g. portion with a 100-ml. portion of 1 *M* salt for 1 hr. This was repeated three times, amounting to a 200-fold excess with respect to the resin capacity. The resin was then equilibrated with a 0.01 *M* solution by shaking it successively with three 100-ml. portions. The halide salts were always used.

The data of Table I show how equilibrium conditions are approached. First, the hydrogen resin is treated with 1 *M* potassium chloride to place it in the potassium state as described above. The number of millimoles of hydrogen ions displaced by each portion of salt solution is given in the four columns on the left. Here the liberated acid was titrated. Then the same resin samples were treated with the dilute solutions; these results are shown in the three columns on the right. Here analyses were performed with the flame photometer.

C. Capacity Determination for Inorganic Ions

The capacity of the resins, equilibrated with 0.01 *M* solutions, was determined by drawing off the excess solution by suction, followed by displacement of the cation from the resin. Since the capacity taken (2 mmoles) is very large compared to the amount of cation contained in as much as 1 ml. of solution, it is not necessary to free the resin of all adhering droplets. For the hydrogen capacity, displacement with 1 *M* potassium chloride, followed by titration, was used. All results reported refer to 1 g. of dry hydrogen resin.

For the lithium, sodium, and potassium capacity, the resin was equilibrated with 0.01 *M* solution, the alkali cation was displaced with a large excess of 1 *M* hydrochloric acid, and the solution was evaporated to dryness in a crucible. The potassium and sodium chlorides were ignited over a Bunsen burner. The crucible containing the lithium chloride was flashed to red heat while covered, and was then weighed. In the case of

TABLE I
Equilibration of Resin with Potassium Chloride Solutions

DVB resin	Weight (hydrogen state)	Millimoles of hydrogen ion displaced by 100-ml. portions of 1 <i>M</i> KCl					Concentration of solution after shaking with 100-ml. portions		
		1	2	3	4	Total	2	2	3
	<i>g.</i>						<i>M</i>	<i>M</i>	<i>M</i>
2	0.3216	1.630	0.036	0.000	0.000	1.666	0.0242	0.0114	0.0112
10	0.3391	1.620	0.028	0.000	0.000	1.648	0.0176	0.0113	0.0112
26	0.3612	1.563	0.053	0.006	0.000	1.622	0.0182	0.0113	0.0112

ammonium chloride, the acid solution was evaporated to dryness at 100°C. and weighed as such. The magnesium content was routinely determined by Blacher titration of the hydrochloric acid eluate. In some cases, magnesium was also analyzed for, using 8-hydroxyquinoline. The two methods always agreed within experimental error.

The accuracy of each of the gravimetric analytical procedures described above is greater than $\pm 0.5\%$, while that for the Blacher titration is about $\pm 1\%$. When other cations were present, sodium and potassium concentrations were determined with the flame photometer (Perkin-Elmer, Model 52A). The precision of this instrument when used in the standard manner is about $\pm 2\%$. Higher precision is obtained by regulating the air pressure at the compressor tank at 58–60 lb., and reducing it down to 10 lb. with two reducing valves. In this manner, the air pressure fluctuations can be kept at a minimum. The gas pressure is similarly controlled. Also, calibration curves are made at the same time as the analysis itself, with all of the components of the solution adjusted to substantially the

same concentrations as in the unknown. In this manner, the precision of the instrument can be extended to $\pm 1.0\%$.

D. Capacity Determination for Organic Ions

The capacity of the resins to various quaternary ammonium ions was determined by shaking the hydrogen resin vigorously and continuously with an excess of the hydroxide, followed by back-titration of portions of the solution. This procedure was used rather than that already described for the inorganic cations, because very large excesses of the quaternary ammonium salts would be required. The uptake of potassium hydroxide was also studied, using the same general technique.

The quaternary salts included the tetramethyl-, tetraethyl-, tetra-butyl(*n*)-, and trimethylphenylammonium halides. These were purified by recrystallization from alcoholic media, and converted to the hydroxides with silver oxide. Then 0.2–0.3 g. (dry wt.) of the hydrogen resin, corresponding to a capacity of about 1.5 mmoles was weighed out. It was shaken with 100 ml. of a 0.0300 *M* solution of the base, representing a 100% excess. The amount of base absorbed was determined by back-titration of 5-ml. portions of the solution, carried out at various times. Thus the base concentration at equilibrium was approximately 0.015 *M*. The rate of potassium hydroxide uptake was followed conductometrically.

The particle diameters of the various resins in the potassium state were measured directly with a microcomparator.

EXPERIMENTAL RESULTS

The hydrogen capacities of the various resins is shown in Table II; the capacity, calculated assuming one sulfonic group per benzene ring in the monomers, is also shown. Sulfur determinations lead to calculated capa-

TABLE II
Hydrogen Exchange Capacity

Resin		Calculated mmoles/g.	Capacity	Experimental mmoles/g.
DVB	0.4	5.42		6.85
	2	5.40		5.18
	4	5.37		5.16
	6	5.35		5.09
	8	5.32		5.06
	10	5.29		4.86
	13	5.36		4.94
	15	5.22		5.07
	17	5.19		4.87
	23	5.13		4.24
	26	5.06		4.49
	36	4.90		4.24
Dowex 50				4.90

cities which are in close agreement with the experimental values. In Table III, the exchange capacities to the various inorganic ions for Dowex 50 is given.

When the resin phase contains two different univalent inorganic cations, the total exchange capacity is unchanged, as is shown in Table IV. However, the exchange capacity is somewhat different for divalent ions, or

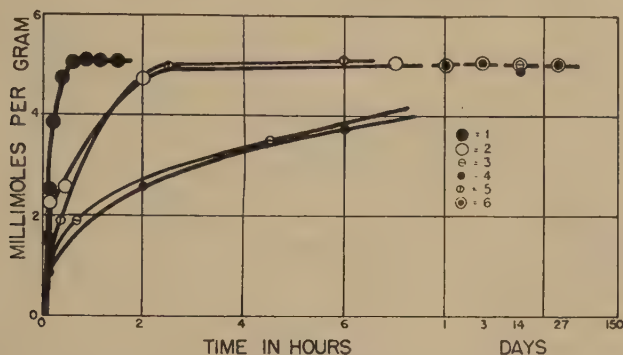


FIG. 1. Uptake of potassium and quaternary ammonium hydroxides from 100 ml. of 0.30 *M* solutions by 0.25–0.3 g. of various hydrogen resins. Symbols are as follows: 1 = potassium; 2 = tetramethylammonium; 3 = tetraethylammonium; 4 = tetrabutylammonium; 5 = trimethylphenylammonium; 6 = all cations; DVB 6.

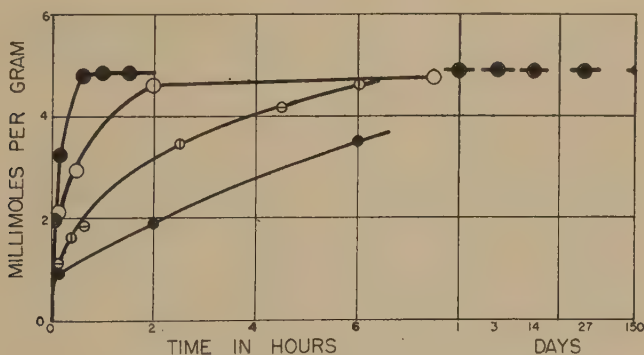


FIG. 2. DVB 10. See Fig. 1 for explanation.

mixtures of divalent and univalent ions. The data of Table V gives the capacity of Dowex 50 in the magnesium and magnesium–potassium states.

The uptake of quaternary ammonium ions by various DVB resins is shown in Figs. 1–5. Here the reaction goes to completion as the quaternary base enters the resin phase. When an excess of quaternary halide is shaken with the resin, the reaction is very much slower. With Dowex 50, identical

capacities were obtained with both tetraethylammonium bromide and the corresponding hydroxide.

In order to compare the rates of uptake of the various quaternary ammonium ions, diffusion coefficients have been calculated. Resin particle sizes were determined with the microcomparator for eight randomly selected particles in each series. The resins were in the potassium state. The size of the particle enters into the diffusion equation as the reciprocal

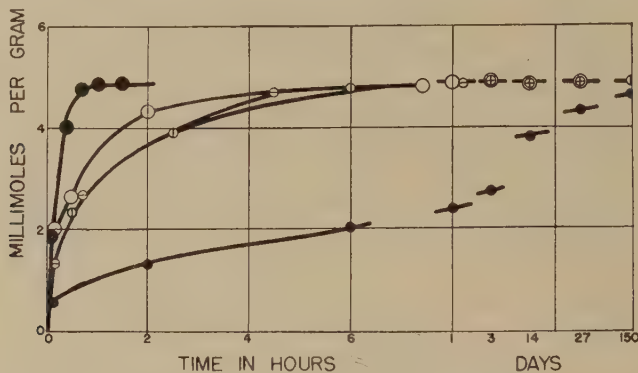


FIG. 3. DVB 17. See Fig. 1 for explanation.

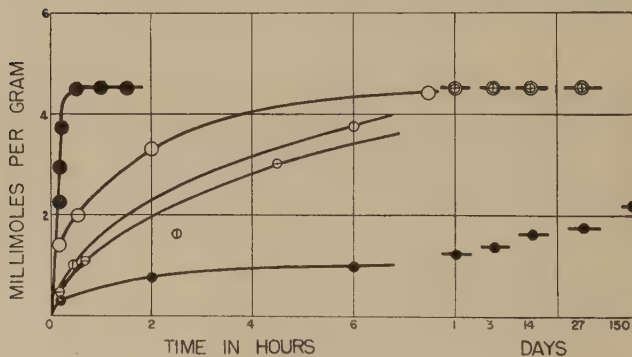


FIG. 4. DVB 26. See Fig. 1 for explanation.

of the radius (r); values of $1/r$ and their average deviations in cm.^{-1} are as follows: DVB 6, 3.7 ± 0.6 ; DVB 10, 5.9 ± 0.8 ; DVB 17, 7.1 ± 0.4 ; DVB 26, 5.0 ± 0.9 ; DVB 36, 19 ± 8.0 .

The equations for diffusion from solution into a sphere are well known (1). The initial portion of the diffusion process is adequately described by the simplified expression $Q_t/Q_\infty = 6/r (D_i t/\pi)^{1/2}$, where Q_t and Q_∞ are the amounts absorbed at time t and at equilibrium, respectively, r is the radius of the particle, and D_i the diffusion coefficient within the resin phase.

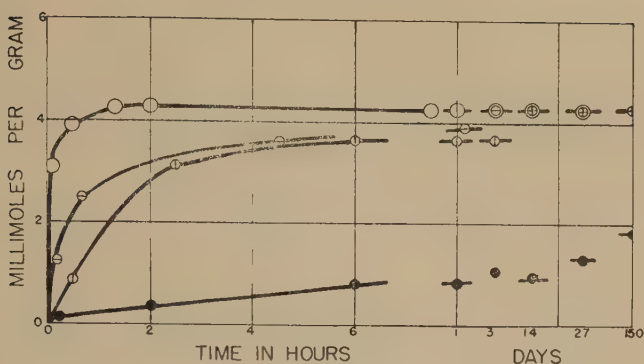


FIG. 5. DVB 36. See Fig. 1 for explanation

This equation has been applied by other investigators (2,3,8) with some success. For the purposes at hand, values of D_i are calculated by taking the half time, i.e., the point where $Q_t/Q_\infty = 0.5$, and substituting it into the diffusion equation. A discussion of the validity of this calculation will be deferred to a later section. These calculated values of D_i are given in Table VI. Included are values of D_o , the diffusion coefficient for the cation in dilute solution, calculated from the conductance data of Hale and DeVries (5) for the quaternary ammonium cations. Also included is the ratio D_i/D_o for the cations in question.

The diffusion equation predicts that the plot of Q_t/Q_∞ should be linear with $t^{1/2}$ for the initial uptake; the data for DVB 10 and DVB 26 are plotted in this manner in Figs. 6 and 7.

DISCUSSION

The various DVB resins show a high degree of uniformity as regards sulfonic acid content. In the case of DVB 0.4, which is a very soft gel, there are about 1.26 sulfonic acid groups per benzene ring. In the range DVB 2-17, there are 0.94 sulfonic acid groups per benzene ring, while in the range DVB 23-26 there are 0.86 groups per ring. These differences in capacity may reflect different susceptibilities of the various resins to the sulfonating agent. The more tightly cross-linked material is sulfonated with more difficulty.

TABLE III

Capacity of Dowex-50 in Different Inorganic Cationic States

Cation	Capacity mmoles/g.
Li^+	4.87
Na^+	4.88
K^+	4.90
NH_4^+	4.91
H^+	4.90

The data of Table III show that for univalent cations, a single cation is absorbed for each exchange site. Thus no complex ions or mixed salts appear to be present, at least in appreciable quantities. Similar data are obtained for resins of higher degrees of cross-linking with these inorganic ions. The data of Table IV show that where two univalent cations are present in the resin phase, the total capacity is unchanged. This is further evidence against complex- or mixed-salt formation.

TABLE IV
Capacity of Dowex-50 in Potassium-Sodium States

Potassium mmoles/g.	Sodium mmoles/g.	Total mmoles/g.
4.90	1.00	4.90
3.91	1.00	4.91
3.62	1.28	4.90
3.40	1.51	4.91
2.50	2.39	4.89
1.48	3.42	4.90
0.82	4.08	4.90
0.0	4.90	4.90

The resin capacity to divalent ions is somewhat greater than its univalent ion capacity. In Table V, the magnesium capacity is shown to be about 7% greater than the potassium capacity. When both potassium and magnesium are present in the resin phase, the total equivalent capacity is approximately that towards magnesium when the majority of the exchange sites are occupied by the divalent ion. The capacity then decreases continually with decreasing mole fraction of magnesium, until it is about that of potassium when the mole fractions reach 0.5. These effects, namely, an increased resin capacity are observed in the case of other alkaline earth cations.

The interpretation of this effect is highly speculative at this time. A possible explanation is that the divalent ions form complex ions, of the

TABLE V
Capacity of Dowex-50 in Magnesium-Potassium States

Magnesium mequiv./g.	Potassium mequiv./g.	Total mequiv./g.
5.23	0.0	5.23
4.81	0.35	5.16
4.41	0.82	5.23
4.13	1.14	5.27
2.46	2.67	5.13
2.10	2.99	5.09
1.76	3.18	4.94
1.39	3.51	4.90
0.0	4.90	4.90

form MgCl^+ or MgOH^+ . The very high concentrations within the resin phase make this plausible.

The exchange capacity of the various DVB resins toward the quaternary ammonium ions is equal to the hydrogen capacity, with the possible exception of the tetra-*n*-butylammonium ion. After 150 days, the inorganic ion capacity is almost reached for this ion with resin DVB 17. Resins DVB 26 and DVB 36 appear to continue absorbing this ion, and may reach the inorganic capacity eventually. Therefore, it appears that there is no "screening" effect with these resins for ions up through the tetraethyl- or trimethylphenylammonium ion sizes. The fact that the capacity is never greater than the number of exchange sites shows that molecular adsorption as such is not present to an appreciable extent.

The variations in the rates of adsorption are of considerable interest. The calculated values of D_i are suitable for qualitative comparisons only,

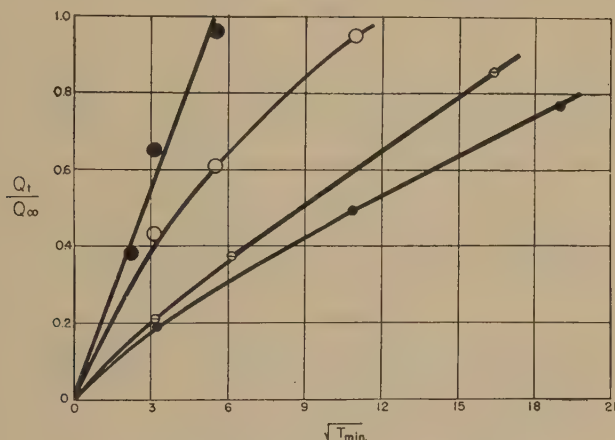


Fig. 6. Uptake of various bases by resin DVB 10.

because (a) the diffusion equation used is valid only for the initial uptake even under ideal conditions, (b) the radius of the resin particles increases with the absorption of the large, quaternary ammonium ions, and (c) the resin permeability is certainly altered by this uptake and swelling. The concentration of base in solution, a parameter which also determines the rate, is continually changing. Furthermore, this is a process of base absorption combined with that of cation exchange, although the rate-determining step is very probably the diffusion of the large organic ion.

As can be seen in Figs. 6 and 7, considerable deviations from linearity occur. For that reason, D_i is calculated from t_i , so that it corresponds to an average value of the diffusion coefficient over the first 50% of the uptake. The inaccuracies in the calculated values of D_i are such as to make only gross differences significant.

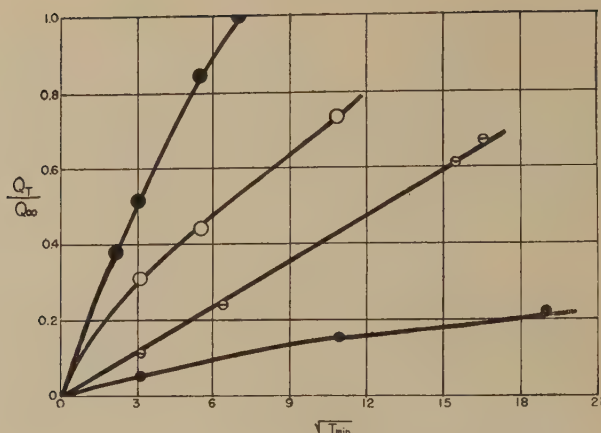


FIG. 7. Uptake of various bases by resin DVB 26.

Table VI does, however, show some striking differences. It is interesting to note that D_i for the potassium ion is about the same for all of the resins. The absolute magnitude of D_i for potassium is in qualitative agreement with values reported for sulfonic acid resins (2,3). For resin DVB 6, the permeability coefficient, D_i/D_0 , is approximately the same for all cations. The value of D_i/D_0 is somewhat lower in resin DVB 10 for all of the ions, particularly for the $(C_2H_5)_4N^+$ and $(C_4H_9)_4N^+$ ions. Resin

TABLE VI

Calculated Values of Cationic Diffusion Coefficients in the Resin Phase (D_i), in the External Solution (D_0), and Their Ratios

Quantity	DVB resin	K ⁺	Me ₄ N ⁺ ^a	Et ₄ N ⁺ ^b	Bu ₄ N ⁺ ^c	Me ₃ PhN ⁺ ^d
$D_i \times 10^7$	6	26	14	2.9	.25	7.8
$D_i \times 10^7$	10	15	6.5	1.5	0.86	1.5
$D_i \times 10^7$	17	14	4.0	2.2	0.048	2.0
$D_i \times 10^7$	26	16	3.4	0.88	0.0070	0.88
$D_i \times 10^7$	36	—	3.3	0.25	0.000026	0.13
$D_0 \times 10^7$		185	89	57	24	—
$D_i/D_0 \times 10^2$	6	14	16	5.1	11	—
$D_i/D_0 \times 10^2$	10	8.1	6.5	2.5	2.2	—
$D_i/D_0 \times 10^2$	17	7.6	4.5	3.9	0.20	—
$D_i/D_0 \times 10^2$	26	8.7	3.4	1.6	0.028	—
$D_i/D_0 \times 10^2$	36	—	3.7	0.44	0.00010	—

^a Tetramethylammonium ion.

^b Tetraethylammonium ion.

^c *n*-Tetrabutylammonium ion.

^d Trimethylphenylammonium ion.

DVB 17 shows the first strong evidence of sterically hindered diffusion, for D_i for the $(C_4H_9)_4N^+$ ion is reduced by an order of magnitude over values for the other ions. With resin DVB 26, a still stronger retardation is found, and resin DVB 36 shows a tenfold retardation for the $(C_2H_5)_4N^+$ ion. The permeability of the resin to the $(C_4H_9)_4N^+$ ion is but 10^{-4} of that to the $(CH_3)_4N^+$ ion. These sharp differences suggest that separations might be effected in favorable cases on a kinetic basis alone.

It is also of interest to note that D_i for the $(CH_3)_3C_6H_5N^+$ ion is between values for the $(CH_3)_4N^+$ and $(C_2H_5)_4N^+$ ions in resin DVB 6, is equal to D_i for $(C_2H_5)_4N^+$ with resins DVB 10, 17, and 26, becoming less in resin DVB 36. This effect may be connected with the asymmetry of this ion, and also with diffusion in the absorbed state. A following paper will show that this ion is strongly absorbed at the exchange site.

Thus it appears that these ion-exchange resins, which are cross-linked polyelectrolytes, behave like concentrated electrolytic solutions. The fact that the univalent cation capacity is the same for all ionic species shows that electroneutrality is observed, that all exchange sites are available, and that molecular adsorption plays a negligible role. It is known that the sequence of selectivity coefficients follows the sequence of (hydrated) ionic volumes. In view of the above, this selectivity effect cannot be explained on the basis that some exchange sites are unavailable to the larger ions.

The fact that (a) there is on the average one sulfonic acid group per benzene ring, (b) that all exchange sites are occupied, even for very large ions, (c) that the capacity is very nearly the same for particles of all sizes having the same degree of cross-linking, and (d) that microscopic examination of split particles shows no observable inhomogeneity, points up the homogeneity of these systems. The kinetic studies of other workers corroborates this point of view (2,3,8).

This paper is the first of a series which deals with the fundamental properties of ion-exchange systems. Future papers will consider the particle volume, the distribution coefficient, the freezing point, and the vapor pressure of these systems.

SUMMARY

1. The preparation of a series of sulfonated polystyrene-divinylbenzene cation-exchange resins is described.

2. Exchange capacities are found to be identical to all inorganic and organic univalent cations studied, with the possible exception of the tetra-(*n*)-butylammonium ion. The divalent cation capacities are slightly larger in every case.

3. Studies of rates of uptake are presented, and diffusion coefficients calculated. The rate of uptake is correlated with both the ionic volume and the degree of cross-linking of the resin structure.

REFERENCES

1. BARRER, R. M., *Diffusion In and Through Solids*. Macmillan Co., New York, 1941.
2. BAUMAN, W. C., AND EICHHORN, J., *J. Am. Chem. Soc.* **69**, 2830 (1947).
3. BOYD, G. E., ADAMSON, A. W., AND MYERS, L. S., JR., *J. Am. Chem. Soc.* **69**, 2836 (1947).
4. GREGOR, H. P., HELD, K. M., AND SUNDHEIM, B. R., in preparation.
5. HALE, C. H., AND DEVRIES, T., *J. Am. Chem. Soc.* **70**, 2473 (1948).
6. HOHENSTEIN, W. P., VINGIELLO, M., AND MARK, H., *India Rubber World* **110**, 291 (1944).
7. KUNIN, R., *Anal. Chem.* **21**, 87 (1949).
8. KUNIN, R., AND MYERS, R. J., *J. Phys. & Coll. Chem.* **51**, 1111 (1947).
9. TOPP, N. E., AND PEPPER, K. W., *J. Chem. Soc.* **1949**, 3299.
10. RICHARDSON, R. W., *Nature* **164**, 916 (1949).

THE MEASUREMENT OF THE FLOW PROPERTIES OF A PSEUDOPLASTIC WITH A CONCENTRIC CYLINDER VISCOMETER

Carl G. Lindquist and William C. Sierichs¹

Stanford University, Stanford, California

Received October 30, 1950

INTRODUCTION

The flow characterization of pseudoplastic and other non-Newtonian systems has been determined in most cases by employing more or less standard viscosity-measuring instruments and comparing empirical results with similar measurements for other systems. Few, if any, measurements have been known to permit determination of the absolute flow properties of pseudoplastic systems. It has been often suggested that if one will employ concentric cylinders of very large diameter the rate of shear will be essentially constant across the annular space and a close approximation to a true shear force-rate of shear curve may be determined. This is certainly sound reasoning but it is difficult to know, a priori, how large the cylinders must be, what clearance between cylinders is allowable, and how close the resulting approximation is to the facts.

It is the purpose of this paper to demonstrate the type of measurements which can be made to closely approximate the true shear stress-rate of shear curve for a pseudoplastic system for which the rate of shear in laminar, steady flow is, at a fixed temperature, a function of the shear stress only. Measurements will be described which were made on an aqueous methylcellulose system in this laboratory by one of us (1).

THEORY

In the case of a Newtonian liquid the absolute viscosity can be determined with a concentric cylinder viscometer such as the MacMichael viscometer. This is possible because the functional relation between rate of rotation and rate of shear is readily evaluated (2). In the case of non-Newtonian systems the rate of shear is not known at any radial distance between the two cylinders since the functional relation between rate of rotation and rate of shear cannot be evaluated.

However, if for a pseudoplastic system one carries out a set of measurements at different rates of rotation for a number of inner cylinders of

¹ Now at Allied Chemical and Dye Corp., Hopewell, Va.

different diameter holding the outer cylinder diameter constant, data are obtained which may be extrapolated to zero clearance between the two cylinders. As the clearance between the two cylinders becomes smaller the difference between the terminal rates of shear becomes less, so that we approach at the limit a constant rate of shear across the annular space.

The rate of shear (due to fluid friction) at any point in the annular space is $r \frac{d\omega}{dr}$.

$$r \frac{d\omega}{dr} = \frac{dv}{dr} - \omega. \quad [1]$$

The rate of shear at the inner cylinder wall is $\frac{dv}{dr}$, since $\omega = 0$. The apparent shear rate at the inner wall might be defined then as $\frac{\Delta v}{\Delta r} = \frac{R_2 \Omega}{R_2 - R_1}$. If for a series of inner cylinders we hold the shear force per unit area at the inner cylinder wall constant the apparent shear rate, $\frac{R_2 \Omega}{R_2 - R_1}$, will approach the true shear rate as the clearance approaches zero.

The shear rate at the outer cylinder wall is $\frac{dv}{dr} - \Omega$ and the apparent shear rate may be defined as $\frac{R_2 \Omega}{R_2 - R_1} - \Omega = \frac{R_1 \Omega}{R_2 - R_1}$. If we hold the shear force per unit area at the outer cylinder wall constant the quantity $\frac{R_1 \Omega}{R_2 - R_1}$ should then approach the true shear rate as the clearance approaches zero. However, since $R_1 = R_2$ at zero clearance, it should be possible to extrapolate τ_1 vs. $\frac{R_1 \Omega}{R_2 - R_1}$ (τ_2 constant) and τ_2 vs. $\frac{R_2 \Omega}{R_2 - R_1}$ (τ_1 constant) to the same intercept at zero clearance.

Whether we employ a constant shear stress at the inner cylinder wall or at the outer cylinder wall should be immaterial with respect to the extrapolated value obtained. However by employing both separately one can obtain a guide to the correct form of the extrapolation curves, as will be demonstrated below.

One should bear in mind that with non-Newtonian systems the dispersed aggregates may become large relative to the clearance between the cylinders as the clearance becomes small. If this were the case one would expect to find deviations in the curves of apparent shear rate versus clearance at small clearances. In the work reported here a minimum clearance of 0.12 cm. was employed and we found no such deviation. Accordingly, it is believed that the bulk shear properties were being measured.

LIST OF SYMBOLS

- r Radius to a point in the concentric cylinder viscometer.
 ω Angular velocity at r .
 v Linear velocity at r .
 R_1 Radius of inner cylinder.
 R_2 Internal radius of cup or radius of outer cylinder.
 Ω Angular velocity of outer cylinder or cup.
 τ Shear stress at r in the concentric cylinder viscometer.
 τ_1 Shear stress at inner cylinder wall.
 τ_2 Shear stress at outer cylinder wall.
 $r \frac{d\omega}{dr}$ Frictional rate of shear at r .
 $\left(r \frac{d\omega}{dr} \right)_1$ Frictional rate of shear at inner cylinder wall.
 $\left(r \frac{d\omega}{dr} \right)_2$ Frictional rate of shear at outer cylinder wall.
 G Apparent rate of shear, $\frac{R_1 \Omega}{R_2 - R_1}$ or $\frac{R_2 \Omega}{R_2 - R_1}$.
 Ω_1, Ω_2 Angular velocities which produce the same shear stress at the outer and inner cylinder walls, respectively.

EXPERIMENTAL

A standard Eimer and Amend, Model 1037, MacMichael viscometer, was employed with the following modifications:

- (a) A cup of 7 cm. internal diameter was provided.
- (b) Inner cylinders having diameters of 6.18 cm., 6.38 cm., 6.60 cm., and 6.76 cm. were provided. These cylinders were made with flat bottoms.
- (c) The circular disk for measuring the angular displacement of the inner cylinder was replaced with an enlarged disk to facilitate accurate reading of the displacement.

Temperature measurement was made with a thermocouple immersed in the test liquid in the annular space between the cylinders. A Type K Leeds and Northrup potentiometer was used to measure the electromotive force (e. m. f.). The thermocouple was removed just prior to a shear force-rate of rotation reading and replaced for a second temperature check just after the reading. The data reported below have all been corrected to a temperature of $30 \pm 0.1^\circ\text{C}$.

This correction was made by utilizing all data taken at $29.5 \pm 0.1^\circ\text{C}$., $30.0 \pm 0.1^\circ\text{C}$., and $30.5 \pm 0.1^\circ\text{C}$. Three shear stress-apparent rate of shear curves for each pair of cylinders were drawn from four to seven experimental points at each temperature. The complete and final curve, at $30.0 \pm 0.1^\circ\text{C}$., was then obtained by interpolation. In a few cases, where there were more than seven experimental points at 30.0°C .,

interpolation was not necessary. No investigation of the effect of rate of shear upon the temperature coefficient of apparent viscosity was made.

The test liquids were 5% aqueous solutions of Dow Methocel [25 centipoises (cps.) and 100 cps.]. The change in apparent viscosity with time which may be due in part to degree of dispersion, and in part to hydrolysis, and in part to unknown causes was carefully checked and all readings were taken over a period in which this change was not significant.

Fischer and Lindsley (3) have done work on the same chemical system employing two different outer cylinders in a Stormer viscometer. They recommend the use of a small clearance and a mean shear rate based on Newtonian characteristics, along with a mean shear stress, to give results correct to within an estimated 10% of apparent viscosity, the latter being reckoned as the slope of the shear stress-rate of shear curve. They did not, however, report any conclusions regarding the absolute or "true" flow properties of the system, nor establish the magnitude of error involved in their method.

The measurements here were made employing two different quantities of sample with each inner cylinder. A micrometer-syringe buret was used to measure sample volumes. Thus measurements were available for two different wetted areas of the cylinders. Torques were subtracted for the same rates of rotation to eliminate the bottom correction. Whether this method, similar to that of Searle (4), is a correct procedure for cylinders of limited length (4 cm.) may be questioned. However, it proved satisfactory for a Newtonian liquid and is believed to be sufficiently accurate for the present purposes. This procedure was chosen when it was found that reproducibility with the usual cone-bottom cylinders was impossible to obtain, presumably because of unequal wetting within the cone.

The ratio between torque and deflection was determined for each wire used by calibration with a Bureau of Standards standard viscosity oil. The shear stress at the inner cylinder wall, the outer cylinder wall, or at any concentric area between these is then obtained by applying the difference in torque for two volumes of the test material to the differential wetted area involved.

RESULTS

The results are shown graphically in Figs. 1 and 2, for one of the three test liquids. The curves in these figures have been extrapolated to the origin, the minimum shear stress varying from 80 to 150 dynes/cm² for the different clearances. In Fig. 1 the shear stress at the inner cylinder wall (called τ_1) is plotted against $\frac{R_1 \Omega}{R_2 - R_1}$, and the shear stress at the outer cylinder wall (τ_2) is plotted against $\frac{R_2 \Omega}{R_2 - R_1}$. The dotted curve

shown on Fig. 1 and also on Fig. 2 will be explained below. In Fig. 2 the solid curves represent plots of τ_1 vs. $\frac{R_2 \Omega}{R_2 - R_1}$ (upper set) and of τ_2 vs. $\frac{R_1 \Omega}{R_2 - R_1}$ (lower set). In Fig. 3 the data from the solid curves of Figs. 1 and 2 have been employed to extrapolate the apparent rate of shear to zero clearance in order to find the "true" rate of shear. The intercepts of Fig. 3 are then taken to derive a true $\left(\tau \text{ vs. } r \frac{d\omega}{dr}\right)$ curve and this has been shown as the dotted curve on Figs. 1 and 2.

The procedure by which the "true" flow properties were thus obtained is, of course, laborious but no other procedure appears to have been suggested to date. Whereas the employment of a single pair of cylinders will not lead to absolute flow properties the accuracy of the data obtained, if properly interpreted, can be determined.

ACCURACY OF DATA FROM A SINGLE PAIR OF CYLINDERS

It is apparent from Fig. 3 that for any finite clearance τ_1 vs. $\frac{R_2 \Omega}{R_2 - R_1}$ is more accurate (closer to the true curve) than τ_1 vs. $\frac{R_1 \Omega}{R_2 - R_1}$, and also

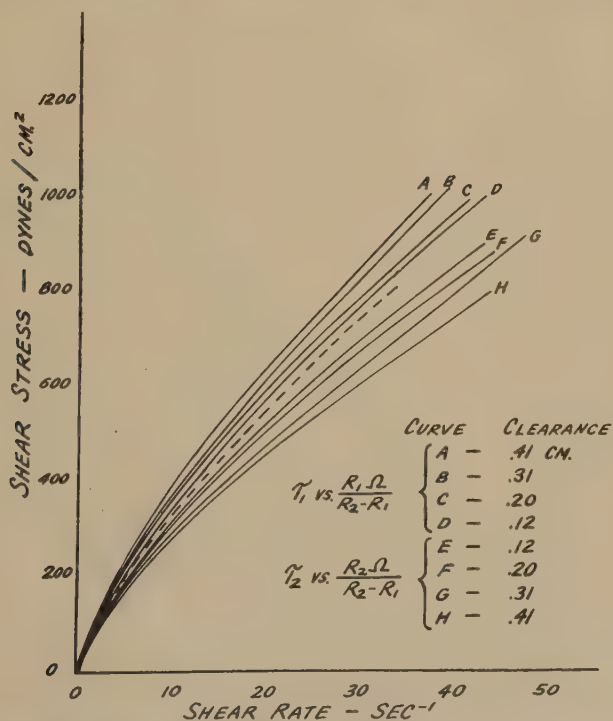


FIG. 1. Shear stress versus apparent shear rate for 5% 100-centipoise Methocel at 30°C.

that τ_2 vs. $\frac{R_1 \Omega}{R_2 - R_1}$ is more accurate than τ_2 vs. $\frac{R_2 \Omega}{R_2 - R_1}$. That this is generally true for a pseudoplastic can be readily shown.

Consider any particular pair of cylinders with the rotating cylinder in motion at a uniform speed. Since τ_1 is greater than τ_2 ($\tau r^2 = \text{constant}$), $\left(r \frac{d\omega}{dr}\right)_1$ must be greater than $\left(r \frac{d\omega}{dr}\right)_2$. But since $R_1 < R_2$, $\left(\frac{d\omega}{dr}\right)_1$ must be greater than $\left(\frac{d\omega}{dr}\right)_2$. Accordingly, $\frac{\Delta\omega}{\Delta r} = \frac{\Omega}{R_2 - R_1}$ must $< \left(\frac{d\omega}{dr}\right)_1$ and $> \left(\frac{d\omega}{dr}\right)_2$. Therefore, $\frac{R_1 \Omega}{R_2 - R_1} < \left(r \frac{d\omega}{dr}\right)_1$ and $\frac{R_2 \Omega}{R_2 - R_1} > \left(r \frac{d\omega}{dr}\right)_2$. The curves τ_1 vs. $\frac{R_1 \Omega}{R_2 - R_1}$ and τ_2 vs. $\frac{R_2 \Omega}{R_2 - R_1}$ therefore bracket the true curve, τ vs. $\frac{r d\omega}{dr}$. The curve τ_1 vs. $\frac{R_2 \Omega}{R_2 - R_1}$ must lie to the right and below τ_1 vs. $\frac{R_1 \Omega}{R_2 - R_1}$ and to the left and above τ_2 vs. $\frac{R_2 \Omega}{R_2 - R_1}$. The curve τ_2 vs. $\frac{R_1 \Omega}{R_2 - R_1}$ must lie to the left and above τ_2 vs. $\frac{R_2 \Omega}{R_2 - R_1}$ and to the right and below τ_1 vs. $\frac{R_1 \Omega}{R_2 - R_1}$.

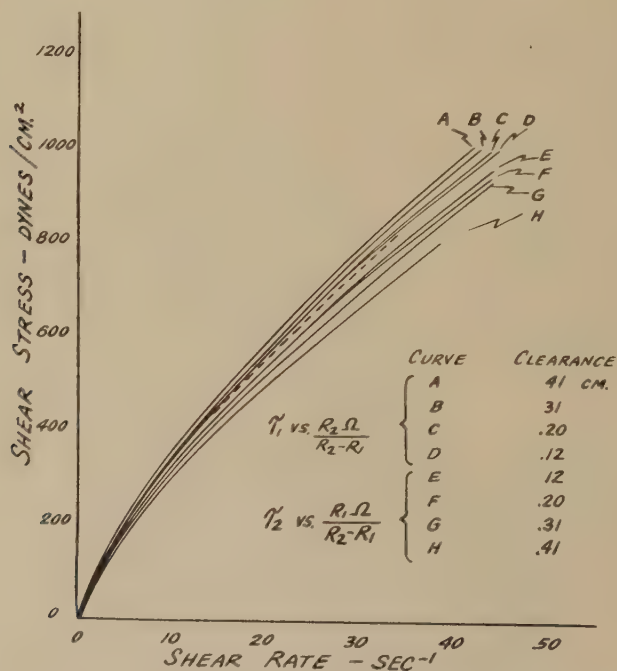


FIG. 2. Shear stress versus apparent shear rate for 5% 100-centipoise Methocel at 30°C.

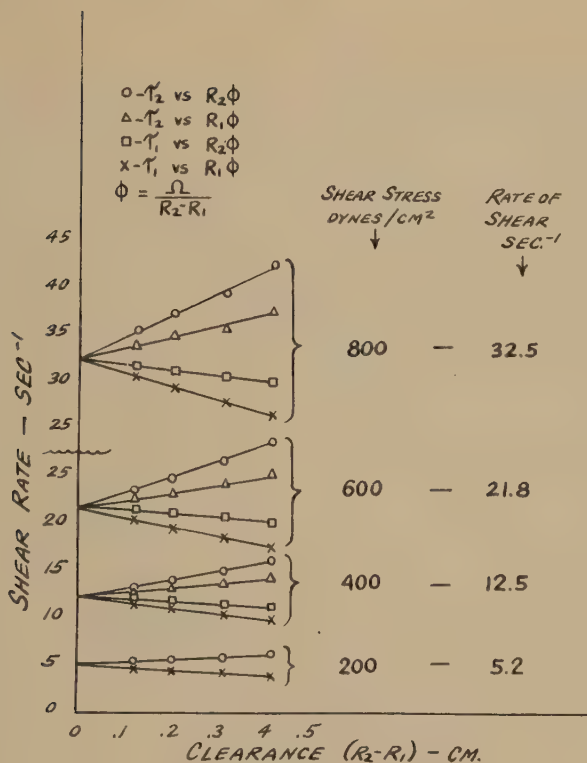


FIG. 3. Determination of true shear rate from data of Figs. 1 and 2.

Now consider a particular pair of cylinders and hold the inner cylinder displacement (torque) constant. For a Newtonian liquid $\left(r \frac{d\omega}{dr}\right)_1 >$

$\frac{R_2 \Omega}{R_2 - R_1}$. But for a pseudoplastic the angular velocity of the outer cup must be less than for the corresponding Newtonian liquid.² Hence for a pseudoplastic $\left(r \frac{d\omega}{dr}\right)_1 > \frac{R_2 \Omega}{R_2 - R_1}$. In a similar manner it can be shown that $\left(r \frac{d\omega}{dr}\right)_2 < \frac{R_1 \Omega}{R_2 - R_1}$.

For any fixed pair of cylinders it is, therefore, expedient to plot τ_1 vs. $\frac{R_2 \Omega}{R_2 - R_1}$ and τ_2 vs. $\frac{R_1 \Omega}{R_2 - R_1}$. Between these two curves will lie the true curve.

The plot, Fig. 4, is drawn from the data obtained on a single pair of cylinders. All four possible plots of shear stress vs. apparent rate of

² The "corresponding" Newtonian liquid is one having a viscosity equal to the ratio of shear stress to rate of shear of the pseudoplastic at the inner cylinder wall.

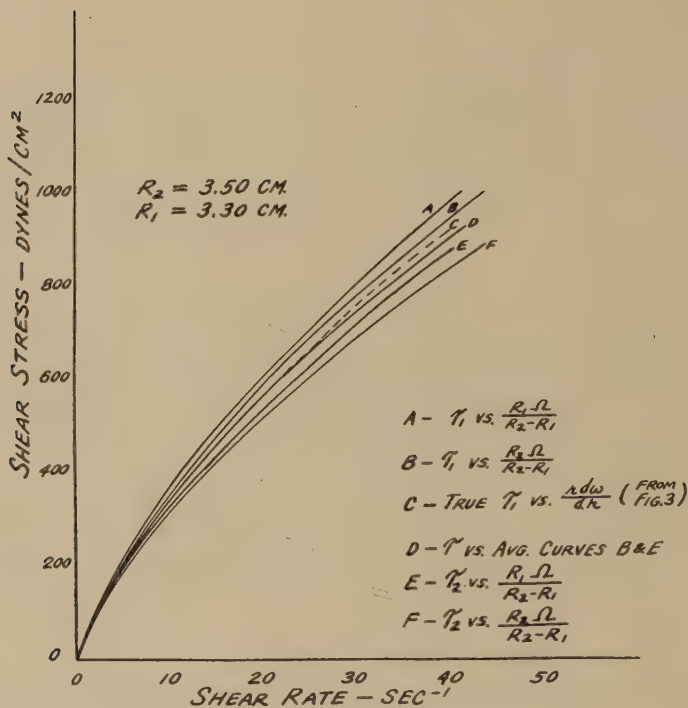


FIG. 4. Determination of an approximate shear stress-shear rate curve from data on a single pair of cylinders.

shear are shown as curves A, B, E, and F. Curve D is obtained by taking the average rate of shear for curves B and E at several values of shear stress. It may be compared with curve C, the "true" shear stress-rate of shear relation as determined from the intercepts in Fig. 3. Other averaging methods may, of course, be applied to the curves B and E.

That the averaging method employed in Fig. 4 to obtain curve D will always result in as close an approximation to the true curve as it did here is not to be assumed. What may be assumed is that this method will yield an averaged curve which must be at least as close to the true curve as it is to either of the curves $\left(\tau_1 \text{ vs. } \frac{R_2 \Omega}{R_2 - R_1}, \text{ or } \tau_2 \text{ vs. } \frac{R_1 \Omega}{R_2 - R_1} \right)$ from which it was produced. In other words, assuming negligible experimental error, the true rate of shear at any shear stress is that of this averaged curve $\neq \frac{\Delta G}{2}$, where ΔG is the difference $\frac{R_1 \Omega_1}{R_2 - R_1} - \frac{R_2 \Omega_2}{R_2 - R_1}$, Ω_1 and Ω_2 being the rates of rotation which produce the shear stress in question at, respectively the outer and inner cylinder walls.

DISCUSSION

The extrapolation procedure described will serve to obtain the absolute flow properties of any pseudoplastic system using standard concentric cylinder instruments. It should be noted that one of the two cylinder diameters should be kept constant since the ratio R_1/R_2 affects the deviation from the true curve as well as the clearance $R_2 - R_1$. The averaging of the inner bracketing curves, Fig. 4, will serve as a general method for approximating the absolute flow properties of any pseudoplastic system to a known degree of approximation, while employing only one pair of cylinders. Obviously the smaller the clearance between cylinders the closer this approximation will be, other factors remaining fixed, and providing the clearance remains large relative to the size of the dispersed aggregates in the system.

Whereas it is true that one may employ large cylinders and small clearance to obtain a close approximation to the true shear stress-rate of shear curve regardless of whether one plots τ_1 or τ_2 against $\frac{R_1 \Omega}{R_2 - R_1}$ or $\frac{R_2 \Omega}{R_2 - R_1}$ it has been shown here how to obtain the best approximation and be able at the same time to judge the degree of approximation.

REFERENCES

1. SIERICHS, W. C., Measurement of Shear Properties of Aqueous Methyl Cellulose and Application to Flow in Tubes. Engineer's Thesis, Stanford University, 1949.
2. PAGE, L., Introduction to Theoretical Physics, p. 262. D. Van Nostrand, New York.
3. FISCHER, E. K., AND LINDSLEY, C. H., *J. Colloid Sci.* **3**, 111 (1948).
4. SEARLE, G. F. C., *Proc. Cambridge Phil. Soc.* **16**, 600-6 (1912).

SOME ASPECTS OF THE RHEOLOGY AND THE STABILITY OF EMULSIONS AND SUSPENSIONS¹

E. W. J. Mardles

Royal Aircraft Establishment, Farnborough, England

and

A. de Waele

Messrs. D. Gestetner, London, England

Received October 13, 1950

I. INTRODUCTION

When two immiscible liquids are shaken together or a finely divided insoluble powder is stirred into a liquid, separation occurs more or less quickly on standing, at a rate mainly dependent on viscosity and density differences. In the case of the two liquids, the interfacial tension, equal to the difference of the surface tensions (Antonoff's rule), is a principal factor governing coalescence and consequent reduction in the interfacial area. Although the rate of separation may be decreased by the selection of liquid pairs of appropriate surface tensions and by decreasing density differences, particle size, concentration, etc., the usual method for obtaining a high degree of stability is to add to the system a small amount of a soluble substance of high molecular weight, which becomes adsorbed at the interface. The character of the liquid-liquid or liquid-solid interface then becomes completely altered, depending on the specific chemical character of the adsorbed film, with a consequent fundamental change in the stability and rheological character of the dispersion. With creams, greases, or pastes of high concentration when the dispersed particles are in close proximity, the effect of the surface film on friction and adhesion between particles outweighs effects directly due to viscosity and density differences. Unfortunately, little is known or understood about these thin interfacial films formed under the influences of surface adhesion forces; data obtained in lubrication studies, with solids rubbed together at high pressures, not likely to be encountered when two droplets or two solid particles in suspension gently collide, are probably not relevant. One of the purposes of this paper is to direct attention to the importance of carrying out investigations on thin films and friction at very low pressures.

¹ Paper presented at a meeting of the British Society of Rheology, London, England, November 1949.

B. Derjaguin (1) gave evidence that for the majority of the liquids he investigated, among which were organic liquids, the pressure exerted by forces of repulsion with thin films decreases to zero only when their thickness is of the order of $0.2\text{--}0.3\ \mu$, which points to the comparatively large radius of action of surfaces upon the neighboring liquid layers. It appears that the forces responsible for these effects are neither of the nature of van der Waals' forces nor of the nature of dipole forces. W. Hardy (2) considered that thin films of liquids at surfaces had special properties due to orientation of the molecules under surface adhesion forces. He reported on the effect of the specific character of the material of optical flats on the force required to pull them apart with a thin film of liquid between. Similar results have been obtained by one of us (3) using a technique rather different from that of Hardy, when it was found that both the rate of radial flow between surfaces and the "adhesion" were affected by the nature of the material of the surfaces. Although roughness, contamination, dust particles, distortion of the plates, etc. may enter into the problem, the departure from current theory cannot be explained by these factors alone, and a good deal of further careful investigation is required in this "discouragingly difficult field," as Hardy describes it. Elton (1948) has shown that thin films of organic liquids, when traces of moisture are present, possess abnormal viscosities due to an electroviscous effect. Film rupture effects also enter into the problem of thin films (4).

II. LYOSPHERES

The depth of penetration into a liquid of surface adhesion forces is not known. Hardy invoked the concept of diachysis, by which it is supposed that the molecules of the liquid behave like a chain of iron filings attached to the pole of a magnet, and so transmit the surface forces to a considerable depth. A. A. Griffith also expressed the view that water molecules could form chains attached to the surface. The properties of these molecular clusters would presumably depend on their mechanical strength, rigidity, etc. Hatschek, in a study of the viscosity of suspensions, suspected that the lyospheres were delicate structures and could be sheared off, so accounting for a decrease in the apparent viscosity with increased rate of shear. Ostwald and Haller considered that variations in the sedimentation volumes with change of dispersion medium were due to the differences in thickness of the lyosphere, but it can be shown that the volume of sedimented particles depends greatly on the friction between the particles, which varies considerably from liquid to liquid. The increased volume of a particle due to the lyosphere becomes noticeable only when the particle size is sufficiently small. Thus the percentage increase in the diameter of a particle $1\ \mu$ with a lyosphere of thickness, say, $0.01\ \mu$ is 2%, while with a particle of size $0.1\ \mu$ the corresponding increase is 20%; but it has been

found experimentally that the ultimate volume of the dispersed phase in closest packing is not the same as demanded by theory, the interstitial layer assuming a friction quite foreign to liquids. In the case of emulsions where an added stabilizer has lowered the surface tension of one of the liquids, say water, the observed interfacial tension differs from the calculated one. There is, however, some difficulty in determining the interfacial tension due to a downward drift with time and the eventual formation of a hazy separating layer or flocculate. It would, therefore, seem reasonable to assume that a correct evaluation of interfacial tension ruling under the conditions of the emulsion at equilibrium cannot be obtained by the usual techniques. Since it is well known that emulsifying agents are heteropolar in character and exhibit at their active ends differences of affinity for the two phases, it is more than likely that we have to deal with a resultant of two interfacial tensions, and that the two main phases are not strictly in contact. There is also considerable evidence to show that the interfacial zone does not exhibit the normal properties of a liquid, but is of non-Newtonian character.

III. THIXOTROPY

A well-known and important property of dispersions is thixotropy, consequent upon the flocculation or aggregation of the dispersed particles, to a greater or less extent, into flocks with lacunae between; these flocks form into a three-dimensional gel structure which can be redispersed by shaking, only to reform after a lapse of time.

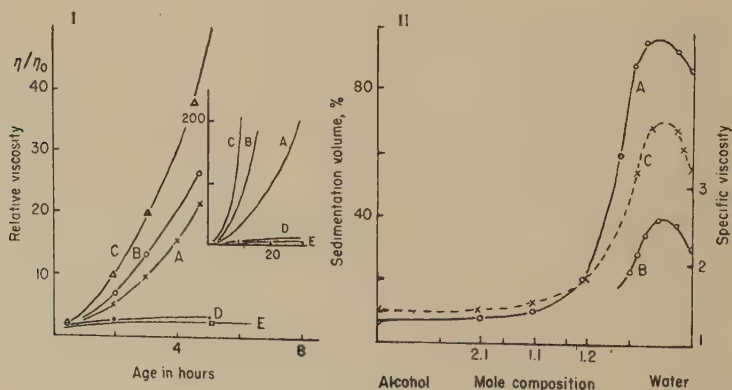


FIG. 1. Bentonite clay in binary mixtures of ethyl alcohol and water. I. Relation between relative viscosity (ordinate) and age in hours (abscissa). Suspending medium: A, water; B, 75% water and 25% alcohol, by vol.; C, 60% water and 40% alcohol, by vol.; D, 50% water and 50% alcohol, by vol.; E, 45% water and 55% alcohol, by vol. II. Relation between composition (mole) and: A, sedimentation volume (per cent suspension) for a concentration of 2 g./100 ml.; B, for a concentration of 0.5 g./100 ml.; C, specific viscosity for concentration of 5 g./100 ml.

With bentonite clay in water the addition of a little alcohol enhances thixotropy although bentonite dispersed in the alcohol itself settles to a relatively small volume as shown in Fig. 1. Similarly, if inert powders such as glass or pigments are dispersed in mixed liquids, the sediment volumes, indicative of the friction and other properties of the lyospheres, vary in an interesting manner with the composition.

In Fig. 2 with binary mixtures of liquids, and Fig. 3 with ternary mixtures, are shown variations in sediment volumes of several solids with composition of media, with and without the addition of stabilizers. Presumably, the surface layer of the molecules of the mixed liquids adsorbed by the surface varies in composition and in thickness with change in the binary mixture composition, especially when the liquid molecules tend to aggregate into molecular clusters as with alcohol and water. The optimum

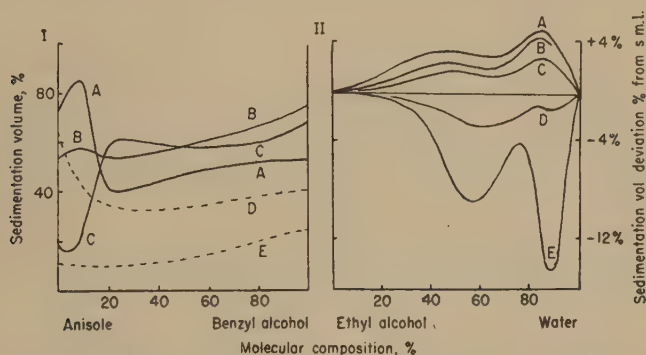


FIG. 2. The variation of the sedimentation volume of powders, per cent total volume suspension, with the molecular composition of binary mixtures of I, anisole and benzyl alcohol, and II, ethyl alcohol and water. I. A, titanium oxide; B, flake aluminum; C, yellow ochre; D, titanium oxide plus 0.5% mastic resin; and E, yellow ochre plus 0.5% wool fat. II. Deviation per cent from simple mixture law values with A, yellow ochre; B, ultramarine; C, potato starch; D, lithopone; and E, zinc oxide.

adsorption would be attained when the molecular aggregation of the mixture was at a minimum and with the best geometrical arrangement of the mixed molecules at the surface (5).

The variations in the properties of a dispersion with the composition of the dispersing liquids, apart from those due to density and viscosity differences, are due presumably to the differences in the properties of the interface, both the adhesion and friction between the particles being affected. This surface effect can be traced even with large particles such as, for example, 1/16-in. diameter steel balls. In Table I are given the coefficient of static friction μ_s (obtained with a small flat steel block on a steel surface, both immersed in the liquid, and the angle of tilt required

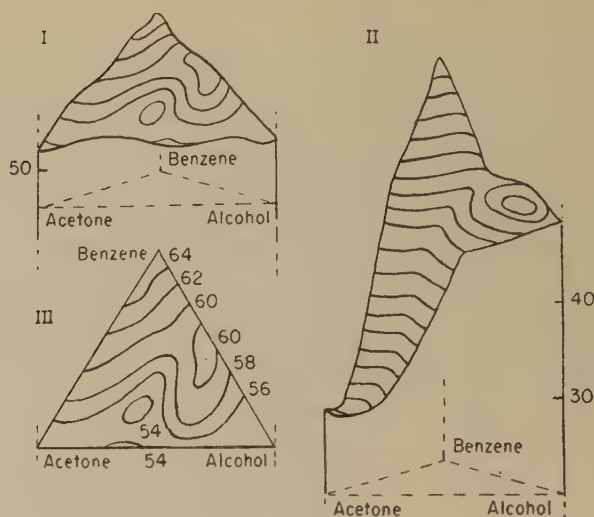


FIG. 3. The sedimentation volumes of kaolin, per cent volume of 15% by vol. concentration suspensions, in ternary mixtures of acetone, alcohol, and benzene. I and II. Perspective view of models I, without, and II, with addition of 0.5% cellulose acetate. III. Ternary mixture diagram corresponding to model I. (The numbers refer to the sedimentation volumes, per cent of suspension.)

to begin motion) together with the sedimentation volume of 2600 balls in an 11-mm. diameter tube, and the angle of repose of the balls in various liquids.

IV. MAXIMUM PACKING OF PARTICLES AND THE RHEOLOGY OF CREAMS AND PASTES

The rheology of the sedimented and centrifuged masses from dispersions can be conveniently investigated by using a small moving plate (edge on) attached to a rigid stem that can freely fall in a vertical guide.

TABLE I

The Influence of Different Liquids on the Sedimentation Volume, etc., of Steel Balls

Liquid	μ_s	Sedimentation volume	Angle of repose
		<i>ml.</i>	<i>deg.</i>
Silicone fluid	0.23	9.5	34
B.P. Medicinal paraffin	0.22	9.3	35
Raw linseed oil	0.20	9.3	31
Light mineral oil	0.18	9.2	30
Light mineral oil + 0.1% stearic acid	0.16	9.2	29

The rate of fall of the plate through the cream or paste can be easily measured with different weights acting on the plate, and a D/τ diagram (relating the rate of shear to shearing force) prepared. The concentrated masses behave as friable solids, yet with gentle and rapid shaking they can become liquid and flow. This behavior can be partially explained on the basis that the coefficient of static friction at light pressures is invariably greater than the kinetic friction; the friction between the moving particles being less than when at rest, the system tends to become liquid and flow.

With increasing rate of shear the concentrated masses show a complex behavior. In addition to a yield value, they can show at first a form of stress thixotropy possibly due to particle orientation, followed by stress hardening due to particle blockage, and finally some kind of rupture of the particle assemblages. The general form of the D/τ diagram obtained is shown in Fig. 4.

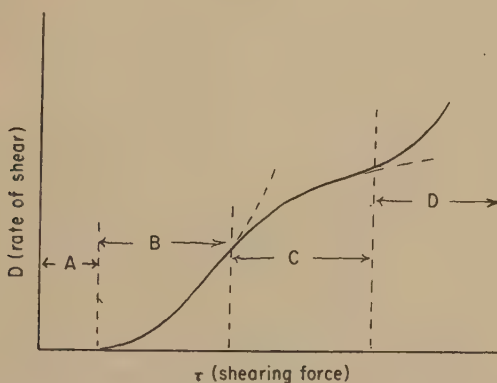


FIG. 4. D/τ diagram for a concentrated dispersion. A, yield value; B, region of stress thixotropy; C, region of stress hardening due to particle blockage; and D, region of rupture of aggregates, etc.

When a suitable dispersator is added to the dispersion medium prior to centrifuging, the above behavior is considerably modified; the friction and adhesion between the particles are reduced with a consequent nearer approach to Newtonian flow. The dispersion also assumes some degree of stability, the rate of sedimentation having been reduced because of the reduction in particle aggregation. With the liquid-liquid system, concentrations up to and even exceeding that corresponding to close packing are readily obtained and may show great stability, due presumably to the distortion of spherical particles in honeycomb fashion with an increased area of interfacial contact.

On the other hand, with solid particles, the pastes of concentrations much below that corresponding to geometrical close packing can be friable

solids. A concentration corresponding to close piling can only be obtained with very coarse particles, and then the system exhibits dilatancy. If, for example, the particles are of the high dispersivity of American carbon black (diameter size 0.025μ), the saturation point of specific absorption may be attained at as low a value as 20% by volume, with no manifestation of dilatancy. Dilatancy at high volume concentrations does not appear when the dispersions comprise a good deflocculating medium, the mass then displays stickiness and stringiness. Dilatancy in coarse powder systems appears to be well marked when the particles approach uniformity of size and at a minimum when the particles are separated by a relatively thick lysosphere.

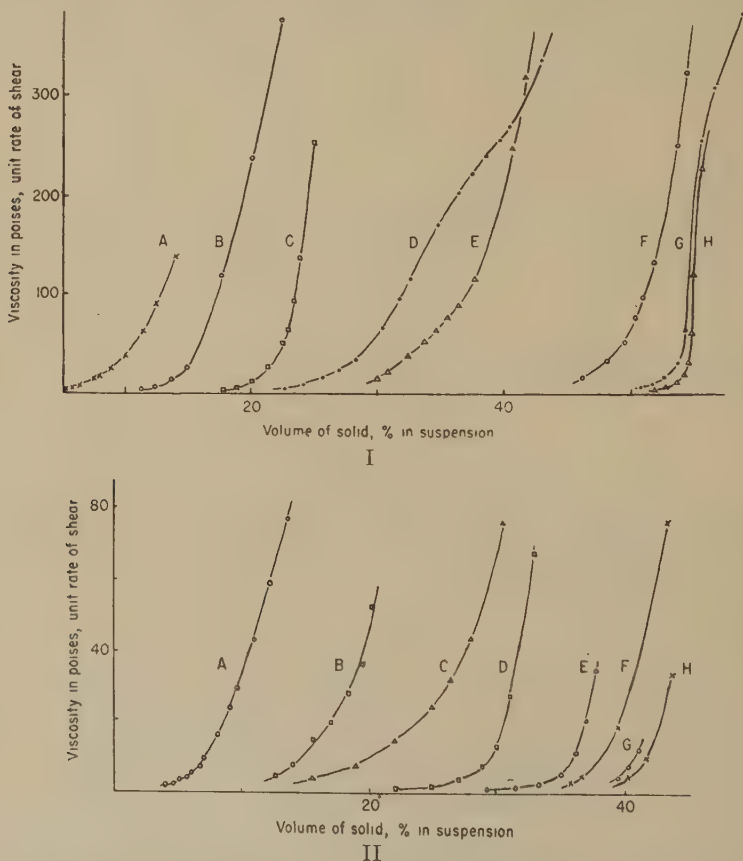


FIG. 5. The viscosity in poises at unit rate of shear of different concentration suspensions. I. A, zinc oxide in water; B, flake aluminum (120-mesh) in light mineral oil; C, flake aluminum (120-mesh) in white spirit; and D, kaolin in water. II. A, zinc oxide in water; B, zinc oxide in raw linseed oil; C, yellow ocher in water; D, yellow ocher in raw linseed oil; E, ultramarine in water; F, lycopodium powder in water; G, ultramarine in raw linseed oil; and H, lycopodium powder in a mixture of chloroform and white spirit.

In close-piled masses the interfacial surface is high and the particles appear to have lost mobility and there is no drift of electrical conductivity with shear. However, at a concentration just below this point of close packing, the skeletal structure is lost during shear, becomes more evenly distributed and less rigid, and has a substantially reduced electrical conductivity to that in its rested condition. These changes occasioned by shear revert to the normal when sufficiently rested.

In Fig. 5, I and II, are given data relating to the effect of concentration on the apparent consistency of some dispersions at unit rate of shear using the moving plate viscometer.

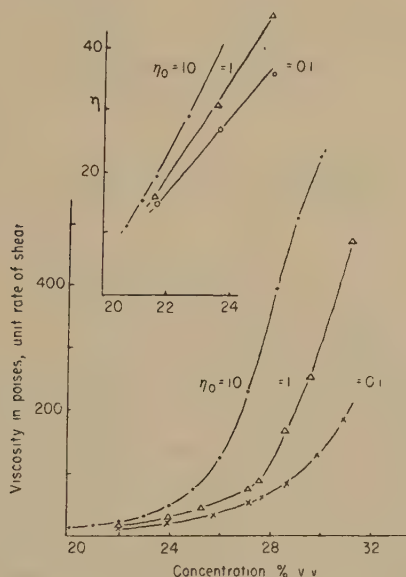


FIG. 6. The viscosity in poises, unit rate of shear, of kaolin at different concentrations in glycerol at three different temperatures when its viscosity $\eta_0 = 10, 1$, and 0.1 poises, respectively.

It will be seen that the highest concentrations are attainable when the particle shape approaches that of a sphere, and that there is then a sudden transition from a liquid suspension to a friable solid with a slight increase in concentration. From the data shown in Fig. 5 it will be seen that zinc oxide gives more fluid suspensions in linseed oil than in water although the viscosity of the oil is greater than water. Similarly, aluminum suspensions are more fluid in white spirit than in a light mineral oil. The viscosities of concentrated dispersions do not appear to be dependent on the Einstein equation or its modifications, particularly since dispersions of any other than vanishingly small concentrations do not exhibit "viscosities" inde-

pendent of the rate of shear. There is a close correlation between the apparent viscosity of a suspension and the sedimentation rate and volume. In general, the more fluid the dispersion the smaller the sediment volume and sedimentation rate. These facts indicate the importance of the film interface: with calcium sulfate which is wetted by water, its dispersions are more fluid than corresponding ones in chloroform which does not wet calcium sulfate very well. Similarly, flake aluminum powder which is scarcely wetted by water forms high-viscosity suspensions, but in chloroform, a good wetting agent in this case, relatively fluid dispersions are obtained.

The independence of the viscosity of concentrated dispersions of the viscosity of the dispersing medium is again illustrated with kaolin suspensions in glycerol over a range of temperature; although the viscosity is changed a hundredfold, the change in viscosity of the suspensions is relatively small (Fig. 6).

In this connection it is important to note that Hardy in his friction studies noted that the coefficient of friction remained practically constant over a wide range of temperature and therefore over a wide range of viscosity for a liquid.

V. THE PROPERTIES OF THIN FILMS

Hardy, from his studies, formed the opinion that liquids in contact with surfaces possessed special properties due to the surface adhesion forces which impart a form of rigidity to a depth beyond the monomolecular layer held by the London-van der Waals' force. The property of the wringing together of flats with a liquid film between has been a source of inquiry for many years, and as Tyndall showed in 1875, the adhesion is practically the same *in vacuo*, and appears to be due to molecular attraction (6). Budgett, in 1911, confirmed measurements made by Reynolds (1877); further data have been obtained by Hardy. More recent data by Darjaguin, (1) Elton (7) and Mardles (3) have shown that the liquid layer between surfaces has abnormal properties which depend on the specific nature of the surface material. Much more careful work is required to reveal the depth of penetration of the adhesion forces and their effect on the rheological properties of the interfacial film. Any results of such investigations will have an important bearing on the stability and rheological properties of dispersions, and will overshadow the usual approach of purely hydrodynamical considerations. From the hydrodynamical side, the approach of two surfaces immersed in a liquid should be in accord with the equation

$$d^2 = ct^{-1}F^{-1}, \quad [1]$$

where,

$$c = 3\pi\eta r^4/4,$$

d is the distance between the particles, t the time elapsed, F the force acting, η the viscosity of the liquid, and r the radius of the approaching surfaces. In a high-viscosity dispersion medium the rate of movement of the dispersed particle is more sluggish in proportion to the viscosity and the energy, proportional to $\frac{1}{2}mv^2$ where v = particle velocity, so that during flocculation or aggregation of particles the rates of approach of a

TABLE II
*Relation Between Coefficient of Static Friction Between Particles and
Their Sedimentation Volume, etc.*

(a) Quartz (Busagh)

Liquid	Angle of tilt, θ	$\mu_s(\tan \theta)$	Sedimentation volume
	deg.		ml./g.
Water	30.1	0.58	0.78
Ether	36.5	0.74	1.05
Chloroform	37.5	0.77	1.15
Toluene	40	0.84	1.21
Benzene	43	0.93	1.23
Carbon tetrachloride	47	1.1	1.25

(b) Aluminum grains (120-mesh)

Liquid	θ	μ_s	Sedimentation volume	Specific absorption
	deg.		ml./g.	ml./g.
Oleic acid	30	0.58	0.58	—
Engine lubricating oil	35	0.7	0.72	—
Acetone	36.5	0.74	0.76	0.31
Benzene	38	0.78	0.82	—
Water	38	0.73	0.80	0.35
Ethyl alcohol	41	0.87	0.82	0.37
Ether	47	0.84	0.84	0.43
White spirit	50	1.2	0.82	0.47
Nujol	50	1.2	0.86	—
White spirit				
Water, 1%	59.5	1.7	1.14	

(c) Aluminum flake (120-mesh)

Liquid	θ	μ_s	Sedimentation volume
	deg.		ml./g.
Chloroform	41	0.87	0.87
Ether	43	0.93	0.93
Acetone	45	1.00	1.00
Aniline	57	1.5	1.54
Oleic acid	>60	1.7	2.5
White spirit	>60	1.7	2.6

particle with the same energy in a liquid, say, water of 0.01 poise and in castor oil of 10 poises are in the ratio $10^6:1$, and the distance between after a time t in the ratio $10^3:1$. These considerations apparently account for the fact that the relative viscosity of dispersions with the same concentration is dependent on the viscosity of the medium and the little yield or no yield values of suspensions in viscous media, such as are produced in the manufacture of glossy enamels. This conclusion, however, is most probably an oversimplification of the facts, since the viscosity of the interstitial phase does not appear to be constant with the distance apart of the particles, nor indeed can it be regarded as a purely viscous fluid. Moreover, the complication arises that when comparing one medium with another, increased viscosity is accompanied by increase in molecular size and complexity, and hence in general greater deflocculating power.

In addition, explanations of thixotropy and the flocculation and aggregation of dispersed particles must involve knowledge of the interfacial thin films and their highly specific chemical character. Busagh studied the adhesion of quartz particles in suspensions by noting the tilt required for a quartz particle to begin slipping down a quartz surface immersed in the liquid. Similar experiments have been described by ourselves (8) and further data are shown in Table II, relating adhesion indicated by the coefficient of static friction and sedimentation volumes, etc.

VI. EMULSION STABILITY

Coming now to stability in practice it is necessary to remark that other factors being equal enhanced stability results when the parent dispersing phase is semisolid or plastic in character, although such plasticity is inadequate to constitute the unique factor ensuring stabilization. Thus, semisolid petroleum jelly does not form emulsions with water in the absence of a dispersing agent, but a hydrocarbon oil solution of wool grease or its derivatives leads to high degrees of stability accompanied by rigidity. The heteropolar nature of the sterols contained in this material suggests its suitability as an obvious link between oil and water phases. The oleates and stearates of di- and tervalent metals are also good dispersing agents, and similarly depend for their efficacy on their heteropolar nature, while the monooleates of polyhydric alcohols form the basis of several very efficacious proprietary dispersing agents. Solutions of lecithin or kephalin in mineral oils present an interesting case of emulsifying action in both W/O and O/W emulsions. The heteropolar nature of these molecules indicates their effectiveness as a transition body between the phases, and their applicability to both types of W/O and O/W emulsions may well suggest a reason for their known great stability when due care is taken to select suitable concentration of the substance in solution, heteropolar balance, and conditions of preparation.

These heteropolar, water-insoluble substances, while sometimes but not necessarily effecting some reduction of surface tension of the aqueous phase, yet invariably show a considerable lowering of interfacial tension of pure hydrocarbon oils against water. Increase of stability and further reduction of interfacial tension are often attained in emulsions made with a dispersing agent if the polar nature of the water be reduced by addition to it of polyhydric alcohols, e.g., glycerol or glycol, and this may have its explanation in the closer approximation of balance between the polarities of the two phases. Several cases are known when increased stability and emulsifying power are obtained by the seeming paradox of additional incorporation of a substance tending to form an emulsion of opposite type, e.g., alumina gel added to *W/O* emulsion, etc.

A synergic effect obtained by the combined use of two or more emulsifying agents has often been observed, but the selection of these components is at present largely empirical. It would seem, however, that the respective forms, sizes, and molecular configurations of the components in relation to the nature and concentration of the emulsion, will prove to be the determining factors.

In the binary mixtures comprising medium and dissolved emulsifying agent, the latter has been shown to be not exclusively adsorbed. Hence the concentration of dispersing agent in solution in a nonpolar oil is more important than the volume ratio of the two phases.

In general, molecules of large size and complexity are the best dispersing and emulsifying agents. These not only favor adsorption potential, but when disposed interfacially, ensure sufficient separation between the dispersed units to reduce largely their mutually opposing fields of force.

Stabilization of a *W/O* emulsion by mere addition of a solid powder of suitable heteropolar nature never results in that degree of stability obtainable by interfacial adsorption of a dissolved substance. Powders may often, however, increase the stability of emulsions.

While several interdependent factors may account for stability of *O/W* systems, *viz.*, reduction of interfacial tension following on lowered surface tension of the outer aqueous phase, and also electrostatic effects, it is difficult to conceive of a mechanism whereby the necessary raising of the outer phase tension may be obtained in the case of *W/O* emulsions. In this connection, it is interesting to recall that Ostwald and Rath (9) observed an increase in surface tension in the dineric surface of a China clay-water suspension.

Following on Bartell's conclusions that the affinity of a solid to water and to an organic liquid is conditioned by the interfacial tension of the former to the two respective liquids, an evaluation which he obtained from the specific absorption values, it would seem to be a less daring

speculation were the hydrophility factor of any given powder to be taken as a criterion of its stabilizing effect on an emulsion.

The authors have in a previous communication (8) referred to the technique of high-speed centrifuging of a suspension, whereby the effects of friction in the resulting sediment could be substantially minimized or eliminated, and lyosorptive effects thereby rendered dominant. If, therefore, the specific absorptions of a well-wetted dispersion of the powder in water and in benzene be determined by such method, the degree of dispersity as a variable is eliminated in the ratio of the one to the other. The ratio (specific absorption to benzene)/(specific absorption to water) will then give a measure of the hydrophility factor (Table III).

TABLE III

Hydrophility Factors and Their Influences on a W/O Emulsion Stabilized by Lecithin

Powder	Hydrophility factor	Effect on lecithin W/O emulsion
American carbon black	0.90	Stabilizes
Antimony oxide pigment	0.95-1.02	Some increase of stability or no change
Insoluble yellow dye	Unwetttable by water	Stabilizes
Insoluble red dye	Unwetttable by water	Stabilizes
Titanium oxide, standard	1.50	Destabilizes
Titanium oxide "hydrophile"	3.50	Destabilizes
Titanium oxide rutile, "oleophile"	1.21	Destabilizes
Milori blue	1.47	Destabilizes

An exact correlation does not always obtain, as solubility of an active substance in either phase, degree of dispersity, etc., are, naturally enough, not shown in the hydrophility factor. The selection of a suitable concentration of any given powder is dependent on its attendant specific surface.

Powders with hydrophility factors of less than unity are few, and in general find little application other than in printing inks.

Experimental evidence goes to show that fineness of subdivision of a powder is an important requisite of its stabilizing efficacy, and it is clear that such condition is essential for the arrangement of the interstitial film to its densest packing. Even distribution in the interface is attained by ensuring the minimum internal friction of the powder in the outer oil phase, a criterion of which may be established from the rheological data on the paste or suspension.

VII. MECHANICAL ASPECTS

While the formation of an emulsion involving the breaking-up of bulk liquid to a condition of discrete droplets of high dispersity is dependent

primarily on the mechanical treatment given, the dispersion of solid powders involves no real change in the magnitude of their surfaces. Whatever the size of the ultimate units or primary particles of a powder before dispersion, they always exist as more-or-less aggregated, secondary clusters. The mutual attachment of these primaries is in no way different from a flocculation, and while the ultimate effect of dispersion to a stable condition involves a mechanism of protection, this need not necessarily accomplish disintegration to primaries. The separation of mutually cohering primaries involves an exchange of their natural surface for that of another medium exhibiting greater adhesion to it. While this exchange may in many cases be obtained by a mechanical effect, the selection of a dispersing agent with a high wetting tension, or the addition to it of a substance with a high spreading coefficient and high vapor pressure, is often resorted to. We have in a previous communication referred to the initial treatment of a powder with a volatile solvent miscible with the medium and exhibiting good wetting properties, as a preliminary step to assisting the disintegration of secondary aggregates.

The mechanical treatment and history of preparation of emulsions have often been referred to in the older literature as a potent factor in determining stability. Thus, the slow addition of the emulsified phase to the dispersing liquid is generally agreed to be essential, while experience has further shown that intermittent agitation often assists dispersion and stability. The velocity gradient of shear would appear from this to be a possible determinant, as well as the rate of adsorption and interstitial orientation. It is therefore preferable in all emulsifications that the desired final degree of subdivision be not attempted in one stage of operation. Accordingly, emulsions to be prepared in cone-valve emulsifiers ("homogenizers") should undergo a preliminary dispersal at low shear, to be followed by repeated passage through the homogenizer at diminishing settings of the valve clearance. The same remarks apply to dispersions of solid powders to suspensions in oil media. Thus, if the two component phases be initially subjected to the high velocity gradients ruling in the narrow gap of the so-called colloid mills, very poor dispersion results.

It is interesting to note that a very coarse but stable emulsion of water in oxidized fatty oil may be obtained to a concentration of up to 80% when it is prepared by slow addition in a Werner Pfleiderer mixer. On its subsequent treatment in any form of apparatus involving a small shearing gap, i.e., 3-roller mill, cone mill, Hurrell mill, or homogenizer, the emulsion breaks down into a semisolid cream of the *W/O* type with liberation of the bulk of the water. It is here evident that the amount of *true* emulsifying material in the oil, while adequate to cover and protect the small interstitial area of the coarse emulsion, fails to stabilize the larger area developed by more intense shear.

There has been a considerable diversity of opinion on the question of the existence of electrostatic charges in systems having a nonionic continuous phase, although it is not immediately evident why a charge should not derive from an inner aqueous phase. One of the authors has established the existence of charges by methods involving examination under the microscope in an electric field, and indeed there is a fair evidence to show that additions to the inner water phase of positively charged lyophilic sols result in a substantial increase in stability. Among such examples may be quoted colloidal ferric hydroxide, positively-charged aqueous dye sols, etc.

SUMMARY

The rheological behavior of emulsions and suspensions is considered in relation to the properties of surface films adsorbed on the dispersed particles. With change of composition in mixed liquids or with small additions of high molecular weight substances, important variations in thixotropy, etc., of a dispersion are recorded which are due to changes in the character of the interfacial surface film. Friction increases between the particles, for example, result in larger sedimentation volumes and higher specific viscosity. This aspect of the theory of emulsions and suspensions, especially for the more concentrated systems, outweighs the usual approach of purely hydrodynamic considerations. It is concluded that future progress in this field depends on results of studies on the properties of thin films of liquid adsorbed on surfaces, including friction measurements at low pressures.

REFERENCES

1. DERJAGUIN, B., *Trans. Faraday Soc.* **36**, 203 (1939).
2. HARDY, W., *Proc. Roy. Soc. (London)* **A108** (1925).
3. MARDLES, E., *Nature* **164**, 324 (1949).
4. MARDLES, E., Physics of Lubrication Conference, Manchester, Institute of Physics, 1950; special issue *Brit. J. Applied Phys.* (1951).
5. BIELAK, E., MARDLES, E., AND TINGLE, E., Physics of Lubrication Conference, Manchester, Institute of Physics, 1950; special issue *Brit. J. Applied Phys.* (1951).
6. ROLF, F. H., *Gauges and Fine Measurements*. MacMillan, London, 1929.
7. ELTON, G. A. H., *Proc. Roy. Soc. (London)* **A192**, 259 (1948).
8. DE WAELE, A., AND MARDLES, E., *Proc. 1st Congress in Rheology*. Holland, 1948.
9. OSTWALD, W., AND RATH, *Kolloid-Z.* **36**, 243 (1925).

THE VOLUME REQUIREMENTS OF POLYMER MOLECULES.

I. THE APPARENT SPECIFIC VOLUME OF POLYSTYRENE IN SOLUTION

Wilfried Heller and Arthur C. Thompson¹

Chemistry Department, Wayne University, Detroit, Michigan

Received December 18, 1950

INTRODUCTION

The apparent specific volume of polymers in solution is of interest for several reasons. Its probable variation with the nature of the solvent is bound to reflect the respective variation of the empirical interaction constant, μ . An isothermal comparison between the apparent specific volume of a polymer in solution and the specific volume of the same polymer in the liquid state should give immediate information on the sign and on the relative magnitude of the heat of mixing. An isothermal comparison between dissolved and solid polymer below the temperature of an apparent second-order transition should yield information on the nature of this transition. An investigation of the apparent specific volume as a function of polymer concentration might provide a criterion for the assumption of configurational changes of polymer molecules during the transition from moderately concentrated to highly dilute solutions (6).

In view of this variety of promising aspects, it is surprising that only very few accurate data are available in the literature on the apparent specific volume of polymers in solution. This is particularly true for polystyrene, one of the favored models in polymer research. In connection with their ultracentrifugal studies, Signer and Gross (12) carried out pycnometric density determinations on solutions of polystyrene of varied molecular weight and concentration in chloroform and in six other solvents. The partial specific volume obtained—apparently pertinent to 20°C.—varied between 0.88 and 0.91 cm.³g.⁻¹. Unfortunately, however, the error varied between ± 0.01 and ± 0.05 so that no distinct trend can be detected for any one of the variables. The authors give 0.91 cm.³g.⁻¹ as the characteristic value and they conclude that this value is identical with the specific volume of solid polystyrene. In connection with his extensive viscosity measurements on polystyrene solutions in benzene, Danes (4) carried out a large number of measurements on the solution density rela-

¹ Present address: Department of Physical Sciences, University of Idaho, Moscow, Idaho.

tive to benzene. No attempt was made, however, to use these data for evaluating the apparent specific volume or the apparent density of the polymer or of the solvent. An analysis of his data from this point of view, together with a comparative analysis of the intrinsic viscosities derived, will be given in a sequence to the present paper. It will be seen that, on varying concentration, temperature, and molecular weight, the apparent specific volume varies between 0.919 and 0.938 in a partially erratic and a partially systematic manner. In connection with their swelling studies on polystyrene, Boyer and Spencer (1) compiled data for the partial density of polystyrene in toluene, which, if converted to partial specific volumes (13) yield the values of 0.909, 0.913, and 0.918 at 0, 20, and 40°C., respectively, omitting the fourth and fifth decimal places. There are, finally, a few interesting dilatometric data by Breitenbach and Franck (3), which we will have occasion to discuss extensively.

The present paper gives a few preliminary results on the apparent specific volume of polystyrene in solution as derived from precise density measurements. The main emphasis is placed on their significance with respect to the problem of the apparent second-order transition of polymers and to the problem of solvent-solute interaction.

I. THE DERIVATION OF APPARENT SPECIFIC VOLUMES FROM DENSITY MEASUREMENTS

The generally favored equation for calculating the apparent specific volume of a solute, ϕ_2 , is based upon the statement of fact that

$$\frac{1}{\rho_{12}} = \phi_{12} = c_1 \phi_1 + c_2 \phi_2, \quad [1]$$

where ϕ_1 is the specific volume of the pure solvent, ϕ_{12} the specific volume of the solution, ρ_{12} its density, and c is the weight fraction. On rearrangement

$$\phi_2 = \frac{\phi_{12} - (1 - c_2) \phi_1}{c_2} \quad [1a]$$

The related statement

$$V_{12} = V_1 + V_2, \quad [2]$$

where V is the absolute volume, gives on rearrangement

$$\phi_2 = \frac{\phi_{12} - \phi_1}{c} + \phi_1, \quad [2a]$$

which yields

$$\phi_2 = \frac{\Delta\rho}{\rho_1 \rho_{12} c_2} + \frac{1}{\rho_1} = \frac{\Delta\rho}{\rho_1 c_2'} + \frac{1}{\rho_1}, \quad [2b]$$

where $\Delta\rho = (\rho_1 - \rho_{12})$ and c_2' is the solute concentration in grams per cubic centimeter of solution. Equation [2b] is used throughout the present work.

Equations [1a] and [2b] have in common that the specific volume of the solvent in solution must be assumed to be identical with that of the pure solvent, a requirement which gives to the derived ϕ_2 the character of an apparent quantity. Any change in ϕ_2 as a function of an experimental variable is therefore subject to several interpretations: It may be due (a) to a true change in the space requirement of the solute molecules or it may be due, instead, (b) to a change in the space requirement of the solvent molecules immediately adjacent to, adsorbed by, or pervading the solute molecules, the latter possibility applying only to nonrigid polymer molecules. Finally, (c) again in the case of nonrigid polymer molecules, one may have to deal with a change in the number of unoccupied spaces inside the molecule. In contradistinction, a change in the number of unoccupied spaces in volume elements containing solvent only, can be discounted as experimentally undetectable except on selecting temperature as the experimental variable.

If sufficient data are available on the variation of ϕ_{12} with c_2 , an alternate solution is possible. As shown by Lewis and Randall (9), the partial specific volume

$$\bar{v}_2 = \frac{\partial \phi_{12}}{\partial c_2} = \phi_{12} - c_1 \frac{d \phi_{12}}{d c_1} = \phi_{12} + c_2 \frac{d \phi_{12}}{d c_1}. \quad [3]$$

It will be seen from our data that, at least for $c > 0.01$, ϕ_2 is practically identical with the thermodynamically more significant \bar{v}_2 . As regards the interpretation of changes in \bar{v}_2 , the situation is identical with that outlined for ϕ_2 .

Still another equation, based on the evident fact of weight additivity,

$$W_{12} = W_1 + W_2 \quad [4]$$

yielding

$$\rho_{12} = v_1 \rho_1 + v_2 \rho_2 \quad [4a]$$

or, transformed

$$\rho_2 = \frac{\Delta\rho'}{v_2} + \rho_1, \quad [4b]$$

where v is the volume fraction and $\Delta\rho' = (\rho_{12} - \rho_1)$, is of no particular use for the immediate purpose, but is of interest for calculating, from the density data, the apparent volume fraction of the solute

$$v_2 = \Delta\rho' \frac{\phi_1 \phi_2}{\phi_1 - \phi_2}. \quad [4c]$$

It is apparent that the type and number of pycnometric density measurements to be carried out depend on the equation to be used. Equation

[3] requires only the determination of ϕ_{12} , but determinations at varied c_2 are necessary in order to arrive at a sufficiently well defined value of \bar{V}_2 characteristic for a given c_2 . The number of necessary determinations increases with the deviation of ϕ_{12} (c) from a straight line. By contradistinction, Eq. [2b] does not require more than one set of data for a given c_2 , but it is necessary to determine either both ϕ_{12} and ϕ_1 , or the difference ($\phi_1 - \phi_{12}$). In the latter case, it is sufficient to know ϕ_1 with a moderate degree of accuracy, i.e., the number of significant figures for ϕ_1 does not need to exceed by more than one the number of significant figures wanted for ϕ_2 . The present, preliminary, data were obtained by the conventional method of individual pycnometric density measurements, but the obvious advantages of the differential method invite its substitution in the forthcoming extension of the present work.

II. EXPERIMENTAL

1. Precision Requirements

The literature data quoted show that it is desirable to obtain three significant figures for the apparent specific volume; only then is the effect of experimental variables apt to show up clearly. This defines the necessary accuracy of both absolute and differential density determinations. Discussing here in detail only the former, more exacting, method, it is required that the uncertainty in individual density measurements in, say, 1% solutions be limited to the sixth decimal place if the density difference between solvent and solute is 0.1. It is, therefore, necessary to provide a sufficiently large value for $(\rho_1 - \rho_2)$ if exploration of more dilute solutions is intended. This was done by selecting, for the more precise work, bromobenzene as the solvent. The value of $(\rho_1 - \rho_2)$ is here 0.40. This value is so much larger than in the former instance that it is possible, with the exception of highly dilute solutions, to aim for six significant decimal places. It is necessary for this purpose that both the weight and the volume in pycnometers of practical size and capacity (25 cc.) be determined with an individual error not in excess of $\pm 2.5 \times 10^{-5}$ g. and cc., respectively.

2. Volume Determinations

The pycnometers used held slightly more than 25 cc. of liquid. They were of the bicapillary type (Fig. 1). The main body of the pycnometers was spherical which is preferable to the conventional, more strained flat-bottom type. The capillaries were calibrated with a traveling microscope by the conventional method of moving a small mercury column stepwise along their entire length. The pycnometers were filled by injection with a medical syringe until each of the two menisci was near a horizontal razor mark on each capillary. After complete thermal equilibrium had been established, the height difference between each meniscus and the respective mark was determined by means of a cathetometer reading to ± 0.01 mm. The error in volume measurements by this technique was defined by $\pm 1.5 \times 10^{-5}$ cc.

3. Weight Determinations

The apparent weight of the pycnometers was determined with a semimicrobalance whose sensitivity at full load amounted to $\pm 1.5 \times 10^{-5}$ g. The conversion to true weights followed the well-known conventional procedure (application of the four different buoyancy corrections pertinent in the present instance and equalization of the surface moisture

film on filled and tare pycnometer). It is worthwhile adding that most of the very critical buoyancy corrections would cancel in the case of differential measurements.

4. Temperature Control

In view of the large cubic expansion coefficient of organic liquids, a rigorous temperature control was necessary, an inconvenience which would be largely eliminated by the differential method. A volume of 25 cc. of bromobenzene, for instance, increases by 2.3×10^{-6} cc. if the temperature increases from 25.000 to 25.001°C. It was, therefore, necessary to keep the temperature fluctuations in the pycnometers below this value and to reproduce in each experiment the temperature within the limits of accuracy of a Beckman thermometer read with the cathetometer mentioned above. A thermoregulator of sufficiently high sensitivity and sufficiently low inertia was obtained by winding 800

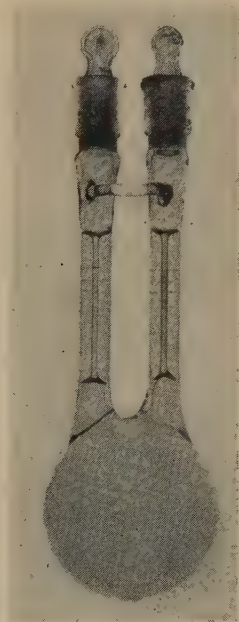


FIG. 1. Pycnometer.

cm. of thin-walled glass tubing, with a capacity for approximately 3 kg. of mercury, to a spiral of approximately 40 cm. diameter which terminated in a narrow capillary. The temperature fluctuations in the well-insulated thermostat, heated with a carbon-filament lamp of low heat capacity, were too small to be detectable with the Beckman thermometer. Considering the difference in heat capacity of the mercury in the thermometer and of the polymer solution in the pycnometer and taking into account the mass differences, it followed that the temperature fluctuations inside the pycnometer were well below 0.001°C., discounting even the additional favorable fact of a pronounced difference in heat conductance. All the following experiments were carried out at $25.00 \pm 0.001^\circ\text{C}$. The omission of a third decimal place means that, while it is a significant relative figure, its absolute value is not known.

5. Precision Achieved

The total error for density measurements with a given pycnometer derives as slightly less than $\pm 1 \times 10^{-6}$. The actual error found, on very careful work, was not in excess of $\pm 2.5 \times 10^{-6}$, the difference being due most likely to uncertainties in the buoyancy corrections. The use of a single pycnometer for all measurements introduces a slight systematic error of unknown magnitude. All experiments were, therefore, carried out with two or, if advisable, with three pycnometers. The mean values obtained with different pycnometers did, on careful work, not differ by more than $\pm 4 \times 10^{-6}$. An example is given in Table I. The limits of error to be given in the Tables are defined as the mean deviation of the mean results obtained from different pycnometers.

III. THE APPARENT SPECIFIC VOLUME OF POLYSTYRENE IN CHLOROBENZENE SOLUTION

Unfractionated Dow polystyrene was purified by reprecipitation from a solution in dioxane. To this effect, the solution was extruded from a medical syringe into continuously agitated water. The finely divided precipitate obtained was easy to dry to constant weight. Chlorobenzene, preferred to benzene because of its lower vapor pressure, was purified by

TABLE I

Sample of Actual Density Data Obtained in Bromobenzene Solution

\bar{M}_w of polystyrene = 356,000; $T = 25.00^\circ\text{C}.$; $c = 0.007535 \text{ g./g.}$; $c' = 0.011165 \text{ g./cc.}$

Pycnometer	ρ_{12}	$\bar{\rho}_{12}$
II	1.481740	1.481737
II	1.481735	
III	1.481732	1.481733
III	1.481735	
IV	1.481730	1.481729
IV	1.481728	

1.481733 \pm 0.000004

fractional crystallization and subsequent distillation. The density of the final product was 1.10102₃ (25.00°C.). (This and all other density data are relative to water at 4°C.) The three solutions investigated cover a concentration range from 1.0–5.2 g. of polymer/100 cc. of solution. They were made up by weighing, to within $\pm 0.2 \text{ mg.}$, first the dry polymer and subsequently the solution. The weight fractions, c , are, therefore, the primary concentration data.

The apparent specific volumes obtained are compiled in Table II. They are, in a first approximation, constant within the concentration range investigated and warrant therefore the compilation of a mean value for this range. However, an examination of the individual data clearly indicates a very slight, but definite, increase of the apparent specific volume with decreasing concentration, disregarding the data pertinent to the low-

TABLE II

*Apparent Specific Volume of Unfractionated Polystyrene^a in
Chlorobenzene Solution at 25.00°C.*

<i>c</i>	<i>c'</i>	Pycnometer	ϕ_2 (Individual mean for respective pycnometer)	ϕ_2 (Over-all mean)
0.00972	0.01017	III	0.92 ₄	0.922 ± 0.002
0.00972	0.01017	IV	0.92 ₀	
0.02314	0.02547	II	0.922 ₇	0.9230 ± 0.0005
0.02314	0.02547	III	0.923 ₇	
0.02314	0.02547	IV	0.922 ₇	
0.04734	0.05208	III	0.921 ₇	0.9213 ± <0.0004
0.04734	0.05208	IV	0.920 ₉	
				0.922 ± 0.002

^a From Dow Chemical Co.

est concentration which are inconclusive in this regard because of the wider spread of the limits of error:

IV. THE SPECIFIC VOLUME OF POLYSTYRENE IN BROMOBENZENE SOLUTION

In order to verify this slight concentration dependence of the apparent specific volume, bromobenzene was used in the subsequent set of experiments. The increase in experimental accuracy associated with the larger ($\rho_1 - \rho_2$) value warranted the use of a fractionated sample of polystyrene of definite molecular weight. A 5-g. sample of fractionated Dow polystyrene of $\bar{M}_w = 356,000$ was kindly provided for this purpose by Dr. R. S. Spencer of the Dow Chemical Company, Midland, Michigan. The bromobenzene was the "Eimer and Amend Tested Purity Reagent" certified by the National Bureau of Standards. Its freezing point is given as $-31.053 \pm 0.002^\circ\text{C}$. It was used without further purification. Its density was found to be 1.48590₉ at 25.00°C.

The results, given in Table III, again indicate a slight increase in specific volume with decreasing concentration, which verifies this effect.

A comparison between Tables II and III shows that the apparent specific volume of the unfractionated polystyrene in chlorobenzene and of the high molecular weight fraction of it in bromobenzene, though nearly the same, differ by more than can be accounted for by the experimental error. This finding will be discussed somewhat later in connection with Table VI.

V. THE PROBLEM OF HIGHLY DILUTE SOLUTIONS

As a solution of randomly kinked polymer molecules decreases in concentration, it changes from a continuous system to a discontinuous one. In the former case, there are polymer contacts throughout the solution, in the latter case volume elements containing polymer and solvent alternate with elements containing solvent only. This transition should be expected (6) to occur in or near the range of concentrations investigated above. It became therefore of particular interest to explore still more dilute solutions.

Since the stock solutions prepared from the small sample of polystyrene had been used up during the preceding experiments, it became necessary to use either another fraction of polystyrene or to re-use the saved contents of pycnometers which had been emptied and carefully rinsed repeatedly in order to avoid as much as possible a loss of polymer. The latter procedure was adopted since, at that time, no sufficiently reliable information was available on the quantitative effect of molecular weight upon the apparent specific volume. The pycnometer contents of the $c = 0.007535$ series were used for two independent secondary stock solutions of $c = 0.004334$ and $c = 0.002016$, respectively, and the pycnometer contents of the $c = 0.03207$ series were used for two additional independent secondary stock solutions of $c = 0.01788$ and $c = 0.009007$, respectively. The concentrations of these secondary stock solutions also were determined by weighing, after proper dilution with bromobenzene.

Figure 2 shows that $(\rho_1 - \rho_{12})/c$ is, in a good approximation, a constant over the whole range of concentrations considered, irrespective of whether the data originated from primary or secondary stock solutions. The appar-

TABLE III

*Apparent Specific Volume of Fractionated Polystyrene^a ($\bar{M}_w = 356,000$)
in Bromobenzene Solution at 25.00°C.*

c	c'	Pycnometer	ϕ_2 (Mean for respective pycnometer)	ϕ_2 (Over-all mean)
0.007535	0.011165	II	0.925 ₄	0.9247 \pm 0.001
0.007535	0.011165	III	0.923 ₅	
0.007535	0.011165	IV	0.925 ₃	
0.032067	0.047087	II	0.923 ₀	0.9231 \pm 0.0001
0.032067	0.047087	III	0.923 ₁	
0.032067	0.047087	IV	0.923 ₂	
				0.924 \pm 0.001

^a From Dow Chemical Co.

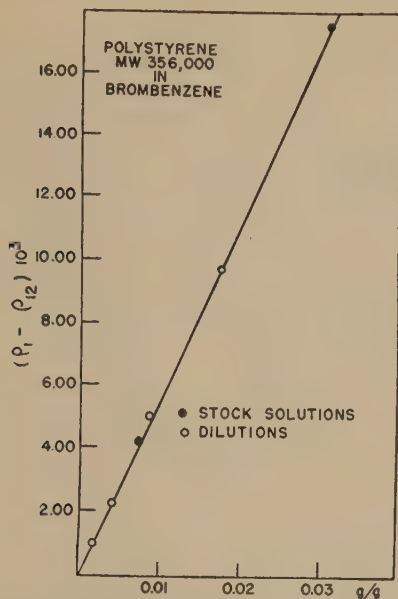


FIG. 2. Density decrement, as a function of concentration in bromobenzene solutions of polystyrene. \bar{M}_w : 356,000; T : 25.00°C.

ent specific volume, however, which is sensitive to differences in the higher decimals of the densities, is not a constant, but seems to rise with concentration at concentrations below 1%. This follows from Fig. 3 which gives the reciprocal, i.e., the apparent density of the polymer. This trend is opposite to that observed at concentrations in excess of 1%, and it is much stronger. It is therefore inviting to consider the concentration range characterized by a maximum in the apparent specific volume as the transition range in the sense pointed out above. However, in view of the fact that the data in highly dilute solutions were obtained with secondary stock solutions only, it is necessary to make due reservations and to await confirmation of the results, in this range, by additional experiments.

VI. THE ISOTHERMAL SPECIFIC VOLUMINA OF DISSOLVED AND VIRTUAL LIQUID POLYSTYRENE AT 25°C.

In order to compare the apparent specific volume of dissolved polystyrene and the specific volume to be expected from bulk polystyrene if it could be obtained as a liquid at room temperature, advantage is taken of the results of Flory and Fox (7) obtained during their recent density studies on sharp polystyrene fractions between room temperature and 217°C.² In confirmation and extension of earlier results [see the literature

² We are indebted to Professor Flory for making his data available to us prior to their publication.

under Ref. (2)], these authors found that the specific volume of liquid polystyrene increases strictly linearly between the transition temperature and 160°C. They found, in addition, that the temperature coefficient of liquid polystyrene is independent of molecular weight, and they established a quantitative relation on the isothermal variation of the specific volume of liquid polystyrene with molecular weight. From the latter relation, it follows that the isothermal specific volume of a polystyrene of $\bar{M}_w = 356,000$ ought to differ by not more than 0.02% from that of a polystyrene of $\bar{M}_w = \infty$. The former two findings allow, in addition, an extrapolation of the $\phi(T)$ curve of liquid polystyrene of $\bar{M}_w = 356,000$ to 25.00°C. The value obtained can be considered as practically identical

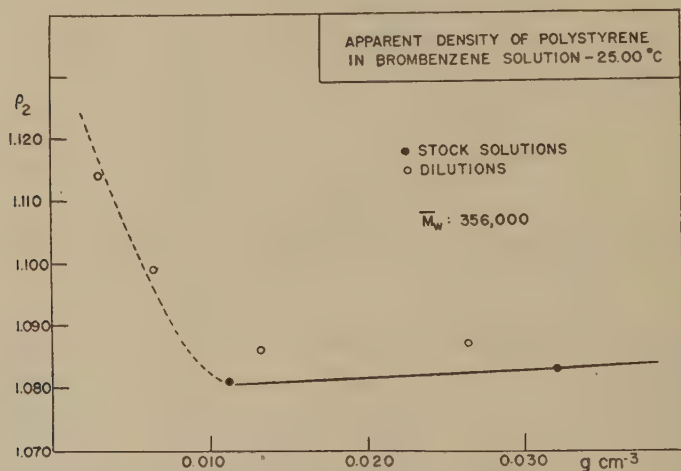


FIG. 3. The apparent density of polystyrene in bromobenzene solution; $\bar{M}_w: 356,000$; $T: 25.00^\circ\text{C}$.

with the specific volume, at 25.00°C., of the corresponding virtual polystyrene liquid. The specific volume thus obtained for the virtual liquid agrees surprisingly well with the apparent specific volume of polystyrene in a 1–5% bromobenzene solution, the apparent difference being less than 0.5% (Table IV and Fig. 4). The true difference—on extrapolating to 100% polystyrene—is bound to be somewhat larger due to the fact that the apparent specific volume decreases slightly with increasing polymer concentration. In order to increase the significance of the comparison in Table IV and Fig. 4, it is important to have some information on the rate of change of the apparent specific volume of dissolved polystyrene with temperature. To this effect the numerous density data of Danes (4) were evaluated in this respect. A brief subsequent paper on this subject will show that these data, in spite of the appreciable scattering

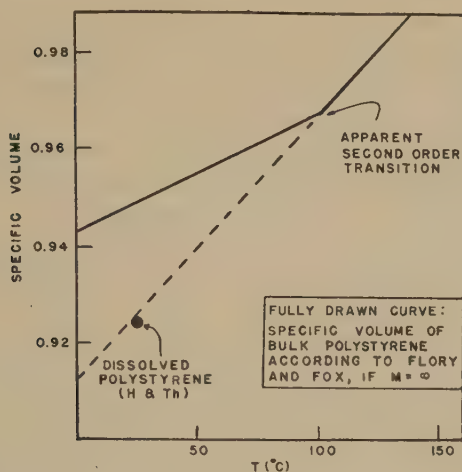


FIG. 4. The specific volume of solid, virtually liquid, and dissolved polystyrene.

of the results, allow the definite conclusion that the slope $d\phi/dT$, of polystyrene dissolved in benzene approximates satisfactorily the slope of the extrapolated data of Flory and Fox.

It is, therefore, possible to state that, at temperatures below the transition point, the molecular space requirement of dissolved polystyrene, in a solvent of equal or similar cohesive energy density, is at least very similar to the molecular space requirement in a virtual liquid of bulk polystyrene. This agrees with the findings of Spencer and Gilmore (13) to the effect that the expansion coefficient of polystyrene in toluene closely approximates the "instantaneous" expansion coefficient of solid bulk polystyrene.

It follows implicitly from the preceding result that the space requirements of polystyrene molecules in a good solvent are, in a first approximation, the same as in actual bulk polystyrene if the temperature of isothermal comparison is above the transition temperature. In order to gen-

TABLE IV
Specific Volume of Polystyrene at 25.00°C.

State of polymer	\bar{M}_w	Specific volume	Authors
Actual bulk	$\approx 100,000$	0.957	Flory and Fox (7)
Virtual bulk (No transition on cooling of liquid)	$\approx 100,000$	0.927	Flory and Fox (7)
Dissolved in chlorobenzene	356,000	0.922 ± 0.002	Heller and Thompson
Dissolved in bromobenzene	356,000	0.924 ± 0.001	Heller and Thompson

eralize, one may state that the isothermal volume occupied by a nonrigid polymer molecule is, in a first approximation, independent of whether it is surrounded and pervaded by identical molecules or by low-molecular-weight solvent molecules provided that the cohesive energy density of the solvent is the same. It is clear that this represents supporting evidence in favor of the basic assumptions made by Flory and by Huggins in their thermodynamic treatment of polymer solutions.

VII. THE ISOTHERMAL SPECIFIC VOLUME OF DISSOLVED AND SOLID POLYSTYRENE AT 25°C.

Signer and Gross (12) assumed that the partial specific volume of dissolved polystyrene is identical with that of solid polystyrene. Table IV and Fig. 4 show that such a general statement cannot be made. Using again data by Flory and Fox (7), the specific volume of solid polystyrene of $\bar{M}_w = 356,000$ interpolates to 0.957 at 25.0°C. This value is more than 3% larger than that of isothermal dissolved polystyrene. The real difference is even somewhat larger due to the concentration dependence of the latter value.

This result is of significance as regards the controversial nature of the apparent second-order transition. It should be expected that the specific volume of bubble-free, noncrystalline solid polystyrene is, at constant pressure, identical with the apparent specific volume of polystyrene dissolved in a solvent of equal cohesive energy density. The lack of identity suggests that solid polystyrene is not in a state of thermodynamic equilibrium which agrees with the point of view advanced by a few other authors [see the reviews under Refs. (2) and (7)].

The large excess volume of more than 3% in solid polystyrene at room temperature apparently supports (13) and may be explained by the assumption of extensive cavities, e.g., of a network of capillaries across the solid. The second-order transition point would then represent the temperature of inception for these fissures. Possible reasons for their formation will be given presently.

Significant, as to the nature of the transition, is the phenomenon of volume relaxation, above the transition temperature, which is observed on change in temperature at constant pressure. The rate of this process decreases rapidly as the transition temperature is approached (7). This shows that the system requires time to acquire its most probable state characteristic for the respective temperature, more so the lower the temperature. Since the molecules are mutually entangled, this means that a critical packing density is reached somewhat above the transition temperature, which imposes upon the system a measurable delay in quantitative configurational rearrangement. On reducing the temperature further, a rearrangement in the configuration of neighboring chain segments of

different molecules toward a state of higher probability is possible only whenever and wherever the dampened internal Brownian movement of the entire mass leads to local fluctuations in the potential barriers large enough to allow, in a given volume element, the necessary rotation or sequence of rotations about valence bonds. The probability of such an event (and still more that of translation of an entire molecule) will decrease rapidly with decreasing temperature. As a result, volume elements with more probable configurations of neighboring segments (of different molecules) will alternate with volume elements where the configurations are less probable. We propose to consider this quasi-permanent alternation of configurational probability from volume element to volume element as the pertinent and characteristic property of state at and below the temperature of the apparent second-order transition. This alternation of configurational probability contrasts with the fluctuation of configurational probability in a given volume element of a true liquid which consists of the same entangled polymer molecules. Such a local alternation is equivalent to an alternation in density and, implicitly, in cohesive energy. On application of a sufficient stress, the solid is therefore bound to shatter randomly along irregular internal areas, in contrast to crystals.

A necessary consequence of an alternation in configurational probability is the development of a "microstrain" near the transition temperature, if a polymer molecule occupies, as it generally will, a sequence of volume elements. This microstrain should obviously decrease with decreasing molecular weight of a given polymer and it should also decrease with increasing molecular rigidity, i.e., with an increase in intramolecular steric hindrance to rotations about valence bonds. In either instance, the limiting case should be—and actually is—a strain-free first-order transition. This microstrain can, in general, lead only to an unsymmetrical strain in the entire system and it can therefore not be expected to produce birefringence.

Such an unsymmetrical strain is apt to lead to localized internal ruptures, i.e. cavitation, in the system "frozen in" on a molecular scale. Some preliminary support for the occurrence of such ruptures by strain may be seen in the observation by Schallamach (11) that rapid cooling of rubber below the transition temperature was accompanied by a clicking noise. The simultaneous sharp drop in thermal conductivity (11)—which simulates a first-order transition—finds a very simple explanation on this basis. Limiting ourselves to only one additional example, it is clear that the concept of microstrain and of concomitant cavitation allows also a ready explanation of brittleness and of its dependence on molecular weight, temperature, and polymer structure.

The lack of symmetry of the strain can be removed partially by partial flow orientation of polymer chains prior to rapid cooling below the tran-

sition temperature. This lowers (10), as expected, the transition temperature itself and it leads to an anisotropy of both cohesive energy and strain. The symmetry axis for either phenomenon should be defined by the direction of orientation, and one should expect that the system is uniaxial negative as regards the strain. This seems to be borne out by the well-known phenomenon of anisotropic brittleness of extruded polystyrene which shatters into a multitude of fibers when tested for brittleness.

VIII. THE SIGNIFICANCE OF DILATOMETRIC VOLUME CHANGES OBSERVED ON MIXING OF POLYMER AND SOLVENT

It is apparent from Fig. 4 that a volume contraction will occur whenever solid polystyrene is mixed with a good solvent at a temperature below the transition point. The observation of a volume change will, therefore, not have any thermodynamic significance unless it differs in magnitude or sign from that to be expected. According to Fig. 4, a minimum contraction of 0.037 cc./g. polystyrene is bound to occur on mixing solid polystyrene at room temperature with bromobenzene. A contraction of this magnitude would indicate a zero heat of mixing rather than a positive heat of mixing. It is worthwhile to emphasize this point since the volume change observed on mixing of solid polymers with solvents has repeatedly been taken as a thermodynamic criterion.

There are, obviously, two ways of excluding an ambiguity of dilatometric results: the best one is to study the effect of mixing above the transition temperature; the alternate one consists of an interpretation of dilatometric results on the basis of previously established $\phi(T)$ relationships such as given in Fig. 4. The usefulness of the latter procedure will be tested in the subsequent section.

IX. THE EFFECT OF SOLVENTS UPON THE APPARENT SPECIFIC VOLUME OF POLYSTYRENE

Although the agreement between the apparent specific volume of polystyrene in bromobenzene and the specific volume of virtually liquid polystyrene at 25°C. is quite close (Table IV), a definite, though small difference exists between the two values. The difference is larger than our experimental error. It would become still larger on extrapolating to a concentration of 100% of polystyrene. The difference is therefore significant on the assumption that the extrapolated temperature function of virtually liquid polystyrene is correct not only in a first, but also in a higher approximation. Granting this, the conclusion would be that either the space requirement (the number of vacant internal sites) of a polymer at equilibrium is slightly reduced in the presence of a good solvent of low molecular weight or that the solvent molecules immediately adjacent to or pervading the polymer molecules assume a slightly higher packing

density than in the solute-free volume elements of the solution. The latter explanation is equivalent to assuming a slight solvation of the polymer molecules, and a minor positive heat of mixing even in a solvent of similar cohesive energy density. Since only the London dispersion forces are operative here, such an effect could not be very pronounced. This agrees with the smallness of the effect observed.

The probability of such a solvent effect is supported by a proper evaluation of dilatometric results obtained by Breitenbach and Franck (3) on studying the volume changes during partial swelling of polystyrene (containing 0.12% *p*-divinylbenzene) in four solvents at 20°C. On converting their data to dimensions and units to fit those adopted here, one obtains a volume contraction of 0.056 cc./g. polymer for swelling in chloroform. This is 51% more than one would expect on the basis of Fig. 4. Complete dissolution instead of partial swelling would probably lead to a still larger difference. In other words, the apparent specific volume at $c = 0.03$ is $\bar{v} \geq 0.901$ which agrees with the direct data of Signer and Gross (12) on pure polystyrene. There is therefore little doubt that a thermodynamic volume contraction occurs for this solvent-solute combination. It is now interesting that the volume contraction observed in benzene amounts to only 0.008 cc./g. polymer. This is only slightly more than 20% of the nonthermodynamic volume contraction expected from Fig. 4 and it is equivalent to an apparent specific volume of $\bar{v} \geq 0.949$ at $c = 0.046$. This value is larger than that for chloroform. The same holds for the direct data obtained in benzene by Danes (4). It seems, therefore, quite definite that the apparent specific volume varies with the nature of a good solvent. The same follows from the compilation in Table V in spite of the considerable uncertainties inherent in some of the data.³

It is very noteworthy that an opposite solvent effect seems to prevail in poor solvents. One of the swelling agents used by Breitenbach and Franck (3), cyclohexane, is a poor solvent. In this case a volume expansion was found on mixing. The effect is, in our units, 0.0033 cc./g. polymer. This indicates that there are here cavities inside the dissolved polymer molecules and that these cavities are not only equal, but even approximately 10% in excess of those present in bulk polystyrene at 25°C. This, in turn, seems to prove that the molecules of poor solvents do not penetrate and pervade the coil of a polymer molecule as easily and as fully as those of good solvents. This is in perfect agreement with the well-known fact of a reduced intrinsic viscosity in poor solvents since a reduction in free solvent drainage across the polymer molecule brings it closer to the

³ According to a private communication by Dr. Boyer, a recent study by D. J. Streeter and R. F. Boyer has shown that the partial specific volume of polystyrene actually varies with the nature of a good solvent and exhibits a minimum in a solvent of intermediate goodness. This study will be published in another periodical.

TABLE V

Apparent Specific Volume of Polystyrene in Various Solvents
 $c > 0.01$; $T = 20-25^{\circ}\text{C}$.

Solvent	ϕ_2	Reference
Chloroform	0.895 ± 0.05	(12)
Chloroform	$\cong 0.901$	Derived from data in Ref. (3)
Toluene	0.913	(13)
Benzene	0.929 ± 0.01	(4)
Benzene	$\cong 0.949$	Derived from data in Ref. (3)
Chlorobenzene	0.922 ± 0.002	This paper
Bromobenzene	0.924 ± 0.001	This paper
Ethyl methyl ketone	$\cong 0.954$	Derived from data in Ref. (3)
Cyclohexane	$\cong 0.960$	Derived from data in Ref. (3)

behavior of an Einstein sphere. This behavior should be approached more the higher the molecular weight and the lesser the steric hindrance to rotations about valence bonds, i.e., the more the molecule exhibiting limited solvent drainage approximates the shape of a sphere. It is clear that all this adds strong support to recent concepts on the viscosity of polymer solutions (5,8).

X. THE EFFECT OF MOLECULAR WEIGHT UPON THE APPARENT SPECIFIC VOLUME

Contradictory and inconclusive data in the literature on the effect of molecular weight upon the apparent specific volume of dissolved polystyrene make it desirable to clear up this question in order to evaluate the importance of working with sharp polymer fractions in this type of studies. A preliminary solution of the problem is possible by following again the procedure adopted and justified in Sec. VI; the data obtained by Flory and Fox for bulk polystyrene of systematically varied molecular weight are extrapolated to 25.0° . In this manner, both the apparent specific volume of polystyrene dissolved in bromobenzene and the actual densities of these solutions are calculated as a function of molecular weight. The results, computed by W. J. Pangonis,⁴ are given in Table VI. It follows that, even with bromobenzene as the solvent, the effect of molecular weight is too small for weights in excess of 80,000 in order to be detected in accurate density measurements with 1% solutions. This explains the good agreement of the data obtained with chlorobenzene and bromobenzene, respectively (Tables II and III). In addition, the small difference between the respective mean values of the apparent specific volume appears now as significant because a complete absence of low-molecular-weight material in the chlorobenzene solution would, according

⁴ A Graduate Student at Wayne University.

to Table VI, enhance the difference in the apparent specific volumes obtained in the two solvents. The apparent specific volume of polystyrene is therefore definitely larger in bromobenzene than in chlorobenzene. The essential result is that, in general, sharp fractions appear unnecessary in studies of the apparent specific volume provided that the molecular weights are within the order of magnitude of 10^6 .

On the other hand, it is apparent from Table VI that the solution density is very sensitive to molecular weight if the latter is less than 30,000, even if the experimental accuracy, in 10% solutions, is limited to four decimal places. This may suggest the use of the densitometric method for rapid molecular weight determinations on material of a low degree of polymerization.

TABLE VI

The Effect of Molecular Weight upon the Apparent Specific Volume of Polystyrene in Bromobenzene Solution and upon the Solution Densities

$T = 25^\circ\text{C}.$

Extrapolation by means of the equation of Flory and Fox (7)

$M \times 10^{-3}$	Φ_2	ρ_{12} (10%)	ρ_{12} (1%)
356	0.924 ₀	1.43248 ₀	1.48038 ₈
100	0.924 ₅	1.43237 ₈	1.48037 ₇
80	0.924 ₇	1.43233 ₇	1.48037 ₂
50	0.925 ₁	1.43221 ₄	1.48035 ₉
30	0.925 ₈	1.43213 ₂	1.48035 ₀
20	0.926 ₈	1.43194 ₇	1.48033 ₁
10	0.929 ₃	1.43139 ₄	1.48027 ₁
8	0.930 ₅	1.43114 ₈	1.48024 ₅
6	0.933 ₈	1.43047 ₂	1.48017 ₃
5	0.934 ₆	1.43030 ₉	1.48015 ₆
4	0.937 ₂	1.42977 ₇	1.48009 ₈
3	0.941 ₆	1.42887 ₈	1.48000 ₂

The foregoing statements are not affected by the possibility that an experimental check may lead to minor revisions of the numerical data in Table VI, since only the trend of the data, i.e., their relative values, are pertinent to the conclusions drawn. As regards the absolute values given, it is noteworthy that an extrapolation to the molecular weight of the monomer yields a specific volume, at $25.0^\circ\text{C}.$, of 1.433, which differs from the mean value of 1.108, obtained by a minor extrapolation, to the same temperature, of the various data available in the literature on the specific volume of styrene. A close examination of the data by Flory and Fox suggests that this discrepancy may be due to a nonvalidity of their $\phi(\bar{M})$ equation below the lowest molecular weight checked, i.e., below $\bar{M}_w = 3000$.

SUMMARY

The apparent specific volume of polystyrene was determined at 25.00°C. in chlorobenzene and bromobenzene. The results are compared with and discussed on the basis of recent density measurements of bulk polystyrene by Flory and Fox. It follows that at least 3% of the volume of solid bubble-free bulk polystyrene at room temperature consists of cavities and that the specific volume of bulk polystyrene at room temperature would be nearly the same as that of polystyrene dissolved in a good solvent if the apparent second-order transition could be avoided for the former. The results indicate that care must be taken in interpreting volume changes observed on mixing solid polymers with solvents. It is proposed to characterize the apparent second-order transition by an alternation of configurational probability in neighboring volume elements. The resulting "microstrain" and cavitation allow a simple explanation of phenomena associated with an apparent second-order transition such as brittleness. Slight divergencies between the apparent specific volume observed and expected in solution and an analysis of pertinent literature data show that the apparent specific volume changes appreciably with the nature of the solvent. It follows, in particular, that the number of vacant sites within a polystyrene molecule in solution is small in good solvents—where conceivably a slight solvation exists—and is very large in poor solvents. In the latter case, the free volume may exceed that found in bulk polystyrene at room temperature. The probable effect of molecular weight upon solution densities and the question of density measurements for rapid molecular weight determinations are discussed briefly by means of extrapolations from data obtained by Flory and Fox.

REFERENCES

1. BOYER, R. F., AND SPENCER, R. S., *J. Polymer Sci.* **3**, 97 (1948).
2. BOYER, R. F., AND SPENCER, R. S., *High Polymer Physics*, pp. 170–185. Chemical Publishing Co., Inc., Brooklyn, 1948; *Advances in Colloid Science*, II, pp. 1–57. Interscience Publishers, Inc., New York, 1946.
3. BREITENBACH, J. W., AND FRANCK, H. P., *Monatsh.* **79**, 531 (1948).
4. DANES, V. Z., *Kolloid-Z.* **68**, 110 (1934); see also YAMAGUCHI, B., *ibid.* **72**, 54 (1935).
5. DEBYE, P., *J. Chem. Phys.* **14**, 636 (1946); DEBYE, P., AND BUECHE, A. M., *ibid.* **16**, 573 (1948).
6. FLORY, P. J., *J. Chem. Phys.* **13**, 453 (1945).
7. FOX, T. G., JR., AND FLORY, P. J., *J. Applied Phys.* **21**, 581 (1950).
8. KIRKWOOD, J. G., AND RISEMAN, J., *J. Chem. Phys.* **16**, 565 (1948).
9. LEWIS, G. N., AND RANDALL, M., *Thermodynamics*, McGraw-Hill, New York, 1923.
10. MUELLER, F. H., *Kolloid-Z.* **95**, 138 (1941).
11. SCHALLAMACH, A., *Proc. Phys. Soc. (London)* **53**, 214 (1941).
12. SIGNER, R., AND GROSS, R., *Helv. Chim. Acta* **17**, 65 (1944).
13. SPENCER, R. S., AND GILMORE, G. D., *J. Applied Phys.* **20**, 502 (1949).

AN INTERIONIC ATTRACTION THEORY APPLIED TO THE DIFFUSE LAYER AROUND COLLOID PARTICLES. I¹

Arthur L. Loeb

Massachusetts Institute of Technology, Cambridge, Massachusetts

Received August 23, 1950

ABSTRACT

Interionic forces in dilute electrolytic solutions have been successfully treated by Debye and Hückel (1), but their theory is not directly applicable to regions of solutions near plane surfaces, especially when these surfaces are highly charged, as in the case of lyophobic colloid particles treated by Langmuir (2). It is shown that even when the total potential is high, that part dependent on an ion being at any given location still obeys approximately a linear differential equation. The concentration distribution and forces between the particles are derived, and compared with the results that Langmuir obtained neglecting interionic forces. In the *Appendix* the extended interionic attraction theory is applied to uncharged or slightly charged surfaces in equilibrium with electrolytic solution.

INTRODUCTION

According to the Debye-Hückel theory, the activity coefficient of the ions in a dilute solution is depressed below its ideal value by a characteristic stabilizing mechanism involving the formations of ionic atmospheres. In the interior of such a solution the normal (i.e., time average) potential is zero everywhere, but when there is an ion at a given point, its presence induces a local space charge of opposite sign nearby, with which an ion interacts, so that its potential energy is lower than the value corresponding to the normal potential.

In the neighborhood of a fixed charge, as on the surface of a colloid particle, the normal potential no longer vanishes. It is produced by the wall charge and the normal diffuse countercharge, and is responsible for the main term in the potential energy of an ion in this region. The stabilizing mechanism must operate to lower this energy, indeed more strongly than in the interior of the solution because the mean ion concentration is greater, and the atmosphere that is formed is more compact.

¹ This article outlines the research done in partial fulfillment of the requirements for the degree of Doctor of Philosophy at Harvard University. The author wishes to express his appreciation for the inspiration and guidance received from Dr. A. Sprague Coolidge. Copies of the complete thesis are filed at Harvard University, the Massachusetts Institute of Technology, Columbia University, the University of Pennsylvania, the University of Amsterdam, and the University of Utrecht (the Netherlands), in each case in the Physical Chemistry Library.

In addition to inducing the stabilizing space charge in the solution, an ion also induces image forces in a nearby surface of discontinuity in the dielectric constant. In previous discussions of the structure of the diffuse layer the ion concentration has been calculated by the Boltzmann law, using for the potential energy only the main term. It is our purpose to estimate the magnitude of the stabilization and image terms and their effect on the ion distribution in the layer.

For the first purpose we must calculate the configuration of the atmosphere formed by an ion near the wall. As compared with the problem solved by Debye and Hückel, the computation is complicated by the absence of spherical symmetry, by the high value of the potential invalidating the linear approximation to the Poisson-Boltzmann equation, and by the need to consider the image terms.

We shall, in our first calculations, use in the Boltzmann exponent for the ions in the atmosphere the potential arising from the wall charge, the diffuse layer, the ion whose atmosphere is to be calculated, the atmosphere to be calculated, and those image terms which can be included automatically by imposing appropriate boundary conditions.

To calculate the potential near a colloid particle, we use Poisson's law

$$\nabla^2 \psi = -\frac{4\pi}{D} \rho, \quad [1]$$

where ψ is the potential, the charge density is ρ , and the dielectric constant is D . The charge density is given for binary electrolytes by the Boltzmann equation:

$$\rho = En^0 z (e^{\eta^+} - e^{\eta^-}); \quad [2]$$

since we are interested only in one kind of ions, the assumption is made that they come from binary electrolytes.

n^0 = bulk concentration of each kind of ions,

E = magnitude of electron charge,

z = valence of ions, and

$\eta_{\pm} = -\frac{U_{\pm}}{kT}$, called the Boltzmann exponent.

U_{\pm} is the work needed to remove an ion from the bulk of the solution to the environment of the charged surface.

If we designate the normal potential by ψ^0 and define $\eta^0 \equiv \frac{Ez\psi^0}{kT}$, we can represent Langmuir's approximation by $\eta_{\pm} = \pm \eta^0$.

This leads at once to an equation for ψ^0 which can be solved. We make the better approximation $\eta_{\pm} = \pm \eta^0 + \eta'$, where η' includes stabilization and image effects and is the same for both ions, depending only on the distance from the wall, and not upon the possible proximity of

other ions. The self-consistency of this assumption can be shown. We do not here account for stabilization terms for the ions that make up the ionic atmosphere; in the bulk of the solution such neglect of stabilization can be justified on the basis of linear approximation, by the argument that solutions of the equation are superimposable, so that the atmosphere of an ion (and therefore its stabilization) is not altered when it takes part in forming the atmosphere of another ion.

This is certainly not true for an atmosphere formed near a charged wall, but it seems probable that a useful first approximation can be obtained by omitting this refinement.

It is now necessary to proceed by successive approximations. Langmuir's value of ψ^0 can be used for approximate calculation of η' , as described in the next paragraph. This can then be used for improved calculations of ψ^0 and of η' itself.

The quantity η_{\pm} is proportional to the work required to transfer an ion reversibly from a position in the bulk of the solution to one near the wall. By a familiar argument, this can be thought of as being done by discharging the ion in its original position and recharging it in the final position. The electrostatic work of the first step is given by the standard theory. For the second step we must first calculate the potential of the atmosphere accumulated by an ion of variable charge $\pm\lambda E$ at a point near the wall.

Under these circumstances let the potential at a point near the ion be:

$$\psi = \psi^0 + \psi',$$

also:

$$\rho = \rho^0 + \rho',$$

where ψ^0 , the "average potential," is independent of the position of the ion, and ψ' , the "perturbation potential," is due to the ion, its atmosphere, and the images.

Equations [1] and [2] hold both for ψ and ρ , and for ψ^0 and ρ^0 ;

$$\begin{aligned}\nabla^2\psi &= \frac{8\pi}{D} En^0ze^{\eta'} \sinh \frac{Ez\psi}{kT}, \\ \nabla^2\psi^0 &= \frac{8\pi}{D} En^0ze^{\eta'} \sinh \frac{Ez\psi^0}{kT}.\end{aligned}$$

The theorem of mean value tells us:

$$\sinh \frac{Ez\psi}{kT} - \sinh \frac{Ez\psi^0}{kT} = \frac{Ez\psi'}{kT} \cosh \left(\frac{Ez\psi^0}{kT} + \mu \frac{Ez\psi'}{kT} \right),$$

where $0 < \mu < 1$

$$\therefore \nabla^2\psi' = \tilde{K}^2\psi', \quad [3]$$

where $\tilde{K}^2 = K^2e^{\eta'} \cosh \frac{Ez\psi^0}{kT}$; $K^2 = \frac{8\pi E^2z^2n^0}{DkT}$.

Equation [3] is analogous to the Debye-Hückel equation, but \tilde{K}^2 here depends on the distance from the charged surface, instead of being constant; the ionic atmosphere is most compact where \tilde{K}^2 (i.e., ψ^0) is largest, namely, near the wall.

To solve Eq. [3], we must know η' and ψ^0 ; a first approximation to ψ^0 can be found by assuming $\eta = 0$, so that $\nabla^2\psi^0 = \frac{8\pi Ez n^0}{D} \sinh \frac{Ez\psi^0}{kT}$, which is the equation that Langmuir (2) used for the potential near charged surfaces. To proceed with the second-order approximation, define $\eta^0 \equiv \frac{Ez\psi^0}{kT}$, so that $\nabla^2\eta^0 = K^2 \sinh \eta^0$ and $\nabla^2\psi' = K^2 \cosh \eta^0 \psi'$.

For simplicity we shall continue with Langmuir's approximation neglecting all ions whose charge has the same sign as that on the wall; this limits the region of our approximation to that where Eq. [4] holds, though in principle our method could be extended through the use of elliptic integrals, as Langmuir did.

$$\sinh \eta^0 \doteq \cosh \eta^0 \doteq \frac{1}{2}e^{\eta^0} = \frac{\pi^2}{2K^2c^2} \sec^2 \frac{\pi x}{2c}, \quad [4]$$

where x is measured perpendicular to the walls from the median plane between them, and where c is an arbitrary constant, depending on the charge or potential on the wall.

$$\therefore \nabla^2\psi' = \frac{\pi^2}{2c^2} \sec^2 \frac{\pi x}{2c} \times \psi'. \quad [5]$$

Equation [5] has various significant features: even though the total potential is high, the perturbation potential ψ' still obeys approximately a linear equation; this approximation may be justified by the same reasoning that is used by Debye and Hückel, and by Onsager (3) in his analysis of the Debye-Hückel theory.

Equation [5] also shows that K^2 is independent of the bulk concentration of the solution, and depends only on the coordinate x , and on the electrical properties of the wall.

Equation [5] must be solved in the cylindrical coordinates x and ρ to fit boundaries at the parallel, plane, charged surfaces and at a pole of unit order at the central ion. A finite charge density produces a continuous, smooth potential, and since the charge density of the atmosphere does not go to infinity anywhere, the function $\left(\psi' \mp \frac{\lambda Ez}{Dr}\right)$ is everywhere continuous and smooth, so that the pole in ψ' must be just equal to that in $\frac{Ez}{Dr}$.

$$\frac{Ez}{Dr} = \frac{Ez}{2D} \int_0^\infty \frac{ds^2}{s} e^{-|x-x_p|s} J_0(s\rho) \quad (4). \quad [6]$$

A solution to Eq. [5] may be written in the form

$$\psi' = \int_0^\infty ds^2 X(s, x) J_0(s\rho), \quad [7]$$

where $X(s, x)$ is a solution of

$$\frac{d^2 X^0}{dx^2} = \left(\frac{\pi^2}{2c^2} \sec^2 \frac{\pi x}{2c} + s^2 \right) X. \quad [8]$$

Therefore the requirement that the function $\left(\psi' \mp \frac{\lambda Ez}{Dr} \right)$ be smooth and continuous, means that $\left(\pm \frac{\lambda Ez e^{-|x-x_p|s}}{2Ds} - X \right)$ must be smooth and continuous. The function $\frac{e^{-|x-x_p|s}}{s}$ has a break in slope equal to 2 at $x = x_p$; in order to compensate for this break, we must make a break in the slope of X at $x = x_p$ of magnitude $\frac{\pm \lambda Ez}{D}$.

The function $X(s, p)$ is shown schematically in Fig. 1. Possible boundary conditions at the walls are $\psi' = 0$ (constant potential), or $\frac{\partial \psi'}{\partial x} = 0$ (constant charge), the truth probably lying between (5). The equations of the walls are $x = \pm d$; the function \tilde{K}^2 goes to infinity at the planes

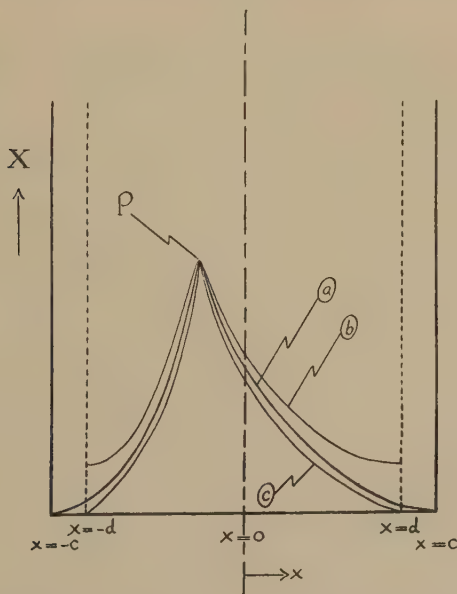


FIG. 1. X as a function of x . (a) $X = dX/dx = 0$ when $x = \pm c$. (b) $dX/dx = 0$ when $x = \pm d$. (c) $X = 0$ when $x = \pm d$. P = location of pole. $x = \pm c$: asymptotes of \tilde{K}^2 . $x = \pm d$: walls or surfaces of colloid particles.

$x = \pm c$. In the extreme case that $c = d$, corresponding to infinite wall potential, both possible conditions are satisfied simultaneously, because of the singularity in K^2 . The resulting form of X is shown schematically in Fig. 1a. When $c > d$, the two cases lead to curves b and c , for the same value of s . It appears from Langmuir's calculations that actual wall charges are usually so high that c is not much greater than d . Then the difference between curves a , b , and c at x_p will be very small, except when x_p is very nearly equal to d ; if we use curve a to calculate η' , the error will be very small, except near the wall, where the precise value of η' has little effect on the course of the ψ^0 curve. We therefore consider only the case $c = d$.

Physically the curve a represents complete shielding of the central ion from the wall; since both field and perturbation potential are zero at the wall in this case, the central ion does not induce any charge at the surface. The curves b and c represent partial shielding, while when $c \doteq d$, we have nearly complete shielding.

We have used three methods for solving Eq. [5] subject to the boundary conditions just described:

(A). We may venture to predict a comparison between the atmosphere formed under these conditions and that which would be formed in a homogeneous solution with constant K equal to $\tilde{K}(x_p)$ (6). The bulk of the constant K atmosphere is contained within a sphere with radius of the order of K^{-1} .

$$\tilde{K}^2(x_p) = \frac{\pi^2}{2c^2} \sec^2 \frac{\pi x_p}{2c} > \frac{2}{(c - x_p)^2},$$

$\therefore K^{-1}(x_p) < 0.7(c - x_p)$, so that wherever the ion is, there is room for such a sphere between it and the walls; a constant K atmosphere would therefore not be seriously mutilated by being cut off at the walls. As to the distortion produced by the actual variation in \tilde{K} , we note, first, that this variation is confined to one of the three principal directions (namely, that perpendicular to the walls), and second, that its first-order effect on the potential (the term proportional to $\frac{\partial \tilde{K}}{\partial x}$) must vanish by symmetry, as otherwise its sign would depend on the choice of the positive direction for x . We conclude that, for purposes of computing η' , the constant K approximation should be quite good. Actually it turns out to be in error by only a few percent.

The resulting expression for ψ' is:

$$\psi' = \frac{\pm \lambda E z}{D r} e^{-\frac{\pi r}{c\sqrt{2}}} \sec \frac{\pi x_p}{2c}, \quad [9]$$

where r = distance from the pole.

(B). For an analytical approximation to Eq. [5], we solve exactly

an equation that approximates Eq. [8]:

$$\frac{d^2X}{dx^2} = \left\{ \frac{2}{(c-x)^2} + \frac{\pi^2}{6c^2} + s^2 \right\} X, \quad [10]$$

which gives as an approximate solution:

$$X(x = x_p) = \frac{\pm \lambda E z}{D \sqrt{s^2 + \frac{\pi^2}{6c^2}}} P(P - Q), \quad [11]$$

where

$$\begin{aligned} P &= \cosh \left\{ \sqrt{\frac{\pi^2}{6c^2} + s^2} (c - x_p) \right\} \\ &\quad - \frac{1}{\sqrt{\frac{\pi^2}{6c^2} + s^2} (c - x_p)} \sinh \left\{ \sqrt{\frac{\pi^2}{6c^2} + s^2} (c - x_p) \right\} \\ Q &= \sinh \left\{ \sqrt{\frac{\pi^2}{6c^2} + s^2} (c - x_p) \right\} \\ &\quad - \frac{1}{\sqrt{\frac{\pi^2}{6c^2} + s^2} (c - x_p)} \cosh \left\{ \sqrt{\frac{\pi^2}{6c^2} + s^2} (c - x_p) \right\}. \end{aligned}$$

The exact function for X vanishes with zero slope at $x = \pm c$, while the approximate one does so at $x = -c$ and at $x = +\infty$; yet the latter lies between the two very nearly equal curves b and c in Fig. 1, and is as acceptable as curve a for the same reasons as those given above. Substituting into Eq. [7], and integrating, we find:

$$\begin{aligned} \psi' &= \frac{\pm \lambda E z}{D} \left[\frac{\pi}{\sqrt{6}c} - \frac{\sqrt{6}c}{\pi(c-x)^2} (e^{-\sqrt{\frac{2}{3}} \frac{\pi(c-x)}{c}} - 1) \right. \\ &\quad \left. - \frac{1}{2(c-x)} e^{-\sqrt{\frac{2}{3}} \frac{\pi(c-x)}{c}} - K \right]. \quad [12] \end{aligned}$$

(C). Equation [5] may be solved by a series expansion of X ; in this expansion each coefficient is a series in s^2 . Since this series must be integrated over an infinite range of s^2 , we cannot use it directly, but will rather check the integrands of the solutions obtained under (A) and (B) against it. (Using Eq. [7], we can expand the expression for ψ' obtained under (A) into an integral in s^2 .) I am indebted to Dr. A. S. Coolidge for the following analysis of the discrepancies between the two approximate solutions and the result of the series expansion.

If we call the two approximate solutions in question X_A and X_B , and their differences from the exact solution $\Delta_A \equiv X - X_A$, and

$\Delta_B \equiv X - X_B$, respectively, we may rewrite Eq. [5] for the two cases:

$$\frac{d^2 X}{dx^2} = \left(s^2 + \frac{2}{\sin^2 x_p} - \frac{2}{3} \right) X + 2A(x)X,$$

where $A(x) = \frac{1}{\sin^2 x} - \frac{1}{\sin^2 x_p}$ for case A , and

$$\frac{d^2 X}{dx^2} = \left(s^2 + \frac{2}{x^2} \right) X + 2B(x)X,$$

where $B(x) = \frac{1}{\sin^2 x} - \frac{1}{x^2} - \frac{1}{3}$, for case B . But

$$\left. \begin{aligned} \frac{d^2 X_A}{dx^2} &= \left(s^2 + \frac{2}{\sin^2 x_p} - \frac{2}{3} \right) X_A \quad \text{and} \\ \frac{d^2 X_B}{dx^2} &= \left(s^2 + \frac{2}{x^2} \right) X_B, \end{aligned} \right\}$$

$$\therefore \left. \begin{aligned} \frac{d^2 \Delta_A}{dx^2} &= 2A(x)X_A + \left(s^2 + \frac{2}{\sin^2 x_p} - \frac{2}{3} \right) \Delta_A \quad \text{and} \\ \frac{d^2 \Delta_B}{dx^2} &= 2B(x)X_B + \left(s^2 + \frac{2}{x^2} \right) \Delta_B. \end{aligned} \right\} \quad [13]$$

$A(x)$ and $B(x)$ can be expanded in a series in $(x - x_p)$, and the Δ functions in a rapidly converging series, in $(x - x_p)$ when $x > x_p$, or in $(x_p - x)$ when $x < x_p$, the boundary conditions being that Δ be smooth and continuous everywhere, even at $x = x_p$. Thus the Δ functions can be expressed as a series in the form:

$$\Delta = e^{-s|x-x_p|} \sum_n k_n s^n |x - x_p|^n$$

k_n being evaluated from the differential equations in [13].

For both Δ_A and Δ_B the integral over the entire range of s converges, even when $x = x_p$, and hence the discrepancies between (A) and (B) with the exact result can be approximated as closely as we please.

Table I lists, for various values of x_p , the values of ψ' as approximated by methods (A) and (B), and the corrections applied as just described.

Since both approximations (A) and (B) were made by neglecting higher terms in the expansion of \tilde{K}^2 , we have under-estimated the compactness of the atmosphere, and consequently the numerical results are too low. For any value of x_p , therefore, the better approximation is the one whose numerical value is higher. Thus when the ion is near the center, the constant solution (A) is better, whereas when it is near the wall, (B) gives a superior result. The value obtained by (A) never deviates by more than 5% from the exact solution. The percentage difference at $x_p = c$ was found by expanding ψ_A' and ψ_B' for very small values of $(c - x_p)$, and comparing the coefficients of the leading terms in the series in $(c - x_p)$.

TABLE I

Values of the Perturbation Found Approximately by Methods A and B, and the Corrected Values Obtained by Method C, Labeled, Respectively,
 ψ_A' , ψ_B' , ψ_{CA}' and ψ_{CB}'

$\frac{\pi x_p}{2c}$	$\frac{D\psi_A'}{\pm \lambda Ez} - \frac{1}{r}$	$\frac{D\psi_B'}{\pm \lambda Ez} - \frac{1}{r}$	Difference	$\frac{D\psi_{CA}'}{\pm \lambda Ez} - \frac{1}{r}$	$\frac{D\psi_{CB}'}{\pm \lambda Ez} - \frac{1}{r}$
0	-1.4142	-1.2500	per cent 13.2	-1.4749	-1.4757
$\frac{\pi}{2} - 1$	-1.6806	-1.7042	-1.39	-1.7620	-1.7609
$\frac{\pi - 1}{2}$	-2.9498	-3.1082	-5.10		-3.1147
$\frac{\pi}{2}$	∞	∞	-5.72		

The last two columns show that the two methods when corrected give good agreement.

To find η' from ψ' , we integrate over λ from zero to unity. Since ψ' obeys a linear differential equation, and is therefore proportional to λ , $\frac{\psi'}{\lambda}$ is independent of λ .

$$\therefore kT\eta' = \int_0^{\pm 1} \psi' d(Ez\lambda) = Ez \int_0^{\pm 1} \frac{\psi'}{\lambda} \lambda d\lambda = \frac{Ez\psi'}{+\lambda} \int_0^{\pm 1} \lambda d\lambda = \frac{Ez\psi'}{\pm 2\lambda}.$$

Case (A), for instance, gives

$$\eta' = \frac{E^2 z^2}{2DkT} \left(\frac{\pi}{c\sqrt{2}} \sec \frac{\pi x}{2c} - K \right). \quad [14]$$

Using the more convenient approximation for η' , the one obtained by method (A), we proceed to find a better approximation for η^0 and for the concentration distribution of ions between the walls.

$$\nabla^2 \eta^0 = K^2 e^{\eta'} \sinh \eta^0 = \frac{K^2}{2} e^{\eta'}.$$

Since η^0 and η' are functions of x only:

$$\frac{d^2 \eta}{dx^2} = \frac{K^2}{2} e^{\eta} + \frac{d^2 \eta'}{dx^2}.$$

Langmuir did not distinguish between η^0 and η ; his solution $\eta = L$ obeys the equation:

$$\frac{d^2 L}{dx^2} = \frac{K^2}{2} e^L, \quad \therefore e^L = \frac{\pi^2}{K^2 c^2} \sec^2 \frac{\pi x}{2c}.$$

Defining the correction function $\delta \equiv \eta - L$, we derive the following differential equation for it by substituting in the last two equations:

$$\frac{d^2\delta}{dx^2} \equiv \frac{d^2\eta}{dx^2} - \frac{d^2L}{dx^2} = \frac{K^2}{2} (e^\eta - e^L) + \frac{d^2\eta'}{dx^2}.$$

when $\delta \ll 1$, $e^\eta - e^L = \delta e^{L+\mu\delta} \doteq \delta e^L$, $0 < \mu < 1$.

Substituting in $\frac{d^2\eta'}{dx^2}$ for η' the function given by Eq. [14] and for e^L Langmuir's expression given above, then

$$\frac{d^2\delta}{dx^2} = \frac{\pi^2}{2c^2} \sec^2 \frac{\pi x}{2c} \times \delta + \frac{E^2 z^2}{\sqrt{2} D k T} \left(\frac{\pi}{2c} \right)^3 \left\{ 2 \sec^3 \frac{\pi x}{2c} - \sec \frac{\pi x}{2c} \right\}$$

δ is therefore independent of the bulk concentration of the solution if its boundary conditions are. One boundary condition is that δ be even in x , so that $\frac{d\delta}{dx} = 0$ when $x = 0$. To choose the second condition, we note that of the three quantities wall separation, surface charge or negative potential, and potential in the median plane, two are independent, the third one being found approximately by the Langmuir expression, which is corrected in this article. We may either find a correction to the potential in the median plane corresponding to a certain wall charge or wall potential and separation, or we may correct the wall separation that corresponds to a given wall charge or potential and median plane potential. It is most convenient to start so the $\delta = 0$ when $x = 0$, i.e., from the same Boltzmann factor at the median plane.

An excellent approximation to the solution of Eq. [12] obeying the boundary conditions $\frac{d\delta}{dx} = \delta = 0$ when $x = 0$ is given by:

$$\delta \doteq \frac{E^2 z^2}{2\sqrt{2} D c k T} \left\{ 3 \sec \frac{\pi x}{2c} - 3 - \frac{\pi x}{2c} \tan \frac{\pi x}{2c} \right\},$$

which deviates from the exact solution by the series

$$\frac{E^2 z^2 \pi}{2\sqrt{2} D c k T} \left[\frac{12}{6!} \left(\frac{\pi x}{2c} \right)^6 + \frac{28}{8!} \left(\frac{\pi x}{2c} \right)^8 + \dots \right],$$

which is small in the region of interest, namely, where $\delta \ll 1$, which is where $\frac{\pi x}{2c}$ is not very large.

The concentration distribution is now found:

$$n = n^0 e^\eta = n^0 e^{L+\delta} \doteq n^0 e^L (1 + \delta) \doteq \frac{\pi D k T}{8 E^2 z^2 c^2} \sec^2 \frac{\pi x}{2c} + \frac{\pi^2}{16\sqrt{2} c^3} \sec^2 \frac{\pi x}{2c} \left(3 \sec \frac{\pi x}{2c} - 3 - \frac{\pi x}{2c} \tan \frac{\pi x}{2c} \right).$$

The first term is that given by Langmuir, while the second term depends on c only, and is otherwise universal.

The last step in finding the force between colloid particles necessitates another correction to Langmuir's theory. So far, our modifications consisted of introducing the function η' into the concentration distribution formula, and of finding a better approximation to the average potential and hence to the relation between median plane potential, wall separation, and surface charge or negative potential. Langmuir found the force between the parallel planes by considering the thermal bombardment of the median plane, remembering that for mechanical equilibrium the force on any plane must be the same. Since we are correcting for the interionic

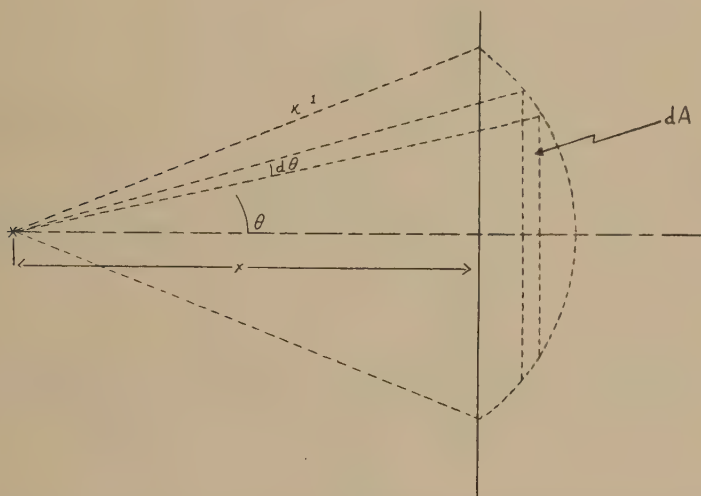


FIG. 2. Ion and a portion of a sphere of radius K^{-1} , showing a ring element of area dA .

attractions, we must subtract from the thermal force at the median plane the force that all ions on one side of it experience from their ionic atmosphere beyond the median plane. To estimate this force, take an ion at a distance x from the median plane, surrounded by an atmosphere regarded as concentrated on a sphere at a distance \tilde{K}^{-1} from the ion, as shown in Fig. 2. The force that the ion experiences from the atmosphere can then be calculated by finding the charge on that part of the atmosphere that is beyond the median plane. The charge on the entire sphere of radius \tilde{K}^{-1} is $-Ez$, hence, the charge density on the sphere is $-\frac{Ez\tilde{K}^2}{4\pi}$.

The sphere is now subdivided into elements by planes parallel to the median plane. Each ring element has an area $dA = \frac{2\pi}{\tilde{K}^2} \sin \theta d\theta$; its charge

is $dq = -\frac{Ez}{4\pi} \tilde{K}^2 dA = -\frac{Ez}{2} \sin \theta d\theta$, which exerts a force on the central ion given by $dF = -\frac{E^2 z^2}{2D} \tilde{K}^2 \sin \theta \cos \theta d\theta$.

Integrating, we get for the force on an ion due to that part of its atmosphere that is beyond the median plane:

$$\begin{aligned} F &= -\frac{E^2 z^2 \tilde{K}^2}{2D} \int_0^{\cos^{-1} \tilde{K}x} \sin \theta \cos \theta d\theta \\ &= \frac{-E^2 z^2 \tilde{K}^2}{4D} (1 - \tilde{K}^2 x^2) \quad \text{for } 0 \leq \tilde{K}x \leq 1, \\ &= 0 \quad \text{for } \tilde{K}x \geq 1. \end{aligned}$$

A justification for treating the ionic atmosphere as a charge concentrated on a sphere may be found in the *Appendix*, where the osmotic pressure of a dilute electrolytic solution is found by the same method, and agrees with that derived by Debye and Hückel. Actual integration over the space-distribution of charge can be shown to lead to the identical result even in the case presently under discussion.

The attraction per unit area between all ions on one side of the median plane and their atmospheres beyond that plane is determined by integration:

$$P = \frac{E^2 z^2 \tilde{K}^2}{2D} \int_0^{\tilde{K}x=1} n(1 - \tilde{K}^2 x^2) dx.$$

Thus the total repulsion between the parallel walls is given by:

$$\Pi = \frac{\pi D}{8E^2 z^2 c^2} (kT)^2 + \frac{E^2 z^2}{4D} \int_0^{\tilde{K}x=1} n \tilde{K}^2 (\tilde{K}^2 x^2 - 1) dx, \quad [15]$$

where

$$\begin{aligned} n &= \frac{\pi D k T}{8E^2 z^2 c^2} \sec^2 \frac{\pi x}{2c} \left\{ 1 + \frac{E^2 z^2 \pi}{2\sqrt{2} D c k T} \left(3 \sec \frac{\pi x}{2c} - 3 - \frac{\pi x}{2c} \tan \frac{\pi x}{2c} \right) \right\}, \\ \tilde{K}^2 &= \frac{\pi^2}{2c^2} \sec^2 \frac{\pi x}{2c} \left\{ 1 + \frac{E^2 z^2 \pi}{2\sqrt{2} D k T} \left(3 \sec \frac{\pi x}{2c} - 3 - \frac{\pi x}{2c} \tan \frac{\pi x}{2c} \right) \right\}, \end{aligned}$$

\tilde{K}^2 containing the correction term included in n , since $\tilde{K}^2 \propto n$.

When $D = 81$, $T = 293^\circ\text{K}$., $z = 1$, this becomes:

$$\Pi = \left(\frac{2.23 \times 10^{-7}}{c^2} - \frac{6.19 \times 10^{-15}}{c^3} \right) \text{ dynes/cm.}^2,$$

where c is expressed in centimeters.

The second term is relatively small in the region of c for which our various assumptions hold

$$\left(8 \text{ \AA.} \ll c \ll \frac{10 \text{ \AA.}}{\sqrt{\text{molar concentration}}} \right)$$

TABLE II

The Average Potential as a Function of Position between Walls $z = 1$; $D = 81$; $T = 293^\circ\text{K}$.; $Kc = 1$; $0.01M$ solution

x/c	$\frac{Ez}{kT} L$	$\frac{Ez\psi^0}{kT}$	Difference
0.0	2.289	1.939	-0.350
0.1	2.314	1.964	-0.350
0.2	2.389	2.039	-0.350
0.3	2.520	2.170	-0.350
0.4	2.713	2.367	-0.346
0.5	2.982	2.642	-0.340
0.6	3.352	3.027	-0.325
0.7	3.869	3.579	-0.290
0.8	4.638	4.434	-0.204
0.9	6.000	6.098	+0.098
1.0	∞	∞	∞

but it does introduce an attraction term that might become relatively important when c becomes very small.

To find the actual repulsion between colloid particles, we subtract from the force given above that due to bombardment of the opposite sides of the particles, namely $\left(2n^0kT - \frac{E^2z^2K}{3D}\right)$. This finally gives us the desired relation between the repulsion, the charge or potential, and the separation of the colloid particles by means of the two parametric

TABLE III

The Concentration Distribution between the Walls $z = 1$; $D = 81$; $T = 293^\circ\text{K}$.; $c = 30\text{\AA}$; concentration solution immaterial

x/c	Langmuir's concentration	Modified concentration	Difference
	<i>g.-ions/l.</i>	<i>g.-ions/l.</i>	<i>g.-ions/l.</i>
0.0	0.102	0.102	0.000
0.1	0.104	0.104	0.000
0.2	0.113	0.114	0.001
0.3	0.128	0.131	0.003
0.4	0.156	0.166	0.010
0.5	0.204	0.216	0.012
0.6	0.295	0.316	0.021
0.7	0.495	0.534	0.039
0.8	1.068	1.144	0.076
0.9	4.168	4.361	0.193
1.0	∞	∞	∞

Eqs. [14] and [15]:

$$\frac{Ez\psi^0}{kT} = \ln \frac{\pi^2}{K^2c^2} - 2 \ln \cos \frac{\pi x}{2c} + \frac{E^2z^2\pi}{2\sqrt{2}DckT} \\ \times \left(2 \sec \frac{\pi x}{2c} - 3 - \frac{\pi x}{2c} \tan \frac{\pi x}{2c} \right) - \frac{E^2z^2K}{2DkT}, \quad [16]$$

c is approximately equal to the semi wall separation; if we set c equal to d in Eq. [14], we have a direct approximate relation between Π and d , independent of the wall charge or negative potential. As demonstrated previously, the wall charge is indeed relatively unimportant.

Tables II, III, and IV demonstrate the difference between Langmuir's value and our second-order approximation for the average potential, concentration distribution, and the pressure, basing our correction on the same value for η_M , and hence of the median plane concentration, as that of Langmuir.

TABLE IV

The Net Pressure between the Walls as a Function of c
 $z = 1$; $D = 81$; $T = 293^\circ\text{K}$.; concentration solution 0.01M

c	Langmuir pressure	Langmuir pressure minus $2n^0kT$	Modified pressure	Mod. pressure minus $\left(2n^0kT - \frac{E^2z^2K}{3D}\right)$	Discrepancy
$^\circ\text{K}$.	$\times 10^5 \text{ dynes/cm.}^2$	$\times 10^5 \text{ dynes/cm.}^2$	$\times 10^5 \text{ dynes/cm.}^2$	$\times 10^5 \text{ dynes/cm.}^2$	$\times 10^5 \text{ dynes/cm.}^2$
5	892	887	393	390	-497
10	223	218	161	158	-60
20	55.8	50.9	48.1	45.0	-5.9
30	24.8	19.9	22.5	19.4	-0.5
40	14.0	9.1	13.0	9.9	0.8
50	8.92	4.05	8.42	5.31	1.26
60	6.20	1.33	5.91	2.80	1.47
70	4.55	-0.32	4.38	1.27	1.59
80	3.48	-1.39	3.38	0.27	1.66
90	2.75	-2.12	2.64	-0.47	1.65

Extrapolation down to 5 Å. in Table IV is obviously not justified, since the correction to Langmuir's result for the pressure is no longer small there; it was shown above that c must be greater than 8 Å. The extrapolation is included because it demonstrates, at least qualitatively, a tendency for the pressure to change its sign when particle separation becomes very small, which may be significant in coagulation.

APPENDIX

A by-product of the presented line of reasoning, and actually the first test application of our method, is the derivation of the osmotic pressure

of a dilute electrolytic solution by electrostatic means, and a study of the charge distribution near discontinuities in the dielectric constant of the medium. In all applications discussed in this appendix we assume $\sinh \frac{Ez\psi}{kT} \doteq \frac{Ez\psi}{kT}$; the potential then obeys the Debye-Hückel equation.

Any discontinuities in \tilde{K}^2 or in D are to occur along planes; such discontinuities may be due to a discontinuity in solvent (e.g., two immiscible solvents) or to a mechanical exclusion of ions from one region (e.g., by means of a semipermeable membrane).

$$\nabla^2\psi = K^2\psi;$$

writing as before $\psi = \psi^0 + \psi'$ and

$$\begin{aligned}\nabla^2\psi^0 &= K^2\psi^0, \\ \nabla^2\psi' &= K^2\psi'.\end{aligned}\tag{17}$$

we obtain

Unlike in the high potential case, the perturbation potential now obeys the same equation as the total potential does, and is independent of ψ^0 . In other words, ψ^0 and ψ' are linearly superimposable. Near a plane surface we must solve Eq. [16] in cylindrical coordinates.

$$\psi = \int_0^\infty ds^2 X(x, s) J_0(s\rho),$$

where X must obey the following boundary conditions: at the surface X is continuous, and $\frac{d}{dx}(Dx)$ continuous as well (D = dielectric constant),

at the pole the break in slope of X is $\frac{Ez}{D}$, and at infinity X vanishes.

For a semipermeable membrane separating pure solvent with dielectric constant D from a solution with the same dielectric constant, we obtain by the same splicing method described before,

$$X = \frac{Ez}{2D\sqrt{K^2 + s^2}} \left\{ \frac{\sqrt{K^2 + s^2} - s}{\sqrt{K^2 + s^2} + s} e^{-2\sqrt{K^2 + s^2} x_p} + 1 \right\},$$

where x_p is the distance between pole and membrane.

For an ion at the membrane ($x_p = 0$):

$$\eta' (= \eta \text{ for uncharged membrane}) = -\frac{KE^2z^2}{6DkT}$$

$$\therefore n_+ = n_- = n^0 e^{-\frac{KE^2z^2}{6DkT}} \doteq n^0 \left(1 - \frac{KE^2z^2}{6DkT} \right).$$

In the absence of electrical forces acting on the membrane the osmotic pressure is proportional to the local concentration of ions at the membrane,

$$\therefore \Pi = 2n^0kT - \frac{E^2z^2K}{3D} n^0,$$

which agrees exactly with the result obtained by Debye and Hückel by means of a free energy method.

Corollary

η' is defined as the work done by the system in bringing an ion from infinity inside the solution to the region near the wall, and in this case a negative quantity. We also found η' for the pure solvent region by assuming a pole in the region where $K = 0$ instead of in the solution. The result was that $\eta' = \frac{KE^2z^2}{3D}$, so that the work necessary to take an ion from ∞

inside the solution to ∞ outside is indeed $\frac{KE^2z^2}{2D}$, in agreement with the limiting law for activity coefficients. The interesting relationship is the ratio 2:1 for the portions of the path inside and outside the solution.

A third method for obtaining the osmotic pressure consists of finding the combined electrical and thermal forces acting on a plane in the bulk of the solution. This method is described above (see Fig. 2), and gives the same result as the other two methods for a dilute solution.

The case of a discontinuity in the dielectric constant is treated in two extreme cases, namely perfectly conducting and perfectly insulating walls.

Let there be two walls separated by a distance $2d$. In the perfectly conducting wall an ion induces an opposite charge, in an insulator an equal one. From the consideration of the whole series of mirror images induced into the two parallel walls, we find for the potential at the central ion caused by a term like $\frac{Ez}{Dr} e^{-Kr}$ for each induced charge as well as the central ion itself:

$$\lim_{r \rightarrow 0} \left(\psi - \frac{Ez}{Dr} \right) = \frac{Ez}{D} \left[-K - \frac{1}{2d} \ln(1 - e^{-4Kd}) \right. \\ \left. \pm \sum_{l=0}^{\infty} \frac{e^{-2K\{(2l+1)d+a\}}}{2\{(2+1)d+a\}} \pm \sum_{l=0}^{\infty} \frac{e^{-2K\{(2+1)d-a\}}}{2\{(2+1)d-a\}} \right],$$

where a = the distance between the central ion and the median plane.

When $a = 0$:

$$\varphi \equiv \lim_{r \rightarrow 0} \left(\psi - \frac{Ez}{Dr} \right) = -\frac{Ez}{Dd} [Kd + \ln(1 \pm e^{-2Kd})],$$

where (+) refers to conducting walls, and (−) to insulating walls.

When the walls are sufficiently far apart that the undistorted ionic atmosphere fits between them, $Kd > 1$. Then $\ln(1 \pm e^{-2Kd})$ is negligible compared with Kd , so that the central ion is effectively screened from the walls by its ionic atmosphere, and the concentration at the median plane

is not appreciably affected by the walls. Actually the dielectric properties of the walls lie somewhere between the extremes described above, in which case the screening is at least as great as that described for the extremes.

When there is only one wall, $d = \infty$, but $d - a$ can be kept finite. The results then agree with those of Onsager and Samaras (5) for a free air solution surface.

REFERENCES

1. DEBYE, P., AND HÜCKEL, *Physik Z.* **24**, 305 (1923).
2. LANGMUIR, I., *J. Chem. Phys.* **6**, 873 (1938).
3. ONSAGER, L., *Chem. Revs.* **13**, 73 (1933).
4. See, for instance, BATEMAN, *Partial Differential Equations*. Cambridge Univ. Press, Cambridge, 1932, p. 410.
5. COOLIDGE, A. S., *J. Am. Chem. Soc.* **71**, 2164 (1949).
6. A similar assumption was made by WAGNER, C., *Physik Z.* **25**, 474 (1924).
7. VERWEY, E. J. W., AND OVERBEEK, J. T. G., *Theory of the Stability of Lyophobic Colloids*, Elsevier Publishing Company, Inc., Amsterdam, 1948.

Though this last reference appeared after research for this paper had been completed, the author has subsequently found it invaluable, and recommends *Part II* and the *Appendix*, especially for a fundamental background.

BINGHAM AWARD TO W. F. FAIR, JR.¹

The third annual Bingham Medal was presented to Dr. W. F. Fair, Jr., of the Mellon Institute and Koppers Company and past president of the Society of Rheology, by W. H. Markwood, Jr., the Society's editor. The award was made "for notable contributions to colloid chemistry, to the technology of bituminous materials, and to the science of rheology; for distinguished services to the American Society for Testing Materials in establishing standards; for his counsel in his position as a member of the governing board of the American Institute of Physics; and for his guidance of the affairs of the Society of Rheology in various positions and finally that of president for the years 1945 to 1949."

ACCEPTANCE OF THE BINGHAM MEDAL²

W. F. Fair, Jr.

I am very proud and very happy to have been selected by your committee for the Bingham Medal Award for 1950. I want to thank you sincerely for this honor which I appreciate so much. I am all the more appreciative of receiving the Bingham Medal Award because of my respect and admiration for the man in whose memory this medal was established. Professor Bingham was an ever constant source of help and advice to me and to many others interested in rheological problems.

I would like to take this occasion to mention briefly the importance of rheological investigations for industry. We all know that there are general problems connected with rheology in all kinds of industries; many of us know particularly the problems in detail in one industry; others of us only have general information over a wider field of interest. Undoubtedly a great deal of progress can be made in the field of industrial rheological research and I fully believe that such development will help the progress of industry and rheology, and should benefit our Society. I cannot speak for industry as a whole, but I can speak with some intimate knowledge of rheological problems in the bituminous materials industry, and I would like to cite a few of current interest. Coal-tar pitches and petroleum and natural asphalts differ markedly in many important physical and chemical properties; but they are generally used as binders for construction installations where water impermeability, weather resistance, binder strength, and adhesion are important. Affecting such properties and the design and service life of the installation are the initial and final flow characteristics of these binders.

In road building the viscosity and viscosity-temperature susceptibility of the binder are important. The engineer must design his installation and select his aggregate gra-

¹ Presented at the Annual Meeting of the Society of Rheology, New York, N. Y., November 3-4, 1950.

² Presented at the Annual Meeting of the Society of Rheology, New York, N. Y., November 3-4, 1950.

dation always keeping in mind the particular viscosities and viscosity-temperature susceptibilities of the bituminous binders specified.

For the construction of built-up roofs, the rheological properties of the binder are extremely important. For flat-roof construction a material of suitable viscosity, high-temperature susceptibility and Newtonian flow is preferred because such a roof heals every summer by resealing itself effectively, the value of which is shown by the extreme service durability of such roofs. A material of similar consistency but of non-Newtonian flow characteristics may crack in the winter time and be unable to seal itself in subsequent hot weather, and thus may exhibit early failure. In steep-roof construction different properties are required. Here high consistency, non-Newtonian flow, and appreciable yield values are needed to prevent the binder and cover aggregate from sliding off the roof.

The flow properties of hot applied coatings are extremely important in the corrosion protection of pipelines, thousands of miles of which have been and are being constructed in this country and other parts of the world. Cold flow before back-filling is undesirable of course. Properties must be tailored in manufacturing the enamel to withstand service conditions and geographical locations. Alternate wetting and drying of clayey soil with simultaneous changes in stress on the protective coating and subsequent damage, is frequently encountered in certain parts of this country and obviously constitutes a double-barreled rheological problem. Attack on this problem may involve attempts to change the soil characteristics, or to develop materials more resistant to higher soil stresses, while retaining the other properties necessary for effective protection against the corrosion environment.

Another interesting rheological problem in connection with bituminous materials is the use of joint sealers. Here the preferred material should be high melting, should not exhibit cold flow under service temperatures underground, should adhere to the pipe surfaces, should not be so hard as to be brittle, and most important of all, should not be so soft as to permit root penetration.

Still another interesting field of rheological importance concerns the development of coatings which will be corrosion resistant to marine immersion and will be resistant to the attack of barnacles. Here it is necessary to develop a coating or system which will be adherent to steel, which will not spall off during pile-driving, for instance, which will be corrosion resistant in marine environments, and which will resist barnacle penetration permanently. Obviously the rheological properties of the constituents of the system will control the solution of this problem.

An entirely new field of rheological problems is encountered with cold-applied protective coatings. This refers not only to the conventional paint-type systems with which you are all familiar, but also the more recently developed distinctive bituminous base coatings intentionally manufactured to produce very thick films, much thicker than ordinary paint systems. For instance, cold-applied thixotropic solvent-type and emulsified bituminous coatings made with and without fillers and fibers have found wide acceptance as protective coatings against extremely severe corrosive environments. Many of these products have such apparently high consistencies that one would expect them to be difficult, if not impossible to apply; however, by using suitable equipment, and by having the appropriate degree of thixotropy and consistency, these materials become momentarily liquefied in positive displacement equipment and can be sprayed as heavily as 50 to 60 sq. ft. to the gallon, leaving coatings which do not exhibit sag because of the rapid recovery of false body after spraying.

I mention the above type of rheological problems in the bituminous field. There are many more that could be cited, particularly by Dr. Traxler. I am sure that similar types of applications could be mentioned by many interested in other industries, or interested purely from an academic point of view. With no intention of minimizing the importance

of pure research in rheology, which is in obviously capable hands, I dwell upon this matter of industrial rheology because I think there is a tremendous field for important work in such research, and I also confidently believe that the growth of the Society of Rheology will depend to a certain extent upon the growth of rheological interest in industry.

On the engineering side of this subject we can note some progress, slow but definite. Many American Society for Testing Materials specifications include provisions dealing with the flow properties of materials of construction. This will be expanded undoubtedly, and, it is to be hoped, will result in putting viscosity and consistency specifications upon a more fundamental basis than is now the case. In this connection mention should be made of Mr. Markwood's work in preparing most of the manuscript, and editing all of the copy, for a proposed American Society for Testing Materials report on various methods of determining absolute viscosity.

I hope that you will all take any opportunity which presents itself to point out the value to industry of intelligent research and development work in rheology.

During the past several years much progress has been made in developing the Society of Rheology which has been experiencing a conservative but strong and steady growth. This could not have been accomplished were it not for the interest, hard work, and earnest cooperation of our elected and appointed officers and committee chairmen, from whom we may and do expect continued sound administration in the future.

Before closing, I want to express my thanks to Dr. Weidlein and Dr. Cretcher of Mellon Institute, and to Mr. Rhodes, Dr. Volkmann, and Dr. Sturrock of Koppers Company for their advice and suggestions on our research, and for providing the opportunity for attention to Society matters; and to Messrs. Beck, Calderwood, Falce, and McKee for their able assistance in our investigations.

Again I wish to thank you sincerely for having honored me with the Bingham Medal for 1950.

SECONDARY STRESSES IN VISCOELASTIC FLOW¹

M. Mooney

United States Rubber Co., Passaic, New Jersey

Received January 26, 1951

ABSTRACT

Theoretical equations are developed for secondary stresses in a shearing viscoelastic fluid. The theory assumes that the elastic stresses developed by the continuous shear also relax continuously in accordance with Maxwell's relaxation theory of viscosity. The steady-state strains are analyzed by the theory of superelasticity. The final equations predict pressure effects to be expected in rotating viscometers of cylindrical, plate, and conical form. In the absence of thixotropy in the test liquid, the secondary stresses are quadratic in the angular velocity. Thixotropy leads to more complicated equations and permits agreement with more complex experimental results.

INTRODUCTION

K. Weissenberg (1,2) has described a number of experiments in which viscoelastic liquids, subjected to continuous shear, developed stresses other than the shearing stress indicated by classical hydrodynamics. The liquid, sheared between concentric cylinders or between parallel rotating plates, assumed various levels and shapes at free surfaces which revealed clearly the action of abnormal stresses.

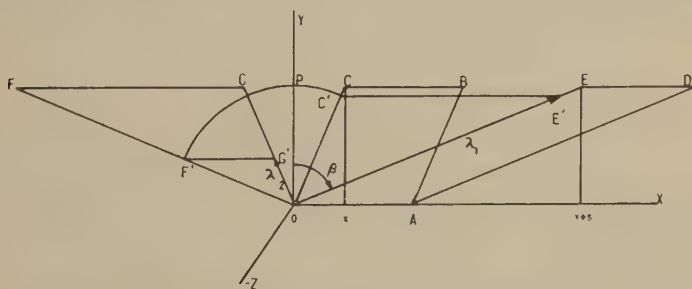
In order to understand such results and to evaluate the experimental method as a research tool, some valid, quantitative theory of the phenomenon is required. Weissenberg's theory (2), except in brief summary (1), has not so far been available to the present writer. On the other hand, recent articles by R. S. Rivlin (3,4) offer a phenomenological explanation which postulates a more general stress-strain-velocity relation than that employed in classical hydrodynamics. From the more general postulate, Rivlin shows that there are normal stresses on the shear planes, proportional to the square of the rate of shear. In another article (5) the same author presents a theory for the origin of the normal-stress coefficient. This theory is based on the configuration and orientation kinetics of the long-chain molecules of a high polymer dissolved in a liquid solvent.

While Rivlin (3) denies Weissenberg's theory (1), based on the elastic properties of a viscoelastic liquid, Rivlin's own theory (5) assumes molecular mechanisms which would be expected to produce elastic properties.

¹ Contribution No. 110 from the General Laboratories of the United States Rubber Company.

In view of this situation it seemed worth while to examine theoretically the elastic effects in viscoelastic liquids. Weissenberg's theory assumes proportionality between elastic stresses and recoverable strains. As applied to elastomers or concentrated solutions of elastomers such an assumption is probably too simple. In the present analysis we shall employ the theory of superelasticity (8) for the relationships between stresses and the state of elastic strain in the viscoelastic liquid. We thus avoid making radical *ad hoc* assumptions. What we do assume in the present theory is that, in a viscoelastic liquid subjected to continuous simple shearing deformation at a constant rate, the elastic stresses that develop are those corresponding to a constant simple shear in a superelastic body. The magnitude of this postulated elastic shear increases with the rate of the continuous shearing of the liquid. Its value is determined by a balance between the continuous increase in the elastic stress caused by the continuous deformation, and the continuous decrease in the elastic stress caused by stress relaxation. This balance point is the same as that at which the rate of strain relaxation equals the rate of the imposed continuous shear.

For later stress analyses we shall need to know the magnitudes and directions of the principal stretches² corresponding to a given simple shear. The magnitudes can be easily obtained from formulas given in standard published analyses of finite strain (9); but the directions cannot. We therefore develop here an analysis of finite simple shear which gives



² Principal stretch = 1 + principal extension.

both the magnitudes of the principal stretches and their angles with respect to the shear axes.

Referring to Fig. 1, we consider a simple X shear in the XY plane, of magnitude s . A parallelogram $OABC$ is thereby transformed into parallelogram $OADE$. The Y -dimension OP is taken as unity. Let us impose the condition that OE , the final direction of the left side of the parallelogram, is to coincide with the direction of a principal stretch. This means that, with a given s , the x -coordinate of point C must be so chosen that $\overline{OE}/\overline{OC}$ is a maximum or a minimum. That is

$$\frac{d}{dx} \left[\frac{1 + (x - s)^2}{1 + x^2} \right]^{\frac{1}{2}} = 0.$$

The solution is

$$x = \frac{1}{2} (\pm \sqrt{s^2 + 4} - s). \quad [1]$$

Taking first the $+$ and then the $-$ sign in the general relation

$$\lambda_i = \left[\frac{1 + (x + s)^2}{1 + x^2} \right]^{\frac{1}{2}}, \quad [2]$$

we find

$$\begin{cases} \lambda_1 = \frac{1}{2} [\sqrt{4 + s^2} + s], \\ \lambda_2 = \frac{1}{2} [\sqrt{4 + s^2} - s] = 1/\lambda_1, \\ \lambda_3 = 1. \end{cases} \quad [3]$$

The third of the above equations results from the fact that there is no Z -component of strain. From the first two of Eq. [3],

$$\begin{cases} \lambda_1 - \lambda_2 = s, \\ \lambda_1 + \lambda_2 = \sqrt{4 + s^2}. \end{cases} \quad [4]$$

For β , the angle between the longer principal stretch axis and the Y -axis, we have

$$\begin{aligned} \cos^2 \beta &= 1/[1 + (x + s)^2], \\ &= \frac{1}{2} \left[1 - \frac{s}{\sqrt{s^2 + 4}} \right]. \end{aligned} \quad [5]$$

STRESSES IN FINITE SIMPLE SHEAR

From the theory of superelasticity (8) we have the principal stresses expressed in the form

$$\begin{cases} \sigma_1 = -p + \frac{G}{2} (\lambda_1^2 - \lambda_2^2) + \frac{H}{6} s^2, \\ \sigma_2 = -p + \frac{G}{2} (\lambda_2^2 - \lambda_1^2) + \frac{H}{6} s^2, \\ \sigma_3 = -p - \frac{H}{3} s^2 = \sigma_z, \end{cases} \quad [6]$$

where p is the mean pressure, G is the modulus of rigidity, and H is the second superelasticity constant.

By the classical theory of stress relations at a point (9), the normal stresses on the Y - and X -planes are

$$\begin{cases} \sigma_y = \sigma_1 \cos^2 (\pi/2 - \beta) + \sigma_2 \cos^2 \beta, \\ \sigma_x = \sigma_1 \cos^2 \beta + \sigma_2 \cos^2 (\pi/2 - \beta). \end{cases} \quad [7]$$

Then from Eqs. [3] to [7]

$$\begin{cases} \sigma_x = -p + \frac{H}{6} s^2 + \frac{Gs^2}{2}, \\ \sigma_y = -p + \frac{H}{6} s^2 - \frac{Gs^2}{2}, \\ \sigma_z = -p - \frac{H}{3} s^2. \end{cases} \quad [8]$$

Again from the theory of superelasticity (8) we have the shearing stress on an X - or Y -surface,

$$\tau_{xy} = Gs. \quad [9]$$

STRAIN IN A VISCOELASTIC MATERIAL

The stress equations of the previous section apply only to elastic deformations; and hence in dealing with a continuous deformation of a viscoelastic material, we must estimate or evaluate in some way the instantaneous state of elastic deformation. In order to make this evaluation we adopt Maxwell's relaxation hypothesis. Considering a viscoelastic liquid undergoing continuous shear, we assume, firstly, that at shear rate g the elastic structure is undergoing elastic shear at the same rate g and therefore developing elastic shearing stress τ_e at the rate Gg , and secondly, that simultaneously the stress is relaxing at a rate proportional to the instantaneous stress. Thus

$$\frac{d\tau_e}{dt} = Gg - \rho\tau_e. \quad [10]$$

In the steady state $\frac{d\tau_e}{dt} = 0$, and

$$\tau_e = \frac{Gg}{\rho}. \quad [11]$$

Then the instantaneous elastic deformation is

$$s = \frac{\tau_e}{G} = \frac{g}{\rho}. \quad [12]$$

The total shearing stress is

$$\tau = \eta_0 f(\phi)g + \tau_e = \left[\eta_0 f(\phi) + \frac{G}{\rho} \right] g, \quad [13]$$

and the viscosity is

$$\eta = \eta_0 f(\phi) + \frac{G}{\rho}. \quad [14]$$

Here η_0 is the viscosity of the solvent, the purely viscous component of the liquid, and $f(\phi)$ is the relative viscosity which a solution of concentration ϕ would have if the elastic component could suddenly cease resisting the deformations of which it is capable. The viscosity relationships, it may be noted, imply Newtonian behavior of the viscoelastic solution.

THEORY OF SECONDARY STRESS MEASUREMENT

We consider first a rotating cylinder viscometer operating on a viscoelastic liquid. Assume that the outer cylinder, of radius b , is fixed and that the inner cylinder, of radius a , is rotating at angular velocity Ω under a torque C . Let the submerged length of the cylinders be L . With cylindrical coordinates r, θ, z , the stress Eqs. [8] and [9] take the forms

$$\begin{cases} \sigma_r = -p - \left(\frac{G}{2} - \frac{H}{6}\right) s^2, \\ \sigma_\theta = -p + \left(\frac{G}{2} - \frac{H}{6}\right) s^2, \\ \sigma_z = -p + \frac{H}{3} s^2. \end{cases} \quad [15]$$

and

$$\tau_{r\theta} = -Gs. \quad [16]$$

The appropriate equation of equilibrium is (9)

$$\frac{1}{r} \frac{d}{dr} (r\sigma_r) - \frac{\sigma_\theta}{r} = Df_r, \quad [17]$$

where D is the density and f_r is the r -acceleration. If ω is the local angular velocity of the liquid

$$f_r = -r\omega^2. \quad [18]$$

If we now eliminate σ_θ and f_r from Eqs. [13], [17], and [18] we obtain

$$\frac{d\sigma_r}{dr} - \frac{Gs^2}{r} = -D\omega^2 r. \quad [19]$$

The local rate of shear is

$$g = r \frac{d\omega}{dr} = -\frac{C}{2\pi L \eta r^2}, \quad [20]$$

and hence, by [12]

$$s = -\frac{C}{2\pi L \eta r^2 \rho}. \quad [21]$$

Integration of [20] yields

$$\omega = \frac{C}{4\pi L\eta} \left(\frac{1}{r^2} - \frac{1}{b^2} \right). \quad [22]$$

We note here incidentally that the angular velocity of the inner cylinder is

$$\Omega = \frac{C}{4\pi L\eta} \left(\frac{1}{a^2} - \frac{1}{b^2} \right). \quad [23]$$

By eliminating s and ω from [19], [21], and [22] we obtain

$$\frac{d\sigma_r}{dr} = \frac{C^2}{4\pi^2 L^2 \eta^2} \left[\frac{G}{\rho^2 r^5} - \frac{rD}{4} \left(\frac{1}{r^2} - \frac{1}{b^2} \right)^2 \right]. \quad [24]$$

The solution satisfying the appropriate boundary condition is

$$\sigma_r(b) - \sigma_r(a) = \Omega^2 \left[\left(\frac{G}{\rho^2} - \frac{Da^2}{2} \right) \frac{b^2 + a^2}{b^2 - a^2} + \frac{2Da^4 b^2}{(b^2 - a^2)^2} \ln \frac{b}{a} \right]. \quad [25]$$

Some simplification of this equation is obviously possible if a/b is small or if $1 - a/b$ is so small as to be negligible.

Equation [25] predicts the difference in pressure to be observed in two manometers connecting with two small holes in the sides of the two cylinders, provided that the manometer connected to the inner cylinder rises straight up so that the meniscus is at the radial distance a from the axis of rotation. If this manometer extends inward so that the meniscus lies on the axis, we may then ignore the terms in D in Eq. [25].

From the first and third Eqs. [15], and Eqs. [21] and [23] it is possible to obtain the equation

$$\sigma_r(r) - \sigma_z(r) = - \left(G + \frac{H}{3} \right) \frac{2\Omega^2 a^4 b^4}{\rho^2 (b^2 - a^2)^2 r^4}. \quad [26]$$

This equation predicts a difference in the r - and z -pressures which varies inversely as r^4 . In particular, if $r = b$, it predicts a pressure difference which will be indicated by the level in the b -manometer in comparison with the liquid level in the viscometer at the outer cylinder.

The liquid level at the inner cylinder will be higher than that at the outer cylinder; but the theoretical expression for this difference would not be valid, due to the disturbing effects of radial flow and spattering.

If the viscometer is operated with a rotating outer cylinder and a stationary inner cylinder, instead of vice versa, the changes in the above equations, beginning with [22], are easily made. Equation [26] remains unaltered; in Eq. [25] a and b are interchanged.

ROTATING PLATE

The second experimental device we shall analyze is that of a pair of parallel, coaxial circular plates immersed in a viscoelastic liquid, the

upper plate being rotated about their common axis. Again we use cylindrical coordinates, but Eqs. [15] and [16] no longer apply, since the axes of shear are now in the θz surfaces instead of the $r\theta$ surfaces. Referring back to Eqs. [8] and [9], we write for the present case,

$$\begin{cases} \sigma_r = -p - \frac{H}{3}s^2, \\ \sigma_\theta = -p + \left(\frac{G}{2} + \frac{H}{6}\right)s^2, \\ \sigma_z = -p - \left(\frac{G}{2} - \frac{H}{6}\right)s^2. \end{cases} \quad [27]$$

$$\tau_{\theta z} = -Gs. \quad [28]$$

Equations [17] and [18] still apply, although ω now is not a function of r , but is a function of z of the form

$$\omega = \frac{z\Omega}{Z}, \quad [29]$$

where Ω is the angular velocity of the rotated plate, and Z is its distance from the stationary plate. The corresponding difference in centrifugal force at different levels will cause some radial flow to be superimposed on the circular flow; but we shall ignore the radial flow and treat the flow as purely circular.

Then from Eqs. [17] and [18] and the first two of Eqs. [27] we find

$$\frac{d\sigma_r}{dr} = \frac{(G+H)s^2}{2r} - D\omega^2 r. \quad [30]$$

The local rate of shear is

$$g = r \frac{\Omega}{Z}, \quad [31]$$

and hence, by [12]

$$s = \frac{r\Omega}{\rho Z}. \quad [32]$$

Substituting for s in Eq. [30] and integrating, we obtain

$$\sigma_r(r) = \sigma_r(b) - \left[\frac{(G+H)\Omega^2}{4\rho^2 Z^2} - \frac{D\omega^2}{2} \right] (b^2 - r^2), \quad [33]$$

where b is the outer radius of the circular plates. Let us suppose there is a central hole of radius a in one or both plates. The mean pressure on the cylindrical surface, within the liquid, of radius a and height Z involves the mean value of ω^2 ,

$$\bar{\omega^2} = \frac{1}{Z} \int_0^Z \omega^2 dz = \Omega^2/2. \quad [34]$$

Then, from [34],

$$\bar{\sigma}_r(a) = \bar{\sigma}_r(b) - \left[\frac{G + H}{4\rho^2 Z^2} - \frac{D}{6} \right] \Omega^2(b^2 - a^2). \quad [35]$$

This equation indicates the liquid level to be expected in a manometer attached at a central hole of radius a .

If a manometer is connected to a small hole at radius r in the stationary plate, where $\omega = 0$, the appropriate stress equation can be obtained by use of Eqs. [27.1], [27.3], [32], and [33]. The solution is

$$\sigma_z(r) = \sigma_r(b) - \left[\frac{G + H}{4} (b^2 - r^2) + \frac{G - H}{2} r^2 \right] \frac{\Omega^2}{\rho^2 Z^2}. \quad [36]$$

Since the radial flow has been ignored, the equations in this section are approximations which require, for their validity, that

$$D \ll \frac{G + H}{\rho^2 Z^2}. \quad [37]$$

EFFECTS OF THIXOTROPY AND NON-NEWTONIAN VISCOSITY

Solutions of the viscoelastic type are generally more or less non-Newtonian and thixotropic, not Newtonian as was assumed above. If we wish to take into account these departures from the laws of a simple liquid, we are faced with the difficulty that the laws of thixotropy and non-Newtonian viscosity are not known in detail. We are forced to assume a rather crude, empirical law.

Let us assume that in the right member of the viscosity Eq. [14] the factors η_0 , $f(\phi)$, and ρ are independent of rate of shear; while G , the modulus, is reduced by thixotropic breakdown at high rates of shear and follows a law of the form,

$$G = \frac{G_0}{1 + k|g|}, \quad [38]$$

where G_0 and k are constants. We assume likewise that

$$H = \frac{H_0}{1 + k|g|}. \quad [39]$$

Corresponding to Eq. [14] we would then have

$$\eta = \eta_0 f(\phi) + \frac{G_0}{(1 + k|g|)}. \quad [40]$$

This form of equation represents to a fair approximation the viscosity of concentrated high polymer solutions as a function of rate of shear.

Substitution from [40] in [20] leads to a differential equation for ω which is difficult. A formal solution is possible in either of two forms, as a

power series in k , or in $1/k$; but no such solution has been worked out as yet.

If the clearance between cylinders in the cylindrical viscometer is small compared with the radius, an approximate solution can be obtained without any integration. Thus, if the difference $\sigma_r - \sigma_z$ is obtained from Eqs. [15.1] and [15.3], and if G and H from Eqs. [38] and [39] and s from [12] are substituted, we obtain

$$\sigma_r - \sigma_z = - \left(\frac{G_0}{2} + \frac{H_0}{6} \right) \frac{g^2}{\rho^2(1 + k|g|)}. \quad [41]$$

The rate of shear is approximately

$$g = \frac{\Omega(b + a)}{2(b - a)}. \quad [42]$$

Hence

$$\sigma_r - \sigma_z = - \left(\frac{G_0}{2} + \frac{H_0}{6} \right) \frac{h^2 \Omega^2}{\rho^2(1 + kh\Omega)}, \quad [43]$$

where $h = \frac{1}{2} \times \frac{b + a}{b - a}$. This equation predicts the pressure indicated by a manometer attached to the side of a cylindrical viscometer with small cylinder clearance.

Turning our attention now to the circular plate apparatus, we substitute from [38] and [39] in [30] and find a differential equation for σ_r which can be solved in closed form. The result for the average pressure is

$$\bar{\sigma}_r(a) - \bar{\sigma}_r(b) = \frac{(G_0 + H_0)\Omega}{2\rho^2 kZ} \left\{ (a - b) - \frac{Z}{k\Omega} \ln \left[\frac{1 + k\Omega a/Z}{1 + k\Omega b/Z} \right] \right\} - \frac{D\Omega^2}{9} (a^2 - b^2). \quad [44]$$

This equation predicts the difference in radial pressure between the inner and the outer edges of annular plates of inner and outer radii a and b .

The corresponding equation for σ_z at the bottom plate is

$$\sigma_z(r) = \sigma_z(b) + \frac{(G_0 + H_0)}{2\rho^2 kZ} \left\{ (r - b) - \frac{Z}{k\Omega} \left[\ln \frac{1 + k\Omega r/Z}{1 + k\Omega b/Z} \right] \right\} + \frac{(G_0 - H_0)\Omega^2}{2\rho^2 Z^2} \left\{ \frac{b^2}{1 + k\Omega b/Z} - \frac{r^2}{1 + k\Omega r/Z} \right\}. \quad [45]$$

This equation predicts the variation in normal pressure on the stationary plate. At small values of $K\Omega b/Z$, this equation approaches Eq. [36]. At large values of $k\Omega r/Z$, Eq. [45] is approximately linear in r , provided that $H_0 \neq 0$.

ROTATING CONE AND PLATE

Suppose that a cone is rotated at angular velocity Ω , with its axis normal to a stationary plate and its apex in the plane of the plate. Let α

be the angle between a generator, or radial line, of the cone and the projection of the generator in the plate. Then if α is small, the rate of shear in a viscoelastic liquid between cone and plate is nearly uniform and has the value Ω/α .

Following the previous method of analysis, we obtain for the pressure in a manometer connecting to a central hole of radius a ,

$$\bar{\sigma}_r(a) = \bar{\sigma}_r(b) - \frac{(G_0 + H_0)\Omega^2}{2\rho^2\alpha^2(1 + k\Omega/\alpha\rho)} \ln \frac{b}{a} + \frac{D\Omega^2}{6} (b^2 - a^2). \quad [46]$$

Neglecting inertial effects we find for the normal stress on the plate

$$\sigma_z(r) = \sigma_r(b) - \frac{\Omega^2}{2\rho^2\alpha^2(1 + k\Omega/\alpha\rho)} \left[(G_0 + H_0) \ln \frac{b}{r} + (G_0 - H_0) \right]. \quad [47]$$

COMPARISON WITH EXPERIMENT

In the above analysis of secondary stress in the absence of thixotropy, the stress is found to be a homogeneous quadratic function of the angular velocity Ω . It is an even function of the radius, r , wherever r enters as a variable.

When thixotropic effects are admitted, the solution becomes much more complicated; and a great variety of theoretical curves can be derived, depending on the value assumed for k . However, the value assumed for k must also give a good fit of Eq. [40] to viscosity measurements over the appropriate range of rates of shear.

Published quantitative data on secondary viscous stress are apparently nonexistent. In Weissenberg's (10) paper presented at the 1948 International Congress on Rheology, a photograph, 12*d*, is shown of the rotating plate arrangement. This photograph indicates the z -pressure to be approximately a linear function of the radius. This requires that, in Eq. [45],

$$\begin{cases} \frac{kb}{Z} \gg 1, \\ H_0 \neq 0. \end{cases}$$

In a private communication Dr. T. W. DeWitt has reported some secondary stress measurements with solutions of Vistanex in Tetralin in a cylindrical apparatus. According to these data the secondary z -stress is approximately of the form

$$\sigma_z(r) = C\eta'\Omega(r - b),$$

where η^1 is the limiting viscosity of the solution at zero rate of shear and C is a constant. All the requirements of this empirical equation are

satisfied by the theoretical Eq. [45] provided that

$$\begin{cases} \frac{k\Omega b}{Z} \gg 1, \\ H_0 = G_0, \\ \eta_0 f(\phi) \ll \frac{G_0}{\rho}. \end{cases}$$

The last inequality here is required, according to Eq. [40], in order that G_0 shall be approximately proportional to η' , or to $\eta_0 f(\phi) + G_0/\rho$.

While we thus show that Eq. [45] can fit DeWitt's secondary stress data, we cannot proceed further and evaluate the various parameters. To do so would require data on the viscosity as a function of rate of shear which have not yet been supplied.

DISCUSSION

There are four parameters occurring in the preceding equations: G_0 , H_0 , ρ , and k ; or three parameters: G , H , and ρ , if $k = 0$. In the first case, $k \neq 0$, viscosity measurements over a wide range of shearing rate will determine k and the ratio G_0/ρ . The secondary stress measurements will theoretically determine G_0/ρ^2 and H_0/ρ^2 , if the theory is valid. In the second case, $k = 0$, the determination of G/ρ depends upon a known or assumed value of the hypothetical relative viscosity $f(\phi)$. Considering the peculiar definition of this relative viscosity, its value will presumably be uncertain, at best.

According to the kinetic theory of superelasticity we should expect to find that $H/G = 1$, or $H_0/G_0 = 1$. Experimental determination of the exact ratio of these elastic constants may be quite difficult, as it has proved to be so far in cured gum elastomers.

When this theoretical investigation was undertaken it was expected that, by comparing the final equations in our theory with those obtained by Rivlin (3), a relationship would be obtained between his normal-stress coefficient and our constants of viscoelasticity. However, this does not turn out to be the case. The reason becomes evident when we examine closely the initial, postulated equations in the two theories.

From our Eq. [8] we can write

$$\begin{cases} \sigma_x = \sigma_z + \frac{s^2}{2}(G + H), \\ \sigma_y = \sigma_z - \frac{s^2}{2}(G - H). \end{cases} \quad [48]$$

From Rivlin's Eqs. (14.3) we can write, in our notation

$$\sigma_x = \sigma_y = \sigma_z + \frac{s^2}{2}\psi, \quad [49]$$

where ψ is Rivlin's normal-stress coefficient. Obviously these two sets of equations can agree only if $G = 0$. We conclude that Rivlin's postulates rule out elastic rigidity as a source of secondary stress in viscous flow. Hence, there can be no correspondence between Rivlin's normal-stress coefficient and any parameter or combination of parameters in our own theory, which is based on the assumed elasticity of the test liquid.

In one (5) of Rivlin's papers thixotropy is discussed as a possible disturbing factor, but no effort is made to analyze thixotropic effects. Here again, therefore, there is no basis for comparison of the two theories.

REFERENCES

1. WEISSENBERG, K., *Nature* **159**, 310 (1947); also Proceedings of the International Rheological Congress, Holland, 1948. North Holland Publishing Co., Amsterdam, 1949.
2. WEISSENBERG, K., Conference of the British Rheologists' Club, 1946.
3. RIVLIN, R. S., *Proc. Roy. Soc. (London)* **A193**, 260 (1938).
4. RIVLIN, R. S., *Proc. Roy. Soc. (London)* **A200**, 168 (1950).
5. RIVLIN, R. S., *Trans. Faraday Soc.*, **45**, 739 (1949).
6. FERRY, J. D., *Rev. Sci. Instruments* **12**, 79 (1941).
7. MASON, W. P., BAKER, W. O., McSKIMIN, H. J., AND HEISS, J. H., *Phys. Rev.* **75**, 936 (1949).
8. MOONEY, M., *J. Applied Phys.* **11**, 582 (1940).
9. LOVE, A. E. H. *Theory of Elasticity*. Dover Publications, New York, 1944.
10. WEISSENBERG, K., Proceedings of the International Rheological Congress, Holland, 1948. North Holland Publishing Co., Amsterdam, 1949.

SINTERING OF SYNTHETIC LATEX PARTICLES ¹

R. E. Dillon, L. A. Matheson and E. B. Bradford

Dow Chemical Company, Midland, Michigan

Received November 13, 1950

INTRODUCTION

Recent developments in the use of synthetic latices in the paint, paper, and textile industries (1,2) have focused attention upon the mechanism by which polymer particles, at comparatively low temperatures, are welded together into a coherent film. These industries are using synthetic latices containing approximately 50% solids dispersed in water; the average particle size is about 0.2μ in diameter. Some of the materials are film forming at room temperature, others must be formulated and dried at elevated temperatures. The film is formed by coating with the latex, usually containing some form of thickener; as the water evaporates, the colloidal polymer particles are deposited upon the surface where they fuse into a film. It is this mechanism whereby the individual particles are united in the film that we will discuss.

The field of powder metallurgy has long been concerned with a fabrication process which has certain elements in common with the formation of a film from colloidal polymer particles. This is the sintering of powdered materials, which Kuczyński (5) has described as follows: "This phenomenon of bonding of two or more particles with the application of heat only and at temperatures below the melting point of any component of the system will be called sintering, although the powder metallurgists use this term in a broader sense, including the presence of a molten phase and of pressure." The analogy is not completely parallel as the metal particles are considerably larger than the polymer particles; also, much higher temperatures are necessary in metal sintering. The sintered metal product is more porous than latex-formed films.

EXPERIMENTAL METHODS

Kuczyński (6) has made a study of the sintering of glass by observing the welding of glass spheres (0.05 cm. in diameter) to glass blocks. Using conventional optical methods, he made measurements of the neck formed between the spheres and the plate as related to time and the size of

¹ Presented at the Annual Meeting of the Society of Rheology, New York, N. Y., November 3-4, 1950.

particles. The size of the latex particles prevents using the same technique; however, other methods are available. For any given particle, the wider the neck, the less the height of the particle. The height and diameter of the particles were obtained by observing shadowed (8) specimens with an electron microscope. The specimens were prepared by diluting the 50% solids latex to a concentration of approximately 20 p.p.m. in water, which usually gave a dispersion such that individual particles were observable. The diameters and shadow lengths were then measured on the electron microscope plates with the aid of a 10-power measuring magnifier. With this technique the particles were sintered to a plane collodion film, rather than to the same material as was done in the case of the glass spheres.

When considering the forces producing a film, the relationship of the forces between the particles involved is much more obscure than the behavior of isolated particles. A qualitative relationship was obtained by observing thin films which were shadowed with metal. Much more detail in the film was observable with the electron microscope in the case of

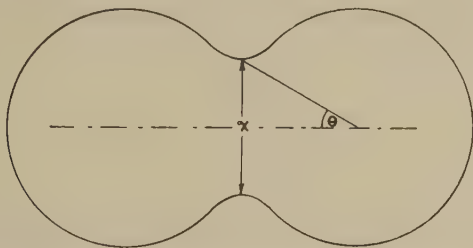


FIG. 1. Schematic representation of the cross section of sintered spherical particles.

shadowed films. This method may be simplified by observing an isolated pair of particles which are in contact with each other. In this case a neck is formed between the two particles which can be measured at the same time the radius is measured.

Figure 1 is a schematic representation of two sintered particles, showing the notation which we used. The radius of the latex particles is indicated by (r). Shaler (7) used a similar method to follow the coalescence of copper spheres.

Considerable trial and error work was necessary to adjust the concentration of the latex to produce a suitable dispersion for electron microscope samples. The finding of isolated pairs of particles of the same size was a tedious task.

Forces Between Latex Particles in Drying

Kuczyński (6) has pointed out that several mechanisms of sintering are possible: (a) viscous flow, (b) evaporation-condensation, (c) volume

diffusion, and (d) surface diffusion. The most obvious of these mechanisms to apply to the sintering of synthetic latex particles is that of viscous flow. In order for viscous flow to take place between the particles, a shearing stress is necessary. When a film is produced from a latex, no external stress is applied and thus some mechanism within must be responsible for the necessary shearing stress. If one considers the change in surface area that takes place when latex particles are united in a film, it is apparent that here is a large source of energy which may well produce shearing stresses of such magnitude that viscous flow will result.

Surface tension γ is a measure of the force on a surface tending to minimize that surface. γ is approximately 70 dynes/cm. for water and approaches 25–30 for relatively nonpolar materials; e.g., most organic liquids and plastics or water containing surface-active agents.

The excess pressure, P , due to surface tension inside a spherical surface of radius, r , over that outside the surface may be calculated. The surface tension γ operating over the circumference $2\pi r$ tends to pull the two halves together with a force $2\pi r\gamma$. In the case of a bubble in a liquid this force causes a higher pressure within the bubble than outside. This differential pressure, P , operating over the area of circle of radius, r , results in a force of $\pi r^2 P$ pushing the two halves apart. Equating,

$$\pi r^2 P = 2\pi r\gamma \quad [1]$$

or

$$P = \frac{2\gamma}{r}, \quad [2]$$

where r is the spherical radius of curvature. This may be expressed in the more general form

$$P = \gamma C, \quad [3]$$

where

$$C = \frac{1}{r_1} + \frac{1}{r_2} \quad [4]$$

and r_1 and r_2 are the principal curvatures of the surface.

In the case of latices with particle diameters 300–600 Å., the approximate size of the largest hole to be expected between the particles is about 50 Å. radius during the drying operation. For a surface tension of 25 dynes/cm., as in a typical latex, the resulting pressure is 100 atm., or 1500 lb./in.².

A hole in an organic liquid or plastic of the above 50 Å. radius would be in equilibrium with a gas pressure of 1500 lb./in.² within it. However, these holes can maintain no such pressure. They were formed at atmospheric pressure, and plastics have a finite permeability for air and water vapor so that in general over a period of time the internal pressure in such a hole is only a little above atmospheric.

With no internal pressure in the hole, surface tension exerts a tensile force on the surrounding solid of the same magnitude. This force is a radial tensile force on the surface but becomes a combination of radial tensile and circumferential compression at a distance from the surface. The actual forces distant from the surfaces depend on the mechanical properties of the medium; e.g., the various moduli and the viscosity.

Frenkel (4) has developed the following relationship for the coalescence of spheres by purely viscous flow:

$$\theta^2 = \frac{3\gamma t}{2\pi\eta r}, \quad [5]$$

where θ is the angle shown in Fig. 1, γ is the surface tension, η is the viscosity coefficient, and r is the sphere radius. For any given field viewed in an electron micrograph, r and θ are the only variables, so that a plot of θ^2 , measured in radians, against $1/r$ should lie on a straight line passing through the origin. Figure 2 shows this relationship for a latex containing

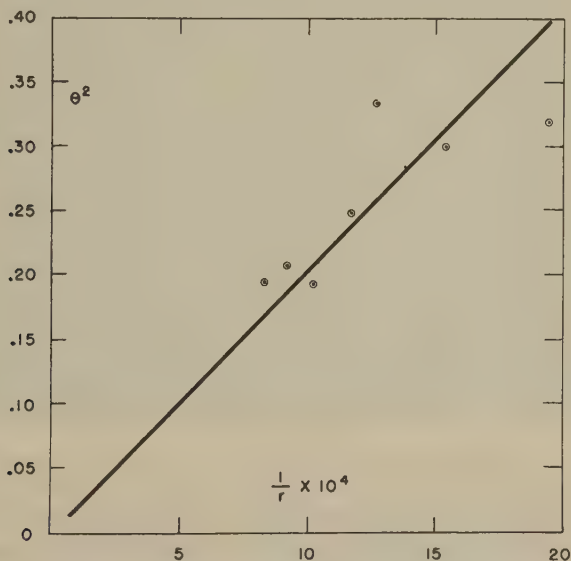


FIG. 2. Effect of particle size upon the angle of contact (θ) of sintered Saran latex particles.

75% polyvinyl chloride and 25% polyvinylidene chloride.² The points shown are individual measurements rather than averages, so some experimental scatter of the points is to be expected. Figure 3 is the same type of plot for a polystyrene latex; here the points are averages of a number of measurements, and so a better fit is obtained.

² Saran.

Experimental difficulty was experienced with the above method in obtaining pairs of particles by a trial and error method. A good dispersion of individual particles was easily obtained and then shadowed, as shown in Fig. 4. The data obtained in this fashion, shadow length and diameter, can be fitted to Eq. [3] by following Frenkel's (4) analysis of the coalescence of two spheres. He has shown that when two spheres coalesce, the decrease in distance between the center of each sphere and the surface of its contact with the other sphere is $r(1 - \cos \theta) \approx \frac{1}{2}r\theta^2$. This will also apply to the sintering of a particle to a plane film, as in the case of particles

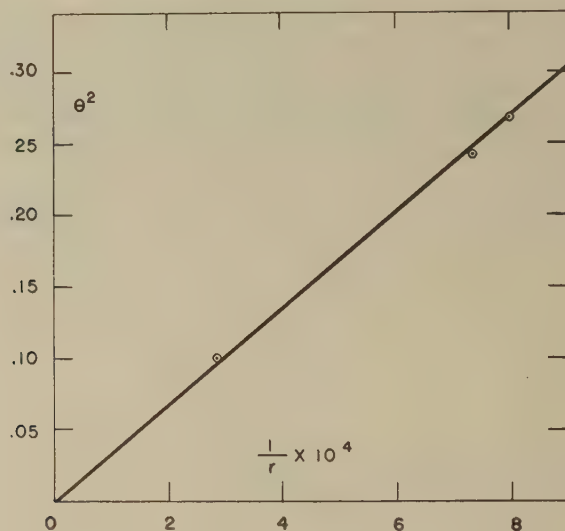


FIG. 3. Effect of particle size upon the angle of contact (θ) of sintered polystyrene latex particles.

deposited upon a film in the preparation of electron microscope samples. The height of the particle is equal to the diameter minus the decrease of the distance between the center of a sphere and the surface of its contact with the other sphere, or film. Thus,

$$H = 2r - \frac{1}{2}r\theta^2 \quad [6]$$

substituting Eq. [5],

$$H = 2r - \frac{3\gamma t}{4\pi\eta} \quad [7]$$

or

$$\frac{H}{2r} = 1 - \frac{3\gamma t}{8\pi\eta r} \quad [8]$$

In any given sample prepared for the microscope, $3\gamma t/8\pi\eta$ is constant; thus we may write

$$\frac{H}{2r} = 1 - K \frac{1}{r}. \quad [9]$$

From Eq. [7] the ratio of the height to diameter plotted against the reciprocal of the radius is a straight line with an intercept of 1 and a negative slope. The data of Fig. 2 were recalculated and plotted in this manner and are shown in Fig. 5. Here, again, it must be remembered that the points were measurements of individual pairs rather than averaged values.

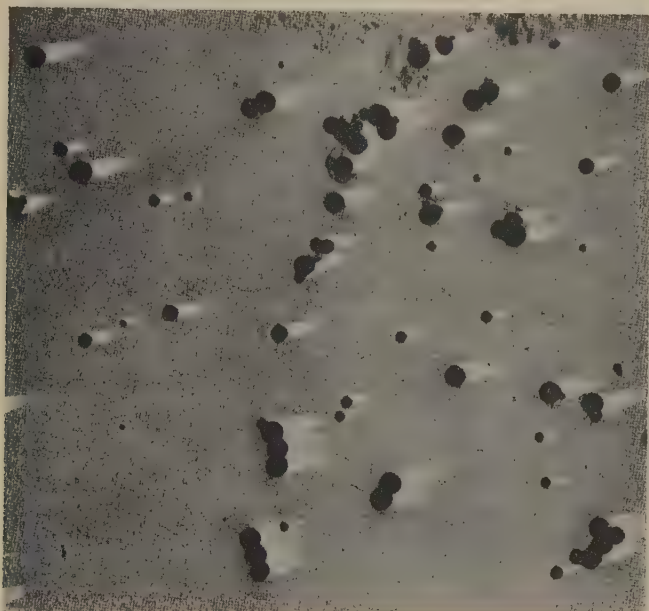


FIG. 4. Electron micrograph of shadowed Saran latex particles ($\times 23,000$).

The data obtained from electron micrographs such as Fig. 4 can now be plotted as the ratio of height, or shadow length, to the diameter versus the reciprocal of the radius. Figure 6 is this type of plot of data obtained from Fig. 4 for which the shadow length was used rather than height inasmuch as the exact shadow angle is difficult to determine from the method of preparation.

The above relationships fit individual particles or pairs of particles, but the real interest is in the way in which particles behave during the formation of a film. The relationship between the particles which enter into a film is much more complicated, and at present only a qualitative interpretation of these results is possible.

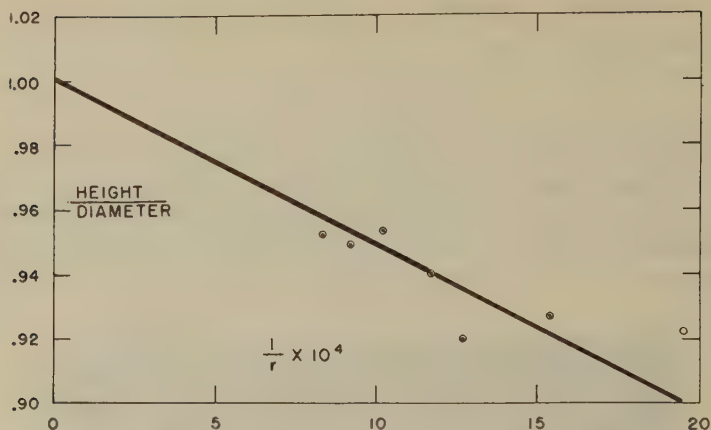


FIG. 5. Effect of particle size upon the flattening of sintered Saran latex particles.

During the drying process the concentration of solids increases until they are in contact with each other, and then the water evaporates from between the particles. The small voids then exert a shearing stress on the surrounding polymer, as shown in Eq. [2], which increases as the size of the void decreases.

A shadowed electron micrograph of a continuous film is shown in Fig. 7. This material formed a film at room temperature without the addition of any formulation materials. The film was thin enough so that a suitable microscope sample was obtained, which was then shadowed. The main body of the film was made up of many small particles which had been deformed so that they had almost lost their identity. The larger particles

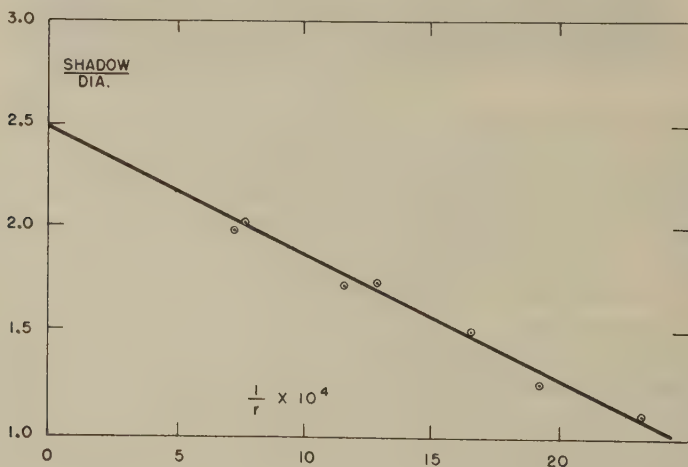


FIG. 6. Flattening of Saran latex particles as determined from shadowed specimens.

were changed in shape only a small amount and appeared to enter into the film only to a small extent. Some of the large particles were embedded in the film as noted by the absence of any shadows from these particles. Others were on the surface of the film and cast a shadow.

The latex used in making this film was more dilute than the commercial latex, and during the drying process not all of the particles were deposited together. A few particles were left in isolated positions. The range in particle size was from 185 A. to 1150 A. in diameter.

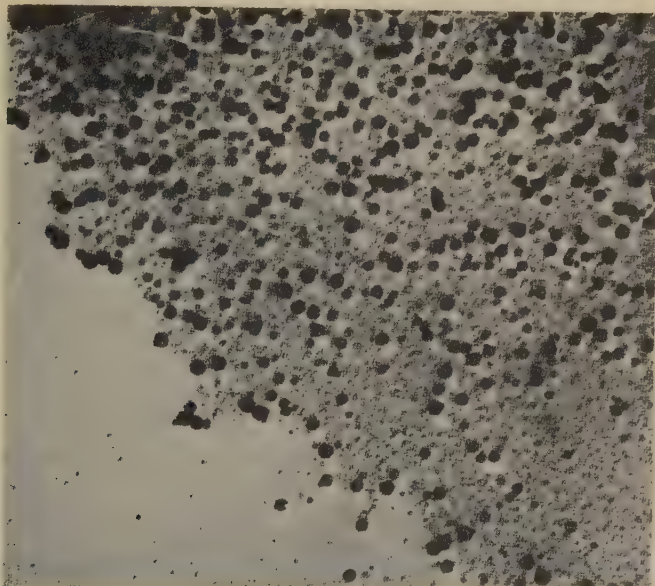


Fig. 7. Shadowed electron micrograph of Saran latex film ($\times 29,200$).

The angle θ is a valuable measure of the action of the latex particles and relates to the physical properties of the film. As θ increases, the voids in the film become smaller; this results in increased tensile strength. From Eq. [5], we can see that a decrease in either r or η will increase θ . For practical purposes in commercial use, the time variation permissible is limited. In any latex, r is fixed and varies only with the distribution of particle size in the latex. η can be changed in the formulation of the latex by the addition of plasticizers or by the application of heat.

The addition of plasticizer and the resulting decrease in viscosity and increase in θ produce a film which is more completely fused in the given length of time. Increased tensile strength of the film is an indication of better fusion of the particles. An increase in the plasticizer content increased the tensile strength of the material to some maximum value and

then fell off as a greater amount of plasticizer was added. Figure 8 shows the relationship between the tensile strength and the amount of plasticizer (3). Since the small particles have a large value of θ without the use of plasticizer, the plasticizer will produce the greatest effect on the large particles.

A further increase in θ may be obtained through decreasing the viscosity by increasing the temperature. The tensile strength of the material of Fig. 8 was increased by short heating periods in those cases in which the plasticizer content was below 15%. This is an even more significant fact when it is considered that some of the plasticizer diffuses out during the heating period, which in this plasticizer concentration range would be

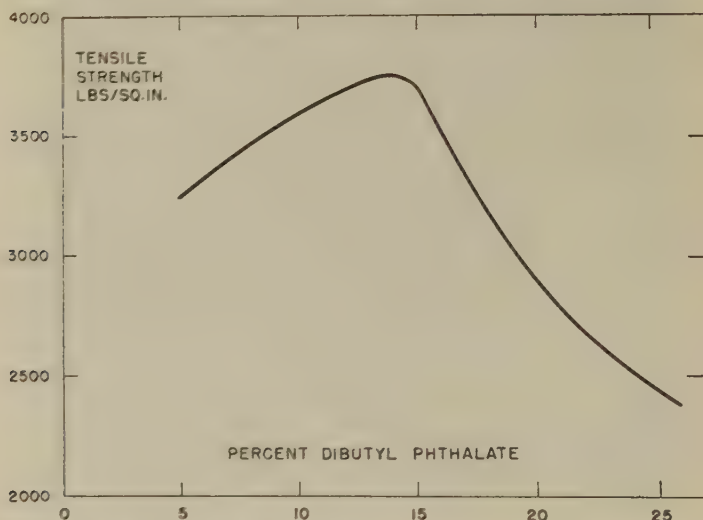


Fig. 8. The effect of dibutyl phthalate plasticizer on the tensile strength of Saran F122 latex films.

expected to reduce the tensile strength. Above 15% plasticizer, the increased fusion and loss of plasticizer both work in the same direction and their effects are not easily separated.

SUMMARY

The sintering of synthetic latex particles takes place by the viscous flow of the polymer, the surface tension of the plastic furnishing the necessary shearing stress. The flow of the polymer under the influence of surface tension follows Frenkel's equation

$$\theta^2 = \frac{3\gamma t}{2\pi\eta r}. \quad [5]$$

The particle size distribution in the latex provided a method of experimentally observing the relationship between θ and r . η was varied by changing the temperature and by addition of plasticizer. The tensile strength of the material under these conditions was used as an indication of the voids in the material, or θ . Over a limited plasticizer range, the tensile strength increased with increasing plasticizer concentration. The conclusions drawn from observations of the sintering of pairs of particles and individual particles were shown to apply in a qualitative manner to the formation of films.

REFERENCES

1. DOW CHEMICAL Co., Coatings Technical Service Bulletin, Dow Latexes 512-K, 512-O and 529-K.
2. DOW CHEMICAL Co., Coatings Technical Service Bulletin, Dow Latex 744.
3. DOW CHEMICAL Co., Dow Coating Materials Technical Data, Saran F122 Latex.
4. FRENKEL, J., *J. Phys.* (U. S. S. R.) **9**, 385 (1943).
5. KUCZYŃSKI, G. C., *J. Inst. Metals* **75**, 169 (1949).
6. KUCZYŃSKI, G. C., *J. Applied Phys.* **20**, 1160 (1949).
7. SHALER, A. J., *Trans. Am. Soc. Metals* **185**, 796 (1949).
8. WILLIAMS, R. C., AND WYCKOFF, R. W. G., *J. Applied Phys.* **17**, 23 (1946).

SOME FLOW PHENOMENA IN THE INJECTION MOLDING OF POLYSTYRENE¹

R. S. Spencer and G. D. Gilmore

Dow Chemical Company, Midland, Michigan

Received November 13, 1950

ABSTRACT

The steps in an injection molding cycle comprise dead time, filling, packing, discharge sealing, sealed cooling, and mold open time. Those steps involving polymer flow are discussed in this paper.

The filling time is directly proportional to the polymer melt viscosity, and inversely proportional to a power of the ram pressure. Raising the mold wall temperature lowers the filling time. Reducing friction between the solid polymer and metal lowers the filling time, but only if the cylinder ahead of the heating chamber is cool.

Studies with a glass-window mold show that hot polymer flows only in a central region, there being stationary layers next to the mold walls. When flowing polymer reaches the advancing front it contacts the mold wall, cools, and ceases flowing. In a typical case the thickness of the central region was 40% of the total thickness.

An approximate equation is presented for calculating maximum pressure in the mold during packing. Agreement with experimental values is good. Approximate treatment of sealing by "freezing" in the gate leads to a linear relationship between temperature and pressure in the mold at the sealing point.

INTRODUCTION

Injection molding is one of the major methods by which thermoplastics are fabricated. Despite its technological importance, little basic work has been done to elucidate the varied phenomena encountered in injection molding. This may be attributed, in part, to the complexity of many of the problems with which one is faced. Consider for a moment the difficulties inherent in attempting a rigorous solution of the problem of a hot, non-Newtonian, compressible liquid flowing through a geometrically complex channel, the walls of which are much colder than the liquid. Little wonder that, in the past, injection molding has been left to develop as an empirical art, for the most part. It has been our feeling, however, that the situation is far from hopeless. Granted that exact solutions of many (or even most) injection molding problems are impractical, yet, much insight into the process may be gained by the use of crude approximations and idealizations which result in only semiquantitative agreement with experience.

¹ Presented at the Annual Meeting of the Society of Rheology, New York, N. Y., November 3-4, 1950.

Such an approach may be used to sketch in the broad forms of relationships to be expected, and the details to be filled in by suitable experiments.

The present paper considers, in this manner, some phenomena having to do with flow during injection molding. A certain amount of preliminary discussion will be necessary. A few basic facts about injection molding, and the sequence of events which takes place therein, will be presented. The general flow behavior of polystyrene will be discussed briefly. This will be followed by a more detailed account of the filling of a mold, the pattern of flow, and the dependence of fill time on temperature, pressure, and polymer viscosity. Finally, some attention will be given to packing, that slow flow of polymer into the mold when pressure is maintained subsequent to filling.

INJECTION MOLDING FUNDAMENTALS

An injection molding machine might be thought of as consisting of six component parts; (a) a feeding mechanism for metering out a constant amount of polymer for each cycle, (b) a plunger, or ram, to move the polymer through the machine and to apply pressure, (c) a tunnel section for heating the polymer uniformly to a temperature at which it flows readily, (d) a precision-built mold, in two or more sections so that it may be opened and the article removed, (e) a clamping mechanism to keep the sections of the mold together, and (f) a system of timers for controlling the sequence of operations in the molding cycle. Figure 1 illustrates schematically the assembly of these components. In operation, the mold is closed and the set amount of polymer introduced ahead of the plunger. The plunger moves forward and forces the polymer into the heating zone, at the same time forcing already heated polymer out of the tunnel and into

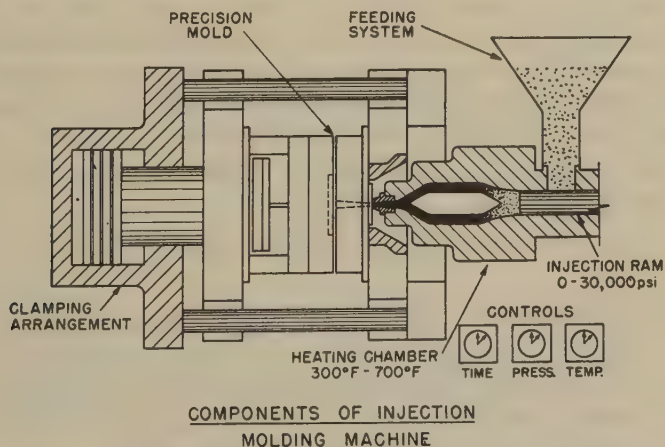


FIG. 1. Schematic drawing of an injection molding machine, comprising: (a) feeder, (b) plunger, (c) tunnel, (d) mold, (e) clamping device, and (f) controls.

the mold. Pressure is maintained on the plunger for some time after the mold has been filled to permit build-up of adequate pressure in the mold. Cooling water is circulated through channels in the mold so as to keep the mold cavity walls at a temperature which is usually between room temperature and the softening temperature of the polymer. Thus, the hot polymer begins to cool as soon as it enters the mold. When it has cooled to a state of sufficient rigidity the mold is opened and the piece is removed. After a short time during which the mold remains open the cycle is repeated.

Six major controls are available to the operator of a molding press: (a) the pressure applied by the plunger, (b) the temperature of the heating section, (c) the temperature of the mold, (d) the plunger forward time, (e) the mold closed time, and (f) the mold open time. Other usually less important controls are available on specific molding presses. Adjustment of these controls and the choice of the polymer to be used are the means by which the acceptability of the finished article is determined. Unfortunately, these controls are indirect and operate interdependently to determine a more primary set of variables which are more directly related to the acceptability of the molded piece. The first part of our program of injection molding research has been to provide means of measuring the primary variables, study their relationships with the control variables, and determine the sequence of events in a molding cycle.

Among those quantities which are of importance in determining the quality of the piece are the pressure, average temperature, and density of the polymer in the mold just before the mold is opened. In general, we wish to know the values of these quantities as a function of time, after the mold has been filled. Knowing the geometry of the mold, the temperature at which the polymer enters the mold, and the mold temperature, the average temperature of the piece may be computed as a function of time from heat conduction theory. This may involve approximations, but a sufficiently close result can be obtained in most cases, leaving the pressure and density to be determined. Fortunately, it is not necessary to measure both of these quantities, inasmuch as they are related through the following equation of state,

$$(P + \pi) \left(\frac{V}{M} - \omega \right) = RT, \quad [1]$$

where P is the pressure, V/M the specific volume, T the average temperature, the π , ω , and R are constants which have been determined for some of the common polymers (7,8). Faced with the choice of measuring pressure or density, pressure was chosen. Details on the means by which this pressure was measured may be found in an earlier paper (2).

Figure 2 shows a typical mold pressure curve for one molding cycle, and indicates the sequence of events, or cycle steps, in injection molding.

The usual subdivision of molding cycle into plunger forward time, mold closed time, and mold open time comes about by considering what the machine is doing throughout the cycle. The subdivision of molding cycle into the steps of Fig. 2 is based, for the most part, on consideration of what the polymer is doing. During the first step, the *dead time*, the polymer is doing nothing, a fixed length of time being required for the plunger to advance far enough to begin forcing polymer into the mold. The second step is that during which polymer is flowing into the mold, eventually *filling* it. The third step is *packing*, during which polymer flows into the mold relatively slowly. The fourth step is *discharge* of polymer back out of the mold after the plunger has ceased to apply pressure to the polymer. After some discharge, *sealing* takes place (at point five) by solidification of polymer in the gate, which is a constriction at the entrance to the mold

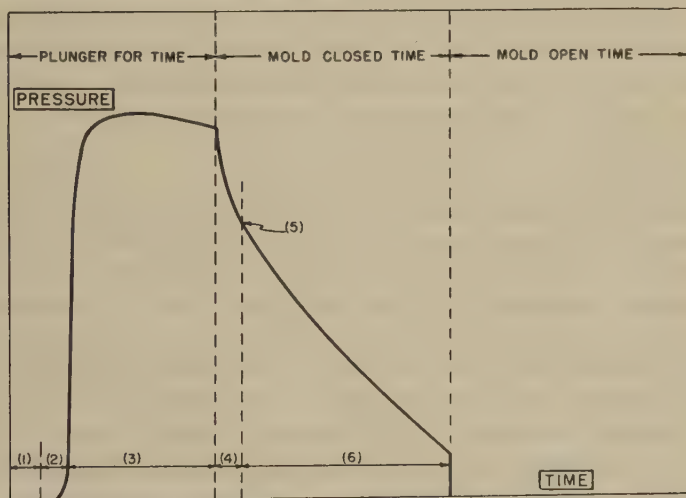


FIG. 2. Pressure in the mold during a typical cycle. Sequence of events is: (1) dead time, (2) filling, (3) packing, (4) discharge, (5) sealing, and (6) sealed cooling.

cavity. Step six consists of *sealed cooling* under conditions of constant mass (and constant volume unless the pressure reaches zero during cooling). The present paper will be concerned largely with steps two and three, filling and packing.

It should be emphasized at this point that much of this and later discussion does not apply, without modification, to situations in which the molded piece is made up of very thin sections. In such cases a somewhat different approach to the problem must be made.

FLOW OF MOLTEN POLYSTYRENE

It is fairly well recognized by now that molten polystyrene is a non-Newtonian fluid. That is to say, the rate of flow is not proportional to the

driving force; rather, the rate of flow increases much more than proportionately with increasing driving force. It has been found (6) that the flow of polystyrene through a capillary may be described by the following empirical equation:

$$Q = \frac{\pi R^4 P}{8L\eta} \left\{ 1 + k\tau + \frac{k^2\tau^2}{2!} + \frac{k^3\tau^3}{3!} + \frac{k^4\tau^4}{4!} \right\} \quad [2]$$

where Q = volume rate of flow,
 R = radius of capillary,
 L = length of capillary,
 P = pressure drop, and
 τ = shearing stress at capillary wall = $PR/2L$.

Two constants characteristic of the polymer appear in this equation. Of these, η is the Newtonian viscosity, and k is a constant proportional to the highly elastic compliance (5). The factors determining these two constants have been studied in some detail, and it is now possible to predict with some accuracy the flow behavior of polystyrene of a given molecular weight, containing a certain amount of solvent, at a given temperature (1,5,6).

Actually, this picture is more detailed than is necessary in considering most commercial polystyrenes. Commercial polystyrenes fall within a rather limited range of average molecular weight. The constant, k , is only directly proportional to molecular weight and is independent of temperature. The net result is that the form of the dependence of flow rate upon pressure is not too different for various commercial polystyrenes unless they differ appreciably in content of plasticizer, lubricant, or low-molecular-weight polymers. The Newtonian viscosity, however, is very sensitive to changes in molecular weight or temperature and thus serves as the major index of flow behavior.

A further simplification is possible. The pressure differentials of interest in injection molding cover, generally, less than one cycle of ten. Under these circumstances, and aided by the fact that the shearing stresses during flow in molding are relatively high, the flow equation can be reasonably well approximated for our purposes by a power law. Thus

$$Q = AP^\alpha/\eta, \quad [3]$$

where the constant A depends on the geometry of the channel through which the polymer flows. For a given channel and given pressure range, one would not expect A and α to depend much upon the temperature or the choice of commercial polystyrene. Further, one would expect this form of relationship to be preserved fairly well even in going over to channels of noncircular cross section.

Now consider an array of channels in series, taking approximate account of the effect of the connecting points by replacing them with equivalent channels. Thus we arrive at an equivalent array in which end effects can be neglected. Suppose that this array is only partially filled with polymer, the forward-moving surface being in the k -th channel at a distance L from the channel entrance. Then we can write

$$Q = \frac{(\Delta P_i)^\alpha}{\eta g_i^\alpha} \quad [4]$$

for the i -th full channel, and

$$Q = A_k \frac{dL}{dt} = \frac{L_k^\alpha (\Delta P_k)^\alpha}{\eta g_k^\alpha L^\alpha} \quad [5]$$

for the partially filled k -th channel,

where $\Delta P_i, \Delta P_k$ = pressure drops along channels,
 g_i, g_k = geometrical factors for channels,
 A_k = cross-sectional area of k -th channel, and
 L_k = length of k -th channel.

These expressions may be solved for the pressure drops along each channel and the pressure drops summed to give the total applied pressure, which we are assuming to be constant, thus,

$$P = \sum_{i=1}^k \Delta P_i = \left(\frac{g_k L}{L_k} + \sum_{i=1}^{k-1} g_i \right) \left(\eta A_k \frac{dL}{dt} \right)^{1/\alpha}. \quad [6]$$

This may be integrated to give the time required for the polymer front to traverse the k -th channel,

$$t_k = \eta P^{-\alpha} \frac{A_k L_k}{(\alpha + 1) g_k} \left[\left(\sum_{i=1}^k g_i \right)^{\alpha+1} - \left(\sum_{i=1}^{k-1} g_i \right)^{\alpha+1} \right]. \quad [7]$$

The total transit time for the r -th through the s -th channels is then

$$t = \eta P^{-\alpha} \sum_{k=r}^s \frac{A_k L_k}{(\alpha + 1) g_k} \left[\left(\sum_{i=1}^k g_i \right)^{\alpha+1} - \left(\sum_{i=1}^{k-1} g_i \right)^{\alpha+1} \right]. \quad [8]$$

The complicated summation is nothing but a geometrical factor which is a constant for a given array; hence Eq. [8] could be written as

$$t = B \eta P^{-\alpha}. \quad [9]$$

Comparing this with Eq. [3] it is seen that the form of the simple flow relationship is maintained even for an array of channels in series.

FILLING THE MOLD

Pursuing the train of thought of the end of the preceding section, let us consider first the fill time, f . This is defined as the length of time between

the instant the polymer begins moving into the mold and the instant the mold becomes full. A detailed consideration of this problem should take into account the geometrical complexity of the channels of flow and the fact that the polymer is being cooled during filling. Needless to say, this makes the problem very difficult, if not completely impractical, of solution. The geometrical complexity presents no problem if we are content with an approximate expression, for we can refer to Eq. [9] and write

$$f = B\eta P_M^{-\alpha} \quad [10]$$

where P_M is the pressure applied to the polymer by the plunger, and η is the viscosity of the flowing polymer. This last quantity raises a further question, for there can be no doubt that the polymer is cooled somewhat while filling the mold and the viscosity is highly dependent upon temperature. For the moment, let us defer this question and merely compute η at the temperature of the polymer just before it enters the mold.

The constants B and α must be evaluated from experimental data. Our only a priori expectation, from Eq. [2], would be that α should be somewhere between 4 and 5 for high shearing stresses. This turned out to be the case for our press and mold, for we found $\alpha = 4.4$ and $B = 11.4$ when we expressed f in seconds, η in poises, and P_M in units of one thousand pounds per square inch (kp.s.i.). Equation [10], with these values of the constants, was in good agreement with observed fill times when the mold temperature was 90°F. (32°C.), as shown in Table I. It was found

TABLE I
Comparison of Equation [10] and Observed Fill Times
Mold temperature = 90°F. (32°C.)

P_M	η	$f(\text{calcd.})$	$f(\text{obs.})$
kp.s.i. ^a	poises	sec.	sec.
19	38,600	1.05	1.2
19	80,500	2.20	1.7
19	115,000	3.14	2.7
19	210,000	5.75	6.7
16	80,500	4.60	4.7
14	9,100	0.94	1.2
14	14,500	1.49	1.2
14	62,500	6.42	6.7
12	12,960	2.63	2.7
12	14,300	2.90	2.7
10	9,100	4.13	4.7
10	12,960	5.88	6.7
10	14,300	6.50	6.7

^a Thousand pounds per square inch.

that raising the mold temperature to 120°F. (49°C.) reduced the fill times, and this corresponded to a value of $B = 6.15$.

There is a limitation on fill time for many molding presses which must be considered. The plunger forward motion is produced by pumping oil at a constant rate into a cylinder which drives the plunger. A pressure control by-passes the pumps when the oil pressure reaches a maximum predetermined value, and subsequently maintains the pressure constant. This corresponds to the pressure P_M . If this maximum pressure is set high enough on the control, it is not attained during filling. Instead, the mold fills at a constant rate under some lower pressure. This filling rate is determined by the oil pumping rate and the ratio of polymer displacement to oil displacement. The *minimum fill time* is determined by this filling rate and the volume of the mold. The filling pressure can be calculated from Eq. [10] by setting f equal to the minimum fill time. The minimum fill time can be calculated, as just outlined, although it is readily determined experimentally.

Thus far we have assumed that viscous flow is the mechanism by which polymer moves everywhere within the molding press. This assumption is valid only if that section, through which the incoming cold granules move during filling, is heated so as to soften the surface of the granules contacting it. If this section of the cylinder is not heated there will be a pressure drop through the granular zone due to frictional effects. It has been shown (9) that this will reduce the pressure at the forward-moving end of the granular zone to

$$P_M^* = P_M e^{-\frac{4\mu L_0}{D}}, \quad [11]$$

where μ = the coefficient of friction of the polymer on the cylinder wall, L_0 = the uncompressed length of the granular zone, and D = the cylinder diameter. Substituting this in Eq. [10] gives

$$f = B e^{\frac{4\alpha\mu L_0}{D}} \eta P_M^{-\alpha}. \quad [12]$$

Thus, only the apparent value of the constant B is altered; the form of the filling equation is preserved. Consider now the effect of adding a lubricant to the surface of the polymer granules. This would lower the coefficient of friction μ and hence would decrease the time required to fill the mold, according to Eq. [12]. If, on the other hand, the cylinder section is heated, frictional effects do not enter into the picture and the fill time is unaltered.

To gain a better insight into the process of filling, a special mold was constructed. Specially annealed glass plates, 1- $\frac{1}{4}$ in. thick, were set into the two sides of the mold and appropriate windows were cut out. The piece molded was a disk, 2 in. in diameter and 0.1 in. thick. The entire mold cavity was visible through the windows and slow motion movies could be

taken of the filling process and other phenomena occurring within the mold. Observation was facilitated by the admixture of a few granules of black polystyrene with the clear polymer used. In this way the flow of polymer during filling, packing, and discharge was made visible.

The pattern of flow during filling was discernible from the movies made in this manner. During filling, the front of hot polymer advanced across the mold, as shown in Fig. 3. The volume of polymer in the mold increased with time, as indicated in Fig. 4. To make clearer what was happening in the mold let us trace one bit of polymer. After passing through the gate it traveled across in a region centrally located between the parallel glass walls. Its velocity was greater than the velocity of the advancing front.

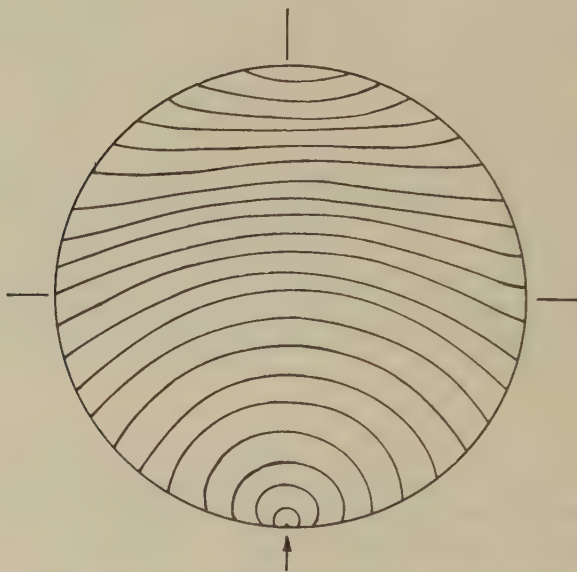


FIG. 3. Successive positions of the polymer front during filling of a disk mold (2 in. diameter, 0.1 in. thickness). The time interval between positions is 0.078 sec.

Its temperature did not drop very much in traversing the mold, unless flow was quite slow or the walls were very close together. When our bit of polymer caught up with the advancing front it was forced outward against the mold wall. Here it was chilled quite rapidly, and here it remained motionless, while the front passed on to traverse the rest of the mold. Thus, in the full portion of the mold we find two regions: a cool, motionless shell, and a relatively hot, flowing core. At the front, the hot, flowing polymer was being converted into a stationary shell. The subsequent phenomena of packing and discharge occurred within the central core. As soon as the mold was full, of course, the core began to cool more rapidly and the shell increased in thickness.

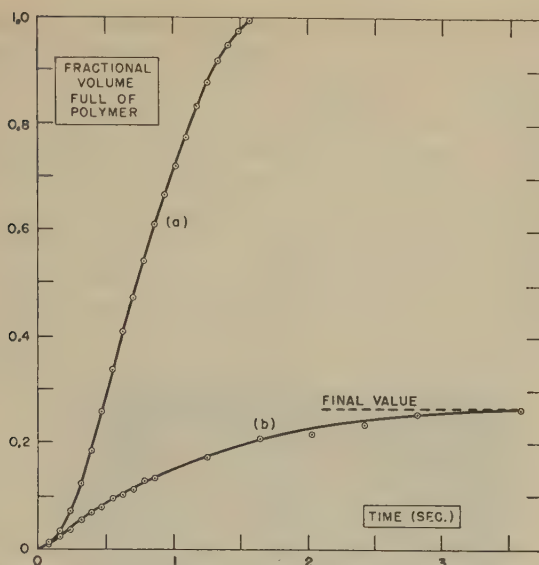


Fig. 4. Volume fraction of polymer in mold during filling; for (a) complete filling, (b) a short shot.

Both packing and discharge have been observed in the glass-window mold. To get some idea as to the relative polymer flow rates during these processes, measurements of lineal velocity in the neighborhood of the gate were made from movies taken during filling, packing, and discharge. The velocities measured are listed in Table II. Comparison of lineal velocities in the full part of the mold with the velocity of the front permits calculation of the thickness of the hot, flowing core. In a typical case this is estimated to be 40% of the thickness of the disk.

With relatively small gates another phenomenon is sometimes observed, which we have termed "jetting." The first polymer entering the mold has such kinetic energy that it shoots out into the cavity in the form

TABLE II

Approximate Lineal Polymer Velocities at About 1 cm. from the Gate in the Glass-Window Mold

Process	Velocity cm./sec.
Filling (about half full)	15-20
Filling (almost full)	6
Packing	3
Discharge	1
Jetting	70 ^a

^a This is the observed lineal velocity of the jet. For comparison with the preceding values, this corresponds to 1.7 cm./sec. lineal velocity 1 cm. from the gate if the mold were full of polymer.

of a jet. The jet continues until the resulting filament of polymer becomes rigid enough, through cooling, to deflect the flow of polymer from the gate. Filling then proceeds in something like the normal pattern, slightly complicated by the presence of the polymer filament. A typical jet is shown in Fig. 5, which is a frame from a movie taken of this phenomenon. The appearance of the filament is very much like that of polystyrene filaments extruded at high shearing stresses (6). The velocity of this jet is indicated in Table II. The dimensions of the gate used in securing Fig. 5 were $0.020 \times 0.030 \times 0.040$ in. land. We believe that jetting is responsible for a characteristic type of surface blemish in the molded article. When filling proceeds too slowly after jetting, the filament cools to such an extent that

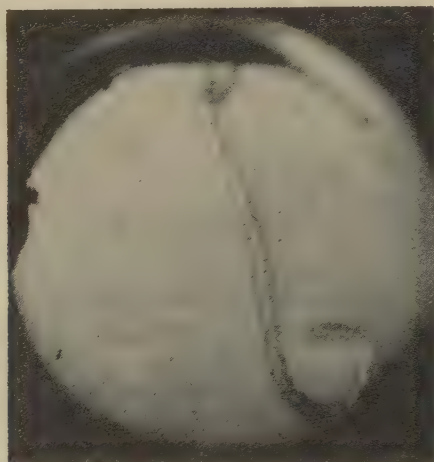


Fig. 5. Polymer jetting into mold during the early stages of filling. The gate dimensions in this case were 0.020 in. \times 0.030 in. \times 0.040 in. land.

it will not weld perfectly with the incoming hot polymer, leaving imperfections in the surface of the article.

PACKING THE MOLD

After the mold is full, there is still a flow of polymer into the mold, which we have termed "packing." To get a better understanding of this process let us idealize the situation somewhat. Consider a long flow channel connected to a cavity of volume V . Let M = the mass of polymer in the cavity, T = the temperature of polymer in the cavity, P = the pressure in the cavity, and P_M = the constant pressure at the other end of the channel. Equation [1] may be rewritten as

$$M = \frac{V}{\omega + \frac{RT}{P + \pi}}. \quad [13]$$

During packing, M is increasing, P is increasing (at first), and T is decreasing. Differentiating the above,

$$\frac{dM}{dt} = \frac{V}{\left(\omega + \frac{RT}{P + \pi}\right)^2} \left\{ \frac{RT}{(P + \pi)^2} \frac{dP}{dt} - \frac{R}{P + \pi} \frac{dT}{dt} \right\}. \quad [14]$$

From the filling equation we can also write

$$\frac{dM}{dt} = \frac{MP_M^{-\alpha}}{\beta f(P_M - P)^{-\alpha}}, \quad [15]$$

where f is the fill time preceding packing, and β is a numerical factor the value of which is determined by the relative resistance to flow in the channel and the cavity. The range of β is from 1 to $(\alpha + 1)$.

Combining Eqs. [10], [14], and [15], we could arrive at a differential equation which would define the pressure-time curve during packing, since the temperature-time curve is known. However, we are not much interested in the details of the shape of the packing curve. One thing in which we are interested is what has been termed the injection pressure, P_i , which might now be defined as the maximum pressure reached in the mold during packing. At this point $dP/dt = 0$. A number of reasonable approximations may now be introduced which permit combination of Eqs. [14] and [15] to give

$$P_i/P_M = 1 - \left[\frac{f(T_i - T_0)}{\gamma} \right]^{1/\alpha}, \quad [16]$$

where T_i = temperature at which polymer enters the mold, and T_0 = mold wall temperature. The magnitude of the constant γ depends upon the cooling characteristics of the mold, the value of β , and a little on the way the approximations are carried out. For our mold, $\alpha = 4.4$ and $\gamma = 18,300$, when f is expressed in seconds and the temperatures in degrees Fahrenheit.

This may be extended quite readily to the case in which a cold granular zone just ahead of the plunger is characterized by a pressure transmission coefficient $e^{-4\mu L_0/D}$ (see Eq. [11]). In this event, all that is necessary is to multiply the entire right-hand side of Eq. [16] by this pressure-transmission coefficient. In our case this was not necessary.

Equation [16] describes the facts fairly well, as may be seen in Table III. There, data are presented on two polystyrenes under a variety of molding conditions. Comparison of calculated and observed values of P_i points out the wide range of application of Eq. [16].

At the end of the packing operation the plunger is returned. This means that there is a certain pressure in the cavity and zero pressure at the other end of the channel. The flow in the channel is now reversed and

TABLE III

Comparison of Equation [16] and Observed Injection Pressures for Two Polystyrenes

Polymer	T_0	T_i	f	P_M	P_i	$P_i(\text{calcd.})$
	$^{\circ}\text{F.}$	$^{\circ}\text{F.}$	<i>sec.</i>	<i>kp.s.i.^a</i>	<i>kp.s.i.^a</i>	
1	90	490	1.2	14.0	9.0	7.9
1	90	490	2.7	12.0	6.1	5.7
1	90	490	6.7	10.0	3.5	3.5
1	90	480	1.7	14.0	8.0	7.4
1	90	460	1.7	16.0	8.9	8.6
1	90	441	1.7	18.0	9.8	9.7
1	90	430	1.7	19.0	10.4	10.3
1	90	450	1.2	19.0	11.3	10.9
1	90	417	4.7	16.0	6.0	6.9
1	90	405	2.7	19.0	8.7	9.5
2	90	400	1.2	20.0	11.8	11.8
2	90	400	1.6	18.0	10.8	10.1
2	90	400	2.7	16.0	8.7	8.1
2	90	400	6.4	14.0	5.5	5.6
2	90	350	4.9	20.0	9.4	9.1
2	120	500	1.6	10.0	5.1	5.3
2	120	450	1.2	14.0	8.7	8.2
2	120	450	2.8	12.0	5.3	5.9
2	120	400	1.6	16.0	9.5	9.1
2	120	400	3.1	14.0	6.4	7.0
2	120	350	7.0	18.0	6.7	7.6

^a Thousand pounds per square inch.

the mold discharges. It is easy to set up a differential equation, as indicated before, which defines the pressure-time curve during discharge, but it is not so easy to solve this equation. Fortunately, there appears to be little need, as yet, for such a solution.

As the pressure drops during discharge the rate of discharge also drops. Finally, the rate becomes low enough so that the polymer passing through the gate is cooled sufficiently to "freeze." Suppose that this sealing takes place when the average temperature of the discharging polymer is T_s when it has just passed through the gate. We are now faced with the problem of computing the amount of cooling during flow of a hot polymer through a cold channel. An approximate solution has been derived for the case in which the cooling during transit is not too extreme (3). Combining this with some published engineering data (4), it may be shown that

$$1 - \theta = K \left(\frac{L}{Q} \right)^{\frac{1}{2}}, \quad [17]$$

where L = length of capillary, Q = flow rate, and θ = reduced average outlet temperature. The quantity K is a known function of the thermal

diffusivity and the ratio of the average viscosity to the viscosity at the wall temperature. This quantity has been computed for polystyrene, under various temperature conditions.

If now the average outlet temperature is taken at T_s at the sealing point, eq. [17] becomes

$$\frac{T_i - T_s}{T_i - T_0} = K \left(\frac{L}{Q} \right)^3. \quad [18]$$

After introducing several values of temperature into Eq. [18], with appropriate values of K , it is possible to make several generalizations, as rough approximations:

(a) The quantity Q/L may be taken as independent of the inlet temperature, over a considerable range.

(b) Q/L will be significantly dependent upon T_0 and T_s , although T_s may not vary too much in practice.

(c) Thus, for a given gate, there will be an effective Q value characteristic of sealing, relatively independent of the polymer inlet temperature.

The third conclusion means that the pressure and temperature in the mold at the instant it seals will be related to each other as given by some particular fill line ($f = \text{constant}$), corresponding to this critical rate of flow. Thus, we should find $\eta P^{-\alpha} = \text{constant}$ at the sealing point. This has been verified experimentally, but it turns out that an equally good, and more useable, approximation is simply a straight line

$$P = A - BT \quad [19]$$

inasmuch as the fill lines are also approximately straight. For a typical polystyrene in our box mold we found

$$P(\text{kp.s.i.}) = 22.5 - 0.066T(^{\circ}\text{F.}). \quad [20]$$

Thus, the pressure sealed into the mold depends upon how much cooling has gone on before discharge.

Two exceptions must be noted. If the pressure in the mold at the end of the packing period is less than that given by the above equation, only very slight discharge will result, and essentially all of the pressure will be sealed into the mold. The other case may arise if the plunger forward motion is unduly prolonged. After considerable cooling has taken place the rate of flow into the mold during packing is greatly diminished. If this becomes low enough the gate will seal during the plunger forward motion, and there will be no discharge at all. This phenomenon has been observed.

SUMMARY

The sequence of events during an injection molding cycle consists of dead time, filling, packing, discharge, sealing, sealed cooling, and mold

open time. Those steps in this sequence which involve flow of the polymer have been discussed in this paper.

The time required to fill the mold was found to be directly proportional to the melt viscosity of the polymer, and inversely proportional to a power (between 4 and 5) of the ram pressure. Raising the temperature of the mold walls decreased the filling time. Lowering the coefficient of friction of the polymer on the cylinder wall decreased the filling time, but only if the cylinder wall was not hot enough to soften the polymer. The filling time cannot fall below a certain minimum value which is determined by the characteristics of the molding press.

The pattern of flow during filling was studied with a special mold in which the entire cavity was visible through glass windows. It was found that hot polymer entering the mold flows only in a central region, there being a relatively cool, stationary region next to each mold wall. When the flowing polymer reaches the advancing front it contacts the wall, cools, and ceases flowing. In a typical case the thickness of the central flowing region was estimated to be about 40% of the total thickness. Packing and discharge were also observed in the glass-window mold.

An approximate equation was developed for the calculation of the maximum pressure developed in the mold during packing. Comparison of calculated and experimental values showed the wide range of usefulness of this equation. Sealing of the mold by "freezing" of polymer in the gate was found to be characterized by a critical rate of flow, for a given gate, polymer softening point, and mold wall temperature. This led to an approximately linear relationship between the temperature and pressure in the mold at the sealing point.

REFERENCES

1. FOX, T. G., AND FLORY, P. J., *J. Am. Chem. Soc.* **70**, 2384 (1948).
2. GILMORE, G. D., AND SPENCER, R. S., *Modern Plastics* **27**, 146 (April 1950).
3. MARSHALL, W. R., AND PIGFORD, R. L., *The Application of Differential Equations to Chemical Engineering Problems*, p. 140. University of Delaware, Newark, Delaware, 1947.
4. SIEDER, E. N., AND TATE, G. E., *Ind. Eng. Chem.* **28**, 1429 (1936).
5. SPENCER, R. S., *J. Polymer Sci.*, in press.
6. SPENCER, R. S., AND DILLON, R. E., *J. Colloid Sci.* **4**, 241 (1949).
7. SPENCER, R. S., AND GILMORE, G. D., *J. Applied Phys.* **20**, 502 (1949).
8. SPENCER, R. S., AND GILMORE, G. D., *J. Applied Phys.* **21**, 523 (1950).
9. SPENCER, R. S., GILMORE, G. D., AND WILEY, R. M., *J. Applied Phys.* **21**, 527 (1950).

THE MIXING OF VERY VISCOUS LIQUIDS ¹

R. S. Spencer and R. M. Wiley

Dow Chemical Company, Midland, Michigan

Received November 13, 1950

INTRODUCTION

The problem of mixing two or more materials, so as to produce a relatively homogeneous mass, is a very common one in chemical technology. When the only nondisperse components are low viscosity liquids solution of the problem is fairly straightforward. Turbulence and diffusion provide randomizing phenomena which may be utilized to advantage in designing mixing equipment. Although a theoretical treatment might prove difficult, yet the general principles are understood and practical know-how has produced many useful types of equipment.

When the materials to be mixed are very viscous liquids the situation is quite different. Neither diffusion nor turbulence can assist very much in mixing. Rather, mixing must be effected by some complex, continuous deformation which serves to disperse the components to the desired degree. This might be termed *streamline mixing*, to distinguish it from *turbulent mixing*. Examples of this type of mixing might include making up rubber formulations on compounding rolls, using an extruder as a mixer, kneading bread dough, and pulling taffy.

The lack of a randomizing factor in streamline mixing introduces both difficulties and advantages. One cannot depend upon the randomizing process to give satisfactory dispersion, if only sufficient time is allowed. The process of deformation must be carefully designed to do just the job required. This has the advantage, however, of permitting the engineer to design very efficient mixing processes.

Because streamline mixing is so different, in many respects, from turbulent mixing, this discussion will begin by defining certain fundamental concepts. These will then be discussed in some detail and a few general conclusions drawn. Finally, the different basic types of mixers will be discussed briefly, and a few simple examples considered.

STREAMLINE MIXING

To discuss mixing, it is first necessary to define what it is that the operation is designed to accomplish. Such vague terms as "homogeneity,"

¹ Presented at the Annual Meeting of the Society of Rheology, New York, N. Y., November 3-4, 1950.

"uniform composition," etc., are of little use in a detailed study of mixing. The concepts which we shall be using are derived from the notion of "visual homogeneity," so let us begin with that.

To start with, the system consists of masses of, say, two materials which are distinguishable in some way. For the purpose of discussion, let us assume that one material is red and the other is transparent. After the mixing operation has been performed our eyes inform us that the material is now of a uniform red color throughout. Just what does this really mean? The starting system contained surfaces of discontinuity of color. After a continuous deformation, however complex, the material must still contain surfaces of color discontinuity, assuming that diffusion is negligible. The deformation, or mixing operation, must have brought these surfaces closer together, at every point, than the limit of resolution of the eye. However, this is not a sufficient guarantee of homogeneity, for the eye may still find longer range fluctuations in intensity of the red color. That is to say, there may still be variations in the relative amounts of clear and red material within different volume elements. Thus it may be seen that an efficient mixing process must accomplish two things so as to keep fluctuations in average composition below some desired level: (a) subdivision of the materials present, and (b) distribution of the subdivided materials.

In general, the definition of what constitutes "apparent continuity" will be determined by the nature of the specific mixing problem at hand. *Visual* continuity provides a simple illustrative example. Assume that the limit of resolution is r . Now divide the material up into little cubes of dimensions $r/2$ on a side. The condition of apparent continuity requires that some of the surface between the components pass through every one of these cubes. Again it is necessary to specify further that the local average composition of the cubes shall not fluctuate too much. That is, the mixing process must create enough new interfacial surface to satisfy the "space-filling" condition of apparent continuity, and must distribute that surface within certain limits of uniformity.

The space-filling condition on the creation of new interfacial surface can be formulated more precisely. Consider any point on the interfacial surface, after mixing has taken place, and erect a normal to the surface. Proceed along the normal a distance $r/2$ from the surface, into the *red* material. The locus of such points is a new surface which is "parallel" to the interfacial surface, and separated from it by a distance $r/2$. The volume contained between this new surface and the interfacial surface must be greater than or equal to the total volume of *red* material present. This is a necessary requirement for apparent continuity. Similarly, proceed along the normal a distance $r/2$ from the interfacial surface, into the *clear* material. The volume between the surface so defined and the interfacial surface must be greater than or equal to the total volume of the

clear material. This also is a necessary requirement for apparent continuity. These two requirements tell us only that enough interfacial surface is available, not that it is distributed properly. In a given mixer it may be necessary to create more surface than this minimum in order to achieve proper distribution. The next section will discuss the question of interfacial surface in more detail.

INTERFACIAL SURFACE

Let us set up coordinate axes x_1, x_2, x_3 and define the interfacial surface in the starting material by the relationship

$$F(x_1, x_2, x_3) = 0. \quad [1]$$

The direction cosines of the normal to this surface, at a point, will be of the form

$$\cos \alpha_i = \frac{\frac{\partial F}{\partial x_i}}{\sqrt{\sum_i \left(\frac{\partial F}{\partial x_i} \right)^2}}. \quad [2]$$

After deformation the new interfacial surface will be defined by some relationship

$$F'(x_1', x_2', x_3') = 0. \quad [3]$$

The direction cosines will be of the form

$$\cos \alpha_i' = \frac{\frac{\partial F'}{\partial x_i'}}{\sqrt{\sum_i \left(\frac{\partial F'}{\partial x_i'} \right)^2}}. \quad [4]$$

Now proceeding along the normal into, first, the red material and then the clear material, two new surfaces may be defined by

$$F' \left(x_1' \pm \frac{r}{2} \cos \alpha_1', x_2' \pm \frac{r}{2} \cos \alpha_2', x_3' \pm \frac{r}{2} \cos \alpha_3' \right) = 0, \quad [5]$$

where the plus or minus signs are chosen so as to proceed into the desired material. It is the volumes contained between these two new surfaces and the deformed interfacial surface which are to be compared with the total volumes of red and clear material.

If the deformed interfacial surface were a plane, the desired volumes would be simply $S'r/2$, where S' is the surface area of the deformed interface. If the average radii of curvature of the interfacial surface are considerably more than $r/2$, this is still a fairly good approximation. Thus, the limiting conditions on interfacial surface area could be written as:

$$S'r/2 \geq V_1 \text{ and } S'r/2 \geq V_2, \quad [6]$$

where V_1 and V_2 are the volumes of the two components being mixed. Our problem is now that of computing the deformed interfacial area from a knowledge of the original surface and the process of deformation.

Let the deformation be described by defining a displacement vector, $\mathbf{u}(x_1, x_2, x_3)$, at each point in the undeformed material, and let the components of this vector be $u_1(x_1, x_2, x_3)$, $u_2(x_1, x_2, x_3)$, and $u_3(x_1, x_2, x_3)$. The deformed surface can now be defined in terms of the undeformed surface, thus,

$$F'(x'_1, x'_2, x'_3) = F(x_1, x_2, x_3) = 0, \quad [7]$$

where $x_i = x'_i - u_i(x_1, x_2, x_3)$, and (x'_1, x'_2, x'_3) and (x_1, x_2, x_3) are corresponding points in the deformed and undeformed material, respectively. Knowing F and \mathbf{u} , Eq. [7] defines the deformed surface and thereby the surface area.

In many cases of practical interest the following approach is useful in computing the interfacial area. Using Eq. [7], we compute the direction cosines of the normal to the surface $F' = 0$ at a point (x'_1, x'_2, x'_3) , in terms of the direction cosines of the normal to the surface $F = 0$ at the corresponding point (x_1, x_2, x_3) . These turn out to be of the form

$$\cos \alpha'_k = (\cos \alpha_k) \times \frac{1 - \sum \left(\frac{\partial u_i}{\partial x_k} \right) \frac{\cos \alpha_i}{\cos \alpha_k}}{\sqrt{1 - 2 \sum_i \sum_j \left(\frac{\partial u_i}{\partial x_j} \right) \cos \alpha_i \cos \alpha_j + \sum_i \sum_j \left(\frac{\partial u_i}{\partial x_j} \right)^2 \cos^2 \alpha_i}} \quad [8]$$

Then the deformed surface area is given by

$$S' = \iint_{S'_{ij}} \frac{dx'_i dx'_j}{\cos \alpha'_k}, \quad [9]$$

where the integration is over S'_{ij} , the projection of the surface S' on the i, j -plane. In unidirectional shear, however complicated otherwise, the projection of the interfacial surface on the plane normal to the displacement vectors is unchanged by the deformation. In such a case Eqs. [8] and [9] provide a convenient means of computing S' .

Consider now a simple example which will serve to illustrate an important point. Let the deformation be simple shear, such that all of the partial derivatives of the components of the displacement vector are zero except for $\partial u_1 / \partial x_2$, which is constant. The projected area S_{23} is unchanged by the deformation, so that Eqs. [8] and [9] can be combined to give

$$S' = \iint_{S_{23}} \sqrt{1 - 2 \left(\frac{\partial u_1}{\partial x_2} \right) \cos \alpha_1 \cos \alpha_2 + \left(\frac{\partial u_1}{\partial x_2} \right)^2 \cos^2 \alpha_1} \frac{dx_2 dx_3}{\cos \alpha_1}. \quad [10]$$

If, further, the interfacial surface is some section of a plane, the direction cosines are independent of the coordinates and Eq. [10] becomes

$$S' = S \sqrt{1 - 2 \left(\frac{\partial u_1}{\partial x_2} \right) \cos \alpha_1 \cos \alpha_2 + \left(\frac{\partial u_1}{\partial x_2} \right)^2 \cos^2 \alpha_1}. \quad [11]$$

The above equation tells us that the deformed surface is directly proportional to the undeformed surface, and that the proportionality factor depends upon the orientation of the surface prior to deformation. Now suppose that the space-filling requirements specify, through Eqs. [6], the surface ratio S'/S that is needed. What orientation of the undeformed surface will result in the predetermined ratio S'/S with a minimum

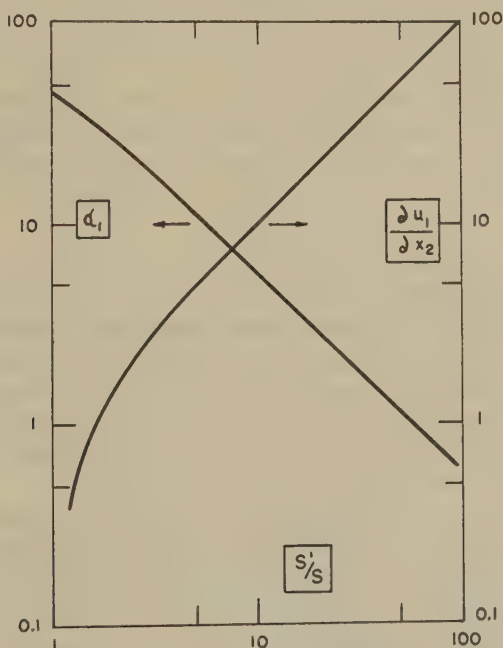


Fig. 1. Optimum orientation angle and minimum shear strain for increasing interfacial surface area. (Eqs. [13] and [14].)

amount of shear? That is to say, what orientation enables us to produce the required new surface most efficiently? Inspection of Eq. [11] shows that $\cos \alpha_1$ cannot be zero and further, that $\cos \alpha_2$ should be negative and as large in absolute magnitude as possible. This latter condition is achieved when $\cos \alpha_3 = 0$, and accordingly $\cos \alpha_2 = -\sin \alpha_1$. Substituting this in Eq. [11] and solving for $\partial u_1 / \partial x_2$, we find

$$\left(\frac{\partial u_1}{\partial x_2} \right) = \sqrt{\left(\frac{S'}{S} \right)^2 \sec^2 \alpha_1 - 1} - \tan \alpha_1. \quad [12]$$

Differentiating this with respect to α_1 and setting the derivative equal to zero, we find the orientation requiring minimum shear to be defined by

$$\tan \alpha_1 = \left(\frac{S}{S'} \right). \quad [13]$$

The minimum shearing strain corresponding to this orientation is

$$\left(\frac{\partial u_1}{\partial x_2} \right) = \left(\frac{S'}{S} \right) - \left(\frac{S}{S'} \right). \quad [14]$$

These two relationships are shown in Fig. 1. Here we see that very small increases in surface area are best achieved by orienting the surface 45° to the displacement vectors, whereas for very large surface ratios the undeformed surface should cut perpendicularly across the displacement vectors. This point is a useful generalization in designing mixers.

Shears are not the only deformations which can be used to create new interfacial surface. Tensile strains can be used to "stretch" the surface. For most efficient production of new surface the undeformed surface should lie parallel to the tensile components of the displacement vectors.

DISTRIBUTION

The problem of the proper distribution of material (or interfacial surface) during mixing is rather different from that of creating new surface. Definitions can be set up as to what constitutes adequate distribution, from whatever point of view may be adopted, but it hardly seems worth while to attempt a formulation of the general problem. The concept involved is a relatively familiar one and the simple problems which are likely to arise can be handled as individual cases.

One comment should be made before continuing. Let us go back to our picture of the problem as that of trying to disperse a small quantity of red material in a relatively larger quantity of clear material. The process of deformation might be described by specifying a pattern of streamlines. Needless to say, these streamlines do not cross one another. Ideally, the red material should cut across all of these streamlines in the undeformed state. However, it will be permissible to leave gaps in the pattern, provided that the streamlines defining the boundaries of a gap are no farther apart than r , the limit of resolution, in the final deformed state. This condition is necessary, but not sufficient, for good distribution.

Now let us consider a rather special type of mixing, which might be termed *repetitive mixing*. By this we mean the following type of process: A mass of material is subjected to a certain unit mixing operation. After this deformation the mass is reassembled into the same gross form as in the beginning. The unit mixing operation is again carried out and the cycle repeated as many times as necessary. The effect of each mixing

operation is just superimposed upon the effect of all preceding operations. An example might be the mixing of something like biscuit dough by alternate rolling and folding over.

The problem of distribution in repetitive mixing can be handled quite conveniently by matrix methods. Subdivide the mass of material into N discrete cells of the same size. Assign numbers, 1 through N , to these cells. Let $a_j^{(n)}$ be the concentration of red material in the j -th cell after n mixing cycles. Now define a distribution matrix for one unit mixing operation, $[D_{ij}]$, where D_{ij} is that fraction of the material originally in the i -th cell which is to be found in the j -th cell after the mixing operation. If $a_i^{(0)}$ is the initial concentration in the i -th cell, the concentrations in the cells after n operations are given by the elements of the matrix

$$[a_j^{(n)}] = [a_i^{(0)}][D_{ij}]^n \equiv [a_i^{(0)}][D_{ij}^{(n)}]. \quad [15]$$

In the foregoing equation the concentration matrices are 1-row, N -column matrices, and the distribution matrices are $N \times N$. If the distribution matrix possesses an inverse, we can write

$$[a_i^{(0)}] = [a_j^{(n)}][D_{ij}]^{-n} \quad [16]$$

and thereby calculate the initial distribution necessary to get to any desired final distribution. It would be well to interject a word of caution at this point. There is a temptation to set $[a_j^{(n)}] = k[1 \ 1 \ 1 \ 1 \ \cdots 1]$, i.e., assume perfect mixing, and try to calculate the corresponding initial distribution. This will not work. If we represent the elements of $[D_{ij}]^{-n}$ as $D_{ij}^{(-n)}$, the perfect mixing condition would lead to

$$a_j^{(0)} = k \sum_i D_{ij}^{(-n)}.$$

Now $\sum_i D_{ij}$ is a constant for all j 's, and this property is preserved during inversion and during raising to the n -th power. Thus the above equation merely tells us that we must start out with perfect mixing. It is true that there are mixing operations which will give perfect mixing (insofar as our subdivision into cells is concerned) in a finite number of cycles, but the distribution matrices of such operations do not possess inverses.

Equation [15] can be written in another way, namely,

$$[a_j^{(n)}] = \sum_k a_k^{(0)} [D_{kj}^{(n)}]. \quad [17]$$

In practice we shall probably be most interested in the case where all non-zero elements of $a_j^{(0)}$ have the same value, say a_0 . Equation [17] then becomes

$$[a_j^{(n)}] = a_0 \sum_{\substack{k \\ (a \neq 0)}} [D_{kj}^{(n)}], \quad [18]$$

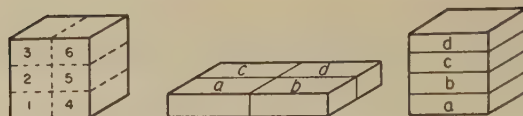


FIG. 2. Example of repetitive mixing operation.

where the summation is over all values of k for which $a_k^{(0)} \neq 0$. Thus, much guidance on the problem of deciding the best initial distribution can be obtained by merely inspecting the rows of the matrix $[D_{ij}^{(n)}]$. If it is desired to have red material in only one cell initially, that cell would be chosen which corresponded to the row in $[D_{ij}^{(n)}]$ along which the elements fluctuate the least. Or perhaps two cells whose rows fluctuate in opposite directions could be chosen to give even better distribution.

Let us consider a very simple example as an illustration. Specify six cells in a cube of material, as shown in Fig. 2. Let the mixing operation consist of compressing the cube to one-fourth its original height, cutting into quarters, and reassembling into a cube as indicated in Fig. 2. The matrix for this operation will be

$$[D_{ij}] = \frac{1}{4} \begin{bmatrix} 1 & 1 & 0 & 1 & 1 & 0 \\ 1 & 1 & 0 & 1 & 1 & 0 \\ 1 & 0 & 1 & 1 & 0 & 1 \\ 1 & 0 & 1 & 1 & 0 & 1 \\ 0 & 1 & 1 & 0 & 1 & 1 \\ 0 & 1 & 1 & 0 & 1 & 1 \end{bmatrix}. \quad [19]$$

Successive powers of this matrix are

$$[D_{ij}]^2 = \frac{1}{16} \begin{bmatrix} 3 & 3 & 2 & 3 & 3 & 2 \\ 3 & 3 & 2 & 3 & 3 & 2 \\ 3 & 2 & 3 & 3 & 2 & 3 \\ 3 & 2 & 3 & 3 & 2 & 3 \\ 2 & 3 & 3 & 2 & 3 & 3 \\ 2 & 3 & 3 & 2 & 3 & 3 \end{bmatrix},$$

$$[D_{ij}]^3 = \frac{1}{64} \begin{bmatrix} 11 & 11 & 10 & 11 & 11 & 10 \\ 11 & 11 & 10 & 11 & 11 & 10 \\ 11 & 10 & 11 & 11 & 10 & 11 \\ 11 & 10 & 11 & 11 & 10 & 11 \\ 10 & 11 & 11 & 10 & 11 & 11 \\ 10 & 11 & 11 & 10 & 11 & 11 \end{bmatrix},$$

$$[D_{ij}]^4 = \frac{1}{256} \begin{bmatrix} 43 & 43 & 42 & 43 & 43 & 42 \\ 43 & 43 & 42 & 43 & 43 & 42 \\ 43 & 42 & 43 & 43 & 42 & 43 \\ 43 & 42 & 43 & 43 & 42 & 43 \\ 42 & 43 & 43 & 42 & 43 & 43 \\ 42 & 43 & 43 & 42 & 43 & 43 \end{bmatrix}.$$

This mixing operation evidently distributes material uniformly and rapidly, as indicated by the appearance of the above matrices. This is substantiated by the fact that if the starting material were 1 in. thick, with a single sheet of red material in the center, four of these mixing cycles would result in bringing successive sheets of red to only 0.004 in. apart. The approach to uniform distribution may be better appreciated by referring to Table I, which lists standard deviations for one row of each of the above matrices. It may be seen that the fluctuations die out quite rapidly.

To illustrate a little different type of situation, let us consider a more irregular distribution matrix

$$[D_{ij}] = \frac{1}{6} \begin{bmatrix} 0 & 1 & 2 & 3 \\ 1 & 2 & 0 & 3 \\ 5 & 0 & 1 & 0 \\ 0 & 3 & 3 & 0 \end{bmatrix}. \quad [20]$$

The first few powers of this matrix are as follows:

$$[D_{ij}]^2 = \frac{1}{36} \begin{bmatrix} 11 & 11 & 11 & 3 \\ 2 & 14 & 11 & 9 \\ 5 & 5 & 11 & 15 \\ 18 & 6 & 3 & 9 \end{bmatrix},$$

$$[D_{ij}]^3 = \frac{1}{216} \begin{bmatrix} 66 & 42 & 42 & 66 \\ 69 & 57 & 42 & 48 \\ 60 & 60 & 66 & 30 \\ 21 & 57 & 66 & 72 \end{bmatrix},$$

$$[D_{ij}]^4 = \frac{1}{1296} \begin{bmatrix} 252 & 348 & 372 & 324 \\ 267 & 327 & 324 & 378 \\ 390 & 270 & 276 & 360 \\ 387 & 351 & 324 & 234 \end{bmatrix}.$$

This operation mixes material much less uniformly than the previous one, as may be seen by referring to Table I. If four mixing cycles were being used, cell two would be the logical place to put the red material initially. If it were permissible to start out with red material in two cells, a much better job of mixing could be done. For example, if both cells one and three were used, the resulting standard deviation after four cycles would be 0.0091, which is a factor of three better than the best that can be obtained by starting with only one cell.

The examples which have been used are, of course, very simple ones. In practice, rather large and unwieldy matrices would be encountered. Fortunately, the necessary operations of inversion, matrix multiplication, etc., can be carried out quite readily by using punched card methods. It would seem that this matrix approach would be particularly useful in

TABLE I
Fluctuation in Rows of Distribution Matrices for Repetitive Mixing

Distribution matrix	Power of matrix	Row	Standard deviation
Eq. [19]	$[D_{ij}]$	Any	0.1179
Eq. [19]	$[D_{ij}]^2$	Any	0.0295
Eq. [19]	$[D_{ij}]^3$	Any	0.0074
Eq. [19]	$[D_{ij}]^4$	Any	0.0018
Eq. [20]	$[D_{ij}]$	1	0.2357
		2	0.2357
		3	0.3727
		4	0.2887
	$[D_{ij}]^2$	1	0.0962
		2	0.1227
		3	0.1179
		4	0.1559
	$[D_{ij}]^3$	1	0.0556
		2	0.0471
		3	0.0651
		4	0.0916
	$[D_{ij}]^4$	1	0.0346
		2	0.0296
		3	0.0394
		4	0.0437

those complex cases which do not yield readily to analysis, and in which recourse must be had to laboratory studies of models to determine the way in which the mixing operation distributes material.

TYPES OF MIXERS

A consistent, complete scheme of classification for streamline mixers may be out of the question, but the following works fairly well, with a few exceptions. First, let us distinguish between (A) batch and (B) continuous mixers. Each of these can be subdivided according to whether there is (a) a continuous change in gross shape, (b) a cyclic change in gross shape, or (c) no change in gross shape. Finally, a distinction can be made, if desired, between the use of shear and tensile deformations.

An example will be given for each of the six major types indicated above. Before doing so, it would be well to make two general comments: (a) Continuous mixers differ from batch mixers only in that an additional deformation process is added to provide continuous transport of material. Additional complications which may arise are usually associated with this transport deformation. (b) Mixers involving a continuous change in shape are usually impractical. Large increases in interfacial area are required, ordinarily, and this necessitates large deformations. To carry these out

by a continuous change in shape would require equipment so large in some dimension as to be impractical.

Typical batch mixing with a continuous change in shape (*Aa*) would be something like pressing out the material between very large platens into a very thin sheet. As pointed out above, this would probably require prohibitively large platens, or a rather good dispersion already in the starting material. Batch mixing with a cyclic change in shape (*Ab*) is well illustrated by a mechanical taffy puller or a biscuit rolling operation (successive rolling and folding). Batch mixing with no change in gross shape (*Ac*) might be done by shearing the material between a stationary platen and a rotating, parallel platen.

Continuous mixing with continuous change in shape (*Ba*) might be done by flowing the material through a channel of diminishing cross section and finally extruding in the form of fine filaments. A continuous mixer with cyclic change in shape (*Bb*) might consist of something like an extruder with pierced baffle plates mounted periodically along the screw. Finally, a typical continuous mixer with no change in shape (*Bc*) might consist of two coaxial cylinders, one rotating with respect to the other, with material flowing through the annular region between them.

Now let us consider the case of simple shear in a little more detail. Suppose that the initial interfacial surface is oriented in the optimum manner, and that a surface ratio S'/S is required. The corresponding shearing strain is given by Eq. [14]. Assuming that both materials being mixed are Newtonian and have the same viscosity, the power required for mixing is given by

$$P = \frac{\eta Q^2}{V} \left(\frac{S'}{S} - \frac{S}{S'} \right)^2, \quad [21]$$

where η = viscosity, Q = processing rate in volume mixed per unit time, and V = volume being mixed. Thus we see that the power required depends upon the square of the processing rate and the square of the degree of mixing required. This points out the advantage of having the initial interfacial area as large as possible to permit reducing power consumption or increasing output.

This may be carried over to the case of a rotating coaxial cylinder continuous mixer, provided the diameters of the cylinders are large compared with the separation between them. Two things are going on at once. The rotation of one of the cylinders deforms the material in a way which we shall approximate by simple shear. Simultaneously, a pressure gradient along the axis of the annular region is forcing material continuously through the mixer; this problem may be approximated by that of flow between stationary parallel plates. When the materials are Newtonian we can invoke the superposition principle, solve the two problems separately, and combine the results. Before doing so let us make a clear distinction

between mixing flow and transport flow. In principle, transport flow can be used for mixing. However, it will be remembered that one of the conditions for good distribution was that the initial interfacial surface should cut across all the streamlines, with minor exceptions. When the streamlines involved are those used for transport of material this poses a practical problem. The only solution would seem to be to feed the two materials intermittently in sheets, cutting across the streamlines. This procedure is so unattractive that it seems preferable to make it a general rule to keep the mixing streamlines and transport streamlines quite distinct.

In treating the coaxial cylinder mixer it must be remembered that material leaving the mixer at different points on the annular cross section will, in general, have been sheared by different amounts. Let us assume that the initial interfacial surface, or "feed" surface, cuts perpendicularly across the rotatory mixing streamlines. Then the S'/S ratio will be a minimum for material leaving the cross section midway between the cylinders. Specifying that this minimum S'/S shall be equal to the necessary degree of mixing, the power required for mixing is

$$P_M = \frac{9\eta Q^2}{4V} \left[\left(\frac{S'}{S} \right)^2 - 1 \right] \quad [22]$$

and the power required for transport is

$$P_T = \frac{12\eta Q^2}{V} \left(\frac{L}{d} \right)^2. \quad [23]$$

In these equations Q = volume rate of flow through mixer, V = the inventory volume of the mixer, L = length of the cylinders, and d = separation between the cylinders. These are of the same general form as Eq. [21] for simple shear, and the same comments apply here. In addition, we can define a sort of mixing efficiency, as follows,

$$\text{Efficiency} = \frac{P_M}{P_M + P_T} = \frac{1}{1 + \frac{16}{3} \left(\frac{L}{d} \right)^2 \frac{1}{\left[\left(\frac{S'}{S} \right)^2 - 1 \right]}}.$$

Thus, in designing a mixer of this type, one would keep the L/d ratio as small as practical.

Other streamline mixers can also be treated by the type of approach just outlined for these simple examples.

SUMMARY

Turbulence and diffusion are negligible factors in the mixing of liquids of high viscosity. Instead, the mixing must be accomplished by some sort of continuous deformation; this has been called *streamline*

mixing. Such mixing can be considered as consisting of two processes: (a) increasing the surface area of the interface between the liquids being mixed, and (b) distributing that interface throughout the volume of the material. Knowing the initial form of the interfacial surface and the type of deformation, the deformed interfacial surface can be computed. This leads to several general rules on orienting surfaces for efficient creation and distribution of interfacial surface. The advantage of using matrix methods in considering certain types of distribution problems was pointed out. Examples of different types of mixers were given, and one simple type of continuous mixer discussed in more detail.

THE RHEOLOGY OF CARBOXYMETHYLCELLULOSE DISPERSIONS IN WATER ¹

D. L. Salt,² N. W. Ryan and E. B. Christiansen

Department of Chemical Engineering, University of Utah, Salt Lake City, Utah

Received December 12, 1950

INTRODUCTION

The rheology of non-Newtonian fluids is of ever increasing industrial importance. Among the numerous industrial applications is the design of piping systems for non-Newtonian fluids. In this application, the principal problem is that of predicting the pressure loss in a specific piping system for a given flow rate, or that of predicting the flow rate under a fixed pressure differential. Quite satisfactory means for predicting these quantities have been developed for the flow of Bingham-plastic fluids (2).

The work reported here represents the initial part of a research program having as its objective the development of a convenient and accurate pressure drop, flow-rate relationship for pseudoplastic fluids. As in the formulation of the Hagen-Poiseuille equation, a primary requirement in the development of a pressure drop flow-rate relationship is an accurate relationship between the unit shearing stress, f , and the rate of shear, du/dr . This paper presents the initial results of the phase of the program dealing with the $f/(du/dr)$ relationship for pseudoplastic fluids. Theoretical equations for the $f/(du/dr)$ relationship are presented, followed by a description of experimental equipment and procedures used in determining rheological data for two carboxymethylcellulose (CMC) dispersions in water. Finally, experimental verification of the equations is presented.

By definition, pseudoplastic fluids do not have a yield point and the relationship between du/dr and f is approximately exponential at moderate rates of shear and linear at higher rates. Powell and Eyring (3) applied the relaxation theory of viscous flow to pseudoplastic systems by postulating that flow involves the breaking of weak bonds characteristic of Newtonian behavior and strong bonds which cause non-Newtonian behavior at moderate stresses. The shearing stress, f , necessary to produce a given rate of shear is then the sum of the two stresses, the stress, f_1 , required to break the weak bonds, and the stress, f_2 , required to break the

¹ Presented at First Annual Meeting of the West Coast Section of the Society of Rheology, November 4, 1949.

² Present address: Utah Oil Refining Company, Salt Lake City, Utah.

strong bonds.

$$f = f_1 + f_2. \quad [1]$$

According to the relaxation theory of viscous flow (1),

$$du/dr = A \sinh bf, \quad [2]$$

which reduces to

$$du/dr = f/\eta \quad [3]$$

for Newtonian fluids. Hence Eq. [1] becomes

$$f = \eta \frac{du}{dr} + \frac{1}{b} \sinh^{-1} \left(\frac{du/dr}{A} \right). \quad [4]$$

An alternative point of view is that Eq. [2] applies directly, but that the free energy of activation, which is included in A in a factor $e^{-\Delta F^\ddagger/RT}$ is itself a function of the rate of shear. In the case of pseudoplastic fluids, the free energy of activation may change with increased rates of shear due to a change in the orientation, structure, or size of the flow unit, to a change in the average nature of the bonds surrounding the flow unit, to failure of the flow unit to reach equilibrium following motion, or to a combination of these and other factors.

Assuming that ΔF^\ddagger is a linear function of the rate of shear according to the equation,

$$\frac{\Delta F^\ddagger}{RT} = \frac{\Delta F_0^\ddagger}{RT} + b\eta \frac{du}{dr},$$

then Eq. [2] becomes

$$\frac{du}{dr} = A_0 e^{-[b\eta(du/dr)]} \sinh bf,$$

where ΔF_0^\ddagger applies to zero rate of shear and A_0 differs from A in that $e^{-\Delta F_0^\ddagger/RT}$ replaces $e^{-\Delta F^\ddagger/RT}$. Hence,

$$f = \eta \frac{du}{dr} + \frac{1}{b} \ln [\alpha + \sqrt{\alpha^2 + e^{-2y}}], \quad [5]$$

where

$$\alpha = \frac{1}{A_0} \frac{du}{dr}, \text{ and } y = b\eta \frac{du}{dr}.$$

If $y \ll 1$, Eq. [5] becomes identical with Eq. [4]. For the condition that $\alpha^2 \gg e^{-2y}$ in the case of Eq. [5] and $\alpha^2 \gg 1$ in the case of Eq. [4], Eqs. [4] and [5] reduce to

$$f = \eta \frac{du}{dr} + \frac{1}{b} \ln 2\alpha, \quad [6]$$

or

$$f = \eta \frac{du}{dr} + \frac{1}{b} \ln \frac{du}{dr} + B. \quad [7]$$

Powell and Eyring (3) found that Eq. [7] represented the data for a lime-base grease very well. It will presently be demonstrated that these

equations based on the relaxation theory of viscous flow also fit the data for 0.67% and 1.01% dispersions of carboxymethylcellulose in water.

NOMENCLATURE

- A = constant, * sec.⁻¹
 b = constant, * cm.²/dyne
 B = constant*
 η = constant, * dyne-sec./cm.²
 f = total shearing stress, dynes/cm.²
 f_1 = shearing stress acting on type 1 (Newtonian) bonds
 f_2 = shearing stress acting on type 2 (non-Newtonian) bonds
 r = distance, measured along velocity gradient vector, from point in fluid to shearing surface, cm.
 u = fluid velocity at r , cm./sec.
 T = absolute temperature, °K.
 ΔF^\ddagger = free energy of activation, flow process.
 R = gas constant in units of ΔF^\ddagger /°K.

Note: Those constants marked with an asterisk, namely, A , b , B , η , which are characteristic of a fluid may also be functions of temperature and concentration.

EXPERIMENTAL

The equipment used in obtaining the data (4) consisted of a rotating cylinder consistometer, a drawing of which is shown in Fig. 1. The outer

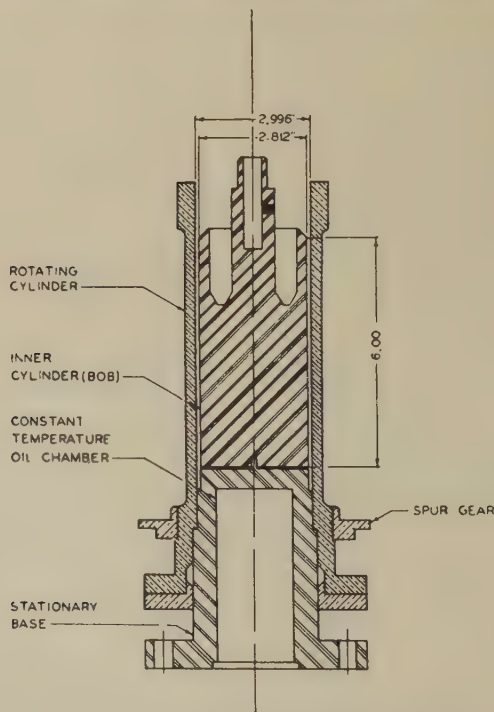


Fig. 1. Cross section of rotating cylinder consistometer.

rotating brass cylinder was driven by a $\frac{1}{4}$ horsepower synchronous motor, through a "Graham" variable speed reducer and spur gears, at speeds varying from 0 to 148 r.p.m. The mild-steel fixed base was machined hollow so that a constant-temperature fluid could be circulated through it.

The inner stationary steel cylinder or "bob" was suspended from a rigid frame by interchangeable torsion wires. These torsion wires were constructed of $\frac{1}{16}$ in. and $\frac{3}{32}$ in. piano wire, both ends of which were soldered into small steel cylinders held rigidly in place in the "bob" and frame by set screws. The length of torsion wire between the steel cylinders in which the ends were soldered was $13\frac{1}{4}$ in.

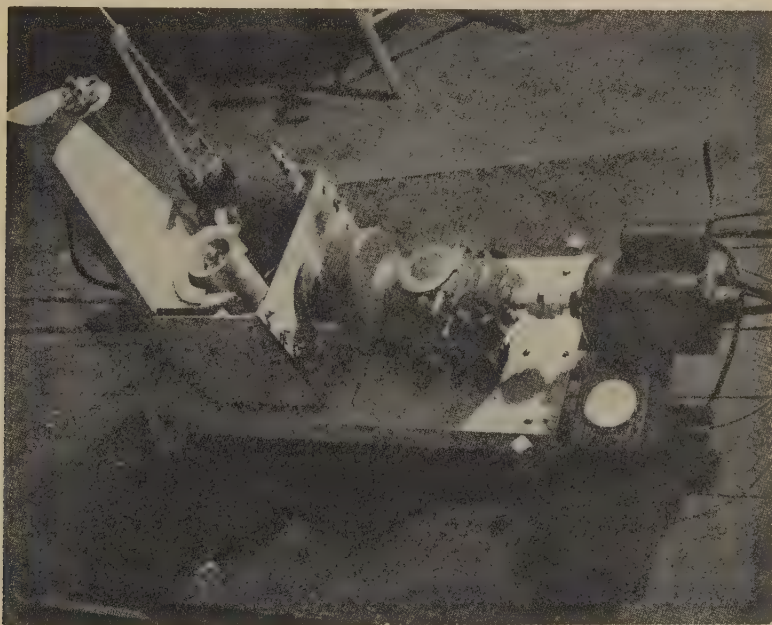


Fig. 2. Consistometer and auxiliary equipment.

Torsion-wire calibrations made before and after the experimental work were identical, indicating that the method of mounting the wires was satisfactory. The angle of rotation of the inner cylinder or "bob" was determined by the position of a needle mounted on the "bob" above a scale mounted on the supporting frame. The rotation rate of the outer cylinder was determined using a stop watch and a revolution counter geared to the cylinder drive. Shearing rates and stresses were then calculated from the deflection angle, the rotation rate, and the constants of the equipment.

A photograph of the assembled consistometer, including the integral constant-temperature oil bath and other accessories, is shown in Fig. 2. The temperature of the thoroughly agitated oil bath was maintained constant within $\pm 0.1^\circ\text{C}$. by means of a water-cooling coil and an immersion heater, the latter controlled by a mercury thermostat through a relay.

In preliminary tests, the viscosities of two standardized oils, as determined by this instrument, were found to be within $\pm 1.8\%$ of their values as reported by the National Bureau of Standards. Also, at a constant rotational speed it was found that the "bob" deflection was a linear function of the fluid depth, which indicated that within the accuracy of the measurements, the end effect had been eliminated.

TABLE I
Experimental Data
Fluid: 0.67% carboxymethylcellulose

f dynes/cm. ² 27.9°C.	du/dr sec. ⁻¹	f dynes/cm. ² 33.8°C.	du/dr sec. ⁻¹
26.3	21.2	21.8	21.0
51.9	55.4	45.1	55.7
80.4	101.2	72.2	100.2
102.2	138.8	111.2	180.4
133.0	193.8	136.8	246.0
154.8	247.7	112.7	190.6
121.0	175.0	73.7	108.5
85.7	109.4	41.3	47.5
38.3	36.8		
36.8°C.		41.0°C.	
23.3	24.0	27.8	37.5
48.9	66.3	50.4	83.9
70.6	112.8	72.2	131.5
95.5	168.0	93.2	189.3
117.3	221.6	112.7	240.6
127.0	247.2	116.5	248.9
106.0	193.8	94.7	191.4
73.7	116.2	66.9	120.3
31.6	37.5	33.8	45.5

The two fluids studied were prepared by mixing a sodium salt of high viscosity, carboxymethylcellulose (CMC), donated by the Hercules Powder Company, and Salt Lake City tap water in the proper proportions to yield 0.67% and 1.01% dispersions by weight.

Data-taking cycles were completed for each fluid at each of four different temperatures. In each cycle, the speed of rotation of the outer cylinder was increased in steps to the maximum and then reduced in similar steps, measurements being made at each consecutive step. This

procedure was followed to determine the extent of hysteresis, if any. No hysteresis effect was observed.

Values of the shearing stress, f , and the rate of shear, du/dr , calculated from the data are presented in Tables I and II.

TABLE II
Experimental Data
Fluid: 1.01% carboxymethylcellulose

f dynes/cm. ² 28.0°C.	du/dr sec. ⁻¹	f dynes/cm. ² 32.2°C.	du/dr sec. ⁻¹
30.1	6.2	36.8	10.4
65.3	19.1	65.3	23.2
108.9	38.9	119.0	52.7
147.2	59.4	162.0	84.9
194.6	96.3	214.0	127.0
229.3	122.0	261.0	174.0
273.4	159.0	324.0	244.0
324.4	214.8	275.0	191.0
352.8	246.7	224.0	140.0
297.9	188.6	130.0	62.8
227.4	123.6	48.1	15.4
168.9	78.5	23.5	5.5
95.5	35.7		
41.4	10.4		
36.6°C.		42.2°C.	
20.3	5.6	27.8	10.3
61.6	24.9	65.3	34.5
95.5	47.1	108.9	67.2
153.3	90.7	148.8	107.8
207.8	138.5	186.5	149.2
238.1	177.7	224.4	198.6
275.4	222.1	263.6	244.1
296.0	246.6	241.1	217.2
252.8	196.0	198.0	165.0
207.8	144.3	129.4	86.2
129.2	73.8	80.5	45.7
75.2	35.1	38.3	15.5
33.8	9.9		

Experimental points, for the highest and lowest temperatures for each fluid, are compared graphically with Eq. [4], represented by the solid lines, in Figs. 3 and 4. It is evident from these figures that the data can be satisfactorily represented by Eq. [4]. Experimental values of f for the 1.01% CMC dispersion at 314.2°K. are compared with those calculated using Eqs. [4], [5], and [6] in Table III. These equations appear to be equally satisfactory with the exception of Eq. [6] at low shear rates.

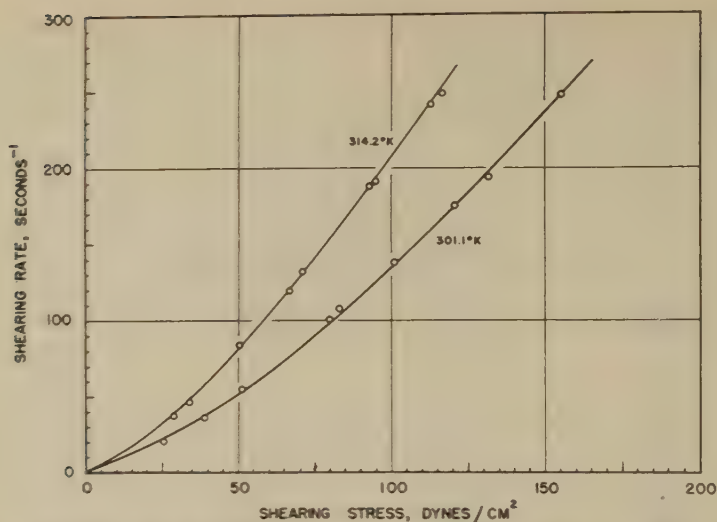


FIG. 3. Shearing stress-shearing rate data for 0.67% suspension of CMC in water.

Constants for Eqs. [4] and [6] are tabulated in Tables IV and V. Although the constants for Eq. [4] appear to be consistent and to show trends, it is believed that data covering larger temperature ranges and higher CMC concentrations should be studied before conclusions can be safely reached regarding the variation of the constants with temperature

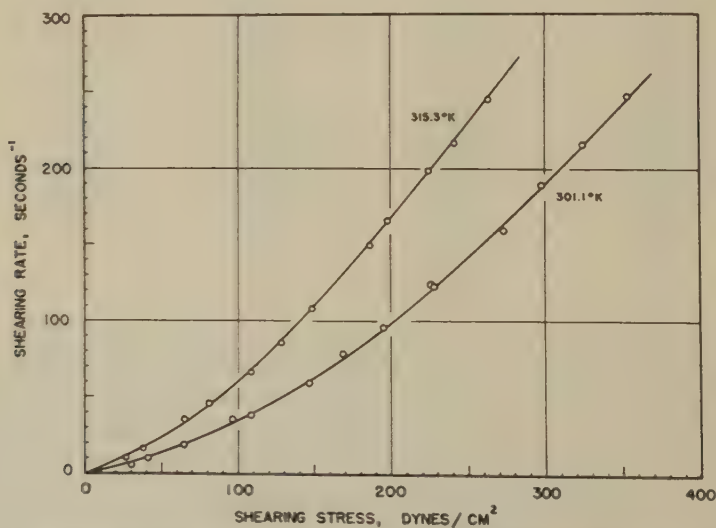


FIG. 4. Shearing stress-shearing rate data for 1.01% suspension of CMC in water.

TABLE III

Comparison of Equations [4], [5] and [6]

Run 4.

Temperature: 315.3°K.

Fluid: 1.01% (wt.) sodium carboxymethylcellulose.

du/dr	f , dynes/cm. ²			
	Experimental ^a	Calculated by		
		Eq. [4]	Eq. [5]	Eq. [6]
sec. ⁻¹				
10	26	24.7	22.7	14.8
30	60	61.3	60.2	60.1
60	100	100	100	100
120	159	160	160	160
180	211	211	211	211
240	259	260	259	259

^a Smoothed data.

TABLE IV

Constants for Equation [4]

$$f = \eta \frac{du}{dr} + \frac{1}{b} \sinh^{-1} \frac{du}{dr} \frac{1}{A}$$

0.67% CMC in water

Temp. °K.	A	b	η
301.1	19.4	0.0563	0.394
307.0	18.7	0.0716	0.378
309.9	18.3	0.0797	0.337
314.2	21.6	0.0777	0.302

1.01% CMC in water

Temp. °K.	A	b	η
301.1	22.5	0.0167	0.691
305.4	21.0	0.0204	0.701
309.7	19.1	0.0248	0.678
315.3	15.0	0.0349	0.667

and concentration. Little significance can be attached to the decrease of A with increasing temperature shown for the 1.01% dispersion in Table IV. For this dispersion and within the limits of experimental error, it is possible to obtain another set of values for b (of about the same magnitude and showing a similar but less pronounced temperature dependence) for which the corresponding values of A (of about the same magnitude) show the opposite trend with increasing temperature. Data on higher

TABLE V
Constants for Equation [6]

$$f = \eta \frac{du}{dr} + \frac{1}{b} \ln \frac{du/dr}{B'}$$

0.67% CMC in water

Temp. °K.	B'	b	η
301.1	7.36	0.0637	0.404
307.0	7.67	0.0770	0.382
309.9	8.01	0.0849	0.345
314.2	8.24	0.0911	0.313

1.01% CMC in water

Temp. °K.	B'	b	η
301.1	9.10	0.0183	0.701
305.4	8.99	0.0222	0.728
309.7	13.2	0.0193	0.587
315.3	7.29	0.0352	0.667

CMC concentrations may make it possible to distinguish between Eqs. [4] and [5] and thus contribute to the picture of the flow mechanism.

CONCLUSIONS

It has been demonstrated that equations based on the relaxation theory of viscous flow accurately represent the pseudoplastic $f / \frac{du}{dr}$ relationship for 0.67% and 1.01% dispersions of carboxymethylcellulose (CMC) in water in the temperature range of 300 to 315°K.

Also, it is believed that these equations are suitable as a basis for the development of a convenient and reliable method for predicting pressure losses in the pseudoplastic flow of fluids in pipes.

REFERENCES

1. GLASSTONE, S., LAIDLER, K. J., AND EYRING, H., *Theory of Rate Processes*, pp. 480-483. McGraw-Hill, New York, 1941.
2. McMILLEN, E. L., *Chem. Eng. Progress* **1**, 537 (1948).
3. POWELL, R. E., AND EYRING, H., *Nature* **154**, 429 (1944).
4. SALT, D. L., *Pressure Losses in the Flow of a Pseudoplastic Fluid*. M. S. Thesis, University of Utah, 1949.

DIELECTRICS AND RHEOLOGY OF DISPERSED MAGNETIZED PARTICLES ¹

Andries Voet and Louis R. Suriani

Research Department, Ink Division, J. M. Huber Corporation, New York, New York

Received November 13, 1950

I. INTRODUCTION

In a previous paper it was shown (1) that the dielectric constant of a dispersion is closely connected with the shape and the orientation of its particles. It was demonstrated that application of shear to more concentrated dispersions may result in a marked decrease of the dielectric constant, a change attributed to the breaking-up of particle aggregates. In addition, it was shown that orientation of nonspherical particles may cause changes in the dielectric constant. It appeared that the orientation of such particles perpendicular to the direction of the electric measuring field caused a decrease in the dielectric constant, in agreement with theoretical considerations of Bruggeman (2).

Rheological investigations showed that in the absence of particle agglomeration and/or orientation, a Newtonian flow pattern exists. Non-Newtonian behavior becomes apparent where agglomeration and/or orientation occurs.

In more concentrated dispersions particle agglomeration usually occurs. Rheological investigations often fail to reveal this condition since the shearing required for the measurements generally breaks up the existing structures. Dielectric measurements carried out in solutions in a quiescent condition are more suitable for revealing the formation of particle agglomeration.

II. MAGNETIZED IRON DISPERSIONS

Attempts were made to obtain a more direct experimental evidence of the correlation between dielectric constant, particle agglomeration, and orientation. This was done by selecting a disperse system which could be changed at will from a nonagglomerating to a strongly agglomerating system, and vice versa.

The materials selected for the dispersion were the fairly uniform and perfectly spherical iron particles prepared by thermal decomposition of

¹ Presented at the Annual Meeting of the Society of Rheology, New York, N. Y. November 3-4, 1950.

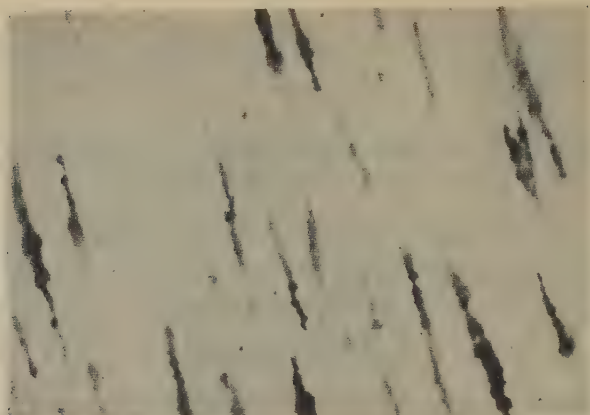


FIG. 1.

iron carbonyl in the gas phase. The fraction selected had an average particle size of $3\ \mu$. The globules were dispersed by thorough agitation, in a concentration of 30% by weight, in a heated mixture of equal parts by weight of a viscous white mineral oil and oleic acid dimer, a vehicle chosen for its excellent dispersing characteristics for the iron particles. The system formed was rather stable, showing some settling after a few hours, without flocculation. Slight agitation restored the original condition.

The dispersion was examined microscopically in a 20-fold dilution with the vehicle, to allow a proper observation by means of the hanging-drop method. The spherical particles were easily observed and were found to move freely in the liquid. Double and triple complexes could be seen at this dilution (Fig. 1, enlargement 500 \times).

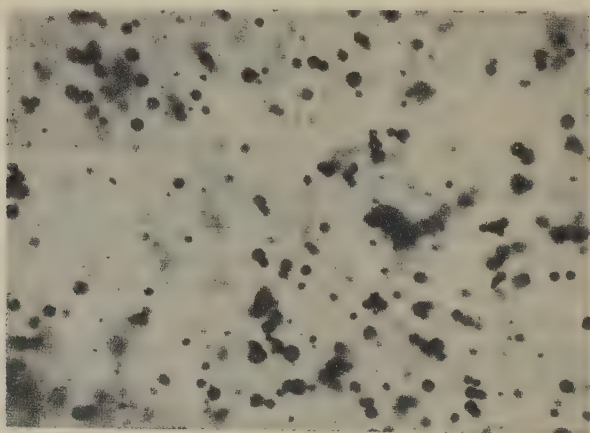


FIG. 2.

Upon bringing the dispersion in the field of a small Alnico permanent magnet, however, remarkable changes occur. The iron globules, having become magnetic, rapidly join together and form long, perfectly linear particle chains, strongly suggesting the image of stretched linear polymers (Fig. 2, enlargement 500 \times). These chains, in turn, are all orientated along the magnetic lines of force and follow a change in their direction. Upon removing the field, however, it appears that there is enough residual magnetism left in the particles to cause the "linear polymers" to remain in existence, although they rapidly lose their orientation and change into a random distribution of the chain direction (Fig. 3, enlargement 500 \times). They can be brought back into the original condition by agitation, indicating that the residual magnetism is apparently insufficient to re-form the particle chains in the absence of a magnetic field.

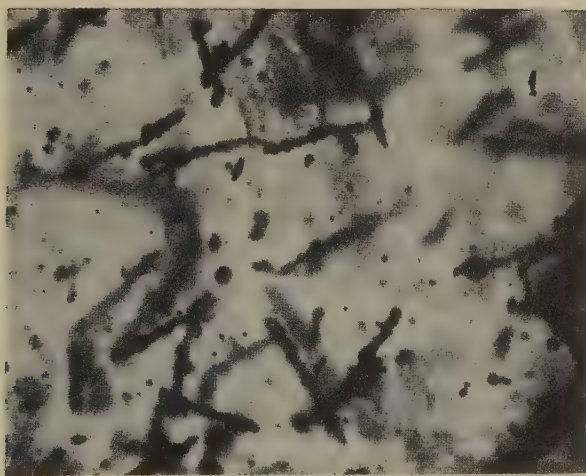


FIG. 3.

It is apparent that the simple dispersion of spherical iron globules is able to exist in different conditions of agglomeration and orientation, each of which is expected to be characterized by a different dielectric constant and by different rheological characteristics.

They are as follows:

Type A

This type is represented by the original, unmagnetized, "virgin" dispersion, shown in Fig. 1, in a quiescent condition. Most of the particles are single, but some agglomeration occurs, which is more pronounced in more concentrated dispersions.

Type B

This condition is found when the "virgin" dispersion is subjected to shear. The agglomerates are then broken up and generally single spherical particles are present at higher shear.

Type C

This type is the magnetized dispersion in the absence of an outside magnetic field, where the particle chains are orientated at random, as shown in Fig. 3.

Type D

The magnetized particle chains of the dispersion are orientated in a magnetic field, as is shown in Fig. 2.

Type E

The magnetized dispersion is subjected to shear in the magnetic field. This may destroy the structures partly or completely, depending upon the rate of shear. A return in the direction of type *B* may be expected.

III. THE RHEOLOGY OF MAGNETIZED IRON DISPERSIONS

Fig. 4 shows the rheological diagrams obtained with the unmagnetized and magnetized iron particles. The measurements are equilibrium data obtained with the aid of a precision rotational viscometer (3), in the absence of a magnetic field.

It appears that the rheological data indicate an identical Newtonian behavior, with a viscosity of 12.0 poises at 30°C., for both dispersions.

In view of the structures observed microscopically in the magnetized

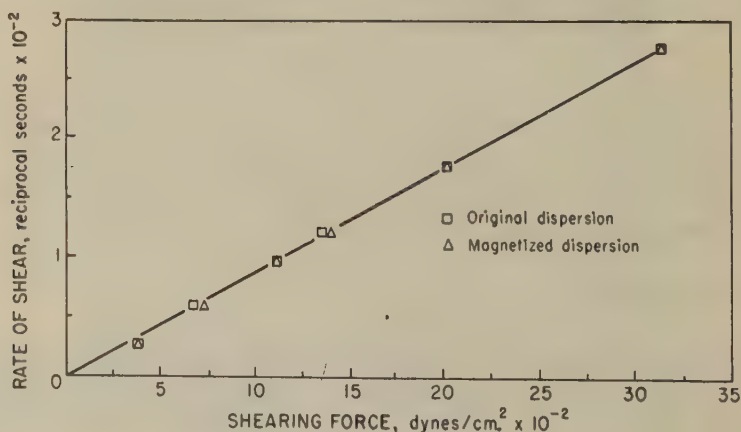


FIG. 4.

dispersions, a Newtonian behavior is unlikely. Upon further microscopic observation it appears that the original structure is eliminated in the viscometer, even at the lowest measurable shear applied. It is thus apparent that the rheological method is not very well suitable to detect changes in particle structure, since the measurement itself destroys the effect which it is intended to measure.

The influence of a magnetic field on the viscosity of the dispersion, however, is very pronounced. While it was impossible to apply a magnetic field to the dispersion in the rotational viscometer in our arrangement, due to the interaction of the steel parts of the instrument in the presence of a magnetic field, flow tests were made in a glass tube held between the poles of a magnet.

About 10 ml. of the dispersion of iron particles was poured into a cylindrical glass tube of about 8 mm. inner diameter, open on both ends, and placed in the field of a small Alnico magnet above the lower end. It was noticed that the liquid did not pass the field of the magnet by gravity flow, as it would do instantaneously in the absence of the magnetic field. Upon prolonged standing, vehicle separation was observed and oil drops were slowly released at the end of the tube, but the pigment held its position in the magnetic field, orientated along the magnetic lines of force.

Air pressure was then applied and increased slowly. At a pressure of about 5 cm. mercury the liquid moved slowly and continued its flow, notwithstanding the presence of a magnetic field. Thus the minimum pressure necessary to cause flow, corresponding to a yield value, is about 5 cm. mercury, equivalent to 6.8×10^4 dynes/cm.². Thus, there appears to be a striking change from Newtonian to non-Newtonian flow in a dispersion of iron particles upon application of a magnetic field.

IV. THE DIELECTRICS OF MAGNETIZED IRON DISPERSIONS

We have attempted to measure the dielectric constants of the dispersion in the various conditions described. Measurements were made by means of a Schering bridge, at 3000 cycles/sec., allowing an accuracy of $\pm 0.2\%$. Measurements in quiescent solutions were made in a conventional three-electrode cell, while measurements under shear were made in a double cylindrical cell, the outside cylinder of which was rapidly rotated. The maximum rate of shear obtained was 650 sec.⁻¹.

The resistivity of these dispersions was of the order of 10^{12} ohms/cm.³. Complications due to dielectric losses were thus avoided. All measurements were made at 25°C., thermostatically controlled.

The magnetic field was produced by introducing the permanent Alnico magnet near the cell. The results obtained are shown in Table I.

TABLE I
Data Summary

Type	Disperison	State of motion	Magnetic field	Dielectric constant
A	Original "virgin"	Quiescent	Absent	2.82
B	Original "virgin"	Sheared	Absent	2.71
C	Magnetized	Quiescent	Absent	3.06
D	Magnetized	Quiescent	Parallel to electric field	3.33
E	Magnetized	Sheared	Parallel to electric field	2.71

It appeared impossible to obtain an orientation of the particles perpendicular to the electric field in our arrangement.

Upon withdrawal of the magnet in the magnetized type *D* dispersion, the parallel-chain orientation changes into the random distribution of type *C*. A relaxation time of about 3 min. was observed for this change.

Upon discontinuation of shear in the unmagnetized type *B* dispersion, a return to the partly agglomerated type *A* condition was observed. The relaxation item for this change was about 20 sec.

V. DISCUSSION

The above experiments appear to confirm the views previously expressed (1). Both orientation as well as agglomeration of particles are reflected in the dielectric constant of the dispersion.

The anticipated differences in dielectric constant clearly exist between the single unmagnetized particles and the agglomerated magnetized particles of the dispersions.

In addition, it was observed that particle orientation markedly affects the dielectric constant. In accordance with Bruggeman's theory the highest value of the dielectric constant was found where the particles were orientated in the direction of the electric field, which occurs when electric and magnetic fields coincide in direction, as in type *D*.

The lowest value of the dielectric constant, lower even than for random orientation, is expected for particles orientated perpendicular to the electric field, a condition which could not be realized in our apparatus.

From the above it appears that the dielectric constant is a direct and sensitive reflection of the inner structure of a dispersion. Rheological characteristics, requiring shear, cannot reveal structures existing nearly exclusively in quiescent summary dispersions.

SUMMARY

A dispersion of iron globules in a nonaqueous vehicle showed only little particle agglomeration. When placed in a magnetic field, however,

the particles showed strong agglomerating tendencies, leading to the formation of linear particle chains. These chains are orientated in a magnetic field, but show a random orientation in the absence of a magnetic field.

Dielectric characteristics gave a more accurate picture of the inner structure of the dispersion than did rheological data, since the shear necessarily applied in the latter case destroys the particle agglomeration.

REFERENCES

1. VOET, A., *J. Phys. & Colloid Chem.* **51**, 1037 (1947).
2. BRUGGEMAN, D. A. G., *Ann. Physik* **24**, 636 (1935).
3. BUCHDAHL, R., *et al.*, *Rev. Sci. Instruments* **18**, 168 (1947).

THE VISCOSITY OF A CONCENTRATED SUSPENSION OF SPHERICAL PARTICLES¹

M. Mooney

General Laboratories of the United States Rubber Company, Passaic, New Jersey²

Received November 13, 1950

ABSTRACT

Einstein's viscosity equation for an infinitely dilute suspension of spheres is extended to apply to a suspension of finite concentration. The argument makes use of a functional equation which must be satisfied if the final viscosity is to be independent of the sequence of stepwise additions of partial volume fractions of the spheres to the suspension. For a monodisperse system the solution of the functional equation is $\eta_r = \exp\left(\frac{2.5\phi}{1 - k\phi}\right)$, where η_r is the relative viscosity, ϕ the volume fraction of the suspended spheres, and k is a constant, the self-crowding factor, predicted only approximately by the theory. The solution for a polydisperse system involves a variable factor, λ_{ij} , which measures the crowding of spheres of radius r_i by spheres of radius r_j . The variation of λ_{ij} with r_i/r_j is roughly indicated. There is good agreement of the theory with published experimental data.

INTRODUCTION AND THEORY

Since the publication of Einstein's basic analysis of the viscosity of a dilute suspension of rigid spheres in a viscous liquid, numerous equations have been developed in efforts to extend Einstein's formula to suspensions of higher concentrations (1-4). The various resulting formulas differ considerably from each other; and no one of them agrees with both sets of experimental data discussed later in this paper. Some papers deal with nonspherical particles, or with nonrigid particles such as dissolved polymer molecules.

The present analysis is limited to rigid, spherical particles. Also, the approach is partly empirical in that the interaction parameters are left for experimental determination, no effort being made to obtain their values from hydrodynamic theory. What the present analysis does consider is the space-crowding effect of the suspended spheres on each other; and there is no restriction imposed on the concentration or particle size distribution.

The Crowding Factor

The Einstein viscosity equation postulates a suspension so dilute that there is no appreciable interaction between the spheres. In extending this

¹ Presented at the Annual Meeting of the Society of Rheology, New York, N. Y., November, 3-4, 1950.

² Contribution No. 113.

equation to higher concentrations, we must take into account at least the first-order interaction. We may describe this interaction as essentially a crowding effect. That is, in a two-component system, for example, spheres of size r_1 and partial volume concentration ϕ_1 crowd spheres of size r_2 into the remaining free volume $1 - \lambda_{12} \phi_1$. The crowding factor, λ_{12} , may be different from unity as will be explained later.

We assume that λ_{12} is a function of the ratio r_1/r_2 , but is independent of the value of ϕ_i . In making this assumption we are neglecting second and higher order interactions. We shall use k to denote the particular value λ_{ii} , the self-crowding factor.

Monodisperse Suspension of Finite Concentration

If spheres all of radius r_1 are added to a suspension in two volume fractions ϕ_1 and ϕ_2 , the addition of the first fraction will increase the viscosity by a factor $H(\phi_1) = \frac{\eta_1}{\eta_0}$. All we know at present concerning H is that it must reduce to Einstein's formula for the relative viscosity at small values of ϕ_1 .

If the second fraction, ϕ_2 , is now added, there will be a further increase in viscosity. Part of this increase we may consider as being an increase, caused by ϕ_2 , in the viscosity of the remaining liquid in the space not occupied by ϕ_1 . This increase will therefore be of the form $H(\psi_{21})$, where $\psi_{21} = \frac{\phi_2}{1 - k\phi_1}$ is the concentration of ϕ_2 in this remaining liquid, allowance being made for a crowding factor, k , different from unity.

But the crowding of fractions ϕ_1 and ϕ_2 being mutual, introducing ϕ_2 reduces the free volume accessible to ϕ_1 , and the effective concentration of ϕ_1 in the liquid is then $\psi_{12} = \frac{\phi_1}{1 - k\phi_2}$. To take account of this effect we must now replace $H(\phi_1)$ by $H(\psi_{12})$. The product $H(\psi_{12}) \times H(\psi_{21})$ is the viscosity of a suspension of total concentration, $\phi_1 + \phi_2$, and hence this product must be equal to $H(\phi_1 + \phi_2)$. This is

$$\begin{aligned} H(\phi_1 + \phi_2) &= \frac{\eta_{12}}{\eta_0} = H(\psi_{12}) \times H(\psi_{21}) \\ &= H\left(\frac{\phi_1}{1 - k\phi_2}\right) \times H\left(\frac{\phi_2}{1 - k\phi_1}\right). \quad [1] \end{aligned}$$

It is found that this functional equation is satisfied if H has the form

$$H(x) = \exp\left(\frac{2.5x}{1 - kx}\right). \quad [2]$$

$H(x)$, in conventional terminology, is the relative viscosity, η/η_0 . The constant 2.5 is chosen to agree with Einstein's equation for very dilute

suspensions, when ϕ approaches zero. To check Eq. [2] mathematically, it can be verified that

$$\begin{aligned} \exp\left(\frac{2.5\phi}{1-k\phi}\right) &\equiv \exp\left[\frac{2.5(\phi_1 + \phi_2)}{1-k(\phi_1 + \phi_2)}\right] \\ &\equiv \exp\left[\frac{2.5\left(\frac{\phi_1}{1-k\phi_2}\right)}{1-k\left(\frac{\phi_1}{1-k\phi_2}\right)}\right] \exp\left[\frac{2.5\left(\frac{\phi_2}{1-k\phi_1}\right)}{1-k\left(\frac{\phi_2}{1-k\phi_1}\right)}\right]. \quad [3] \end{aligned}$$

More generally, if ϕ is divided into n small fractions, it is easily verified that

$$\exp \frac{2.5\phi}{1-k\phi} \equiv \prod_1^n \exp \left[\frac{\frac{2.5\phi_i}{1-k(\phi-\phi_i)}}{\frac{k\phi_i}{1-k(\phi-\phi_i)}} \right]. \quad [4]$$

Suspension of Spheres of Two Different Diameters

For spheres of different diameters, the crowding factor will be different from k , and will be different, also, depending on which spheres are considered as being crowded, the large ones or the small ones. Hence in modifying the right-hand member of Eq [3] to fit this case, we must substitute $\lambda_{21} \phi_2$ for $k\phi_2$ in the first exponential term, and $\lambda_{12} \phi_1$ for $k\phi_1$ in the second exponential. Simplification of the resulting expression then leads to

$$H(\phi_1 + \phi_2) = \exp\left(\frac{2.5\phi_1}{1-k\phi_1-\lambda_{21}\phi_2}\right) \times \exp\left(\frac{2.5\phi_2}{1-k\phi_2-\lambda_{12}\phi_1}\right). \quad [5]$$

Polydisperse Suspension

If we have a suspension of n groups of spheres, each group of a different diameter, we may write, by extension of Eq. [5],

$$\ln H(\phi) = 2.5 \sum_{i=1}^n \frac{\phi_i}{1 - \sum_{j=1}^n \lambda_{ji}\phi_j}. \quad [6]$$

For a continuous distribution of diameters, Eq. [6] becomes in the limit

$$\ln H(\phi) = 2.5 \int_0^\phi \frac{d\phi_i}{1 - \int_0^\phi \lambda_{ji} d\phi_j}. \quad [7]$$

Let

$$\begin{cases} \sigma = \ln \frac{r}{\bar{r}}, \\ d\phi = P(\sigma)d\sigma, \\ \int_{\sigma_1}^{\sigma_2} P(\sigma)d\sigma = 1, \end{cases} \quad [8]$$

where \bar{r} is a mean radius, defined anyhow, and σ_2 and σ_1 are the upper and lower limits of σ . Then Eq. [7] takes the form,

$$\ln \frac{\eta}{\eta_0} = \ln H = 2.5\phi \int_{\sigma_1}^{\sigma_2} \frac{P_i d\sigma}{1 - \phi \int_{\phi_1}^{\sigma_2} \lambda_{ji} P_j d\sigma}. \quad [9]$$

With regard to the physical significance of the preceding equation, it may be clarifying to point out that the first integral sign does not represent the successive additions of the different components of the suspended material. Rather, it represents the successive evaluations of the effects of the different components, each component operating in the presence of all of the other components.

$$\text{Properties of } \lambda_{ij} \left(\frac{r_i}{r_j} \right)$$

While there will be no attempt here to determine by theoretical analysis the precise properties of λ_{ij} as a function of the radius ratio, $\rho_{ij} = r_i/r_j$, we can easily deduce certain important features of this function. For the case $\rho_{ij} \rightarrow 0$, $\rho_{ji} \rightarrow \infty$, the suspension of the small spheres in the liquid between the large spheres behaves towards the large spheres like a homogeneous liquid of increased viscosity. Hence the large spheres are not crowded at all by the small ones; and the small spheres are crowded into the space left unoccupied by the large ones. Therefore

$$\lim_{\rho_{ij} \rightarrow 0} \lambda_{ij} = 0, \quad [10]$$

$$\lim_{\rho_{ij} \rightarrow \infty} \lambda_{ij} = 1, \quad [11]$$

If we use these values of λ_{ij} in Eq. [5], letting ϕ_1 be the component of small radius and ϕ_2 the component of large radius, we find

$$\eta = \eta_0 \exp \frac{2.5\phi_1}{1 - k\phi_1 - \phi_2} \exp \frac{2.5\phi_2}{1 - k\phi_2}. \quad [12]$$

The same equation can be obtained from two applications of Eq. [2], if we recognize only that the volume accessible to the fraction ϕ_1 is $1 - \phi_2$. Thus Eqs. [10] and [11] are checked.

The value of λ_{ij} , or k , is obviously of considerable importance. We can make a rough estimate of k from the following considerations. Densely packed spheres, in a face-centered cubic lattice, for example, would exhibit infinite viscosity, simply because of mechanical interlocking. The fractional volume, ϕ_c , of the spheres in such packing is 0.74. Hence, if $H(\phi_c)$ by Eq. [2] is to be infinite, we must have

$$k \doteq 1/0.74 = 1.35. \quad [13]$$

This method of estimating k gives a lower limit. A rough estimate of an upper limit can be similarly obtained by assuming that the densest packing which will permit continuous movement is simple cubic. For this case $\phi_c = \pi/6$, and

$$k \doteq 6/\pi = 1.91. \quad [14]$$

From this purely geometric argument we therefore conclude that

$$1.35 < k < 1.91. \quad [15]$$

This simple analysis of space-filling and crowding action at high concentrations does not in itself prove much about the value of k at low

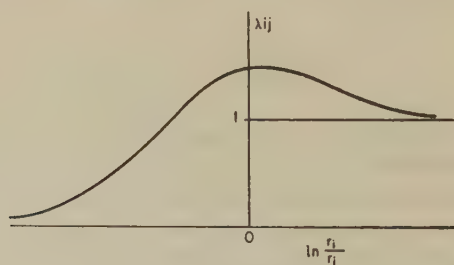


FIG. 1. Properties of λ_{ij} , the effective crowding of spheres of radius r_j by spheres of radius r_i .

concentrations. However, space-filling action cannot vary greatly with concentration, and if the associated crowding action is a major part of particle-to-particle hydrodynamic interaction, then we may expect that k will vary only slightly with ϕ , if at all, and will have a value of approximately 1.5. Presumably the function $\lambda_{ij}(\rho_{ij})$ has a maximum at or near $\rho_{ij} = 1$.

The properties of λ_{ij} , so far as they have been deduced, are shown in Fig. 1.

EXPERIMENTAL CHECK

The above theory provides three equations, [2], [5], and [9] or [6], by which the theory can be tested. Unfortunately the published literature does not provide the data necessary for rigorous tests of the more general equations. Relatively little work has been done at high concentrations of

rigid suspended spheres; and the control of particle diameter leaves much to be desired. Particles small enough to form colloidal solutions are increased in size by an adsorbed stabilizing layer of unknown thickness.

The best experimental data for testing Eq. [2] are those published by V. Vand (3) on nearly monodisperse suspensions of glass spheres, of diameters ranging from 0.010 to 0.016 cm. His suspension medium was an equally dense solution of zinc iodide in a mixture of water and glycerol.

The upper curve of Fig. 2 shows Vand's data for relative viscosity, η_r , or in our notation, $H(\phi)$, plotted against ϕ . The curve fitted to these points represents Eq. [2] with $k = 1.43$. The agreement seems to be within experimental error over the full range of the data. The two branches of the experimental curve above $\phi = 0.35$ represent two variations in experimental technique. Curve *S* was obtained by stirring the suspension immediately before measuring; curve *N* by not stirring.

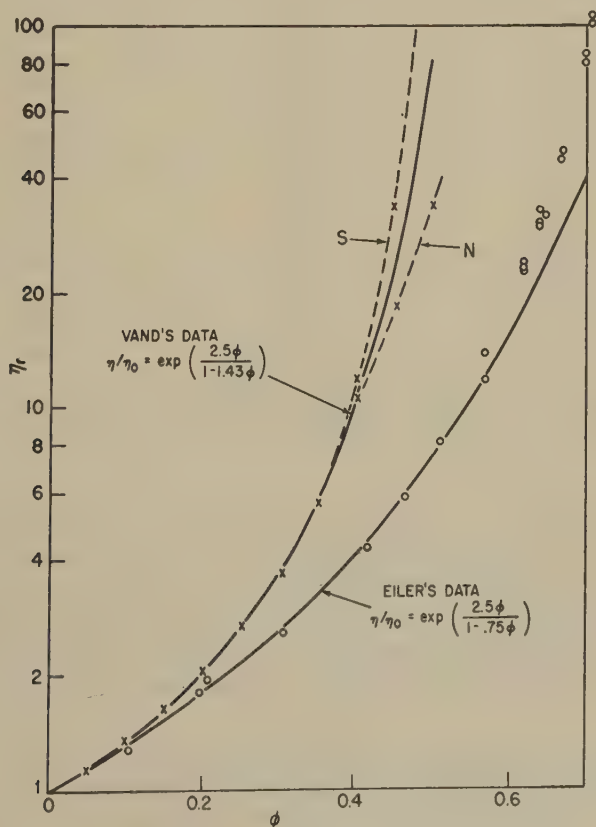


FIG. 2. Theoretical curves fitted to experimental data by Vand (x) and by Eilers (o).

The comparison between observed and calculated viscosity is shown more exactly in Table I.

This experimental test of the theory shows that, in spite of the slight spread in diameter of Vand's glass spheres, the theoretical equation fits the data with a constant value of k over the total variation in ϕ from 0 to 0.5. Furthermore, the value of k comes within the limits set by the inequalities (see Eq. [15]).

H. Eilers (5) has published a series of viscosity measurements on concentrated emulsions of a bituminous material of high softening point, such that at room temperature the droplets were essentially rigid. The

TABLE I
Vand's Data: Observed and Calculated^a

Concentration ϕ , %	η_r (obs.)	η_r (calcd.)
0	1.000	1.000
5	1.145	1.144
10	1.342	1.340
15	1.621	1.613
20	2.024	2.016
25	2.632	2.648
30	3.636	2.716
35	5.556	1.75
40N	10.53	10.36
40S ^b	11.77	10.36
45N ^b	18.18	23.48
45S ^b	33.33	23.48
50N ^b	33.33	80.35
50S ^b	200.00	80.35

^a Calculations by the formula $\ln \eta_r = \frac{2.5\phi}{1 - 1.43\phi}$.

^b S signifies that suspension was stirred just before being measured; N signifies not stirred.

diameters varied from 1.6 to 4.7 μ , except for about 1% by volume of diameter less than 1.6 μ . The emulsions must therefore be considered as polydisperse. If we knew the λ_{ij} function in detail, and if we knew the $P(\sigma)$ function for Eilers' material, we could then use Eq. [9] to express the viscosity as a function of the concentration. Lacking this information, we proceed to develop Eq. [9] as a power series in ϕ , obtaining

$$\ln \frac{\eta}{\eta_0} = 2.5\phi \left[1 + \sum_1^{\infty} \phi^n \lambda_n \right], \quad [16]$$

where

$$\lambda_n = \int_{\sigma_1}^{\sigma_2} P_i \left[\int_{\sigma_1}^{\sigma_2} \lambda_{ji} P_j d\sigma \right]^n d\sigma. \quad [17]$$

To the second degree in ϕ , Eq. [16] may be written

$$\ln \frac{\eta}{\eta_0} = \frac{2.5\phi}{1 - \lambda_1\phi}, \quad [18]$$

which is of the same form as Eq. [2]. The lower curve in Fig. 2 shows Eilers' data, and also Eq. [18] with $\lambda_1 = 0.75$. The agreement is quite satisfactory in view of the fact that Eq. [18] is only an approximation, not expected to be valid at high concentrations. The fact that λ_1 (Eilers) $< k$ (Vand) also is in agreement with the theory.

DISCUSSION

The crowding theory of viscosity that has been presented here yields an equation for the relative viscosity of a monodisperse suspension of spheres which agrees with the best published experimental data over the full concentration range from 0 to 0.5. In addition to the Einstein coefficient for dilute suspensions, the equation involves one adjustable parameter which is correctly predicted as to order of magnitude. In view of this success of the theory, the conclusion seems justified that the interaction between the spheres in a suspension is primarily the simple geometric crowding action which is the basis of the theory. The mutual disturbance of flow lines around two near particles is therefore a matter of secondary importance.

From Eqs. [17] and [18], and also from the two curves in Fig. 2, it is clear that the second-degree coefficient in the viscosity-concentration equation must be a function of the particle size distribution. This is a point which has been ignored in other published theories. For example, we have the following paradoxical situation. In de Bruijn's theory of viscosity (1) an unknown parameter is determined by assuming infinite viscosity for a suspension of spheres of volume concentration 0.74, corresponding to close packing of spheres of uniform size (just as, for example, we obtained Eq. [13] above). De Bruijn's fluidity formula was found to give excellent agreement with Eilers' data on bitumen suspensions. We would here consider these suspensions to be polydisperse systems, and would not expect good agreement. De Bruijn's formula should agree, on the other hand, with Vand's data, published in 1947; but the disparity between the two curves of Fig. 2 above shows that de Bruijn's formula agreeing with Eilers' data could not agree with Vand's data.

Presumably the equations of the present theory could be elaborated to apply to other than rigid, spherical particles; but before such an extension of the theory is attempted it would be desirable to have the necessary experimental data for a rigorous test of the theory as it now stands. This requires close control of particle size, and measurements on single-

dual-, and multiple-component suspensions covering a wide range of particle diameters and concentrations.

While this manuscript was in preparation a recent paper by James V. Robinson (6) came to the writer's attention. Robinson measured the viscosities of suspensions of glass spheres in S. A. E. No. 30 motor oil, S. A. E. No. 50 motor oil, castor oil, ethylene glycol, a sucrose solution, and corn sirup. Sphere diameters were mostly from 10 to 30 μ . All of Robinson's data are well fitted by Eq. [18] with $\lambda_1 = 0.833$, except for the initial points, at $\phi = 0$, on the curves for ethylene glycol, sucrose solution, and corn sirup. These three initial points do not fit well with the other experimental points on their respective curves, and some systematic error in the data seems to be indicated.

Robinson developed a theoretical viscosity equation of the form

$$\frac{\eta}{\eta_0} = 1 + \frac{Ak\phi}{1 - S\phi},$$

where A and S are adjustable constants. The product $S\phi$ is interpreted as the sedimentation volume of the glass spheres, and $1 - S\phi$ as the "free" volume of liquid. Obviously, in order to agree with Einstein's equation, A must have the value 2.5; but Robinson finds that, in order to fit his experimental data, he must choose various values of A from 3 to 5.

The concept of free volume introduced by Robinson is developed more rigorously in the present paper. The improvement in the present analysis, compared with Robinson's, is indicated in one way by the fact that, while fitting experimental data at high concentrations, we still agree with Einstein's equation at low concentrations.

Note added in proof. As a result of some correspondence with Professor F. R. Eirich, the author wishes to add a remark concerning V. Vand's (3) theoretical work. Equation [2] of the present paper occurs as an intermediate equation in Vand's theory. However, Vand's theory gives a value for k of .61, which is too low to make the equation fit his data. After further theoretical development Vand arrives at a final equation which fits his data quite well, but is in the form of a power series terminating with the second degree in the concentration.

There is, in this author's opinion, a serious error in Vand's theory of the collision effect. Vand assumes that after collision two spheres will separate along rectilinear paths; but it can be shown that the paths of recession must be curvilinear and are the mirror images of the paths of approach. Correction of this error in Vand's theory would lead to a higher theoretical value of k .

REFERENCES

1. DE BRUIJN, H., *Rec. trav. chim.* **61**, 863 (1942).
2. GUTH, E., AND SIMHA, R., *Kolloid-Z.* **74**, 266 (1936).
3. VAND, V., *J. Phys. & Colloid Chem.* **52**, 277 (1948).
4. SIMHA, R., *J. Reserch Natl. Bur. Standards* **42**, 409 (1949).
5. EILERS, H., *Kolloid-Z.* **97**, 313 (1941).
6. ROBINSON, J. V., *J. Phys. & Colloid Chem.* **53**, 1042 (1949).

RHEOLOGICAL PROPERTIES OF A LUBRICATING GREASE ¹

C. R. Singleterry and E. E. Stone

Naval Research Laboratory, Washington, D. C.

Received January 30, 1951

INTRODUCTION

McKee (1) has described the construction and use of a worker-consistometer for lubricating greases which makes use of the small sample size and the high shear rates of the Hain microworker (2) in connection with arrangements for following shear breakdown in the grease by capillary flow measurements without removing the grease from the worker or terminating the shear-breakdown process. The evaluation of breakdown phenomena obtained with this equipment is handicapped by the fact that most other data concerning shear-breakdown and thixotropy of greases have been reported in terms of the penetration readings on the American Society for Testing Materials (ASTM) penetrometer, using either the standard cone or the micropenetrometer cone described by Kaufman *et al.* (3). Both of these devices give empirical values which depend largely on the yield value of the grease, whereas measurements of capillary flow are profoundly influenced by the viscosity of the liquid phase present.

The possession by a grease of a bona fide yield value which must be exceeded by the shearing stress before any flow will occur is almost its defining characteristic. The possibility that greases are Bingham bodies whose flow behavior can be analyzed to obtain absolute values of the yield point and of the limiting viscosity is attractive because such an analysis would characterize each material uniquely in terms of two numerical constants of obvious physical significance instead of in terms of a locus of apparent viscosities calculated from a formula inapplicable to the system measured. The flow of grease in capillaries has been investigated by many workers (4-9). Early attempts to interpret capillary flow data for Bingham bodies were based on the mistaken assumption that the flow pressure curve for a true plastic in a capillary would take the linear form indicated by the dotted line *AB* of Fig. 1 (10). This would have allowed a direct graphic solution for the yield pressure and the limiting viscosity. Failure to find the expected linear behavior diverted attention toward the concentric cylinder type of viscometer, for which Reiner (12)

¹ The opinions or assertions contained in this communication are the authors' and are not to be construed as official or reflecting the views of the Navy Department.

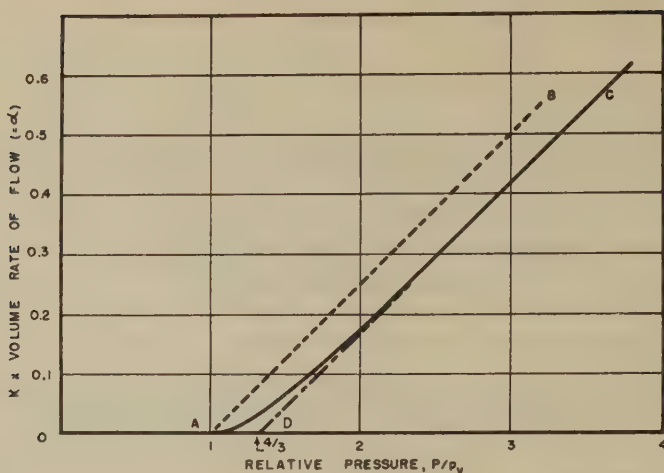


FIG. 1. Generalized curves for plastic flow.

showed that linear flow-stress plots resulted under suitable conditions of measurement. An adequate mathematical analysis of the effects of a yield value on the distribution of velocity gradients in the tube, with resulting plug flow of a central unsheared portion, was made by Buckingham (11).

Buckingham's equation, omitting any correction term for slippage, may be written:

$$V = \frac{\pi a^4 m}{8L} (P - 4p_y/3 + p_y^4/3P^3), \quad [1]$$

where

V = volume rate of flow (cc.-sec.⁻¹),

a = radius of the tube (cm.),

m = mobility of the grease = $1/\eta_\infty$ (poises⁻¹),

L = length of the tube (cm.),

P = pressure drop in the tube (dynes-cm.⁻²),

p_y = yield pressure at which flow begins (dynes-cm.⁻²).

This relation is plotted as the solid curve AC of Fig. 1. It is evident that the plot of V as a function of P/p_y is sensibly curved at values of P less than $2.5 p_y$ and that at high relative pressures the curve approaches an asymptote which intersects the horizontal axis at $P = 4p_y/3$.

Caldwell and Babbitt (13), working with clay slurries, pointed out that division of the term in parentheses; (Eq. 1) by the total pressure drop, P , gave rise to a dimensionless term which was a function only of the relative extent of plug flow, i.e.,

$$V = \frac{\pi a^4 m P}{8L} (1 - 4p_y/3P + p_y^4/3P^4). \quad [2]$$

These investigators also noted that at high rates of flow $p_v^4/3P^4$ becomes negligible, and they assumed that by working with systems in which $p_v/P < 0.5$ they were justified in neglecting the fourth-power term.

McMillen (14), using dimensionless quantities, derived expressions for the flow behavior as a function of the relative size, c , of the unsheared central plug ($c = b/a$, where b is the radius of the unsheared plug in a tube of radius a). He set up a number of dimensionless functions of c that were useful in analyzing flow data and provided tables and graphs from which appropriate numerical values of these derived functions could be read. His solution of the Buckingham equation was then made by fitting the experimental data to the equation in a trial-and-error process that was substantially simplified by his use of the functions.

We have modified this method by a graphical device that eliminates the trial-and-error procedure and permits a straightforward derivation of the rheological constants from measurements at two suitably selected flow rates. We have also made use of McMillen's dimensionless treatment to tabulate a set of generalized solutions of the Buckingham equation for convenient values of P/p_v which will permit rapid computation of the flow-pressure curve for any Bingham plastic in any tube. These computational tools have made it feasible to attempt the derivation of the fundamental rheological constants of greases from measurements made in the worker-consistometer.

McMillen restricted the application of his plastic flow equations to a section of pipe sufficiently removed from contraction or expansion points to eliminate end effects, which he found to have a much greater relative magnitude in these systems than in those involving Newtonian flow. Hence, an experimental evaluation of end effects is an essential preliminary to any interpretation of the flow behavior of greases in the consistometer. The nature and magnitude of the piston correction required with greases in this type of instrument and the extent of the temperature rise resulting from shear in highly viscous systems also require evaluation before the validity of the concept of greases as Bingham bodies can be tested.

EXPERIMENTAL PROCEDURES AND MATERIALS

The worker-consistometer described by McKee and White (1) has been modified to obtain a uniform flow rate throughout the power-driven working stroke and to provide close temperature control over a wide working range by means of electric heaters and liquid coolant channels in the cylinder block itself. The machine (Fig. 2) consists of two opposed cylinders (A) 0.5644 in. in diameter connected by a breech lock mechanism (B); each cylinder is fitted with a matching piston (C) of not greater than 0.0002 in. clearance. The cylinders are separated by various 0.2500-in.-thick orifice plates (D) containing 0.0135-in.-diameter holes. One plate

contains 1 hole and another, 10 holes. A third plate 0.125 in. thick, containing 11 holes of the same diameter as the previous plates, and an auxiliary spacer or clearance plate of equal thickness, with an opening of 0.566 in. diameter, are provided for the study of end effects. Another spacer plate 0.2500 in. thick, with an opening 0.566 in. in diameter, allows direct measurement of the correction for piston drag. The temperatures of the upper and lower cylinder walls at a point near the orifice plate are

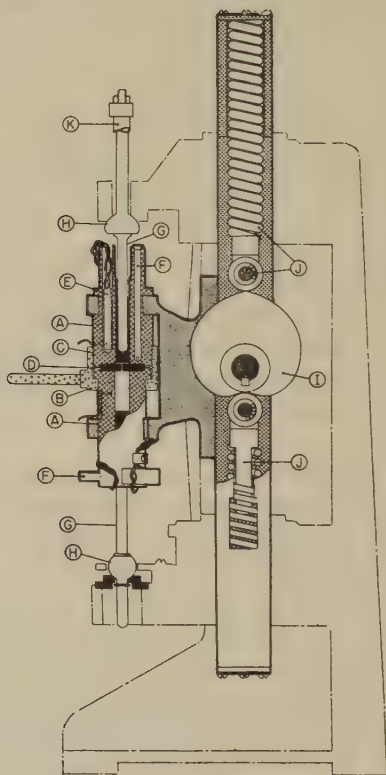


FIG. 2. Worker-consistometer, cross-section. *A* cylinders, *B* lock mechanism, *C* piston, *D* orifice plate, *E* electric heaters, *F* liquid heat exchanger, *G* piston rods, *H* ball and socket joints, *I* cam, *J* overload device, and *K* stirrup suspension.

measured to 0.01° C. by means of thermocouples inserted in 0.062-in.-diameter wells extending to within 0.125 in. of the inner surface.

In operation as a worker, the pistons (*C*) are held fixed by the piston rods while the cylinder assembly is reciprocated by rotation of the power-driven cam, *I*. During measurements of consistency the cylinder assembly is locked in the lower position, the lower piston rod support is removed, and grease is forced from the upper to the lower cylinder cavity by various

loads applied to the upper piston through the stirrup which is rigidly attached at *K*. An auxiliary yoke has been provided which permits the return of grease from the lower to the upper cylinder during the measuring routine at a selected uniform rate controlled by dead-weight loading, so that flow measurements can be conducted in either direction or under total external pressures greater than that of the effective driving load.

The orifice plates were calibrated from measurements of the flow rates of oils of known viscosity. The average diameter of the capillaries in a given plate was obtained by plotting the apparent diameter as a function of the pressure applied, and extrapolating to zero applied pressure to eliminate the effects of heating of the liquid during shear. Corrections were applied for piston drag and for kinetic energy losses. The effective diameters adopted for the three plates studied were: 1-hole 0.25-in. plate, 0.0382 cm.; 10-hole 0.25-in. plate; and 11-hole 0.125-in. plate, 0.0348 cm.

TABLE I

Flow Data for 14G8 Grease After 100 Passes Through the Microworker
Temperature 25.1°C.; all return passes at 10 sec./in.; 10-hole plate.

Pressure	Individual flow times				Average flow time	Average deviation
	1	2	3	4		
<i>dynes-cm.⁻²</i> ($\times 10^{-4}$)					<i>sec./in.</i>	%
12.9	34.0	33.0	32.6	30.2	32.4	2.8
16.0	16.6	16.0	16.1	15.2	16.0	2.5
19.0	10.1	10.2	10.0	9.8	10.0	2.0
22.0	7.5	7.5	7.3	7.3	7.4	1.4

The grease selected for the evaluation of the instrument was a synthetic grease, made in the Naval Research Laboratory (NRL) pilot plant (15) conforming to the Bureau of Ordnance specification 14G8. It consisted of lithium stearate (16%) in di(2-ethylhexyl) sebacate with sorbitan monooleate (1%) and 4-*tert*-butyl-2-phenylphenol (0.2%) as additives. The micropenetration after 10 passes in the Hain microworker (2) was 93. The unworked grease showed some shear breakdown during measuring passes through the consistometer at the highest rates. The measurements reported were made on samples which had been sheared in either the consistometer or the Hain microworker until they showed no progressive change in consistency during a normal measurement cycle at four different rates of shear. The experimental points represent values averaged from at least four such measuring cycles. Data from a representative set of measurements are given in Table I.

SOURCES OF ERROR

Temperature Rise During Flow

During the calibration of the orifice plates with oils of known viscosity it was noted that the plots of η/t against the applied pressure were not linear. Calculation of the work expended on the oil during its passage through the capillary suggested that the apparent decrease in viscosity found with higher driving pressures might well result from a temperature rise in the oil. Hersey and Zimmer (16) have studied such temperature effects in glass capillaries. They concluded that the heat evolution during laminar flow was nearly adiabatic, with the major temperature rise occurring in the zone of high shear near the wall. Our results with capillaries drilled through a steel plate are shown in Fig. 3, in which η/η_0 , the ratio of the observed viscosity to the limiting viscosity at very small driving pressures, is plotted as a function of P .

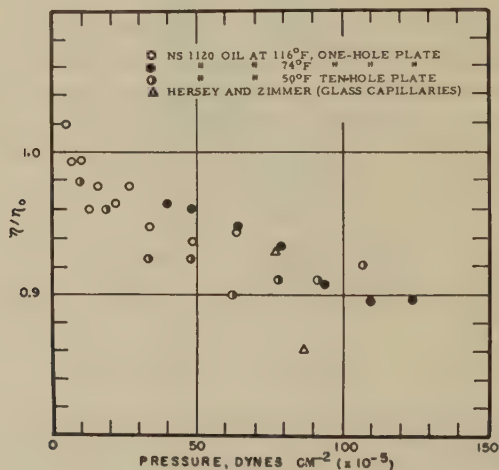


FIG. 3. Changes in relative viscosity resulting from heat generation during flow under pressure.

It is evident that, if errors resulting from temperature rise during the passage of the oil through the capillary are to be held below 1%, the pressure drop in the capillary must be held below 15 or 20 $\times 10^5$ dynes-cm.⁻². The precise limits will depend upon the temperature coefficient of viscosity of the substance under examination. For comparison, two experimental points from the paper of Hersey and Zimmer are plotted to the same scale (open triangles). It is apparent that a metal block is not much more effective than a glass wall in maintaining conditions of isothermal flow under moderate pressure drops. This does not seem surprising when one calculates the residence time of the fluid in the capillary. With the

equipment described here, a flow rate for the piston of 0.1 in./sec. corresponds with the one-hole plate to an average linear velocity within the capillary of about 360 cm./sec., or to a residence time of slightly less than 0.003 sec.

The temperature effect with greases will differ from that with oils because in greases the shear and the resulting evolution of heat are concentrated in the zone outside the central unsheared plug which in practical measurements is likely to have a depth of less than half the radius of the capillary. This will accentuate the decreases in resistance to flow, and the effect will be only partly compensated by the fact that the heated fluid is nearer to the metal wall of the tube than is the case with an oil. Grease 14G8 shows an increase in flow rate of about 3% per degree at a given driving pressure.

This phenomenon has a bearing on measurements made in the SOD viscometer, or in the simplified pressure viscometer described by Brunstrum and Steinbruch (17). The temperature effect does not impair the usefulness of such measurements, which have an essentially empirical significance in any case, but it does clarify the interpretation of data for greases whose liquid components have widely different viscosity indices.

For measuring purposes, there is an inverse relation between the length of a capillary of given radius and the maximum rate of shear attainable before temperature effects impair the reliability of the results. The range of shearing rates accessible for measurement can be extended by shortening the capillary, and this fact seems to justify the use of a capillary with a smaller ratio of length to diameter than the 40-to-1 ratio established for the SOD viscometer.

End Effects and Pressure Drops External to the Capillary

The correction for piston drag with a material of finite yield value is of a different magnitude and character than that found with oils (1). Curves *A* and *B* of Fig. 4 represent flow rates observed when the orifice plate was replaced by an opening of the same diameter as the cylinder. Curve *C* is for one of these greases with the 10-hole plate in position.

It can be seen that the piston effect is large at all useful flow rates but that it is not a constant independent of the flow rate. The flow properties of the grease in the annular space between piston and wall evidently do not correspond exactly to those of the bulk material. This may result because of shearing to some characteristic lower consistency in the 0.0002-in. clearance. The calculated yield pressure for movement of the pistons is 3.1×10^5 dynes-cm.⁻², while the yield pressure indicated by extrapolation of the piston-correction data of Fig. 4 does not exceed 1.6×10^5 dynes-cm.⁻².

When the rate at which the grease and pistons are returned to their upper position is changed (from, for example, 5 sec./in. to 20 sec./in.), a definite decrease is observed in the flow rate at any given pressure for the succeeding measurement. The effect is most marked when the succeeding measurement is made at a pressure giving a low flow rate (see Table II). The effect of previous history was much more pronounced when the clearance plate replaced the 10-hole plate and the major resistance to flow was thus offered by the shearing of grease between the piston and cylinder walls. The variations appear to reflect the consistency to which the grease film between piston and wall has been reduced by shear. After intervals as

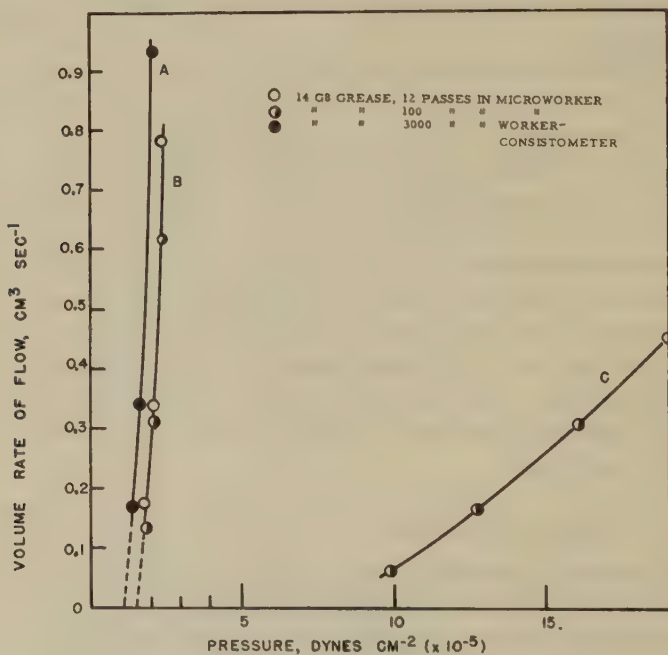


FIG. 4. The piston correction for a grease.

long as 3 days, the consistometer was found still to retain a definite "memory" of whether the preceding return pass was rapid or slow. A standard return rate comparable with the highest measuring rate used has been found to give the smallest and most reproducible piston correction, but during measurements at slow rates of flow the piston correction actually increased during the stroke. Because of this difficulty it is best to make timing measurements as early in the timing stroke as one can be certain of uniform flow conditions, and to make measurements at very low flow rates on a very short distance (0.1 in.) near the beginning of the stroke.

The finite yield value of greases implies that pressure drops associated with flow external to the capillary cannot be negligible at even the slowest flow rates. The major points of external resistance are the zone of shear between the grease plug and the cylinder wall, and the spaces near the entrance and exit of the capillary. Zimmer and Patberg (18) concluded that entrance effects were mainly responsible for the lack of agreement between the apparent viscosities of greases determined in capillaries of length to diameter ratio of 12 to 1 and the corresponding viscosities measured in a 40 to 1 capillary. These authors estimated the magnitude of the effect from measurements of the flow through an orifice of the same diameter as the capillary but with a length to diameter ratio of 1 to 1. McMillen (14) studied pressure losses in a system consisting of an aluminum soap gel in a hydrocarbon during passage from a 2-in. to a 0.75-in. pipe and from a 0.75-in. to a 0.125-in. pipe and found the pressure drop to be nonlinear up to 50 diameters from the point of contraction.

TABLE II

Effect of Return Rate of Piston Assembly on the Succeeding Measurement at a Pressure of 9.9×10^5 dynes-cm.⁻²

Seconds/inch for return stroke	Seconds/inch for succeeding measured stroke
20	26.6
8	24.8
5.6	23.0

Entrance losses in the worker-consistometer were studied by using two comparable multihole plates, one having a thickness of 0.25 in. (18 diameters) and the other of 0.125 in. (9 diameters). The effective average diameter of the holes, as determined from calibration with a viscous oil, was 0.348 cm. for both plates. Comparisons were made with samples of grease which had been worked until further breakdown would not occur during the measuring passes in the consistometer. The results for one case are presented in Table III and plotted in Fig. 5, which shows the uncorrected pressure-flow curves *A* and *B* for both plates and the plot *C* of the difference between the pressures producing equal flow rates through the two plates. This latter curve is essentially the pressure-flow curve for the second half of the longer capillaries, separated from piston drag, entrance effects and changing pattern of flow in the first 9 diameters of the capillary. The combined magnitude of the piston and end effects is obtainable as the difference between curves *B* and *C*. It will be seen that the external effects produce a pressure drop comparable in magnitude with that resulting from flow through 0.125 in. of capillary and that these effects have a considerable magnitude at any finite rate of flow.

The assumption that a distance of 9 diameters from the entrance is

TABLE III

Flow Data for 14G8 Grease After 100 Passes in the Microworker
 Temperature, 25°C. Volume of cylinder, 4.11 cm.³/in. of length.

0.250-in. plate			0.125-in. plate		
<i>P</i>	<i>t</i>	<i>V</i>	<i>P</i>	<i>t</i>	<i>V</i>
<i>dynes-cm.⁻²</i> ($\times 10^{-5}$)	<i>sec./in.</i>	<i>cm.³-sec.⁻¹/hole</i>	<i>dynes-cm.⁻²</i> ($\times 10^{-5}$)	<i>sec./in.</i>	<i>cm.³-sec.⁻¹/hole</i>
12.9	32.4	0.0127	9.9	18.9	0.0198
16.0	16.0	0.0256	11.1	13.1	0.0285
19.0	10.0	0.0403	12.9	8.45	0.0442
22.0	7.4	0.0555			

adequate to establish equilibrium conditions of flow in the tube may not be justified. It is believed, however, that for a material with a yield value as high as that of even a soft grease, the pressure drop in spaces actually external to the capillary is large as compared with any departure from a linear pressure gradient within the tube, and that the flow beyond 9 diameters will be so nearly steady state as to permit a test of the Buckingham equation.

This belief is supported by visual examination of the flow of a specially prepared transparent grease in a glass analog of the consistometer, using polarized light to detect zones of shear and small suspended particles to indicate the direction and velocity of flow. The main mass of grease in the

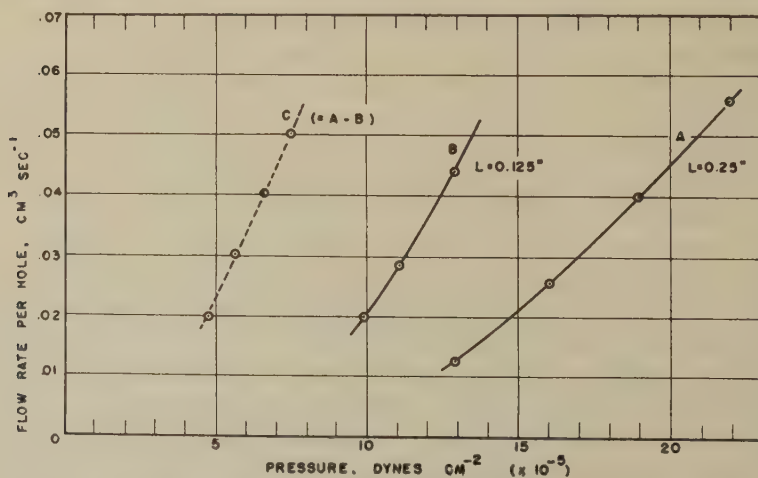


FIG. 5. Comparison of flow rates in capillaries of different length to evaluate the external pressure drop. A, length of 18 diameters; B, length of 9 diameters; C, difference between A and B. 14G8 grease, worked 100 passes in microworker.

cylinder can be seen to flow almost as a solid plug until it reaches a point approximately equal to the diameter of the cylinder away from the plate containing the capillary. At this point an extensive deformation and relative shearing of the grease can be seen to set in, with grease from different parts of the cylinder converging toward the central capillary at varying velocities. At the same time the pattern of birefringent bands, which has been moving down the cylinder with even its minor irregularities unchanged, is destroyed and replaced by a slowly changing pattern characteristic of the convergence toward the capillary.² There is also a slight radial flow inward just in front of the advancing piston as slowly moving or stationary layers of grease next to the cylinder walls are peeled off by the advancing piston and flow inward to force the main plug slightly more rapidly towards the capillary end of the apparatus. Beyond the exit of the capillary this flow process is repeated approximately in reverse, although the details of the geometry of flow, and of the resulting birefringence pattern differ in minor aspects.

A further modification of the glass device permitted visual determination of the distance required to establish a state of steady flow in a glass capillary 0.16 cm. in diameter with a square-edged entrance. The un-sheared central section could be observed as a dark zone extending from wall to wall as it entered the tube but tapering gradually to one-third its original diameter as a complex birefringence pattern of alternating lighter and darker bands developed along the walls. Because of the rigidity of the soap structure in the grease, the pattern persisted unchanged when the flow was suddenly interrupted, and could be studied at leisure with a microscope carrying a micrometer eyepiece. The birefringent pattern next to the walls of the capillary became fully resolved at a distance of about 10 diameters from the entrance. Measurements of the distance between corresponding bands in the pattern outside the central dark section indicated that they moved very slightly closer to the center between the 10th and the 15th diameters from the entrance and persisted unchanged from that point to the end of the tube.

CALCULATION OF THE BINGHAM YIELD VALUE AND MOBILITY FROM CAPILLARY FLOW DATA

McMillen's treatment of the Buckingham equation in terms of the dimensionless quantity c (the relative radius of the un-sheared central plug) makes it possible to derive the Bingham yield value and mobility and to test the conformity of experimental results with the equation without a prohibitive expenditure of time. McMillen's paper (14) should be

² The birefringence observed is produced by orientation of anisotropic soap crystals and not by elastic strain; it persists unchanged after the pressure is released and flow has ceased.

consulted for the derivation of his equations, but for convenience some of his dimensionless functions and the practical equations in which their use is convenient are summarized below, together with definitions of the symbols used.

- a = radius of the tube in centimeters,
 b = radius of the unsheared central plug in centimeters,
 $c = b/a$ (the basic dimensionless quantity of the treatment),
 V = volume rate of flow in $\text{cm}^3\text{-sec.}^{-1}$,
 P = pressure drop in the capillary in dynes-cm.^{-2} ,
 p_y = pressure required to initiate flow ($p_y = Pc$),
 L = length of tube in centimeters,
 f = yield value in dynes-cm.^{-2} ,
 m = mobility (reciprocal of limiting apparent viscosity at high rates of shear), poises^{-1} ,

$$\alpha = \frac{c^4 - 4c + 3}{12c}, \quad [3]$$

$$f = Pac/2L, \quad [4]$$

$$m = V/\pi a^3 f \alpha, \quad [5]$$

$$V = \pi a^3 f m \alpha. \quad [6]$$

For a given material it follows from Eq. [6] that the function α is proportional to the volume rate of flow in a given tube, i.e., $V_1/V_2 = \alpha_1/\alpha_2$. This establishes the ratio of the α 's for any two measured rates of flow. Equation [4] indicates that, for a given material and tube, P is inversely

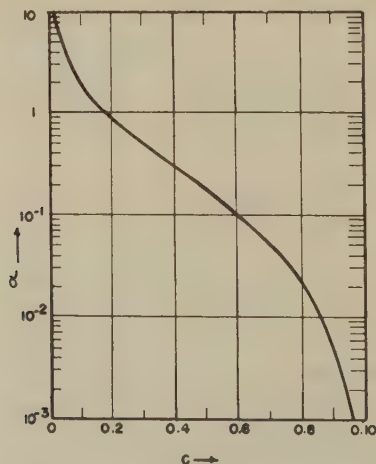


FIG. 6. Plot of α as a function of the dimensionless quantity, c (after McMillen).

proportional to c , or that $P_2/P_1 = c_1/c_2$. McMillen pointed out that for such a system there was only one set of values of c_1 and c_2 for which α_1/α_2 would equal V_1/V_2 when $c_1/c_2 = P_2/P_1$. This pair of values he found by a trial-and-error process of assuming values of c_1 and c_2 that satisfied the relation $c_1/c_2 = P_2/P_1$ and testing whether the corresponding functions α_1 and α_2 as read from his table or graph of α as a function of c (Fig. 6) satisfied the relation $\alpha_1/\alpha_2 = V_1/V_2$. By a further elaboration of McMillen's tables it is possible to select convenient fixed ratios of c_1/c_2 , such as 1.25, 1.50, 1.75, and 2.00, and for each of these ratios to calculate and plot α_1/α_2 as a function of c_2 . These plots are given on a reduced scale in Fig. 7. For actual computations the functions should be plotted from Table IV to a scale that will permit reading points from the curve to within 1%.

The determination of the Bingham body constants of a grease from measurements of flow in a capillary then involves the following steps:

1. Obtain pressure-flow relations for which the Buckingham equation could be expected to hold by applying to the raw data suitable corrections for external pressure drops. Plot the corrected data to show V as a function of P , and draw the best smooth curve through the points.
2. Select one of the established ratios of $P_2/P_1 (= c_1/c_2)$ that will allow utilization of the major portion of the experimental range, assign corresponding values for P , and read from the PV curve the corresponding values of V_1 and V_2 . (Comparisons between different substances will be more reliable if V_1 and V_2 fall in a similar range for the two substances.)
3. From the plot of $\alpha_1/\alpha_2 (= V_1/V_2)$ as a function of c_2 (Fig. 7) determine the c_2 value that applies. From the relation $c_1/c_2 = P_2/P_1$ compute c_1 .
4. From the plot of α as a function of c (Fig. 6) determine α_1 and α_2 . Compute α_1/α_2 for comparison with V_1/V_2 as a check on the accuracy of the operations.
5. Calculate f by Eq. [4], in which P and c may be any corresponding pairs of values. (Note that $a/2L$ is a constant of the capillary used.) The yield pressure, p_y , may be calculated from the relation $p_y = P \times c$. Calculate $m (= 1/\eta_\infty)$ by Eq. [5] rearranged to

$$m = \frac{1}{\pi a^3} \times \frac{V}{f\alpha},$$

where V and α are for a single flow rate and $1/\pi a^3$ is again a constant of the instrument.

If it is desired to plot the curve for the Buckingham equation having the f and m just determined, suitable points may be computed from Eq.

[6] where α is a function of c , which is equivalent to p_y/P , and may be read from McMillen's table for convenient values of p_y/P . For convenience of reference, a short tabulation of the function α for selected values of the more convenient quantity, the relative pressure P/p_y , is given in Table V.

A significant test of the conformity of greases to the Bingham body type of flow can best be made on measurements taken at a pressure drop of 20×10^5 dynes-cm.⁻² or less, using a constant return rate and applying an over-all correction for piston and end effects obtained by a comparison between the flow behavior through a 0.25-in. plate and that through a 0.125-in. plate. The data presented in Fig. 5 conform closely to the above requirements.

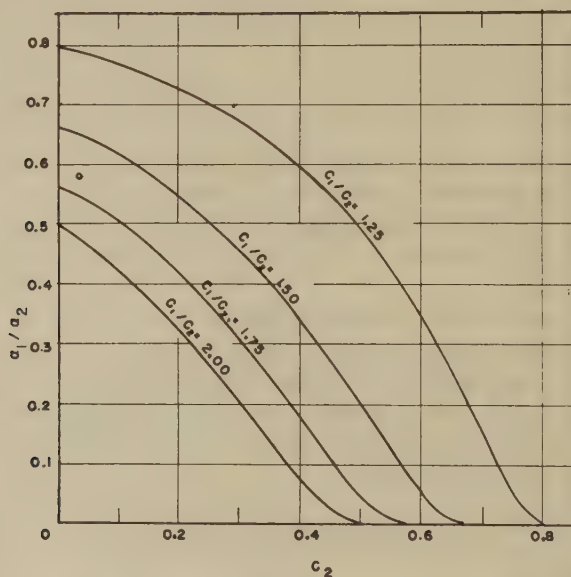


Fig. 7. Plots of α_1/α_2 as a function of c_2 for various ratios of c_1/c_2 .

Applying the successive steps, we obtain the points of curve *C* of Fig. 5 as the result of step 1. These points are replotted as curve *B* of Fig. 8. Steps 2 to 5 lead to the yield values and mobilities shown in Table VI. Computing convenient values of V as a function of P by Eq. [6] and Table V we obtain curve *B* of Fig. 8 originating at $V = 0$ when $P = p_y$.

The points on curve *A* present the corrected flow data for a grease that had been worked in the consistometer for 3000 passes through the 10-hole 0.25-in. plate at an apparent shear rate of $250,000 \text{ sec.}^{-1}$, together with the flow curve computed from the Buckingham equation.

The closeness with which the experimental points can be fitted by the Buckingham equation argues for the validity of the concept of greases as Bingham bodies. It must, however, be noted that most of the experimental

points lie at relative pressures higher than two, where a nearly linear relation between pressure and flow is predicted. The points would be equally well fitted by any other equation requiring a linear relation between pressure and flow rate at high relative pressures. To remove uncertainty requires either reliable flow data at relative pressures lower than two or an independent measurement of the yield value for comparison with that determined from the Buckingham equation. Measurements of flow at very low relative pressures are unsatisfactory because of the large and

TABLE IV
 α_1/α_2 as a Function of c_2

$c_1/c_2 = 1.25$		$c_1/c_2 = 1.50$		$c_1/c_2 = 1.75$		$c_1/c_2 = 2.00$	
c_2	α_1/α_2	c_2	α_1/α_2	c_2	α_1/α_2	c_2	α_1/α_2
0.784	0.00784	.6600	.00072	0.5600	0.00158	.4800	.00412
0.7600	0.03953	.6400	.01025	0.5200	0.02632	.4400	.03119
0.7200	0.11545	.6000	.05126	0.4800	0.06969	.4000	.07351
0.6800	0.19765	.5600	.10733	0.4400	0.12300	.3600	.12327
0.6400	0.27589	.5200	.16791	0.4000	0.17641	.3200	.17561
0.6000	0.34695	.4800	.22872	0.3733	0.21300	.2800	.22754
0.5600	0.41015	.4400	.28689	0.3200	0.28344	.2400	.27727
0.5200	0.46599	.4000	.34118	0.2667	0.34808	.2000	.32377
0.4800	0.51510	.3600	.39110	0.2400	0.37785	.1600	.36653
0.4400	0.55830	.3200	.43653	0.2000	0.41917	.1200	.40542
0.4000	0.59623	.2800	.47756	0.1600	0.45657	.0800	.44041
0.3600	0.62964	.2400	.51446	0.1067	0.50062	.0400	.47183
0.3200	0.65905	.2000	.54751	0.0800	0.52033	.0200	.48629
0.2800	0.68499	.1600	.57705	0.0533	0.53863	.0100	.49325
0.2400	0.70790	.1200	.60345	0.0000	0.57143	.0000	.5000
0.2000	0.72817	.0800	.62686				
0.1600	0.74610	.0400	.64788				
0.1200	0.76206	.0267	.65438				
0.0800	0.77612	.0133	.66064				
0.0533	0.78469	.0000	.66667				
Limit	0.8000						

variable piston correction associated with the present piston design. However, some measurements of the yield value of a freshly sheared grease have been made with a modification of the ASTM penetrometer which employs a thin blade instead of the standard cone.³ At equilibrium the grease supports a known weight by means of its contact with a measurable area of the blade. The absolute yield value of the grease can be calculated directly from the area and the weight applied. A sample of 100-pass grease similar to that used in obtaining the data for curve *B* (Fig. 8)

³ Details of this device will be reported elsewhere.

gave a directly measured yield value⁴ of 6.5×10^3 dynes-cm.⁻². This value is in better agreement with the 6.31×10^3 dynes-cm.⁻² obtained from the Buckingham equation than with the value of 8.2 dynes estimated by a simple extrapolation through the corrected data points to the axis of zero flow.

Green (4) concluded from measurements with a Bingham plastometer that greases and soap-thickened oils showed the plastic type of flow, but his interpretation of the data was made before Buckingham's analysis of the nature of plastic flow in tubes and assumed a relation of the type of curve *AB* of Fig. 1 for plastic flow in a capillary. Moses and Puddington

TABLE V
α as a Function of P/p_y for Calculation of Flow Rates by Eq. [6]

P/p_y	α
1.02	.00023
1.05	.00113
1.10	.0043
1.20	.0149
1.30	.0296
1.50	.0663
1.70	.1088
2.00	.1771
2.20	.2245
2.40	.2727
2.60	.3214
2.80	.3705
3.00	.4198
3.2	.4692
3.4	.5188
3.6	.5685
3.8	.6182
4.0	.6680
4.5	.7926
5.0	.9172
6.0	1.1671

(8) used a similar instrument to study calcium greases. They interpreted their measurements in terms of Goodeve's (19) theory of thixotropy during flow (which is formally equivalent to Bingham's assumption of a yield value) and concluded that the greases studied conformed. They explicitly identified Goodeve's coefficient of thixotropy with the hardness or yield value of the grease, but made no reference to the complex nature of plastic flow in a capillary. They ignored the curvature at low flow rates in determining flow constants from their plotted data, which was equivalent to Green's treatment of his data. Neither Green nor Moses and Pud-

⁴ The yield stress obtained with either the consistometer or the blade penetrometer is a dynamic value; it corresponds to the second yield stress of Blott and Bonner (20).

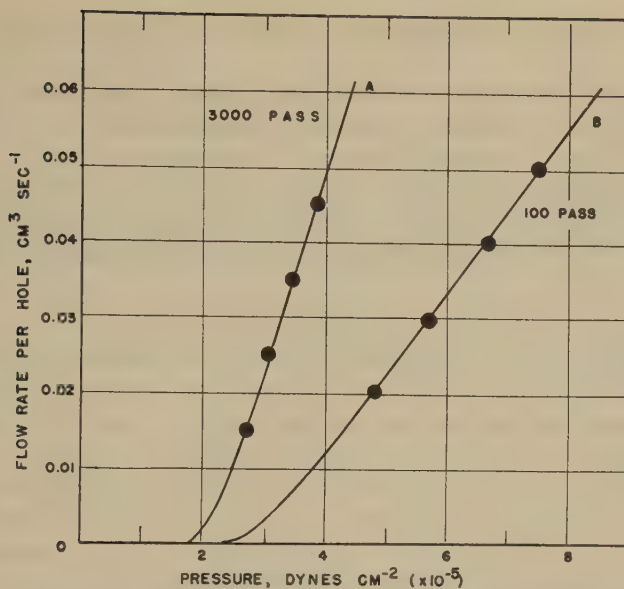


Fig. 8. Comparison of flow data corrected for external pressure drop (circles) with Buckingham equation for plastic flow (solid lines). A, 14G8 grease after 3000 passes through worker-consistometer; B, 14G8 grease after 100 passes in Hain microworker.

dington reported any correction for entrance effects. Arveson (5) stated explicitly that his results did not fit the Buckingham equation, but his measurements covered such a range of pressures and shear rates that the temperature rise must sometimes have been considerable. Replotting of his data to show volume rate of flow as a function of pressure gives curves which become continually steeper as the pressure is increased, as would be expected if the grease were being appreciably heated by shear in the capillary. McMillen found approximately plastic flow with a dispersion of an aluminum soap in a hydrocarbon, although the situation was compli-

TABLE VI

Rheological Constants for 14G8 Grease at Two Stages in the Process of Shear Breakdown

Stage in breakdown	Yield value, f , Eq. 4	Yield value, by blade-pene- trometer	Mobility, m	Limiting viscosity, $1/m$
	dynes-cm.^{-2} ($\times 10^{-3}$)	dynes-cm.^{-2} ($\times 10^{-3}$)	poises^{-1}	poises
100 passes in Hain micro- worker	6.31	6.5	1.00	1.00
3000 passes in worker- consistometer	4.8	4.5	2.42	0.41

cated by the elastic phenomena characteristic of many aluminum soap systems.

In general these publications seem to indicate that the plastic flow behavior found for the lithium soap-diester grease studied here will be exhibited by many commercial greases of the buttery type if they are examined under suitable experimental conditions. It goes without saying that greases subject to appreciable shear breakdown during the act of measurement cannot be characterized by simple Bingham constants.

SUMMARY

The results here described show that when the phenomena of flow in a capillary are separated from accompanying effects such as piston drag, entrance losses, and temperature rise during flow, a shear-stable grease of the 14G8 type behaves substantially as a Bingham plastic whose flow can be specified in terms of yield value and mobility. The yield value so obtained is in reasonable agreement with that measured directly. The reciprocal of the mobility, which can be identified with the limiting apparent viscosity approached at high rates of flow, is from two to five times the viscosity of the diester fluid present in the grease. These magnitudes are reasonable in the light of the volume and particle shape of the suspended soap phase.

A graphic method has been developed for the analysis of flow data for Bingham plastics in terms of the Buckingham equation for plastic flow in tubes of circular cross section. This treatment permits direct computation of both the yield value and the mobility of such a plastic from data for flow under two suitable pressures without resort to the trial-and-error operations previously employed for this purpose.

ACKNOWLEDGMENTS

The authors wish to acknowledge their indebtedness to S. A. McKee and H. S. White, both of the National Bureau of Standards, for helpful discussion of the present design of the worker-consistometer.

REFERENCES

1. MCKEE, S. A., AND WHITE, H. S., *ASTM Bull.* **No. 153**, 90 (1948).
2. HAIN, G. M., *ASTM Bull.* **No. 147**, 86 (1947).
3. KAUFMAN, G., FINN, W. J., AND HARRINGTON, R. J., *Ind. Eng. Chem., Anal. Ed.* **11**, 108 (1939).
4. GREEN, H., *Am. Soc. Testing Materials, Proc.* **20**, 451 (1920).
5. ARVESON, M. H., *Ind. Eng. Chem.* **24**, 71 (1932); *ibid.* **26**, 628 (1934).
6. BEERBOWER, A., SPROULE, L. W., PATBERG, J. B., AND ZIMMER, J. C., *Inst. Spokesman* **6**, No. 8, 9 (1942); *ibid.* **6**, No. 10, 11 (1943).
7. WILSON, J. W., AND SMITH, G. H., *Ind. Eng. Chem.* **41**, 770 (1949).
8. MOSES, G. B., AND PUDDINGTON, I. E., *Can. J. Research* **27B**, 616 (1949).
9. PIGOTT, R. S. J., *Inst. Spokesman* **11**, No. 9, 4 (1947).

10. GREEN, H., *Industrial Rheology and Rheological Structures*, p. 10. John Wiley and Sons, New York, 1949.
11. BUCKINGHAM, E., *Am. Soc. Testing Materials, Proc.* **21**, 1154 (1921).
12. REINER, M. J., *J. Rheol.* **1**, 5 (1929).
13. CALDWELL, D. H., AND BABBITT, H. E., *Ind. Eng. Chem.* **33**, 239 (1941).
14. McMILLEN, E. L., *Chem. Eng. Progress* **44**, 537 (1948).
15. HAIN, G. M., JONES, D. T., MERKER, R. L., AND ZISMAN, W. A., *Ind. Eng. Chem.* **39**, 500 (1947); HAIN, G. M., AND STONE, E. E., *Ind. Eng. Chem.* **39**, 506 (1947).
16. HERSEY, M. D., AND ZIMMER, J. C., *J. Applied Phys.* **8**, 359 (1937).
17. BRUNSTRUM, L. C., AND STEINBRUCH, R., *Inst. Spokesman* **13**, No. 8, 10 (1949).
18. ZIMMER, J. C., AND PATBERG, J. B., *Inst. Spokesman* **9**, No. 5, 1-5 (1945).
19. GOODEVE, C. F., AND WHITFIELD, G. W., *Trans. Faraday Soc.* **34**, 511 (1938).
20. BLOTT, J. F. T., AND BONNER, W. B., *Proceedings of the International Congress on Rheology*, Holland, 1948, p. II-265. North-Holland Publishing Co., Amsterdam, 1949.

A MODERN THEORY ON THE STRUCTURE AND CAKING PROPERTIES OF COAL FROM THE RHEOLOGICAL VIEWPOINT

Katsuya Inouye

From Nenryo-Kenkyujo (Fuel Research Institute), Saitama-Kawaguchi, Japan

Received May 16, 1950; revised December 29, 1950

INTRODUCTION

Concepts as to the physical structure of coal have been obtained from several points of view. From microscopic observations, we recognize the heterogeneity of coal texture. From measurements of adsorption capacity or heat of wetting, we can calculate the colloid-chemical surface area of coal. Also, the techniques of the x-ray diffraction gives information on the fundamental molecular (or atomic) arrangement with incoal (1). Each method, accordingly, gives us a particular manner of observing the micro or macro structures. But information is unfortunately lacking as to what structure is fundamental to the essential properties of coal, although the x-ray studies of H. L. Riley *et al.* (2) have thrown light on this problem.

In the viewpoint of the present author, the essential properties of coal are clearly manifested in the so-called "caking properties" of coal, and, accordingly, if any one theory on the structure of coal cannot explain the caking properties, the theory lacks basic meaning. In the present paper, the term "caking" refers to the phenomenon of coal's softening or fusing and swelling within a certain range of temperature, say within 400–500°C., during carbonization. This is a necessary condition for obtaining coke from coal. By "coking" (of wider meaning than "caking") is included the concept of strength of the coke; this is a somewhat different view from that of certain other authors.

The above described methods of study are insufficient for evaluating essential properties of coal. In this regard, the classical chemical studies have given rather more valuable information on this fundamental problem. In the present stage, the theories of caking properties of coal may be summed up as follows:

(a) The bitumen theory has its origin in the work of F. Fischer *et al.* (3), who reported that the amount of the "bitumen" in coal, i.e., the portion soluble in benzene by pressure extraction in an autoclave, primarily accounts for the caking properties of coal.

(b) The gamma theory of R. V. Wheeler and co-workers (4) sought to explain the caking properties by the presence of the "gamma" portion, namely the portion extractable by pyridine and chloroform.

(c) W. A. Bone and others (5) suggested that not only the extractable portion but the nature of the residual matter or the mutual relationship between extractable and unextractable parts is important.

It does not seem, however, to be of fundamental physical significance to seek the origin of the caking properties of coal in some limited form of matter, because each extracted or unextracted portion is formed within a continuous series of materials; for example, the so-called α -, β -, and γ -portions and the bitumen and residue are all of essentially the same meaning in the "turbostratic" molecules, as H. L. Riley *et al.* have recently proved by x-ray diffraction studies (2), and a practical separation by extraction among them merely means a fractionating process. If we continue such fractionation, we can divide the complex material such as coal into many portions, and, as a consequence of this course of study, we may understand coal as a substance of extreme complexity. This appears to be the reason why studies on the essential properties of coal have been more or less inactive for more than 20 years.

IMPORTANCE OF THE RHEOLOGY OF COAL

From the above introduction, there remains little doubt as to the necessity for studying coal from the rheological viewpoint, especially when we observe its behavior during carbonization. When a typical caking coal is carbonized in the oven, gases are distilled off at the lower temperatures; then at 400–500°C. the coal fuses and swells with the evolution of more gases by pyrolysis; during this gradually continuing process a porous coke is formed. The essential problem is to determine why caking coal fuses and swells. The present author believes that a certain weakness of the intermolecular forces of coal is necessary to realize these properties, as will be shown in the following experiments. In 1937 R. Houwink (6) pointed out that the strength or type of bonds in solid substances is evaluated rather logically from rheological studies. He stated that Young's modulus is a measure of bond strength in solids; for example, metals, glasses, and silk, possess chiefly strong primary bonds showing higher values, say 10^{11} – 10^{12} dynes/cm.², in contrast with the lower value *ca.* 10^{10} dynes/cm.², shown by natural and artificial resins having more secondary or van der Waals' bonds. If Young's modulus is considered as representing the stiffness of springs, in solids this will represent the binding forces existing among their constituent substances; thus, we are able to recognize Houwink's idea as a modern physical viewpoint for solids.

EXPERIMENTAL

Young's Modulus of Elasticity of Coal

As a first stage in studying the rheological properties of coal, experiments on Young's modulus of elasticity were carried out. The correct values of Young's modulus of coal are unfortunately not known. O. Müller (7) reported two values of Young's modulus for German coals of unknown origin. More recently, D. H. Bangham and F. A. P. Maggs (8) obtained three values for British coals. These values, however, seem to be of limited significance, because they are measured by the static compression method and may contain some influence of plasticity. Furthermore, as seen from the following experiments, one is hardly able to discuss coal of every rank and variety from two or three coals. Therefore, the first aim of the present work was to find a suitable method for measuring Young's modulus of coal and obtaining correct values applying to all varieties of coals.

Resonant Frequency Method for Determining Young's Modulus for Coal

A dynamic resonant frequency method, schematically shown in Fig. 1, was used.

Measurement of Young's modulus of solids by the resonant frequency method has been used since 1935 in the field of building materials (9), and also, more recently in the rubber industry (10). In these experiments, the specimens can be prepared in almost any desired dimensions. With coal specimens, however, it is hardly possible to obtain desired dimensions, because of the presence of cracks or flaws and also because of the anisotropic texture of the coal sample. Nevertheless, many prismatic coal specimens were prepared with an accuracy of 1% in each dimension, by using a motor-grinder, a motor-driven polishing apparatus, sandpaper, and a glass plate together with carborundum. The length of specimens obtained varied from several centimeters to 2 cm.

A calibrated audio-frequency oscillator of the C-R type, a 3.2-w. power amplifier, a Rochelle salt pick-up, and a voltage amplifier of 55

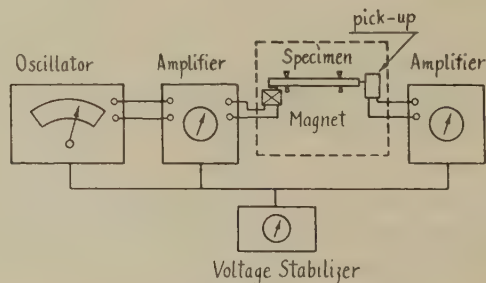


FIG. 1. Experimental apparatus.

decibles were used. The specimen was supported by wedge-shaped rubber supports at the two nodes of the first fundamental flexural vibration of the bar (0.224 of the length from each end). The specimen vibrates due to the action of a small magnet coil and a light iron plate cemented on the bottom side of the specimen in a position opposite to the magnet. To avoid vibration from the floor, the apparatus enclosed by the dotted line of Fig. 1 was fixed on a thick board and suspended by rope and rubber cords. The not-too-tight support of the specimens and the placing of the pick-up needle lightly are important features of the measuring technique. The resonant frequency is readily detected by observing the maxima of output voltage from the Rochelle salt crystal at n , $n/2$, $n/4$, etc., where n cycles/sec. is the resonant frequency (usually in the order of kilocycles). From the resonant frequency we can calculate Young's modulus by using Pickett's equation (11):

$$E = C W n^2, \quad [1]$$

where,

E = Young's modulus,

W = weight of the specimen in grams,

n = the resonant frequency in cycles/second, and

C = a factor which depends upon the shape and size of the specimen, the mode of vibration, and Poisson's ratio.

The following is a sample calculation:

Sample: Shosaku anthracite.

Dimensions of specimen: length, 5.88 cm.; width, 1.629 cm.; thickness, 0.592 cm.

Weight of specimen: 8.422 g.

Resonant frequency measured: 4050 cycles/sec.

For the first mode of vibration of a prism of rectangular section, we find from the value of ratio of depth to length an intermediate factor T_1 to be 1.06, using Fig. 2 of Pickett's paper [see p. 853 of Ref. (11)].

Hence,

$$\begin{aligned} E &= \frac{0.002453 \times (5.88)^3 \times 1.06 \times 8.422 \times 2.204 \times 10^{-3} \times (4050)^2}{1.629 \times 0.3937 \times (0.592)^3} \\ &= 1.21 \times 10^6 \text{ lb./in.}^2 \\ &= 8.29 \times 10^{10} \text{ dynes/cm.}^2. \end{aligned}$$

By this method the author obtained Young's modulus values for wood, ebonite, gypsum, chalk, paraffin, resins, etc., and all showed expected values. The error of measurement in the value of E appears to be within 2 or 3%.

RESULTS AND DISCUSSION

Influence of Orientation of Specimen

Table I shows the orientation effect with respect to the bedding planes of coal. These data were selected from samples of clearly visible orientation, but, in general, especially with bituminous coals, the orientation is not markedly apparent.

TABLE I

Orientation Effect of Specimens on Young's Modulus

Sample	Orientation	$E \times 10^{-10}$
Bituminous (Omine)	Parallel	6.48
	Perpendicular	5.43
Bituminous (Shishimachi)	Parallel	6.62
	Perpendicular	2.19
Bituminous (Yubari)	Parallel	4.25
	Perpendicular	3.75
Bituminous (American)	Parallel	3.95
	Perpendicular	3.71

The specimens orientated parallel to the bedding planes show higher values than specimens orientated perpendicularly. The E values reported are measured from specimens parallel to the bedding planes.

Influence of Moisture

In order to determine the influence of moisture in coal on Young's modulus, values of representative specimens of each rank were examined after storing them in desiccators at various relative humidities for 10 to 15

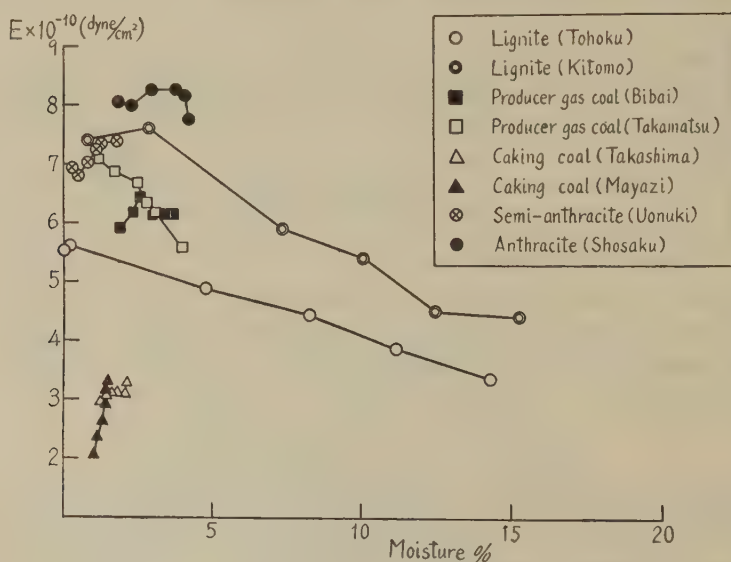


FIG. 2. Effect of moisture.

days. Temperatures were maintained at $10 \pm 4^\circ\text{C}$. throughout these measurements.

Figure 2 shows the change of E with moisture content determined from weight differences of powdered samples of each specimen caused by heating 1 hr. at 105°C .; Fig. 3 shows the effect of relative humidity. The values of E of lignites and producer gas coal increase linearly with a decrease of moisture, in contrast to bituminous coals or anthracite. This remarkable influence of the moisture of younger coals is due to two causes, one of which is the presence of active peripheral groups such as carboxyl and hydroxyl (phenolic) which strengthen the intermolecular forces (these forces are weakened by binding the water molecules by

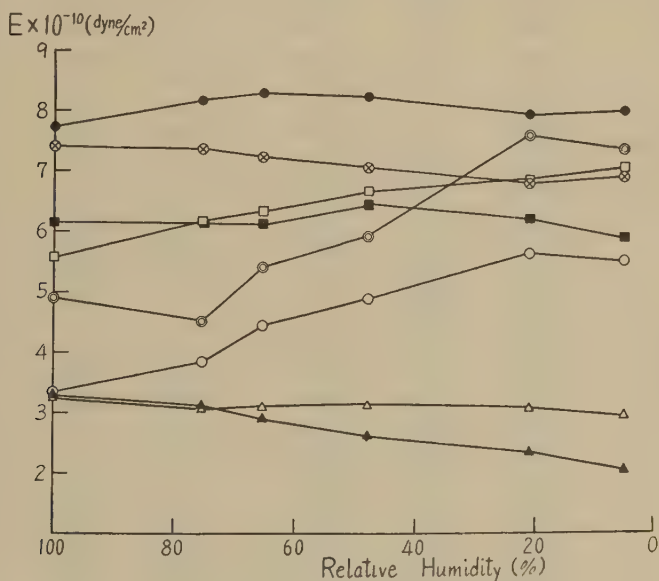


FIG. 3. Young's modulus and relative humidity.

hydrogen bond), and the other is the possibility of shrinkage. With the higher-rank coals the removal of moisture means the appearance of new inner surfaces which results in a decrease of Young's modulus.

It was decided that the specimens in all experiments would be put in the 76% relative humidity desiccator (over NaCl-saturated water) for 3 days in order to equalize the influence of humidity.

Young's Modulus and the Grades of Coal

To date Young's modulus has been determined for more than 120 samples of coals of every grade from young lignite to anthracite, and from Japan, China, and the United States. Table II and Fig. 4 show the rela-

TABLE II
Young's Modulus and Grade of Coal

Sample	Proximate analysis				Volatile matter, dry, ash-free	Young's Modulus $\times 10^{-10}$
	Moisture	Ash	Volatile matter	Fixed carbon		
					%	<i>dynes/cm.²</i>
Shosaku	3.96	16.52	6.10	73.42	7.65	8.19
Uonuki	0.82	8.52	14.79	75.87	16.31	7.37
Kanbayashi	0.62	24.50	20.11	54.77	26.86	5.14
American	1.51	4.36	30.53	63.60	32.40	2.04
Oshima	0.99	10.47	35.78	52.76	36.98	1.76
Takashima	1.43	8.01	34.31	56.25	37.47	3.20
American	1.33	4.80	36.38	57.49	38.75	3.98
Shimameguri	2.80	8.25	35.40	53.55	39.80	6.62
Mojiri	2.81	11.24	34.86	51.09	40.56	2.02
Sakito	2.02	11.61	36.02	50.34	41.72	3.57
Kamiutashinai	3.08	8.10	39.50	49.32	44.47	0.971
Yubari	1.19	2.47	43.08	53.26	44.72	4.25
Horonai	4.29	4.40	41.20	50.11	45.12	3.98
Toro	2.84	13.15	38.39	45.64	45.70	4.70
Noborikawa	2.06	6.46	42.93	48.55	46.93	5.54
Omine	2.61	3.75	43.98	49.66	46.97	6.48
Miike	0.58	6.74	44.17	48.51	47.66	3.79
Teshio	14.22	6.89	37.65	41.24	47.72	2.66
Takamatsu	3.87	18.84	37.15	40.14	47.96	4.39
Wakkanai	15.37	4.83	38.76	41.04	48.57	3.49
Nishikine	2.37	5.86	45.43	46.34	49.50	5.47
Mayaji	1.07	4.55	47.16	47.22	49.97	2.53
Yamada	2.39	24.34	37.01	36.26	50.51	4.17
Miike	0.99	13.83	44.42	40.76	52.15	2.26
Shigeuchi	11.19	21.80	35.25	31.76	52.60	4.26
Kitomo	11.97	12.63	42.56	32.84	56.45	5.70
Tajima	12.03	11.87	43.54	32.56	57.20	7.09
Takasaki	12.62	2.69	49.78	34.91	58.78	5.03
Shiba	14.89	8.64	45.72	30.75	59.79	3.36
Ochiai	9.63	28.47	39.64	22.26	64.04	2.96
Tomowo	7.86	36.85	35.52	19.77	64.24	4.44
Terukoshi	11.34	1.37	56.63	30.66	64.88	3.88
Yubetsu	3.11	11.76	50.36	34.77	65.85	7.08

tionship between Young's modulus and the grade of coal for those coals whose volatile-matter content had been determined. The volatile matter was determined from the loss in weight at 950°C. minus the weight of moisture determined at 105°C. and was calculated to the dry, ash-free basis. These values, in the order of 10^{10} dynes/cm.², are reasonable, considering the rheological properties of coal. As a whole, we observe a relationship between values for Young's modulus and grade, namely, the

higher moduli shown for anthracites having little volatile matter, gradually decrease for bituminous coal, again increase for producer gas coal and brown coal, and finally decrease for young lignite. The disadvantage of using volatile matter as an expression of rank is that the content of volatile matter does not correlate directly with the difference in caking properties of the coals. Strongly caking coals showed lowest E values, nearly 2×10^{10} dynes/cm.², the lower-caking coals showed higher E values. This trend seems to be sufficient to explain the actual characteristics of all coals. The strongly caking coals fuse and swell because of a weakness of their intermolecular forces, and the caking properties diminish

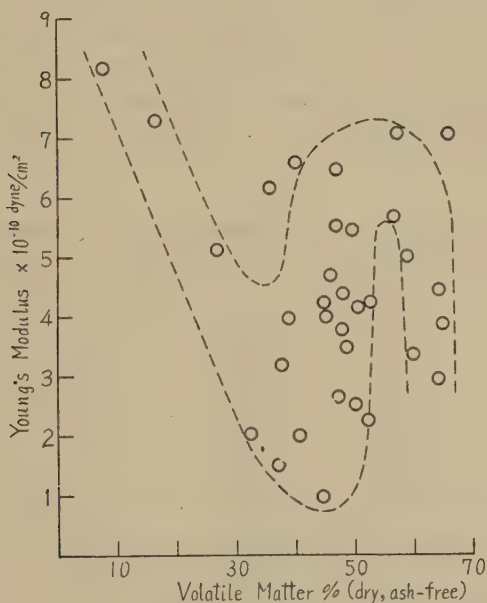


FIG. 4. Young's modulus and the grade of coal.

gradually as the intermolecular forces become stronger, reaching higher E values for producer gas coal or brown coal because of the presence of groups containing oxygen which strengthen the intermolecular forces; consequently, the coal molecules decompose without fusing when carbonized. On the other hand, anthracites having no caking properties have larger values for the development of the carbon lattice. The reason for low E values for the young lignites is due to the influence of flaws or a micro-inner structure in the solid, as explained later in this paper.

It is interesting to note that Young's modulus of strongly caking coals, *ca.* 2×10^{10} dynes/cm.², is nearly the same as that of thermo-

plastics, because both materials have similar rheological properties, i.e., their molecules become mobile at some elevated temperature. According to R. Houwink (12) values below $ca. 2 \times 10^{10}$ dynes/cm.² can be taken as characteristic of nonhardening resins with globular micelles, considering the micelles of such solids to be held together only by relatively weak forces of the van der Waals' type.

Relation of Ash to Coal Molecules

With the exception of moisture, coal may be considered as being constructed of organic molecules and ash. From the measurements of Young's modulus of many specimens with various ash contents, a very interesting relation was found to exist between ash and organic coal molecules. It is concluded that Young's modulus is a linear function of ash content expressed in volume percentage, based on the assumption that the density of ash is 2.0 and that of pure coal is 1.2. The ash contents, of course, were

TABLE III
Young's Modulus and Ash Contents in Volume Percentages

Sample	Ash, dry basis (A)	Ash, dry basis (ϕ)	Young's modulus $\times 10^{-10}$
	wt.-%	vol.-%	dynes/cm. ²
American	4.41	2.49	2.01
	18.69	12.14	2.03
	3.26	1.98	2.04
	28.05	18.96	3.92
	9.60	5.99	3.98
	11.05	6.94	4.60
	82.87	74.37	6.86
	28.05	18.96	9.20
	44.49	32.50	13.80
Takashima (Kyushu, Japan)	6.81	4.21	2.83
	3.32	2.02	2.86
	6.89	4.26	3.04
	3.43	2.09	3.56
	15.82	10.13	4.19
	2.42	1.47	4.49
Shishimachi (Kyushu, Japan)	14.70	9.37	2.59
	43.41	31.52	4.53
	47.38	35.08	4.53
	29.77	20.28	7.20
	62.43	49.93	8.54
	51.23	38.67	9.73
	54.87	42.29	9.96

TABLE III—*Continued*

Sample	Ash, dry basis (<i>A</i>)	Ash, dry basis (ϕ)	Young's modulus $\times 10^{-10}$
	<i>wt.-%</i>	<i>vol.-%</i>	<i>dynes/cm.²</i>
Toro (Saghalien, now U.S.S.R.)	12.85	8.13	3.95
	7.26	4.48	3.96
	32.45	22.46	4.70
	38.82	27.57	5.56
Yubetsu (Hokkaido, Japan)	27.76	18.74	3.63
	14.46	9.21	3.75
	12.78	8.08	5.11
	21.54	19.46	6.98
	36.55	25.69	7.23
	57.79	45.10	9.24
Nakago (Joban, Japan)	53.38	40.72	4.51
	19.02	12.35	4.56
	86.14	78.26	9.23
Taiheiyo (Hokkaido, Japan)	6.48	3.99	4.02
	7.30	4.51	4.35
	5.81	3.57	4.96
	7.71	4.89	5.04
Shosaku (China)	38.30	27.17	6.43
	9.39	5.63	6.86
	6.75	4.17	7.45
	5.72	3.49	8.09
	10.05	6.29	8.26
	5.91	3.64	8.29

determined on the same specimens on which the Young's modulus values were measured.

A sample calculation of the ash content in volume percentages, ϕ , is shown as follows:

Analytical data of a specimen:

Moisture %	Ash %	Ash, dry basis (<i>A</i>) %
3.84	5.68	5.91

$$\begin{aligned}
 \phi &= \frac{A/\text{density of ash}}{(A/\text{density of ash}) + [(100 - A)/\text{density of pure coal}]} \\
 &= \frac{5.91/2.0}{5.91/2.0 + (100 - 5.91)/1.2} \\
 &= 3.64.
 \end{aligned}$$

Table III, and Figs. 5 and 6 show this relationship for eight coals. It is noteworthy that if this relation is expressed by the linear equation,

$$E = E_0(1 + K\phi), \quad [2]$$

where,

E = Young's modulus of the specimen,

E_0 = Young's modulus of "pure" coal,

K = a constant for the coal representing the inclination of the line, and

ϕ = the ash concentration in volume percentage,

the influence of ash to coal molecules can be represented by the values of K .

Equation [2] is in the same form as the equation for filler effect on Young's modulus of rubber derived recently by H. M. Smallwood (13) and E. Guth (14). It is necessary to recognize that this equation can be derived formally as E. Guth stated in this paper and holds not only in rubber-carbon black systems but in all other analogous ones. The constant K represents the degree of solvation of organic molecules with "filler" particles suspended in the matrix. On the other hand, E_0 is a measure of the intermolecular forces between "pure" organic molecules.

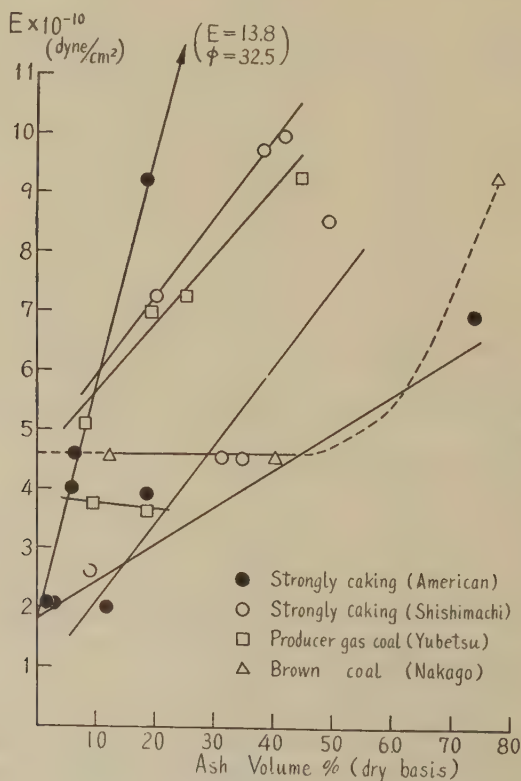


Fig. 5. Young's modulus and ash concentration.

As we see from the values of K and E_0 in Table IV and also from Figs. 5 and 6, these values evaluate quantitatively the essential rheological properties of coals of every grade. In general, the strongly caking coal have low E_0 and high K values, lower-caking coal larger E_0 and smaller K values, and anthracite the largest E_0 and zero or negative K .

This is one of the absolute expressions of the idea that the essential properties of coal can be considered from the concept of intermolecular forces, as already stated in the previous section. The strong solvation of caking coals seems interesting to compare with the discovery by the x-ray diffraction study of H. L. Riley *et al.* (2) that a maximum in the c -dimension is observed in the range of the higher grade bituminous coals.

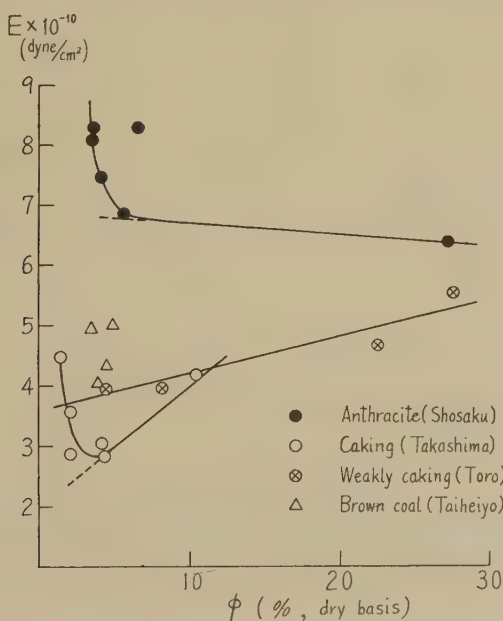


Fig. 6. Young's modulus and ash concentration (*cont.*).

As shown by the above data, the American strongly caking coal of unknown origin (which is used in Japan for improving the caking properties of Japanese caking coals), a Japanese strongly caking coal (Shishimachi), and a producer gas coal (Yubetsu) have more than one series of E - ϕ relationship. Shishimachi coal and Yubetsu coal are said to be mined from two series of coal seams, respectively. As an explanation of the difference in Young's modulus values between these two series of the same ash concentration, it is suggested that the elemental analysis of two specimens of almost similar ash contents from Yubetsu producer gas coal shows some difference in oxygen (plus sulfur and nitrogen) contents, as

TABLE IV
 Values of E_0 and K

Sample	E_0 $\times 10^{-10}$	K $\times 10^2$	E_0/K $\times 10^{-12}$	Caking properties
	<i>dyne/cm.²</i>			
Anthracite (Shosaku)	7.0	-2	-3.5	Noncaking
Bituminous (American)	1.8	38	0.047	Strongly caking
	1.8	6	0.30	Weakly caking
Bituminous (Shishimachi)	0.8	14	0.057	Strongly caking
	4.7	13	0.36	Noncaking
Bituminous (Takashima)	2.0	20	0.10	Caking
Bituminous (Toro)	3.6	7	0.51	Weakly caking
Producer gas coal (Yubetsu)	4.5	13	0.35	Noncaking
	3.9	-1	-3.9	Noncaking
Brown coal (Nakago)	4.6	0	—	Noncaking

shown in Table 5; these atoms, especially oxygen, naturally will strengthen the intermolecular forces.

Effect of Bitumen

Considering the classic bitumen theory of caking properties and the fact that coal in its simplest division can be said to consist of "bitumen" and "residue," the effect of bitumen was examined for several kinds of coal.

Bitumen content was determined on the same specimens previously used for measuring Young's modulus. The specimen was powdered to

 TABLE V
 Elemental Analysis and E of Yubetsu Producer Gas Coal

$E \times 10^{-10}$	Elemental analysis, dry basis				O + etc., dry, ash-free basis
	Ash	C	H	O + etc.	
<i>dynes/cm.²</i>					
6.98	21.54	62.78	5.50	12.97	16.53
3.63	27.76	59.31	5.57	10.19	14.11

pass a 60-Tyler mesh, dried 1 hr. at 105°C., weighed, and 5 g. of the sample and 100 ml. of pure benzene were put in an autoclave. The autoclave was shaken automatically throughout the extraction, heated electrically up to 300°C. in 2.5 hr. and retained at this temperature for 3 hr. The pressure was about 50 atm. The extracted sample was washed with benzene in a Soxhlet apparatus and then dried. The bitumen content was determined from the difference of ash contents between the original and this extracted sample, assuming no ash was present in the bitumen.

A remarkable relationship between the bitumen content (dry, ash-free basis), namely, the percentage of bitumen in the organic portion of coal and Young's modulus is shown in Fig. 7. The experimental data plotted in Fig. 7 are shown in Table VII in a later section, in a comparison with

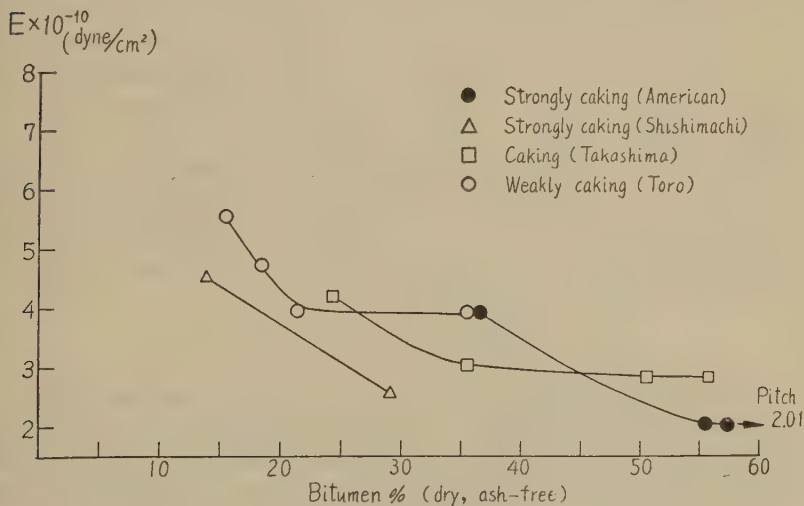


FIG. 7. Effect of bitumen.

the calculated values. This supports the idea that the bitumen molecules with weak intermolecular forces act as a kind of plasticizer agent to weaken the total forces and thus determine the caking properties; at the same time the physical mechanism of the old chemical theory is clearly understood from these curves.

The $B-E$ curves are of a saturation type and on the whole of the shape of a fan, whose pivot is at $ca. 8 \times 10^{10}$ dynes/cm.², the Young's modulus of anthracite which contains no bitumen. The formulation of these curves is found in a later section, but it is interesting to note that in the strongly caking coals (American coal and Takashima coal) the effect of bitumen is different than in the weakly caking (Toro) coal, the latter shortly reaching the saturation condition of the bitumen effect with

TABLE VI
Young's Modulus and Gamma Contents

Sample	Caking properties	Gamma, dry, ash-free	Young's modulus $\times 10^{-10}$
		%	dynes/cm. ²
Kanbayashi	Noncaking	0.28	5.98
Yamada	Almost noncaking	2.4	4.17
American, 1	Caking	10.9	3.98
Takashima	Strongly caking	11.6	2.83
Miike	Strongly caking	12.6	2.26
American, 2	Strongly caking	18.4	2.04

a small amount of bitumen; Young's modulus at this condition is rather high. This is the evidence of the classical theory of W. A. Bone (5), mentioned in the *Introduction*, that the mutual relation between the bitumen and residue properties is important. To improve the caking properties of Toro coal, the addition of more bitumen, even if it is possible by any treatment, is without effect, but improvement of the residue or bitumen-residue relationship by weak hydrogenation or solvent treatment at high temperature, for example, as is in part already practiced industrially in Japan, is effective. These processes result in a weakening of the intermolecular forces of the "residue" and at the same time promote an affinity with the existent bitumen.

Physical Meaning of the Gamma Theory

To define the physical meaning of the classical gamma theory of caking properties, the amounts of γ -portion were determined on several specimens. Determination of the γ -fraction was carried out by the generally used Soxhlet extraction method (4) and the difference $100 - (\alpha + \beta)$ was regarded as γ . Table VI and Fig. 8 show the γ - E relation.

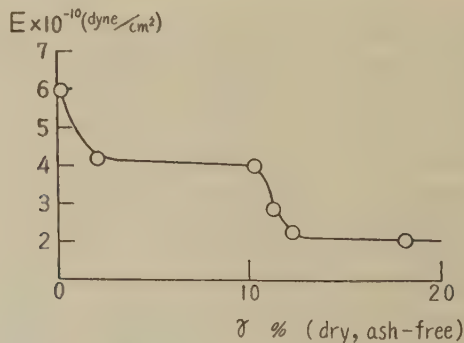


FIG. 8. Gamma effect.

In the region of γ under 10%, *i.e.*, of noncaking or weakly caking coals, Young's modulus decreased to a kind of halfway saturation. Also, in this respect the importance of not only the γ -portion but other (α and β) residual portions is suggested.

Formulation of Caking Properties

From the exact determinations of ash and bitumen on many bituminous coals it was ascertained that a definite relationship exists between ϕ and B (bitumen, %, dry, ash-free basis). This curve (Fig. 9) can be expressed by the equation,

$$\gamma = a/B^b, \quad [3]$$

where a and b are constants applicable to all bituminous coals. Taking logarithms of both sides of the equation, we have a linear relation between

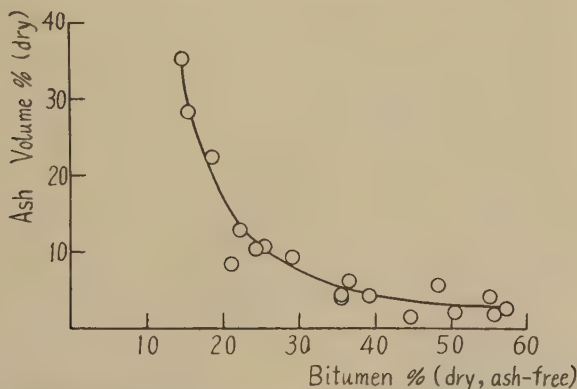


FIG. 9. Ash-bitumen relation.

$\log \gamma$ and $\log B$, as shown in Fig. 10. Hence, the constants are calculated as

$$\phi = 7.5 \times 10^3/B^2. \quad [4]$$

Substituting ϕ of Eq. [2] by ϕ of Eq. [4], we have,

$$E = E_0 \left(1 + K \frac{7.5 \times 10^3}{B^2} \right). \quad [5]$$

Young's modulus of specimens of known bitumen concentration in several coals which have previously known K and E_0 values were calculated by Eq. [5]. Calculated and experimental values of these Young's moduli are compared in Table VII.

If K and E_0 are previously determined for any coal species (or coal seam), E , B , and ϕ are easily calculated, at least approximately, with determination of any one of these three factors, of which the ϕ (ash) determination is easiest, from Eqs. [2], [4], and [5].

Accordingly, from these relations the caking properties of any coal are estimated with fair accuracy without the laborious and indirect tests used in the coke industry.

Necessary Conditions for Caking

From the above description the essential conditions for caking properties are known to be a small E_0 and a large K . When these two conditions are satisfied, all other relations between E , B , and γ can be derived by the above equations. This means that the caking properties of coal can be expressed in absolute units.

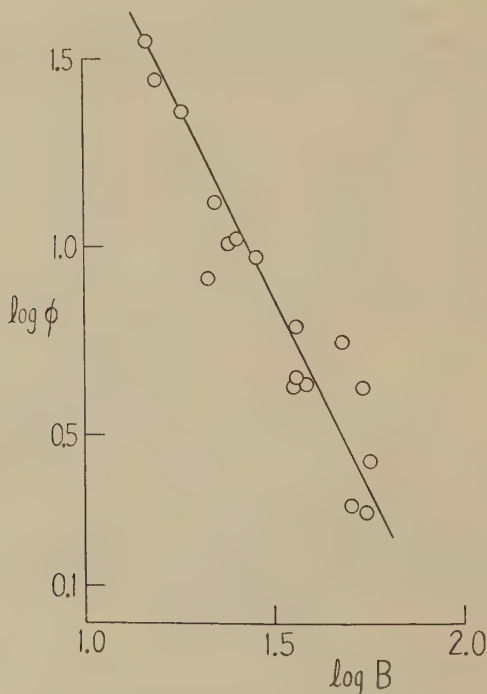


FIG. 10. $\log \phi$ vs. $\log B$.

The physical meaning of these fundamental conditions is that the intermolecular forces of coal molecules should be weak and that the molecules should solvate as strongly as possible around the ash particles.

New Essential Models of Coal Structure

In order to illustrate these facts and considerations, new structural models for coals of different grades have been proposed, as shown in Fig. 11a-d.

TABLE VII
Calculated and Experimental Young's Modulus

Sample	E_0 $\times 10^{-10}$	K $\times 10^2$	B	$E_{\text{calcd.}}$ $\times 10^{-10}$	$E_{\text{exptl.}}$ $\times 10^{-10}$
Bituminous (Toro)	3.6	7	%		
			15.58	4.4	5.56
			18.50	4.2	4.70
			21.37	4.0	3.95
Bituminous (American)	1.8	38	35.61	3.8	3.96
			36.67	5.6	3.98
			55.63	3.5	2.04
			57.44	3.4	2.01
Bituminous (Shishimachi)	0.8	14	14.89	4.6	4.53
			29.21	1.8	2.59
Bituminous (Takashima)	2.0	20	24.30	7.1	4.19
			35.72	4.4	3.04
			50.53	3.2	2.86
			55.06	3.0	2.83

It should be noted first that these models represent the essential properties of coal, not the real texture. Thus, an explanation of the difference between fusain and durain by means of these models would lack essential meaning.

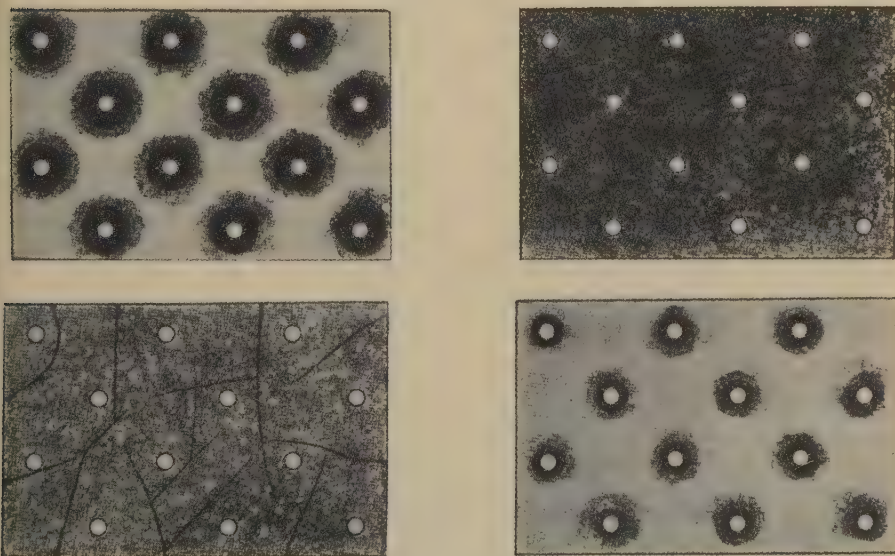


FIG. 11. New proposed models for coal structure.

Throughout Fig. 11 the concentration of blackening means the strength of intermolecular forces, and the circles represent ash particles as skeletons. A high concentration around the circles means a strong solvation, *i.e.*, large K values; a strong blackening of the background suggests strong forces between coal molecules, *i.e.*, large values of E_0 . In the young coals (from lignite to brown coal) in Fig. 11a, complex colloidal inner surfaces are illustrated by black random lines, whose existence often results in a lower Young's modulus instead of strong intermolecular forces (see the next section).

The blackening of the ground and solvated regions changes continuously since the coal consists of essentially the same molecules in the "turbostratic system" 2, 15), but of only continuously changing intermolecular forces. There can be little doubt that the molecules of weaker forces are hence easily extracted.

Young's Modulus and a Practical Measure of Caking Properties

As a comparison of Young's modulus with a practical measure of caking properties, the so-called Lessing indexes were measured on many coals. The Lessing index is the ratio of the height of carbonized coal after

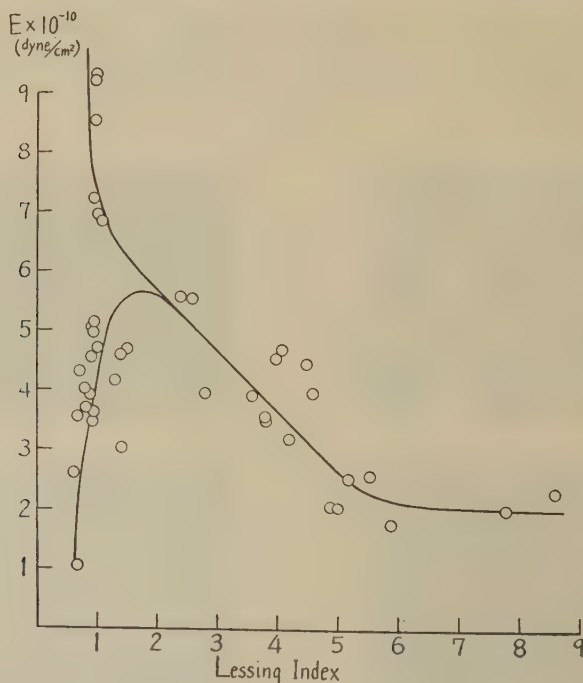


FIG. 12. Lessing index and Young's modulus.

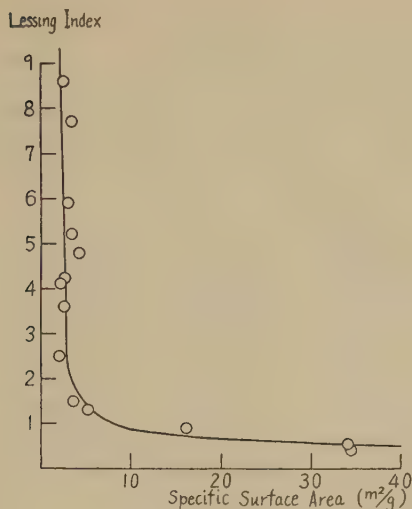


FIG. 13. Lessing index and the inner surface.

heating for 7 min. at 900°C. in a silica retort to the height of 1 g. of the original coal of minus 30 Tyler mesh. As shown in Fig. 12 the coals with large Lessing indexes have lower Young's moduli. In the region of low Lessing indexes, two branches are recognized, of which the left branch is for anthracite and the right branch is for younger coals which show a low modulus because of their complex inner surfaces.

Figure 13 shows the relation of Lessing indexes to specific surface areas calculated from the iodine adsorption method (16); the coals of high Lessing indexes have little inner structure, and vice versa.

ACKNOWLEDGMENTS

The author acknowledges with sincere thanks the enthusiastic assistance of Hideo Tani and Mitsuo Abiko during the course of the investigation.

He is also indebted to Dr. Y. Kobashi of the Kobayashi Physical Institute for his suggestions on the sonic measurement method, and to Dr. T. Shimmura, Dr. M. Kurokawa, and Mr. A. Baba, all of this Institute, for their encouragement.

He is further deeply thankful to Dr. H. L. Riley (England), Dr. D. T. A. Townend (England), Dr. D. H. Bangham (England), and Dr. G. Pickett (U. S. A.) for their kind information on studies which are not available in this occupied country.

REFERENCES

1. Excellent papers were published on these problems in 1944. See the Proc. Conf. Ultra-Fine Structure Coals and Cokes, British Coal Utilisation Research Assoc., London, 1944.
2. BLAYDEN, H. E., GIBSON, J., AND RILEY, H. L., Proc. Conf. Ultra-Fine Structure Coals and Cokes, p. 176. British Coal Utilisation Research Assoc., London, 1944; BLAYDEN, H. E., GIBSON, J., AND RILEY, H. L., *Inst. Fuel (London) Wartime Bulletin* 1945, 177.

3. FISCHER, F., BROCHE, H., AND STRAUCH, J., *Brennstoff-Chem.* **5**, 299 (1924); *ibid.* **6**, 33 (1925); *idem*, *Fuel* **5**, 466 (1926).
4. CLARK, A. H., AND WHEELER, R. V., *Trans. J. Chem. Soc.* **103**, 1704 (1913); JONES, D. T., AND WHEELER, R. V., *Trans. J. Chem. Soc.* **109**, 707 (1916).
5. BONE, W. A., PEARSON A. R., AND QUARENDON, R., *Proc. Roy. Soc. (London)* **A105**, 608 (1924); BONE, W. A., *Trans. J. Soc. Chem. Ind.* **44**, 291T (1925).
6. HOUWINK, R., *Elasticity, Plasticity and Structure of Matter*, p. 141. Cambridge University Press, London, 1937.
7. MÜLLER, O., *Glückauf* **66**, 1601, 1946 (1930).
8. BANGHAM, D. H., AND MAGGS, F. A. P., *Proc. Conf. Ultra-Fine Structure Coals and Cokes*, p. 118. British Coal Utilisation Research Assoc., London, 1944.
9. GRIME, G., *Phil. Mag.* **20**, 304 (1935); GRIME, G., AND EATON, J. E., *Phil. Mag.* **32**, 96 (1937); POWERS, T. C., *Proc. Am. Soc. Testing Materials* **38**, Part 2, 460 (1938); BAAB, K. A., AND KRANER, H. M., *J. Am. Ceram. Soc.* **31**, 318 (1948).
10. DILLON, J. H. PRETTYMAN, I. B., AND HALL, G. L., *J. Applied Phys.* **15**, 309 (1944); WITTE, R. S., MROWCA, B. A., AND GUTH, E., *J. Applied Phys.* **20**, 481 (1949); LYONS, W. J., AND PRETTYMAN, I. B., *J. Applied Phys.* **18**, 586 (1947).
11. PICKETT, G., *Proc. Am. Soc. Testing Materials* **45**, 846 (1945).
12. HOUWINK, R., *Elasticity, Plasticity and Structure of Matter*, p. 141, 154. Cambridge University Press, London, 1937.
13. SMALLWOOD, H. M., *J. Applied Phys.* **15**, 758 (1944).
14. GUTH, E., *J. Applied Phys.* **16**, 20 (1945).
15. BISCOE, J., AND WARREN, B. E., *J. Applied Phys.* **13**, 364 (1942).
16. INOUE, K., *J. Fuel Soc. Japan* **29**, 112 (1950).

ERRATA

In the article by Arthur L. Loeb entitled, "An Interionic Attraction Theory Applied to Diffuse Layer Around Colloid Particles," which appeared in Volume 6, Number 1, pp. 75-91, the following corrections should be noted:

- | | |
|---------------|---|
| p. 78, line 6 | read: " $\eta' = 0$ " for " $\eta = 0$ " |
| 78, line 25 | read: " \tilde{K}^2 is independent" for " K^2 is independent" |
| 80, line 3 | read: "singularity in \tilde{K}^2 " for "in K^2 " |
| 84, line 4 | read: "When" for "when" |
| 85, line 8 | omit "negative" |

THE MECHANISM OF BIMOLECULAR REACTIONS IN SOLUTIONS

J. A. Christiansen

Physicochemical Institute of the University, Copenhagen, Denmark

Received January 8, 1951; revised March 28, 1951

A bimolecular reaction between molecules A and B in a solution may be described by means of the following picture:

Let the molecule A be surrounded by a surface, the critical surface being of a certain form and extent; and let us introduce the admittedly very crude assumption that the surface is a sphere with radius r . The interaction between A and B must then be described as a reaction taking place in two steps. The first step is that the center of molecule B by diffusion reaches the critical surface, and the second is the chemical reaction proper.

According to well-known principles, the reciprocal $1/s$ of the resulting velocity of reaction then is a sum of two reciprocal velocities, one corresponding to the first step and one corresponding to the second step.

In very fast reactions, *i.e.*, reactions with low activation energies, the reciprocal velocity belonging to the first step will be predominant. In this case, the temperature coefficient of the resulting reaction will be determined by the viscosity of the solvent, *i.e.*, it will be the same for different (fast) reactions in that solvent. In the other limiting case, where the activation energy of the reaction is high and thus the resulting velocity low, the reciprocal velocity belonging to the second step will be predominant. In this case, the effect of the viscosity of the solvent disappears, and the temperature coefficient will be determined by the activation energy of the reaction in question; *i.e.*, it will be characteristic for the reaction in the solvent in question and may thus very well be different for different reactions in the same solvent.

Finally, if both reciprocal velocities are of the same order of magnitude, both members must be taken into account with the result that the velocity will not obey the Arrhenius equation. It can be seen that at high temperatures the apparent "heat of activation" of the reaction will approach the low value, namely, the "heat of activation" of the viscosity; and conversely at low temperatures it will approach the high value, namely, the heat of activation of the chemical reaction. On account of the properties of exponential functions this intermediate case will appear only exceptionally, as in most cases, either one or the other member in the sum will predominate. The proof of this statement is as follows:

Let the velocity constant k of the total reaction be connected with two velocity constants k_1 and k_2 by the equation

$$1/k = 1/k_1 + 1/k_2.$$

Let furthermore $k_1 = f_1 \exp(-A_1/T)$; $k_2 = f_2 \exp(-A_2/T)$, where f_1 and f_2 are frequency factors.

We then get

$$\ln(k/f_1) = -\ln[\exp(+A_1/T) + \beta \exp(+A_2/T)]; \beta \equiv f_1/f_2.$$

The Arrhenius diagram will then qualitatively be the one in Fig. 1, *i.e.*, the curvature will always be as shown. The intersection of the two asymptotes will be at the temperature where

$$\exp(A_1/T) = \beta \exp(A_2/T)$$

and the corresponding point on the curve will lie $\ln 2 \simeq 0.7$ below the point of intersection.

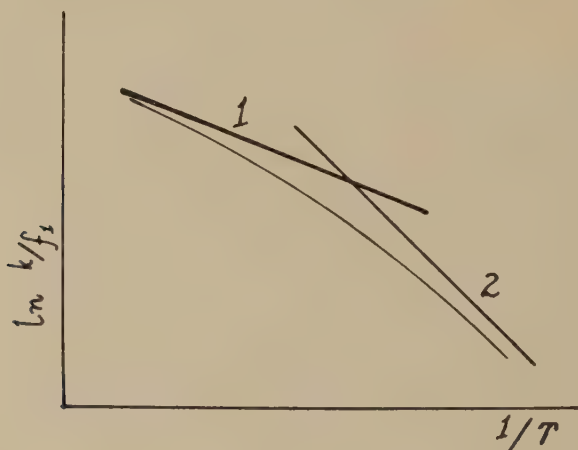


FIG. 1.

Such considerations show that there is no real discrepancy between the statements concerning frequency factors on the one hand by Debye (1) and on the other hand by earlier authors, *e.g.*, the present (2). Following Smoluchowski, Debye arrives at an expression for the probability/sec. for collision with molecules B

$$Z = 8RTb/3\eta \times 1000,$$

where b is the concentration in moles/l. of B and η the viscosity of the medium.

The old assumption was that the frequency factor could reasonably well be represented by the classical gas kinetic collision number. It ap-

appears now from the above considerations that in the case of fast reactions (e.g., quenching of fluorescence) Debye's collision probability must be used, while in the case of slow reactions, i.e., reactions with a considerable heat of activation, the ordinary collision number must be applied.

To sharpen the argument, the chain of reasoning will be repeated below by means of mathematical symbols.

Let us write in a purely formal way the sequence of reactions under consideration:



where the symbol (+1) will refer to the forward reaction and (−1) to the same reaction reversed. Let further the probability per unit time for an A to react according to (+1) be w_1 and let the probabilities (per unit time) for an X to react according to (−1) and (+2), respectively, be w_{-1} and w_2 . If the intermediate X has a very short life, its amount must be stationary, and denoting the concentration of A by a , we therefore get for the reciprocal over-all velocity of the process (1/s), the expression

$$1/s = 1/aw_1 + w_{-1}/aw_1w_2.$$

The fraction w_{-1}/aw_1 is a purely thermodynamic quantity measuring the reciprocal equilibrium concentration x^0 of X , defined by

$$aw_1 = x^0w_{-1};$$

1/s may therefore be rewritten as

$$1/s = 1/aw_1 + 1/x^0w_2.$$

It is obvious that w_1 and x^0 both contain the concentration b of B , and furthermore, that if x^0w_2 is small as compared to aw_1 , the over-all velocity of the reaction will be determined by the former. It may be emphasized once more that x^0 is an equilibrium quantity which therefore cannot depend on the viscosity.

To give the symbols w definite meanings we must consider our picture more closely. As stated above, the first step in the reaction is the crossing of the center of B of the critical surface of A , where the radius r is the reaction distance. In other words, r is the distance between the centers of A and B when the reaction takes place. Debye (1) calculates w_1 from the Smoluchowski diffusional treatment applied originally to coagulation of neutral colloidal particles. Apart from electrostatic influences, w_1 becomes

$$w_1 = 8RTb/3\eta \times 1000,$$

where R is the usual gas constant, η is the viscosity of the solvent, and b is reckoned in moles/l.

With the values $R = 8.31 \times 10^7 \text{ erg/}^\circ\text{K}$; $T = 298^\circ\text{K}$, $b = 1 \text{ mole/l.}$, $\eta = 8.94 \times 10^{-3} \text{ dyne-sec./cm.}^2$ (the viscosity of water) we get

$$w_1 = 7.39 \times 10^9 \text{ sec.}^{-1}$$

which shows that for chemical reactions with directly measurable velocities, $1/w_1$ must always disappear as compared to w_{-1}/w_1w_2 . As the temperature dependence of η is usually small, the same will be true also at higher temperatures.

We thus get $s = x^0w_2$ with an error which is far below the experimental inaccuracy. Now X in our case simply means a complex AB with the prescribed distance r between the centers of the two molecules. x^0 must therefore be a times the equilibrium concentration $b(r)$ of B -molecules having a distance r from A . In the case where there are no forces between the molecules, $b(r)$ is of course the same as b ; if not, the appropriate correction must be introduced. At any rate, $b(r)$ is proportional to b .

The probability w_2 is the probability per unit time that a molecule B placed at the distance r from A will react with A . Following the old idea (from the first decade of this century) of M. Trautz and others, this probability may be set equal to the number of times the center of B passes the critical surface in the right direction times the usual exponential function, which represents the fraction of "active" molecules. We may try to define the situation somewhat more sharply by specifying the assumptions. We may, for example, assume that the necessary and sufficient condition for B to react with A is that the center of B passes the critical surface with a momentum p directed against the center of A and exceeding a certain threshold value p_0 . Denoting the reduced molar mass

$\frac{M_A M_B}{M_A + M_B}$ by μ , we get for the kinetic energy E_p of the complex X (AB)

$$E_p = \frac{1}{2\mu} p^2.$$

According to the canonical equations, this yields for the velocity \dot{q} corresponding to p

$$\frac{\partial E_p}{\partial p} = \dot{q} = p/\mu.$$

In our case, \dot{q} must equal r ; i.e., $p = \mu \dot{r}$. For an element $d\sigma$ of the critical surface, we get from statistical mechanics an expression for the inward flow f of particles obeying the above assumption,

$$f = d\sigma \int_{-P_0}^{-\infty} P \dot{q} dp, \text{ where } P = C \exp(-p^2/2\mu RT)$$

or

$$f = Cd\sigma \int_{E_0}^{\infty} \exp(-p^2/2\mu RT) dE_p \\ = Cd\sigma \int_{E_0}^{\infty} \exp(-E_p/RT) dE_p = Cd\sigma RT \exp(-E_0/RT)$$

This flow integrated over the whole surface becomes

$$s/a = 4\pi r^2 RTC [\exp(-E_0/RT)].$$

The constant C is determined by the condition that the integral $C \int_{-\infty}^{+\infty} P dp$ must be equal to $b(r)$.

$$b(r) = C \int_{-\infty}^{+\infty} \exp(-p^2/2\mu RT) dp = C\sqrt{2\pi\mu RT}.$$

This gives

$$s = ab(r)2r^2\sqrt{2\pi RT/\mu} \times \exp(-E_0/RT).$$

This formula and its derivation are practically identical with those derived by Krüger (3) (1908), Goldschmidt (4) (1909) and K. F. Herzfeld (5) (1919).

The main difference is the replacement of b by $b(r)$ which becomes necessary when intermolecular forces come into play.

If, for example, A and B are ions and the solution so dilute that the Debye-Hückel approximation can be applied, we may place $b(r) = b\gamma$, where b is the molar concentration of B in the solution and γ a factor whose logarithm is

$$\ln \gamma = -\frac{z_1 z_2}{\epsilon k T r} \exp(-\kappa r),$$

where κ is the well-known Debye factor defined by

$$\kappa^2 = 8\pi N^2 e^2 I / \epsilon RT \times 1000$$

and where e is the electronic charge in electrostatic units (e.s.u.), I is the ionic strength, z_1 and z_2 are the charges in e.s.u. of the colliding ions, and ϵ is the dielectric constant of the medium (2). As the argument leading to this expression is only valid when κr is a small fraction, $\ln \gamma$ may be re-written

$$\ln \gamma = -\frac{z_1 z_2}{\epsilon k T r} + \frac{z_1 z_2 \kappa}{\epsilon k T}.$$

For a similar reason the factor added by G. Scatchard (6) $[\exp(a\kappa)/(1+a\kappa)]$ is superfluous, as in the approximation considered it is equal to one.

It may be added that although r and a are of the same order of magnitude, their meanings are quite different: r is the "reaction distance" which of course is characteristic for the reaction in question while a is a

parameter representing some average distance (also of the order of magnitude of molecular dimensions) which is characteristic for the solution but not for the reaction. This is correctly stated by Scatchard but sometimes one meets in the literature a confusion of r and a .

REFERENCES

1. DEBYE, P., *Trans. Electrochem. Soc.* **82**, (1942). (A more detailed derivation is given by UMBERGER AND LA MER, *J. Am. Chem. Soc.* **67**, 1099 (1945) who treat the problem of quenching of fluorescence.)
2. CHRISTIANSEN, J. A., *Z. physik. Chem.* **113**, 35 (1924).
3. KRÜGER, *Nachr. Ges. Wiss. Göttingen* p. 1 (1908).
4. GOLDSCHMIDT, *Physik. Z.* **10**, 206 (1909).
5. HERZFELD, K. F., *Ann. Physik* **59**, 635 (1919).
6. SCATCHARD, G., *Chem. Revs.* **10**, 229 (1932).

A MICROMETHOD FOR DETERMINATION OF CATION-EXCHANGE CAPACITY OF CLAY

Robert C. Mackenzie

The Macaulay Institute for Soil Research, Craigiebuckler, Aberdeen, Scotland
Received January 5, 1951

INTRODUCTION

During investigations on clays and minerals, of which only small amounts were readily available, it became necessary to find an accurate micromethod for determining cation-exchange capacities. Usual methods, which are far too numerous to detail here (1), require considerably more than the 10–50 mg. of material that could be spared. Three possible methods were tested, *viz.* (a) an adaptation of the manganese method of Bower and Truog (2); (b) a method employing saturation with strontium and utilizing spectrographic determination of the sorbed strontium; (c) an adaptation of the usual ammonium acetate method (3,4).

Method (c) proved most satisfactory and consequently the other two methods, although referred to in the discussion, will not be described in detail.

EXPERIMENTAL

A sample of 10–50 mg. of the clay, depending on the expected cation-exchange capacity, was accurately weighed out by means of a semi-microbalance into a 15-ml. centrifuge tube, shaken up with 10 ml. normal ammonium acetate solution of pH 7 and allowed to stand overnight. In the morning the suspension was again shaken, centrifuged, and the supernatant liquid was removed by gentle suction. A further 10 ml. of the ammonium acetate solution was added, the clay redispersed by shaking, shaken for a further 5 min., recentrifuged, and the supernatant liquid was again removed. This procedure was repeated a further four times giving six washings in all. A little ammonium chloride was added to the last washing to give Cl^- as a tracer.

The clay was washed free from excess ammonium salts with neutral 95% alcohol using the centrifuge procedure. To ensure complete removal, one wash was given after no Cl^- was detected in the supernatant liquid. Normally 4–5 washings suffice.

The clay was then washed into a Markham microdistillation apparatus (5) with the minimum amount of distilled water, the tube and stopper being thoroughly rubbed with a rubber policeman to ensure complete removal of clay. With care this procedure can be performed with as little

as 20 ml. water. The NH_4^+ was steam-distilled off in the usual manner with 50% NaOH, the distillate being collected in 2 ml. 4% boric acid solution containing a mixed indicator of methyl red and bromocresol green. About 15–20 ml. of distillate was collected and titrated with approximately 0.0067 *N* (*N*/150) H_2SO_4 , using a 1-ml. microburet and compressed-air stirring. A blank determination on the distilled water was run before and after every set, and a solution of known NH_4^+ content was occasionally used as a check on the accuracy of the apparatus and acid.

The whole process is relatively rapid, the last 5 washings with ammonium acetate solution and the alcohol washings being completed in one morning and the distillation in the afternoon. Normally six samples are run at once, the number being limited by the size of the centrifuge. As with all micro techniques, great care has to be taken to avoid loss of any material, but the method is now being used here as routine.

All reagents, except the boric acid and indicators, are of AnalaR standard. The ammonium acetate is made up by dissolving the requisite amounts of concentrated ammonia and glacial acetic acid in distilled water, making up to volume and adjusting to pH 7 using bromothymol blue as indicator.

RESULTS AND DISCUSSION

The manganese and strontium methods, referred to in the *Introduction*, were selected primarily because the ions employed easily lend themselves to quantitative microdetermination. Difficulties were soon encountered, however, because of the high cation-exchange capacities obtained, presumably due to sorption of the ion as $\text{M}(\text{OH})^+$ rather than as $\text{M}^+ + (6)$, a feature which is likely to be accentuated when dealing with clays of low cation-exchange capacity, where it would be difficult for polyvalent ions to bridge two or more exchange spots relatively far apart. It appears, therefore, that unless alcoholic solutions of these salts are used (6), reasonably accurate results are likely to be obtained only by the use of univalent ions.

The results of Golden, Gammon, and Thomas (7) indicate that, using ammonium acetate, the sum of the cations removed is greater than the total cation-exchange capacity. In their experiments they removed the sorbed NH_4^+ from the ammonium-saturated clay with neutral normal KCl solution and determined the NH_4^+ in the solution. This method, we have found, gives consistently lower results than direct distillation (3,8) of the ammonium-saturated clay with NaOH or MgO, presumably because some of the NH_4^+ becomes "fixed," or at least difficult to remove by K^+ . For example, a normal saturation of a sample of montmorillonite, of cation-exchange capacity 78 mequiv./100 g. by direct distillation of the ammonia, gave a capacity of only 73 mequiv./100 g. using the usual KCl

technique (4,7) (six washings), while distillation of the clay after the KCl washings revealed that 3-4 mequiv./100 g. of NH_4^+ were still present in the clay and could be removed by direct distillation. With kaolinite of cation-exchange capacity 5 mequiv./100 g. the amount of NH_4^+ left in the clay was about 0.5 mequiv./100 g. Results with vermiculite also showed a smaller cation-exchange capacity using the KCl technique than that obtained by direct distillation. Incomplete removal of NH_4^+ by K^+ has been discussed by Bower (9) in a paper which has appeared since this work was completed.

In view of these results it appears that direct distillation of the ammonium-saturated clay, free from excess ammonium salts, is the best method to employ for cation-exchange capacity determination, and it is this method we have adapted to the micro scale. In addition, it is difficult to employ the KCl technique on the micro scale because of dilution difficulties.

Using direct distillation, it is essential to ensure that the clay does not contain organic matter, which might liberate, or absorb, ammonia during the distillation. Consequently, soil clays have to be treated several times with H_2O_2 on the steam bath before using the above-described method.

In Table I are listed cation-exchange capacities for kaolinite, illite, and montmorillonite determined by the micromethod and by the macromethod normally employed here. This is similar to that of Jackson and Truog (4), except that, for the reasons noted above, direct distillation of the ammonium-saturated clay with MgO is employed.

TABLE I

Comparison of Cation-Exchange Capacities as Determined by Macro- and Microtechniques

Clay	Cation-exchange capacity		Difference ^a
	Macro	Micro	
	mequiv./100g.	mequiv./100g.	%
Kaolinite	5.0	4.8	-4.0
Illite	37.1	36.6	-1.3
Wyoming bentonite	77.9	77.0	-1.2

^a Expressed as percentage of results by macromethod.

For both methods, the results quoted in Table I are the means of duplicate determinations. The agreement is sufficiently good for normal purposes; even for single determinations the error should not exceed about 5%.

In conclusion, it may be remarked that the distillation should be carried out as soon as possible after the alcohol washings. From some

results obtained, it appears that standing overnight after the last alcohol washing has been removed (even though the centrifuge tubes are stoppered) tends to give low results.

SUMMARY

A method is described for the determination of cation-exchange capacities of clays on samples of 10-50 mg. The method is discussed and the results obtained compared with those using the normal method employed here for samples of 0.2-1.0 g. clay.

REFERENCES

1. See, e.g., KELLEY, W. P., *Cation Exchange in Soils*. Reinhold, New York, 1948.
2. BOWER, C. A., AND TRUOG, E., *Ind. Eng. Chem., Anal. Ed.* **12**, 411 (1940).
3. SCHOLLENBERGER, C. J., AND DREIBELBIS, F. R., *Soil Sci.* **30**, 161 (1930).
4. JACKSON, M. L., AND TRUOG, E., *Soil Sci. Soc. Am. Proc.* **4**, 136 (1939).
5. MARKHAM, R., *Biochem. J.* **36**, 790 (1942).
6. BOWER, C. A., AND TRUOG, E., *Soil Sci. Soc. Am. Proc.* **5**, 86 (1940).
7. GOLDEN, L. B., GAMMON, N. AND THOMAS, R. P., *Soil Sci. Soc. Am. Proc.* **7**, 154 (1942).
8. KELLEY, W. P., AND BROWN, S. M., *Agri. Expt. Sta. Calif. Tech. Paper No. 15*, (1924).
9. BOWER, C. A., *Soil Sci.* **70**, 375 (1950).

THE BEHAVIOR OF NONIONIC SURFACE ACTIVE AGENTS IN SALT SOLUTIONS

Todd M. Doscher, George E. Myers,¹ and Don C. Atkins, Jr.²

Department of Chemistry, University of Southern California, Los Angeles, California

Received December 4, 1950

INTRODUCTION

This investigation was carried out to determine whether alkali metal ions and alkaline earth metal ions have different effects on the properties of solutions of nonionic surface-active agents. It had already been observed (8,9) that in the presence of the alkaline earth metal ions these surface-active materials are capable of stabilizing suspensions of clay in oil and water media for use as drilling fluids, whereas the alkali metal ions had a coagulating effect.

The nonionic surface-active agents used in this investigation are those produced by reacting hydroxylic or acidic water-insoluble compounds with ethylene oxide under such conditions that the ethylene oxide condenses to form a polyethylene oxide chain attached to the nonpolar residue. The products have formulas of the type: $R-O-(C_2H_4O)_n-C_2H_5OH$, where n may have average values between 3 and 20, and R may be (a) an alkyl-aryl residue, such as the isoöctyl-phenyl group in Triton X-100 (Rohm and Haas Co.); (b) a fatty acid residue, such as the mixed fatty and rosin acids derived from Tall Oil in Renex (Atlas Powder Co.); or (c) a partial ester of hexitol anhydride and a fatty acid, in which case there are several polyethylene oxide chains attached to each molecule of the ester, as in the Tweens (Atlas Powder Co.).

These surface-active agents owe their solubility in water to the hydration of the polyethylene oxide chain; solubility increases and surface activity decreases with increasing length of the chain. At temperatures above 60°C. solutions of most of these compounds become turbid due to dehydration and consequent association of the molecules into larger colloidal aggregates. It has been demonstrated that the osmotic coefficient of solutions of these materials exhibits similar behavior to that of colloidal electrolytes (11); and, further, that solutions of these nonionic compounds solubilize water-insoluble dyes (12), and a long x-ray spacing is obtained

¹ Part of this work was performed under the auspices of a National Lead Company (Baroid Division) Fellowship, and was submitted as part of the Master of Science thesis. Present address: Harvard University, Cambridge, Mass.

² Present address: Crest Laboratories, Burbank, Calif.

at moderate concentrations in water and benzene solutions (5). Earlier experiments (11) have shown that concentrations of alkali chlorides below 1% have no effect on the colligative properties of dilute solutions of these materials. However, the observation that the ability of these nonionic materials to suspend clay could be enormously varied by the use of different salts suggested that at relatively high bulk concentrations of salts, or when dilute solutions are in contact with a solid surface, at which a higher than bulk concentration of salt may exist due to adsorption, the behavior of these nonionic materials might then be affected differently by different salts.

All three types of water-soluble, nonionic materials mentioned above were found to act similarly in the earlier studies; and the materials chosen to typify their respective classes were Renex and Tween 80 (monoöleate ester), both of which contain 10 moles of ethylene oxide/mole of nonpolar residue (2), and Triton X-100. The number average molecular weight of the latter, determined from its freezing point depression in dry benzene, was 680. All the materials, as received, contained slight traces of electrolytes, which had been introduced as condensation catalysts. These were removed by electrodialysis of 10% solutions, and the solutions were then concentrated by evaporation *in vacuo* between 15° and 25°C.

EXPERIMENTAL AND RESULTS

Turbidity and Viscosity

A clear indication that the properties of solutions of these nonionic colloids can be influenced differently by different salts was obtained by studying the turbidity and viscosity of their solutions. The turbidity of solutions of Triton X-100 was determined with the Phoenix Light Scattering Instrument at a wavelength of 437m μ . In order to remove dust from the solutions, since the colloids could not be recrystallized and filtered, advantage was taken of the facts that dust in aqueous solutions is usually negatively charged and that the colloids are nonionic. A sintered-glass disk was sealed into the bottom of a glass U-tube, and a collodion membrane was deposited on one side of the disk. Platinum gauzes were suspended on both sides of the disk and connected to a source of 100 v. d.c., the positive pole in the unfiltered solution. The electrodialyzed, 10% solution of Triton X-100 was sucked very slowly through the disk. The filtered solution was then transferred to a container fitted with a rubber serum seal, and measured quantities were withdrawn as needed, and transferred to the light-scattering cell with a hypodermic syringe. Water or the appropriate salt solutions, which had been prepared from recrystallized salts and a supply of water obtained by subliming ice, were similarly stored and transferred to the light-scattering cell.

The relative viscosities of the solutions were determined with an Ostwald pipet which had a delivery time for water of 121.2 sec. at 20.0°C.

The turbidities of solutions of Triton X-100 are greatly increased by the addition of sodium chloride; see Fig. 1; calcium chloride, however, has very little effect, and may act either to raise or lower the turbidity slightly depending upon the ratio of salt to surface-active material. When the turbidimetric data are replotted as reduced transparencies, Hc/τ (15)

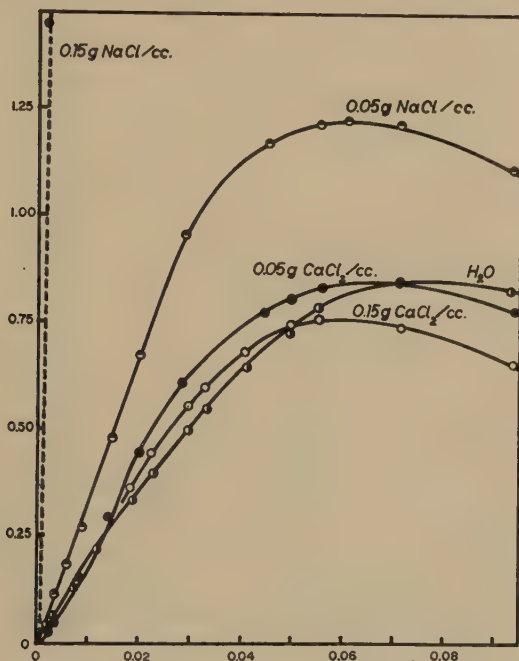


Fig. 1. Turbidity $\times 10^3$ vs. concentration of Triton X-100, g./cc.

(Fig. 2), significant differences are observed in the slopes of the curves. The small slope for the sodium chloride solution is indicative of the fact that the sodium chloride solution is a comparatively poor solvent for the Triton X-100, whereas concentrated calcium chloride solutions appear to be better solvents than pure water (7). The dissymmetry coefficients at concentrations of Triton X-100 above 0.5% are zero, but at lower concentrations were observed to vary in an erratic manner. It is therefore not feasible at this time to extrapolate the turbidimetric results to zero concentration and report molecular weights of the aggregates in the various solutions.

The viscometric results, shown in Fig. 3, are in accord with those obtained turbidimetrically. The viscosities of solutions of all of the non-ionic surface-active agents are abnormally raised by moderate concentra-

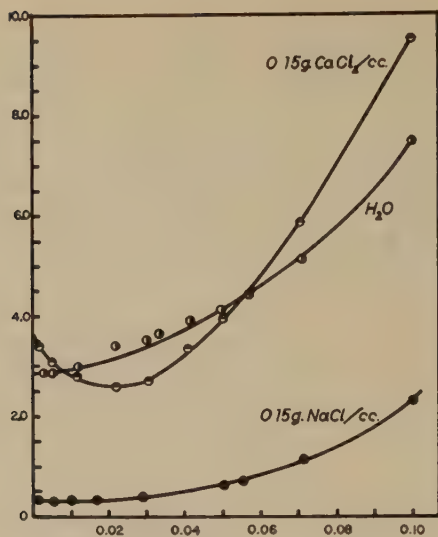


FIG. 2. Reduced transparency $\left(H \frac{c}{\tau}\right) \times 10^4$ vs. concentration of Triton X-100, g./cc.

tions of sodium chloride, but calcium chloride has only a slight effect. Other salts were studied in less detail than the sodium and calcium chlorides: the nitrates of these cations, on the basis of chemical equivalents, have the same effect as the chlorides; lithium is considerably less effective in raising the turbidity and viscosity than sodium; and potassium salts are only slightly less effective than sodium salts. Barium and magnesium produce slightly higher viscosities and turbidities than does calcium, but aluminum salts give somewhat lower values.

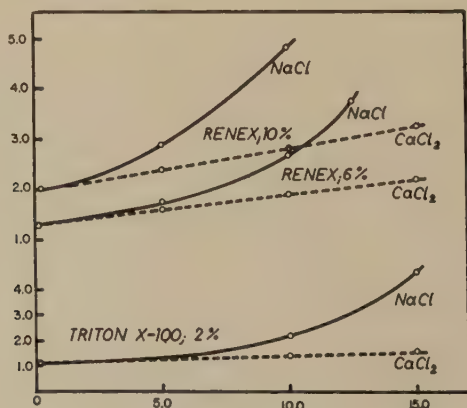


FIG. 3. Relative viscosity at 20°C. vs. salt concentration, wt. per cent.

Solubilization

The solubilization of the dye, Orange OT, was studied in solutions of Triton X-100 containing calcium and sodium chlorides. The determinations were carried out by shaking a suspension of the solid dye in the solution, settling and centrifuging at approximately $2000 \times g$, and finally analyzing the supernatant liquid with a colorimeter. The results are shown in Fig. 4. Both sodium and calcium raise the solubility in 0.5% solutions of Triton X-100, but sodium chloride does so only slightly more than the

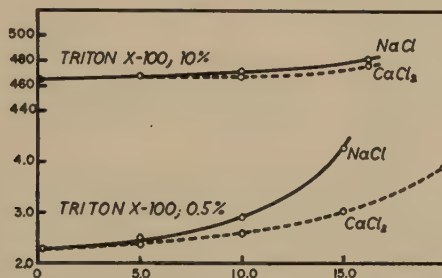


FIG. 4. Solubility of Orange OT, mg./100 cc., vs. salt concentration, weight per cent.

calcium salt. As the solutions become more concentrated in Triton X-100, the effect of both salts decrease. Attempts to measure the solubility of Orange OT in very dilute solutions of Triton X-100 met with failure because the solid dye was so well peptized in pure water and calcium chloride solutions that the suspensions could not be clarified with the available apparatus.

Surface Tension, Protective Power and Cataphoretic Velocity

The surface tension of Triton X-100 and Renex at various concentrations of sodium and calcium chlorides was determined with the DeNuoy tensiometer, and making the appropriate ring corrections (22). The results are tabulated in Table I. The surface tension increases gradually with an increasing ratio of calcium chloride to surface-active material and decreases with increasing sodium chloride concentration.

The nonionic colloids were found to serve as protective colloids for Lange's gold sol, and the protective power of the colloid was determined against the coagulating effect of sodium and calcium chlorides. The coagulation of the red gold sol was determined photometrically with a Klett photometer employing a blue filter. One ml. of the appropriate solution of the colloid was added to 5 ml. of the standard gold sol, and the solution was then gently shaken for 5 min. and allowed to stand for 10 min. more. The photometer was balanced to read 100% transmission and then 1 ml. of the salt solution was added, the tube shaken for 1 min. and then returned to the instrument. A decrease in transmission of 10% was

TABLE I
Surface Tension in Salt Solutions
 (dynes/cm.)

Surface-active agent	Sodium chloride concn.				Calcium chloride concn.				
	0	5%	10%	15%	0	5%	10%	15%	25%
Renex, 0.02%	40.3	39.8	39.3	39.1	40.3	40.4	40.9	41.3	42.6
2.0%	38.5	38.5	38.4	38.4	38.5	39.2	40.0	40.8	41.2
6.0%	38.0	38.0	38.1	37.9	38.0	38.1	38.4	39.5	41.0
Triton X-100, 0.2%	29.4	—	29.2	29.1	29.4	29.6	—	—	31.4
2.0%	29.3	29.2	—	29.0	29.3	29.4	—	29.9	30.2
10.0%	29.4	—	28.6	28.4	29.4	29.3	29.5	29.9	29.9

adopted as a convenient standard for the occurrence of coagulation since solutions showing such a decrease in transmission could be visually identified as having been coagulated.

The results obtained with Renex are shown in Fig. 5. The calcium is a far stronger coagulant than the sodium for the unprotected gold sol, but upon the addition of the nonionic colloids the coagulating power of the calcium is eventually reduced to a value below that of sodium. It should be pointed out that 1 g. sodium chloride and 1 g. calcium chloride are within 5% of being chemically equivalent to each other.

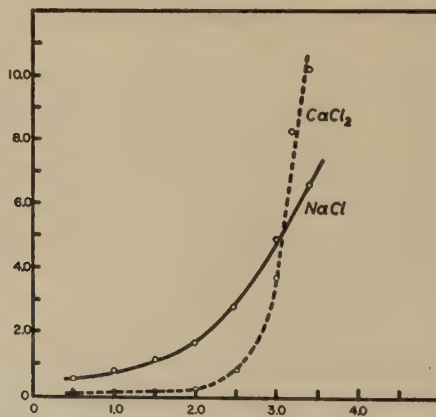


FIG. 5. Salt concentration, weight per cent, to coagulate gold sol *vs.* Renex concentration, per cent $\times 10^4$.

In order to observe the effect of combinations of the nonionic surface-active materials and various salts on the electrical properties of suspensions, a sample of kaolin was used. The kaolin consisted of particles less than $1\ \mu$, and it was electrodialyzed and neutralized with sodium hydrox-

ide. The use of kaolin had several advantages: observations could be made in a microelectrophoretic cell (3) with normally incident light, and the kaolin has definite exchange sites at which cations may be held. The results at various concentrations of Renex and added salts are shown in Fig. 6.

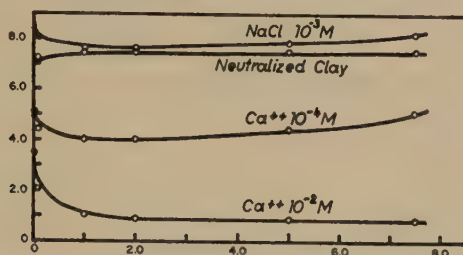


FIG. 6. Cataphoretic mobility of kaolin ($\mu/\text{sec.}/\text{volt}/\text{cm.}$) vs. Renex concentration, weight per cent.

It is apparent that the addition of Renex to the neutral sodium clay has little effect on the cataphoretic velocity; low concentrations of sodium chloride itself raise the cataphoretic velocity, as expected, and the addition of Renex to the sodium chloride-clay suspension lowers the cataphoretic velocity very slightly. Calcium chloride, at low concentrations, lowers the cataphoretic velocity; but its effect is magnified by the addition of very small quantities, less than 0.1%, of Renex. As the concentration of Renex is further increased its effect is ambiguous: at $10^{-2} M$ concentrations of calcium, the cataphoretic velocity decreases, then attains an asymptotic value; whereas in more dilute calcium solutions the mobility reaches a minimum value and then rises with further addition of Renex.

Solubility of Calcium Salts and Isolation of Calcium Salt Complexes

A direct determination of the activity of calcium ion in the presence of a nonionic colloid was attempted by measuring the solubility of calcium sulfate in aqueous solutions of the colloid. To preclude the possibility that the results would be influenced by any effect of the nonionic colloid on the rate of solution of the solid (6), the solubility was determined both by adding solid dihydrate to prepared detergent solutions and by adding detergent to solutions which were originally supersaturated with respect to the dihydrate. (The latter were prepared with the hemihydrate, which is more soluble than the dihydrate, and which reverts to dihydrate in water). The solubility is reported on the basis of 1 g. water, and is shown in Fig. 7.

The observed solubilities may be corrected, to a first approximation, for the amount of water bound to the nonionic molecule, and therefore unavailable for solution of the calcium sulfate, by comparing the observed specific viscosity with that predicted by Einstein's equation. Such a cor-

rection would tend to be too large since any display of non-Einsteinian viscosity in these systems would be due to such factors as nonsphericity, nonrigidity, and interaction of the colloidal aggregates, as well as being due to abnormal hydration. Notwithstanding these complications, solubility corrections calculated on the basis of the Einstein equation are not sufficient to compensate completely for the observed decrease in solubility.

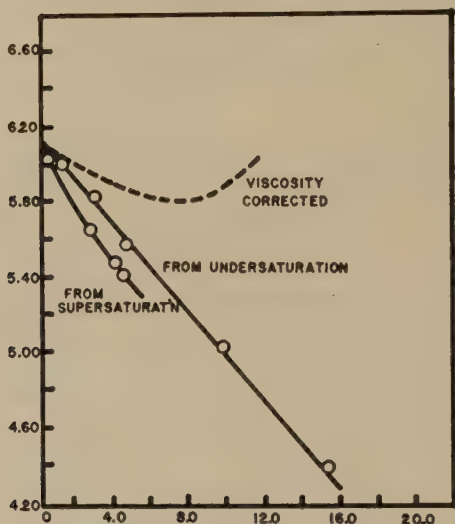


FIG. 7. Solubility of $\text{CaSO}_4 \cdot 2\text{H}_2\text{O}$ (g. Ca/g. H_2O) $\times 10^3$ vs. Renex concentration, weight per cent.

Unfortunately, the salts of the alkali metals salt out the nonionic colloid before the solution is saturated with the salt, so that direct comparison of the decrease in solubility of sodium and calcium salts cannot be made.

When 30% or more calcium chloride is added to moderately concentrated (about 5%) solutions of several of the nonionic surface-active materials, a solid material slowly precipitates. The two materials which produce such a precipitate most readily are Renex and JH-331 (a homolog of Triton X-100, which contains a greater number of moles of ethylene oxide/mole nonpolar residue). The precipitate is readily soluble in water, indicating that it is not a product of hydrolysis. It is also soluble in alcohols (*n*-amyl was the highest used), but is insoluble in acetone, dioxane, and ethyl ether, whereas the original colloids are themselves soluble in all of these liquids. The precipitates were filtered, recrystallized from isopropanol, and finally washed with ether to remove any excess isopropanol. After two or three such recrystallizations, the solid loses its amorphous appearance and a pale-yellow nonhygroscopic powder is obtained. Analysis of the solid revealed that calcium and chlorine are present in

stoichiometric proportions, and that the composition of the powder obtained from Renex was 23.7% CaCl_2 , and 20.2% volatiles at 100°C. The volatiles were identified as water by drying the material in a closed system so that the vapors could be condensed and collected. Assuming a molecular weight of 750 for the Renex, the molar ratios in the recrystallized complex are approximately 3 CaCl_2 , 15 H_2O , 1 Renex.

In order to determine whether the nonionic portion of the complex was the same as that left in the mother liquor or whether it was a different molecular weight fraction, an attempt was made to recover the two. The calcium was removed by precipitation as the oxalate, and the solutions were concentrated by freeze-drying at 0°C. The concentrates were then extracted with ether. The two nonionic oils recovered from the precipitate and the mother liquor had refractive indices within 0.0004 of a unit of each other. This result was rather unexpected, since it is known that the starting material is not homogeneous.³

Finally, to determine whether the solid was merely a mixture of calcium chloride and the original material, x-ray powder diffraction patterns were obtained from the recrystallized solid and a frozen specimen of the original substance. The d/n values of the important diffraction lines are shown in Table II. The short spacings of the solidified Renex and the solid complex are strikingly different. Those of the latter were compared with the d/n values of calcium chloride and its hydrates (1) without finding any correspondence.

TABLE II

d/n Spacings for Calcium Chloride-Renex Complexes

Frozen Renex—2% water ^a	3.87	4.69	30.2 (60.4/2?)	60.9
Recrystallized complex	3.96	6.92		59.7
Dehydrated complex	—	—		54.8
Rehydrated (60°C.) complex	3.96	6.92		74.9–80.0
Recrystallized, dehydrated complex	4.30 ^b	5.98 ^b		
Calcium chloride-isopropanol residue	4.30	5.98		

^a The diffraction pattern obtained from the anhydrous material was not as sharp as that obtained from the system containing 2% water. The halos were, however, centered at 3.9, 4.7, and 55.

^b Very weak.

After dehydrating the recrystallized complex at 100°C. *in vacuo*, no sharp short spacings could be obtained, but a long spacing was again identified. The dehydrated material was rehydrated at 60°C. and the

³ Work in progress has shown that it is possible to fractionate the raw materials by adsorption on charcoal.

sharp spacings were restored and the long spacing increased. The dehydrated material was also dissolved and reprecipitated in absolute isopropanol; however the solid gave no long spacing and very faint short spacings at d/n values of 4.30 and 5.98. These two spacings were determined to be due to the presence of a calcium chloride-isopropanol complex by dissolving calcium chloride in absolute isopropanol and evaporating the solution to dryness at room temperature. The white, crystalline solid gave spacings of 4.30 and 5.98.

DISCUSSION OF RESULTS

The viscometric and turbidimetric data demonstrate that the nonionic surface-active agents are salted out of aqueous solution by sodium chloride. Desolvation of the colloidal molecules and aggregates is presumably the cause of this phenomenon, and judging by the increase in viscosity, micellar growth must accompany the desolvation. The observed order of salting out for the alkali metal ions, *viz.*, Na, K, Li, is not the usual order for the lyotropic series (13) in which lithium precedes sodium. The observed effect of the heavier metal cations is also contradictory to the usually accepted order for the lyotropic series. These cations, which have relatively high heats of hydration and high electrical charge densities, are usually far stronger coagulants than the alkali metal ions. It may be concluded therefore that the alkaline earth metal ions interact with the polyethylene oxide chain of the nonionic colloids, and thereby product a salting-in rather than salting-out effect. This conclusion is further substantiated by the surface tension data, which show that at high ratios of calcium chloride to colloid the surface tension is increased; and also by the fact that the turbidity in these calcium chloride solutions is actually less than that observed in pure water.

In contrast to the above results the solubilization data show very little difference in the effects of the calcium and sodium salts on the ability of solutions containing more than 0.5% of Triton X-100 to solubilize a water-insoluble dye. This result, together with the turbidimetric and viscometric results, suggests that the organization within the colloidal micelles and the fraction of the surface-active material in the form of micelles is not affected differently by the two salts, but that the salts influence only the size of the micelles and the extent of solvation of the micellar surfaces. The salts may cause an appreciable difference in the amount of aggregated material at concentrations of colloid below 0.1%, when aggregation in pure water may not be as complete, but the extremely high suspending power of the surface-active agents in this low concentration range has prevented the determination of the amount of dye solubilized.

The mechanism of the salting-in effect of the calcium may be assumed to be due to its coordination with the ethereal oxygen atoms of the polyethylene oxide chain. Although the polar moment of the nonionic molecules is not known, it is undoubtedly less than that of the water molecule, and preferential solvation of the calcium ion by the water molecule therefore would be expected (10). On the other hand, the water molecules solvating the calcium ion will be favorably oriented (with their positive poles outward) for coordinating with the negative ethereal oxygens (14). A dioxanate (dioxane is the dimer of ethylene oxide) hydrate of calcium chloride has been isolated with the composition $\text{CaCl}_2 \cdot 2\text{H}_2\text{O} \cdot \text{C}_2\text{H}_4\text{O}$ (5), whereas no anhydrous dioxanates have been isolated.

The isolation of a reproducible, crystalline complex of calcium chloride, water, and Renex is further evidence for this suggested mode of coordination. The role of water in forming this complex is made evident by the fact that dehydration destroys the crystalline spacings. It is also significant to note that the recrystallized complex exhibits larger short spacings but a long spacing very similar to that shown by the Renex itself. Only after an excess of water is added by hydrating the complex at 60°C . does the long spacing increase. It therefore appears quite definite that the hydrated calcium ions do coordinate along the polyethylene oxide chains.

The experiments on electrophoresis and protective power involved the introduction of a solid-liquid interface. The enhancement of the protective power of the nonionic colloid by calcium ion can be ascribed to the primary adsorption of the solvated calcium ions by the gold particles followed by the anchoring of the nonionic colloid via the hydrate shell of the calcium ion to the colloidal particle. Pauli (19) has already suggested such a mechanism to account for his observations that gelatin and gum arabic acted as protective colloids for hydrosols only in the presence of small quantities of heavy metal ions. It is also known that calcium aids in the fixation of organic colloids to clay (17).

The sharp reduction in electrophoretic mobility observed upon the addition of Tween 80⁴ to a suspension of clay in dilute calcium solution is similar to the observed reduction in electrophoretic mobility produced by a combination of calcium chloride and glucose on cholesterol (21). It may also be accounted for by the above hypothesis: the inclusion of the nonionic molecule in the solvate envelope surrounding the clay particle will result in a reduction of the dielectric constant of the diffuse layer with a consequent decrease in ionization of the calcium ion and a lowered charge density. Also, assuming that the potential on a colloidal particle can be calculated using the Debye-Hückel equations, it can be shown that the electrophoretic mobility will be proportional to the square root of the dielectric constant. A similar reduction of the dielectric constant in the

⁴ Polyoxyalkylene derivative of sorbitan monoöleate.

solvate shell of the calcium ion may explain the observed increase in activity coefficient and solubility of the calcium sulfate.

The increase in electrophoretic mobility upon increasing the Renex concentration in dilute calcium solution suggests that the Tween 80 adsorbed onto the clay particle at low concentrations is stripped from the clay surface at higher concentrations. This may be brought about by the growth of micelles in the bulk of the solution at larger concentrations and their competition with the clay for the calcium ion (20). It may be noted at this point that very stable petroleum oil-in-water emulsions have been prepared at concentrations of Tween 80 of 0.01%, but that such emulsions were very unstable at higher concentrations and at zero concentration (18).

The preceding results and their interpretation indicate that the efficacy of these nonionic materials in improving detergency in hard water (4) is due to the following factors: (a) formation of soluble complexes with calcium, thus preventing the formation of insoluble calcium soaps, and (b) enhanced formation of a protective layer of the nonionic colloids on the solid surfaces at which calcium and other heavy metal cations are adsorbed.

SUMMARY

1. Sodium chloride and other salts of the alkali metals have been found to salt-out nonionic surface-active agents, whereas soluble calcium salts and other soluble salts of heavy metals salt-in these colloids.

2. A crystalline complex of a nonionic surface-active agent, calcium chloride, and water has been isolated.

3. The nonionic surface-active agents appear to coordinate with hydrated calcium ions both in solution and at solid-liquid interfaces.

REFERENCES

1. AM. SOC. TESTING MATERIALS, Card Index. Philadelphia, 1945.
2. ATLAS POWDER Co., private communication.
3. ABRAMSON, H. A. A., MOYER, L. S., AND GORIN, M. H., *Electrophoresis of Proteins*. Reinhold Publishing Corp., New York, 1942.
4. BARKER, G. E., *J. Am. Oil Chemists' Soc.* **26**, 304 (1949).
5. BOGARDOS, H. F., AND LYNCH, C. C., *J. Phys. Chem.* **47**, 650 (1943).
6. BRINTZINGER, H., AND SCHALL, A., *Kolloid-Z.* **71**, 300 (1935).
7. DEBYE, P., *Ann. N. Y. Acad. Sci.* **51**, 575 (1949).
8. DOSCHER, T. M., *Oil Gas J.* **48**, 75 (1945).
9. DOSCHER, T. M., *J. Phys. & Colloid Chem.* **53**, 1362 (1949).
10. FUOSS, R. M., AND KRAUSS, C. A., *J. Am. Chem. Soc.* **55**, 2387 (1933).
11. GONICK, E., AND MCBAIN, J. W., *J. Am. Chem. Soc.* **69**, 334 (1947).
12. GREEN, A. A., AND MCBAIN, J. W., *J. Phys. Chem.* **51**, 286 (1947).
13. KRUYT, H. R., *Colloid Science*, Vol. II, pp. 564 ff. Elsevier, New York, 1949.

14. MCBAIN, J. W., Colloid Science, pp. 133 ff. Heath, New York, 1950.
15. MARK, H., in Chemical Architecture, Chap. V. Interscience, New York, 1948.
16. MARSDEN, S. S., AND MCBAIN, J. W., *J. Phys. & Colloid Chem.* **52**, 110 (1948).
17. MYERS, G., M.S. Thesis, Univ. of Southern Calif., 1950.
18. MYERS, H. E., *Soil Sci.* **44**, 331 (1937).
19. PAULI, W., AND SZPER, L. S., *Trans. Faraday Soc.* **35**, 1316 (1939); and PAULI, W., AND ZENTNER, H., *ibid.* **35**, 1234 (1939).
20. REICHENBERG, D., *Trans. Faraday Soc.* **43**, 467 (1947).
21. REMSOW, I., *Biochem. Z.* **218**, 86, 170 (1930).
22. ZOIDEMA, H. H., AND WATERS, G. W., *Ind. Eng. Chem., Anal. Ed.* **13**, 312 (1941).

IONOGRAPHY: SOME ASPECTS OF ION MIGRATION ON PAPER IN AN ELECTRIC FIELD

Hugh J. McDonald, Matthew C. Urbin¹ and Martin B. Williamson

*Department of Biochemistry, The Graduate School and the Stritch School of Medicine,
Loyola University, Chicago, Illinois*

Received January 22, 1951

INTRODUCTION

In previous reports (1,2) experiments were described in which a strip of filter paper moistened with buffer solution served as a path along which ions or charged particles migrated under the influence of a potential gradient. This technique has come to be known by the term *ionography*. It shows great promise in the fields of separation and identification of biological materials. It is being used to separate amino acid mixtures, protein mixtures, to determine transference numbers, to determine isoelectric points of amino acids and proteins, and to study complex-ion formation in solution.

A number of recent papers have appeared in which some aspects of this subject have been discussed (3-8). In order to utilize ionography to its fullest extent, it is necessary to elucidate the factors which influence the migration on paper of charged particles in solution in an electric field. This study is concerned with the effect of such factors as potential gradient, time, pH of the buffer solutions, and ionic strength on the rate of migration.

EXPERIMENTAL METHODS

During the course of these studies, a number of modifications were made on the original apparatus (1). Although these modifications increased the reproducibility and accuracy of the measurements, the apparatus remained basically the same.

The apparatus consists essentially of three main component parts: (a) an enclosed vessel containing one or more filter paper strips,² (b) the buffer vessels, and (c) the electrode vessels. In Fig. 1 is shown a later modification of the apparatus, with common buffer vessels and electrodes. It is made of a polymerized methyl methacrylate plastic,³ fitted with a

¹ Graduate Research Fellow, Standard Oil Company (Indiana).

² The filter paper used was Eaton and Dikeman, No. 613, 8 mm. wide, in rolled strip form.

³ Lucite.

removable Bakelite frame, and can accommodate seven strips simultaneously. The strips are held in place by Bakelite screws. A microammeter is connected in series with the paper strips, buffer vessels, agar-KCl salt bridges, and electrodes. By separating the electrode vessels from the buffer vessels with an agar-KCl bridge (1% sterilized agar in 1 *M* KCl solution), all need for contact of the metal electrodes with the strip itself was removed, and the products of the electrode reactions, especially the hydroxyl ion in the vicinity of the cathode, were effectively separated from the paper.

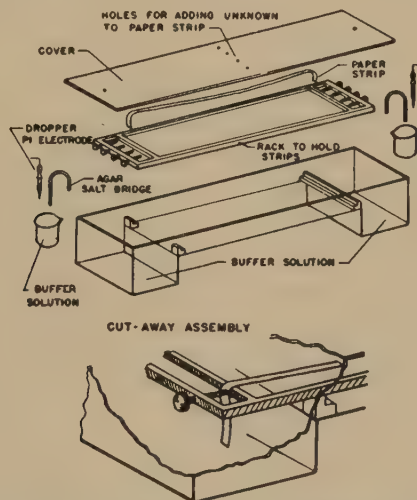


Fig. 1. An ionograph with common buffer vessels and electrodes. The level of the buffer solution in the left hand buffer reservoir is raised so as to cover the floor of the chamber and displace as much of the air as possible.

In use, an electrical potential, provided by from three to fifteen 90-v. radio B-batteries, is applied across the ends of the filter paper strips, previously saturated by immersion in a buffer solution. The paper strips were 52.5 cm. from the water level of one buffer vessel to the other. A typical current reading for a single strip would be 70 μ a. The material under study is applied by means of a micropipet, at some previously marked intermediate point on the paper strip. In these experiments, approximately 0.05 ml. of a 0.05 *M* solution of the amino acid was placed on the paper.

The displacement of the migrating compound is detected by spraying the paper, previously dried in a stream of warm air, with suitable spot test agents to produce colored bands. The bands were about 0.5 cm. in width. In the experiments involving amino acids, a solution of 0.1% ninhydrin in a 5% solution of butanol in water was used to spray the paper. The experiments were so arranged that the migration was usually

from 8 to 10 cm. In replicate experiments, under identical conditions, the displacement of the front edge of the migrating substance, as indicated by the colored bands, varied by less than ± 2 mm.

The purpose of the buffer vessels is to help maintain a constant pH along the paper strip during the course of an experiment. Unless a fairly large quantity of buffer solution is used, it is found that, at low ionic strength values, the pH along the paper strip changes sufficiently so that some substances, particularly ampholytes, may reverse the direction of their migration part way through an experiment. The buffer vessels used held approximately 1 l. of buffer each. In these experiments, the pH of the buffer solutions was determined before and after each run.

RESULTS AND DISCUSSIONS

Despite the superficial resemblance of ionography to paper chromatography, a careful distinction should be maintained between the two separation processes. In chromatography, separation of solution constituents depends on a distribution between a mobile and nonmobile phase. In ionography, separation results from the migration of ions or charged particles at different rates, in an electric field, rather than from distribution equilibria, adsorption-desorption effects, or counter-current processes. The paper strip serves as a carrier for the solvent or dispersion medium and helps to fix the migrating substances in position when the current is turned off, until the paper is dried.

Movement as a Function of Time

In Fig. 2 is shown a plot of the movement of leucine versus time.⁴ The pH, potential, and ionic strength were held constant during the course of the experiment. The movement appears to be a linear function of time. This may be interpreted to mean that equilibrium conditions are being maintained with regard to moisture in the paper strip and in the atmosphere within the apparatus. The method of wetting the paper strips was found to be important in establishing the equilibrium. Although a number of techniques for wetting the paper were tried, it was found that the most reproducible results were obtained when the paper strip was immersed in the buffer solution and the excess liquid was allowed to drain off.

Any fluctuations in the temperature of the moist paper strips, due to the fact that it is conducting a current, is probably controlled by convection currents in the air surrounding the paper. Evaporation of a small amount of water from the paper surface, with a concomitant cooling effect provided by the heat of evaporation, also helps to maintain the temperature.

⁴ All the points shown in Figs. 2-7 represent the average of quadruplicate determinations. The deviation of individual measurements from the average was usually less than 3%.

It might be expected that even a small amount of evaporation of water from the paper strip would cause an increase in the concentration of buffer salts in the paper. That this is not a serious effect is probably due to the fact that since the evaporation is uniform throughout the length of the paper, the potential gradient is maintained constant. The water loss is probably replaced largely by seepage of water from the buffer vessels, and also, to some extent, in the following way. All positive and negative ions in the water sheath surrounding the paper strip, including those derived

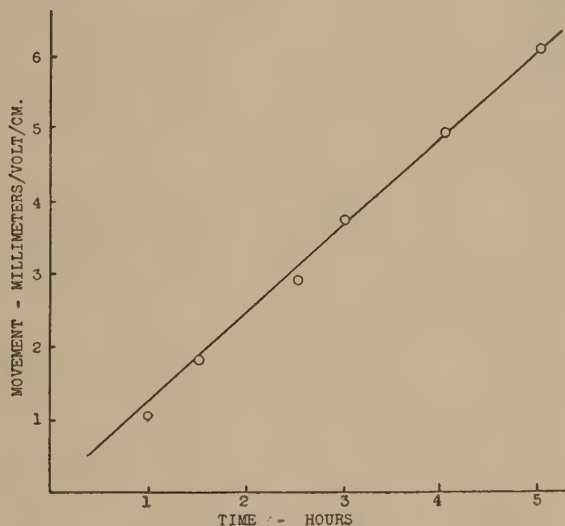


FIG. 2. The movement of leucine as a function of time. Potential gradient, 22.5 v./cm.; pH, 2.8; buffer, acetic acid, 0.1 M; temp., 23–25°C.

from the buffer itself, tend to move toward opposite ends of the paper strip under the influence of the potential, and, of course, carry with them various numbers of molecules of water of hydration. This continual movement of hydrated ions apparently plays an additional role in that it exerts an equalizing action on the over-all ion concentration in the paper, tending to level it out to the same concentration as in the buffer vessels. Whatever the explanation may be, the important point is the experimental observation that a linear relationship between the movement of the migrating compound and time is found.

Movement as a Function of Potential

As is shown in Fig. 3, when movement, in microns per second (μ /sec.), is plotted against potential, in volts per centimeter (v./cm.), applied across the paper strip, under conditions of constant pH, ionic strength and temperature, a linear form is again obtained. The rate of movement, in this case of leucine, is directly proportional to the applied voltage. This

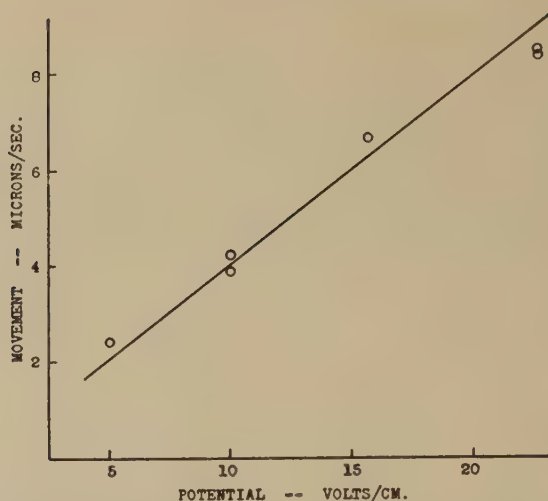


FIG. 3. The movement of leucine as a function of potential. pH, 2.8; buffer, acetic acid, 0.1 *M*; temp., 23–25°C.; time, 3 hr.

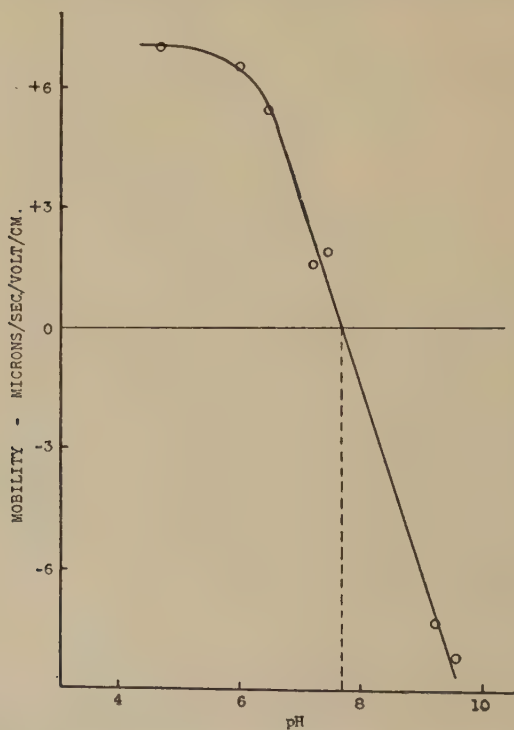


FIG. 4. Mobility of histidine as a function of the pH of the buffer solution. Potential gradient, 15.7 v./cm.; ionic strength, 0.013; buffers: pH 2.2–3.8, potassium hydrogen phthalate-HCl; pH 4.0–6.2, phthalate-NaOH; pH 5.8–8.0, potassium dihydrogen phosphate-NaOH; pH 7.8–10.0, KCl-NaOH; temp., 23–25°C.; time, 3 hr. The vertical broken line represents the isoelectric pH, 7.6.

means that any desired voltage, as well as any convenient length of paper, may be used for this technique, as long as the movement is expressed in terms of *mobility*; i.e., $\mu/\text{sec.}/\text{v.}/\text{cm.}$

Mobility as a Function of pH

The mobilities of histidine and of glutamic acid were studied over a considerable pH range of the buffer solution saturating the paper strip. The ionic strength, time, temperature, and potential were held constant. In Fig. 4, showing the behavior of histidine, mobility of positively charged ions is plotted above, and of negatively charged ions below, the x -axis. It will be seen that at higher pH values, histidine bears a negative charge and exhibits high mobility. As the pH of the buffer solution is lowered, the mobility decreases linearly to zero, represented by the isoelectric pH.

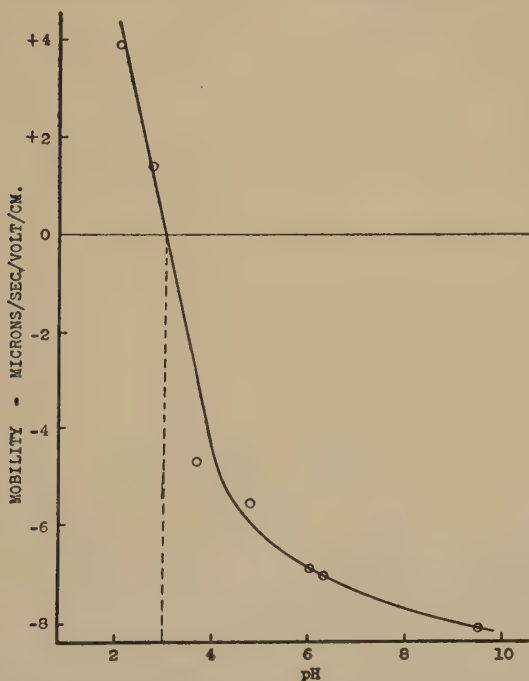


FIG. 5. Mobility of glutamic acid as a function of the pH of the buffer solution. All conditions the same as those shown for Fig. 4. The vertical broken line represents the isoelectric pH, 3.1.

As the pH of the buffer is further lowered, the direction of migration is reversed, the histidine becoming positively charged and moving toward the negative end of the paper. At about pH 6, the mobility decreases sharply with further reduction in pH.

The relationship between pH and mobility, brought out even better in the case of glutamic acid, is shown in Fig. 5. At low pH values, the

glutamic acid acts as a positively charged species and exhibits high mobility. As the pH of the buffer is increased, the mobility decreases linearly, reaching a value of zero at the isoelectric pH. When the pH increases beyond the isoelectric point, the direction of movement is reversed. The mobility again increases linearly up to a pH of about 3.4, then drops off rapidly as the pH increases to a value of 9.4.

This method appears to offer a convenient technique for determining the isoelectric points of amino acids. Preliminary experiments with purified proteins of known isoelectric points indicate that this technique can also be used to establish the isoelectric points of proteins (9).

Mobility as a Function of Ionic Strength

In Fig. 6, the mobility of leucine is plotted as a function of the ionic strength of the buffer solution. It is apparent that the mobility increases with decreasing ionic strength, approaching the y -axis asymptotically.

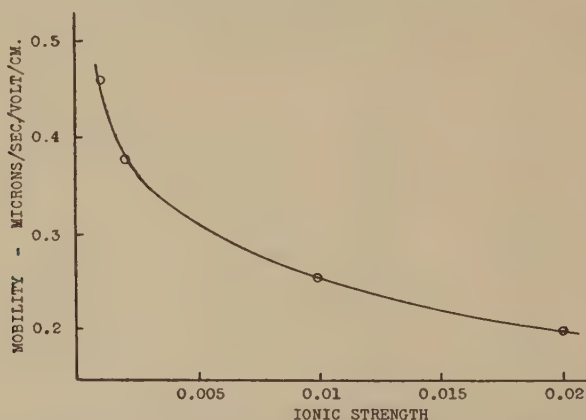


FIG. 6. The mobility of leucine as a function of the ionic strength of the buffer solution. Potential gradient, 15.7 v./cm.; pH, 4.2; buffer, potassium hydrogen phthalate-NaOH; temp., 23-24°C.; time, 3 hr.

This is the result to be expected on the basis of known effects of electrolyte concentration on the ion atmosphere of an ion in solution, or on the zeta potential of a colloid.

It is evident that there should be an optimal value of the ionic strength at which to conduct ionographic measurements. Although mobility of the compounds under study becomes more rapid at lower buffer concentrations, there is a lower margin beyond which it is not profitable to dilute the buffer. When the buffering capacity of the solution drops below a certain value, it is difficult to maintain uniform pH levels along the paper strip throughout an experiment.

If the migrating substance is viewed in the light of the Debye-Hückel theory of strong electrolytes, it can be shown that the zeta potential around a charged particle or ion is related to the ionic strength of the solution in the following way, at 25°C.:

$$\text{Zeta potential} = \frac{4\pi\sigma}{D} \times \frac{1}{0.33 \times 10^8 \sqrt{\mu}},$$

where σ is the surface charge density of the migrating substance; D is, to a fair approximation, the dielectric constant; and μ is the ionic strength. It is evident that the greater the zeta potential, the greater the mobility of the particle should be. It should be possible then to write:

$$\text{Mobility} = \frac{K 4\pi\sigma}{D} \times \frac{1}{0.33 \times 10^8 \sqrt{\mu}},$$

where K is the constant of proportionality between the mobility and the zeta potential. It can be seen from this equation that if the mobility of the migrating substance is plotted against the reciprocal of the square root of the ionic strength, a straight line relationship should obtain. In Fig. 7

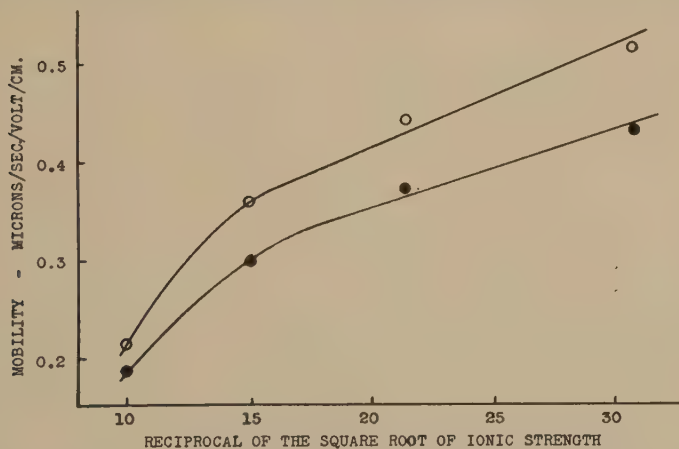


FIG. 7. Mobility as a function of the reciprocal of the square root of the ionic strength of the buffer solution. Upper curve, phenylalanine; lower curve, leucine; potential gradient, 15.7 v./cm.; pH, 3.8; buffer, potassium hydrogen phthalate-HCl; temp., 23-24°C.; time, 3 hr.

are shown the results obtained from a plot of this kind for phenylalanine and leucine. It will be noticed that below a certain value of ionic strength, a good linear relationship between mobility and the reciprocal of the square root of the ionic strength is, in fact, obtained. This behavior might be interpreted to mean that the ions or charged particles act much as they would in the body of the liquid.

SUMMARY

The relationships that exist between the mobility of amino acids migrating on paper under the influence of an electric field, and the pH of the solution, the ionic strength, the time and the voltage across the paper are presented. The rate of migration bears a linear relation to the potential gradient and to the time. The isoelectric points of histidine and glutamic acid have been determined to be 7.6 and 3.1, respectively.

REFERENCES

1. McDONALD, H. J., URBIN, M. C., AND WILLIAMSON, M. B., *Science* **112**, 227 (1950).
2. McDONALD, H. J., URBIN, M. C., AND WILLIAMSON, M. B., Abstracts, Div. Biol. Chem., 118th Meeting Am. Chem. Soc., p. 66C, 1950; see also *J. Am. Chem. Soc.* **73**, 1893 (1951).
3. WIELAND, T., AND FISCHER, E., *Naturwissenschaften* **35**, 29 (1948).
4. DURRUM, E. L., *J. Am. Chem. Soc.* **72**, 2943 (1950).
5. CREMER, H., AND TISELIUS, A., *Biochem. Z.* **320**, 273 (1950).
6. BISERTE, G., *Biochim. et Biophys. Acta* **4**, 416 (1950).
7. KRAUS, K. A., AND SMITH, G. W., *J. Am. Chem. Soc.* **72**, 4329 (1950).
8. TURBA, F., AND ENENKEL, H. G., *Naturwissenschaften* **37**, 93 (1950).
9. McDONALD, H. J., URBIN, M. C., AND WILLIAMSON, M. B., *Federation Proc.* **10**, 218 (1951).

STUDIES ON ION-EXCHANGE RESINS. II. VOLUMES OF VARIOUS CATION-EXCHANGE RESIN PARTICLES^{1,2}

Harry P. Gregor, Fradelle Gutoff and J. I. Bregman³

Department of Chemistry, Polytechnic Institute of Brooklyn, Brooklyn, New York

Received February 9, 1951

INTRODUCTION

In the thermodynamic theory of ion-exchange processes developed by Gregor (4, 5), the free-energy changes involved in swelling or deswelling the resin matrix are considered. These free energies of swelling are a significant, often a critical part of the total free-energy changes involved in ion-exchange processes. This paper describes the volume and composition of various cation exchangers, measured under different conditions. Some of the thermodynamic properties of these systems are calculated from the data. In many instances, however, only qualitative comparisons can be made. Only some of the experimental parameters required to describe these systems have been considered in this and the preceding paper in this series. Future papers will take up the remaining parameters.

EXPERIMENTAL METHODS

A. Exchangers

The cation-exchange systems used included a series of sulfonated polystyrene-divinylbenzene (DVB) resins, prepared using different amounts of the cross-linking agent. These resins are referred to as DVB 0.4, 2, 4, etc., the numbers denoting the weight per cent of divinylbenzene used in preparing the unsulfonated polymer. Three commercial sulfonic acid resins were used: a sulfonated polystyrene resin, prepared using 8% divinylbenzene-Dowex 50 (Dow Chemical Co.); a sulfonated phenolic base resin, Duolite C-3 (Chemical Process Co.); and a phenolic base resin, prepared by the alkaline condensation of phenolsulfonic acid, phenol, and formaldehyde—hereafter referred to as "Phenolic resin." An inorganic cation-exchanging mineral, glauconite, was used; it was made more permeable by treatment with hot alkali (Super Zeo-Dur, Permutit Co.).

¹ Taken in part from the dissertation of J. I. Bregman, submitted in partial fulfillment of the requirements for the degree of Doctor of Philosophy in Chemistry, Polytechnic Institute of Brooklyn, September 1950.

² The authors wish to thank the Office of Naval Research and the Signal Corps, U. S. Army, for the support rendered to this work.

³ Present address: National Aluminate Corp., Chicago, Ill.

Each of these materials was treated in several alternate cycles with an excess of 1 *M* sodium hydroxide and 1 *M* hydrochloric acid, then given a final regeneration with acid, rinsed to an effluent pH of 4.5, and air-dried. The exchangers were screened to $-20 + 30$ mesh size, except some of the DVB resins which were somewhat smaller. A detailed description of the preparative procedures for the DVB resins is given in an earlier paper in this series, together with details of the conditioning procedure (7).

All the data for the resinous exchangers presented in this paper refer to a specific quantity of resin, i.e., 1 g. dry resin in the hydrogen state. Thus the weight and volume of a resin system prepared starting with 1.000 g. of dry hydrogen resin is designated as the specific weight (W_e), the specific volume (V_e), etc. This system of notation makes convenient a comparison of the properties of the same resin in various states.

In practice, the experiments described herein employed 0.5-g. samples of air-dried resin. The moisture content was determined by drying to constant weight over P_2O_5 .

The specific exchange capacities in *m* moles/g. of the various exchangers used were: DVB 0.2, 6.85; DVB 2, 5.18; DVB 4, 5.16; DVB 6, 5.09; DVB 8, 5.06; DVB 10, 4.86; DVB 13, 4.94; DVB 17, 4.89; DVB 23, 4.24; DVB 26, 4.50; Dowex 50, 4.90; Duolite C-3, 2.90; phenolic, 2.84; and glauconite, 0.108. All of these exchangers had the same capacity with respect to all univalent cations as shown in an earlier paper (7). The sole exception was the glauconite exchangers where the hydrogen exchange capacity is lower than the univalent (potassium) exchange capacity. All glauconite data are reported in terms of 1 g. dry potassium exchanger.

B. Volume Determinations

The specific volumes were determined using the centrifugation technique described by Gregor, Held, and Bellin (8). The exchangers were treated with a large excess of the various equilibrating solutions to insure that equilibrium was reached in every case, as described in a previous paper (7). The final equilibration was accomplished in a thermostat at $25.00 \pm 0.05^\circ\text{C}$. Then the resin and some solution were transferred into a drying tube, the narrow end of which rested on the bottom of a 10-ml. pycnometer. The particles of exchanger settled to the bottom of the tube, while the solution filled the pycnometer. Then the drying tube was raised very slowly, and the resin particles settled into the pycnometer. If this latter process is carried out too rapidly, light particles may be washed out of the pycnometer. The pycnometer was then capped, allowed to come to temperature equilibrium in the thermostat, and weighed in the conventional manner.

The resin was then transferred from the pycnometer to a small basket made of 1-cm. polystyrene tubing, with a 60-mesh screen sealed into its bottom. This basket was placed in a centrifuge tube (with a few drops

of solution at the bottom to maintain the vapor pressure) and centrifuged for 3 min. at 3000 r.p.m. when the particles were spherical. If they were irregularly shaped, about 30 min. of centrifugation was required to attain a constant centrifuged weight.

The density of the equilibrating solution was determined pycnometrically, and the specific wet weight, W_e and specific volume, V_e , of the exchanger calculated. The precision of this determination varies from $\pm 0.2\%$ for spherical particles to $\pm 0.5\%$ for irregularly shaped ones. The styrene base resins were spherical; the others were irregularly shaped.

C. Nonexchange Electrolyte

When exchangers are equilibrated with dilute aqueous solutions (0.01 M) the exchange capacity toward univalent cations is the same as shown by Gregor *et al.* (7). But in more concentrated solutions, some additional cations are found in the resin phase, these cations being compensated for electrically by movable anions which have also entered the resin phase (1, 4, 5, 13). This electrolyte is referred to as nonexchange electrolyte. The specific nonexchange electrolyte content (NE) is given in m moles present in the specific volume of resin phase, V_e .

The nonexchange electrolyte content of the resin phase is determined by equilibrating the resin with a specific solution, centrifuging it, then placing the centrifuged resin into a measured volume of water to elute the nonexchange electrolyte. Since, as will be shown later, negligible amounts of nonexchange electrolyte are present in the resin phase when the latter is in contact with dilute solutions, this procedure results in a virtually quantitative elution. The concentration of nonexchange electrolyte in the eluate was determined conductometrically, with an over-all accuracy of about $\pm 1\%$.

D. Matrix Volume Determination

The specific volume of dry exchanger (V_m) is determined using the pycnometric technique, with n -octane as the pycnometric liquid. This liquid does not enter the exchanger phase nor react with any of its components, nor cause it to swell, as was shown by Gregor, Held, and Bellin (8). It is thus an inert pycnometric fluid.

EXPERIMENTAL RESULTS

In all of the experiments described hereafter, the chloride or bromide salts were used, unless stated otherwise. Also, all of the equilibrating solutions used were 0.001 m (molal) unless stated otherwise.

When the exchangers are equilibrated with dilute (0.001–0.01 m) electrolytic solutions, the values of V_e and W_e do not depend upon the nature of the anion present. For the Dowex 50 resin in the sodium state,

the values of V_e and W_e are 1.418 and 1.870, respectively, with the chloride, 1.422 and 1.882 with the hydroxide, and 1.418 and 1.874 with the thiocyanate. In the ammonium state, V_e and W_e are 1.409 and 1.754 with the chloride and 1.411 and 1.756, respectively, with the sulfate. In the tetramethylammonium state, V_e and W_e are 1.623 and 1.931 with the chloride, and 1.638 and 1.943 with the hydroxide. Thus it is evident that in dilute solution the anion does not play a significant role in determining V_e and W_e . The values of V_e and W_e in the hydroxide solutions appear to be very slightly but consistently larger than in the halide solutions. This effect is almost within the range of the errors involved in the determinations. It may result from the presence of a trace of weak acid groups in the resin; results of Gregor and Bregman (6) show that in strongly alkaline media, the exchange capacity of the resin may increase by a very small amount.

Values of V_e , W_e , and V_m for the Dowex 50 resin in equilibrium with 0.001 *m* solutions of various salts are shown in Table I. Corresponding

TABLE I

Specific Volumes, Weights and Dry Volumes for Dowex 50 Resin in Various States

Cation	V_e	W_e	V_m	m
	ml.	g.	ml.	
H ⁺	1.524	1.880	0.696	5.6
Li ⁺	1.503	1.898	0.702	5.6
Na ⁺	1.418	1.870	0.730	6.4
K ⁺	1.357	1.843	0.763	7.4
Rb ⁺	1.368	2.052		7.8
Cs ⁺	1.391	2.292		7.8
NH ₄ ⁺	1.409	1.754	0.792	7.3
(CH ₃) ₄ N ⁺	1.623	1.931	1.130	8.4
(C ₂ H ₅) ₄ N ⁺	1.893	2.201		8.8
(CH ₃) ₃ C ₆ H ₅ N ⁺	1.666	2.070		21.7
Ag ⁺	1.209	2.094	0.685	10.7
Tl ⁺	1.182	2.492		10.3
Mg ⁺⁺	1.456	1.921	0.707	5.7
Ca ⁺⁺	1.372	1.853	0.720	6.4
Sr ⁺⁺	1.345	1.938		6.8
Ba ⁺⁺	1.264	1.946	0.726	7.9

values for a series of DVB resins in the potassium, ammonium, lithium, tetramethylammonium, and tetraethylammonium states are shown in Table II. Table III shows corresponding values for the Duolite C-3, phenolic, and glauconite exchangers. The molality (*m*) of the resin phase, calculated as moles of exchange cation/1000 g. water contained in the resin phase, is also shown.

TABLE II

Specific Volumes, Weights and Dry Volumes for DVB Resins in Various States

Resin	K ⁺				NH ₄ ⁺			Li ⁺			(CH ₃) ₄ N ⁺			(C ₂ H ₅) ₄ N ⁺		
	V _e	W _e	V _m	m	V _e	W _e	m	V _e	W _e	m	V _e	W _e	m	V _e	W _e	m
DVB	ml.	g.	ml.		ml.	g.		ml.	g.		ml.	g.		ml.	g.	
0.4	42.40	42.80	0.769	0.13	44.63	44.95	0.16				33.71	33.90	0.21	33.88	34.10	0.21
2	4.602	5.102	0.783	1.33	4.387	4.726	1.43				4.421	4.700	1.58	4.536	4.815	1.60
4	2.757	3.275	0.818	2.50				2.961	3.395	2.2	3.057	3.340	2.66	3.310	3.610	2.7
6					2.034	2.373	3.95	2.113	2.529	3.4	2.115	2.390	5.10	2.276	2.550	5.8
8	1.618	2.122	0.827	5.5				1.750	2.220	4.3						
10	1.436	1.920		6.7	1.478	1.809	6.7	1.559	1.965	5.2	1.678	1.974	8.0	1.911	2.214	8.4
13	1.302	1.780	0.828	7.4												
17	1.195	1.667	0.799	10.0	1.248	1.582	9.8	1.299	1.700	7.3	1.469	1.784	11.6	1.666	1.976	14.1
23	1.147	1.564	0.871	10.8												
26	1.115	1.582	0.838	11.2							1.302	1.578	18.1	1.542	1.826	18.3

TABLE III

Specific Volumes, Weights and Dry Volumes for Exchangers in Various States

Cation	Duolite C-3		Phenolic			Glaucinite		
	V _e	W _e	V _e	W _e	V _m	V _e	W _e	V _m
	ml.	g.	ml.	g.	ml.	ml.	g.	ml.
Li ⁺	1.606	2.018	1.788	2.183	0.806	0.691	1.299	0.510
Na ⁺	1.484	1.940	1.685	2.075	0.825	0.687	1.297	0.515
K ⁺	1.380	1.857	1.610	1.976	0.834	0.681	1.309	0.517
NH ₄ ⁺			1.609	1.967	0.835	0.682	1.299	0.520
(CH ₃) ₄ N ⁺			1.859	2.211	1.099			
(C ₂ H ₅) ₄ N ⁺			1.925	2.295	1.160			

Values of V_e and W_e for various DVB resins were determined with both potassium and tetramethylammonium ions in exchange positions. Table IV shows these experimental parameters as a function of X_{K^+} , the fraction of exchange sites occupied by the potassium ion.

TABLE IV

DVB Resins in Potassium Tetramethylammonium States

DVB 2			DVB 10			DVB 26		
X_{K^+}	V _e	W _e	X_{K^+}	V _e	W _e	X_{K^+}	V _e	W _e
	ml.	g.		ml.	g.		ml.	g.
1.00	4.602	5.102	1.00	1.436	1.920	1.00	1.115	1.582
			0.83	1.535	1.959	0.72	1.147	1.508
0.44	4.441	4.797	0.46	1.610	2.002	0.54	1.191	1.529
0.25	4.441	4.751	0.31	1.678	2.039	0.32	1.216	1.523
0.00	4.421	4.700	0.00	1.678	1.974	0.00	1.302	1.578

TABLE V
Deswelling of Resins in Ammonium Chloride Solutions
DVB 0.4

Molality	W_0 g.
0.001	44.95
0.012	42.23
0.22	22.09
0.50	15.60
1.00	12.63
3.06	7.88
4.45	6.58
5.24	5.85

DVB 2

Molality	V_0	W_0	NE	m_{Cl^-}	$m_{NH_4^+}$	γ_{\pm}
	<i>mL.</i>	<i>g.</i>	<i>mmoles</i>	<i>m</i>	<i>m</i>	
0.001	4.387	4.726				
0.012	4.320	4.658	0.0071	0.0020	1.46	0.204
0.12	4.097	4.440	0.172	0.051	1.60	0.370
0.74	3.271	3.619	0.970	0.392	2.49	0.495
1.44	2.943	3.301	1.76	0.832	3.29	0.548
2.09	2.680	3.059	2.48	1.35	4.18	0.542
3.76	2.322	2.705	3.92	2.79	6.49	0.533
5.75	2.177	2.580	5.59	4.68	9.03	0.534

DVB 6

0.001	2.034	2.373				
0.012	2.021	2.358	0.0040	0.0031	3.99	0.100
0.12	1.997	2.340	0.022	0.0175	4.05	0.344
0.74	1.862	2.207	0.231	0.209	4.79	0.490
1.44	1.773	2.118	0.504	0.498	5.53	0.545
2.09	1.709	2.058	0.781	0.835	6.28	0.560
3.76	1.592	1.946	1.50	2.13	8.40	0.535
5.75	1.517	1.871	2.30	3.44	11.05	0.561

DVB 10

0.001	1.478	1.809				
0.012	1.474	1.802	0.004	0.0055	6.79	0.058
0.12	1.463	1.794	0.009	0.0126	6.88	0.303
0.74	1.435	1.762	0.110	0.165	7.35	0.445
1.44	1.389	1.723	0.247	0.390	8.13	0.507
2.09	1.387	1.706	0.366	0.603	8.70	0.516
3.76	1.314	1.648	0.764	1.45	10.7	0.575
5.75	1.275	1.606	1.31	2.87	13.6	0.554

TABLE V (Continued)

DVB 17						
Molality	V_e	W_e	NE	m_{Cl^-}	$m_{NH_4^+}$	γ_{\pm}
	<i>ml.</i>	<i>g.</i>	<i>mmoles</i>	<i>m</i>	<i>m</i>	
0.001	1.248	1.582				
0.012	1.243	1.572	0.004	0.008	9.96	0.040
0.12	1.225	1.563	0.009	0.0186	10.17	0.205
0.74	1.210	1.558	0.080	0.169	10.5	0.365
1.44	1.186	1.524	0.133	0.305	11.5	0.484
2.09	1.189	1.522	0.251	0.585	12.0	0.485
3.76	1.134	1.474	0.497	1.35	14.7	0.508
5.75	1.120	1.450	0.838	2.62	17.9	0.505

Dowex 50						
0.01	1.409	1.754				
0.12	1.399	1.738	0.0130	0.020	7.58	.236
0.61	1.382	1.712	0.0705	0.113	7.98	.435
1.23	1.346	1.689	0.149	0.252	8.55	.53
2.05	1.318	1.661	0.294	0.530	9.35	.57
3.34	1.290	1.633	0.501	0.970	10.5	0.63
4.86	1.253	1.618				
5.81	1.247	1.613				
7.14	1.223	1.573	1.297	3.13	15.0	0.63

The deswelling of resins in ammonium chloride solutions is shown in Table V. The specific nonexchange electrolyte content is also given. The results of similar experiments with Dowex 50 resins and other electrolytic solutions are shown in Table VI; Table VII shows values for Duolite C-3 resins.

TABLE VI
Deswelling of Dowex 50 in Various Solutions

Solution	V_e	W_e	NE
Hydrochloric acid			
<i>m</i>	<i>ml.</i>	<i>g.</i>	<i>mmoles</i>
0.005	1.524	1.880	
0.12	1.502	1.871	
0.49	1.495	1.858	
0.78	1.505	1.870	
2.68	1.408	1.775	
3.34	1.362	1.727	
4.21	1.348	1.711	
5.03	1.314	1.676	
6.65	1.287	1.641	

TABLE VI (Continued)

Solution	V_e	W_e	NE
Lithium chloride			
0.001	1.503	1.898	
0.075	1.504	1.896	0.024
0.73	1.486	1.880	0.018
1.51	1.437	1.833	0.057
2.64	1.368	1.766	0.383
3.46	1.342	1.738	
3.47	1.334	1.730	
4.60	1.289	1.687	0.507
6.18	1.240	1.650	
6.40	1.121	1.511	
7.02	1.092	1.485	0.889
7.32	1.064	1.461	
12.4	1.019	1.437	
18.1			3.290
Sodium thiocyanate			
m	$ml.$	$g.$	$mmoles$
0.01	1.418	1.874	
0.10	1.403	1.860	
0.68	1.368	1.834	
1.02	1.371	1.835	
3.36	1.295	1.778	
6.17	1.236	1.745	
7.95	1.197	1.727	
16.0	1.169	1.742	
Ammonium sulfate			
0.005	1.411	1.756	
0.065	1.401	1.700	
0.41	1.390	1.738	
0.41	1.385	1.737	
0.76	1.427	1.776	
0.96	1.366	1.712	
1.21	1.349	1.699	
1.79	1.338	1.684	
1.79	1.335	1.684	
2.60	1.289	1.667	
3.29	1.274	1.640	
4.28	1.256	1.630	
4.78	1.241	1.617	

TABLE VII

Deswelling of Duolite C-3 in Various Solutions

Hydrochloric acid		Lithium chloride		Sodium chloride		Potassium chloride	
Molality	V_e	Molality	V_e	Molality	V_e	Molality	V_e
<i>m</i>	<i>ml.</i>	<i>m</i>	<i>ml.</i>	<i>m</i>	<i>ml.</i>	<i>m</i>	<i>ml.</i>
0.003	1.643	0.0075	1.606	0.003	1.456	0.003	1.377
0.012	1.643	0.075	1.609	0.01	1.453	0.01	1.380
		0.76	1.555	0.03	1.459	0.03	1.379
0.12	1.640	1.55	1.532	0.10	1.445	0.10	1.378
				0.30	1.452	0.30	1.379
1.27	1.600			1.03	1.423	1.04	1.358
3.19	1.487	4.97	1.446	2.10	1.412	2.17	1.332
6.87	1.462	6.88	1.424	3.23	1.394	3.30	1.328

DISCUSSION

The thermodynamic theory of ion-exchange processes (4, 5) considers the resin system as a cross-linked polyelectrolyte, where the free energy of the swelling process is of appreciable magnitude. As a first approximation, a simple relationship between the osmotic pressure π (equal to the swelling pressure) and the external resin volume V_e is postulated, namely,

$$V_e = a\pi + b.$$

Here a is related to the bulk modulus of the resin system and b represents the sum of the matrix volume V_m plus a "rest volume" term, where π is zero. The osmotic pressure is defined in the conventional manner,

$$\pi = \frac{RT}{\bar{V}_w} \ln \frac{a_{w_o}}{a_{w_i}},$$

where the subscript " w " refers to the solvent (water) and " i " and " o " refer to the inner or resin phase and the outer solution phases, respectively. When the resin is in equilibrium with a dilute electrolytic solution, the concentration of fixed negative groups within the resin phase is so high as to virtually exclude all movable anions from the resin phase. Under these circumstances, $a_{w_o} \cong 1$, and

$$V_e = - \frac{aRT}{\bar{V}_w} \ln a_{w_i} + b.$$

This equation, which holds that V_e is a function solely of a_{w_i} when various cations occupy the exchange positions in the resin, assumes that the mechanical behavior parameters a and b are not specifically affected by the presence of these cations. In other words, it assumes that the entropy of the polymer chains is unaffected by the nature of the exchange cation,

aw_i being the same. This assumption appears to be valid especially with inorganic and low-molecular-weight organic cations. High-molecular-weight organic cations do appear to affect the chain entropy to some extent; evidence for this effect will be presented in a later paper.

In Fig. 1 the volume data shown in Table I are plotted against the logarithm of the hydrated molar ionic volume of the univalent exchange cations. For bivalent cations the hydrated equivalent ionic volumes are used. These hydrated ionic volumes are calculated from conductance data (3). Table I and Fig. 1 show that the specific resin volume is proportional to the hydrated ionic volumes in the case of the alkali metal ions and the quaternary ammonium ions. The somewhat lower values of

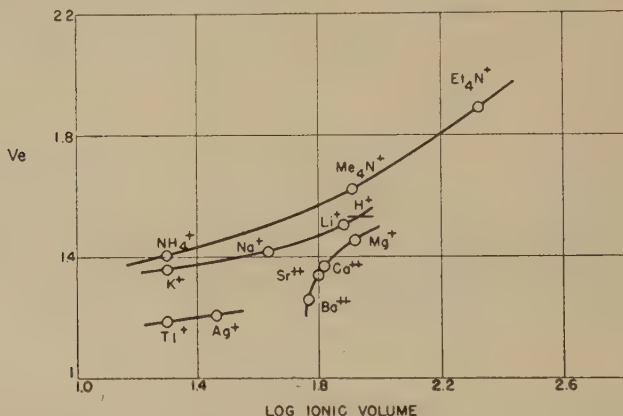


FIG. 1. Specific resin volume (V_e) as a function of the logarithm of the equivalent (hydrated) ionic volume for a Dowex 50 resin. Me = CH_3 ; Et = C_2H_5 .

V_e for the alkali metal cations as compared with those for the ammonium and quaternary ammonium ions may be due to the fact that in these highly concentrated systems a partial dehydration of the hydrated ions has taken place. It is known that while the potassium ion and the ammonium ion are almost the same size in dilute aqueous media, the former is somewhat hydrated while the latter is not. The same comparison obtains for the lithium and the tetramethylammonium ions.

It is of interest to note that the value of V_e for the hydrogen ion is slightly larger than that for the lithium ion, suggesting that in the resin phase these two ions are of about the same size. This is as expected from a consideration of ion-dipole forces.

The fact that V_e follows the sequence of increasing hydrated ionic volumes, plus the fact that selectivity coefficients also follow this sequence (the smaller ion being preferred), is consistent with the modern theories of electrolytic solutions, plus a consideration of pressure-volume effects (5). The Bjerrum (2), Harned (10), Stokes-Robinson (12) theory holds

that concentrated electrolytic solutions depart from ideal behavior as a result of electrical work, as calculated by Debye and Hückel, and in addition, binding n moles of water to each mole of solute. Thus there is a Debye-Hückel term, and a bound solvent term.

For ions of the same valence, in solutions of the same concentration, differences in the ionic activity coefficients due to the Debye-Hückel term depend entirely upon differences in angstrom units (A.), the distance of nearest approach. However, the corresponding difference in activity coefficient is small. For example, for potassium halides $A. = 4$; for lithium halides $A. = 5$. In eight molal solutions, to draw an analogy to the resin systems, $\gamma_{\pm}^{\text{KCl}} = 0.50$, and $\gamma_{\pm}^{\text{LiCl}} = 0.56$, considering only the Debye-Hückel term.

The solvent term makes for the major differences which are found for the various salts. Here values of n are calculated by curve fitting. Since the anions (particularly the halides) are not appreciably hydrated, the n values can be attributed almost entirely to the cations. For lithium, n is 8, for sodium n is 4, and for potassium n is 2 (12). However, n values calculated from conductivity data (3) are considerably lower. For example, the hydrated molar values are 20 ml. for potassium, 43 ml. for sodium, and 76 ml. for lithium. Thus $n^{\text{K}^+} = 1$, $n^{\text{Na}^+} = 2$, $n^{\text{Li}^+} = 4$. This is expected, for the conductance measurement itself probably strips off some of the hydration shell.

The Bjerrum, Harned, Stokes-Robinson theory thus holds that heavily hydrated solutes (high n values) make for lower solvent activities, and as a consequence have higher ionic activity coefficients; the converse also obtains. A simple treatment, based upon the same general considerations as this theory, considers the bound solvent as part of the solute, and expresses the composition of the solution in terms of only the free or unbound solvent. As regards the solvent term of the Bjerrum theory, the two treatments are equivalent. This is the same as counting the bound solvent as part of the solute, and the n terms drop out. Then, in comparing the thermodynamic properties of electrolytic solutions of the same valence type at about the same concentration, the Debye-Hückel contribution to activity coefficients will be about the same for all. The ionic activity coefficients will be about the same and differences in the activities of the solvent can be assumed to be a function solely of differences in the mole fraction of free solvent in the various solutions (5).

It follows that V_e will be the same for all cations having the same (hydrated) ionic volumes, for under these circumstances the same amount of free water (which defines aw_i) will be present. For equal quantities of resin, moles of components other than solvent are always the same. V_e will increase as aw_i decreases, and decrease as aw_i increases. For the alkali metal cations, the atomic volumes of which are small compared to their

hydrated ionic volumes (see Table VIII which follows later), V_e is determined largely by the extent of hydration. For the ammonium series of cations, which are not appreciably hydrated, V_e is determined by the ionic volumes, for here less solvent can be present in the same volume of solution.

These effects would be observed even if no pressure-volume free-energy considerations applied to these systems. The pressure-volume effect will decrease aw_i , or force free solvent from the resin phase. This effect will be strongest where V_e is largest, for here π is largest. Therefore, the differences in V_e are probably smaller than the actual differences in hydrated ionic volumes would indicate.

From Fig. 1 it then appears that since V_e is the same for the ammonium and the sodium resins, that the (hydrated) volume of the latter is equal to that of the former, which is not appreciably hydrated and is equal to about 20 ml./mole. Then for sodium, the n value is 1. For lithium, where V_e is equal to the mean V_e values for the ammonium and tetramethylammonium ions, n is calculated to be 3. In the case of potassium, there is no corresponding V_e value for an unhydrated cation which is of the same size or smaller, and thus unfortunately no reference scale exists. However, n is obviously considerably smaller than in the case of sodium. These n values all appear to be reasonable, considering the extremely high molalities (5–9 m) for these systems.

It is of interest to note that the matrix volumes follow the order of increasing atomic volumes rather than that of hydrated ionic volumes. Table VIII lists molar ionic volumes taken from the V_m data of Table I,

TABLE VIII
Comparison of Molar Atomic and Ionic Volumes

Ion	$V_m - V_m [H^+]$ ml./mole	Atomic volume ml./mole
Li ⁺	1.2	0.56
Na ⁺	6.8	2.2
K ⁺	15.4	4.9
NH ₄ ⁺	19.2	20
(CH ₃) ₄ N ⁺	86.8	81

calculated assuming that the value for the hydrogen state ($V_m[H^+]$) represents the matrix volume itself. These values are compared with molar atomic volumes, taken from crystallographic data (11). The resin values are considerably larger than the atomic volumes for the small alkali metal ions, but agree rather well with them for the larger ions. This is as expected, for the polymer chains are large compared with the size of unhydrated alkali metal ions.

The low values of V_e for the thallium and silver resins undoubtedly reflect ion-pair formation between the sulfonate group and an ion with

which it forms a slightly soluble compound in solution. Here ion-pair formation results in a decrease in the concentration of osmotically active movable cations with an increase in the activity of the water. Similar effects are observed in the case of the alkaline earth metals, where the order of decreasing values of V_e follows the order of decreasing solubility of the sulfonate salts.

In Fig. 2 the logarithm of the specific resin volume V_e is plotted against the DVB percentage. Since the molecular weights of the monomer

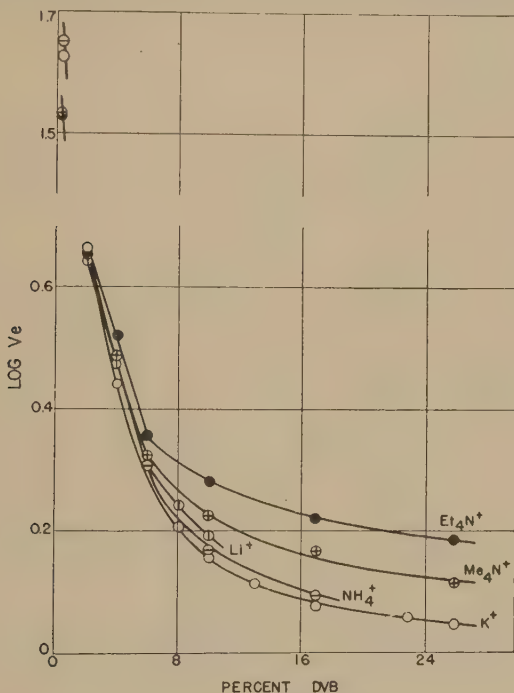


FIG. 2. Logarithm of the specific resin volume (V_e) as a function of the per cent DVB in the polymer, for various DVB resins.

and cross-linking agent are not very different, the per cent DVB corresponds roughly to the per cent cross-linking. From Fig. 2 it is seen that V_e rises sharply as the degree of cross-linking decreases, and that the molality of exchange cations (m) falls from 11 to 0.1. This is as expected from a consideration of the swelling pressure as resulting from a thermodynamic osmotic pressure. For resins prepared from styrene-divinylbenzene copolymers using a suspension polymerization technique, the percentage of divinylbenzene originally present in the emulsion is larger than the amount available for cross-linking, because the cross-linking agent is slightly soluble in the water used as suspensions medium. This is

particularly the case for low divinylbenzene contents. For this reason, the percentages of DVB listed are no doubt too high.

DVB 0.4 is a very soft, gelatinous material, almost transparent when suspended in water. As the DVB content increases, the resin changes from a firm gel (DVB 2) to very hard, brittle granules. A comparison of DVB 0.4 with similar products prepared using bulk polymerization techniques where the effective divinylbenzene content is known, indicates that a product prepared using 0.1% DVB has about the same gel properties. The DVB 2 products appears to be about the same in both cases.

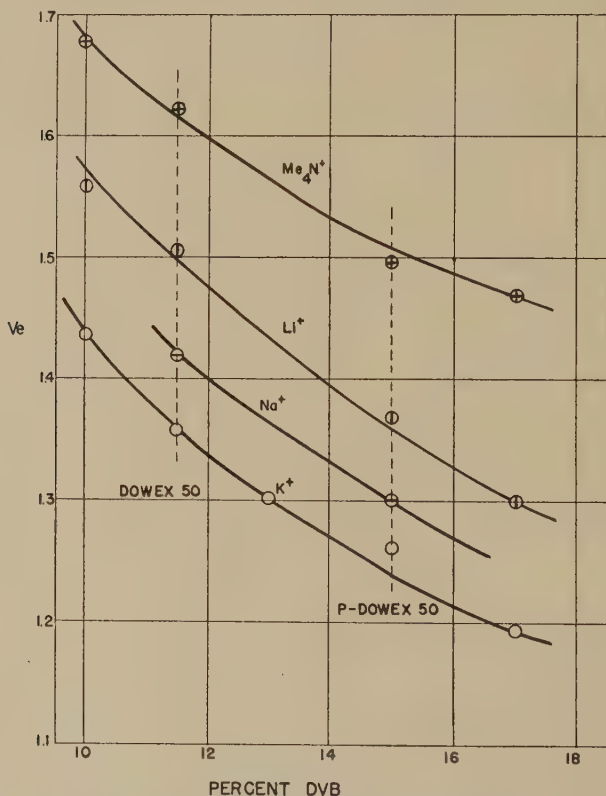


FIG. 3. A comparison of V_e values for two Dowex 50 resins with values for the DVB resins.

From Table II and Fig. 2 it should be noted that the V_e values follow the order of increasing (hydrated) ionic volume at the higher degrees of cross-linking, but that a "cross-over" is encountered at low DVB values. With DVB 0.4, V_e for potassium and ammonium is significantly larger than V_e for the very much larger quaternary ammonium ions. Also, while V_e for the tetraethylammonium ions is larger than that for the tetra-

methylammonium ions at high degrees of cross-linking, the two are virtually identical for DVB 0.4 and 2. All of these effects are related to the activity coefficients of these ions in the resin phase; they will be discussed in a quantitative manner in a subsequent paper in this series.

In Figs. 2 and 4, the specific volumes and densities of a series of DVB resins in various states are compared with corresponding values for two samples of Dowex 50, one obtained in 1947 (Table I) and another labeled P-Dowex 50, obtained in 1949. In Fig. 3 values of V_e for the DVB resins are plotted against the per cent DVB. The corresponding values for the Dowex 50 resins were fitted to the curves by shifting their values along

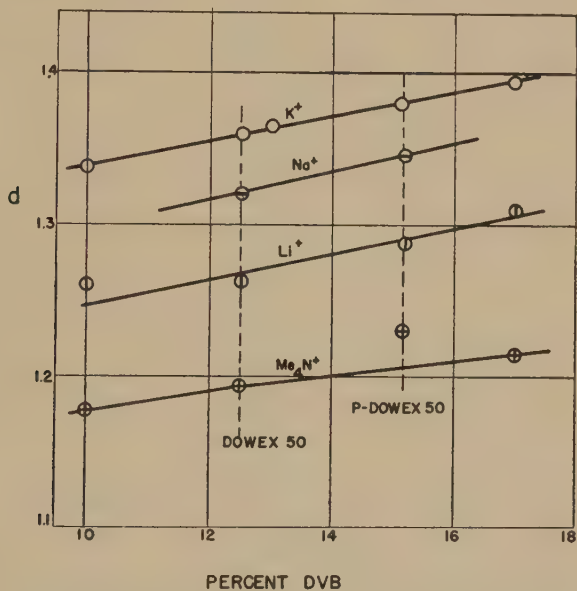


FIG. 4. A comparison of densities for two Dowex 50 resins with values for the DVB resins.

the abscissa until the closest match of potassium and tetramethylammonium V_e values was effected.

It is apparent from Fig. 3 that the relative V_e values for the same resin in different states are very nearly the same for the four resins described. This is as expected, although small differences which exist may be the result of different degrees of sulfonation. The two commercial resins are different in their physical properties, one corresponding to 11.5, the other to 15% cross-linking, based on the DVB resin scale. It appears that the establishment of an arbitrary scale of per cent DVB based upon V_e values rather than methods of polymerization would be useful in comparing data obtained with different resin systems. Since the rate of exchange (7) and

also the selectivity coefficient (5) are functions of the mechanical properties of an ion-exchange resin, the establishment of such standards is important.

In Fig. 4 the density of the resin particles, $d = W_e/V_e$, is plotted in the same manner as in Fig. 3. The density of the Dowex 50 resins also fits the DVB scale. The potassium resin is the most dense, the density decreasing as the atomic weight of the alkali metal cation decreases. This

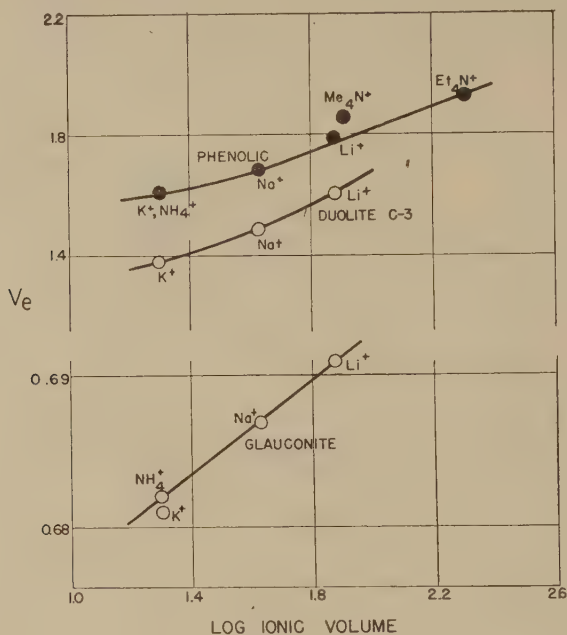


FIG. 5. Specific exchanger volume (V_e) as a function of the logarithm of the molar (hydrated) ionic volume for three exchangers.

is because the density of the ion decreases with its extent of hydration, and also because V_e is proportional to the hydrated ionic volume. The tetramethylammonium resin is lightest, as expected.

The data of Table III is shown graphically in Fig. 5; V_e values are plotted against hydrated ionic volumes. Here the same relationships are observed as in the case of the polystyrene resins. For the phenolic resin, the values of V_e for the quaternary ammonium resins are lower, relative to values for the alkali metal ions. This effect is probably due to a stronger adsorption of the organic ions onto the less polar matrix of these resins. Their sulfonic acid capacity, or ratio of polar sulfonic groups to hydrocarbon matrix, is less than for the sulfonated polystyrene resins; greater absorption hereby obtains with the lower capacity resins.

The glauconite exchanger also appears to swell as large hydrated ions occupy exchange positions. This is not sufficient evidence that the same swelling mechanism operated in both types of exchange systems, but the data may point to that conclusion.

The data of Table IV, relating the fraction of exchange positions occupied by the potassium ion ($X_{K_i^+}$) to V_e values, are shown plotted in Fig. 6. Here it is seen that the volume is a smooth function of the com-

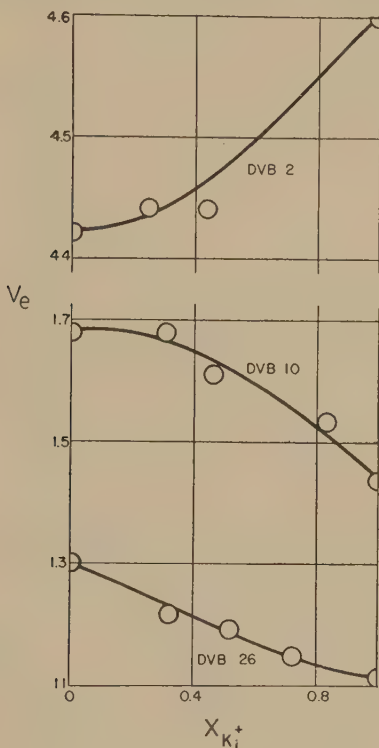


FIG. 6. Specific resin volume (V_e) as a function of the fraction of exchange sites occupied by the potassium ions ($X_{K_i^+}$), for potassium tetramethylammonium exchange with various DVB resins.

position of the resin phase. This suggests that the activity coefficients of the exchange cations are not strongly dependent upon their relative concentrations.

The data of Table IV allow the calculation of some of the parameters of the fundamental thermodynamic equation describing cation exchange processes (5). Taking, as a typical example, the exchange of tetramethylammonium ions for potassium ions,



where g is the moles of water moving from the solution phase to the resin phase; the thermodynamic equation is (5),

$$RT \ln \left[\left(\frac{m_1}{m_2} \right)_i \left(\frac{\gamma_1}{\gamma_2} \right)_i \left(\frac{a_2}{a_1} \right)_o \left(\frac{a_{w_i}}{a_{w_o}} \right)^g \right] = \pi (\bar{V}_2 - \bar{V}_1 - g\bar{V}_w).$$

Here the subscripts 1 and 2 refer to the potassium and tetramethylammonium ions, respectively; γ is the ion-activity coefficient; a_o is the activity of the electrolyte in the solution phase; and \bar{V} is the partial molar volume of the ion in the resin system.

While the individual values of \bar{V} cannot be evaluated because of electroneutrality considerations, the net partial molar volume ΔV can be determined.

The net partial molar volume for the exchange process is,

$$\bar{V}_2 - \bar{V}_1 - g\bar{V}_w = \Delta V = \frac{\partial V_e}{\partial n_2} - \frac{\partial V_e}{\partial n_1} - \frac{g \partial V_e}{\partial n_w},$$

where n refers to the numbers of moles and $\partial V_e / \partial n$ is the change in volume which takes place in a resin system of infinite volume when a mole of exchange ions enters the resin phase. If the data of Table IV are plotted as V_e against the moles of potassium in the resin phase, as is shown in Fig. 7,

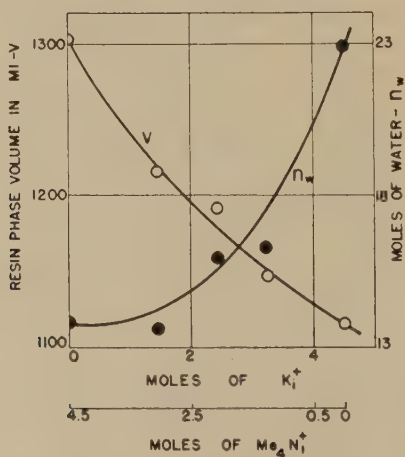


FIG. 7. Plot of the resin volume (V) and moles of water present (n_w) for DVB 26 resin, as a function of moles of potassium ions present in the resin phase.

and the slope taken at any $X_{K_i^+}$ then that slope is ΔV in ml./mole for that composition. At $X_{K_i^+} = 0.5$, for resin DVB 26 it is -38 ml./mole, for DVB 10 it is -47 ml./mole, and for DVB 2 it is 39 ml./mole.

The values of g can be determined in a similar manner, by plotting the moles of water present in the system as a function of moles of K_i^+ , and $g = (\partial n_w / \partial n_{K^+})_i$. The data for resin DVB 26 are also plotted in Fig. 7 as

a function of the moles of water present in the resin phase; here g is 1.5 at $X_{K_i^+} = 0.5$.

When the resin system is in equilibrium with a concentrated electrolytic solution, some nonexchange electrolyte enters the resin phase and a deswelling takes place. For a system containing a cation (C^+) and a movable anion (A^-), the reaction which can occur is,

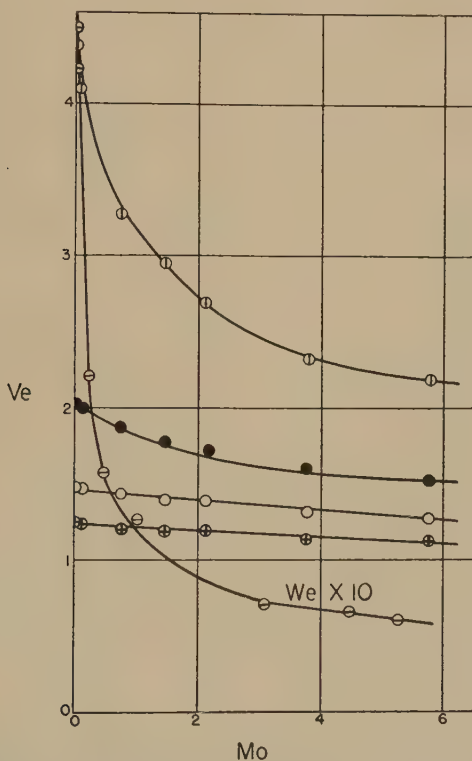


FIG. 8. Deswelling of various resins as a function of the molality of ammonium chloride in the solution phase. DVB 0.4, \ominus ; DVB 2, \oplus ; DVB 6, \bullet ; DVB 10, \circ ; DVB 17, \oplus .

The Gibbs-Donnan equation which applies to this equilibrium is (5),

$$RT \ln \left[\frac{m_o^2 \gamma_{\pm o}^2}{m_i^+ m_i^- \gamma_{\pm i}^2} \left(\frac{a_{w_o}}{a_{w_i}} \right)^g \right] = (\bar{V}_{CA} + g\bar{V}_w) \pi,$$

where m is the molality of the ionic components, and \bar{V}_{CA} the partial molar volume of the salt, C^+A^- . Eliminating the solvent terms which constitute an identity,

$$RT \ln \frac{m_o^2 \gamma_{\pm o}^2}{m_i^+ m_i^- \gamma_{\pm i}^2} = \pi \bar{V}_{CA}.$$

If π is zero, the latter equation reduces to the familiar Donnan equation, and γ_i^\pm can be calculated from the data. If π is of appreciable magnitude, then it and \bar{V}_{CA} must be known to evaluate γ_i^\pm . For a salt such as ammonium chloride where \bar{V} is about 40 ml./mole, if π is 100 atm. the ratio of solute activities a_o/a_i is about 1.2; if π is 200 atm., the ratio is above 1.4. These values of π are of the estimated magnitude for these systems (5).

These equations predict that as the concentration of electrolyte in the solution phase increases, the exclusion of movable anions from the resin phase as a result of the Donnan effect will make for a counter osmotic pressure, which will deswell the resin. The data of Table II show this effect. Here the molality of both the chloride (m_{Cl^-}) and the ammonium ($m_{NH_4^+}$) ions are calculated. This calculation takes into consideration the weight of the nonexchange electrolyte present in the resin phase. The value of γ_i , the mean activity coefficient of ammonium chloride in the resin phase, is calculated from the relationship, $\gamma_i = a_o/(m^+m^-)_i^{\frac{1}{2}}$, which assumes that π is zero.

Figure 8 shows the deswelling effects which occur as m_o , the molality of ammonium chloride in the resin phase, increases. The curve for DVB 0.4 is reduced by a factor of ten, to allow a comparison. It should be noted that w_e rather than V_e is reported, because the extreme softness of this resin gel makes volume determinations very difficult. Figure 8 shows that the low DVB resins are deswelled much more strongly, the result of considerably lower thermodynamic osmotic pressures, and lower exchange-ion concentrations. Figure 9 shows the same volume data as well as the molality of chloride within the resin phase, plotted against the logarithm of m_o . As m_o increases, measurable amounts of nonexchange electrolyte enter the resin phase only when m_o is an appreciable fraction of the concentration of fixed exchange groups.

The nonexchange electrolyte values are reasonably accurate. The amount of nonexchange electrolyte contained in the resin phase is greater, by at least an order of magnitude, than the amount of electrolyte that could be contained in a solution film covering the resin particles after centrifugation. For resin DVB 6 in 0.12 m solution, the specific nonexchange electrolyte is 0.022 m moles. This amount of salt is contained in about 0.2 ml. solution. Since V_e is 1.997 ± 0.004 ml., the amount of solution required to account for all of the nonexchange electrolyte, 0.2 ml., is more than twenty times the maximum experimental variation in the volume of the resin (0.008 ml.). A similar calculation performed for higher or lower DVB resins shows that the maximum error in NE is less than 10%, calculated in this manner.

Recently Gregor, Pope, and Collins (9) determined the amount of various neutral molecules contained in the resin phase by equilibrating

the resin with a dilute aqueous solution of the molecule, followed by centrifugation and elution. The amount of neutral molecule contained in the resin phase was also determined by following its rate of diffusion from the resin, extrapolating to zero time, and calculating the amount present initially. Here it was found that both methods gave the same results within experimental error; this is further verification of the validity of the nonexchange electrolyte content values, which are probably accurate to at least 2%.

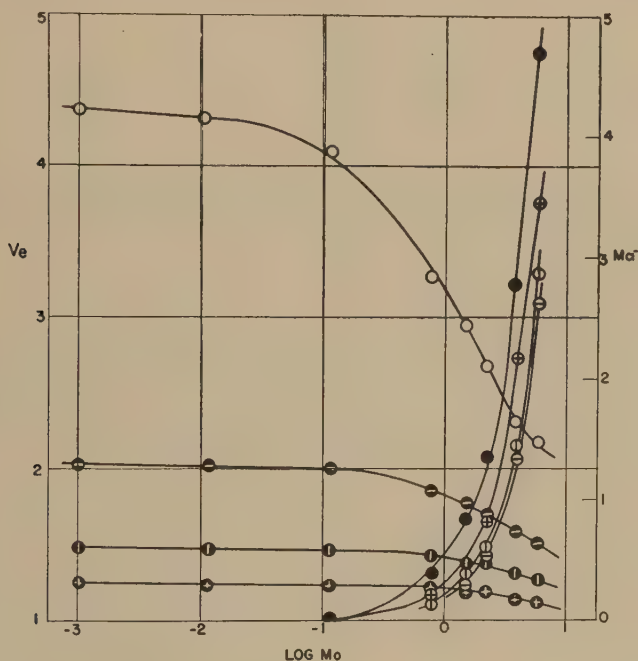


FIG. 9. Deswelling and nonexchange electrolyte content of various DVB resins, as a function of the logarithm of the molality of ammonium chloride in external solution. Values of V_e and m_{Cl^-} are, respectively, DVB 2, \circ and \bullet ; DVB 6, \bullet and \oplus ; DVB 10, \bullet and \odot ; DVB 17, \oplus and \ominus .

The calculated values of the mean activity coefficient of ammonium chloride within the resin phase (γ_i) appear quite interesting. While pressure-volume effects make the simplified calculation of γ_i somewhat inaccurate, a strong effect is observed, in that γ_i decreases as $m_i^+m_i^- = m_i^2$ increases, as shown in Fig. 10. This is as expected, for the movable anion acts as a "bridge" for the movement of an exchange cation away from its exchange site. Therefore, the activity coefficient (here largely the cationic activity coefficient) increases sharply as the number of "bridges" increases. In Fig. 11 the activity coefficient γ_i is plotted against the logarithm of the molality of chloride "bridges" in the resin phase. Figure 12 shows the same

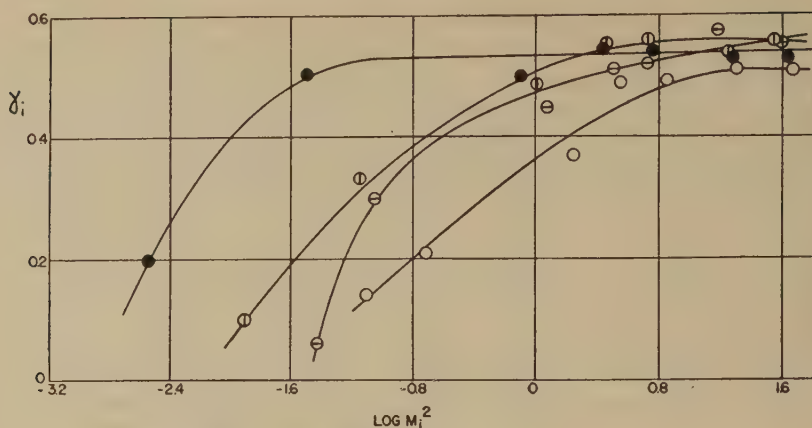


FIG. 10. Mean activity coefficient (γ_i) of ammonium chloride in the resin phase as a function of the logarithm of the product of the cationic and anionic molalities. Resins are: DVB 2, \bullet ; DVB 6, \oplus ; DVB 10, \ominus ; DVB 17, \circ .

data plotted against the logarithm of the ratio of the molalities of the ammonium and chloride ions in the resin phase. Data for Dowex 50 are also included here. The mathematical theory which deals with these systems, and in particular the theoretical significance of the plots shown, will be given in one of the next papers in this series.

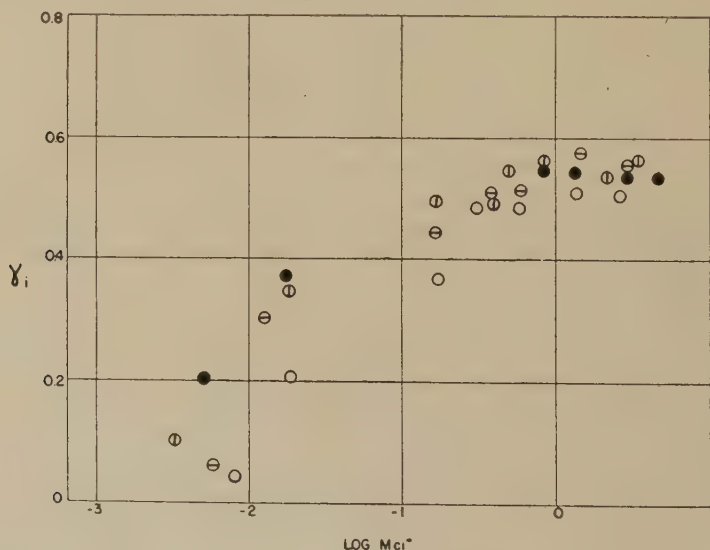


FIG. 11. Plot of γ_i against logarithm of molality of chloride in the resin phase (m_{Cl^-}). See Fig. 10.

Figures 11 and 12 show a remarkable uniformity in γ_i values, considering the range of DVB resins considered. Since π decreases as the per cent DVB decreases, and is apparently rather low for DVB 2 (5), the

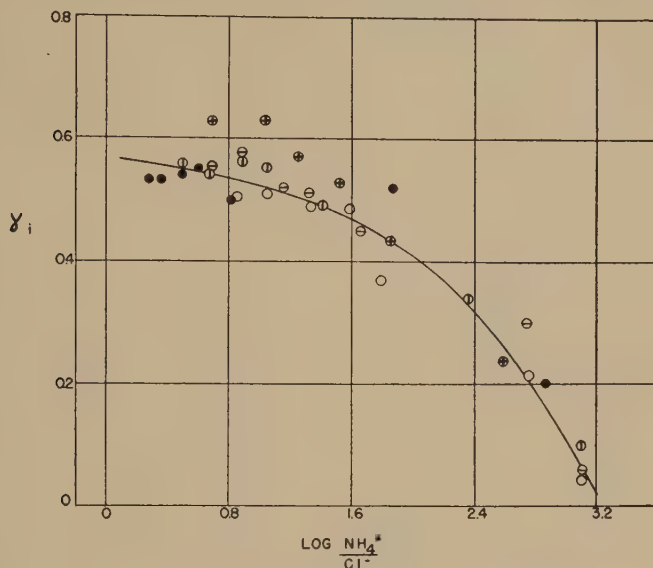


FIG. 12. Plot of γ_i against logarithm of ratio of ammonium and chloride molalities in the resin phase. See Fig. 10, Dowex 50, \oplus .

similarity of the curves indicates that the $\pi\bar{V}$ correction may be a small one. The mean activity coefficient of ammonium chloride in solutions ranging from 2 to 8 molal is in the range 0.60 to 0.62. Thus it appears that the γ_i values approach this value as a limit.

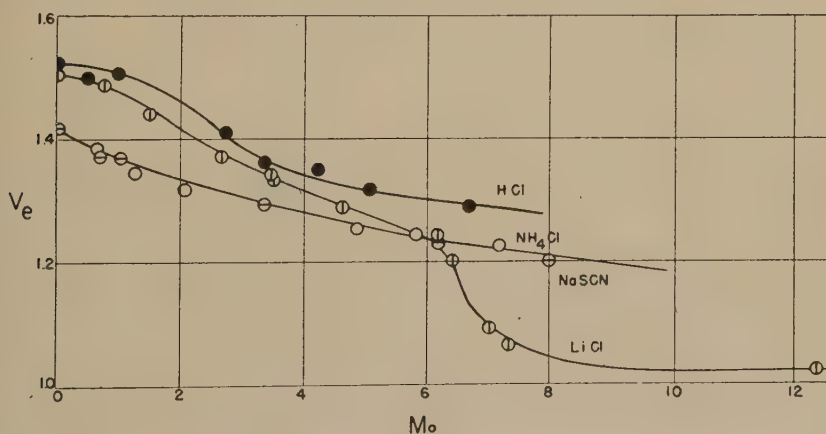


FIG. 13. Deswelling of Dowex 50 resins in various electrolytic solutions.

The deswelling of Dowex 50 resins in various electrolytic solutions is shown graphically in Fig. 13. The curves for hydrochloric acid, ammonium chloride, and sodium thiocyanate all appear normal. The lithium chloride curve does show a sharp break at $m_o = 6$; this discontinuity may reflect a sharp change in the hydration of the lithium ion.

In Fig. 14 the deswelling of Dowex 50 resin in ammonium chloride and ammonium sulfate solutions is shown, plotted against the activity of the

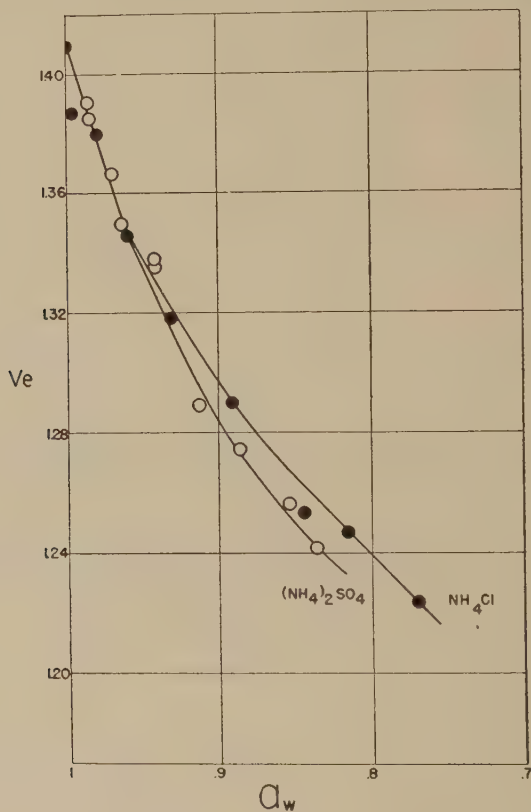


FIG. 14. Deswelling of Dowex 50 resin in ammonium chloride and ammonium sulfate solutions, plotted as a function of the activity of the solvent in the solution phase.

solvent in the external solution phase. The coincidence of the two curves at high values of a_{w_o} is expected, for in this range a_{w_i} should be a function of only a_{w_o} and the nature of the exchange cation. As appreciable amounts of nonexchange electrolyte enter the resin phase, the two curves deviate. The deswelling of Duolite C-3 resins in various electrolytic solutions is shown in Fig. 15. Here results are observed which are quite similar to those encountered with the other exchangers.

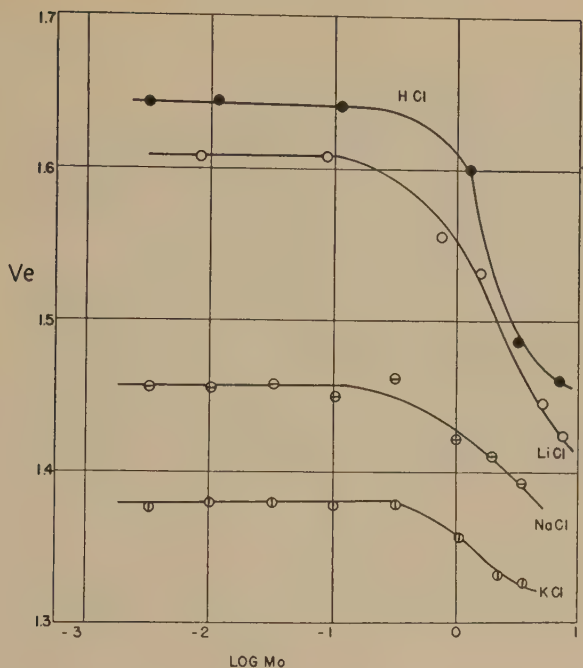


FIG. 15. Deswelling of Duolite C-3 resins in various electrolytic solutions.

SUMMARY

1. The volume and composition of a number of cation-exchange resins, measured under various experimental conditions, have been described. For a particular resin, the volume increases with the (hydrated) ionic volume of the exchange cation (except where ion-pair formation takes place). This phenomenon is discussed in terms of the Bjerrum, Harned, Stokes-Robinson theory.

2. The swelling of resins having different degrees of cross-linking is described in terms of an osmotic model. Various sulfonated polystyrene-divinylbenzene resins are compared.

3. The swelling and composition of a resin phase containing more than one species of exchange cation is described. Net partial molar volumes are calculated.

4. The deswelling of resins in concentrated electrolytic solutions is described, and the mean ionic activity coefficient of the movable electrolyte within the resin phase calculated. This activity coefficient decreases sharply as the concentration in the external solution phase decreases.

REFERENCES

1. BAUMAN, W. C., AND EICHHORN, J., *J. Am. Chem. Soc.* **69**, 2830 (1947).
2. BJERRUM, N., *Z. anorg. Chem.* **109**, 275 (1920).
3. GORIN, M. H., *J. Chem. Phys.* **7**, 405 (1939).
4. GREGOR, H. P., *J. Am. Chem. Soc.* **70**, 1293 (1948).
5. GREGOR, H. P., *J. Am. Chem. Soc.* **73**, 642 (1951).
6. GREGOR, H. P., AND BREGMAN, J. I., *J. Am. Chem. Soc.* **70**, 2370 (1948).
7. GREGOR, H. P., BREGMAN, J. I., GUTOFF, F., BROADLEY, R. D., BALDWIN, D. E., AND OVERBERGER, C. G., *J. Colloid Sci.* **6**, 20 (1951).
8. GREGOR, H. P., HELD K., AND BELLIN, J., *Anal. Chem.* (in press).
9. GREGOR, H. P., POPE, M., AND COLLINS, F. C., In preparation.
10. HARNED, H. S., in TAYLOR, H. S., *Treatise on Physical Chemistry*, 1st Ed. D. Van Nostrand and Co., New York, 1924.
11. PAULING, L., *Nature of the Chemical Bond*. Cornell University Press, Ithaca, N. Y., 1939.
12. STOKES, R. H., AND ROBINSON, R. A., *J. Am. Chem. Soc.* **70**, 1870 (1948).
13. WALTON, H. F., *J. Phys. Chem.* **49**, 471 (1945).

LIGHT SCATTERING OF POLYVINYLPIRIDINE-NITROMETHANE SOLUTIONS¹

W. M. Cashin

Department of Chemistry, Cornell University, Ithaca, New York

Received March 26, 1951

This paper is a résumé of some experimental light-scattering work done on nitromethane solutions of a sample of polyvinylpyridine. The typical viscosity curve for a polyelectrolyte was found; light scattering clearly indicates an increase of polymer size with dilution, and the effect of additives on size has been studied.

The poly-2-vinylpyridine used was a sample of emulsion polymer furnished by Dr. V. S. Chambers of the U. S. Rubber Company. The molecular weight as determined by light scattering in dioxane was 650,000; R (the square root of the averaged square of the distance from beginning to end of the polymer chain) in this solvent was found to be 940 Å. by dissymmetry measurements.

The nitromethane was a c.p. grade redistilled immediately before use. The light used in the measurements was the blue line of mercury (4358 Å.).

In Fig. 1 are shown plots of $(\ln t/t_0) c$ against c for the polymer in nitromethane and dioxane (c is in g./cc., and t and t_0 are the flow times of solution and solvent). The curve for the polymer in nitromethane is typical of polyelectrolytes (1). It may be readily understood how this system will give the results indicated when one considers the nature of the solvent and solute. Nitromethane can behave as a weak acid (2), while polyvinylpyridine, like pyridine, is a base; consequently, there will be some ionization of the polymer (increasing with dilution) with a concomitant increase in size. The results of the angular light scattering measurements are summarized in Table I. It appears that the dissymmetry increases with dilution up to a certain point and levels off. The constancy in dissymmetry does not mean that the size is not increasing. At such sizes the dissymmetry is no longer a good measure of the size, having reached a constant value for any size (larger than 1 wavelength). This is a fundamental limitation of the dissymmetry method of size determination.

¹ The work herein reported was done in connection with the Government Research Program on Synthetic Rubber under contract with the Office of Rubber Reserve, Reconstruction Finance Corporation.

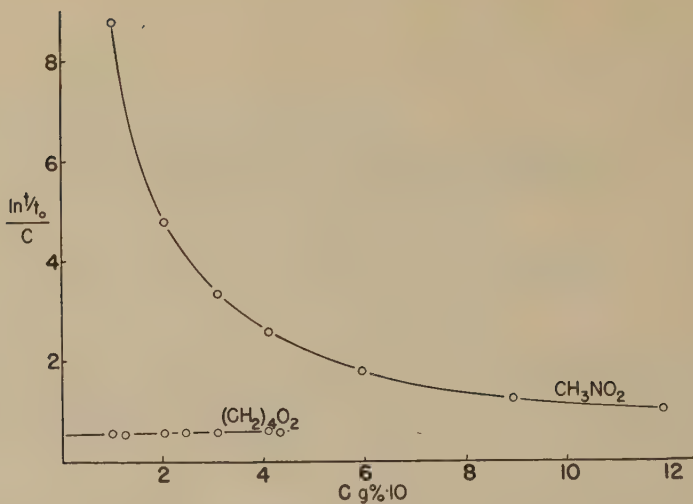


FIG. 1. Viscosity data for nitromethane and dioxane solutions of polyvinylpyridine; plot of $(\ln t/t_0)/c$ vs. c .

TABLE I

Dissymmetry (I_{45}/I_{135}) and Sizes of Polyvinylpyridine in Nitromethane for Different Concentrations

Conc. of polymer %	I_{45}/I_{135}	$R\mu_0/\lambda$
0.95	3.9	0.8
0.71	4.3	0.9
0.48	4.8	>1
0.24	4.7	>1
0.10	4.7	>1

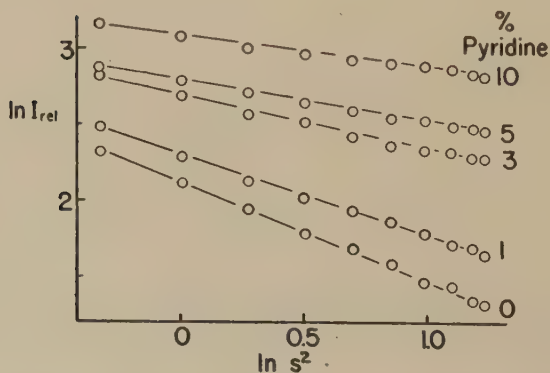


FIG. 2. Light scattering of polyvinylpyridine in nitromethane with added pyridine, plotted $\ln I_{rel}$ vs. $\ln s^2$.

The effect of the addition of pyridine to the system was also studied. The results of the light-scattering measurements are shown in Fig. 2. The concentration of the polymer is 0.9% for amount pyridine equal to zero. In other solutions it is less by the factor cc. pyridine/100. In this plot of $\ln I$ vs. $\ln s^2$ ($s = 2 \sin \theta/2$) increasing negative slope shows increased size. The size change is believed due to the decreased ionization of the polyvinylpyridine on the addition of pyridine.

Preliminary viscosity data on the polymer in nitromethane with added small amounts of tetramethylammonium iodide (a weak electrolyte in nitromethane) also shows a size decrease with added salt. This effect of added salt has not yet been investigated further. It was also noted that all the angular scattering curves obtained showed that a linear coiling polymer model assumption best fitted the experimental data.

REFERENCES

1. FUOSS, R. M., AND STRAUSS, U. P., *J. Polymer Sci.* **4**, 97 (1949).
2. TURNBULL, D., AND MARON, S. H., *J. Am. Chem. Soc.* **65**, 212 (1943).

TWO-DIMENSIONAL ELECTROPHORESIS AND IONOPHORESIS ¹

E. L. Durrum ²

Army Medical Service Field Research Laboratory, Fort Knox, Kentucky

Received December 15, 1950

ABSTRACT

The author has reported recently a unidimensional microelectrophoretic technique in which an electrical potential is applied across the ends of strips of filter paper saturated with buffer or other electrolyte solutions. To these strips are applied at intermediate areas, mixtures of charged substances to be separated. The present report is concerned with the extension of this method of separation in a manner analogous to two-dimensional paper chromatography. The method depends upon the fact that certain charged materials exhibit relative differences in mobilities at different pH values under the influence of an electrical field.

The phenomenon of "mobility equilibrium" is described and a hypothesis proposed to explain it.

INTRODUCTION

In previous reports (1,2) a unidimensional method for the separation of many types of charged substances by electrophoresis or ionophoresis on filter paper strips which had been saturated with buffer or other electrolyte solutions was described. The purpose of this report is to describe an extension of this method in order to increase its applicability and its efficiency. This has been carried out by operation in a manner analogous to two-dimensional paper chromatography as developed by Consden, Gordon, and Martin (3).

The separations obtained in the present process are based upon the principle that certain charged substances, for example, amino acids, migrate at quite different relative rates when subjected to an electrical potential on filter paper saturated with buffer or other electrolyte solutions which have different pH values. Thus, in brief, a separation is effected along one axis in accordance with mobility relationships which occur at a given pH followed by a successive separation at some other pH (where different mobility relationships hold) at an axis of 90° to the

¹ Most of the subject matter of this paper was presented before the American Society of Biological Chemists, April 20, 1950, in Atlantic City, N. J. This paper is based on U. S. Army Medical Service Field Research Laboratory Report of same title, Project No. 6-64-12-06-(38) dated October 9, 1950.

² Present address: Army Medical Service Graduate School, Army Medical Center, Washington 12, D. C.

original axis. The process can best be described by referring to the table and figures.

Table I shows the order of migration for amino acids on filter paper (S. & S. No. 413) in two electrolytes of different pH value. The groups identify amino acids which have mobilities so close to one another under the usual conditions of unidimensional operation as not to be separable,

TABLE I

Relative Order of Migration for Amino Acids on Filter Paper (S. & S. No. 413)

Toward cathode in 1.0 <i>N</i> acetic acid (pH 2.3)	Toward anode 0.2 <i>N</i> ammonium hydroxide (pH 11.3)
Lysine	Aspartic acid
Histidine	Glutamic acid
Arginine	Cystine
Glycine	
Alanine	Glycine
	Serine
Valine	Threonine
Isoleucine	Hydroxyproline
Leucine	Tyrosine
	Methionine
Serine	Histidine
Threonine	Phenylalanine
Methionine	Alanine
Tryptophan	Valine
	Isoleucine
Phenylalanine	Leucine
Glutamic acid	Tryptophan
Tyrosine	
Proline	
Cystine	Proline
Aspartic acid	Lysine
Hydroxyproline	
	Arginine

although individual amino acids within the different groups can be separated readily from individual amino acids in other groups by unidimensional methods.³ An inspection of this table suggests that two-dimensional separations should be attainable at these pH values, at least in cases where the amino acids fall into different mobility groups. Therefore, to carry out two-dimensional separations, it was only necessary to evolve

³ In Table I, in the case of the amino acids grouped with glycine in the anode migration column, the more rapidly migrating members are separable from the slower ones, although closely neighboring members are not separable by unidimensional means under the conditions cited.

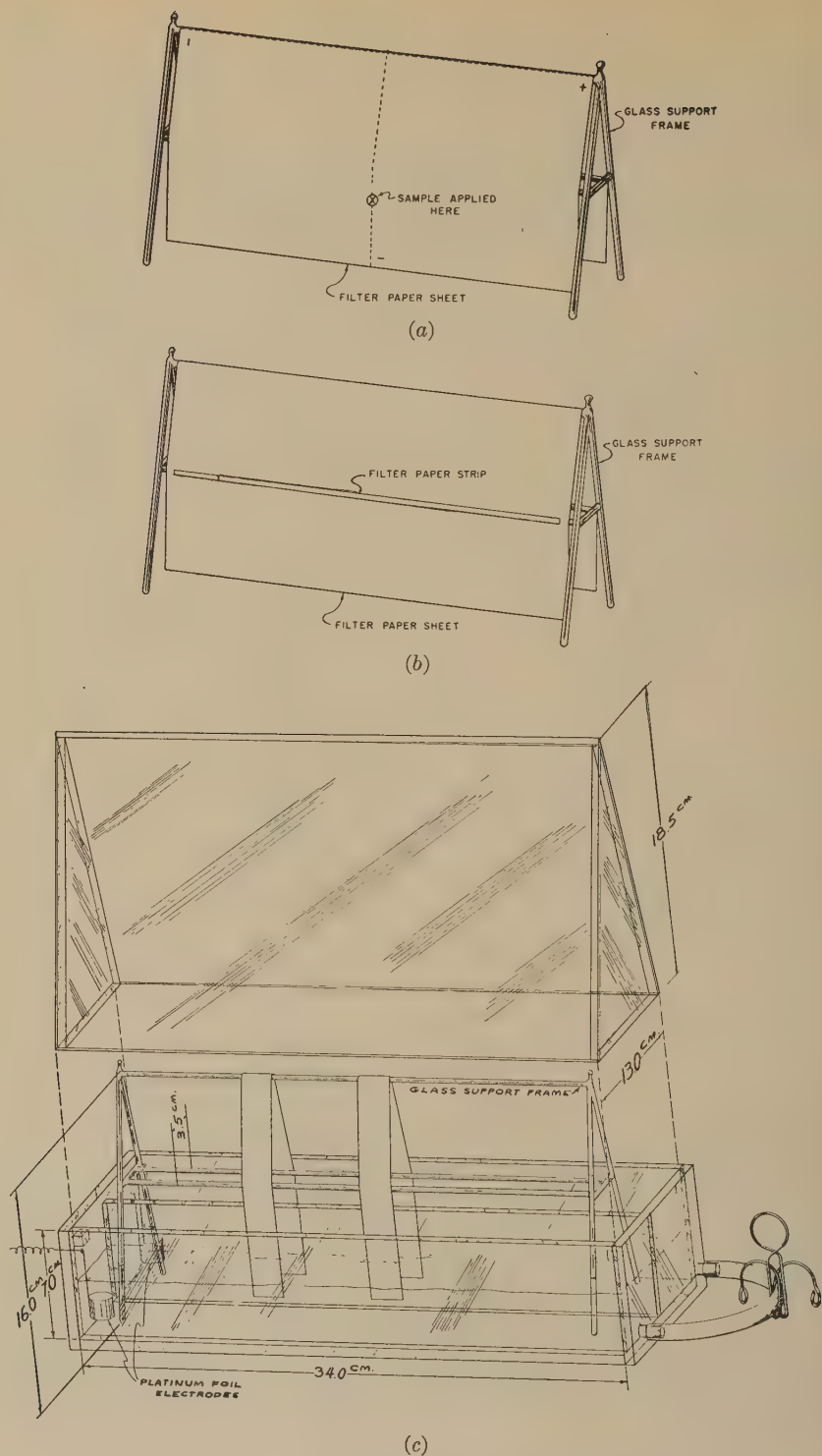


FIG. 1. Apparatus for two-dimensional electrophoresis and ionophoresis.

a technique which permitted convenient handling of wide sheets of filter paper in accordance with the above-mentioned principles.

EXPERIMENTAL

An apparatus which has been found to be suitable for this two-dimensional technique is illustrated in Fig. 1. It consists of a Lucite box with a center partition dividing the box into anode and cathode compartments. Platinum foil electrodes dip into the electrolyte solution in the anode and cathode sides. The two compartments are connected by a piece of Tygon tubing to permit initial equilibration of the liquid level of anolyte and catholyte in order to prevent electrolyte flow currents due to "siphoning," which may be pronounced when the levels of electrolyte differ appreciably in the two compartments. During operation, this tubing is clamped shut. In Fig. 1c, single narrow strips are illustrated being supported by a glass support frame with their ends dipping into the electrolyte compartments. In two-dimensional runs, a wide sheet of filter paper, as is shown in Fig. 1a, is substituted for the narrow strips.

A multiple cell adapted to handle simultaneously seven sheets of paper has also been used extensively. A manifold system of glass and rubber tubing connects the various electrolyte compartments and permits initial equilibration of electrolyte levels. By clamping the rubber tubing connections at appropriate positions, sheets may be run either in parallel or in series. A peaked roof of the cover of this cell permits any electrolyte condensing on the cover to drain back into the electrolyte compartments without dripping upon the filter paper sheets.

In general, two distinct methods are employed in separations, depending upon whether or not the first electrolyte system is volatile. The following example illustrates the technique in volatile electrolyte systems.

Example 1 (Partial Separation of Amino Acid Mixture)

A sheet of Whatman No. 2 filter paper, 30 × 30 cm. was folded double and creased, then opened and folded double a second time at right angles and creased. The creases thus established 90° axes which were marked by dotted lines with a pencil. One end of each line was marked with a plus sign and the other end of each line marked with a negative sign. At a point 10 cm. from the apex toward the cathode side of one axis was placed a reference mark X. The sheet was draped over a glass support frame as is illustrated in Fig. 1a. The paper was then washed by directing copious amounts of distilled water along the apical axis; then it was permitted to drain and dry. One liter of 0.2 N ammonium hydroxide (pH 11.3) was then poured into the cell illustrated in Fig. 1c, the clamp being removed from the Tygon tubing. The dried filter paper sheet supported upon its rack was then placed in the cell, and the paper was saturated with elec-

trolyte which was applied to the paper with a glass syringe. The Lucite top portion of the cell was replaced, and after standing for 5 min. to permit drainage of excess electrolyte from the paper, the tubing clamp was replaced.

A 5-mm. disk⁴ of filter paper containing approximately 270 $\mu\text{g.}$ of a mixture of 19 amino acids (arginine, lysine, histidine, glycine, alanine, valine, isoleucine, leucine, serine, tryptophan, threonine, methionine, phenylalanine, tyrosine, glutamic acid, proline, cystine, hydroxyproline, and aspartic acid) was placed on the reference mark X where it adhered by capillary attraction. A potential of 400 v. was then applied across the platinum electrodes for a period of 90 min. At the end of this period the



FIG. 2. Partial separation of amino acid mixture (example 1).

cell was opened and the filter paper and rack were removed and placed in a drying oven for 2 min. at 110°C. After 2 min. the paper (which was still slightly damp) was removed and the axis shifted 90° on the rack. The sheet and rack were replaced in the oven for an additional period of 5 min. to complete drying.

In the meantime, the cell was emptied and rinsed with tap water and filled with 1 l. of 1.0 *N* acetic acid (pH 2.3). The dried filter paper sheet and rack were now replaced in the cell and the top was replaced. After

⁴ An equimolecular aqueous solution 0.04 *M* in each of the amino acids enumerated was prepared with the aid of a few drops of concentrated ammonium hydroxide. Approximately 1/40 ml. of this solution was applied to disks of Whatman No. 2 filter paper 5 mm. in diameter, which were permitted to dry in the air at atmospheric temperature. The resulting disks contained approximately 270 $\mu\text{g.}$ of the amino acid mixture.

standing about 45 min., capillary forces caused the acetic acid solution to flow up both limbs of the paper, the two fronts eventually coalescing along the apical axis. This method of operation (except when "mobility equilibrium" separations are carried out, as explained later in this paper) is extremely important inasmuch as it "gathers up" amino acids (which have tended to diffuse on either side of the first axis in the course of the first part of the separation) to result in their distribution as a fine starting line which has been observed to result in more efficient separations. (Ordinarily, if one is careful the process of effecting coalescence of the two electrolyte fronts ascending on either side of the axis can be hastened by carefully applying electrolyte to both sides of the apex with a glass syringe and only requiring that capillarity effect the last 30 to 40 mm. of ascent.)

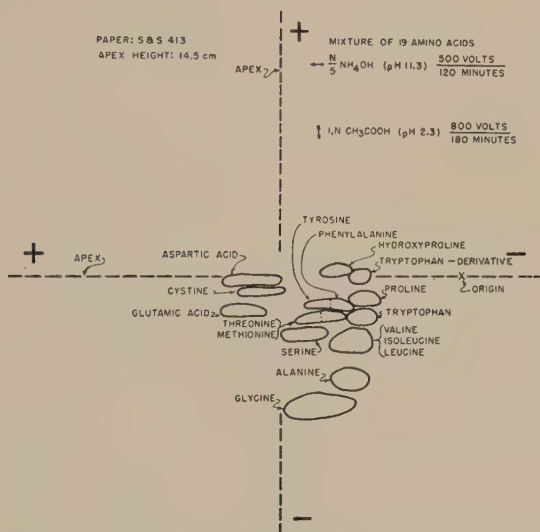


FIG. 3. Separation of amino acid mixture (example 2).

After the acetic acid electrolyte fronts had coalesced, a potential of 1000 v. was applied across the platinum electrodes. After 30 min., the rack and paper were removed and placed in a drying oven at 110°C. for 5 min. After drying, the sheet was sprayed with 0.1% ninhydrin solution in 95% ethyl alcohol, and replaced in the oven for 5 min. A tracing of the resulting sheet prepared by utilizing transmitted light is given in Fig. 2. It will be noted that in this example an ionophoresis period of short duration in acetic acid sufficed to permit identification of the basic amino acids as well as glycine, glutamic acid, aspartic acid, cystine, and hydroxyproline. Longer periods are required to separate the remaining mono-aminomonocarboxylic acids.

Example 2 (Separation of Amino Acid Mixture)

Figure 3 illustrates an experiment wherein 800 v. was applied for 180 min. in 1.0 *N* acetic acid during the second phase of separation. In Fig. 3, it will be noted that the basic amino acids have migrated completely off the paper into the cathode compartment. The monoaminomonocarboxylic acids (except valine, leucine, and isoleucine) methionine and threonine and phenylalanine and tyrosine are completely separated as distinct zones.

Example 3 (Separation of Casein Hydrolyzate)

Figure 4 illustrates a similar experiment carried out under the conditions indicated, for a pancreatic casein hydrolysate. It will be seen that the type of separation effected is exactly analogous to that which occurs



FIG. 4. Separation of casein hydrolyzate (example 3).

with known amino acid mixtures. Inspection indicated that there existed a definite correlation between the intensity and size of the amino acid zones with the known quantitative amino acid composition of casein. In Fig. 4, it will be noted that four zones (indicated with a question mark) exist which do not correspond to any of the 19 amino acids investigated; these presumably are due to peptides or other amino acids. One other point deserves mention. Under the conditions described, apparently all the amino acids, with the exception of tryptophan, are stable. However, some of the tryptophan has been observed to react, apparently during one of the periods of heating in the oven. This portion of tryptophan which has reacted or is otherwise bound to the filter paper is indicated as "tryptophan derivative," whereas the excess of tryptophan which does not react

is found between the proline and the valine-isoleucine-leucine zones. Fortunately, this instability does not appear to interfere with the identification of other amino acids.

In the previously described separations, the first electrolyte used was volatile and, therefore, eliminated prior to the second stage of the separation. In our experience, however, when the first electrolyte utilized was not volatile, it was impossible to obtain clean-cut separation of the amino acids in experiments of ordinary duration. Presumably, this was due to the fact that residual (nonvolatile) electrolyte which remained on the paper during the second phase of separation interfered. It was demonstrated, however, that if a run was continued sufficiently long, satisfactory

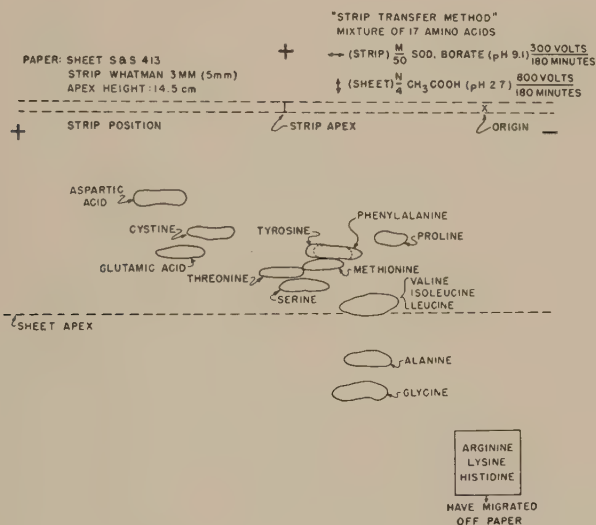


FIG. 5. Separation of amino acid mixture by "strip transfer method" (example 4).

separation could be effected in some cases where a nonvolatile electrolyte or buffer system was employed in the first phase—the extra time required being presumably utilized to "clear" the paper of the salts of the background electrolyte before separation could proceed in accordance with desired second-stage conditions. If the first separation is carried out with a nonvolatile buffer system, it is preferable to carry out the first separation on a narrow strip of paper and then transfer the narrow strip to an appropriate position on a sheet for the second stage.

In this "strip transfer method," difficulties due to the entire sheet's containing the residual nonvolatile electrolyte are avoided inasmuch as conditions usually can be chosen so that the residual ions of the first buffer

system then migrate as a continuous band either in front of or behind the other substances being separated and do not interfere appreciably with pH, ionic strength, and other conditions which it may be desired to control.

There is ordinarily no reason to dry the strip between runs; indeed it is much easier to cause a narrow strip to adhere to the sheet by capillary action when both sheet and strip are moist. However, it is possible to transfer a dry strip to a moist sheet and both types of transfer have been successfully employed.

Example 4 ("Strip Transfer Method")

Figure 5 illustrates an experimental separation carried out according to this process. In this experiment, the strip was applied to the sheet as is shown in Fig. 1b.

Example 5 (Combined Chromatography and Ionophoresis)

It is evident that when separations are performed in this manner it is very easy to combine conventional unidimensional chromatography as the first phase of the separation with paper ionophoresis as the second phase of the separation. In special cases, this is a useful method of procedure. (For example, a more complete separation between methionine and

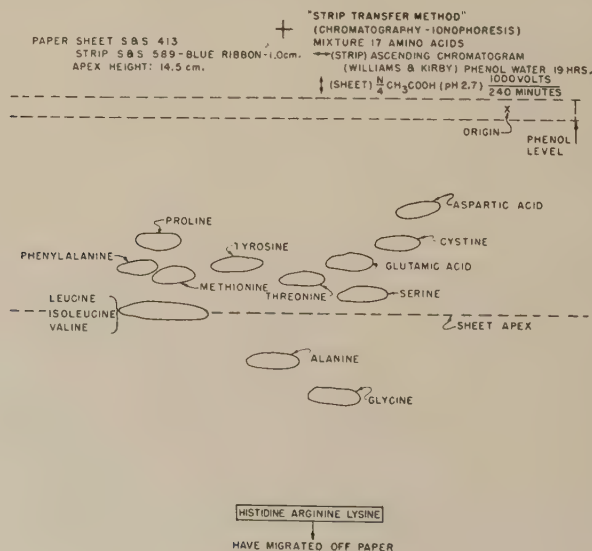


FIG. 6. Separation of amino acid mixture by chromatography and ionophoresis (example 5).

threonine is attained than in the examples described above.) In this method of operation, we have found it convenient first to run a chromatogram on a relatively narrow strip of paper, for example, according to the method of Williams and Kirby (4), and then apply the strip to a wide sheet of paper which has been saturated with appropriate electrolyte and drained causing the chromatogram to adhere by capillarity, as is illustrated in Fig. 1b. Figure 6 illustrates the results of such an experiment wherein the chromatogram was developed in water-saturated phenol.

During the course of the present investigation, the question arose as to whether or not the serum proteins in blood fractions would interfere with the separation of amino acids under the experimental conditions ordinarily used since it might be expected, at the pH values employed, that some of the serum proteins would have mobilities comparable to the mobilities of the various amino acids. Early experiments showed that ordinarily a volume of human serum of the order of 0.01 ml. does not contain sufficient amounts of amino acids to be readily detectable by the ninhydrin procedure. It is evident, therefore, that the determination of amino acids in blood derivatives would ordinarily require their concentration. In this connection, it seemed desirable to determine whether or not it would be necessary to deproteinize serum or other biological fluids prior to applying the present process. To answer this question, experiments were performed in which known amino acid mixtures were added to serum or plasma samples and the resulting patterns compared with patterns from control experiments in which only the amino acid mixture was separated.

The resulting protein-amino acid and amino acid (control) sheets were sprayed with ninhydrin in the usual manner. This procedure permitted localization of the amino acid zones (ninhydrin under the condition used gives only faint colors with proteins). Under these conditions, the basic patterns of the zones in both the protein-amino acid and amino acid control experiments were essentially the same. The amino acid zones thus having been located, the position of the superimposed protein pattern was established by dyeing with bromophenol blue⁵ as described in previous reports (1,2) which gave rise to the protein patterns (which it is believed merit separate discussion).

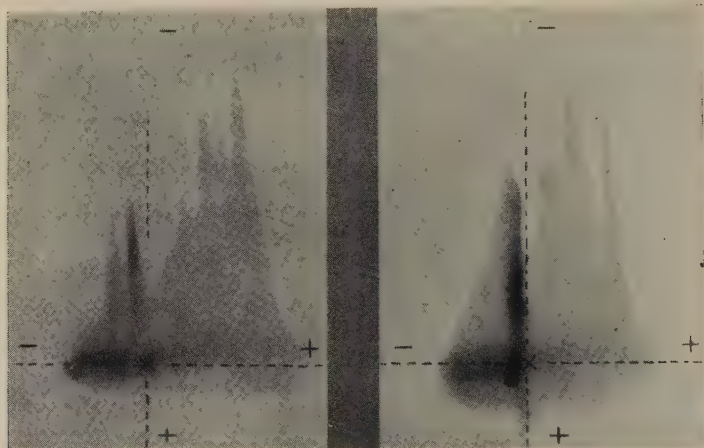
The foregoing experiments with mixtures containing 17 amino acids showed that in the case of separations carried out in 0.2 *N* ammonium hydroxide followed by 0.25 *N* acetic acid, the serum protein mobilities (or mobilities of derived substances, see footnote 6) are such that they partially overlap the amino acid zones. Aspartic acid, cystine, glutamic

⁵ We presently use 0.01% bromophenol blue in aqueous solution, 5% in each mercuric chloride and glacial acetic acid for 60 min. followed by washing in running tap water from 3-5 min. (for thin papers such as Whatman No. 2).

acid, serine, threonine, tyrosine, glycine, arginine, lysine, and histidine fall outside the protein zone. On the other hand, proline, phenylalanine, methionine, leucine, isoleucine, valine, and alanine fall entirely or partially within the zone encompassed by the pattern produced by the serum protein constituents.

Example 6 (Serum Protein Patterns)

Figure 7 illustrates two typical protein zone patterns obtained when different human sera were subjected to conditions described above (in



Human Sera
 $\leftrightarrow \frac{N}{5} \text{NH}_4\text{OH}$ (pH 11.3) $\frac{500 \text{ volts}}{90 \text{ minutes}}$
 Air Dried
 $\updownarrow \frac{N}{4} \text{CH}_3\text{COOH}$ (pH 2.3) $\frac{265 \text{ volts}}{180 \text{ minutes}}$
 Paper: Whatman No. 2
 Apex Height 14.5 cm.

FIG. 7. Two-dimensional human serum patterns (see text) (example 6).

this case in the absence of added amino acids). These patterns appear to be reproducible and are quite characteristic for a given serum. Reproducibility of the protein zones, however, does depend upon very careful attention to details of the process particularly with respect to the duration and degree of drying between the first and second phases of the operation. It has been observed that the form of these patterns was quite different on successive days for the same serum sample when marked changes in humidity occurred. The importance of the conditions of drying suggest that surface denaturation phenomena may be involved in their produc-

tion. It is hoped that further study will permit them to be correlated with various blood protein changes, and conceivably they may prove to be of some use clinically as a diagnostic tool. However, it is to be emphasized that they are purely empirical and the proteins of course receive drastic treatment in the course of their development under these particular experimental conditions which would be expected to result in secondary changes.⁶

The foregoing considerations led to investigations of two-dimensional separations of serum proteins under conditions such that alteration of the proteins would not be anticipated during separation. Two-dimensional separations of serum proteins were effected at low temperature. The initial phases were carried out in acetate buffers at pH 5–5.6 followed by shifting the axis of the paper sheet without drying and followed by the second phase of separation at pH 8.6 in barbiturate buffers. As was expected, the difficulties discussed above in relation to clearing background electrolyte from the paper were encountered. Nevertheless, distinct zone separations were achieved but as might have been predicted from pH–mobility curves for serum proteins the individual protein constituent zones were distributed along a fairly straight diagonal line—presumably in the same relative order as occurs in unidimensional separations within this pH range. The applicability of two-dimensional separations to other protein mixtures and within other pH ranges appears promising and is being investigated further.

During the course of development of the present technique, further insight into the underlying mechanisms of the basic unidimensional process has been attained. The following two examples are cited to illustrate certain phenomena that have been observed and are discussed fully in the following section.

Example 7 (Mobility Equilibrium Illustrated by Serial Strips)

This experiment was carried out by arranging ten 2-cm. strips of filter paper (S. & S. No. 413) in the apparatus illustrated in Fig. 1c. The cell was charged with 1 l. of 0.25 *N* acetic acid. On each strip, a test mixture comprising a few micrograms of a mixture of equimolecular proportions of arginine, glycine, alanine, valine, serine, threonine, phenylalanine, proline, and aspartic acid was applied at a point 5 cm. from the apex, toward the anode side of each strip. A potential of 1000 v. was applied across the

⁶ That the drastic conditions of pH and drying here used for amino acid separations may cause secondary reactions in proteins was illustrated when a single pure protein, crystalline zinc insulin (26.5 units/mg.), was subjected to the same conditions described in Fig. 7. In this case, a multizoned pattern was obtained which probably represents breakdown products of insulin. This subject is under further investigation; also, G. Perlmann and D. Kaufman (5) have reported that serum is denatured in the presence of acetic acid at pH values below 4.

electrodes. The strips were removed at intervals and then were sprayed with ninhydrin to develop color in the usual manner. The pH of electrolyte in the anode compartment at the end of 240 min. was 2.62, and in the cathode compartment 2.67. At the end of the experiment (1410 min.) the pH in the anode compartment was 2.62 while that in the cathode compartment was 2.67. The pH at the beginning of the experiment was 2.64 in both electrolyte compartments. When the strips were mounted side by side to facilitate comparison it was observed that all the amino acids had migrated toward the cathode compartment. However, arginine migrated at a very much faster rate than the remaining amino acids and at the end of 90 min. had already migrated off the paper into the cathode compartment. All the remaining amino acids migrated to positions corresponding to their equilibrium positions which they all had attained at the end of 240 min. These positions were all measured from the point of application to the center of the zone and were: glycine, 91 mm.; alanine,

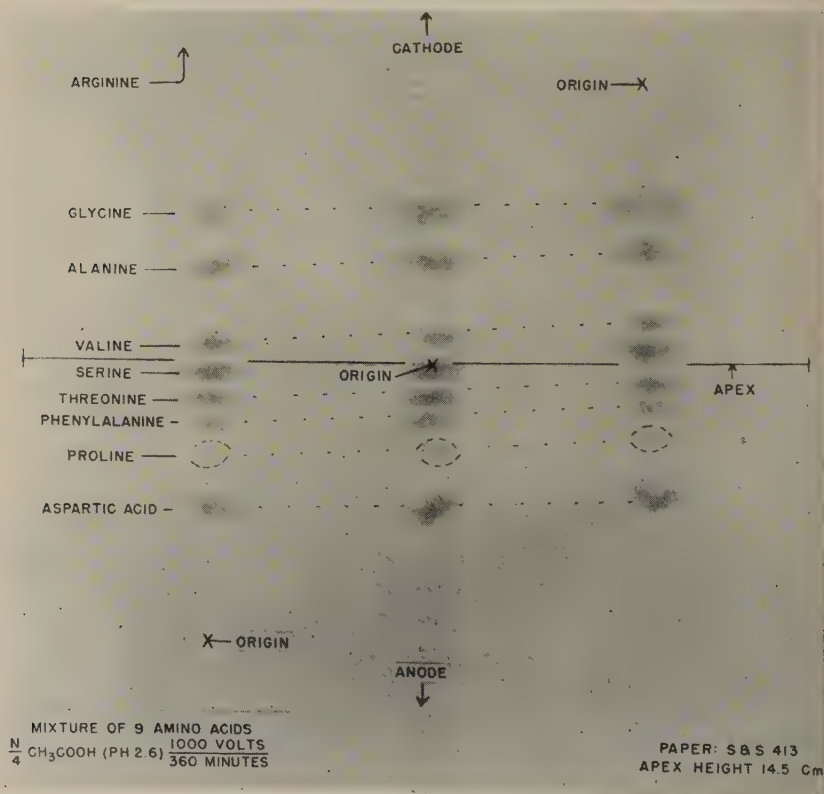


FIG. 8. Mobility equilibrium attained from different points of application (see text) (example 8).

75 mm.; valine, 51 mm.; serine, 48 mm.; threonine, 40 mm.; phenylalanine, 33 mm.; proline, 27 mm.; aspartic acid, 11 mm. The strips removed at 1410 min. showed practically no further progression of any of these substances.

Example 8 (Mobility Equilibrium Attained from Different Points of Application)

A single sheet of S. & S. No. 413 paper was placed in the apparatus of Fig. 1c. The same test mixture used in Example 7 was applied at three different positions on the paper, *viz.*, 10 cm. below the apex on the anode side, at the apex in the center, and laterally on the other side 10 cm. toward the cathode from the apex. After 1,000 v. had been applied for 360 min., the sheet was removed and color developed with ninhydrin. The initial pH was 2.66 in both electrolyte compartments. After 360 min., the anode compartment pH was 2.64 while the cathode compartment pH was 2.71. Figure 8 illustrates results of this experiment. (The position of proline has been indicated in Fig. 8 by dotted lines because it does not show up clearly on the photograph.)

DISCUSSION

In previous reports (1,2) certain theoretical aspects of separation according to the present method were discussed and data presented to show that the rate of migration of certain ions was not a linear function of time. Further experience with this method of separation has shed additional light upon underlying mechanisms which appear to be quite important under certain experimental conditions.

During the course of separations, according to this method, heat is developed in the strip as a consequence of the passage of the electrical current. Under ordinary operating conditions the heat developed may be sufficient to result in gross distillation of electrolyte from the paper. Since the paper is dried by this procedure and thus its state of capillary saturation is decreased, capillary forces continuously "siphon" fresh electrolyte from the electrolyte compartments into the paper. Inasmuch as each succeeding increment of filter paper beyond the electrolyte compartment receives less volume of electrolyte by that amount which has been evaporated in the preceding increment, there results a successive decrease in volume of flow as the center is approached. Since the actual cross section of the paper is constant, a flow rate gradient results in the fluid flow along the length of the filter paper strip from each electrolyte compartment, decreasing as the center of the paper is approached (electroendosmosis augments this flow rate on the anode side of center and diminishes it on the cathode side). Then, in analogy, the ions applied in the center of the paper must "swim" against a current which is constantly increasing in

swiftness as the electrode compartments are approached. Therefore, it might be anticipated that if the mobility of a given ion happened to fall within the range of the extreme values of a given gradient that it would seek a position at which its tendency to flow "upstream" due to its charge in the electric field was exactly balanced by the countercurrent flow of electrolyte toward the center of the paper. Under such conditions, it would be anticipated that the final position of migration would be quite independent of the point of application of such an ion to the paper. Examples 7 and 8 illustrate results of experiments which were performed under these conditions and which support these conclusions. In view of the insignificant pH change which occurred in examples 7 and 8, it is believed that the observed equilibrium migration positions cannot be explained by changes in this factor during the course of the experiment.

Example 8, illustrated in Fig. 8, was designed to attempt to rule out adsorption as an explanation of the observed phenomena. It is believed that the results provide striking evidence in support of the proposed equilibrium mobility hypothesis. It is evident that the amino acids have aligned themselves in almost parallel columns as they approach their mobility equilibrium positions within the gradient ranges on either side of the apex, notwithstanding the fact that their positions of application varied by as much as 20 cm. Arginine, which has a mobility greater than any counterflow of electrolyte from the cathode compartment, under these experimental conditions migrated off the paper. The individual amino acids were identified and their correspondence in the different columns established by their distinctive colors and spacing. (Thus, phenylalanine gives a characteristic slate-blue color, and proline, a yellow color as compared to the mauve of the other amino acids under the conditions used.)

In the experiments described above, the electrolyte was volatile. In separations where nonvolatile buffer materials are employed (e.g., serum protein separations in barbiturate or phosphate buffers), an added complication which augments the above effect has been noted. This is apparently due to the fact that the electrolyte concentration is constantly being increased on the paper strip as the water evaporates. Thus, the protein anions not only migrate against a stream of increasing swiftness but into a stream which is progressively increasing in ionic strength as the electrolyte compartment is approached. This of course is an independent mechanism reducing mobility.

The tendency for serum protein constituents to reach a temporary equilibrium position has been striking even when distillation from the strip has been held to a minimum by permitting only very low currents to flow. Undoubtedly, under these conditions, the added slowing effect resulting in mobility equilibrium, was due to migration into zones of increasing ionic strength gradient. Experiments with serum proteins, par-

ticularly in barbiturate buffers at pH 8.6, have shown that the equilibrium positions do not remain indefinitely fixed but the condition of equilibrium is apparently eventually destroyed as a result of buffer salts reaching certain concentrations with perhaps actual precipitation of buffer constituents with consequent shifts in pH value.

It may be imagined that after a given ion has migrated to its position of equilibrium and if a steady state is maintained that the only process tending to move it is diffusion. Then, if an ion happened to diffuse to a position on one side of the equilibrium line it would be driven back by the electrolyte flow, and if it happened to diffuse on the other side, would be pulled back by its migration tendency due to its charge in the electric field. No such "restoring forces" against diffusion would exist with respect to lateral diffusion. And, indeed, in cases where experiments of long duration have been carried out on wide sheets of paper, lateral elongation of the mobility equilibrium zones is quite pronounced. Of course, when narrow strips of paper are employed lateral diffusion is limited, and there result remarkably uniform rectangular equilibrium mobility zones if the experiments are permitted to run for long periods and conditions of temperature and applied potential are maintained constant.⁷

The foregoing discussion applying to the phenomenon of mobility equilibrium is of primary importance in the consideration of experiments of long duration under conditions favorable for its development (e.g., relatively high current flow with volatile electrolyte systems). It is obvious that either unidimensional or two-dimensional separations may be effected also under conditions where this phenomenon does not play an important role (e.g., in experiments of short duration where the ions being separated have sufficient differences in mobility so that the desired separation can be obtained before an ion reaches a position of mobility equilibrium). This could occur theoretically either in the case where the experimental conditions afforded a mobility gradient of very gentle slope or wherein the mobility of an ion under consideration fell outside the total gradient range.

The above considerations suggest practical modifications of the method to improve resolution, e.g., operation at lower temperature might be expected to give sharper zones at equilibrium. Experiments have been performed in which the cell was maintained at low temperature which confirm this.

⁷ It has recently been reported by H. J. McDonald *et al.* (6) that valid mobility measurements can be made in paper-electrolyte systems similar in essential details to those described herein. Experiments performed in this laboratory failed to confirm their results. The above considerations suggest some of the reasons why this system is not suitable for measuring true mobilities unless further experimental modifications are made to prevent evaporation from the paper and thus eliminate the condition giving rise to the mobility equilibria described. It is also necessary to take into account adsorption and electroendosmosis in any system wherein ionic mobilities are measured on paper. For further discussion of these factors see Ref. (7).

Perhaps a more promising approach is to attempt to make the mobility equilibrium gradient cover a wider range. Thus, it has been found that increasing the apical angle, which may be carried out in specially designed wider and flatter cells, somewhat improves resolution, although other practical considerations such as convenience in handling and drying multiple racks has made the employment of cells with racks of steeper angles preferable. Reducing the applied electrical field with reduced current likewise improves resolution. However, the equilibrium is achieved much more slowly than under the operating conditions cited and, therefore, a compromise situation has been chosen which favors less time-consuming experimental conditions.

Undoubtedly, better operating conditions will be evolved with more experience and attention to the above considerations. However, it should be emphasized that the experimental conditions reported herein are of practical utility in the separations of even quite complex mixtures.

ACKNOWLEDGMENTS

The author wishes to acknowledge the valuable technical assistance contributed by Miss N. L. Puckett and Mr. R. L. DeArmond.

REFERENCES

1. DURRUM, E. L., U. S. Army Medical Dept. Field Research Lab. Report, Project 6-64-12-06-(18) March 15, 1949.
2. DURRUM, E. L., *J. Am. Chem. Soc.* **72**, 2943 (1950).
3. CONSDEN, R., GORDON, A. H., AND MARTIN, A. J. P., *Biochem. J.* **38**, 225 (1944).
4. WILLIAMS, R. J., AND KIRBY, H., *Science* **107**, 481 (1948).
5. PERLMANN, G., AND KAUFMAN, D., *J. Biol. Chem.* **179**, 133 (1949).
6. McDONALD, H. J., URBIN, M. C., AND WILLIAMSON, M. B., *Science*, **112**, 227 (1950).
7. DURRUM, E. L., *Science* **113**, 66 (1951).

BOOK REVIEWS

Colloid Science. By JAMES W. MCBAIN. D. C. Heath and Company, Boston, 1950. 450 pp. Price \$6.00.

Colloid Science is such a vast field that even a book of 450 pages can only give a general and in certain respects sketchy accounts of facts, ideas, and applications. In a situation like this, the merit and value of a book depend entirely on careful selection and proper balance. Nobody could have brought with him more experience, knowledge, and authority to place and distribute emphasis than Professor McBain, one of the few founders of Colloid Science who is still active in this field.

The Table of Contents lists 27 chapters starting with the description of general phenomena such as emulsions, foams, sorption, etc., progressing to methods of investigation, such as osmotic pressure, ultracentrifuge, viscosity, x-rays, etc., and ending up with the discussion of specific systems such as cellulose and derivatives, rubbers, proteins, and synthetic macromolecules.

The presentation is lively, full of interesting personal remarks and animated by critical sidelights; it blends in a fascinating manner the description of facts and ideas with the names of their originators, most of whom are either colleagues or pupils of the author; it is an account of the present state of colloid science congenially interwoven with a history of its development. Many well-drawn figures help elucidate experimental devices and structural features. Each chapter is concluded by a carefully selected bibliography which assists the interested reader to penetrate into the original literature. Some reviewers will probably not be entirely satisfied with certain passages, such as the rather brief treatment of light-scattering by aerosols on p. 416. A reference to pp. 92-95 might have been in place, where the newer development is adequately and lucidly described. It might also be worthwhile to complete the information given at the bottom of p. 141 by adding that the discussions at the annual meetings of the Society of Rheology are now generally printed in the *Journal of Colloid Science*, of which Professor McBain is himself an editor. These, and other minor inconsistencies and roughnesses weigh nothing against the wide scope of the book, the wealth of information which it contains, and the stimulation which it offers to the reader. Anybody interested in Colloid Science will study it with great profit and pleasure.

H. MARK, Brooklyn, N. Y.

Fluorine Chemistry, Vol. I. Edited by J. H. SIMONS. Academic Press Inc., New York, 1950. xvii + 615 pp. Price \$13.50.

The chapters and their authors are as follows: Foreword, J. H. Simons; Nonvolatile Inorganic Fluorides, H. J. Emeléus; Volatile Inorganic Fluorides, A. B. Burg; The Chemistry of the Fluoro Acids of Fourth, Fifth, and Sixth Group Elements, Willy Lange; The Halogen Fluorides, H. S. Booth; Boron Trifluoride, H. S. Booth and Donald Ray Martin; Hydrogen Fluoride, J. H. Simons; Hydrogen Fluoride Catalysis, J. H. Simons; Preparation of Fluorine, George H. Cady; Physical Properties of Fluorine, George H. Cady; The Theoretical Aspects of Fluorine Chemistry, George Glockler; The Action of Elementary Fluorine upon Organic Compounds, Lucius A. Bigelow; Fluorocarbons and Their Production, J. H. Simons; Fluorocarbons—Their Properties and Wartime Development, T. J. Brice; Fluorocarbon Derivatives, W. H. Pearlson; Aliphatic Chlorofluoro

Compounds, Joseph D. Park; Fluorine Compounds in Glass Technology and Ceramics, W. A. Weyl.

As Dr. Simons has truly stated in his foreword: "The past thirty years have witnessed a tremendous increase in fluorine chemistry both in knowledge and in interest. The field has grown to such a size that no one individual can be considered pre-eminent in all divisions of the subject. For this reason this book has been written by a group of authors each one dealing with that branch of the subject in which he has special knowledge or has made significant contributions. It is extremely fortunate that so many individuals are still available whose scientific activities have contributed to this rapid growth of the subject.

"Two previous books on fluorine chemistry were written by men who at their time were the leading authorities on the entire subject. The first by Henri Moissan dealt mainly with the author's discoveries, and the second by Otto Ruff contained chiefly the advances made to the subject by the author and his collaborators."

The contributors to this work have been themselves responsible for the major part of the rapid progress in fluorine chemistry made during recent years, and they have presented the present state of knowledge in a style and clarity that invites nothing but praise. It would be captious indeed for a reviewer to hunt for minor points of disagreement in a subject still in the making, and in a book so remarkably good. The moderate amount of duplication resulting from multiple authorship is all to the good in offering more than one point of view regarding unsettled questions.

The chemistry of fluorine cuts across the realms of organic, inorganic, and physical chemistry, and any chemist, even a colloid chemist, no matter how he classifies himself, should be able to find in the book much to stimulate his thinking as well as many suggestions for research.

Dr. Simons deserves the gratitude of all chemists for his conception of this work, for assembling so able a group of contributors, and for working together with the publisher, to produce a book so well arranged and printed.

JOEL H. HILDEBRAND, Berkeley, California

CONTRIBUTION TO THE DISCUSSION ON THE SHAPE OF THE POLYSTYRENE MOLECULE IN DILUTE SOLUTIONS BY MEANS OF FLOW BIREFRINGENCE MEASUREMENTS

Roger Cerf ¹

Department of Chemistry, Cornell University, Ithaca, New York

Received June 4, 1951

ABSTRACT

It is usually assumed that a chain molecule like polystyrene in dilute solutions is bent, and the question as to whether it is more or less rolled together has been put forward some time ago. Flow birefringence studies should be a fruitful approach to this question, but the theory of the Maxwell effect for chain molecules is very unsatisfactory.

The author has recently developed the theory of the Maxwell effect for a solution of elastic impenetrable spheres. This model represents a limiting case like the model of a rigid sphere used successfully by Sadron and by Flory in the interpretation of viscosity measurements. The model could be a reasonable first approximation for flexible chain molecules, inasmuch as Debye and Bueche, as well as Kirkwood and Riseman find the impenetrable sphere as a limiting case in their more general theory of viscosity.

The theory of the elastic sphere leads to some conclusions which are in agreement with experiments on the temperature dependence of the extinction angle at low gradients carried out with two samples of polystyrene. These results constitute a strong argument in favor of the model of a rather compact sphere for the polystyrene molecule. Also, the observed effect is completely different from the orientational effect characteristic of rigid molecules like tobacco mosaic virus; for polystyrene the origin of the phenomenon seems to be much more a deformation of an initially isotropic particle rather than an orientation of an elongated molecule.

The results are on the other hand in disagreement with the theory of W. Kuhn and H. Kuhn based on a dumbbell model.

In this short paper the author will summarize the results and put the emphasis on the possibilities of the flow-birefringence technique in the field of flexible chain molecules for the determination of the elasticity and the internal viscosity of these particles. Finally, a general method is suggested in order to check whether a chain molecule in solution is more or less rigid or flexible (extinction angle measurements at low gradients for several solvents with different viscosities).

1. INTRODUCTION

The first studies on streaming double refraction of chain molecules were those of Signer (1, 2, 3) (polystyrene, nitrocellulose). These thorough studies showed that streaming double-refraction measurements should

¹ Fellow of the Rockefeller Foundation, on leave from the "Centre d'Etudes de Physique Macromoléculaire," Strasbourg, France. This paper is to be presented at the International Chemical Conclave New York, September, 1951. It essentially summarizes a study done at Strasbourg.

provide a fruitful method for investigating the shape of long-chain molecules in solution.

It had already been suggested at that time that long-chain molecules should exhibit in dilute solutions the shape of more or less sphere-like clusters, not quite extended and stiff, but also not entirely rolled together.

Let us briefly recall that in the concentric cylinder apparatus the solution is subjected to a two-dimensional flow with constant shear gradient G , the direction oz of the light beam being perpendicular to the plane of flow xoy (Fig. 1).

The optical properties of the flowing solution, i.e., the behavior of the neutral lines (fast and slow axes of the birefringent medium in the plane xoy), as well as that of the magnitude of the birefringence Δn with respect

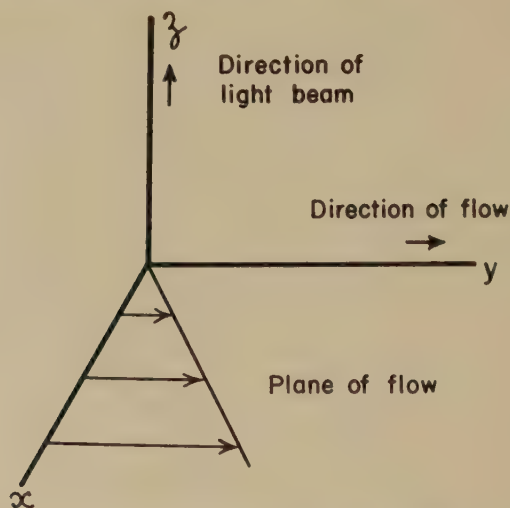


Fig. 1. Velocity field in concentric cylinder apparatus.

to the velocity gradient G give valuable information about the degree of elongation and rigidity of the molecule. In some cases [nitrocelluloses of high molecular weight, $M \sim 10^6$, Signer and Gross (2), Snellman (4)], the curve giving the birefringence as a function of the velocity gradient shows a saturation effect for high values of G . This behavior is similar to that of a rigid particle (orientational effect), and it seems likely that the chain molecule, although being not quite stiff, is rather elongated.

On the other hand, nitrocelluloses of lower molecular weight (2, 4) and polystyrene of intermediate molecular weight ($M \sim 3 \times 10^5$) show a linear dependance of Δn with respect to the velocity gradient G .

For polystyrene of high molecular weight ($M \sim 6 \times 10^5$) and for polyisobutylene [Tsvetkov and Petrova (5), Tsvetkov and Frisman

(6)], the increase of Δn with respect to G becomes even greater than linear; this is evidence for a deformation of the molecule.

The comparison between the behavior of the extinction angle χ characterizing the position of neutral lines and that of the magnitude of the birefringence is in that case particularly instructive. Figure 2 shows

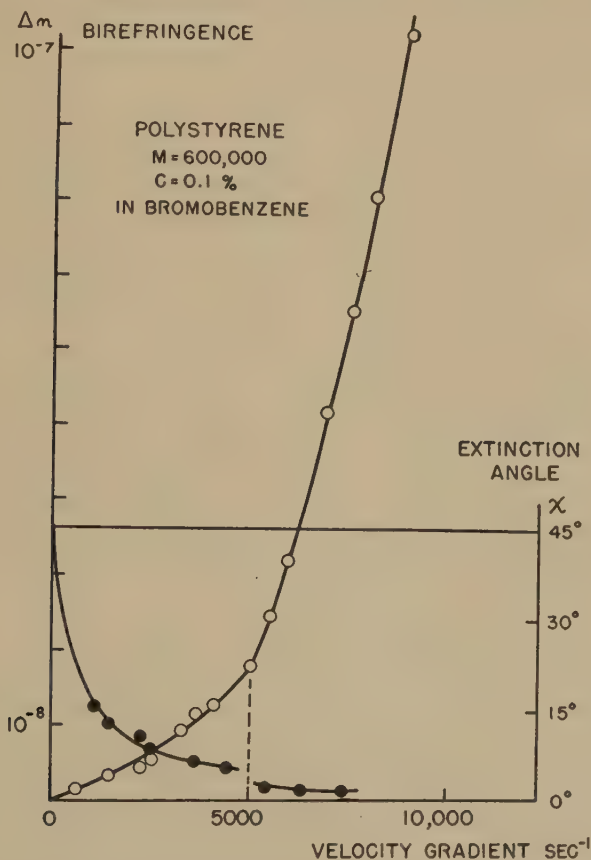


FIG. 2. Polystyrene, $M = 6 \times 10^5$ in bromobenzene. The discontinuities correspond to the appearance of turbulence. For turbulent flow the velocity gradient is no longer constant in the solution. The given G values are derived from the speed of the rotating cylinder using the formula which is valid for laminar flow.

the curves giving Δn and χ as a function of G that we have obtained for a 0.1% solution of polystyrene, $M = 6 \times 10^5$, in bromobenzene, prepared at the laboratory of Professor Signer.

It is to be seen that for velocity gradients higher than 5000 sec^{-1} the extinction angle is almost 0° and the magnitude of the birefringence still increases. Thus the behavior of these chain molecules seems to be quite

like the behavior of a liquid drop subjected to a shear gradient [see G. I. Taylor (7)]. The drop, initially spherical, takes the form of an ellipsoid. For high velocity gradients the major axis of the ellipsoid becomes almost parallel to the direction of flow, and its length still increases when the velocity gradient increases. Thus the Maxwell effect for polystyrene of high molecular weight at high velocity gradients seems to be a deformation effect. A similar behavior of Δn and χ with respect to G has been described for polyisobutylene by Tsvetkov and Petrova (5).

For the following theoretical discussion we shall restrict ourselves to small velocity gradients.

The hydrodynamical problems which arise in the theory of the Maxwell effect are very similar to those which arise in the theory of viscosity of solutions of macromolecules. The question of the choice of a proper model for the chain molecule is here particularly important as the whole interpretation of the phenomenon is changed if one changes the model.

In the theory of viscosity two limiting cases have first been treated. The case of free draining [W. Kuhn and H. Kuhn (8, 9, 10), J. J. Hermans (11), H. A. Kramers (12), P. Debye (13)] and the case of complete impermeability [Sadron (14)]. More recently, Brinkman (15), Debye and Bueche (16), as well as Kirkwood and Riseman (17) treated the intermediate and more likely case of partial draining. It is to be pointed out that for very high molecular weights these authors also obtain in the limit a total impermeability. According to Flory and Fox (29) the limiting case should already be reached for molecular weights as low as 50,000 [see also earlier papers of Flory (30)].

The theory of streaming double refraction exhibits more difficulties than the theory of viscosity because of the fact that the deformation of the particle has to be taken into account whereas for the theory of viscosity one can suppose the particle not to be deformed.

W. Kuhn and H. Kuhn (8, 9, 10) developed the theory of streaming double refraction on the basis of the same model they used for the calculation of the viscosity of a solution of macromolecules, that is to say the dumbbell model. In W. Kuhn and H. Kuhn's treatment the initial birefringence for small velocity gradients appears to be an orientational effect like the well-known effect for rigid particles. The crude approximations involved in this theory have been pointed out by J. J. Hermans (18) and by O. Snellman (4). Moreover, this theory is contradicted by the experiments reported below.²

The author has developed the theory of the elastic sphere model (19) in the field of low velocity gradients. This model has been chosen pro-

² As H. A. Kramers does not calculate the extinction angle in Ref. (12) his theory will not be discussed at this place. See Ref. (21).

visionally in view of the huge difficulties that a complete theory would encounter. It represents the limiting case of total impermeability and should constitute a first approximation for a future, more satisfactory theory of flow birefringence for chain molecules.

As has been shown in Ref. (19), the effect exhibited by a solution of elastic spheres is a deformation effect of a completely different nature than the orientational effect for rigid particles or the effect considered by W. Kuhn and H. Kuhn which for small velocity gradients is like an orientational effect.

Thus if it is possible for a given system to show that the effect is mainly a deformation effect, like the elastic sphere effect, strong evidence will be obtained that the studied molecule has roughly a spherical shape, and is rather compact. If alternatively the solution shows a characteristic orientational effect the dissolved molecule will probably be almost extended and rigid.

In the next paragraph we shall briefly indicate those results of the theory of the elastic sphere which will be useful for our present purpose. They only concern the position of neutral lines; this is directly related to the mechanical properties of the molecule. The results concerning the magnitude of the birefringence will not be referred to here. The next paragraph will then summarize some experimental results we have obtained on polystyrene [see Refs. (20) and (21)] together with the conclusions which can be drawn.

2. SOME RESULTS OF THE THEORY OF THE ELASTIC SPHERE (EXTINCTION ANGLE)

The elastic sphere is supposed to be homogeneous and isotropic, limited by a continuous surface, and the external liquid is also supposed to be a continuous medium.

The two physical coefficients which have to be considered in order to characterize the properties of the sphere are the Lamé elasticity coefficient μ and a quantity already introduced by Haller (22) in his qualitative treatment, the internal viscosity η_i .³

The behavior of a macroscopic elastic sphere in the hydrodynamic field is quite like the behavior of a liquid drop, the latter having been studied by G. I. Taylor (7). The sphere is deformed into an ellipsoid whose section by the plane of flow (Fig. 1) is an ellipse as shown in Fig. 3.

For small velocity gradients the axes of the ellipse make an angle of 45° with respect to the direction of flow. (The corresponding position of the major axis is marked *X* on Fig. 3.) The external contour of the particle

³ An internal viscosity has also been introduced by W. Kuhn and H. Kuhn (8, 9, 10). The internal viscosity considered here differs from that of Kuhn and is defined as the viscosity of a continuous medium.

has a definite form while the matter inside the drop is rotating. For higher values of the velocity gradient the major axis of the ellipse, now marked X' , makes an angle

$$\chi = \frac{\pi}{4} - \delta\varphi$$

with respect to the direction of flow.

The calculation of the departure $\delta\varphi$ requires the knowledge of the terms of second order with respect to G in the stress tensor within the

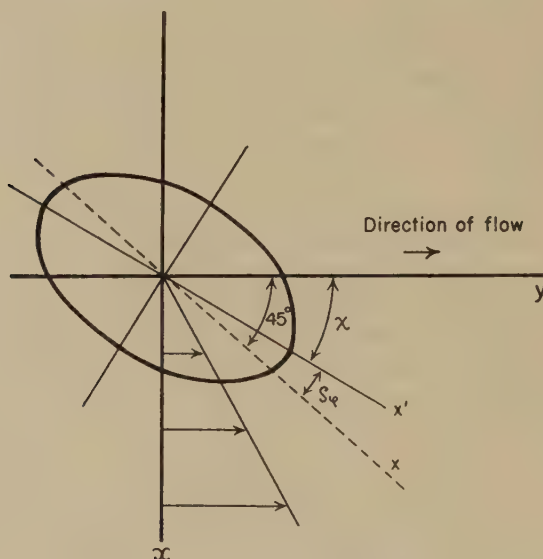


FIG. 3. The deformed particle.

sphere. The result is:

$$\delta\varphi = \frac{1.25}{\mu} (\eta_0 + 0.4 \eta_i) G \quad [1]$$

where μ and η_i have been defined above; η_0 is the viscosity of the surrounding medium.

Equation [1] holds for an infinitely dilute solution, and so far we have considered a macroscopic particle.

The effect of Brownian motion is here completely different from its effect upon the motion of a rigid particle. Without going into any detail, we shall say shortly that for an elastic sphere whose radius is of the order of magnitude of 300 Å. the effect of Brownian motion can be neglected as a first approximation.

Thus the position of the optical preferential axes of the solution or neutral lines is given simply by Eq. [1]. Hence, the initial slope $\tan\alpha$ of

the curve giving χ as a function of G is for an infinitely dilute solution ($c = 0$):

$$(\tan\alpha)_{c=0} = \frac{1.25}{\mu} (\eta_0 + 0.4 \eta_i) \quad [2]$$

The corresponding quantity for a solution of rigid ellipsoids is given by the equation of Peterlin and Stuart (23)

$$(\tan\alpha)_{c=0} = \frac{1}{12D} \quad [3]$$

where D is the rotatory diffusion constant. Since D is inversely proportional to the viscosity η_0 of the solvent, Eq. [3] can also be written

$$(\tan\alpha)_{c=0} = A\eta_0 \quad [4]$$

where the factor A depends only on the temperature and on geometrical

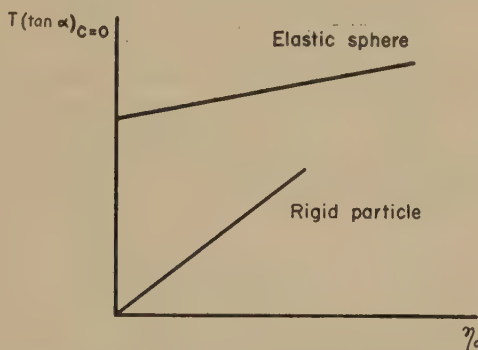


FIG. 4. Theoretical behavior of the extinction angle for an elastic sphere and a rigid particle.

quantities. Thus the quantity $(\tan\alpha)_{c=0}$ shows quite a different behavior with respect to η_0 for a solution of elastic spheres than for a solution of rigid ellipsoids.

For a solution of rigid particles the curve giving $(\tan\alpha)_{c=0}$ as a function of η_0 is a straight line going through the origin (Fig. 4).

For a solution of elastic spheres the curve is also a straight line but the intercept is different from zero. It should be noted that for Kuhn's model, as in the case of a rigid particle, the curve also goes through the origin. It should be pointed out further that while the molecular phenomena are completely different for the two types of molecules the only observable difference between a solution of rigid ellipsoids and a solution of elastic spheres is the one which we just mentioned. The behavior of the magnitude of the birefringence, at least in the field of small velocity gradients, would not show any difference for the two solutions.

Consequently, the experiments which have to be carried out in order to decide whether a given sample is a crumpled coil or a rather rigid and elongated particle are the measurements of $(\tan\alpha)_{c=0}$ as a function of η_0 . Such experiments are difficult to make, the magnitude of the birefringence for chain molecules usually being very small; the determination of the extrapolated quantity $(\tan\alpha)_{c=0}$ therefore requires very accurate measurements [see Refs. (21) and (24)].

It has been found convenient to study the temperature dependence of $(\tan\alpha)_{c=0}$ in order to vary the viscosity η_0 .

The theory of Brownian deformation of the elastic sphere (19) leads to the following formula relating the elasticity coefficient μ to the fluctuation of form of the molecule

$$\mu = \frac{kT}{3v\overline{d_{ii}^2}} \quad [5]$$

where k is Boltzmann's constant, T the absolute temperature, v the volume of the sphere and $\overline{d_{ii}^2}$ the mean square value of the principal deformation of the sphere due to the Brownian deformation. When the model of the elastic sphere is applied to a chain molecule $\overline{d_{ii}^2}$ becomes a quantity which should probably be obtained from the knowledge of the distribution of configurations, although this problem is a difficult one inasmuch as no definition of the quantity d_{ii} exists today for a chain molecule.⁴

However, we can conclude from Eq. [5] that for such molecules for which d_{ii} is a purely geometric quantity, that is to say for chains with free rotation and for chains with steric hindrances and no energetic interactions, μ is proportional to the absolute temperature T . Measurements of the magnitude of the birefringence, which are not reported here, provide an experimental verification of that law. It should be noted that it constitutes for an isolated molecule in solution a law quite analogous to that which is known for some rubberlike materials in the solid state. [See the experiments of Meyer and Ferri (26) and the theoretical work of W. Kuhn (27).]

On the other hand viscosity measurements showed that the intrinsic viscosity of the solutions studied does not vary much in the investigated temperature range. This means that the volume of the particle does not depend very much on the temperature, and we have consequently assumed that the internal viscosity can in a first approximation be taken as a constant.

⁴ Recent investigations in mathematical statistics deal with such problems (25). They only constitute a first approach and no definition for the "mean form" of a coil has yet been obtained.

Equation [2] then becomes

$$T(\tan\alpha)_{c=0} = \frac{1.25T_x}{\mu_x}(\eta_0 + 0.4\eta_i) \quad [6]$$

μ_x being the value of μ for the arbitrary temperature T_x . The factor T_x/μ_x is a constant and the only variable quantity in the right hand member of [6] is η_0 .

Since for a rigid ellipsoid the rotatory diffusion constant is proportional to the absolute temperature, Eq. [3] may be written

$$T(\tan\alpha)_{c=0} = A'\eta_0 \quad [7]$$

where the coefficient A' depends neither on η_0 nor on T . Finally one can see that the quantity $T(\tan\alpha)_{c=0}$ plotted against η_0 shows for a solution of chain molecules and for a solution of rigid ellipsoids a behavior analogous to that represented in Fig. 4 for $(\tan\alpha)_{c=0}$.

3. EXPERIMENTAL RESULTS

Figure 5 shows the quantity $T(\tan\alpha)_{c=0}$ for a sample of polystyrene of average molecular weight, 140,000, in cyclohexanone, together with the corresponding figure for tobacco mosaic virus in suspension in water.

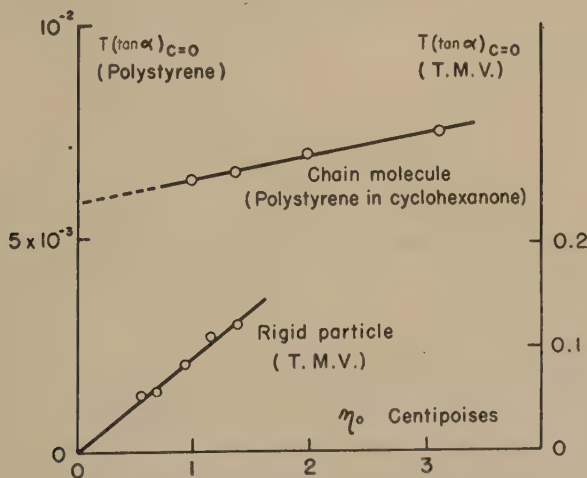


FIG. 5. Behavior of the extinction angle for a chain molecule and a rigid particle.

The former, for which the experiments have been carried out in the temperature range 0–60°C., shows a behavior in agreement with Eq. [6]. It should be noted that similar results have been obtained for a fractionated sample.

The latter, for which the experiments have been carried out in the temperature range 7–50°C., shows a behavior in agreement with Eq. [7].

4. CONCLUSIONS

(a) The preceding results show that it is indeed possible to represent the experimental behavior of polystyrene by means of the two coefficients μ and η_i introduced in the theory of the elastic sphere. This qualitative success seems to indicate that the polystyrene molecule in cyclohexanone is rather crumpled and that the Maxwell effect is indeed rather a deformation effect.

(b) On the other hand the resultant dependence of $T(\tan\alpha)_{c=0}$ on η_0 is not compatible with the theory of W. Kuhn and H. Kuhn where the curve giving $T(\tan\alpha)_{c=0}$ with respect to η_0 goes through the origin and where the slope of that curve can only vary by a factor of three in the whole range of viscosities from zero to infinity. It would however be instructive to carry out measurements in a range of viscosities as large as possible.

(c) If we tentatively assume Eq. [6] to have a semiquantitative value, it is to be seen that streaming double refraction measurements provide a method for evaluating the elasticity constant μ and the internal viscosity η_i , by determining the slope m and the intercept n of the curve giving $T(\tan\alpha)_{c=0}$ with respect to η_0 ; μ_T and η_i are respectively given by the following formulas⁵

$$\begin{cases} \mu_T \sim 1.25 \frac{T}{m} \\ \eta_i \sim 2.5 \frac{n}{m} \end{cases} \quad [8]$$

where μ_T is the value of μ for the temperature T , and where the sign \sim indicates that the preceding equations might only have a semiquantitative value.

For the sample reported here, $\mu \sim 7 \times 10^3$ c.g.s., $\eta_i \sim 0.3$ c.g.s.

The question as to whether formulas [8] have a more or less quantitative value for some types of molecules needs further investigation.

(d) However, even for those molecules for which the elastic sphere model will not be applicable quantitatively, it will be instructive to measure $(\tan\alpha)_{c=0}$ as a function of η_0 since such measurements provide a test for differentiating between a rigid particle and a crumpled coil. The test has the advantage of being independent of an eventual polydispersity of the solution.

⁵ It should be noted that the variation of the viscosity η_0 of the solvent can be obtained by other means than by a variation of temperature.

This method has been recently applied to thymonucleic acids (28). In these experiments the variation of viscosity of the solvent was obtained by using a mixture of salt, water, and glycerol with different concentrations of glycerol.

REFERENCES

1. SIGNER, R. *Z. physik. Chem.* **A150**, 257 (1930).
2. SIGNER, R., AND GROSS, H., *Z. physik. Chem.* **A165**, 161 (1933).
3. SIGNER, R., *Trans. Faraday Soc.* **32**, 296 (1936).
4. SNELLMAN, O., *Acta Chem. Scand.* **1**, 291 (1947).
5. TSVETKOV, V. N., AND PETROVA, A., *J. Tech. Phys. U. S. S. R.* **14**, 289 (1944).
6. TSVETKOV, V. N., AND FRISMAN, E., *Acta Physicochim. U. R. S. S.* **20**, 363 (1945).
7. TAYLOR, G. I., *Proc. Roy. Soc. (London)* **A146**, 501 (1934).
8. KUHN, W., AND KUHN, H., *Helv. Chim. Acta* **26**, 1394 (1943).
9. KUHN, W., AND KUHN, H., *Helv. Chim. Acta* **28**, 1533 (1945).
10. KUHN, W., AND KUHN, H., *Helv. Chim. Acta* **29**, 71 (1946).
11. HERMANS, J. J., *Physica* **10**, 777 (1943).
12. KRAMERS, H. A., *J. Chem. Phys.* **14**, 180 (1946).
13. DEBYE, P., *J. Chem. Phys.* **14**, 636 (1946).
14. SADRON, CH., *J. chim. phys.* **44**, 22 (1947).
15. BRINKMAN, H. C., *Applied Sci. Research* **A1**, 27 (1947).
16. DEBYE, P., AND BUECHE, A. M., *J. Chem. Phys.* **16**, 573 (1948).
17. KIRKWOOD, J. G., AND RISEMAN, J., *J. Chem. Phys.* **16**, 565 (1948).
18. HERMANS, J. J., *Rec. trav. chim.* **63**, 205 (1944).
19. CERF, R., *J. chim. phys.* **48**, 59 (1951).
20. CERF, R., *J. chim. phys.* **47**, 663 (1950).
21. CERF, R., *J. chim. phys.* **48**, 85 (1951).
22. HALLER, W., *Kolloid-Z.* **61**, 26 (1932).
23. PETERLIN, A., AND STUART, H. A., *Z. Physik* **112**, 1 (1939).
24. CERF, R., *Rev. optique* **29**, 200 (1950).
25. FRÉCHET, M., *Ann. inst. Henri Poincaré* **10**, 215 (1948).
26. MEYER, K. H., AND FERRI, C., *Helv. Chim. Acta* **18**, 570 (1935).
27. KUHN, W., *Kolloid-Z.* **76**, 258 (1936).
28. SCHWANDER, H., AND CERF, R., *Helv. Chim. Acta* **34**, 436 (1951).
29. FLORY, P. J., AND FOX, T. G., *J. Am. Chem. Soc.* **73**, 1904 (1951).
30. FLORY, P. J., *J. Chem. Phys.* **17**, 303 (1949).

STUDIES ON ION-EXCHANGE RESINS. III. DIFFUSION OF NEUTRAL MOLECULES IN A SULFONIC ACID CATION-EXCHANGE RESIN ¹

Harry P. Gregor, F. C. Collins and Martin Pope ^{2,3}

Department of Chemistry, Polytechnic Institute of Brooklyn, Brooklyn, New York

Received April 22, 1951

INTRODUCTION

This paper is one of a series on the fundamental structure and properties of ion exchange resins (10, 11). A study was made of the desorption processes of various neutral molecules from a sulfonated polystyrene cation exchange resin. The molecules included: urea; methyl-, ethyl-, and isobutyl acetate; ethyl- and isobutyl alcohol. The resin was in the lithium, sodium, potassium, and tetramethylammonium states. The effect of stirring speed, particle size, neutral molecule concentration, ionic strength, and temperature on the desorption process was studied. Distribution and diffusion coefficients, and energies of activation of the diffusion process were calculated.

Some studies have been made on the sorption of water by high polymeric, polar materials (23) and on the diffusion of neutral molecules into egg cells of marine invertebrates and plants (25). Several papers dealing with the kinetics of the ion exchange process have been published (2, 4, 10, 15). Studies have been made on the use of the cation exchange resin in the hydrogen state as a catalyst (13, 17, 20, 21) in esterification and ester hydrolysis reactions. Reference will be made to some of these articles later.

THEORETICAL DISCUSSION

The equation for diffusion of a substance out of a sphere of radius r_0 into a solution where the concentration of that substance is zero, is

$$\frac{Q}{Q_0} = \frac{6}{\pi^2} \sum_{n=1}^{n=\infty} \frac{1}{n^2} \exp. \left(- \frac{D\pi^2 n^2 t}{r_0^2} \right),$$

where Q and Q_0 are the amounts of diffusate present in the sphere at time t and at $t = 0$, and D is its diffusion coefficient in the sphere (1).

¹ The authors wish to thank the Office of Naval Research for the support rendered to this work.

² Abstracted from the dissertation of Martin Pope, submitted in partial fulfillment of the requirements for the degree of Doctor of Philosophy in Chemistry, Polytechnic Institute of Brooklyn, January, 1951.

³ Present address: Balco Research Laboratories, Newark, N. J.

If $\frac{D\pi^2}{r_0^2}$ be set equal to B , a plot of Q/Q_0 against $(Bt)^{\frac{1}{2}}$ will yield Fig. 1.

In order to obtain a value for B (and hence D), an experimental value of Q/Q_0 for a particular time t is used to obtain the corresponding value of Bt from Fig. 1. The value of D may be calculated using the radius of the particles. As described by Boyd (4), this equation may be written:

$$Q/Q_0 = 1 - 1.08 \sqrt{Bt}.$$

This is sometimes referred to as the parabolic diffusion equation, and is valid for small values of t , large particles, or small diffusion coefficients. This latter equation may be used to obtain a value of Q_0 by extrapolating to $t = 0$ from a plot of Q against $t^{\frac{1}{2}}$, at short desorption times.

Boyd, Adamson and Myers (4) have found that this diffusion equation describes the rate of ion exchange processes in 0.1 N solution, and have

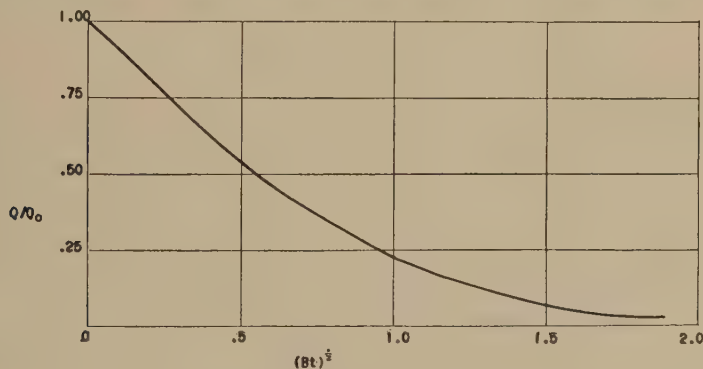


FIG. 1. Theoretical curve for diffusion out of a spherical particle.

detailed methods of calculating D . The applicability of this equation to a rate process is tested by calculating a value of B from each experimental point; a small average deviation in B values indicates that the process is rate controlled, with a constant diffusion coefficient.

EXPERIMENTAL METHODS

A. Preparation and Conditioning of the Resin

All the work described herein was done with a sulfonated polystyrene-divinylbenzene copolymer, available in bead form—Dowex 50 (Dow Chemical Company). Wet screening was employed; only those particles *which were actually lodged in interstices* of 16-mesh and 30-mesh screens were used. In this way, a uniform particle size was obtained. After screening, the resin was air-dried and rolled (3). Conditioning was accomplished by means of three alternate cycles, using 2 M solutions of hydrochloric

acid and sodium hydroxide. Each cycle was of one hour duration with water rinsing between the acid and base treatment. The conversion to each cationic form, determination of moisture content, capacity, and particle radius is described in a paper by Gregor *et al.* (10). The resin had a capacity of 5.20 meq./g. dry hydrogen resin.

Aliquots of resin were used (0.5 g.), the weighed samples being placed in stainless steel wire mesh baskets in which they were kept for the entire series of experiments.

B. Apparatus

In general, there were four steps to each experiment: 1. Equilibration; 2. Desorption; 3. Elution; 4. Analysis. Equilibration is the process whereby a resin sample was brought to equilibrium with a given solution containing neutral molecule and ionic species. Desorption is the process whereby the resin samples were shaken for varying lengths of time in a large volume of solution which was essentially at zero concentration with respect to the particular neutral molecule being studied, and was of the same ionic strength as the equilibrating solution. Elution is the process during which the resin sample was shaken in a known volume of distilled water (50 ml. in most cases) for as long a period as was used in the equilibration. During this process, all the neutral molecule which remained in the resin sample after the desorption process was eluted for analysis. The last step, that of analysis, will be discussed later.

The scheme of the desorption process was as follows: The weighed samples of resin were enclosed in stainless steel wire (60-mesh) baskets, which were held to a device that agitated the baskets with a vertical reciprocating motion in a large volume of water. At appropriate times, each basket was removed in turn from the shaker and dropped into a sample bottle containing a known volume of eluant.

Each desorption experiment was carried out as follows: After the resin was equilibrated in the neutral molecule-salt solution, the baskets were attached to the basket holders, and the latter placed on the vertical shaking device. The basket was kept filled with the equilibrating solution until ready to use. The motor was turned on for a few seconds to shake most of the solution out of the baskets. The motor was then stopped, and the assemblage was lowered into a large vessel containing about 5 liters of desorption solution, containing no neutral molecule. The motor and the stopwatch were then started for the desorption run.

At the end of each predetermined period of time, the basket was removed, shaken twice and placed into the eluting solution. The elapsed time for this step was about two seconds; the residual desorption solution in the basket was negligible.

The desorption experiments were carried out at 43, 25, and 7°C., constant to $\pm 0.1^\circ\text{C}$.

C. Analyses

All solutions were prepared from reagent grade chemicals and laboratory distilled water. All electrolyte concentrations reported are accurate to 1%.

The neutral molecules were determined colorimetrically, using the Klett-Summerson photoelectric colorimeter with appropriate filters. Urea was determined using Nessler's solution. The method of Keenan (14) was used for the esters, with some modifications to suit the dilutions encountered in the eluate. The improved method of Buckles and Thelen (5) was not available at the time this work was carried out. The method of Webb (22) was employed for the alcohol determinations.

All analytical determinations were made in duplicate, with an average deviation of less than 3%. In every case, it was established that the resin itself did not impart to the solutions any color which interfered in the colorimetric determinations.

D. Equilibration with Neutral Molecules

While it is known that ionic equilibrium is reached quite rapidly with these resins, it was necessary to establish the condition of equilibrium between the resin phase and the solution containing the neutral molecule. The general procedure followed was to shake the resin with various solutions for different periods of time, followed by elution of the neutral molecule. When the amount of neutral molecule absorbed was independent of time, it was assumed that equilibrium had been reached.

The minimum volume of solution used for the equilibration was calculated on the basis of the amount of resin being treated. For each gram of wet resin sample, at least 50 ml. of solution was allowed. Since about 40% of the wet weight of the resin was water, a rough estimate of the "free volume" inside the resin would be 0.4 ml. per gram of wet resin sample. Assuming a distribution coefficient near unity, this 50 ml. aliquot represented a 125-fold volume excess over the "free volume" of the resin sample. As an additional check, it was found that the concentration of the equilibrium solution before and after equilibration was the same, within experimental error.

Equilibration in the urea-, ethyl acetate-, and ethyl alcohol-salt solutions was accomplished by overnight shaking. Equilibrium was reached within one hour for urea, as shown in Table I. For ethyl acetate, equilibrium was reached in 4 hours, as shown in Table II. In each case, an experimental equilibration time was used which was substantially longer than the minimum time required. In the case of the tetramethylammonium-form of the resin, a 48-hour equilibration time was employed.

Since the rate of hydrolysis of methyl acetate in solution is relatively high, a 3-hour equilibration time was used. Since the diffusion rate for

methyl acetate is almost double that of ethyl acetate, and a 3-hour equilibration time was shown to be quite adequate for the ethyl acetate, the procedure for methyl acetate is justified. A 48-hour equilibration period was employed in the isobutyl acetate and isobutyl alcohol systems.

The hydrolysis of ethyl acetate in water requires several days to become detectable and 365 days for 95% completion (18). On shaking the

TABLE I
Establishment of Equilibration Time for Resin in Urea Solution
Composition of solution: 0.1 *m* urea; 0.001 *m* NaCl

Equilibration time <i>hours</i>	Elution time <i>hours</i>	Q^* mmoles $\times 10^3$
3.25	18	3.60
6.25	18	3.68
24.31	30	3.68
42.7	45	3.65
114.8	120	3.65
138.9	140	3.60

* Q is millimoles of neutral molecule per gram of dry hydrogen resin.

lithium resin (without the basket) with a 2×10^{-3} *m* ethyl acetate solution for 6 days at room temperature, it was found that the ester concentration had decreased 4.6%. At this rate, 95% of the ester would be hydrolyzed in 339 days. Agreement with the literature value is satisfactory. The catalytic effect of the resin in the salt state was therefore negligible.

TABLE II
Establishment of Equilibration Time for Sodium Resin in Ethyl Acetate Solution
Composition of solution: 0.25 *m* ethyl acetate; 0.001 *m* NaCl

Equilibration time <i>hours</i>	Elution time <i>hours</i>	Q mmoles $\times 10^3$
1	18	6.55
2	18	7.65
3	18	7.70
4	18	7.85
5	18	7.80
24	24	7.80

The effect of the stainless steel basket on the rate of ester hydrolysis and also on the ionic state of the resin was determined by shaking 6 resin samples (3.29 g. dry hydrogen resin) in the tetramethylammonium state for 70 hours with 700 ml. of a solution 0.25 *m* in ethyl acetate and 0.001 *m* in the $(\text{CH}_3)_4\text{N}^+$ ion. At that time the resin samples were found to contain 8.9 per cent of their capacity in the hydrogen state. Under these

conditions, the concentration of acid in the external solution could be estimated since the distribution coefficient for the $\text{H-Me}_4\text{N}$ system is about 1 with this resin. Thus, in 70 hours, 1.75 meq. of H^+ is formed. The original solution contained 175 mmoles of ester, so approximately 1% hydrolyzed during this period. This compares with a value of 2% calculated on the basis of the results on the lithium resin previously reported. The slower rate encountered during the first 70 hours may be due to the induction period which appears in the first part of the hydrolysis due to autocatalytic effects.

Since the normal equilibration time was 14 hours or less, the H^+ content of the resin sample would be about 3%. This amount is negligible. It may be concluded that neither the resin nor the stainless steel baskets had any detectable effect on the process.

The half-time for the hydrolysis of methyl acetate is about 6 days (24). Using first-order kinetic theory, it may be calculated that in 3 hours, 2% of the methyl acetate will disappear. Thus, hydrolysis will have no more effect in this case than in the case of the ethyl acetate.

E. Diffusion Coefficients of Neutral Molecules in Water

For purposes of comparison, determinations were made of the aqueous diffusion coefficient, D_0 , of ethyl- and isobutyl acetate. The diaphragm cell method (7) was used in these measurements. A collection of aqueous

TABLE III
Diffusion Coefficients of Various Neutral Molecules in Water

Neutral molecule	D $\text{cm.}^2 \text{ sec.}^{-1} \times 10^5$	Temperature of measurement $^{\circ}\text{C.}$	Source of data	D Corrected to 25°C. $\text{cm.}^2 \text{ sec.}^{-1} \times 10^5$
Methyl alcohol	1.37	18	(6)	1.67
Urea	1.18	20	(6)	1.36
Methyl acetate	(1.3)	25	Estimated	(1.3)
Ethyl alcohol	1.02	20	(16)	1.17
Ethyl acetate	1.20	25	This paper	1.20
Butyl alcohol	0.88	18	(16)	1.07
Amyl alcohol	0.88	18	(6)	1.07
Isobutyl alcohol	(0.95)	25	Estimated	(0.95)
Isobutyl acetate	0.90	25	This paper	0.90

diffusion coefficients appears in Table III. Corrections to 25°C. were made assuming an energy of activation of diffusion in water of 5 kcal./mole.

F. Breakage of Particles

The particles were not broken to any degree during the course of the experiments. Over a 2-month period during which the resin was in frequent use, the number of broken particles found in a resin sample was

the same, as determined by actual count. The percentage of broken particles (halves) was about 7-8%.

G. Detailed Procedure

Following is a typical example of the exact procedure followed and the calculations made.

The data in Table IV will be used as the example. Here the resin in the potassium state was equilibrated with a standard solution which was approximately 0.25 *m* in ethyl acetate and 0.1 *m* in potassium chloride. The equilibrating solution was prepared by diluting 25.00 ml. of pure

TABLE IV

Data for Typical Procedure

Temperature: 24°C.

Composition of solution: 0.242 *m* ethyl acetate; 0.1 *m* KCl

Volume of eluant: 50 ml.

Volume of aliquot taken for analysis: 3 ml.

Dilution for sample of equilibration solution: 10:1000

Time	Duplicate colorimeter readings		Average colorimeter reading (less blank)	Q_A mmoles $\times 10^2$	Q mmoles $\times 10^2$	Q_0 1.00 g. dry H—0.25 <i>m</i> ester mmoles $\times 10^2$
min.						
0				(7.14)	(11.9)	(22.8)
1	147	147	133	6.06	10.1	
2	142	139	127	5.80	9.66	
3	133	131	118	5.40	9.00	
4	131	130	117	5.35	8.92	
5	124	125	111	5.05	8.42	
10	113	112	99	4.50	7.50	
Equil.						
Sol'n	177	168	159	7.25		
Water	14	14	0			
Molality = $\frac{7.25 \times 10^{-3}}{3 \times 10^{-2}} = 0.242$.						

Concentration of equilibrating solution: 0.242 *m*.

ethyl acetate and 0.50 ml. of 2.0 *m* potassium chloride with 1000 g. of water. After the run, which has been described in a previous section, the samples were placed into 50.00 ml. of water for elution; the system was shaken overnight.

All subsequent analytical procedures were carried out in standard Folin-Wu Blood Digestion tubes. The elution bottles were removed from the shaker and two 3.00 ml. aliquots were withdrawn; each was placed in a Folin-Wu tube. Two aliquots were also taken from the diluted original equilibrating solution. The colorimetric analysis was then performed.

After the analysis, the results were tabulated as shown in Table IV. The colorimeter readings were corrected for the blank. Using the calibra-

tion curve, the amount of ester in the aliquot was determined. These data appear under the column marked " Q_A ." Since the 50.00 ml. eluant volume was used, and a 3-ml. aliquot taken for analysis, the total amount of ester in the eluant and hence the resin sample was 50/3 times that in the aliquot. These data appear in the column marked " Q ."

Data at time $t = 0$ were obtained by either of two methods; centrifugation or extrapolation. The former is described in a previous paper (12). The centrifuged sample was eluted and analyzed along with the other samples. Extrapolated values were obtained by plotting the amount of ester found in the resin against $t^{\frac{1}{2}}$, as described in a previous section. The best straight line through the data for the first 40% of the desorption process was obtained by the method of least squares. An extrapolation of the straight line obtained to time $t = 0$ gave the required result. The

TABLE V
Comparison of Extrapolated and Centrifuged Values of Q_0
Size of sample: 1.00 g. dry hydrogen resin

Equilibrating solution	Q_0 Extrapolated mmoles $\times 10^2$	Q_0 centrifuged mmoles $\times 10^2$	Diff. %
0.1 <i>m</i> urea—			
0.001 <i>m</i> LiCl	11.4	11.9	4
0.1 <i>m</i> urea—			
0.001 <i>m</i> NaCl	8.20	8.35	2
0.25 <i>m</i> ethyl acetate—			
0.001 <i>m</i> NaCl	21.0	21.2	1
0.25 <i>m</i> ethyl acetate—			
0.001 <i>m</i> KCl	21.1	22.0	5
0.25 <i>m</i> ethyl acetate—			
0.001 <i>m</i> LiCl	21.7	22.5	4

agreement between centrifuged and extrapolated values is good, as shown in Table V.

EXPERIMENTAL RESULTS

For convenience, the following abbreviations, definitions, and conventions will be used: All particles are 16-mesh unless otherwise stated; all results are based on 1.00 g. of dry hydrogen resin; the precision of all measurements is reported in terms of the average deviation; all bracketed data are extrapolated values; $(m_0)_i$, $(m_0)_0$, are the molal concentrations of neutral molecule in the resin and solution phases, respectively; K_D is the distribution coefficient of the neutral molecule between the resin and solution phases and is $(m_0)_i/(m_0)_0$; V_e is the specific wet volume, and is the volume occupied by 1.00 g. of dry hydrogen resin in equilibrium with the required solution; W_e , W_m , are the specific wet and dry weights, respectively, of the resin, and refer to 1.00 g. of dry hydrogen resin in the appropriate wet and dry ionic state; W_w is the weight of water in the wet

resin in the appropriate ionic state; E_a is the energy of activation for diffusion in kcal./mole, calculated from $D = D_0 \exp(-E_a/RT)$; ΔH in kcal./mole is calculated from $d \ln K_D / dT = \Delta H / RT^2$.

A. Stirring Rate

In all desorption experiments, it is necessary to insure that the rate of stirring is sufficiently high so as not to be a variable in the diffusion process. In Fig. 2 are given some diffusion coefficients calculated from data collected at four different stirring speeds, varying from 8 cm./sec. to 49 cm./sec. The diffusion coefficient increased with the rate of stirring up to 36 cm./sec.; it was constant thereafter.

Since the rate of diffusion of urea in the resin was greater than that of any of the other neutral molecules studied, any stirring speed which was

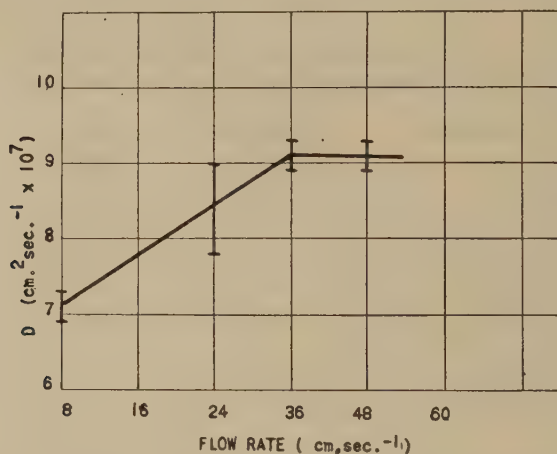


FIG. 2. Variation of diffusion coefficient with flow rate at 25°C.

sufficiently high for urea would also be adequate for the other molecules. A stirring speed of 49 cm./sec. was used in all subsequent experiments.

The above results were obtained for 16-mesh particles. When 30-mesh particles were used, it was found that the calculated diffusion coefficients were the same in both cases within experimental error. This is shown in Table VII, lines 6 and 7. If the stirring speed were too slow for the smaller particles, the diffusion coefficient would be less than that for the 16-mesh particle. It must therefore be assumed that the stirring speed of 49 cm./sec. was also adequate for the smaller size particle.

As a corollary to the above, it follows that the stirring speed was also adequate for experiments made with the 16-mesh particles at 43°C. since the diffusion flux at 43° C. was less than for the 30-mesh particles at 25°C.

The particle size effect was determined with the sodium resin, using urea. The results are shown in Table VII, lines 6 and 7. It is seen that D and Q_0 for both particle sizes were the same within experimental error.

The data followed the classical equation for diffusion out of a spherical particle throughout the experiment. When only 30% of the neutral molecule remained in the resin phase, its concentration in the eluate was so low that the analytical procedure was not reliable. However, in the first 70% of the process, the deviations in B are apparently random, as is shown in Fig. 3. Here Q/Q_0 is shown as a function of Bt for two urea and two ethyl acetate experiments. The experiments selected were those showing a minimum and maximum deviation of B in each series. Agreement between theory and experiment is good for the first 70% of the

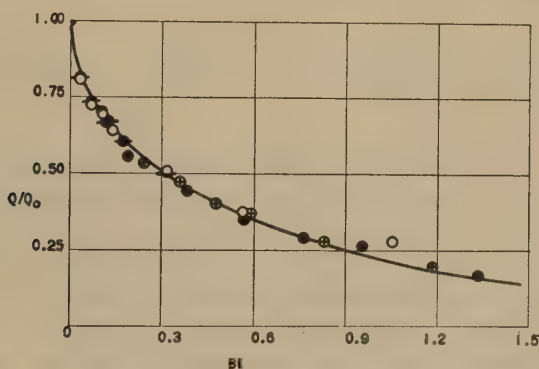


FIG. 3. Rate of diffusion of various neutral molecules in resin at 25°C. (Solid line represents theoretical curve.) ●, Urea in K-resin; ⊕, Urea in Li-resin; ○, Ethyl acetate in Na-resin; ⊗, Ethyl acetate in K-resin.

process. Three of the four superposed curves of Fig. 3 use values of Q_0 obtained by centrifugation. This fact emphasizes the agreement.

B. Volume of the Resin as a Function of the Ionic State

The specific volume of the resin in each ionic state was the same at 25 and 43°C. within 2%. The sequence of these volumes was: $\text{Me}_4\text{N}^+ > \text{Li}^+ > \text{Na}^+ > \text{K}^+$. The amount of water present in the resin in each ionic state was also the same at both temperatures within 2%. The sequence of the water content was $\text{Li}^+ > \text{Na}^+ > \text{K}^+ > \text{Me}_4\text{N}^+$. The equilibrium volume of the resin in ethyl acetate and in urea solutions was the same as in water. These data are given in Table VI.

C. Effect of $(m_0)_0$ on D

The value of K_D and of D does not depend on $(m_0)_0$ for the urea and ethyl acetate systems in the concentration ranges studied. This is shown

TABLE VI
Assembled Values

Ionic state	μ Molal	Neutral molecule	$(m_0)_i$ Molal	Temp. °C.	W_e g.	W_m g.	W_w g.	V_e ml.	r_0^3 $\text{cm.}^3 \times 10^6$	r_0^2 $\text{cm.}^2 \times 10^4$	r_0 $\text{cm.} \times 10^2$
Li	0.001			25	1.762	1.031	0.731	1.370 ± 0.004	251	39.8	6.32
Li	0.001			43	1.754	1.031	0.723	1.370		39.8	
Na	0.001			25	1.750	1.115	0.635	1.301 ± 0.005	238	38.4	6.20
Na	0.001	U	0.1	25	1.753	1.115	0.638	1.291 ± 0.003		38.4	
Na	0.001	E	0.25	25	1.753	1.115	0.638	1.295 ± 0.003		38.4	
Na	0.001			43	1.745	1.115	0.630	1.294			
K	0.001			25	1.742	1.197	0.545	1.263 ± 0.002	231	37.9	6.14
K	0.001			43	1.745	1.197	0.548	1.280		37.9	
Me ₄ N	0.001			25	1.838	1.380	0.458	1.495 ± 0.005	274	42.2	6.50
Me ₄ N	0.001			43	1.838	1.380	0.454	1.525		42.2	
Na*	0.001			25	1.782	1.113	0.669	1.337 ± 0.003	267	8.93	2.99

Abbreviations: U, urea; E, ethyl acetate.

* 30-mesh.

in Table VII, lines 1, 2, and 17, 18. The same table shows that Q_0 was directly proportional to $(m_0)_0$.

D. Effect of Concentration of Electrolyte on D

The effect of the concentration of electrolyte in the equilibrating and desorption solutions on D and K_D was determined for the urea and ethyl acetate systems. D , K_D , and $(m_0)_i$ for the urea system were unaffected by a change in ionic strength from 0.001 m to 0.1 m , both for 16- and 30-mesh particle sizes, as is seen in Table VII, lines 1, 4, and 7, 10, and 11, 13, etc. The work of Gregor, Gutoff, and Bregman (11) shows that V_e is substantially the same in 0.001 m and 0.1 m salt solutions.

In the ethyl acetate system, however, the effect of ionic strength was marked. An increase in ionic strength caused a decrease in D . This is in contrast with the effect noted in the ion-exchange process (4), where an

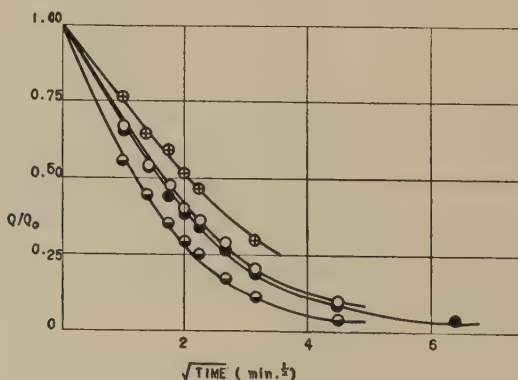


FIG. 4. Rate of desorption of urea from resin at 25°C. \oplus , Me₄N-resin; \circ , Li-resin; \bullet , Na-resin; \ominus , K-resin.

TABLE VII
Assembled Values

Ionic state	Molal	Neutral molecule	(m_0) ₀ Molal	Temp. °C.	B <i>min.</i> ⁻¹	D <i>cm.</i> ² / <i>sec.</i> × 10 ⁷	Q ₀ <i>mmole</i> × 10 ²	(m_0) _i Molal	K _D	E _a <i>kcal./mole</i>	ΔH <i>kcal./mole</i>	D/D ₀
Li	0.001	U	0.1	25	0.118 ± 0.002	8.1 ± 0.2	11.9	0.163	1.63			
Li	0.001	U	0.3	25	0.110 ± 0.006		36.0					
Li	0.001	U	0.1	43	0.22 ± 0.01	14.8 ± 0.8	11.0	0.152	1.52	6.0 ± 0.6	-0.7 ± 0.06	
Li ^a	0.1	U	0.1	25	0.12 ± 0.004		(10.7)					
Na	0.001	U	0.1	25	0.127 ± 0.003	8.5 ± 0.3	8.35	0.131	1.31			
Na	0.001	U	0.1	25	0.126 ± 0.003	8.5 ± 0.3	8.35					
Na ^b	0.001	U	0.1	25	0.52 ± 0.02	8.4 ± 0.3	8.37					
Na	0.001	U	0.1	43	0.26 ± 0.01	17.0 ± 0.7	7.62	0.121	1.21	6.9 ± 0.6	-0.8 ± 0.06	
Na ^a	0.1	U	0.1	25	0.13 ± 0.003	8.7 ± 0.3						
Na ^b	0.1	U	0.1	25	0.52 ± 0.02	8.4 ± 0.3						
K	0.001	U	0.1	25	0.19 ± 0.01	12.2 ± 0.7	7.13	0.131	1.31			0.091
K	0.001	U	0.1	43	0.41 ± 0.02	26.3 ± 1.3	6.62	0.121	1.21	7.7 ± 0.8	-0.8 ± 0.06	
K ^a	0.1	U	0.1	25	0.17 ± 0.003	10.9 ± 0.3	7.0					
Me ₄ N	0.001	U	0.1	25	0.071 ± 0.002	5.1 ± 0.2	8.1	0.172	1.72			
Me ₄ N	0.001	U	0.1	43	0.19 ± 0.02	13.5 ± 1.4	5.3	0.117	1.17	9.7 ± 1.0	-4 ± 0.3	

Abbreviations: U, urea; M, methyl acetate; E, ethyl acetate; I, isobutyl acetate; EA, ethyl alcohol; IA, isobutyl alcohol.

^a Different batch of Dowex 50.^b 30-mesh.

TABLE VII (Continued)

Ionic state	Molal	Neutral molecule	(m_0) ₀ Molal	Temp. °C.	B min.^{-1}	D $\text{cm.}^2/\text{sec.} \times 10^7$	Q ₀ $\text{mmole} \times 10^2$	(m_0) _i Molal	K _D	E ₀ kcal./mole	ΔH kcal./mole	D/D ₀
Li	0.001	E	0.25	25	0.031 \pm 0.001	2.1 \pm 0.1	(21.7)	0.297	1.19			
Na	0.001	E	0.25	25	0.031 \pm 0.002	2.0 \pm 0.1	21.2	0.334	1.33			
Na	0.001	E	0.50	25	0.028 \pm 0.001		(38.0)	0.300	1.20			
Na	0.001	E	0.25	7	0.015 \pm 0.001	1.0 \pm 0.1	(20.8)	0.328	1.31	6.0 \pm 0.6	0 \pm 0.03	
Na	0.1	E	0.25	25	0.018 \pm 0.001		21.2					
Na	0.1	E	0.25	26	0.019 \pm 0.001		(20.7)					
K	0.001	E	0.25	25	0.032 \pm 0.001	2.0 \pm 0.1	(21.1)	0.383	1.53			0.018
K	0.1	E	0.25	24	0.019 \pm 0.001	1.2 \pm 0.1	(22.8)					
K	0.01-0.1	E	0.25	25	0.025 \pm 0.001	1.6 \pm 0.06						
Me ₄ N	0.001	E	0.25	25	0.082 \pm 0.007	5.8 \pm 0.4	(4.1)	0.090	0.36			
K	0.001	M	0.25	25	0.061 \pm 0.002	3.9 \pm 0.1	(19.9)	0.365	1.46			0.30
K	0.001	M	0.25	7	0.021 \pm 0.001	1.4 \pm 0.1	(21.7)	0.398	1.59	9.0 \pm 1.0	-0.7 \pm 0.06	0.023
K	0.001	I	0.025	25	0.0033 \pm 0.0002	0.21 \pm 0.01	(2.7)	0.49	2.0			
K	0.001	I	0.025	7	0.0027 \pm 0.0002	0.17 \pm 0.01	(3.4)	0.63	2.5			
K	0.001	EA	0.5	25	0.13 \pm 0.003	8.3 \pm 0.2	(19.6)	0.359	0.72			0.071
K	0.001	EA	0.5	7	0.072 \pm 0.002	4.6 \pm 0.2	(19.3)	0.354	0.71	4.8 \pm 0.4	0	
K	0.001	IA	0.5	25	0.020 \pm 0.001	1.3 \pm 0.1	(28.4)	0.52	1.04			0.014
K	0.001	IA	0.5	7	0.013 \pm 0.0005	0.83 \pm 0.03	(25.8)	0.47	0.95	3.5 \pm 0.4	0.7 \pm 0.06	

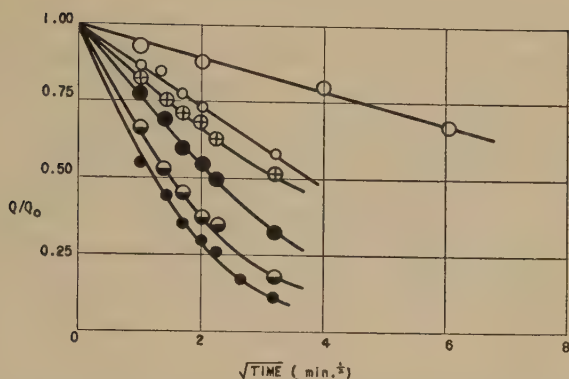


FIG. 5. Rate of desorption of various neutral molecules from K-resin at 25°C. ○, Isobutyl acetate; ○, Isobutyl alcohol; ⊕, Ethyl acetate; ●, Methyl acetate; —, Ethanol; ●, Urea.

increase in ionic strength causes an increase in the rate of exchange. This is shown in Table VII, lines 17, 20, and 22, 23. The values of B given in this table have been corrected to 25°C. where the temperature of the original experiment was different from 25°C. The Q_0 of ethyl acetate was not affected by the change in ionic strength, within experimental error. Desorption curves are shown in Figs. 4 and 5.

DISCUSSION

In the neutral molecule desorption process, there are two possible rate determining steps: (1) diffusion through a thin bounding liquid film; and (2) diffusion in the resin phase. Diffusion in the resin phase may take place in the interstitial liquid or on the resin matrix in the adsorbed state.

The experimental results show that the process in every case can be described by the spherical particle diffusion equation. The average error in D for all the experiments performed is $\pm 5\%$. Excellent agreement is obtained between values of Q_0 determined (a) directly by centrifugation and (b) by use of the radial diffusion equation; this is shown in Table V for the urea and ethyl acetate experiments. Values of D and Q_0 for urea are the same for 30- and 60-mesh particles, where the radius of the particles changes by a factor of 2. As is shown in Table VII, lines 8, 12, and 19, the calculated energies of activation for the desorption process in the urea and ethyl acetate systems are 7 and 6 kcal./mole, respectively, which are of the order expected in a diffusion process. Furthermore, as is shown in Table VII, the ratio D/D_0 for the molecules studied varies from 0.002 to 0.09 whereas D_0 varies by only 50%. It is unlikely that an unstirred film around the resin particles could produce these effects.

The above results indicate that radial diffusion in the resin phase is the rate determining step in the desorption process. A number of conclu-

sions may be drawn from the constancy of D and Q_0 . Chief among these is that the experimental techniques employed were proper. Furthermore, the essential homogeneity of the resin particles of the sizes investigated is strongly indicated, together with the similarity in physical structure of particles of different sizes. The efficacy of the centrifugation method for the separation of the solution and resin phases is also demonstrated.

The external volume of the resin particles does not change markedly with temperature, as shown in Table VII. The composition of the resin

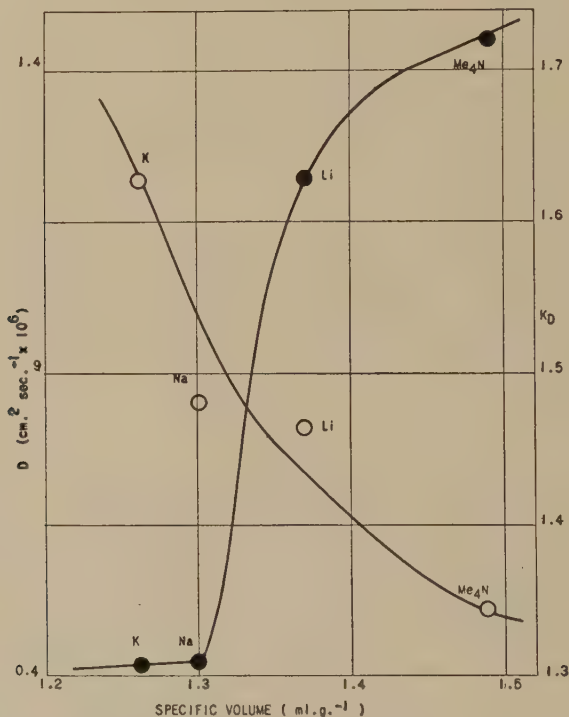


FIG. 6. Diffusion coefficient and distribution coefficient of urea in resin at 25°C. as a function of the specific volume of the resin. ●, K_D ; ○, D .

also changes very little with temperature. The distribution coefficient K_D for urea is larger for lithium than for sodium and potassium resins; it is highest for the Me_4N resin. Since urea is a highly polarizable molecule, it may enter the hydration shell of the ions. Also, because of its organic nature, it may be adsorbed by the tetramethylammonium ion.

As regards D for the urea molecules, diffusion is fastest in the potassium resin, and decreases in the order: sodium, lithium, and tetramethylammonium resins. Since the (hydrated) ionic volumes are in the sequence $\text{Me}_4\text{N}^+ > \text{Li}^+ > \text{Na}^+ > \text{K}^+$, it follows that the "free volume" or volume

of the solvent which is not water of hydration, is in the inverse order. Therefore, D appears to be directly proportional to the free volume, in the case of urea. While this represents a plausible postulate, the absence of reliable values for the hydration of ions in concentrated electrolytic media make a quantitative comparison impossible.

Figure 6 also shows that K_D for urea is related to the specific wet volume V_e and also to the hydrated ionic volume. This implies that urea preferentially enters the hydration sphere of the inorganic ions, or is adsorbed by the quaternary ammonium ion. Again, independent data are lacking for a comparison. Since K_D is greater than unity, a net "salting in" by the resin phase has occurred. Since urea is a polarizable molecule, adsorption onto the hydrocarbon matrix may be neglected.

The energies of activation appear to be significantly higher than corresponding values in free solution. This may be interpreted in general as resulting from two processes: (1) hindered diffusion in the gel and its change with temperature; (2) the energy of activation of the "salting in" process. Since E_a for urea follows the sequence $K^+ > Na^+ > Li^+$, it may be presumed that the hindering effects of the matrix play a major role. Since the dimensions and water content of the resins do not change with temperature, these cannot influence the process. It could be argued that since ion hydration decreases with temperature, the free volume should increase; however, this effect would be largest for the lithium resin. The opposite is observed.

In the case of the tetramethylammonium resin, E_a is abnormally high, 9.7 kcal./mole; this may be the result of significant adsorption processes. The effect of temperature on K_D supports this latter postulate, since "salting in" by the resin phase decreases sharply with temperature.

Table VII shows that K_D is not concentration-dependent for urea and ethyl acetate, at least in the concentration range employed. This is as expected, because the solutions are dilute with respect to the neutral molecules.

The ionic strength of the external solution in the range 0.001 m to 0.1 m does not affect the rate of diffusion of urea in the resin, even for 30-mesh particles. This fact is consistent with the picture that the composition of the resin phase does not change in this ionic strength range. Donnan effects exclude most non-exchange electrolytes from the resin phase, and its wet weight and wet volume are substantially constant. Therefore, these facts indicate that the diffusion of urea across an unstirred surface film is not a rate determining step.

In the case of ethyl acetate, effects are observed which are not capable of explanation at present. In Table VII, it is seen that both for sodium and potassium resins, D is actually larger in 0.001 m than it is in 0.1 m solutions. This effect is quite strong, D varying by a factor of at least 1.5.

The values of K_D are, however, quite independent of ionic strength, whether determined by centrifugation or extrapolation techniques. Another experiment was performed, in which the potassium resin was equilibrated in 0.1 *m* potassium chloride and desorbed in a 0.001 *m* potassium chloride solution. These data, shown in Table VII, line 24, give a value of B which is intermediate between B in 0.1 *m* and B in 0.001 *m* salt solutions.

No explanation can be offered at this time for these results. Since the thickness of the unstirred film may be expected to increase with a decrease in ionic strength, it appears that this is not an unstirred film effect. Since the resin phase is the same in 0.1 as in 0.001 *m* solutions, these effects probably take place at the surface of the particles.

Values of Q_0 , K_D , D , and E_a for the ethyl acetate system are shown in Table VII. Here the values of Q_0 are nearly the same for the resins in the K, Na, and Li states. However, Q_0 in the Me_4N state is but one-fifth of the value in the inorganic states. The values of K_D are in the order $\text{K}^+ > \text{Na}^+ > \text{Li}^+$. The fact that K_D is greater than unity for the inorganic states is probably due to adsorption of the relatively non-polar molecule on the hydrocarbon matrix. It is known that polystyrene adsorbs ethyl acetate strongly. A striking anomaly is found for the resin in the Me_4N state. Here K_D is 0.36 compared with 1.53 for the potassium resin.

The diffusion coefficient of ethyl acetate in the resin in the various ionic states is substantially the same. Again, the Me_4N resin is anomalous. Here D is almost three times the value for the potassium resin. Thus, in the Me_4N system, K_D is abnormally low and D is abnormally high.

The value of E_a for the diffusion process is 6.0 kcal./mole, and ΔH for the partition process is approximately zero for ethyl acetate with the sodium resin. These results are similar to those obtained for E_a and ΔH in the case of urea.

In addition to urea and ethyl acetate, the distribution and diffusion coefficients of a number of other neutral molecules, including methyl and isobutyl acetate, and ethyl and isobutyl alcohol, were investigated with potassium resin, equilibrated with 0.001 *m* solutions. Table VII gives a summary of the results obtained. Here it is seen that K_D is substantially the same for the urea, methyl and ethyl acetate molecules. In the case of isobutyl acetate, it is significantly higher, indicating that this molecule is adsorbed to a greater extent due to its high molecular weight. In the case of ethyl alcohol, K_D is less than 1, while in the case of isobutyl alcohol, it is substantially 1. These data indicate that the lower molecular weight alcohol is "salted out" of the concentrated electrolytic solution. Partial adsorption of the high molecular weight alcohol may account for the increase of K_D . All of these results appear to be consistent with the picture that the polar, highly polarizable urea molecule is "salted in" due to elec-

trical effects, while the other neutral molecules are probably adsorbed by the matrix.

Comparison of the diffusion coefficients shows several interesting effects. The relative diffusion coefficient D/D_0 shows that urea diffusion is about one-tenth as fast in the resin phase as in solution. This result agrees rather well with relative diffusion coefficients of ions in the resin phase (2, 4).

The methyl acetate and ethyl acetate molecules diffuse somewhat more slowly in the resin than does urea. This may reflect their diffusion in the adsorbed state. Ethyl alcohol and urea appear to behave in a similar fashion. Isobutyl acetate and isobutyl alcohol have relative diffusion coefficients much lower than for the other neutral molecules. This strong effect is undoubtedly associated with hindered diffusion.

The energies of activation are low in all cases. The values for urea and ethyl acetate are the most reliable, because the Q_0 value was in all cases checked with centrifugation techniques. In the case of isobutyl acetate, E_a was not calculated because of the large analytical errors encountered in the isobutyl acetate determination.

The evidence of hindered diffusion in this work is in agreement with the results of Gregor *et al.* (10) on the rate of absorption of the various quaternary ammonium bases by hydrogen resins, and also is in agreement with the work of Levesque and Craig (17) who found that large molecules diffused so slowly in the resin phase that only the surface of the resin was effective as a catalyst; for small molecules, the entire resin was effective.

Haskell and Hammett (13) found that diffusion played a minor role in the rate of hydrolysis of various esters by a cation exchange resin. By making suitable corrections for the different particle sizes employed by Haskell and this paper, and assuming that the physical structure of the two resin systems is the same, it is possible to make a rough calculation of the effect of diffusion in the case of ethyl *n*-butyrate, studied by Haskell. Here, Haskell found the specific rate constant to be 0.256×10^{-5} l. mol.⁻¹ sec.⁻¹. On this basis, the half-time of the reaction would be about 1000 minutes. For isobutyl acetate, D is 0.21×10^{-7} cm.² sec.⁻¹, from which it may be calculated that the half-time for the diffusion process would be about 10 minutes. These values are in agreement with the small diffusion effects noted by Haskell.

SUMMARY AND CONCLUSION

The rates of diffusion of a number of neutral molecules in a cation exchange resin in various exchange states were investigated. Distribution coefficients, diffusion coefficients, and energies of activation of the diffusion process were calculated.

It is found that the diffusion process may be described by the equations for diffusion into a spherical particle.

The diffusion coefficients vary from 0.002 to 0.1 of the corresponding values in solution. As the molecular size increases, there is evidence of hindered diffusion with a sharp drop in the diffusion coefficient.

As a rule the molecules are "salted into" the resin phase. This may be the result of either entrance into a hydration sphere in the case of a highly polarizable molecule as urea, or physical adsorption on the matrix as in the case of the nonpolar molecules. Diffusion in the case of the polar molecules appears to be largely through the aqueous phase; with the nonpolar molecules, diffusion in the adsorbed state may be important.

REFERENCES

1. BARRER, R. M., *Diffusion in and through Solids*, p. 39. Cambridge Univ. Press, 1941.
2. BAUMAN, W. C., *et al.*, *Ind. Eng. Chem.* **40**, 1350 (1948).
3. BAUMAN, W. C., AND EICHHORN, J., *J. Am. Chem. Soc.* **69**, 2830 (1947).
4. BOYD, G. E., ADAMSON, A. W., AND MYERS, L. S., *J. Am. Chem. Soc.* **69**, 2836 (1947).
5. BUCKLES, R. E., AND THELEN, R., *Anal. Chem.* **22**, 676 (1950).
6. GLASTONE, EYRING, LAIDLER, *Theory of Rate Processes*, p. 529, McGraw-Hill, New York, 1941.
7. GORDON, A., *Ann. N. Y. Acad. Sci.* **41**, 285-308 (1945).
8. GREGOR, H. P., *J. Am. Chem. Soc.* **70**, 1293 (1948).
9. GREGOR, H. P., AND BREGMAN, J. I., *J. Am. Chem. Soc.* **70**, 2370 (1948).
10. GREGOR, H. P., BREGMAN, J. I., GUTOFF, F., BROADLEY, R., BALDWIN, D., AND OVERBERGER, C. G., *J. Colloid Sci.* **6**, 20 (1951).
11. GREGOR, H. P., GUTOFF, F., AND BREGMAN, J. I., *J. Colloid Sci.* **6**, 245 (1951).
12. GREGOR, H. P., HELD, K., AND BELLIN, J., *Anal. Chem.* **23**, 620 (1951).
13. HASKELL, R. C., AND HAMMETT, L. P., *J. Am. Chem. Soc.* **71**, 1284 (1949).
14. KEENAN, A. G., *Can. Chem. Process Inds.* **29**, 857-8 (1945).
15. KUNIN, R., AND MYERS, R. J., *J. Phys. Colloid Chem.* **51**, 1111 (1947).
16. LANDOLT-BÖRNSTEIN, *Tables of Physical Constants*, p. 228, 5. Auflage, 3. Ergänzungsband, 1. Teil.
17. LEVESQUE, C. L. AND CRAIG, M., *Ind. Eng. Chem.* **40**, 96 (1948).
18. POETHKE, W., *Ber.* **68B**, 1031-7 (1935).
19. SNELL, F. D., *Colorimetric Analysis*. Vol. II, p. 395, D. Van Nostrand Co., New York, 1938.
20. SUSSMAN, S., *Ind. Eng. Chem.* **38**, 1228 (1946).
21. THOMAS, C. G., AND DAVIES, C. W., *Nature* **159**, 372 (1947).
22. WEBB, D. A., *Sci. Proc. Roy. Dublin Soc.* **21**, 281 (1936).
23. WHITE, H. J., JR., AND EYRING, H., *Textile Research J.* **17**, 523-553 (1947).
24. WIJS, E., *Z. physik. Chem.* **12**, 514 (1893).
25. ZWOLINSKI, B. J., EYRING, H., AND REESE, C. E., *J. Phys. Colloid Chem.* **53**, 1426-1453 (1949).

STUDIES ON ION-EXCHANGE RESINS. IV. SELECTIVITY COEFFICIENTS OF VARIOUS CATION EXCHANGERS TOWARDS UNIVALENT CATIONS¹

Harry P. Gregor and J. I. Bregman^{2,3}

Department of Chemistry, Polytechnic Institute of Brooklyn, Brooklyn, New York

Received April 22, 1951

INTRODUCTION

This paper describes the selective uptake of one univalent cationic species over another by various cation exchange materials. The selectivity coefficient is defined as,

$$K_2^1 = \left(\frac{n_1}{n_2} \right)_i \left(\frac{a_2}{a_1} \right)_0,$$

where the n 's refer to moles of cation within the resin phase (i) and the a 's to the activity of the cation in the external, equilibrating solution (0). The notation K_2^1 means that ion (1) is the reference ion, and refers to the exchange process (22), $(1)_0 + (2)_i = (1)_i + (2)_0$. The selectivity coefficient without regard to a particular system is written as K_D . The cationic activities are customarily replaced by mean activities, and in dilute solutions by concentrations. This allows a calculation of K_D directly from experimental quantities.

This paper is one of a series which take up the various parameters in the thermodynamic equations for ion exchange processes (7,8,9,11,14). Previous communications have dealt with the capacity and volume parameters, while forthcoming ones will deal with osmotic pressure and activity coefficient parameters. Since the values of all of these parameters are required for a complete, quantitative evaluation, this paper considers qualitative relationships only.

EXPERIMENTAL METHODS

A. Exchangers

The cation exchange systems used included a series of sulfonated polystyrene-divinylbenzene resins, prepared using different amounts of

¹ The authors wish to thank the Office of Naval Research for the support rendered to this work.

² Taken in part from the dissertation submitted by J. I. Bregman in partial fulfillment of the requirements for the degree of Doctor of Philosophy in Chemistry, Polytechnic Institute of Brooklyn, September, 1950.

³ Present address: National Aluminate Corp., Chicago, Ill.

the cross-linking agent (6). These resins are referred to as DVB 0.4, DVB 2, etc., the numbers denoting the weight percent of divinylbenzene used in preparing the unsulfonated polymer. Three commercial sulfonic acid resins were used: a sulfonated polystyrene resin, prepared using 8% divinylbenzene—Dowex 50 (Dow Chemical Co.); a sulfonated phenolic base resin—Duolite C-3 (Chemical Process Co.); and a phenolic base resin, prepared by the alkaline condensation of phenolsulfonic acid, phenol and formaldehyde—hereafter referred to as Phenolic resin. An inorganic cation exchanging mineral, Glaucinite, was used; it was made more permeable by treatment with hot alkali (Super Zeo-Dur, Permutit Co.).

Each of these materials was treated in several alternate cycles with an excess of 1 *M* sodium hydroxide and 1 *M* hydrochloric acid, then given a final regeneration with acid, rinsed to an effluent pH of 4.5, and air dried. The exchangers were screened to $-20 + 30$ mesh size, except some of the DVB resins which were somewhat smaller. A detailed description of the preparative procedures for the DVB resins is given in an earlier paper in this series, together with details of the conditioning procedure (9).

All of the data for the resinous exchangers presented in this paper refer to a specific quantity of resin, i.e., 1 g. of dry resin in the hydrogen state. Thus the weight, volume, etc., of a resin system prepared starting with 1.000 g. of dry hydrogen resin are designated as the specific weight (W_e), specific volume (V_e), etc. This system of notation makes a comparison of the properties of the same resin in various states convenient.

In practice, the experiments described herein employed 0.5 g. samples of air dried resin. The moisture content was determined by drying to constant weight over P_2O_5 .

The specific exchange capacities in *m* moles per gram of the various exchangers used were: DVB 0.4, 6.85; DVB 2, 5.18; DVB 4, 5.16; DVB 6, 5.09; DVB 8, 5.06; DVB 10, 4.86; DVB 13, 4.94; DVB 17, 4.89; DVB 23, 4.24; DVB 26, 4.50; Dowex 50, 4.90; Duolite C-3, 2.90; Phenolic, 2.84; Glaucinite, 0.108. All the synthetic exchangers have the same capacity with respect to all univalent cations, as shown in an earlier paper (9). For the Glaucinite exchangers the hydrogen exchange capacity is lower than the univalent (potassium) exchange capacity. This exchanger shows the same capacity towards potassium, sodium, lithium and ammonium. All Glaucinite data are reported in terms of 1 g. of dry potassium exchanger.

B. Volume Determinations

The specific volumes were determined using the centrifugation technique described by Gregor, Held and Bellin (12), and in a preceding paper in this series (11).

C. Analytical Procedures

Potassium and sodium were determined using the flame photometer (Perkin-Elmer, model 52A), which has an accuracy of $\pm 1\%$, when proper precautions are taken (9). Where a solution contained a mixture of only lithium and tetramethylammonium chloride, it was analyzed by evaporating to dryness at 100°C . and weighing. The chloride content was determined by potentiometric titration with silver, and the amounts presented calculated. This procedure is accurate to $\pm 2\%$.

E. Determination of K_D

Two methods were employed to determine selectivity coefficients. The first consisted in passing a known solution through a small bed of resin in a column until the effluent composition was that of the influent. The resin was then separated from the solution, the ions eluted from it and analyzed. The second method consisted in shaking a known amount of resin containing a single cationic species with a measured amount of known solution containing a different cation, until equilibrium was attained. The former method is referred to as the column procedure, the latter as the shaking procedure.

The column procedure employed a glass ion exchange column, consisting of a 300-ml. bulb, connected by a short length of rubber tubing to a tube 15 cm. long, 1 cm. in diameter, with an "extra coarse" sintered glass disc near its bottom. Useful tubes could be constructed by fusing a number of 2-mm. glass beads to form a porous disc at the bottom of a tube. The rate of flow through the column was controlled by a Hoffman clamp on a rubber tube, connected to the bottom of the column.

The hydrogen resin was weighed out in 0.5 g. (2 *m* mole) samples, placed in the column and the hydrogen eluted with 1 *M* potassium chloride solution. Titration of the eluate gave the exchange capacity of the resin. While the capacity could be calculated from the amount weighed out and the moisture content, this method was not as accurate as the direct determination of every sample. This may have been because the size of the sample was often too small for perfect sampling. Also, the air-dried resins necessarily had high water contents, to prevent their decrepitation upon re-wetting. As the room temperature varied some of this water would distill over and condense on the sides of the bottle. For these reasons, when air-dried resins were weighed out and their capacity determined at different times, the reproducibility was not satisfactory for an average deviation of $\pm 0.7\%$ was encountered. However, for the same sample of resin the reproducibility of a series of capacity determinations is equal to that of the titration procedure itself ($\pm 0.1\%$).

The resin, now in the potassium state, was then equilibrated successively with various solutions. First, 0.001 *M* potassium chloride solution was

passed through the resin bed; the effluent concentration did not reach that of the influent until 100 ml. had been used, in spite of the fact that the resin was already in the potassium (1 *M*) state. Then 0.01 *M* ammonium chloride was passed through the bed. With resin DVB 2, equilibration required 600 ml. of solution or a threefold excess in terms of equivalents. Resins DVB 13 and 26 required 1200 ml. of solution, or a sixfold excess.

The resin was then equilibrated with a solution 0.005 *M* with respect to potassium chloride and 0.005 *M* to ammonium chloride. Resin DVB 2 required 400 ml. of solution; resins DVB 13 and 26 required 800 ml. of solution. Thus, up to a fourfold excess was required in terms of potassium capacity.

These data show that large excesses are required to establish equilibrium conditions. Routinely, a twenty- to forty-fold excess was employed, more in the case of slow reactions or ones with unfavorable distribution coefficients. The rate of flow in the column was always kept at 0.5 ml./min./ml. of bed, which was sufficiently slow for efficient column operations, i.e., a high number of theoretical plates. The temperature was 24–26°C., unless otherwise stated.

The electrolyte in the resin phase was then eluted. First, excess equilibrating liquid was drawn off by suction. The amount which remained in the column was negligible when dilute (<0.01 *M*) solutions were used. With more concentrated solutions, the resin was removed from the column and centrifuged (11) to remove excess liquid, replaced in a clean column, and then eluted.

The resin was eluted with 200 ml. of 0.1 *M* magnesium nitrate. This salt was used because magnesium does not interfere directly with sodium and potassium determinations with the flame photometer, and because the divalent cation displaces univalent cations efficiently. The amount used represented a large excess.

The shaking procedure involved weighing the resin into flasks, determining its capacity by direct titration, and then equilibrating it with a 0.01 *M* solution of the reference electrolyte (usually potassium chloride). A many-fold excess was used, usually more than was required by the column technique. Then the excess solution was drawn off the resin by suction, and various amounts of 0.01 *M* solutions of the other cation were added, and the system shaken until equilibrium was reached. In every case, the system was shaken for a period of time at least twice as long as the time required for equilibration. With inorganic salts, equilibrium is reached within a few hours; in the case of the quaternary ammonium ions, considerably longer periods of time were required (9). The data of Table I were obtained by adding a 0.01 *M* solution of tetraethylammonium bromide to potassium resin, and shaking in a thermostat. The rate of ex-

change was followed conductometrically, using different dipping electrodes sealed in the flasks. For experiments of this type which involved ions which diffuse slowly in the resins, equilibrating times of at least 50 days were employed.

The distribution coefficients were calculated as follows: In the column experiments, the equilibrium concentrations in the external solution were known. One of the cations in the resin phase was analyzed for directly. When potassium was present, it was determined; otherwise, sodium or hydrogen was determined. The amount of other cation present was then calculated by difference, for the total capacity is known. Thus three of the four quantities making up K_D were determined directly.

TABLE I
*Shaking Equilibration of Potassium Resin with 0.01 M
Tetraethylammonium Bromide*

Time	Resistance of external solution in ohms		
	DVB 2	DVB 10	DVB 26
0 hours	1143.8	1255.0	1035.1
1	1127.0	1253.0	1033.8
2	1118.0	1252.0	1033.2
4	1110.8	1251.5	1033.1
7	1103.3	1246.1	1029.9
1 days	1089.7	1234.2	1021.7
2	1057.3	1210.0	1016.7
3	1041.5	1195.7	1015.8
6	1016.7	1186.8	1013.5
9	1008.7	1185.7	1011.7
16	999.6	1177.9	1013.9
19	996.1	1177.9	1006.6
21	994.2	1176.6	1008.2
24	995.3	1175.0	1005.6
26	994.9	1174.2	1005.3
28	994.7	1176.2	1004.5
30	995.0	1175.0	1004.6
32	994.8	1174.8	1004.8

When the external solution was concentrated (1 M), the electrolyte content of the resin phase was determined by adding water to the centrifuged resin to elute the non-exchange electrolyte, followed by elution, determination of the eluate, and calculation by difference.

When the shaking procedure was used, both the external solution and the eluate were analyzed for the reference ion, usually potassium. Also, the halide content of the external solution was determined as an additional check. Here the amount of ion other than potassium, sodium or hydrogen was calculated by difference; thus two of the four quantities making up K_D were determined directly.

Calculated values of K_D are subject to the errors arising in the various determinations. These errors are largest when the fraction of exchange

sites occupied by each cation is less than 0.3, larger than 0.7. The reproducibility of some K_D determination is shown in Table II, where the capacity fractions are 0.4–0.6. As a rule, the K_D values reported in this paper are reproducible to at least $\pm 5\%$; this represents the upper limit of the error which can result from analytical errors.

TABLE II
*Reproducibility of Duplicate K_D Determinations by Shaking Technique
for Potassium-Tetramethylammonium System*
Ionic strength = 0.01

Resin, DVB	(X_{K^+})	K_D
2	0.44	0.84
2	0.44	0.84
8	0.50	2.54
8	0.51	2.49
17	0.60	7.43
17	0.61	7.45

X_{K^+} is the fraction of exchange sites occupied by the potassium ion in the resin phase.

Most of the experiments involving the alkali metal cations only were carried out using the column technique, while those involving the quaternary ammonium ions used the shaking technique. When both techniques were applied to the same system, the calculated K_D values were the same within experimental error.

The chloride, bromide or iodide salts were always used, unless stated otherwise.

EXPERIMENTAL RESULTS

Most selectivity coefficient measurements were made using potassium as the reference cation. Since the K_D value is usually a function of X_{K^+} , the fraction of exchange sites occupied by the potassium ion, that value is also given. In every case, unless stated otherwise, the ionic strength of the external, equilibrating solution was 0.01.

Selectivity coefficients for various cations, including lithium, sodium, hydrogen, ammonium, tetramethylammonium (Me_4N^+), tetraethylammonium (Et_4N^+), tetra *n*-butylammonium (Bu_4N^+) and trimethylphenylammonium (Me_3PhN^+), measured against potassium with the various DVB resins, are shown in Table III. In Table IV, the effect of the ionic composition of the resin phase upon the selectivity coefficient is shown.

Table V shows that the selectivity coefficient is not a function of the initial state of the system, i.e., that no hysteresis effects are observed. In

TABLE III

Selectivity Coefficients for Various Cations Measured against Potassium with DVB Resins

DVB Resin	Li ⁺		Na ⁺		H ⁺		NH ₄ ⁺		Me ₄ N ⁺		Et ₄ N ⁺		Bu ₄ N ⁺		Me ₃ PhN ⁺	
	X' _K ⁺	K _D	X' _K ⁺	K _D	X' _K ⁺	K _D	X' _K ⁺	K _D	X' _K ⁺	K _D	X' _K ⁺	K _D	X' _K ⁺	K _D	X' _K ⁺	K _D
0.4	0.50	0.96	0.50	1.03	0.55	1.21	0.41	0.69	0.50	0.58	0.44	0.48				
2	0.43	1.38	0.50	1.16	0.60	1.48	0.47	0.90	0.44	0.84	0.47	0.61	0.58	0.40	0.44	0.31
4	0.68	2.10	0.50	1.20	0.61	1.57			0.42	1.06	0.42	1.10				
6	0.48	2.08							0.45	1.67	0.50	2.07				
8	0.74	2.66	0.58	1.60	0.65	1.91	0.52	1.10	0.51	2.52	0.61	4.58	0.60	4.19	0.37	0.78
10	0.52	2.76			0.52	2.29			0.56	3.53	0.51	6.45				
13	0.74	2.64	0.61	1.86	0.70	2.24	0.54	1.19	0.55	4.66	0.60	9.01				
15									0.57	7.03						
17	0.72	2.46			0.71	2.41			0.61	7.44	0.63	11.0	0.65	21.4	0.53	4.17
23	0.57	2.57	0.65	2.24	0.64	1.82			0.62	9.64	0.63	13.6				
26	0.43	0.73	0.56	1.51	0.61	1.55	0.50	1.00	0.64	10.72						
36			0.53	1.34					0.63	11.36						

each case the resin was placed in the initial state with one of the two cations, shaken with a solution of the other, and the K_D value determined. The K_D value is shown to be the same, within experimental error, regardless of the direction from which the equilibrium state was approached. This is shown for four different DVB resins.

TABLE IV

Selectivity Coefficient as a Function of Fraction of Exchange Capacity in Potassium State

DVB Resin	Li ⁺		NH ₄ ⁺		Me ₄ N ⁺		Et ₄ N ⁺		H ⁺	
	X' _K ⁺	K _D	X' _K ⁺	K _D	X' _K ⁺	K _D	X' _K ⁺	K _D	X' _K ⁺	K _D
0.4			0.22	0.81	0.21	0.65	0.20	0.64		
0.4			0.41	0.69	0.50	0.58	0.44	0.48		
0.4			0.63	0.58	0.72	0.41	0.69	0.24		
2			0.25	1.02	0.24	0.92	0.23	0.77		
2					0.44	0.84				
2			0.47	0.90	0.51	0.69	0.47	0.61		
2			0.72	0.88	0.65	0.35	0.70	0.21		
6	0.43	2.12								
6	0.48	2.08								
6	0.53	1.93								
10					0.31	4.52	0.40	8.26		
10					0.54	3.91	0.51	6.45		
10					0.56	3.53				
10					0.72	2.74	0.71	2.39		
23	0.44	3.05			0.32	18.9				
23	0.57	2.57			0.54	13.6			0.52	2.29
23					0.62	9.64				
23	0.66	1.82			0.72	7.75			0.64	1.82

TABLE V
Comparison of Selectivity Coefficients Determined from
Different Initial States

DVB Resin	Initial state	X'_{K^+}	K_D
6	Et_4N^+	0.50	1.97
6	K^+	0.50	2.07
10	Et_4N^+	0.53	5.94
10	K^+	0.51	6.45
13	NH_4^+	0.54	1.16
13	K^+	0.54	1.19
26	NH_4^+	0.51	1.00
26	K^+	0.50	1.00

TABLE VI
Selectivity Coefficients for Potassium-Hydrogen and Potassium-Lithium
Systems at Varying Ionic Strengths

External solution				
Resin	Total ionic strength	X_{KCl}	X'_{K^+}	K_D
DVB		Potassium-Hydrogen		
2	1.0	0.453	0.41	0.98
	0.1		0.46	1.02
	0.01		0.44	0.96
	0.001		0.48	1.10
10	1.0	0.318	0.45	1.81
	0.1		0.49	2.03
	0.01		0.52	2.29
	0.001		0.50	2.19
23	1.0	0.355	0.47	1.63
	0.1		0.55	2.19
	0.01		0.52	2.29
	0.001		0.54	2.11
		Potassium-Lithium		
2	1.0	0.354	0.42	1.31
	0.1		0.42	1.30
	0.01		0.43	1.38
	0.001		0.44	1.42
10	1.0	0.374	0.47	2.40
	0.1		0.49	2.58
	0.01		0.52	2.76
	0.001		0.50	2.68
23	1.0	0.344	0.59	2.68
	0.1		0.56	2.41
	0.01		0.57	2.57
	0.001		0.58	2.64

TABLE VII
Selectivity Coefficients as a Function of Temperature

System	Resin, DVB	Temperature, °C.							
		5		25		40		60	
		X'_{K^+}	K_D	X'_{K^+}	K_D	X'_{K^+}	K_D	X'_{K^+}	K_D
K^+-H^+	2	0.60	2.61	0.60	1.48	0.41	1.09	0.45	0.82
	13	0.54	2.86	0.70	2.24	0.37	1.82	0.45	1.60
	23	0.55	3.21	0.64	1.82	0.48	1.65	0.50	1.25
K^+-Li^+	2	0.68	3.79	0.65	1.82	0.45	1.13	0.50	0.92
	13	0.55	4.15	0.74	2.64	0.45	2.27	0.42	1.41
	23	0.70	5.67	0.57	2.57	0.54	2.17	0.56	1.88
H^+-Li^+	2	0.47*	0.98	0.47*	0.99	0.49*	0.77	0.51*	0.75
	13	0.45*	1.20	0.53*	1.23			0.51*	1.20
	23	0.46*	0.97	0.45*	1.04	0.42*	1.05	0.51*	1.03
$K^+-Me_4N^+$	2	0.48	0.82	0.44	0.84			0.49	0.60
	13	0.48	4.85	0.55	4.66			0.46	3.69
	23	0.54	12.64	0.62	9.64			0.52	9.09

* X'_{H^+} for these.

In Table VI are shown results of K_D determinations in which the ionic strength of the equilibrating solution was varied from 0.001 to 1.0. The total ionic strength of the solution is given, together with the molar

TABLE VIII
Selectivity Coefficients with Various Pairs of Ions

Ions (1) (2)	Resin DVB	X_1 Experimental	K_D
H^+-Li^+	2	0.47	0.99
H^+-Li^+	8	0.59	1.42
H^+-Li^+	13	0.53	1.23
H^+-Li^+	23	0.45	1.04
$H^+-Me_4N^+$	8	0.53	1.45
Na^+-H^+	8	0.59	1.40
Na^+-Li^+	8	0.66	1.85
$Na^+-NH_4^+$	8	0.40	0.66
$Na^+-Me_4N^+$	8	0.46	1.25
$Li^+-Me_4N^+$	0.4	0.51	0.73
$Li^+-Me_4N^+$	4	0.53	0.48
$Li^+-Me_4N^+$	6	0.54	0.74
$Li^+-Me_4N^+$	8	0.45	1.07
$Li^+-Me_4N^+$	10	0.56	1.64
$Li^+-Me_4N^+$	13	0.62	1.81

TABLE IX
Selectivity Coefficients for Phenolic and Glauconite Exchange Systems

Ion system	X ⁺ K ⁺	K _D
Phenolic Resin		
K ⁺ -Li ⁺	0.60	1.34
K ⁺ -Na ⁺	0.57	1.18
K ⁺ -NH ₄ ⁺	0.54	0.99
K ⁺ -Me ₄ N ⁺	0.32	0.25
K ⁺ -Et ₄ N ⁺	0.58	0.10
K ⁺ -Bu ₄ N ⁺	0.54	0.048
K ⁺ -Me ₃ PhN ⁺	0.26	0.041
Glauconite		
K ⁺ -Li ⁺	0.72	1.96
K ⁺ -Na ⁺	0.56	1.65
K ⁺ -NH ₄ ⁺	0.57	0.89

fraction of the electrolyte which was potassium chloride (X_{KCl}). Selectivity coefficients determined at different temperatures, 5, 25, 40 and 60°C., are shown in Table VII. In the previous tables, the potassium ion was used as a reference cation. K_D values determined for a number of other pairs of ions is shown in Table VIII. In Table IX selectivity coefficients for the Phenolic and Glauconite exchangers are shown.

DISCUSSION

The general thermodynamic expression for the equilibrium constant K_m , which applies to ion exchange processes in dilute solution is (7, 8, 11),

$$RT \ln \left[\left(\frac{m_1}{m_2} \right)_i \left(\frac{\gamma_1}{\gamma_2} \right)_i \left(\frac{a_2}{a_1} \right)_0 \left(\frac{a_{wi}}{a_{w0}} \right)^g \right] = \pi(\bar{V}_2 - \bar{V}_1 - g\bar{V}_w),$$

where m is the molality, γ the ion activity coefficient, and a the activity in the resin (i) and external solution (0) phases, respectively, π the thermodynamic osmotic pressure, g the number of moles of solvent involved in the exchange reaction, \bar{V} the partial molar volumes of the exchange ions in the resin phase, and the subscripts 1, 2 and w refer to the two cationic species and the solvent, respectively. For purposes of simplification in a qualitative discussion, this expression can be reduced to (7, 8),

$$RT \ln \left[K'_2 \left(\frac{\gamma_1}{\gamma_2} \right)_i \right] = \pi(v_2 - v_1)_i,$$

where v_2 and v_1 are the hydrated molar volumes of the exchange cations. A previous paper in this series described some of the relationships between the π , γ_i and v_i values. The qualitative correlation between K_D and these parameters is discussed here.

From the latter equation, it is evident that the selectivity coefficient is determined by either the ionic activity coefficient ratio in the resin

phase $(\gamma_1/\gamma_2)_i$, or by π , or by the difference in hydrated ionic volumes $(v_2 - v_1)_i$, or by any combination of these effects. If π is small, then $(v_2 - v_1)_i$ effects are of no consequence and K_D is determined solely by

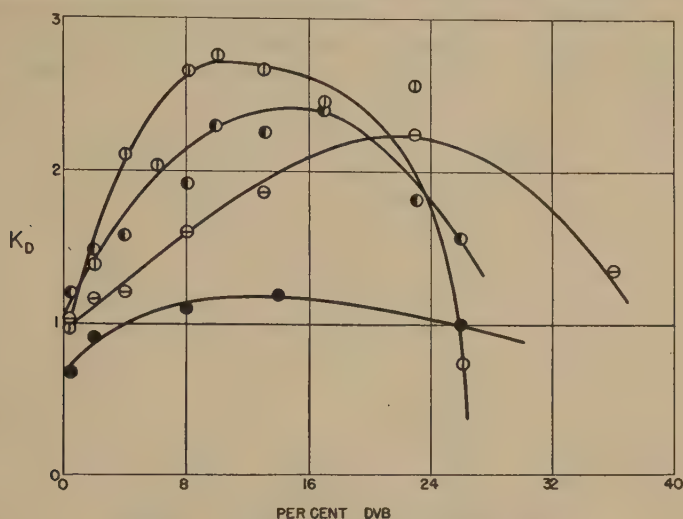


Fig. 1. Selectivity coefficients measured against potassium with various DVB resins. Cations are: \bullet , ammonium; \ominus , sodium; \bullet , hydrogen; \oplus , lithium.

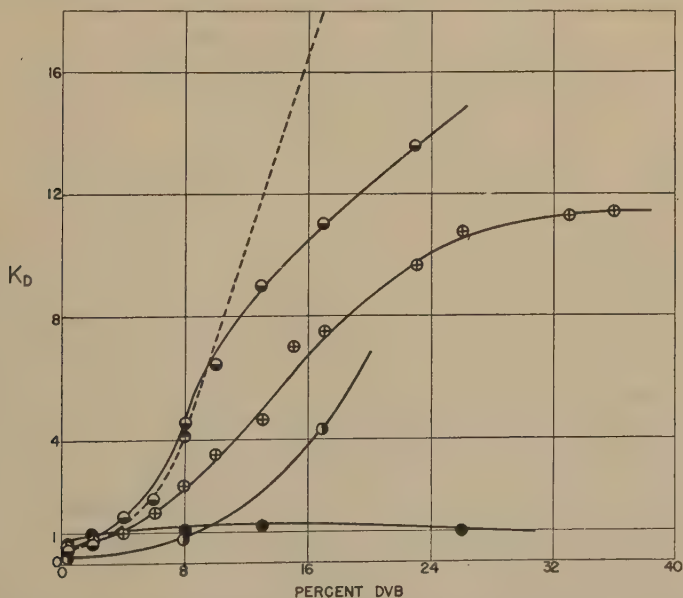


Fig. 2. Selectivity coefficients measured against potassium with various DVB resins. Cations are: \bullet , ammonium; \bullet , trimethylphenylammonium; \oplus , tetramethylammonium; \ominus , tetraethylammonium; \bullet , tetraethylammonium.

$(\gamma_1/\gamma_2)_i$. This would be the case for resins of very low degrees of cross-linking, which are very soft gels. If π is of appreciable magnitude, then at constant values of $(\gamma_1/\gamma_2)_i$ and $(v_2 - v_1)_i$ K_D will increase with π . If $v_2 = v_1$, then the right hand side of the expression is zero, and K_D again is determined by $(\gamma_1/\gamma_2)_i$. Thus K_D may be determined by ion activity effects, by differences in hydrated volumes, and by thermodynamic osmotic pressures.

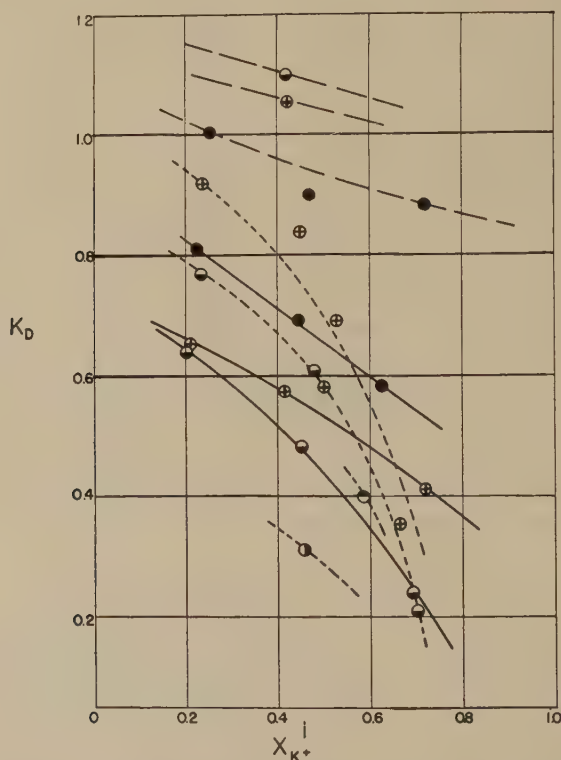


FIG. 3. Selectivity coefficients as a function of the fraction of exchange sites occupied by the potassium ion. Resins are: —, DVB 6; ----, DVB 2; —○—, DVB 0.4. Cations are: ○, tetraethylammonium; ⊕, tetramethylammonium; ●, ammonium; —○, tetrabutylammonium; ●, trimethylphenylammonium.

Selectivity coefficients for the alkali metal and ammonium ions, measured against potassium at $X_{K^+} = 0.4 - 0.7$, are plotted in Fig. 1; comparable values for the quaternary ammonium ions are shown in Fig. 2. The influence of variations of X_{K^+} upon K_D is shown graphically in Fig. 3 for the low DVB resins, in Fig. 4 for the higher DVB resins. These data are from Tables VII and VIII. For the inorganic and ammonium ions, K_D is approximately unity for DVB 0.4; K_D then increases sharply

for the alkali metal ions, reaches a maximum in the DVB range of 9 to 20, and then decreases as the degree of cross-linking continues to increase.

This behavior can be interpreted by considering the thermodynamic expression. As the percentage of the cross-linking agent approaches zero, K_D approaches unity. Since π is very low for these resins, $(\gamma_1/\gamma_2)_i$ is approximately unity. As π increases and if $(\gamma_1/\gamma_2)_i$ remains equal to unity, the pressure-volume effect will make for an increase in K_D , the extent of increase being determined by the volumes of the ions. At the very high

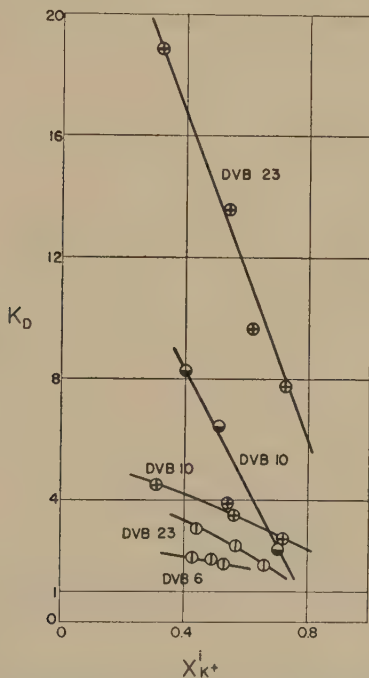


FIG. 4. Selectivity coefficients as a function of the fraction of exchange sites occupied by the potassium ion. Cations are: \oplus , tetramethylammonium; \ominus , tetraethylammonium; \odot , lithium.

molalities which exist in the higher DVB resins (~ 10 molal), a decrease in hydration is encountered. This "stripping of hydration layer" effect is undoubtedly proportional to the extent of hydration. This is indicated by the fact that the down-turn of K_D values occurs at lower DVB values and to a greater extent with lithium than with sodium. The behavior of the hydrogen and sodium ions is consistent with this picture. With DVB 26 resin, the hydrated lithium ion appears to be actually smaller than the hydrated potassium ion. Thus K_D decreases even though π is increasing, because $(v_2 - v_1)_i$ is decreasing in value.

While all of these observed effects could be due entirely to $(\gamma_1/\gamma_2)_i$ effects, with pressure-volume effects playing no role at all, this does not seem probable. First, the swelling pressures generated by these resins are clearly demonstrable (3, 6, 8, 20) and can be calculated from vapor pressure data (8, 13). Second, in solutions of mixed electrolytes, ionic activity coefficients are determined by all of the components (16). Also, in a concentrated solution of two electrolytes having a common anion, the cationic activity coefficients are approximately the same. This is also predicted by the Bjerrum, Harned, Stokes-Robinson theory, which assumes that n moles of water are "bound" to each mole of electrolyte present, and ex-

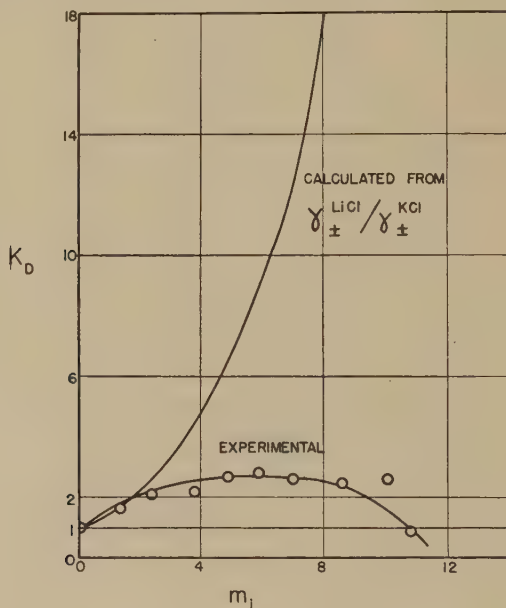


FIG. 5. Selectivity coefficient for potassium-lithium exchange, calculated from activity coefficients of the chloride salts, compared with experimental K_D values as functions of the molality in the resin phase.

presses activity coefficients in terms of effective concentrations. This postulate readily leads to the conclusion that in mixtures of uni-univalent electrolytes, the sole source of differences in activity coefficients lies in differences in Debye-Hückel effects. These latter effects make for minor differences in activity coefficients, of the order of 10 or 20% even under extreme conditions (11).

Another reason for not ascribing K_D effects as being due primarily to $(\gamma_1/\gamma_2)_i$ effects can be seen from the data. Various authors (1, 2, 19) have pointed out that the sequence of K_D values for the alkali metals follows the sequence of mean activity coefficients for the alkali halides.

If K_D values were determined solely by these activity coefficient ratios, it would be predicted, *e.g.*, the case of potassium-lithium exchange, that K_D will rise with the molality of the resin phase. This calculation is shown in Fig. 5, where the function

$$K_m = \left[\frac{m_{K^+} \cdot \gamma_{K^+}}{m_{Li^+} \cdot \gamma_{Li^+}} \right]_i \left[\frac{a_{Li^+}}{a_{K^+}} \right]_0$$

is set equal to unity as required by Donnan considerations in the absence of pressure-volume effects. If $\gamma_{K^+}^i$ is set equal to γ_{\pm}^{KCl} at the same molality (11), and $\gamma_{Li^+}^i = \gamma_{\pm}^{LiCl}$, then $K_D = \gamma_{\pm}^{LiCl} / \gamma_{\pm}^{KCl}$. It is seen that the curve calculated on this basis bears no relationship to experimental values.

The relationship between K_D values and the Debye-Hückel parameter a^0 , and also the Stokes-Robinson n value, have been noted (2, 19). It has been suggested that ion-pair formation is primarily responsible for the K_D values. This does not seem reasonable. First, while the quaternary ammonium ions have low n values, they behave like the large lithium ion rather than like the smaller potassium ion, as will be shown. Also, Heymann (18) has shown that the equivalent conductance of the alkali metal ions in the resin phase is directly proportional to the ionic conductance in solution. This is evidence against ion-pair formation. All of these results and observations appear to be consistent with the Bjerrum, Harned, Stokes-Robinson theory, and a consideration of pressure-volume effects.

The data to be considered next on the ammonium ions, and on the temperature effect to be discussed later, both lend support to the concept that in the absence of interaction between movable cations and fixed anionic groups, the $\pi (v_2 - v_1)_i$ effect primarily determines the selectivity coefficient.

The effect of varying the fraction of exchange positions occupied by the potassium ion upon K_D can be seen from Table IV and Fig. 4. As $X_{K^+}^i$ increases, K_D decreases. This may be due to either (or both) of two effects. Either there is a change in the $(\gamma_1/\gamma_2)_i$ ratio as $X_{K^+}^i$ varies, or else as the resin goes from the swelled lithium state to the relatively relaxed potassium state, π decreases and thus K_D will decrease at constant $(v_2 - v_1)_i$. Similar results are reported by other authors (11). The magnitude of this effect suggests that it is due to changes in π rather than $(\gamma_1/\gamma_2)_i$ for the alkali metal cations.

The behavior of the hydrogen ion appears to be anomalous in ion exchange systems as it is in aqueous solutions. In particular, K_C^H values appear to vary considerably with $X_{H^+}^i$, in a manner as to suggest that the $(\gamma_1/\gamma_2)_i$ ratios are responsible (4, 5, 15, 16). The anomalies appear greatest at very low and very high $X_{H^+}^i$ values. Determinations of K_D values for other pairs of ions at high and low X^i values are not available, largely due to experimental difficulties. The unavailability of these data is

unfortunate; the fact that the V_e vs. X^i curves are normal (11) indicates that $(\gamma_1/\gamma_2)_i$ effects alone must be responsible for any anomalies which may occur.

The behavior of the ammonium ion is best discussed with that of the quaternary ammonium ions. At low DVB values, Fig. 2 shows that these ions are preferred over potassium, but as the degree of cross-linking increases, a sharp and continual rise in K_D results. These results are readily interpreted as the result of interaction between the resin and the organic ions.

The resins possess a polystyrene matrix, and as such adsorption of organic ions upon the matrix is likely. The adsorption of organic molecules and ions upon various resins has been observed (10, 14, 17, 21, 23). The results shown in Figs. 2, 3, and 4 are consistent with adsorption phenomena. As the molecular weight of the ion increases, the adsorptive effect increases according to Traube's rule. As $X^{i_{K^+}}$ increases or as the concentration of the organic ion decreases, the adsorptive effect increases, as is the case in adsorption isotherms. This increase in adsorption with the dilution of the organic ion appears to become somewhat greater as the degree of cross-linking increases. This may be the result of stronger adsorption as the hydrocarbon chains get closer together.

Also, as the polarity of the resin decreases this adsorption effect increases, for the resin becomes a better hydrocarbon adsorbent. The polarity of the resin is a function of its capacity, as will be discussed later.

These adsorptive effects are not the result of molecular adsorption of salts of the organic ion, or of hydrolytic adsorption. The resin capacity is exactly equal to the number of fixed anionic groups, and in no case has an excess capacity been observed (9). The adsorptive effect can be expressed thermodynamically as a lowering of the activity coefficient of the adsorbed ion; in this case the ratio $(\gamma_1/\gamma_2)_i$ is greater than unity, and increases as $X^{i_{K^+}}$ increases.

Thus in the case of the quaternary ammonium ions, as shown in Fig. 2, the pressure-volume effect is opposed to the adsorption effect. At low degrees of cross-linking, adsorption predominates. At higher degrees of cross-linking, the pressure-volume effect overcomes this adsorption effect and results in a preferential uptake of the potassium ion. With the tetrabutylammonium ion, K_D increases by almost two orders of magnitude with a reversal in sign as the mechanical properties of the resin vary from DVB 0.4 to DVB 17.

The behavior of the trimethylphenylammonium ion is of particular interest. Because of its aromatic character and the aromatic character of the matrix, the adsorptive effects are particularly strong. While the cross-over point ($K_D = 1$) occurs at about DVB 3 for the aliphatic ions,

the pressure-volume effect does not compensate for the adsorptive effect with this aromatic ion until DVB 9.

The influence of changes in the ionic strength of the external, equilibrating solution upon K_D is shown in Table VII. Here the potassium-hydrogen and potassium-lithium systems were studied at $X_{K^+}^i = 0.4-0.6$, for resins DVB 2, 10, and 23. When $\mu = 0.1, 0.01$ or 0.001 , K_D is the same within experimental error. Since π and $(v_2 - v_1)_i$ are the same in all cases, it must be concluded that $(\gamma_1/\gamma_2)_i$ is also the same. It does not follow that the individual γ_i values are constant; in fact, these values appear to decrease as μ decreases (11). When $\mu = 1$, π is decreased by the counter-osmotic pressure (8, 11), and changes in the other parameters may occur.

The temperature effect described in Table VII is illuminating. Four sets of ion-pairs were selected, two of the relatively unhydrated potassium ion with the heavily hydrated lithium and hydrogen ions, one composed of these heavily hydrated ions together, and one of the potassium ion with the unhydrated tetramethylammonium ion. From Table VII it is readily observed that K_D decreases with increase in temperature when the two cations are hydrated to a markedly different extent, and that K_D is fairly independent of the temperature when the ions are either not hydrated, or where they are hydrated to the same extent.

While $K_D \left(\frac{\gamma_1}{\gamma_2} \right)_i$ is different from the true equilibrium constant K_m , the two differ only in a \bar{V}_w term. This latter term does not change markedly with temperature, as has been observed by Gregor, Collins and Pope (14). Thus as an approximation the two expressions can be used interchangeably as regards temperature effects. In the case of alkali metal cations, the ratio $(\gamma_1/\gamma_2)_i$ will be fairly constant at different temperatures, for it is defined largely by the Debye-Hückel terms (16). In the case of the quaternary ammonium ions, it might be anticipated that adsorption would decrease with rising temperature, and that K_D would correspondingly increase. This is not verified by experiment; rather, K_D is singularly constant.

For purposes of a qualitative comparison the following expressions can be written,

$$\log K_D = \frac{\pi(v_2 - v_1)_i}{2.3 RT} = A(v_2 - v_1)_i = -\frac{\Delta H}{RT} + C.$$

Since π is directly proportional to T , the substitution of the constant A (a different A for each DVB resin) is made. In Fig. 6 the data of Table VII is shown graphically. In order to condense the graph and show differences in K_D values with temperature, the logarithm of the relative K_D value (K_D/K_D°) , where K_D° is the value at 25°C . for the resin in question,

is used. Also, relative K_D values are plotted without distinguishing between the various DVB resins, because the temperature effect is approximately the same for each resin with a particular set of ions. While there is some scatter of points, probably due in part to the increased experimental difficulties at low and high temperatures, the effects shown are quite consistent.

In the case of potassium-tetramethylammonium exchange, the slope is approximately zero as expected, because v for the tetramethylammonium ion is constant, and potassium is but slightly hydrated. The experimental fact that the volume of the particles does not change significantly

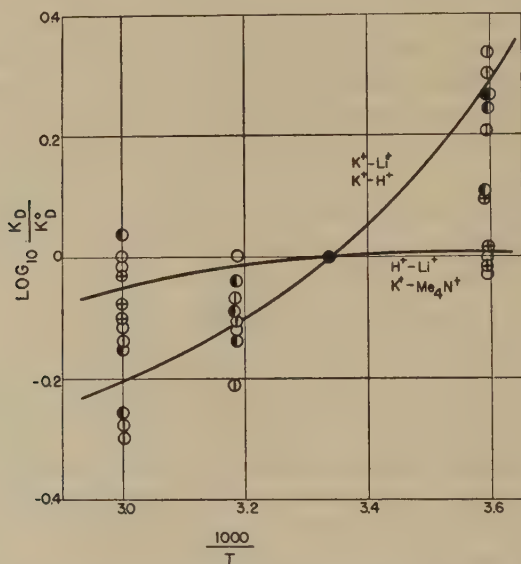


FIG. 6. Effect of temperature upon K_D . Cation pairs are: \circ , lithium and potassium; \bullet , hydrogen and potassium; \oplus , tetramethylammonium and potassium; \circ , hydrogen and lithium.

with temperature (14) is also a case in point. The heat of the exchange reaction ΔH is very low.

In the case of potassium-lithium and potassium-hydrogen exchange, the positive slope which increases with $\frac{1}{T}$ is interpreted as an increase in the value of $(v_2 - v_{K^+})_i$ as the temperature decreases, or conversely as a decrease in $(v_2 - v_{K^+})_i$ as T increases. Since the extent of hydration decreases as the kinetic energy of the solvent dipoles increases with temperature, it can be concluded that the (hydrated) lithium and hydrogen ions become smaller at elevated temperatures, and to the same extent in

both cases. This is consistent with the hypothesis that K_D in these cases is a function of the v 's and π rather than the γ_i values.

Thus ΔH has negative value for the exchange reaction $\text{Li}_i^+ + \text{K}_0^+ = \text{Li}_0^+ + \text{K}_i^+$. Since the lithium ion is leaving the resin phase where it is not strongly hydrated, and enters the external, dilute solution where it interacts with the water dipoles, the negative ΔH value of significant

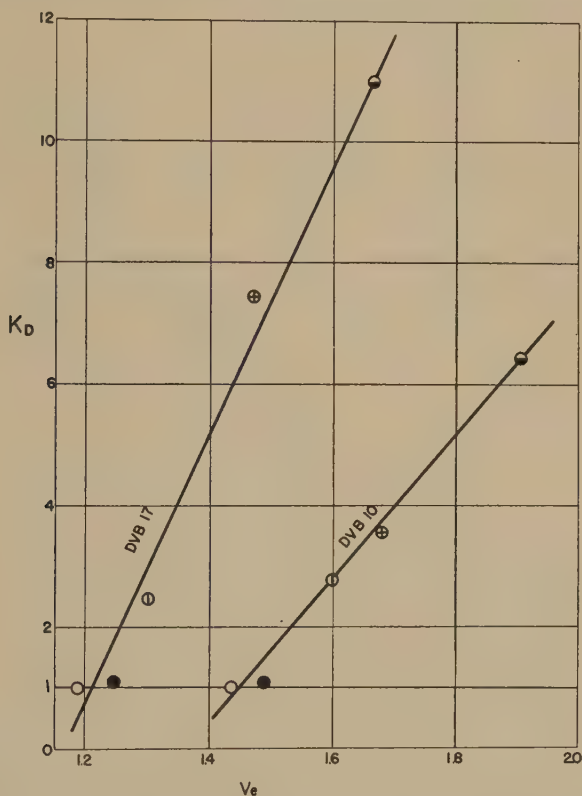


FIG. 7. Selectivity coefficients measured against potassium as a function of specific resin volume for: ○, potassium; ●, ammonium; ⊙, lithium; +, tetramethylammonium; ◐, tetraethylammonium.

magnitude is as expected. While the potassium ion loses water of hydration as it enters the resin phase, this process occurs to a considerably lesser extent, and the concomitant thermal effect is small compared to that for lithium.

With hydrogen-lithium exchange, v_2 and v_1 appear to decrease in the same manner and to the same extent with temperature; the constancy of K_D and the low value of ΔH are as expected, and are consistent with other data (19).

The relationship between the specific external volume (V_e) of an exchange resin with the thermodynamic properties of the exchange cation have been discussed previously (11). In general, for the same resin, V_e will be the same for all cations having the same (hydrated) ionic volume, in the absence of interaction between the movable ions and the resin itself. Where adsorption takes place, V_e is determined by both the ionic volume and the ion activity coefficient.

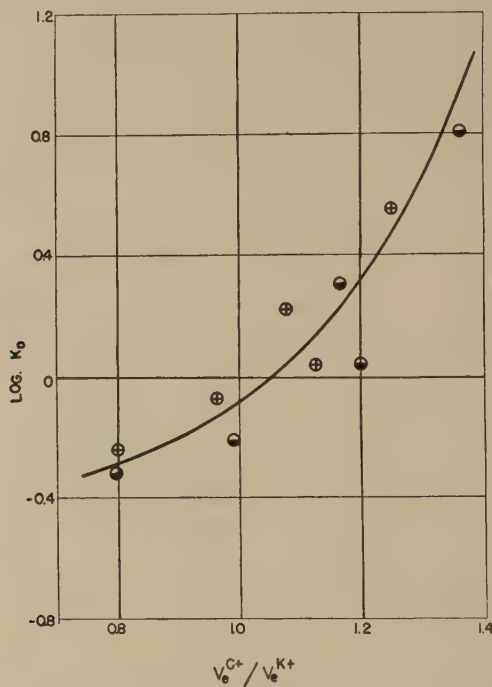


FIG. 8. Selectivity coefficients measured against potassium as a function of relative specific resin volume for the tetramethylammonium (\oplus) and tetraethylammonium (\odot) ions.

Two experimental results are thus predicted: The first is that the resin will select that ion which corresponds to a smaller value of V_e , and second, K_D and V_e should vary in a linear manner with the fraction of exchange positions occupied by a particular ion. An experimental verification of the latter prediction has already been given. In Fig. 7, K_D values for exchange with the potassium ion with two different resins are shown plotted against the V_e values for the corresponding cation. The proportionality between the two parameters is good.

In the case of lower DVB resins, a logarithmic plot of K_D is made against the ratio of the V_e value for the exchange cation to that for

potassium, $V_e^{C^+}/V_e^{K^+}$. The logarithmic plot is used because the K_D values are both greater and less than unity, and the use of the ratio of V_e values makes possible a simultaneous comparison of several different resins. This plot given in Fig. 8, shows that when $V_e^{C^+}$ is smaller than $V_e^{K^+}$, that the C^+ ion is preferred; when $V_e^{K^+} > V_e^{C^+}$, the selectivity coefficient is in favor of potassium. This selectivity rule obtains in most ion exchange reactions. Some exceptions are observed where one of the two ions is very large, so large that it makes for a large V_e value in spite of a low γ_i value (10). This effect is discussed in a later section.

Almost all of the discussion thus far deals with exchange of one cation for the potassium ion. The question now arises whether it is possible to predict K_D values for two ions from K_D values obtained with each of those ions and a third reference ion. The preceding discussion has indicated that for a particular resin, the v values appear to be constant, but that π and $(\gamma_1/\gamma_2)_i$ may vary with the $X_{C^+}^i$ value. Consider exchange processes between two sets of ions, 1, 2 and 1, 3. Let the thermodynamic quantities for the former process be designated by primes ($'$), for the latter by double primes ($''$). Then

$$RT \ln \left[K_2^1 \left(\frac{\gamma_1}{\gamma_2} \right)_i' \right] = \pi'(v_2 - v_1),$$

and

$$RT \ln \left[K_3^1 \left(\frac{\gamma_1}{\gamma_3} \right)_i'' \right] = \pi''(v_3 - v_1).$$

Here the K_2^1 and K_3^1 values are determined by the γ and π values corresponding to each system. If one equation is subtracted from the other,

$$RT \ln \left[\frac{K_2^1}{K_3^1} \left(\frac{\gamma_{3''}}{\gamma_{2'}} \right)_i \left(\frac{\gamma_{1'}}{\gamma_{1''}} \right)_i \right] = \pi'(v_2 - v_1) - \pi''(v_3 - v_1),$$

it is seen that the K_2^1/K_3^1 ratio will be equal to K_3^2 only if

$$\gamma_{1'} = \gamma_{1''}, \gamma_{3''}/\gamma_{2'} = (\gamma_3/\gamma_2)''', \text{ and } \pi' = \pi'' = \pi'''.$$

Therefore two K_D values, corresponding to specific sets of γ and π values, cannot in theory be divided by one another to obtain a third K_D value. An exact solution requires that π and γ be expressed as a function of X_1^i , X_2^i , and X_3^i .

If it is assumed that the γ_i value for a specific ion in a resin is a function of only the $X_{C^+}^i$ value for that cation, then one can eliminate the γ_i problem by experimentally making all $X_{C^+}^i$ values approximately the same, such as 0.5. As regards π , two possibilities present themselves. The first is that for a specific resin, π does not change to a marked extent with $X_{C^+}^i$ (or V_e), this change being smaller than differences in π for different resins. Another is that since K_D is a function of V_e (or π), that K_D be

measured at the same V_e values. While this may be possible from an experimental point of view, the $X_{C^+}^i$ values would not remain at 0.5.

In Table VIII a series of K_D determinations made with various sets of cations not including potassium are compared with K_D values calculated from exchange with the potassium ion. The K_D values were taken at $X_{K^+}^i \cong 0.5$. The agreement between experimental and calculated values is good. This is shown in Table VIII and also in Figs. 9 and 10. In Fig. 9, K_D values for potassium-lithium and potassium-tetramethylammonium exchange with various resins are plotted. Here with low DVB resins tetra-

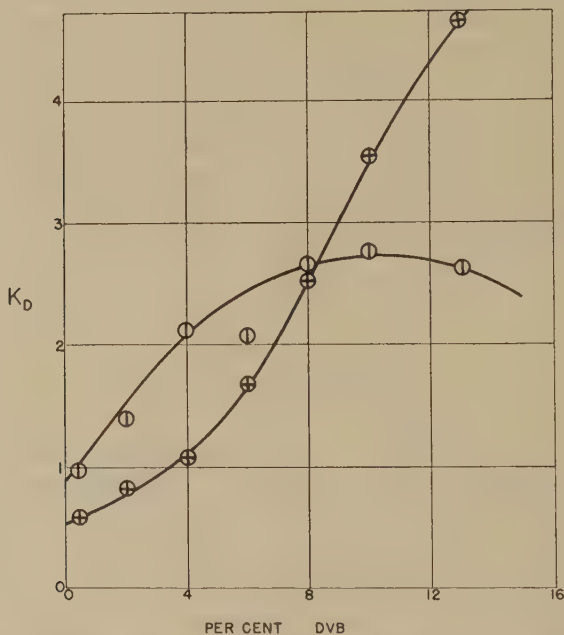


FIG. 9. Selectivity coefficients measured against potassium with various DVB resins. Cations are: ○, lithium; ⊕, tetramethylammonium.

methyammonium should be preferred over potassium, and at DVB 8 an inversion point should occur; above DVB 8, lithium should be preferred over tetramethylammonium. In Fig. 9 the calculated values are compared with those determined by direct experiment.

The good agreement indicates that the previous assumptions are valid. This calculation may not apply where two ions which are both highly adsorbed are compared with one another. In general, one can calculate selectivity coefficients for a pair of ions from values determined using a common reference ion.

Selectivity coefficients for the Phenolic and Glaucinite exchangers, shown in Table IX indicate that these exchangers behave as do the DVB

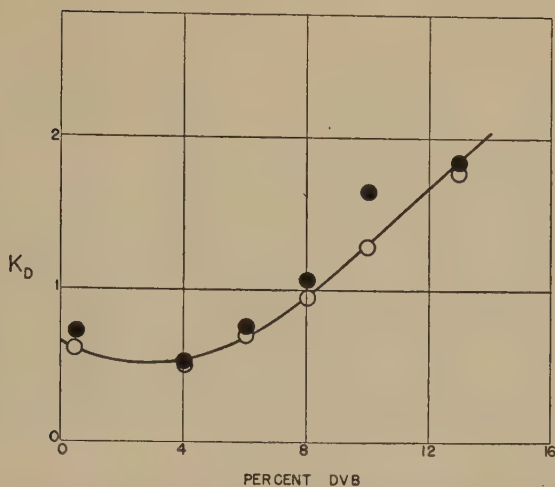


FIG. 10. Selectivity coefficient for lithium-tetramethylammonium exchange with various DVB resins. Experimental points, ●; calculated values from K_D values against potassium, ○—.

resins in the case of the alkali metal and ammonium cations. A plot of K_D against V_e is shown in Fig. 11 for the Phenolic exchanger. Similar results are observed with the Glaucanite exchanger. However, in the case of the

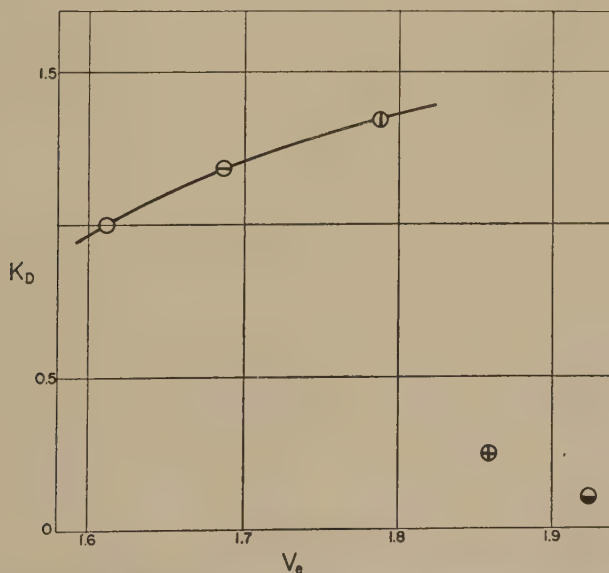


FIG. 11. Selectivity coefficients measured against potassium as a function of specific resin volume for: ○, potassium; ⊖, ammonium; ⊕, lithium; ⊕, tetramethylammonium; ⊖, tetraethylammonium.

quaternary ammonium ions, a marked difference appears. While the sequence of V_e values is as anticipated, the K_D values are less than unity, and decrease with increasing molecular weight. This effect is similar to that found for the low DVB resins, and can be ascribed to being the result of either low π values, or high $(\gamma_K^+/\gamma_C^+)_i$ values.

The role of the thermodynamic osmotic pressure can be ascertained by comparing K_D values for sodium and lithium with those of DVB resins. Resin DVB 2 has a K_D value of 1.38 for lithium and 1.16 for sodium. These agree closely with the corresponding values with the Phenolic resins, and point to the conclusion that the π values are comparable. In the case of the quaternary ammonium ions, however, the corresponding K_D values for the Phenolic resin and DVB 2 are: Me_4N^+ , 0.25 to 0.84; Et_4N^+ , 0.10 to 0.61; Bu_4N^+ , 0.048 to 0.40; Me_3PhN^+ , 0.041 to 0.31. Thus the ratio of K_D values ranges from 1:3 to 1:8 as the molecular weight increases.

This result can be explained by comparing the exchange capacities of the two resins. The "molecular weight" or average monomer weight for the Phenolic resin is 350 compared to 195 for DVB 2. Since the sulfonate group corresponds to 80 units, the hydrocarbon ratio in the matrix becomes 270:115. Thus it is entirely reasonable that the organic ions be adsorbed much more strongly upon the Phenolic resin.

The specific resin volumes (V_e) follow the sequence of increasing molecular weight, because the organic ions are so large as to correspond to an appreciable fraction of the resin volume. In addition, these organic ions may, as a result of the adsorption process, reduce the entropy of the polymer chains and make for an increase in V_e . This reinforcement of the adsorption effect through a lowering of the exchange capacity of the resin is utilized commercially in the preparation of highly adsorbent ion exchange resins.

This discussion has interpreted the experimental data in terms of a Gibbs-Donnan osmotic model (8). The apparent, reasonable agreement between the theoretical treatment and the results observed tempt one to conclude that the model is valid. However, the ion exchange phase, viewed from another point of view, is a water-salt of organic acid mixture, where the fraction of organic monomer units is large, even though the chains themselves have little or no translational degrees of freedom. Thus it is recognized that the treatment given in this paper rests upon a model which may not be a valid one. Only further experimentation can decide.

SUMMARY

1. The thermodynamic theory of ion-exchange processes predicts that the selectivity coefficient is determined by the ratio of the exchange ion activity coefficients in the resin phase, by differences in ionic volumes and by the thermodynamic osmotic pressure.

2. The variation in selectivity coefficient with ionic composition of the resin phase appears to be, in the case of the alkali metal cations, primarily a pressure-volume effect. In the case of the quaternary ammonium ions, ion activity variations, resulting from adsorption of the organic ions on the resin matrix, appear to oppose the pressure-volume effects.

3. The effects of temperature and concentration of the resin phase are consistent with the concept of ion hydration as it affects the pressure-volume term. The constancy of ionic activity ratios for the alkali metal cations is in accord with the Bjerrum, Harned, Stokes-Robinson theory.

4. The selectivity coefficients are not a function of the ionic strength of the equilibrative solutions. In the absence of adsorption effects, the smaller ion is preferred.

5. Selectivity coefficients for a pair of cations can be calculated from selectivity coefficient values for each of these ions with a third reference ion. This indicates that the thermodynamic osmotic pressure varies only slightly with different exchange cations for a given resin, and supports the view that the ionic activity coefficients are determined chiefly by the nature and concentration of the ion and not by interaction between the ions.

6. Adsorption effects of the quaternary ammonium ions are more pronounced in the case of low capacity resins, due to the larger ratio of organic to polar groups.

REFERENCES

1. BAUMAN, W. C., AND EICHHORN, J., *J. Am. Chem. Soc.* **69**, 2830 (1947).
2. BOYD, G. E., SCHUBERT, J., AND ADAMSON, A. W., *J. Am. Chem. Soc.* **69**, 2818 (1947).
3. BREITENBACH, J. W., AND KARLINGER, H., *Monatsh.* **80**, 312 (1949).
4. DUNCAN, J. F., AND LISTER, B. A. J., *J. Chem. Soc.* 3285 (1949).
5. DUNCAN, J. F., AND LISTER, B. A. J., *Faraday Discussion Soc.* No. 7, 4 (1949).
6. D'ALELIO, G. F., U. S. Patent 2,366,007., Dec. 26, 1944.
7. GREGOR, H. P., *J. Am. Chem. Soc.* **70**, 1293 (1948).
8. GREGOR, H. P., *J. Am. Chem. Soc.* **73**, 643 (1951).
9. GREGOR, H. P., *et al.* *J. Colloid Sci.* **6**, 20 (1951).
10. GREGOR, H. P., AND BELLE, J., in preparation.
11. GREGOR, H. P., GUTOFF, F., AND BREGMAN, J. I., *J. Colloid Sci.* **6**, 245 (1951).
12. GREGOR, H. P., HELD, K. M., AND BELLIN, J., *Anal. Chem.* **23**, 620 (1951).
13. GREGOR, H. P., AND HELD, K. M., in preparation.
14. GREGOR, H. P., POPE, M., AND COLLINS, F. C., *J. Colloid Sci.*, in press.
15. HALE, D. K., AND REICHENBERG, D., *Faraday Discussion Soc.* No. 7, 79 (1949).
16. HARNED, H. S., AND OWEN, B. B., *Physical Chemistry of Electrolytic Solutions*. Reinhold, New York, 1950.
17. HASKELL, R. C., AND HAMMETT, L. P., *J. Am. Chem. Soc.* **71**, 1284 (1949).
18. HEYMANN, E., AND O'DONNELL, I. J., *J. Colloid Sci.* **3**, 405 (1948).
19. KRESSMAN, T. R. E., AND KITCHENER, J. A., *J. Chem. Soc.* 1190 (1949).
20. KUHN, W., HARGITAY, B., KATCHALSKY, A., AND EISENBERG, H., *Nature* **165**, 514 (1950).
21. LEVESQUE, C. L., AND CRAIG, M., *Ind. Eng. Chem.* **40**, 96 (1948).
22. REICHENBERG, D., PEPPER, K. W. AND McCAULEY, D. J., *J. Chem. Soc.* 493 (1951).
23. SAMUELSON, O., *Ing. Vetenskaps Akad. Handl.* **179** (1944).

WATERPROOF ADHESIVES FOR CELLULOSE

Robert B. Dean

Department of Chemistry, University of Oregon, Eugene, Oregon

Received May 7, 1951

INTRODUCTION

The present work was undertaken in 1948 as a survey of commercial waterproof adhesives for plywood. To satisfy the tests of the Douglas Fir Plywood Association (D.F.P.A.), the glue line in a waterproof plywood must show at least 90% adhesion after two 4-hr. periods in boiling water separated by a 20-hr. drying period at 35°C.

There exist considerable differences of opinion concerning the mechanism of the gluing of wood. One school holds that mechanical penetration of the glue into the pores of the wood is largely responsible for adhesion. This point of view is reviewed in Refs. (1) and (2). A far more likely hypothesis is that specific adhesion between atoms in the glue and atoms in the wood is responsible for the major effects. Specific adhesive forces between any solid and any liquid which wets it and then solidifies were demonstrated by McBain and Lee (3). In spite of this fact, McBain concluded that mechanical penetration was largely responsible for the adhesion of protein glues to wood. Workers at the Forest Products Laboratory (4,5) did not agree with McBain's conclusions and held that specific adhesion is most important.

Tests of adhesion to flat cellulose surfaces in the form of regenerated cellulose film (cellophane) provide one answer to this question. The surface is smooth and offers no opportunities for mechanical penetration and interlocking. Many substances do adhere to cellophane by specific interatomic adhesion. McLaren (6) tested a large number of polymers and found that those which can form hydrogen bonds with cellulose adhere most strongly. Polyvinyl alcohol showed by far the best adhesion to dry cellophane. However, all the polymers tested by McLaren fail to stick to wet cellophane. In this paper it will be shown that waterproof plywood adhesives do form waterproof bonds with cellulose films and these bonds may even be strengthened by prolonged boiling. Evidence that true chemical bonds are formed between the adhesive and the cellulose will be presented.

EXPERIMENTAL PROCEDURE AND MATERIALS

The thermosetting phenolic adhesives used in this work were commercial resins containing 40-70% solid material. They were used as

shipped even though the final glue mixtures as recommended by the manufacturers did contain various quantities of wood flour or other filler as well as a little water. A number of commercial cold-setting adhesives obtained on the open market were used according to directions on the containers.

The extruded cellulose film, 0.004 cm. thick, was purchased as dialyzer tubing from a scientific supply house. It appeared to be identical with Visking tubing made for sausage casing. This form of cellulose is not treated with waterproofing agents and is as pure a form of regenerated cellulose as can be obtained commercially. For all the adhesion tests the tubing was slit open and the adhesive applied to the inner untouched surfaces. In this way interference by previously contaminated surfaces was believed to be eliminated. The pore diameter of this material is less than 10 Å. when wet with water as shown by diffusion tests. It will retard the free diffusion of sucrose and stop proteins. The pores in the dry film are even smaller.

In most of the work reported here the spread of the adhesive was automatically controlled in the following manner. The adhesive was placed in the fold between two inside surfaces of the cellophane tubing. A piece of 10-mesh iron wire gauze separated from the cellulose by one piece of scratch paper was pressed with the cellulose and the adhesive at 200 lb./in.² in a hot press. The resin flowed out to fill the small hollows produced by the meshes in the wire gauze so that the total area of the bond depended only on the initial volume of the resin. Although this method produces a uniform over-all spread of about 30 lb./1000 sq. ft., the thickness of the adhesive film varied from 0.2 mm. to extremely thin spots which were probably not more than a few microns thick as judged by their optical density. There was no definite evidence that these variations in thickness produced any significant variations in the adhesion.

Adhesion was tested by a crude stripping test which nevertheless showed up large differences between various adhesives. After treatment in the hot press the samples were soaked in water to plasticize the cellulose (dry samples fresh from the press were very brittle). Cold pressed samples were allowed to age at least 1 day. The glued sample was then cut into strips either 10 mm. or 3 mm. wide, depending on the expected strength of the adhesive. It was necessary to have a small unglued area at one end of each strip to start the stripping. After the stripping was started by hand the free ends of the cellophane strips were seized in small, parallel-jaw spring paper clips. One clip was hooked to a light-weight bucket and the other was held in one hand. Water was added to the bucket until the joint began to peel at a perceptible rate. The weight of the bucket and clip was then determined and recorded together with the width of the strip.

In many cases the cellulose film tore diagonally across the adhesive bond. In other cases a multitude of small tears led to immediate rupture of the cellulose film. When this happened a minimum stripping force was recorded.

RESULTS

The results of the stripping tests are recorded in Tables I and II. In general, except as noted, the cellulose appeared to peel away cleanly, indicating that the adhesion of the glue to the cellulose was less than the cohesion of the glue. The cellulose film usually peeled at an angle of 90° to the surface of the adhesive. In any stripping test the thickness and flexibility of the film that is being stripped off controls the true area of rupture and the stripping force. Thus it has been observed that stripping

TABLE I
Stripping Tests on Hot Pressed Adhesives
(Data in g./sq. cm.)

Resin ^a		Wet	Strength after boil tests
Phenol-formaldehyde-alkali	A	40-60	90-180
Phenol-formaldehyde-alkali	B	65	120
Phenol-formaldehyde-alkali	C	55	100
Phenol-formaldehyde-alkali	D	50	50
Phenol-formaldehyde-alkali	E	40-70	30
Phenol-formaldehyde-neutral	F	50	40-60
Melamine-formaldehyde powder	G	40	40
Resin A soaked in 8% NaOH		3	10 ^b
Resin A soaked in 50% NaOH		50 ^b	

^a Resins A-F were commercial plywood adhesives obtained in most cases from plywood mills in Oregon and Washington. It is known that most of the formulas in use at the time this work was done have been subsequently modified. Resin G is Melmac 401 obtained through the courtesy of the American Cyanamid Company.

^b Indicates failure of the cellophane.

forces are linearly proportional to the thickness of the stripped film. (7). In this work the stripped film was ordinarily the cellulose since it was more flexible than the adhesive. The flexibility of the cellulose film was also constant, at least in all experiments with wet bonds. The stripping force as recorded should therefore be proportional to the true adhesive strength of the bond. Even though the proportionality factor is not known, dimensional considerations show that it should vary inversely as the thickness of the film.

The results confirm earlier work which showed that ordinary adhesives do not stick to wet cellulose. The only materials which do adhere to wet cellulose are "thermosetting" resins which are cured in the bond either by the application of heat or catalysts. All of the adhesives tested

showed adhesion to dry cellulose at relative humidities of approximately 50%, confirming the work of McLaren (6) and others.

It is furthermore significant that some of the phenolic adhesives which have high free-alkali contents actually stick better to cellulose after treatment in boiling water than they do before such treatment. This effect is not due to under-cure since it is not produced by prolonged dry heat. Neither is it caused by the leaching of alkali since overnight soaking at room temperature did not increase the strength of the bond.

TABLE II

Stripping Tests on Cold Pressed Adhesives

(Data in g./sq. cm.)

	Dry	Wet	Boiled
Model airplane cement, Lepage's 21	0-5	0	0
Model airplane cement, Comet	0-5	0	0
Model airplane cement, Testor's	0-5	0	0
Rubber cement for paper, Carter's Synthetic	3	0	0
Black rubber adhesive, Miracle	30-100 ^c	0	0
Cellulose tape, Scotch	275	0	0
White "flexible" cement, Casco Flexible	30-40	0	0
Polyvinyl resin glue, Cascorez	500	0	0
Animal glue, Lepage's 10	133	0	0
Casein glue, Casco A ^a	110	0	0
Urea-formaldehyde, Weldwood ^a	275	10 ^c	0
Urea-formaldehyde, Cascamite ^a	260	23	0
Urea-formaldehyde, CascoRez #5 ^b	130	25	20
Resorcinol formaldehyde, Cascophen ^b	60	20	20
Resorcinol formaldehyde, Cascophen ^b RS 216	200	40-60	60

^a Dry adhesive mixed with water before use.

^b Liquid adhesive mixed with "catalyst" before use.

^c Glue fails, does not strip clean from cellophane.

DISCUSSION

In order that an adhesive stick to a smooth surface, bonds must be established between the atoms of the adhesive and the atoms on the surface. McBain and Lee (3) showed that any liquid which wets a surface and subsequently solidifies will adhere to the surface. The forces responsible are the van der Waals' forces including polarization forces and hydrogen bonds. Since all atoms have van der Waals' forces for all other atoms it is not surprising that Loughborough and Hass (8) found that ice would stick to all surfaces, including paraffin and polyethylene. The adhesion of any liquid to any solid is shown by the fact that contact angles of 180° are never observed.

The best adhesives for dry cellulose are those that form hydrogen bonds. McLaren (6) found that polyvinyl alcohol formed stronger ad-

hesive bonds than any other of the materials which he tested. The strengths he reported are comparable in magnitude with those reported in this work. However in the presence of free water even polyvinyl alcohol forms no bond with cellulose. The adhesion of polyvinyl alcohol to cellulose is the result of hydrogen bonds between the —OH groups on the polymer and —OH groups on the surface of the cellulose. This is the same type of bond which renders cellulose insoluble in water. Regenerated cellulose is insoluble only because the chains can fit together into a stable crystalline structure. Any interference with a crystalline structure, such as can be obtained by methylating one-third of the available —OH groups of cellulose, permits water to penetrate and makes the material water-soluble. No adhesive can be expected to have the highly specific structure necessary for it to fit into the crystal structure of regenerated cellulose. Therefore water should be able to replace all hydrogen bonds between cellulose and an adhesive.

The behavior of formaldehyde-linked adhesives on cellulose is different in kind from the behavior of other materials which form hydrogen bonds. Many of the polymers are hard and brittle and unable to follow the changes in dimensions of the cellulose on wetting; these are factors which ordinarily would not be favorable to good adhesion. All other compounds which form hydrogen bonds with cellulose fail to adhere in the presence of water. This includes compounds with —OH groups (polyvinyl alcohol), —COONa groups (carboxymethyl cellulose and proteins), —NH_2 , =NH and =C=O (protein glues). There seems to be no reason why the $\text{C}_6\text{H}_5\text{—OH}$ and $\text{C}_6\text{H}_5\text{—CH}_2\text{OH}$ groups of phenolic resins and $\text{N—CH}_2\text{OH}$ groups of urea and melamine resins should stick any better by hydrogen bonding than the other equally active hydrogen-bonding groups.

The fact that some phenolic resins form bonds which are strengthened by boiling in water suggests that new chemical bonds are being formed. The formation of these new bonds requires both heat and moisture (which softens the cellulose and permits adjustment of the reactive groups). It is highly probable that other formaldehyde-linked polymers also form true carbon-to-carbon or carbon-to-oxygen bonds with cellulose during the curing process. The high reactivity of formaldehyde condensation products is well known. In addition, cellulose itself is oxidized to reactive aldehydes by oxygen in the presence of alkalis (9). These aldehydes could react with the methylol groups of the polymer by the same mechanism that produced polymerization of the original resin. The covalent bonds formed by this reaction would be several times stronger than hydrogen bonds and would be completely resistant to water. The actual number of bonds formed would, however, be less than the number of hydrogen bonds formed with polyvinyl alcohol or similar polymers. The covalent bonds would be reinforced with hydrogen bonds between

—OH or —NH₂ groups on the polymer and hydroxyl groups on the cellulose.

The solvent action of aqueous sodium hydroxide on partially cured phenolic resins is well known. The effect is very apparent in the pH range where phenol dissociates as an acid (pH 11–14). The solvent effect of the NaOH is attributable to the formation of water-soluble phenolate anions on the polymer molecules which have not yet become completely cross-linked. These ions repel one another and the molecules separate and dissolve. Many phenoplasts are apparently not cured to the condition of a completely cross-linked network but stick together primarily through hydrogen bonds. They are, therefore, softened and even dissolved by concentrated alkaline solutions. However, a fully cured alkaline phenolic resin adhesive is not completely dissolved by strong alkaline solutions because it is cross-linked by true covalent carbon-to-carbon bonds. In the case of the phenoplasts, ionic repulsion aids the solution of phenoplast in an alkali. If the adhesion of a phenolic resin adhesive were entirely a matter of hydrogen bonding we should expect the bond to fail in strong alkali. Tests in cold 8% and 50% NaOH showed a bond strength comparable to that of the weakened cellulose (which is greatly shrunk in in 50% NaOH).

SUMMARY

The adhesion of formaldehyde-linked resins to cellulose films (cellophane) is still strong after soaking in water or alkali. It may even be increased by boiling.

The adhesion of these resins appears to be due to the formation of covalent bonds between the resin and the cellulose, possibly by aldehyde formation in the cellulose followed by condensation with reactive groups in the resin.

REFERENCES

1. DE BRUYNE, N. A., *J. Sci. Instruments* **24**, 29–35 (1947).
2. FARROW, C. A., HAMLY, D. H., AND SMITH, E. A., *Ind. Eng. Chem., Anal. Ed.* **18**, 307 (1946).
3. MCBAIN, J. W., AND LEE, W. B., Third Report Adhesives Research Committee. H. M. Stationery Office, London, 1932.
4. BROWNE, F. L., AND BROUSE, D., *Ind. Eng. Chem.* **21**, 74–9 (1929).
5. BROWNE, F. L., AND TRUAX, T. R., *Colloid Symposium Monograph* **4**, 258 (1926).
6. McLAREN, A. D., *J. Polymer Sci.* **3**, 652 (1948).
7. GREEN, H., AND LAMATTINA, T. P., *Anal. Chem.* **20**, 523 (1948).
8. LOUGHBOROUGH, W. K., AND HASS, E. G., *J. Aeronaut. Sci.* **126**, 13 (1946).
9. OTT, E., Cellulose and Cellulose Derivatives, High Polymers, Vol. 5. p. 742. 1943.

PARTICLE MOTIONS IN SHEARED SUSPENSIONS.

I. ROTATIONS

B. J. Trevelyan¹ and S. G. Mason

Pulp and Paper Research Institute of Canada, McGill University, Montreal, Canada

Received May 31, 1951

LIST OF SYMBOLS

- a, b = major and minor axes of prolate spheroid (or cylinder).
 C = orbital constant.
 G = rate of shear.
 N_1, N_2 = r.p.m. of inner and outer Couette cylinders.
 r = axis ratio a/b .
 r_e = axis ratio of equivalent ellipsoid calculated from period of rotation.
 R_1, R_2 = radii of inner and outer Couette cylinders.
 R = radial distance of particle under observation.
 t = time.
 T = period of rotation.
 u, v, w = respective velocity components along X -, Y -, Z -axis.
 λ = azimuthal angle (Y = polar axis).
 θ, ϕ = spherical polar coordinates (Z = polar axis).
 ω = angular velocity of particle about Z -axis.
 Ω = angular velocity of fluid in Couette annulus.

INTRODUCTION

Particles in liquid suspensions subjected to velocity gradients undergo characteristic rotational and translational motions which reveal themselves in a number of ways. The rotations are of interest in connection with the viscosity of the systems (1-4), and with unsymmetrical particles result in preferred orientations which are important in interpreting viscosity (4), thixotropy (5), and streaming birefringence (5,6). The translational motions cause the particles to undergo collisions and, in certain instances, to form aggregates (3,7,8); the formation of aggregates of unsymmetrical particles is also believed to be influenced by rotations (7).

In this communication we describe an experimental study of shear-induced rotations of spheres and cylinders which extends the incidental observations which have been reported by other workers (9,10,11). This work forms part of an investigation of orientation and aggregation phenomena in fiber suspensions being carried out in this laboratory.

¹ Holder of a Canadian Industries Ltd. Scholarship. Present address: Fraser Companies Ltd., Campbellton, N. B., Canada.

A rigorous theoretical treatment of the rotary motion of rigid ellipsoids has been given by Jeffery (2,4). For a single prolate spheroid with center at the origin of an infinite field of laminar fluid motion defined by

$$u = Gy$$

$$v = 0$$

$$w = 0$$

u , v , and w being the respective components of fluid velocity along the X , Y , and Z axes, and G the rate of shear, Jeffery's equations for the angular velocities of the principal axis of the ellipsoid expressed in terms of the spherical polar coordinates θ and ϕ , with the Z axis as the polar axis (Fig. 1), are:

$$\omega = \frac{d\phi}{dt} = \frac{G}{(a^2 + b^2)} (a^2 \cos^2 \phi + b^2 \sin^2 \phi) \quad [1]$$

and

$$\frac{d\theta}{dt} = \frac{G(a^2 - b^2)}{(a^2 + b^2)} (\sin \theta \cos \theta \sin \phi \cos \phi) \quad [2]$$

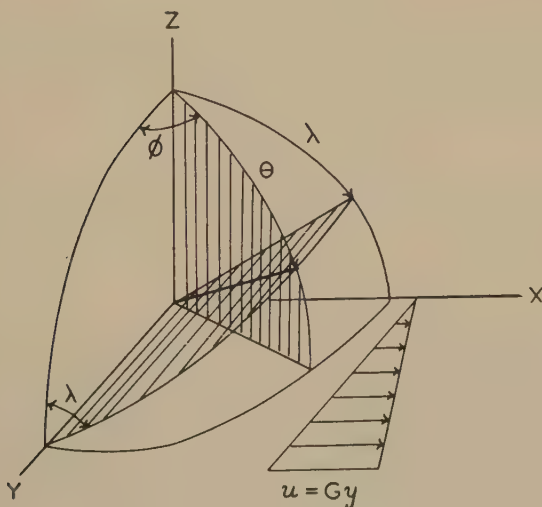


FIG. 1. Coordinate systems for describing particle rotations.

where a is the major axis, and b is the minor axis of the ellipsoid. In deriving these equations, it is assumed that the particles are non-sedimenting, inertial effects are absent, the particles are rigid, and that there is no slip at the particle-liquid interface.

For the simple case of a sphere ($a = b$), the particle rolls in the direction

of motion at a constant angular velocity

$$\omega = G/2 \quad [3]$$

and with a period of rotation

$$T = \frac{4\pi}{G} \quad [4]$$

Equation [3] has been derived independently (1,3) in considering the viscosity of suspensions of spheres.

When $a > b$, Eq. [1] indicates that the angular velocity ω is independent of θ , and is at a maximum when the particle is at right angles to the direction of fluid motion ($\phi = 0$) and a minimum (not zero) when it points in the direction of motion ($\phi = \pi/2$).

Integration of Eqs. [2] and [3] yields

$$\tan \phi = \frac{a}{b} \tan \frac{G a b t}{(a^2 + b^2)} \quad [5]$$

and

$$\tan \theta = \frac{Ca}{\sqrt{(a^2 \cos^2 \phi + b^2 \sin^2 \phi)}} \quad [6]$$

where C is a constant of integration. It follows from Eq. [5] that the rotations about the polar axis are periodic, having as the period of a complete rotation

$$T = \frac{2\pi (a^2 + b^2)}{a b G},$$

which for moderately large values of the axis ratio $r = a/b$ can be written as

$$T = \frac{2\pi r}{G}. \quad [7]$$

Since from Eq. [6], corresponding to a given C , θ is uniquely defined by ϕ , the orbit described by the ends of the particle relative to its center is regular. The orbits of the ends of the particle, defined by Eq. [6], are a symmetrical pair of spherical ellipses whose eccentricity is defined by the parameter C , subsequently referred to as the orbital constant. A family of such curves is shown in Fig. 2. The major and minor axes of the ellipses are defined respectively by

$$\tan \theta_1 = rC \quad [8A]$$

$$\tan \theta_2 = C \quad [8B]$$

The parameter C thus fixes the constants of the ellipse. In the limiting case where $C = 0$, the particle aligns itself along the Z axis. When C is

infinite, the orbit is a great circle lying in the X - Y plane. In this case the particle describes a disk.

In the investigation described here, the rotational velocity of spherical particles at various rates of shear was measured. Instead of prolate spheroids, which are difficult to prepare, glass cylinders were used to verify the predictions embodied in Eqs. [5] and [6]. In order to adhere as closely as possible to the conditions assumed in the equations, small particles and low shear rates were used. Because of our primary interest in the significance of particle rotations in suspensions of wood cellulose fibers, the axis ratios covered the range 20 to 120.

In the experimental method used, observations were made along the Y axis (Fig. 1). With spherical particles this presented no complication.

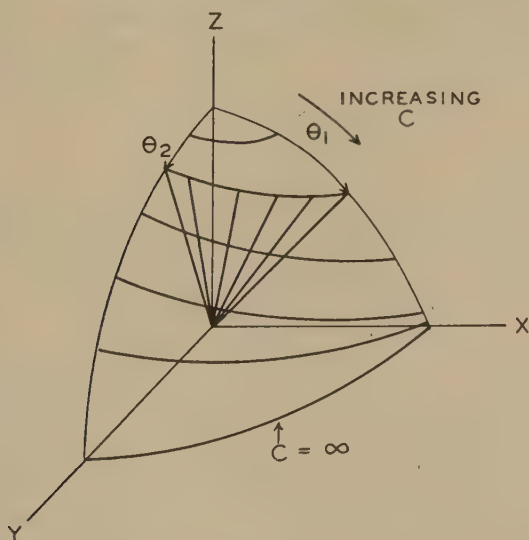


Fig. 2. Spherical elliptic orbits defined by Eq. [6]. After Burgers (4).

With cylindrical particles, however, θ and ϕ could not be determined directly. Instead the projection of the particle on the X - Z plane was viewed. The angular displacement of the projection from the Z axis is the azimuthal angle λ referred to Y as the polar axis (Fig. 1). Using the transformation $\tan \lambda = \tan \theta \sin \phi$, substituting for $\tan \theta$ in Eqs. [5] and [6], and reducing, we obtain

$$\tan \lambda = Cr \sin \frac{2\pi t}{T}. \quad [9]$$

The significance of Eq. [9] is that the particle appears to rock back and forth through an angle $2\lambda_{\max} = 2 \tan^{-1} Cr$ to complete a cycle in the

time T . The maximum angular velocity $d\lambda/dt$ occurs when $\lambda = 0$. From Eq. [8] it follows that the projected length of the particle diminishes from a at λ_{\max} to $a\sqrt{\frac{1}{1+C^2}}$ at $\lambda = 0$.

EXPERIMENTAL PART

Apparatus

Observations were made in a special Couette apparatus in which the two coaxial cylinders were rotated in opposite directions by means of independently variable speed drives. This arrangement (Fig. 3) made it possible to maintain the center of a particle in a stationary position in the field of a microscope whose axis was directed at right angles to the axis of rotation of the cylinders, and in this manner to study the rotary motions of the particles over considerable periods of time.

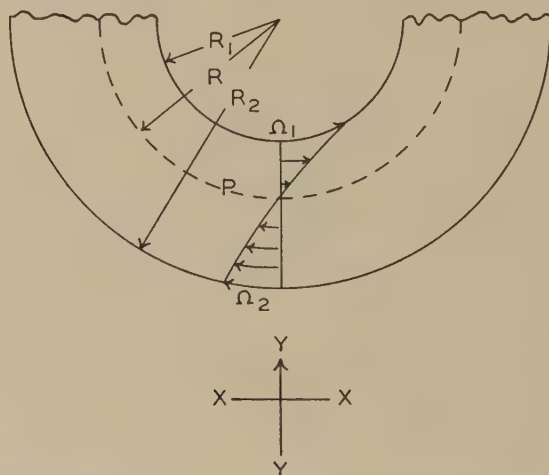


FIG. 3. Principle of the double Couette apparatus. Ω_1 and Ω_2 are manipulated so that $\Omega_R = 0$ and the center of the particle (at P) is stationary. The axis of rotation of the cylinders is parallel to the Z -axis of Fig. 1.

The dimensions of the apparatus were such that the variation in the rate of shear across the annulus between the two cylinders could not be ignored in calculating G . It is readily shown that for laminar flow and Newtonian behavior, the velocity profile is given by the equation

$$\Omega_y = -\Omega_1 + (\Omega_1 + \Omega_2) \frac{(y^2 - R_1^2)}{(R_2^2 - R_1^2)} \frac{R_2^2}{y^2} \quad [10]$$

whence

$$G_y = y \frac{d\Omega}{dy} = 2 \frac{(\Omega_1 + \Omega_2)}{(R_2^2 - R_1^2)} \frac{R_1^2 R_2^2}{y^2} \quad [11]$$

where Ω_y = clockwise angular velocity of the fluid at radius y ,

Ω_1 = counterclockwise angular velocity of the inner cylinder (radius R_1),

Ω_2 = clockwise angular velocity of the outer cylinder (radius R_2),
and

G_y = shear rate at y .

In operation, Ω_1 and Ω_2 were adjusted so that the particle under observation had zero "translational velocity." Denoting the distance of the particle from the Couette axis by R , then $\Omega_R = 0$, and from Eq. [10]

$$\frac{1}{R^2} = \frac{R_1^2 \Omega_1 + R_2^2 \Omega_2}{R_1^2 R_2^2 (\Omega_1 + \Omega_2)}. \quad [12]$$

The shear rate at this point becomes

$$G = \frac{2 (R_1^2 \Omega_1 + R_2^2 \Omega_2)}{(R_2^2 - R_1^2)}. \quad [13]$$

In the apparatus used $R_1 = 1.845$ in. and $R_2 = 2.245$ in. Inserting these values in Eq. [13], and expressing the speeds of the inner and outer cylinders as N_1 and N_2 r.p.m. respectively, G is given by

$$G = 0.436 N_1 + 0.646 N_2 \text{sec.}^{-1}. \quad [14]$$

Thus while the velocity gradient increased by a factor of 1.5 between the outer and inner boundaries of the annulus, G could be accurately calculated from the speeds of the cylinders without measuring the position of the particle. The details of the apparatus are shown in the cross-sectional view in Fig. 4.

The cylinders (1 and 2) were of precision-bore Pyrex tubing and were 8 in. long. The outer surface of the inner cylinder was ground concentric with the inner surface. In assembling the apparatus great care was taken to ensure concentricity of the two cylinders.

The outer cylinder was mounted on the brass block (3) containing a drainage hole (4). The inner cylinder was suspended from the brass block (5) and had at its lower end a brass plug (6). Each block was supported by two bearings in the bearing housings (7) which were integral with the cast aluminum frame (8). The frame was bolted to a sturdy aluminum base.

Each block was geared to its own drive mechanism through the gear box (9). The lower block was geared directly to the input shaft (10) from the drive mechanism. The upper block was geared through the drive shaft (11) to the other input shaft (12).

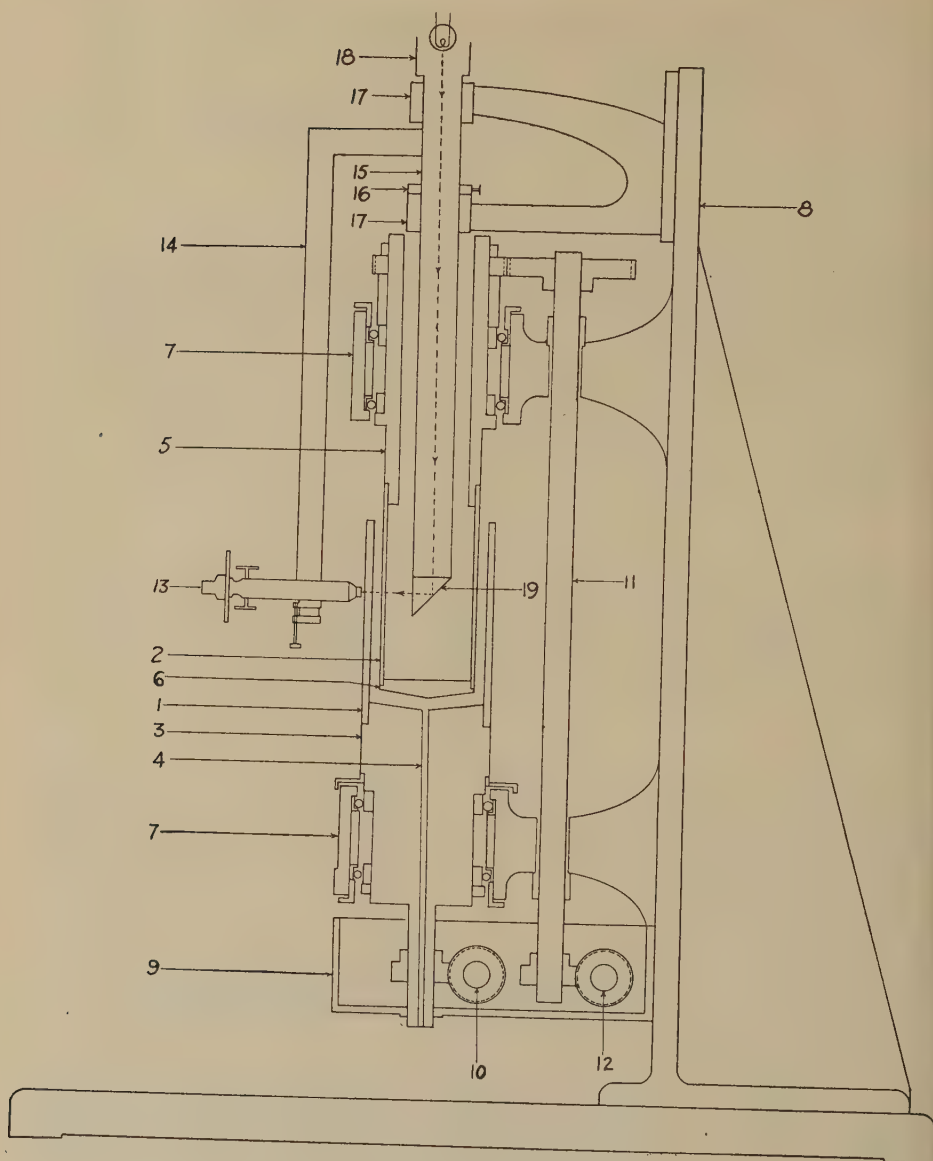


FIG. 4. Details of Couette apparatus.

Each drive mechanism consisted of a variable speed Graham drive, with micrometer speed adjustment, to the input of which was coupled an 1800 r.p.m. synchronous motor and to the output a 50:1 speed reducer. The output of each speed reducer was coupled to one of the input shafts (10 and 12) of the apparatus proper. This arrangement made it possible

to vary the speed of each cylinder continuously from zero to 2 r.p.m. with a sensitivity of better than .001 r.p.m. The upper limit of G was therefore 2 sec.⁻¹.

The microscope (13) for observing the particles was mounted on a U-piece made of stainless steel tubing (14,15) in such a way that it could be readily rotated coaxially with the cylinders. To accomplish this, the tubing (15) was aligned along the axis of the cylinders and held in position by the clamp (16) and the collars (17) in which it was free to rotate. The microscope could be moved vertically by loosening the clamp (16) and sliding the tubing (15) through the collars. For fine vertical adjustments there was a screw on the microscope itself. Illumination of the field was provided by the lamp (18), from which the light was focussed through the prism (19).

Since the microscope was readily movable in all three dimensions, any particle in the annular space could be focused in the field.

Materials

Glass spheres in two size ranges (150 and 290 μ diameter) were obtained in bulk from the Flex-O-Lite Manufacturing Company.

Model cylindrical particles were prepared by embedding bundles of glass fibers (9.5 μ diameter) in Tissuemat and cutting the glass to predetermined lengths in a sliding microtome. The lengths of the particles in a given stock were substantially constant, but because of the wide variations in diameter, it was necessary to determine microscopically the axis ratio of each particle used. This could be done with an accuracy of about 2%.

The liquid medium used was a high-viscosity white corn sirup. The high viscosity of the medium compensated for the low density in preventing gravitational and centrifugal sedimentation of the particles. In the experiments with the spheres both types of sedimentation did occur over long periods of time but this caused no difficulty.

RESULTS

A. Spheres

The steady rotational motion of spherical particles was readily discernible by following optical imperfections within the body of the spheres. These served as convenient reference points in measuring the periods of rotation.

Table I contains a number of observed periods of rotation for both particle sizes at various rates of shear and at various distances from the inner cylinder of the annulus. The last quantity is expressed as $(R - R_1)/(R_2 - R_1)$, i.e. the fraction of the total width of the annulus, and is calculated from the cylinder speeds N_1 and N_2 using Eq. [12].

TABLE I
Periods of Rotation of Spheres

Diameter μ	Speed of rotation		$\left(\frac{R - R_1}{R_2 - R_1}\right)$	G sec.^{-1}	Period	
	Inner cylinder (N_1) <i>r.p.m.</i>	Outer cylinder (N_2) <i>r.p.m.</i>			Observed <i>sec.</i>	Calculated <i>sec.</i>
150	.291	.046	.83	.157	80.1	80.1
	.448	1.22	.21	.984	12.9	12.8
	.72	1.94	.22	1.57	8.12	8.02
290	.121	.024	.79	.0684	185	184
	.115	.380	.18	.296	42.6	42.5
	.330	1.01	.20	.796	15.9	15.8

A plot of T^{-1} versus G for all spherical particles studied is shown in Fig. 5.

The agreement between the observed periods and those calculated from Eq. [4] is seen to be excellent.

These results demonstrate indirectly the validity of the Couette velocity profile Eq. [10].

B. Cylinders

Periods of Rotation. The rocking motion of cylindrical particles through the fixed angle $2\lambda_{\max}$ predicted by Eq. [9] was observed when

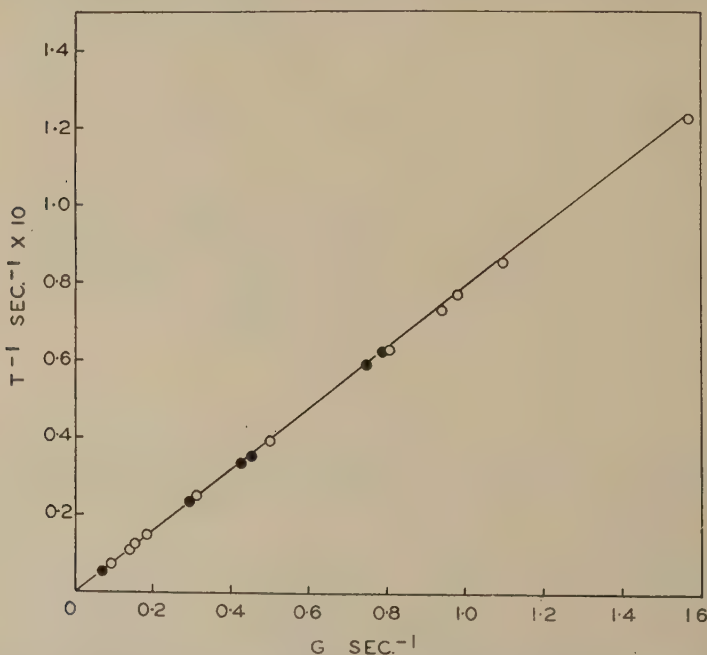


Fig. 5. Periods of rotation of spheres at various shear rates. Open circles 150 μ diameter and closed circles 290 μ diameter. The line is that calculated from Eq. [4].

single particles were introduced into the apparatus by means of a needle probe. The periodic motion of the particles was readily followed in the field of the microscope by using a goniometric ocular with a fixed and a movable cross hair. With the fixed cross hair aligned along the vertical, the axis of the particle could be followed with the movable cross hair. When the orbital constant C was large, the projected length of the particle became smaller as λ approached zero, as would be anticipated from the nature of the predicted orbit.

An extensive series of measurements showed that the period of rotation varies inversely with G . Figure 6 shows a representative series of plots of T^{-1} vs. G for three different particles.

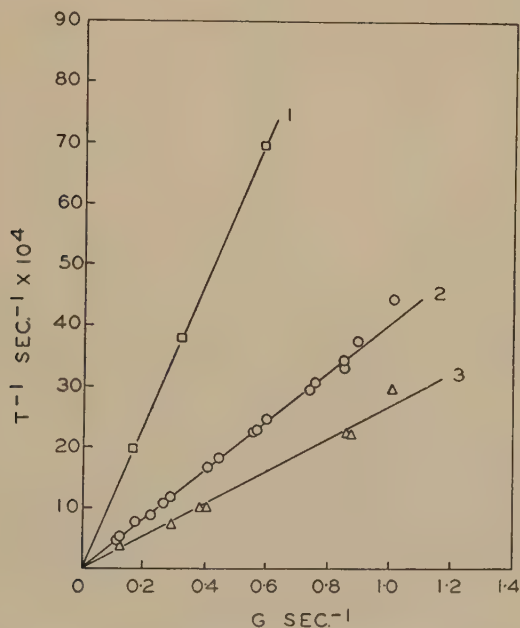


FIG. 6. Periods of rotation of cylinders at various shear rates. Curves 1, 2, and 3 are for axis ratios of 20.0, 60.0, and 105, respectively.

In all cases the period of rotation was less than the value predicted from Eq. [7] for prolate spheroids of corresponding axis ratios. This is illustrated by the summary in Table II of a large number of observations made over a range of shear rates. The quantity r_e is the equivalent ellipsoidal axis ratio calculated from Eq. [7] using the *measured* period of rotation. The ratio r_e/r shows a significant decrease with increasing axis ratio.

The orbital constants were, of course, determined fortuitously in introducing the particles into the annulus. Expressing C in the form (cf.

Eq. [9])

$$C = \frac{1}{r_e} \tan \lambda_{\max}$$

the values of C for the particles in Table II varied over the range 0.03 to 0.50. When the orbital constant of a given particle was varied, r_e remained unchanged (Table III), as predicted by Eq. [7].

TABLE II

*Equivalent Ellipsoidal Axis Ratio of Cylindrical Particles
Calculated from Measured Periods of Rotation*

Measured axis ratio	Mean	
r	r_e	r_e/r
17.8	12.8	.72
19.1	13.4	.70
20.6	13.2	.66
21.5	14.9	.69
53.0	35.0	.66
60	38.6	.64
66	42.2	.64
105	59.4	.57
132	75.0	.57

Details of Orbits. Detailed confirmation of the spherical elliptical orbits was obtained by measuring the variation of the angle λ with time for single particles. In performing these experiments, the rapid succession of events was recorded verbally on a dictating machine, and the times were subsequently measured on the play-back.

Figure 7 shows the variation of λ with t/T for half-rotations of the particle of $r = 66$ for the two orbits given in Table III. The observed values of λ are in close accord with those calculated from Eq. [9]. Similar agreement was shown for particles of axis ratio 20 and 110 in various orbits and at various shear rates.

TABLE III

Effect of Orbital Constant upon Period of Cylindrical Particles

r	G sec. ⁻¹	T sec.	λ_{\max} deg.	C	r_e
20.0	0.311	265	75.0	0.28	13.1
	0.585	145	81.2	0.50	13.5
60.0	0.731	339	53.5	0.035	39.4
	0.224	1118	85.3	0.33	39.8
66.0	0.442	603	55.9	0.034	42.5
	0.473	561	80.1	0.14	42.3

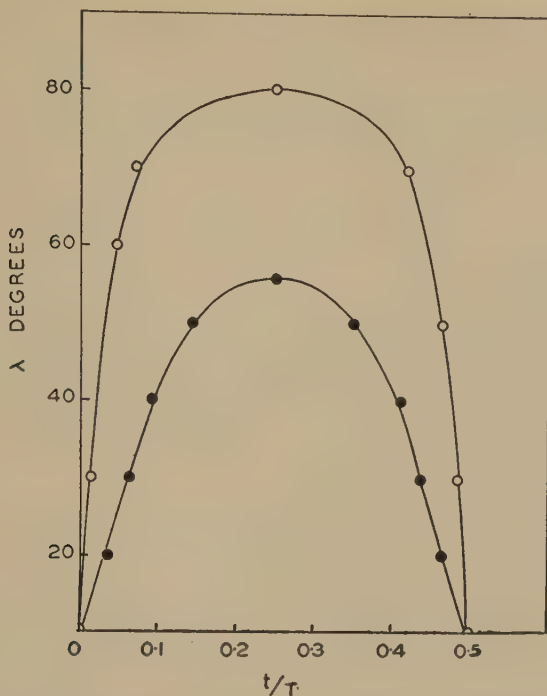


FIG. 7. Variation of angle λ with time of two different orbits (Table III) for a cylinder of axis ratio 66. The curves are calculated from Eq. [9].

DISCUSSION

The agreement between observed and predicted periods for spheres is to be expected on the basis of experimental confirmation of the Einstein viscosity equation (3,12) since the validity of the viscosity relationships for suspensions of spheres is dependent upon the existence of the steady rotational motion described by Eq. [3].

The periodic motions of cylinders follow Jeffery's equations for prolate spheroids except that r_e is significantly less than r , and r_e/r decreases slightly with increasing r . The most obvious explanation for this discrepancy lies in the difference in shape of the two kinds of particle.

Brief reference should, however, be made to a source of error which is inherent in the experimental method. The field of motion in the Couette apparatus does not provide a constant G , as envisaged by Jeffery, but one which increases between the outside and inside ends of the particle. It may be shown, by an argument which we do not reproduce here, that the effect of this distortion of the field is to superpose a translational velocity in the x -direction upon the particle which causes the observed axis of

rotation to shift along the particle from its center to a point toward the outside of the annulus. The G effective in producing rotations, however, can be shown to be that at the center of the particle and is therefore higher than that calculated from [13]. The effect is greatest when $C \rightarrow \infty$ and for this case

$$G_{\text{effective}} = G_{\text{observed}} (1 + a^2/R^2).$$

For the particles used here ($a_{\text{max}}/R = .02$) this introduces a negligible error in calculating r_e .

Burgers (4), in an approximate theoretical analysis of the comparative effects of prolate spheroids and cylinders in disturbing the flow pattern of a fluid subjected to shear, has shown that for two particles of identical length, the disturbance caused by a cylinder of axis ratio r will be reproduced by an ellipsoid of $r_e = 0.74 r$. This agrees approximately with the experimental values reported here.

No mention has been made of the regularity of the orbit. According to the principles outlined in the *Introduction*, the orbit of a particle subjected to prolonged shear should remain unchanged, C being determined by the initial orientation of the particle in the field. A number of observations were carried out on the variation of C for as many as 30 complete rotations of single particles, and of particles selected for observation in particle assemblies. The results were inconclusive; in some instances C remained unchanged, in others it decreased, while in others it varied erratically with time.

The distribution of orbital constants in particle assemblies determines the extent of particle orientation and thus has an important influence upon flow-induced anisotropy of suspensions of asymmetric particles (4).

This point is being investigated further; discussion of this aspect is deferred until more complete results are available.

SUMMARY

Observations of the rotational motion of single rigid spheres and cylinders suspended in a liquid subjected to a velocity gradient have been compared with Jeffery's theoretical equations for ellipsoids of revolution.

The constant angular velocity of spherical particles is proportional to the shear rate, is independent of particle size, and is in excellent accord with theory.

The orbits of cylinders are in good agreement with Jeffery's predicted spherical ellipses. The period of rotation is independent of the orbital constant, and is approximately two-thirds that predicted for a prolate spheroid of the same axis ratio. The latter effect is to be expected from the difference in particle geometry.

REFERENCES

1. EINSTEIN, A., *Ann. Physik* (4) **19**, 289 (1906); **34**, 591 (1911).
2. JEFFERY, G. B., *Proc. Roy Soc. (London)* **A102**, 161 (1922).
3. VAND, V., *J. Phys. & Colloid Chem.* **52**, 277 (1948).
4. BURGERS, J. M., Second Report on Viscosity and Plasticity, pp. 113-84. Academy of Sciences, Amsterdam, 1938.
5. ROBINSON, J. R., *Proc. Roy. Soc. (London)* **A170**, 519 (1939).
6. BOEDER, P., *Z. Physik* **75**, 258 (1932).
7. MASON, S. G., *TAPPI* **33**, 441 (1950).
8. HUBLEY, C. E., ROBERTSON, A. A., AND MASON, S. G., *Can. J. Research* **B28**, 770 (1950).
9. TAYLOR, G. I., *Proc. Roy Soc. (London)* **A103**, 58 (1923).
10. EIRICH, F., BUNZL, M., AND MARGARETHA, H., *Kolloid-Z.* **75**, 20 (1936).
11. BINDER, A., *J. Applied Phys.* **10**, 711 (1939).
12. EIRICH, F., BUNZL, M., AND MARGARETHA, H., *Kolloid-Z.* **74**, 276 (1936).

MEASUREMENT OF PARTICLE SIZE AND CONCENTRATION OF HOMOGENEOUS AEROSOLS

Edward C. Y. Inn

Air Force Cambridge Research Laboratories, Cambridge, Massachusetts

Received May 21, 1951

INTRODUCTION

The measurement of particle number and size of homogeneous aerosols and hydrosols by transmission methods has been previously reported (1, 2, 3). It is the purpose here to describe a very simple adaptation of the Beckman quartz spectrophotometer (model DU) for transmission measurements of homogeneous aerosols, thus obtaining the size, number, and mass concentrations.

EXPERIMENTAL

Standard 10-cm. (quartz window) cells were used in the recommended cell compartment and holder. The cover of the cell housing was replaced with a light-tight black cloth through which two pieces of rubber tubing were passed, the latter being connected to the two outlets of the sample cell. Thus, the rubber tubing and black cloth cover allowed freedom of movement of the cells when it was required to switch from one cell to the other into the line of the monochromatic beam of the spectrophotometer.

Homogeneous glycerin aerosol, prepared in a generator of the La Mer-Sinclair type, was passed into the sample cell through the attached rubber tubing, and the aerosol was collected after passing through the outlet end of the cell. A glass tube containing tightly packed glass wool was used for collecting the aerosol, the amount collected being measured gravimetrically. Transmission measurements were taken over a range of wavelengths from 4000 Å. to about 12000 Å. at intervals of about 500 Å. Higher-order Tyndall spectra measurements were also made using a modified "Owl" (1).

In the actual measurements the spectral transmission was determined while the aerosol flowed continuously through the sample cell as it was being constantly produced in the generator. Thus, any settling of the aerosol particles in the cell was minimized in the flowing stream. Furthermore, the deposition of particles on the cell windows was negligibly small since the cell constant did not change during the transmission measurements.

The spectral transmission measurements were thus plotted on log-log paper and compared with the theoretical scattering curve for glycerin

particles. Since the curves are identical in shape, and by selecting and comparing corresponding points on the theoretical and experimental curves, one can then calculate the particle radius, number, and mass concentration. The following equations illustrate this. Thus:

$$I = I_0 e^{-K_s \pi r^2 n l} \quad [1]$$

or

$$2.303 \log \frac{I_0}{I} = K_s \pi r^2 n l,$$

where $\frac{I_0}{I}$ is the transmission, K_s the scattering coefficient, r the particle radius, n the number concentration, and l the optical path length. Therefore,

$$nr^2 = 2.303 \frac{\log \frac{I_0}{I}}{K_s \pi l}. \quad [2]$$

Now, it can be shown that

$$nr^{p+2} = 2.303 \frac{\left(\lambda^p \log \frac{I_0}{I} \right)}{\left(\frac{K_s}{\alpha^p} \right) (2\pi)^p \pi l}, \quad [3]$$

where p is any positive or negative number (usually integral or half integral); thus for $p = 1$

$$nr^3 = 2.303 \frac{\left(\lambda \log \frac{I_0}{I} \right)}{\left(\frac{K_s}{\alpha} \right) 2\pi^2 l} \quad [4]$$

where we note that nr^3 is proportional to the mass concentration.

Hence, comparing experimental values with the theoretical values we have

$$nr^{p+2} = 2.303 \frac{\left(\lambda^p \log \frac{I_0}{I} \right)_{\text{exp.}}}{\left(\frac{K_s}{\alpha^p} \right)_{\text{theo.}} (2\pi)^p \pi l}. \quad [5]$$

Also

$$r = \frac{(nr^{p+2})_{\text{exp.}}}{(nr^{p+1})_{\text{exp.}}}, \quad [6a]$$

$$n = \frac{(nr^p)_{\text{exp.}}}{(r^p)_{\text{exp.}}}. \quad [6b]$$

Thus, by plotting $\left(\lambda^p \log \frac{I_0}{I} \right)_{\text{exp.}}$ vs. $\frac{1}{\lambda}$ and $\left(\frac{K_s}{\alpha^p} \right)_{\text{theo.}}$ vs. α , both

on log-log paper, and comparing characteristic corresponding points of the two curves we can calculate r , n , and nr^3 by use of Eqs. [4], [6a], and [6b].

We may also calculate r from

$$\alpha = \frac{2\pi r}{\lambda},$$

or

$$r = \frac{(\lambda)_{\text{exp.}}(\alpha)_{\text{theo.}}}{2\pi}, \quad [7]$$

where $(\lambda)_{\text{exp.}}$ is the wavelength of the characteristic point (maximum) of the transmission curve and $(\alpha)_{\text{theo.}}$ the corresponding point on the theoretical scattering curve.

Table I shows some of the results of transmission measurements of glycerin aerosols. The theoretical scattering curve for glycerin particles (index of refraction, $m = 1.473$), was obtained by interpolation from the

TABLE I
Results of Transmission Measurements of Glycerin Aerosols

r_1^a μ	r_2^b μ	r_3^c μ	nr^3^d $\times 10^7$	$n_3r_3^3^e$ $\times 10^7$	n^f $\times 10^{-6}/\text{cm.}^3$	n_3^g $\times 10^{-6}/\text{cm.}^3$
0.34	0.32	0.32	0.57	0.56	1.45	1.72
0.38	0.38	0.36	0.90	0.89	1.64	1.88
0.40	0.41	0.40	0.71	0.64	1.11	1.03
0.43	0.41	0.39	1.45	1.15	1.83	1.89
0.43	0.43	0.38	1.12	1.01	1.41	1.78
0.47	0.45	0.43	1.06	0.86	1.02	1.06
0.51	0.45	0.47	1.76	1.46	1.33	1.40
0.56	0.55	0.55	2.26	1.99	1.33	1.40
0.60	0.59	0.57	1.89	1.59	0.88	0.85
0.67	0.66	0.64	4.28	3.45	1.42	1.34

^a r_1 , particle radius measured by higher-order Tyndall spectra.

^b r_2 , calculated radius using Eq. [7].

^c r_3 , calculated radius using Eq. [6a].

^d nr^3 , measured gravimetrically.

^e $n_3r_3^3$, calculated from Eq. [4].

^f n , from $\frac{nr^3}{r^3}$.

^g n_3 , calculated from Eq. [6b].

table of scattering functions for $m = 1.44$ and $m = 1.50$. This may be permissible since the two latter scattering curves lie close to one another.

It is to be noted that the radius as calculated and obtained by different methods agrees in general within 10%. However, the values of r_1 are in most cases larger than r_3 . This consistent difference may be due to the method of the higher-order Tyndall spectra used to obtain r_1 being subjective, giving consistently high results, or due to the use of interpolated

values of the theoretical scattering curve for glycerin particles. The latter may be also the explanation for the differences of nr^3 (proportional to the mass concentration) as shown in the table of results. However, the lack of a high degree of homogeneity of the aerosol will depress the maximum of the transmission curve which will therefore result in low $n_3r_3^3$ values. The agreement between n and n_3 is surprisingly good.

Although no transmission measurements were made on the Beckman spectrophotometer for homogeneous aerosol particle sizes smaller than $0.3\ \mu$ or larger than $0.7\ \mu$, it should be possible, by the method described above, to determine particle sizes down to about $0.1\text{--}0.15\ \mu$ and up to $0.9\text{--}1.0\ \mu$. The accuracy of this method of course depends on the precision of the Beckman spectrophotometer and spectral transmission measurements made therefrom.

REFERENCES

1. SINCLAIR, D., AND LAMER, V. K., *Chem. Revs.* **44**, 245 (1949).
2. LAMER, V. K., INN, E. C. Y., AND WILSON, I. B., *J. Colloid Sci.* **5**, 471 (1950).
3. LAMER, V. K., AND BARNES, M. D., *J. Colloid Sci.* **1**, 71 (1946); ZAISER, E., AND LAMER, V. K., *J. Colloid Sci.* **3**, 571 (1948).

LETTER TO THE EDITORS

DIFFUSION THROUGH PAPER MEMBRANES

The experimental advantages and the information obtainable with the porous disk diffusion method particularly for the case of biologically active substances, are well known (5,6). While investigating the diffusing properties of the amylases, the usual fritted-glass disk was found impractical.

Recently Gage (2) has shown that Whatman filter paper No. 52 may be used as the porous diaphragm for determining the diffusion coefficient of substances such as glucose and sulfaguanidine. Our use of this particular filter paper for high-molecular-weight substances such as proteins gave erroneous results.

The effect of pore size of the filter paper on the diffusion coefficient of bovine serum albumin¹ was investigated. The diffusion was carried out in a closed all-glass cell with interchangeable ground-glass diffusate compartments, the volume of each compartment being about 5 ml. No mechanical stirring (9) was used other than that resulting from density gradients. The cell was calibrated with 0.1 *M* KCl (3,4) using $d_{25^\circ} = 1.867 \times 10^{-5}$. The concentration of the bovine albumin solutions were determined spectrophotometrically at 280 m μ . The results are summarized in Table I.

TABLE I
Diffusion Coefficient of Bovine Serum Albumin (1%)
pH 6.7; 0.13 *M* phosphate buffer

Paper diaphragm (Whatman No.)	$d_{25^\circ} \times 10^7$ cm. ² -sec. ⁻¹	Average pore size ^a of diaphragm μ	F/L cm. ⁻¹
50	2.7	0.7-1.5	2.6
52	3.5	1.5-2.0	2.9
54	6.91	3-5	3.6
41-H	6.86	3-5	3.2

^a Courtesy of Reeve Angel and Co., New York City.

The diffusion coefficients listed for paper membranes Nos. 54 and 41-H in Table I compare favorably with the free diffusion value of bovine serum albumin at pH 5.0 as given by Putnam *et al.* (7). These authors found $d_{25^\circ} = 7.16 \pm 0.21$ for a 0.7% bovine albumin solution. They also reported a value of $d_{25^\circ} = 7.36$ when the viscosity correction was applied. No such correction has been made for the data in Table I.

¹ Purchased from Armour Laboratories, Chicago, Ill.

Since sintered-glass disks with an average pore size of $2\text{--}5\ \mu$ have been used fairly successfully for several proteins (1,5), the diffusion coefficient of bovine albumin was determined with a glass membrane of this pore size under the conditions given in Table I. The results obtained with the glass disk further substantiate the use of paper membranes Nos. 54 and 41-H for this type of diffusion study.

This work appears to indicate that hardened filter paper of proper porosity may be used for the diffusion and fractionation of high polymers. The great advantage in using filter paper instead of the usual sintered-glass disk is that the time required for diffusion measurements is reduced about ten-fold. This is of particular importance for high-molecular-weight substances such as enzymes which may undergo significant changes with time.

The F/L values (8) listed in Table I are specific membrane constants and may be interpreted as a measure of the efficiency of the membrane in the diffusion cell. In comparison with the values reported by Rosenberg and Beckmann (8), the F/L value for paper No. 54 is appreciably larger than their most efficient membrane. Furthermore, the mechanical and chemical stability as well as the availability of hardened filter paper should lead to extensive use of this material in the construction of fractionating equipment for high polymers.

Department of Chemistry, Columbia University,
New York City, New York

ROBERT J. BURCH
MARY L. CALDWELL

Newark Colleges of Rutgers University,
Newark, New Jersey

BENJAMIN CARROLL

Received June 25, 1951

REFERENCES

1. ATEN, A. H. W., DREVEN, J., AND DREVEN, J. V., *Trans. Faraday Soc.* **44**, 202 (1948).
2. GAGE, J. C., *Trans. Faraday Soc.* **44**, 253 (1948).
3. GORDON, A. R., *Ann. N. Y. Acad. Sci.* **46**, 285 (1945).
4. HARNED, H. S., AND NUTTALL, R. L., *J. Am. Chem. Soc.* **71**, 1460 (1949).
5. NEURATH, H., *Chem. Revs.* **30**, 357 (1942).
6. NORTHRUP, J. N., AND ANSON, M. L., *J. Gen. Physiol.* **12**, 543 (1928).
7. PUTNAM, F. W., ERICKSON, J. O., VOLKIN, E., AND NEURATH, H., *J. Gen. Physiol.* **26**, 513 (1943).
8. ROSENBERG, R. L., AND BECKMANN, C. O., *J. Colloid Sci.* **3**, 483 (1948).
9. STOKES, R. H., *J. Am. Chem. Soc.* **72**, 936 (1950).

BOOK REVIEW

The Physical Chemistry of Dyeing. By T. VICKERSTAFF. Oliver and Boyd, Edinburgh and London, 1950. 416 pp. Price 42 s.

Most of us who are now of middle age grew up under the comfortable shadow of belief in the inevitability of the progress of the human race. The gradual undermining of this faith has been followed by an increasing bewilderment in the face of the confusion, complexity, and incomprehensibility of that stupendous and untidy structure which we call Science. It is therefore a matter of rejoicing when some small measure of comprehension and simplification is possible. During the last quarter of a century, for instance, thanks to the devoted labors of W. H. Carothers, Staudinger, Kraemer, and many others, Colloid Science has been largely taken out of its mystery, until it now forms part of the general framework of physical chemistry. The book under review represents a notable stage in that process of generalization. It would have been a bold man who would have prophesied, in 1900, or even in 1925, that 1950 would have seen the process of dyeing under the spell of the thermodynamics of Willard Gibbs. Yet this is precisely what has been done, and Vickerstaff's book explains, in a critical yet eminently readable manner, this achievement.

The first phase in the work has been one of analysis, where the process of dyeing has been studied out of its dyehouse environment and under such conditions that one factor only is varied, whilst all the others remain constant. In this way a certain insight has been gained into the time rate of dyeing, the effects of salt, and of dye concentration and of temperature, while the relation between dye constitution and affinity still remains largely empirical and obscure. The author has, however, not attempted to follow a historical approach, but to examine the subject solely in the light of the present day. From this point of view the book is comprehensive, indeed the manner of treatment is such as to lead to some repetition and one wonders whether it could not have been curtailed. It is rather a formidable state of affairs when over 400 pages are required to deal with such a narrow field of science. The method of giving references without index numbers is not such as to make the book valuable as a bibliography, and the author disclaims any desire to do this. The book has been written from a broad scientific viewpoint, so far as present knowledge allows, rather than from the more confined outlook of the dyeing technician.

In the application of thermodynamics to dyeing equilibria, one can choose one of two simplified models, that of adsorption on an equipotential surface or that of equilibrium distribution between two bulk phases, each of which is regarded as an equipotential volume.

The author gives a balanced account of both lines of treatment, but appears to lean toward the former. So long as experimental evidence is confined to the determination of adsorption isotherms, a crucial determination will be lacking. In this respect the book suffers under the handicap of having been written in 1946 and published in 1950, so that the most recent work is not included.

The thermodynamic treatment is not so precise, in the matter of strict use of symbols, as could be wished. The use of the chemical potential of the "dye" (p. 98) rather obscures the ionic mechanism of the salt effect. The dye is a strong electrolyte and the chemical potential of the sodium ions is important only because of the difficulty of separating them appreciably from the color ions, which alone have specific affinity for the fiber. The author is clearly aware of this, but his desire to present all points of view in a

comprehensive manner tends to blur the outlines of the picture, discrimination being left to the reader.

The reader not already familiar with the subject may find this state of affairs confusing, at any rate on first reading.

There are a few minor errors which will no doubt be corrected in future editions. Some of these are obvious; for instance, the sudden change of sign which the energy of activation suffers when the reader turns over p. 239. Others, for example the inadequate interpretation of the classical experiment of Donnan and Harris on Congo Red (p. 57), are less so.

The book, however, should find a place in all academic and technological libraries, as well as in the more enlightened dyehouses.

S. M. NEALE, Manchester, England.

ERRATA

In the article by Andries Voet and Louis R. Suriani entitled, "Dielectrics and Rheology of Dispersed Magnetized Particles," which appeared in Volume 6, Number 2, pp. 155-161, the following corrections should be noted:

p. 156, the captions for Figures 1 and 2 should be interchanged

p. 160, fourth line from the bottom of the page, the word "summary" should be deleted

VISCOSITIES OF CONCENTRATED POLYVINYL ACETATE SOLUTIONS IN VARIOUS SOLVENTS

John D. Ferry, Edward L. Foster,¹ George V. Browning²
and W. M. Sawyer³

Department of Chemistry, University of Wisconsin, Madison, Wisconsin

Received August 2, 1951

INTRODUCTION

In previous investigations of the viscosities of concentrated polymer solutions (1-5) the effects of temperature and concentration have been reported, but there have not been many comparisons of viscosities in different solvents. In the present study, polyvinyl acetate was chosen for such a comparison because the thermodynamic (6) and dynamic mechanical (7,8) properties of this polymer had been measured in several different solvents in this laboratory. Moreover, steady-flow viscosity data were required in order to treat the dynamic mechanical properties by the method of reduced variables (9).

Although a complete characterization of the viscous behavior of polymer solutions such as these must include study of deviations from Newtonian behavior at higher shearing stresses (4,10,11), the present study is confined to low stresses where the flow is essentially Newtonian. It is found that the viscosity depends greatly on the choice of solvent if viscosity values are compared at equal weight concentrations, but only slightly if relative viscosities are compared at equal volume concentrations. The dependence on temperature and concentration is similar to that exhibited by solutions of other linear amorphous polymers.

MATERIALS AND METHODS

A sample of unfractionated polyvinyl acetate, AYAX, lot 1232, was furnished through the kindness of Mr. A. K. Doolittle of the Carbide and Carbon Chemicals Division, Union Carbide and Carbon Corporation. Its number-average molecular weight (6) was 140,000. This material was studied in 1,2,3-trichloropropane, methyl isobutyl ketone, methyl ethyl ketone, and cyclohexanone; and at one concentration, representing the minimum solubility, in diisopropyl ketone, with which this polymer is

¹ Present address: Lion Oil Company, El Dorado, Arkansas.

² Present address: Standard Oil Company, Whiting, Indiana.

³ Present address: Shell Development Company, Emeryville, California.

imperfectly miscible. Three rough fractions (6) of polyvinyl acetate were also studied in trichloropropane. Their number-average weights (6) were as follows: **I**, 840,000; **II**, 280,000; **III**, 62,000.

All the solvents except methyl isobutyl ketone were distilled through a 30-plate Oldershaw column. The latter ketone (from Carbide and Carbon Chemicals Corporation) was dried over anhydrous sodium sulfate and used without further purification.

Most of the measurements were carried out by the falling-ball method, using steel bearing balls⁴ in glass tubes. The ball diameter, r ; tube diameter, ρ ; and solution depth were for whole polymer solutions, respectively, 1/16 in., 2 cm., and 12–20 cm.; for the fractions: 1/32 in., 1 cm., and 12 cm. The velocity, v , was measured with a cathetometer and interval timer, and the viscosity η was calculated with the Ladenburg correction for the effect of the tube radius:

$$\rho = \{(2/9)gr^2(d_1 - d_2)/v\}/(1 + 2.4r/\rho), \quad [1]$$

where g is the acceleration due to gravity, and d_1 and d_2 the densities of ball and solution, respectively. The density d_1 was obtained from weighing groups of balls and calculating the volume from the specified diameter, and d_2 was calculated by assuming additivity of the volumes of solvent and polymer (6). The Ladenburg correction is within 1% of the Faxén correction recently used by Cragg, Faichney, and Olds (5).

Some measurements in the viscosity range from 0.3 to 10 poises were made with two capillary viscometers. These were calibrated with a Bureau of Standards oil (N-16, viscosity 9.87 poises at 25 °C.) for which the flow times were 821 and 5236 sec. Under these circumstances, the kinetic energy correction was neglected. For still more dilute solutions, conventional intrinsic viscosity technique was employed.

In both experimental methods the flow can be regarded as Newtonian. The maximum shearing stress (12) at the surface of a falling ball is $(d_1 - d_2)gr/3$, and at the wall of a capillary it is $rP/2l$, where P is the pressure and l the capillary length. In our experiments the numerical values are of the order of 100 dynes/cm.² in both cases. The non-Newtonian behavior of concentrated polymer solutions can be expressed in terms of a critical stress (10,13) which is of the order of 10^3 to 10^4 dynes/cm.²; if the maximum experimental stress is smaller than this value by a factor of three or more, deviation from Newtonian behavior is found to be negligible.

RESULTS

Viscosities of solutions of the unfractionated polymer in the five solvents are given in Table I. The logarithm of the viscosity is plotted against the reciprocal absolute temperature for the trichloropropane solutions in

⁴ Miniature Precision Bearings, Keene, N. H.

Fig. 1. Here, as in the other solvents, a straight line is obtained at each concentration, within experimental error. It is possible, of course, that a wider temperature range would reveal curvature. Values of $Q_\eta [= R d \ln \eta / d(1/T)]$ calculated from these plots are also included in Table I. It increases with increasing concentration; at comparable concentrations the values in the three solvents do not differ greatly.

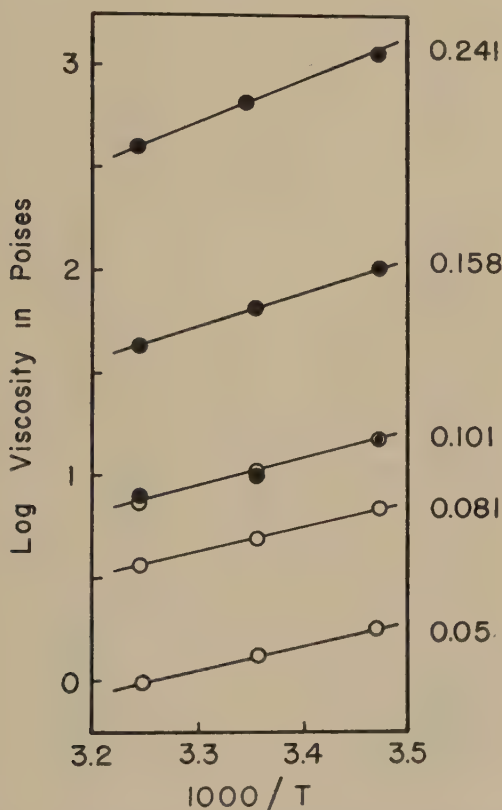


FIG. 1. Logarithm of viscosity plotted against reciprocal of absolute temperature for solutions of unfractionated polymer in trichloropropane. Solid circles, falling ball; open circles, capillary. Figures denote weight fraction of polymer.

The logarithm of the viscosity at 25° is plotted against the square root of the weight fraction (w_2) in Fig. 2. Several investigators (2,3,5,14) have found for various polymers that this type of plot gives straight lines for moderately concentrated solutions, although it is usually obvious that such a line cannot extrapolate into the viscosity of either pure solvent or pure polymer. In our polyvinyl acetate solutions, where w_2 ranges from 0.004 to 0.5, curvature is apparent over this entire concentration range.

TABLE I
Viscosities of Solutions of Unfractionated Polymer

Solvent	w_2	Method ^a	η in poises at			Q_η kcal.
			15°C.	25°C.	35°C.	
1,2,3-Trichloro- propane	0	C		0.22		
	0.050	C	1.76	1.32	0.99	5.1
	0.081	C	6.99	4.95	3.64	5.5
	0.101	C	15.00	10.57	7.53	5.8
		F	15.17	10.22	7.85	
	0.158	F	104	65.3	44.5	7.4
	0.207	F	—	266	—	
	0.241	F	1,150	635	396	9.4
	0.256	F	—	871	—	
	0.300	F	—	2,590	—	
	0.403	F	83,000 ^b	40,300	18,800	15.0
Methyl isobutyl ketone	0	C		0.0055		
	0.0042	C		0.0069		
	0.0063	C		0.0080		
	0.0084	C		0.0087		
	0.0125	C		0.0107		
	0.030	C		0.0232		
	0.050	C		0.0495		
	0.100	C		0.254		
	0.200	C		3.76		
	0.302	F	62.9	40.3	27.6	7.1
	0.338	F	—	101	—	
	0.389	F	—	313	—	
	0.401	F	713	400	240	9.5
	0.466	F		1,641		
	0.508	F	8,600	4,640	2,150	12.7
Methyl ethyl ketone	0	C		0.0039		
	0.0043	C		0.0054		
	0.0084	C		0.0069		
	0.0125	C		0.0089		
	0.030	C		0.0214		
	0.050	C		0.0464		
	0.100	C		0.225		
	0.200	C		2.72		
	0.300	C		23.6		
	0.341	F		51.5		
	0.391	F		143.3		
	0.403	F		194		
	0.506	F		1,608		
	0.514	F		1,732		
Cyclohexanone	0	C		0.0203		
	0.202	F	51.7	32.7	22.6	7.2
	0.351	F	—	1,116	—	—
Diisopropyl ketone	0	C		0.0059		
	0.542	F	—	30,400	—	—

^a C = capillary, F = falling ball.^b At 17.2 C.

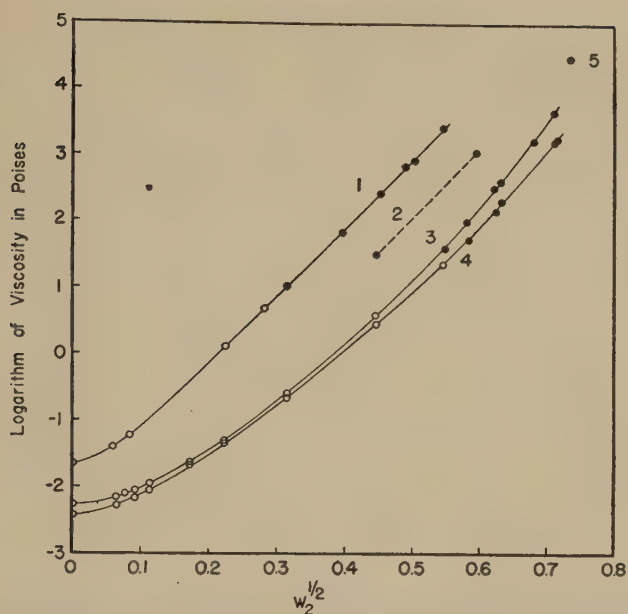


FIG. 2. Logarithm of viscosity at 25°C. plotted against square root of weight fraction of polymer (unfractionated). 1, trichloropropane; 2, cyclohexanone; 3, methyl isobutyl ketone; 4, methyl ethyl ketone; 5, diisopropyl ketone.

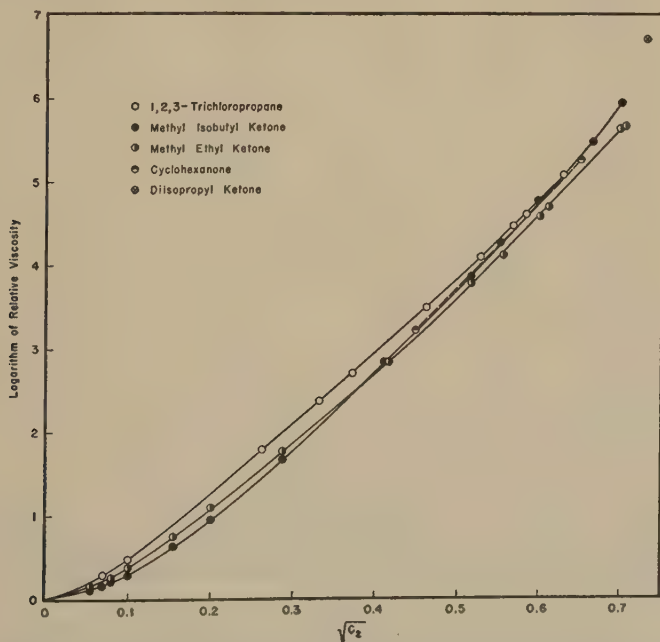


FIG. 3. Logarithm of relative viscosity at 25°C. plotted against square root of volume concentration (g./cc.) of polymer (unfractionated), in five different solvents.

At comparable values of w_2 , the viscosity increases in the order methyl ethyl ketone < methyl isobutyl ketone < cyclohexanone < trichloropropane, and the differences are large, the ratios being of the order of 1:2:16:120.

Part of the solvent dependence can be attributed to the viscosity of the solvent itself; if the logarithm of the relative viscosity (η_r) is plotted

TABLE II
Viscosities of Solutions of Fractions in 1,2,3-Trichloropropane

Fraction	w_2	Method ^a	η in poises at			Q_{η} kcal.
			8°C.	25°C.	50°C.	
I	0.0301	C	2.64	1.55	0.820	
	0.0401	C	5.80	3.29	1.68	
	0.0498	C	11.4	6.31	3.13	
	0.0554	F	16.2	8.76	4.29	5.71
	0.0821	F	75.7	38.4	17.1	6.54
	0.113	F	352	154	67.6	7.28
	0.144	F	1350	570	222	8.02
II	0.0307	C	0.926	0.55	0.30	4.90
	0.0411	C	1.78	1.02	0.541	5.06
	0.0504	C	2.98	1.68	0.860	5.25
	0.0579	F	—	2.59	—	
	0.0772	F	12.8	6.25	3.12	6.18
	0.0965	F	25.8	12.9	5.90	6.36
	0.122	F	62.5	30.2	12.9	6.82
	0.173	F	344	149	55.8	7.75
	0.201	F	858	347	122	8.39
	0.239	F	2640	956	300	9.40
III	0.091	C	1.73	0.946	0.476	5.53
	0.119	C	—	1.92	—	
	0.147	C	7.39	3.64	1.64	6.55
	0.183	C	17.4	7.85	3.36	7.00
	0.247	C	94.8	36.5	12.9	8.57
M ^b	0.0471	C	—	1.90	—	
	0.0765	C	—	8.55	—	
	0.107	C	—	30.3	—	
	0.138	F	—	97.3	—	
	0.173	F	—	316	—	

^a C = capillary, F = falling ball.

^b Mixture of 59% fraction I and 41% fraction III by weight.

against $\sqrt{w_2}$, the curves are brought closer together and the ratios (at $w_2 = 0.2$) are now 1:1:2.5:16. The differences are further diminished by plotting $\log \eta_r$ against the square root of the *volume* concentration, c_2 , in g./cc. (Fig. 3). Here the ratios (at $c_2 = 0.2$) are 1:1.1:1.1:1.7. These plots are also somewhat curved, although for the ketones the curvature is less than in Fig. 2.

Viscosities of solutions in 1,2,3-trichloropropane of the three fractions, and of a mixture of 59% fraction I and 41% fraction III, are given in Table II. The logarithm of the viscosity is plotted against the reciprocal absolute temperature for solutions of fraction II in Fig. 4. Within the temperature range covered, the points are well fitted by straight lines; linear plots were also obtained for fractions I and III. Values for Q_η calculated from the slopes of these lines are included in Table II.

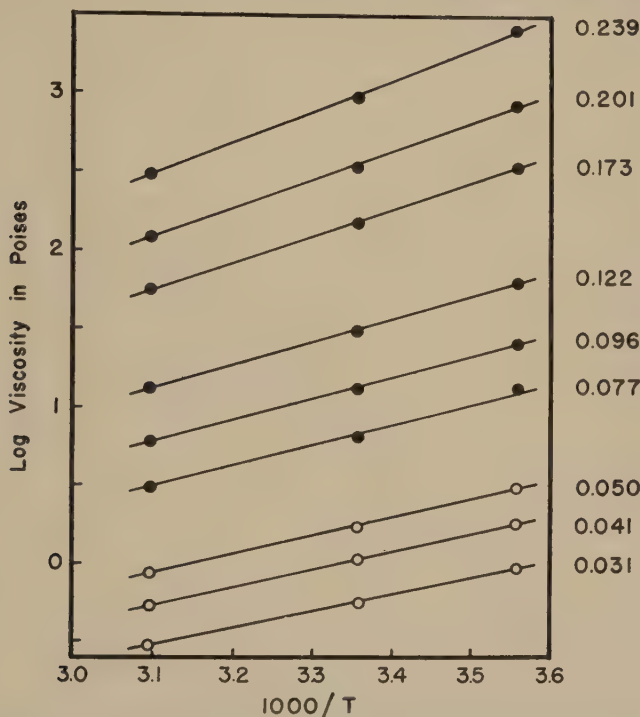


Fig. 4. Logarithm of viscosity plotted against reciprocal absolute temperature for solutions of fraction II in trichloropropane. Key same as in Fig. 1.

The logarithm of the relative viscosity is plotted against the square root of the volume concentration in Fig. 5. These plots show an upward curvature; their slopes increase somewhat with molecular weight.

DISCUSSION

The linear relationships exhibited in Figs. 1 and 4 are no doubt approximations restricted to a limited range of temperature. Over wider ranges, the plot of $\log \eta$ against $1/T$ has been found by Fox and Flory to exhibit curvature for polymer melts (15). Nevertheless, Figs. 1 and 4 serve for calculation of the apparent activation energies, Q_η , which have been given

in the tables. These values are plotted against c in Fig. 6. They increase roughly linearly with concentration, somewhat faster in methyl isobutyl ketone than in trichloropropane, and they increase slightly with molecular weight.

No attempt has been made to describe the concentration dependence of viscosity analytically. In any case, it appears that the dependence on volume concentration is simpler than that on weight concentration, and more instructive for comparison of solvents. In Fig. 3, all the solvents are approximately the same, even diisopropyl ketone, which is so poorly

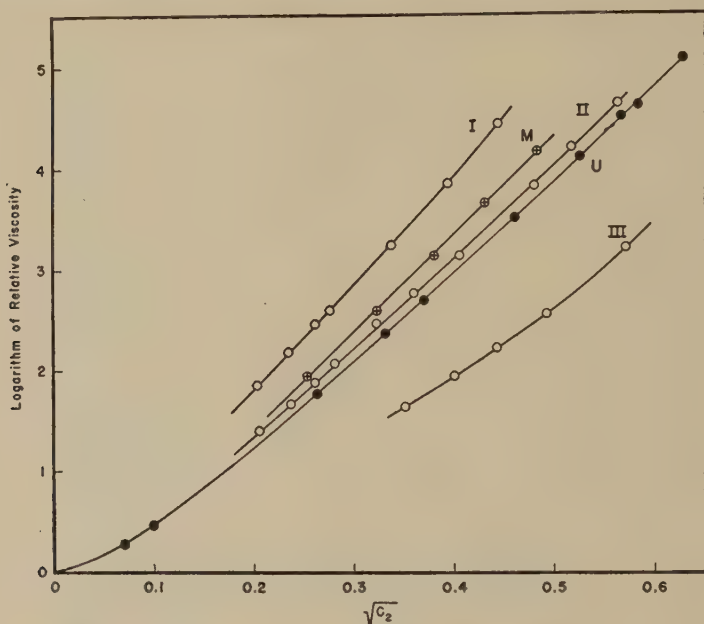


FIG. 5. Logarithm of relative viscosity plotted against square root of volume concentration (g./cc.) of five polymer samples in trichloropropane. Numerals denote fractions; U = unfractionated, M = mixture.

matched in cohesive energy density that it does not mix with the polymer in all proportions. The relatively small differences are expressed by the statement that the curve for methyl isobutyl ketone is the lowest at low concentrations but crosses and becomes the highest at high concentrations, while the curve for trichloropropane lies above that of methyl ethyl ketone throughout. The behavior of methyl isobutyl ketone is consistent with the presence of an aliphatic group which diminishes the polymer-solvent interaction and causes a tighter coil configuration in dilute solution but a tighter entanglement, or even a slight association of polymer segments, in concentrated solution. Similarly, the single point for diiso-

propyl ketone, which has two aliphatic groups, lies quite high. The comparative behavior of trichloropropane and methyl ethyl ketone is consistent with the fact that both are very good solvents, with negative heats of dilution (6), and the former is the better of the two.

It is of interest to characterize these curves of $\log \eta_r$ against $\sqrt{c_2}$ by their slopes, taken at $c = 0.16$ g./cc. Such slopes are summarized in

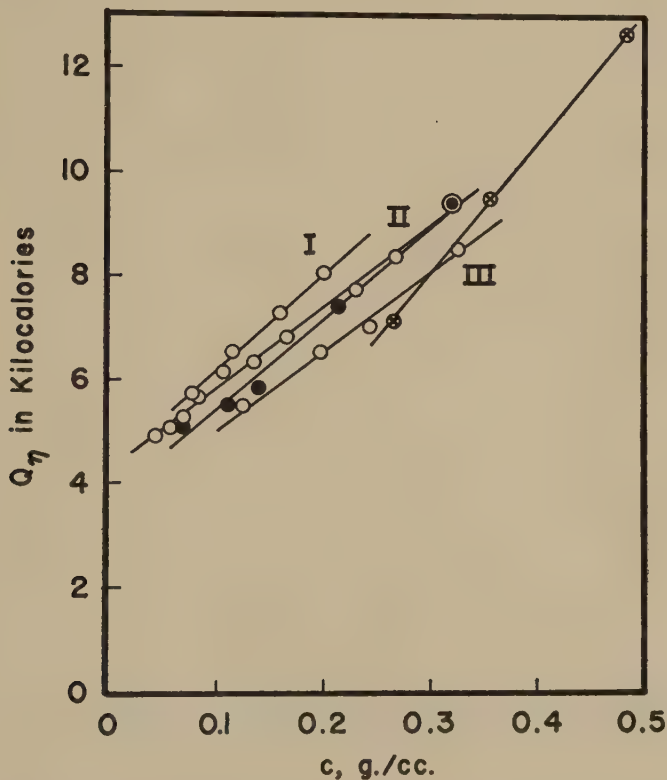


FIG. 6. Apparent activation energy for viscous flow plotted against volume concentration. Numerals refer to open circles and denote fractions in trichloropropane; solid circles, unfractionated polymer in trichloropropane; crossed circles, unfractionated polymer in methyl isobutyl ketone.

Table III for the data of Figs. 3 and 5 and also for several other polymer-solvent systems reported in the literature. They show remarkably little dependence upon the chemical nature of polymer or solvent. Except for the lowest polyvinyl acetate fraction and a butadiene-styrene copolymer of quite high molecular weight, the values at 25° range from 8.7 to 12.4 (g./cc.)^{-1/2}. They increase somewhat with increasing molecular weight.

The molecular weight dependence of the viscosities of various samples in trichloropropane is shown in Fig. 7, where the logarithm of the viscosity

TABLE III
Slopes of Plots of Log η Against $\sqrt{c_2}$, at $c_2 = 0.16$

Polymer	Mol. wt.	Solvent	Temp. °C.	$\frac{d \log \eta}{d \sqrt{c_2}}$	Reference	
Polyvinyl acetate (unfr.)	140,000 ^a	1,2,3-trichloro- propane	15	9.0	Fig. 3	
			25	8.7		
			35	8.5		
		Methyl isobutyl ketone	15	11.3		
			25	10.3		
			35	9.7		
Methyl ethyl ketone	25	9.1				
	Polyvinyl acetate (fraction I)	840,000 ^a	1,2,3-trichloro- propane	8	11.3	Fig. 5
				25	10.6	
50				10.0		
Polyvinyl acetate (mixture)	140,000 ^a		25	9.6		
Polyvinyl acetate (fraction II)	280,000 ^a	1,2,3-trichloro- propane	8	9.4		
			25	9.0		
			50	8.3		
Polyvinyl acetate (fraction III)	62,000 ^a	1,2,3-trichloro- propane	8	6.9		
			25	6.3		
			50	5.7		
Rubber	—	Benzene	15	9.8	2	
			50	9.7		
Butadiene-styrene copolymer	258,000 ^b	Benzene	15	14.3	5	
			25	14.0		
			35	13.7		
Polystyrene	153,000 ^a	Xylene	0	11.4	4 ^c	
			25	10.4		
	101,000	Isopropyl benzene	25	11.5	14	
			Methyl ethyl ketone	25		11.6
Vinyl chloride acetate copolymer (VYHH)	13,000 ^d	Acetone	20	9.3	16	
		Methyl ethyl ketone	20	9.6		
		Methyl <i>n</i> -propyl ketone	20	9.9		
Cellulose acetate	—	Cyclohexanone	25	12.4	1	
		Acetone	25	12.4		

^a Number average from osmotic pressure.

^b Viscosity average.

^c These data were recalculated by extrapolating the viscosity to zero stress by a logarithmic hyperbolic sine plot (10), rather than the linear extrapolation used previously.

^d Number average from ebulliometry [HILL, F. N., AND BROWN, A., *Anal. Chem.* **22**, 562 (1950)].

at $c = 0.16$ g./cc. is plotted against the square root of the number-average molecular weight and also against the intrinsic viscosity. Comparison of the values for fractions with the unfractionated material and the mixture shows that the viscosity in concentrated solution is not determined by the

number-average molecular weight but that it is closely related to the intrinsic viscosity, which reflects an average close to the weight average. This result agrees with the conclusions of Fox and Flory (15) that in undiluted polymer melts the viscosity is determined by the weight-average molecular weight, as long as the latter is not too small.

When dynamic mechanical data on concentrated polymer solutions are expressed in terms of reduced variables according to a scheme recently described (9), values at all different temperatures and concentrations should yield a single composite curve provided that the rates of all relaxation mechanisms have the same temperature and concentration dependence. It is a corollary of these provisions that the temperature and concentration dependence of the steady flow viscosity should be independent of molecular weight. Actually, at a given concentration Q_η depends

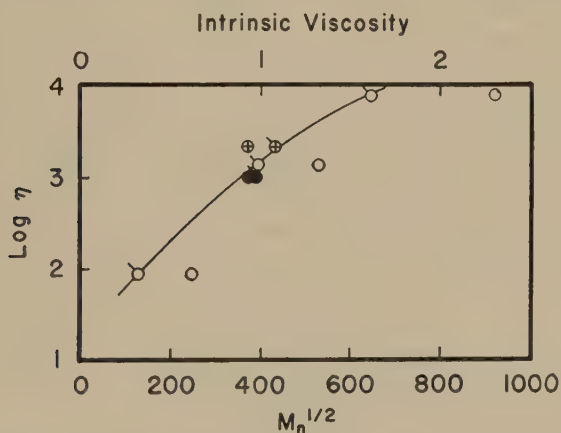


FIG. 7. Logarithm of viscosity at $c = 0.16$ g./cc. in trichloropropane at 25°C. plotted against square root of number-average molecular weight (untagged) and against intrinsic viscosity (tagged). Open circles, fractions; solid circles, unfractionated; crossed circles, mixture.

slightly on molecular weight (Fig. 6), and at a given temperature $d \log \eta / d \sqrt{c_2}$ also depends slightly on molecular weight (Table III). It is to be expected, therefore, that more accurate and extensive applications of the method of reduced variables may reveal imperfect superposition of dynamic data at different temperatures and concentrations, even though the examples treated thus far have appeared to superpose quite closely.

It is hoped that this study may be of use in guiding the development of a theory for the viscosities of concentrated polymer solutions and their dependence on concentration, temperature, and molecular weight. Better theoretical understanding of these phenomena is badly needed.

ACKNOWLEDGMENTS

This work was supported in part by the Research Committee of the Graduate School of the University of Wisconsin from funds supplied by the Wisconsin Alumni Research Foundation, and in part by a grant from Research Corporation.

SUMMARY

Viscosity measurements are reported on concentrated solutions of polyvinyl acetate in 1,2,3-trichloropropane, methyl isobutyl ketone, methyl ethyl ketone, cyclohexanone, and diisopropyl ketone. The logarithm of the viscosity is not a linear function of the square root of either the weight or the volume concentration, although the deviation from linearity is not great for either. When the viscosities are compared directly at equal weight concentrations, the dependence on solvent is enormous; when the relative viscosities are compared at equal volume concentrations, the dependence on solvent is slight. The logarithm of the viscosity is a linear function of the reciprocal absolute temperature within a limited temperature range; the calculated heat of activation increases approximately linearly with concentration and it increases slightly with molecular weight. The derivative of the logarithm of the viscosity with respect to the square root of the volume concentration is of the order of $10 \text{ (g./cc.)}^{-\frac{1}{2}}$ and does not vary much for a number of polymer-solvent pairs reported in the literature. It appears to depend primarily on the chain length rather than on the chemical nature of either polymer or solvent.

REFERENCES

1. MARDLES, E. J. W., *J. Chem. Soc.* **123**, 1951 (1923).
2. ABERNETHY, C. L., *India-Rubber J.* **70**, 775 (1925).
3. FLORY, P. J., *J. Phys. Chem.* **46**, 870 (1942).
4. FERRY, J. D., *J. Am. Chem. Soc.* **64**, 1330 (1942).
5. CRAGG, L. H., FAICHNEY, L. M., AND OLDS, H. F., *Can. J. Research* **26**, 551 (1948).
6. BROWNING, G. V., AND FERRY, J. D., *J. Chem. Phys.* **17**, 1107 (1949).
7. SAWYER, W. M., AND FERRY, J. D., *J. Am. Chem. Soc.* **72**, 5030 (1950).
8. FERRY, J. D., SAWYER, W. M., BROWNING, G. V., AND GROTH, A. H., JR., *J. Applied Phys.* **21**, 513 (1950).
9. FERRY, J. D., *J. Am. Chem. Soc.* **72**, 3746 (1950).
10. SCHREMP, F. W., FERRY, J. D., AND EVANS, W. W., *J. Applied Phys.* **22**, 711 (1951).
11. SPENCER, R. S., AND DILLON, R. E., *J. Colloid Sci.* **4**, 241 (1949).
12. PAGE, L., *Theoretical Physics*. Van Nostrand, New York, 1935.
13. SPENCER, R. S., *J. Polymer Sci.* **5**, 591 (1950).
14. SPENCER, R. S., AND WILLIAMS, J. L., *J. Colloid Sci.* **2**, 117 (1947).
15. FOX, T. G., AND FLORY, P. J., *J. Am. Chem. Soc.* **70**, 2384 (1948).
16. QUARLES, R. W., *Ind. Eng. Chem.* **35**, 1033 (1943).

SURFACE STRUCTURE OF WATER AND SOME OF ITS PHYSICAL AND CHEMICAL MANIFESTATIONS¹

W. A. Weyl

*Department of Mineral Technology, The Pennsylvania State College,
State College, Pennsylvania*

Received April 16, 1951

I. FORMATION OF AN EQUILIBRIUM SURFACE

In previous papers the author (1,2,3) described and explained a number of surface phenomena which were the result of the polarization and deformation of ions (K. Fajans) in the asymmetrical environment which is characteristic for a surface. A nascent surface, for example, one which is the result of a fracture, undergoes several types of changes which lower the surface free energy of the system. The first step, an instantaneous process, consists of the polarization of ions. This process is presented schematically in Fig. 1 where the nascent surface of a NaCl crystal, corresponding to an ideal 100 face (*A*), undergoes a change which leads to an uneven electron density distribution within the surface ions. Scheme *B* indicates by heavier lines that the electron density toward space is higher than average for the Na⁺ ions and lower than average for the Cl⁻ ions. This unequal electron distribution probability is the result of the asymmetry of the environment. The surface Na⁺ ions are backed by chlorine ions of the next deeper layer which, due to their negative excess charge, repel the electron cloud of the Na⁺ ions. The surface chlorine ions, in turn, are polarized in the opposite direction. They are backed by Na⁺ ions which attract their electron clouds, and this deformation leads to a lower than average electron density toward space. Both polarizations, that of the Na⁺ ion and that of the Cl⁻ ion, lower the intensity of the potential fields of the surface ions. As indicated by the length of the arrows, the polarized surface (*B*) has a weaker potential field than the ideal surface (*A*). Just how much the polarization decreases the surface potential of the solid depends on the polarizability of the ions. Compounds, such as HgI₂ or PbI₂, can develop such low surface fields (4) that they are not readily wet by water. As a rule the polarizability of anions is larger than that of cations (5). In our scheme this is indicated by the reduction of the size of the arrows, thus pointing out a considerable weak-

¹ Based on O.N.R. Technical Report No. 19 (August 1950). Contract No. N6 onr 269 Task Order 8 NR 032-265.

ening of the potential fields of the Cl^- ions, but one which is much less for the Na^+ ions.

The lower polarizability of the cations as compared with that of the anions provides an additional means for decreasing the surface energy of the solid; namely, a rearrangement of the surface ions in a fashion which is schematically described in Fig. 1c. The cations are here slightly recessed so that the outer surface layer consists primarily of Cl^- ions. In receding, the Na^+ ions are more completely screened by the anions and this, in turn, decreases the intensity of the unbalanced surface forces.

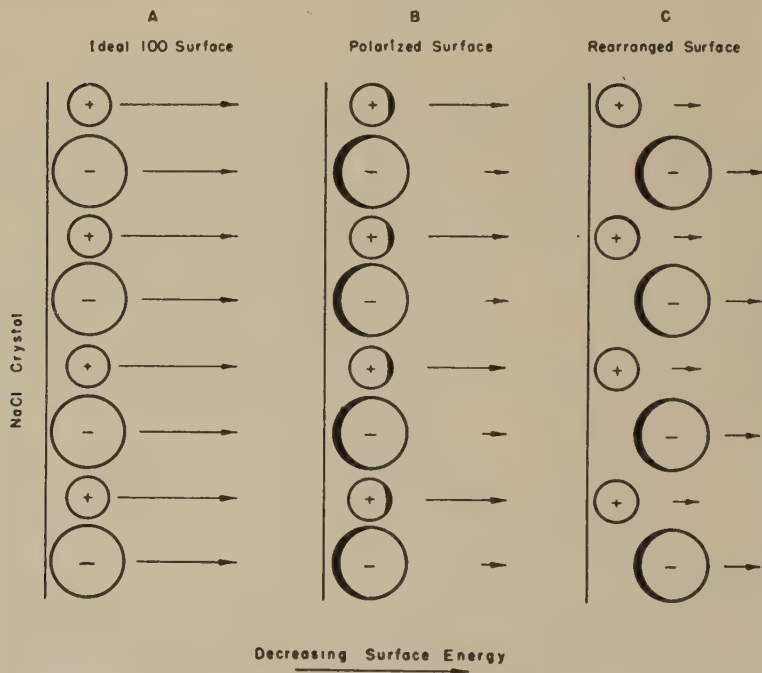


FIG. 1. Electronic deformation and ionic rearrangement in a sodium chloride surface.

It is this difference in the atomic structures of surfaces which is responsible for the reactivity of nascent surfaces and the inertness of those which have reached their equilibrium state.

II. FLUIDIZATION OF SOLIDS

The formation of MgO through the calcination of $\text{Mg}(\text{OH})_2$ or of MgCO_3 should produce a very reactive crystal surface. If the textbooks were correct, the surface of each individual MgO crystal would be pictured as consisting of a checkered positive and negative potential field. The forces emanating from each little cube face should be strong and

should cause the nascent crystals to adhere one to another and, thus, form a solid mass. Precisely the opposite is true. Not only is it impossible to press the freshly formed MgO into a dense body or to sinter pure MgO at temperatures as high as 1800°C., but the crystals seem to repel one another and to form a fluffy powder. The repulsion forces are due to the electrical double layer which must form in order to make it unnecessary for the unpolarizable Mg^{2+} ions to participate in the surface layer.

This fluidization phenomenon is characteristic for those oxides which contain a cation of high potential field and low polarizability (Al^{3+} , Si^{4+} , Mg^{2+}). The mutual repulsion between the individual particles is now being used commercially to fluidize and to move catalysts by viscous flow.

III. SURFACE STRUCTURE OF WATER AND THE FORMATION OF AN ELECTRICAL DOUBLE LAYER

Liquid water and ice have atomic structures which show a close resemblance as far as their geometry is concerned. Liquid water, like other liquids, lacks the long-range order, but in the short-range order of its atoms, there is a far reaching similarity between water and the various forms of silica. Each O^{2-} ion is tetrahedrally surrounded by four protons. According to J. D. Bernal and R. H. Fowler (6), one distinguishes: (a) an ice-like, tridymite-like (four-coordinated) form of water at low temperature, below 4°C.; (b) a quartz-like (four-coordinated) form between 4°C. and 200°C.; and (c) an ammonia-like close packed form at 200–240°C.

These three forms are thought to be types which pass continuously into each other. On this basis Bernal and Fowler were able to explain the abnormal densities of water and the behavior of water under pressure. Silica glass as well as water possesses a negative thermal expansion over a certain low-temperature region. They emphasized that a mere dipole association of H_2O molecules (dihydrol, trihydrol) cannot explain the various phenomena associated with water. The peculiar cohesion of water molecules is due to the geometrical possibility of the fitting together of the H_2O molecules. The presence of two and only two H atoms per molecule allows the possibility of attaching two water molecules by this means and two others by means of their own H atoms, thus mimicking the ionic structure of quartz which has one oxygen between every two silicons instead of one H between every two oxygens.

In spite of the fact that such complete information on the structure of water is now available, our thinking still tends to follow inherited patterns. The information given by Bernal and Fowler is nearly 20 years old and there is no doubt concerning its correctness. In 1941, E. J. W. Verwey (7) suggested some minor modifications, but he stated that the basic conceptions of Bernal and Fowler's theory are both fruitful and substantially correct.

However, Bernal and Fowler's model of the structure of water applies to the bulk structure only and cannot be used for describing the atomic arrangements within thin films or minute droplets. In accordance with his ideas concerning the surface structure of crystals, the author postulates that the extreme outer layer of liquid water or of ice does not contain protons.

A droplet of water, therefore, has its O^{2-} ions in the exterior layer, followed by a second layer which contains the nonpolarizable H^+ ions. A particle which contains OH^- or O^{2-} ions in the surface, followed by a layer which is preferentially positive, can be considered as being covered with dipoles, the negative parts of which point into space, whereas the positive parts are directed toward the interior.

As early as 1879, H. von Helmholtz (8) formulated his "double layer theory," a concept which still forms the basis of the understanding of a large number of electrical surface phenomena, such as electrophoresis, ballo-electricity, electrokinetic potential, stability of lyophobic colloids, aerosols, etc. Other phenomena, not less important, arise from the adsorption of charged particles because of the forces emanating from the Helmholtz double layer. Adsorbed ions (Freundlich and Gouy's diffuse double layer) may provide an excess electrical charge which prevents the aggregation of colloidal particles.

Our considerations show that the assumption made by Helmholtz, namely, that the particle must have an over-all electrical charge, is not necessary. Even electrically neutral particles may develop a double layer if they consist of ions which have widely different polarizabilities, in particular, if the cation has a strong potential field and a low polarizability.

As a result of the electrical double layer, two water droplets repel one another when in close proximity in spite of being electrically neutral. Large droplets unite on collision because of their greater inertia which overcomes the repulsion forces; small droplets may remain separated (fogs, clouds) over long periods of time.

An analog of the repulsion of two water droplets in atomic dimensions can be observed when SO_3 -containing gases are allowed to pass through water. In spite of the highly exothermic character of the reaction



no major absorption occurs. The water surface repels the SO_3 molecule. An SO_3 molecule can be described as an S^{6+} ion surrounded by three O^{2-} ions. The repulsion forces between the O^2 ions of the SO_3 molecule and the O^{2-} ions of the H_2O surface prevent the contact which is essential for the chemical reaction.

IV. FORMATION OF ELECTRICALLY CHARGED PARTICLES OF NON-STOICHIOMETRIC COMPOSITION (ORIGIN OF BALLO-ELECTRICITY)

As long as a water particle is sufficiently large, the excess of anions in the surface film is readily compensated for by a corresponding excess of protons in the bulk structure. With decreasing size of the droplet, however, such an adjustment becomes more and more difficult. This difficulty is encountered in the formation of nuclei in a supersaturated vapor phase. The relation which exists between the particle size of a water droplet and its stability has been described by W. Thomson's equation which correlates the vapor pressure of a droplet with its size and surface tension. Our atomistic interpretation goes one step further and postulates that the mere physical subdivision of water when carried to an extreme leads to particles of non-stoichiometric composition with an excess electrical charge and a different pH value. Formation of nuclei in a supersaturated vapor phase can be increased if oxygen ions are supplied (ionization).

In order to keep the surface energy and, with it, the free energy of the system at a minimum, the smallest water droplets formed by mechanical disintegration must contain more OH^- ions in the surface than can be balanced by the H^+ ions present in its volume. These OH^- ions are missing in the larger droplets, but no spectacular effects are produced by the slight excess of protons in the bulk of the water.

The mechanical disintegration of water in a waterfall or in a spray leads to minute particles which, for this reason, may have an excess negative charge. The bulk of the water having excess protons has, therefore, a positive charge with respect to both the water before its disintegration and to the surrounding atmosphere; the latter contains the negatively charged small droplets. This phenomenon has been extensively studied by P. Lenard (9) who measured the potential of alpine waterfalls. It is known as "waterfall" or "ballo-electricity." The phenomenon has also been examined in the laboratory, and the work of C. Christiansen (10) and of T. Malarski (11) may be cited as examples.

In connection with the waterfall electricity, the question arises: Why do the negatively charged small particles not recombine with the positively charged bulk? The larger particles or the bulk of the falling water has an excess of protons and, as a result, it carries a positive electrical charge. In spite of its positive excess charge, however, a large drop of water may repel the minute negatively charged droplets on close approach because of the repulsion forces originating between the two electrical double layers.

Water surfaces have negatively charged ions in their first layer. In spite of the coulomb attraction forces acting between the positively

charged bulk of the water and the small negatively charged spray particles, reunion cannot be expected because of the mutual repulsion which results from the double layers and exceeds the coulomb attraction. In a recent publication L. R. Sonders, D. P. Enright, and W. A. Weyl (12) described experiments which illustrate the variations in the wettability of water by aqueous solutions containing polarizable cations.

Ballo-electric phenomena are extremely sensitive to impurities. Sodium chloride or heavy metal salts provide ions of greater polarizability than the OH^- ion. As a result, they tend to enter the surface layer and to decrease the surface free energy. This not only decreases the ballo-electric potential, but may even reverse the sign of the excess charge of the small particles.

V. CRYSTALLIZATION OF WATER DROPLETS

If we assume that the water in the interior of a droplet has its normal atomic structure, whereas that of the surface film of the same droplet has a basically different atomic structure, then it follows that a water droplet has to have a certain minimum size in order to be stable. The transition from one type of structure to another type having a different geometry requires a finite distance. This distance must be a function of the temperature, because the structure of water changes with temperature with respect to geometry and internuclear distances. One would also expect that the more rigid structure of ice would require a larger transition layer than the more flexible structure of liquid water. As a result, at a given temperature below the freezing point, a particle size must exist where a droplet of water is stable in the liquid state but not as ice. This is the reason why water droplets of small size (fogs, clouds) can be supercooled very strongly without showing a tendency to crystallize. In a recent report (13) to the National Advisory Committee for Aeronautics, R. G. Dorsch and P. T. Hacker showed that the average spontaneous freezing temperature of water decreased with decreasing size of the droplets. They found that the effect of size on the spontaneous freezing temperature was particularly marked below $60\ \mu$.

At the present time a group of scientists working for the General Electric Company, Schenectady, N. Y., claim that they can produce rain by "seeding" supercooled clouds with a smoke of silver iodide (14a). The crystal structure of AgI resembles that of one of the forms of ice. Based on this similarity between the crystal structure of AgI and H_2O , its effect is interpreted as "seeding" (14b). Whether it leads to rain or not, it is a fact that a supercooled cloud consisting of minute droplets of water having a temperature considerably below the freezing point can crystallize when contaminated by AgI smoke.

Silver iodide provides two polarizable ions. These ions are likely to enter the surface of the water droplets where they lower the surface

energy. The presence of these highly polarizable ions weakens the distorting influence of the electrical double layer so that the atomic structure of the water droplet changes toward that of the normal arrangement, and crystallization becomes possible.

This explanation has recently been tested by C. L. Hosler (15) who found that many iodides, furthermore, silver sulfide and silver nitrate and even ozone, have the same effect upon the supercooled water droplets as the silver iodide. There is no resemblance between the atomic structures of Ag_2S or of AgNO_3 and ice.

That fact that the most polarizable ions enter the surface of water is well established and has been discussed in previous papers in more detail. Analytical proof for this phenomenon was given by A. Stock (16) who discovered, during his microanalytical work on mercury, that the Hg^{2+} ions enter the surface layer of an aqueous solution, leaving the bulk of the liquid with a lower concentration of mercury.

VI. THE STRUCTURE OF THE ICE SURFACE AND SOME OF ITS MANIFESTATIONS

Even if the atomic structure of the liquid water and that of ice show a close resemblance, one has to expect that the distortion of the surface structure of a rigid crystal is energetically much more difficult than a corresponding structural change in a liquid surface. How then can an ice crystal adjust its surface structure in order to avoid the participation of protons in the extreme outer layer?

If we take an ice cube out of our refrigerator and immerse it in carbonated water it acts as a source of copious gas evolution. The ice cube has adsorbed from the atmosphere those molecules which can lower its free energy. The gas evolution indicates that the surface has become hydrophobic and that it behaves like the "clean" mirror in a bathroom which is hydrophobic also and does not condense the water vapor in the form of a continuous film but rather forms individual droplets. Adsorption of "greasy" constituents from the atmosphere is one of the most efficient means which a surface has to lower its free energy.

After the ice cube has had a chance to purify its surface by partly melting, it also loses its power to release carbon dioxide from the super-saturated solution of carbonated water. Filling up the glass with more carbonated water does not produce the copious gas evolution which was characteristic for the ice cube when it first came from the refrigerator. How does a pure ice crystal behave?

Some reflection on this problem leads to the following picture as a probable solution. An ice crystal, even at a temperature of $5-10^\circ\text{C}$. below its melting point, is coated with a film of liquid water. This layer provides a transition from the rigid structure of the bulk of the crystal to the double

layer. This film neither has the normal structure of water nor is it supercooled with respect to ice. Such a film is in equilibrium with its vapor on one side and with the surface of the rigid ice on the other. In order to bridge two basically different atomic structures the film is probably a few hundred molecules thick. The strict coordination requirements of the hydrogen ions and their lack of polarizability make it improbable that such a transition would take place within a short distance.

We, therefore, assume that even at temperatures below $0^{\circ}\text{C}.$, ice is coated by a mobile, noncrystalline film having a thickness of several hundred molecules. The atomic structure of this film is not uniform, but is distorted and its energy content must be higher than that of a corresponding amount of bulk water at the same temperature. Nevertheless, its transition into the normal structure of ice is prevented by the increase of the surface energy which would accompany such a rearrangement.

This concept of the surface of ice being covered with a liquid film which is stable below the freezing point is not new, but has been proposed a hundred years ago by M. Faraday (17) and J. Tyndall (18) in order to explain the phenomenon of "regelation."

1. *Regelation Phenomena*

Who is not familiar with the beautiful picture which a winter landscape offers after a snowstorm? The trees are heavily loaded and on closer inspection one finds that each little branch is covered with a mass of snow crystals, piled up an inch high or even higher. If we were not accustomed to seeing this spectacle every year, if we had not built snowmen or engaged in snowball fights, we probably would stop and wonder about the unique properties and the strange behavior of snow. We would ask questions such as: Which other crystalline powders could be piled up on a thin branch like snow? Is there another homogeneous, powdery and dry material which solidifies under the gentle pressure of children's hands? Is there another substance of high purity whose crystals will combine at a mere touch? Not only do snowflakes stick together and pile up, but two pieces of ice will fuse together on mere contact, even under water.

Faraday and Tyndall were probably the first scientists to think about and experiment with this strange substance, ice. They came to the conclusion that this freezing together, or "regelation" as Tyndall called it, must be the result of a liquid layer covering the ice surface. This water film, they theorized, must have the ability to freeze when bounded by ice on both sides but to remain liquid when bounded by ice on one side only. M. Faraday's experiments are convincing in their simplicity and his diary is full of stimulating observations. For example (19):

"When wet snow is squeezed together, it freezes into a lump (with water between) and does not fall asunder as so much wetted sand or other

kind of matter would do. In a warm day, if two pieces of ice be laid one on the other and wrapped up in flannel, they will freeze into one piece. All this seems to indicate that water at 32° will not continue as water, if it be between two surfaces of ice touching or very near to each other. Also that in such cases, an accumulation of such pieces of ice in one heap or portion can have freezing going on within, whilst no part is below the freezing point and whilst thawing is going on at the outside."

He further observed that two flat pieces of ice floating in water *repelled one another*. However, when they were brought into contact they immediately adhered and froze together. This theory was daring indeed. It was well established that a substance can be supercooled, i.e., prevented from crystallizing below its freezing point, but not in the presence of crystal nuclei. Faraday postulated the presence of a liquid film which is stable not only below the freezing point, but also in contact with the crystalline phase of the same composition. One can easily understand that this explanation met with serious resistance. One of the foremost antagonists of this theory was Lord Kelvin, who attacked it vigorously. However, it was well defended by Faraday.

2. Penetration Phenomena

Ice shows another phenomenon for which no sound explanation has yet been offered. A block of ice can flow through a piece of wire gauze without being damaged. In the same fashion a solid object, a metal ball or a wire, can work its way through a piece of ice without cutting it apart. The velocity of a metal sphere falling through ice was found to depend upon the temperature; it is fast close to the melting point, but even below -10°C . it still falls with a measurable speed. Numerous experiments dealing with this mutual interpenetration have been performed within the last hundred years. N. E. Dorsey (20) gives us an excellent review of the early work and his book should be consulted for more details. The "explanations" given for these phenomena go back to J. Thomson (1861) who assumed (21) that the ice melts under pressure and that the water freezes as soon as the pressure is released. It is surprising that this naive explanation is still used in our textbooks at a time when the phase relationships of water are well established. Penetration has been measured at -11°C ., i.e., at a temperature where a pressure of 1500 atm. is required for melting the ice.

In spite of this obvious discrepancy, skiing, skating, regelation, penetration of ice and solids, including the flow and compression of glaciers through narrow beds, are still being discussed on the basis of J. Thomson's explanation. Sir George Beilby (22) expressed his opinion on this subject very aptly when he stated:

"A theory of the formation and flow of glaciers based on the fusion of ice under pressure, and its regelation on the removal of pressure, has been widely accepted, though many students of the subject have recognized that this theory could only be made to cover all the known facts, *by straining both the facts and the theory.*" The pressure of a wire cutting through ice or of a steel ball falling in ice is supposed to cause local melting of the supporting ice. The necessary heat of fusion is taken from the wire so that its temperature drops. The cold wire is supposed to cause freezing of the water on top of it. Only the water, which has flowed around the wire and now is free of stress, can freeze. Its heat of crystallization warms the wire which conducts the heat to the supporting ice and causes the latter to melt, etc.

The thermal conductivity of the wire or of the steel ball is assumed to play an important role in this cycle. This assumption seemed to be supported by the experiment. It was found that a metal wire cuts through ice fairly fast, but that a string loaded with the same weight at the same temperature takes much longer. There can be no doubt that ice undergoes plastic deformation when sufficiently loaded, but it seems highly improbable that these phenomena can be explained on the basis of plastic flow alone.

3. Slipperiness of Ice

The friction of an ice surface slightly below the melting point is zero. More than one hundred years ago, W. Hopkins (23) measured the flow of an ice block on slabs of both polished and unpolished marble and found the ice to move if the inclination of the unpolished stone surface was less than 0.5° . On the polished surface the ice moved at any inclination which he could detect with a spirit level.

This phenomenon which is effective in skating has also been "explained" on the basis of local melting under pressure and regelation. In order to explain that skating is possible even below -10°C . one has to assume that the area which supports the skates is so small that the local pressure can reach 1500 atm.

4. Scientific Basis of the Faraday-Tyndall Concept of the Ice Surface

All of the phenomena which were discussed in the preceding chapters can be explained easily by the concept that ice is covered by a liquid film, as had been suggested by Faraday and Tyndall. The liquid film must be stable indefinitely in the presence of ice, but can crystallize when sandwiched between ice. The main objection against this postulate, the coexistence of a liquid and a solid phase of a substance below its melting point, seemed to be that it violates a basic law of thermodynamics.

Many physicists and chemists still fail to realize that the dimensions of a solid or of a liquid cannot be decreased beyond a certain limit without affecting those properties which are a function of the atomic structure.

Films of a metal assume a negative temperature coefficient of electrical conductivity; they become semiconductors. In a similar fashion, insulators lose their ability to prevent material and electron transport through their lattices as soon as their dimensions become less than a few hundred angstrom units. The vapor pressure of liquids changes if the size of the droplet decreases; a phenomenon which is attributed to the curvature of the surface. However, the vapor pressure of a non-curved water film is affected by the thickness of the film in a similar fashion. According to I. R. McHaffie and S. Lenher (24), the variation of the vapor pressure of an H_2O film is a function of both its thickness and the nature of its support (glass, platinum). Our modern concept, namely, that the structure of liquids resembles much more that of crystals than that of gases, offers no serious difficulties to account for the apparent discrepancy. The fact that the melting point of silica is 1600°C . for quartz, 1670°C . for tridymite and 1713°C . for cristobalite may be explained on the basis of the different energy contents of the three modifications which, in turn, are the result of the different arrangement of their atoms in space. The surface film which is stable on ice represents a different modification of H_2O and its energy must differ considerably from that of normal water because it has a basically different atomic structure. However, in contrast to the modifications of silica, each of which is homogeneous, the surface film on ice represents a gradual transition between two extreme structures, a layer of oriented dipoles at the one side and a cristobalite-like ice structure at the other. For this reason the structure of the film cannot be described in terms of self-repeating elementary cells. As a result, the surface film has no sharp melting point, but its thickness decreases gradually with decreasing temperature. This leads to the conclusion that the characteristic properties of the ice surface, for example, its slipperiness, change gradually as the temperature is lowered.

Dorsey (20) in his chapter "Sliding Friction of Ice" describes the influence of the temperature on skating and quotes a remark of the arctic explorer Nansen who observed in Greenland that at very low temperatures ice had lost its slipperiness.

Due to its structure-gradient, the free energy of the surface film becomes a function of its thickness. The thickness of the film is a function of the dissimilarity of the two bordering media. For example, the surface film on ice at a given sub-zero temperature should be thicker if it has to bridge two basically different media, such as ice-metal, than if it has to bridge the gap between the structure of ice and a hydrophilic organic material.

The difference in speeds of penetration between a wire (fast) and a string (slow) can thus be explained on the basis of different film thicknesses rather than different thermal conductivities.

Regelation is the result of the crystallization of the surface film when brought in contact with ice on both sides.

The effect of polarizable ions (I^- , Pb^{2+}), atoms (Hg), or polarizable molecules (I_2 , O_3) on the crystallization of supercooled water droplets may be explained on the same basis. Their presence in the surface film makes it unnecessary to distort the normal structure of water to the extent that crystallization becomes improbable.

VII. CHEMISTRY OF THE NASCENT SURFACE OF WATER (SONO-CHEMISTRY)

The deformation of the surface ions and their geometrical rearrangement are not the only ways to decrease the energy of a nascent surface. Frequently the surface energy of a system is lowered by the chemisorption of foreign molecules. For silica it was found (25) that the nascent surface which is obtained either by fracture of quartz or by dehydration of silica gel produces atomic oxygen by breaking up oxygen molecules which had been adsorbed from the air. If that is true for silica, the nascent surface of water should produce a similar reaction.

The cavitation of water in an ultrasonic generator provides a convenient means of studying the behavior of nascent surfaces. W. A. Weyl and E. C. Marboe (26), in a paper on some mechanochemical properties of water, discussed the role of foreign molecules, such as carbon tetrachloride, on the tensile strength of water. A nonpolar molecule can affect the tensile strength of water in much the same manner as a "Griffith defect" affects that of solids. Water under tension stress can be expected to break at those places where dissolved gas molecules (N_2 or O_2) are present. Cavitation of water, which is saturated with air, exposes, therefore, the N_2 and O_2 molecules to its nascent surface or, more specifically, to the strong positive potential field of protons. The resulting electrical field deforms or polarizes the nonpolar molecule to such an extent that a transfer of electrons occurs between the polarized gas molecule and some oxygen ions of the nascent surface. Some of the oxygen ions change into O^- ions by donating electrons, and the O_2 and N_2 molecules enter into chemical reaction with the water.

1. *Sonoluminescence*

The phenomena of triboluminescence and sonoluminescence are closely allied with the chemical reactions which take place at nascent surfaces. Sugar crystals, fractured in air, produce a luminescence which is visible to the dark-adapted eye. This luminescence results from the dissociation of nitrogen molecules in the electrical field of a hydrogen or a carbonium ion which is exposed in the nascent surface of sugar. According to M. Longchambon (27), the triboluminescence spectrum of sugar reveals the recombination of nitrogen atoms. When fractured under xylol, sugar does not

show triboluminescence, according to F. G. Wick (28). The mechanical fracture of sugar leads, therefore, to its chemical reaction with the constituents of the atmosphere.

In the same fashion one can explain the nitrogen glow in cavitating water. E. N. Harvey (29) reviewed the literature in this field and performed a number of pertinent new experiments on "sonoluminescence." Ever since these phenomena were observed, they were treated as if they were the result of an electrical discharge between two electrodes. This explanation is not satisfactory because there is no obvious relation between the behavior of molecules in a discharge tube and those dissolved in water and exposed to a strong ultrasonic field. E. N. Harvey found that O_2 and N_2 show sonoluminescence in cavitating water, but H_2 and Ne do not. Bromine dissolved in water was found to produce the strongest sonoluminescence. The atomistic approach to this phenomenon provides a simple explanation for Harvey's results. In order to satisfy the potential field of the protons, a nonpolar molecule is polarized to such an extent that it breaks up into ions. Nitrogen, for example, can form N^{3-} ions which then combine with the protons to form ammonia. The polarization of neon atoms, however, cannot easily lead to a chemical reaction. Bromine molecules are cleaved into Br^+ and Br^- ions, and the latter are utilized by the nascent surface to satisfy the potential field of the protons.

2. Oxidation Phenomena as a Result of Cavitation

The oxidation phenomena which occur in water when it is exposed to strong ultrasonic radiation are the result of dissolved oxygen molecules reacting with the nascent surface of water. These oxidation phenomena require the presence of oxygen molecules (dissolved air) in the water and an ultrasonic field which is sufficiently strong to produce cavitation, i.e., nascent surfaces. The phenomena themselves are well known and have been studied repeatedly since their discovery by F. O. Schmitt, C. H. Johnson, and A. R. Olson (30). H. Beuthe (31), as well as H. Schultes and H. Gohr (32), found that the formation of hydrogen peroxide is accompanied by an increase in the acidity of the water.

The formation of hydrogen peroxide in cavitating water can be explained on the same basis as the formation of atomic oxygen at the nascent surface of silica. The nascent surfaces of water and of silica contain cations (H^+ and Si^{4+} , respectively) which produce strong potential fields as a result of their small sizes and low polarizabilities.

Oxygen molecules are polarized and attracted to these cations. The polarized O_2 molecule can be described as having an induced dipole, and the part with the higher electron density is oriented toward the cations, whereas the more positive part extends into space. This positive part attracts an electron from an adjoining O^{2-} ion and the resulting electron

transfer produces O_2^- ions as the first step of the chemical reaction. At the surface of silica the O_2^- ion cleaves off atomic oxygen, whereas at the nascent surface of water it forms H_2O_2 instead.

The various oxidation reactions which may follow, for example, the liberation of iodine from KI, are too well known to be reviewed here.

3. *Fixation of Nitrogen as a Result of Cavitation*

As we have seen from the triboluminescence of sugar in air and from the sonoluminescence of water containing dissolved nitrogen, even the stable nitrogen molecule can be broken up in the high potential field of the proton. H. Beuthe (31) found reaction products of nitrogen with water after exposure to ultrasonic radiation. In particular, he obtained positive tests for NH_3 , HNO_2 , and HNO_3 . His findings have been confirmed several times since, and recently A. I. Virtanen and N. Ellfolk (33) published a systematic study on the fixation of nitrogen in an ultrasonic field.

Their work elaborates on previous observations and includes the effects which other substances have upon the oxidation of nitrogen during cavitation. From our point of view it can be easily understood that molecules which are more readily deformed and ionized than the N_2 molecule should interfere with the oxidation, provided the ionization products of these molecules can satisfy the force fields of the protons by a chemical reaction. Indeed, the presence of carbon monoxide, of ether, and of hydrogen prevents nitrogen fixation. The presence of argon, however, does not interfere. Previous attempts to account for the reaction of nitrogen with water assumed the ionization of the nitrogen molecules in an electrostatic field and a subsequent reaction of the N^+ or N_2^+ ions with oxygen in the same fashion as in an electric discharge tube. In a discharge tube hydrogen interferes with the oxidation of nitrogen but so does argon, because both gases have similar ionization potentials. However, the oxidation of nitrogen during cavitation is not materially affected by the presence of argon. Virtanen and Ellfolk write: "In our experiments in the ultrasonic field, however, argon does not, at least appreciably, prevent nitrogen fixation. Since, on the other hand, the inhibitory effect of hydrogen is very strong, and under the experimental conditions the hydrogen molecule has been proved to dissociate into atoms, as the reduction of trivalent iron to bivalent iron shows, the experimental material so far does not give any proof for the idea that the primary reaction in the combination of nitrogen to oxygen in the ultrasonic field is ionization of the nitrogen molecule."

In spite of the similarity of the two processes, a basic difference exists between the excitation of a molecule in a gas discharge tube, on the one hand, and in a cavity formed in water by ultrasonic radiation, on the other. The ionization of molecules in a gas discharge tube is the result of electron transfer between the neutral molecule and the electrode. The

nascent surface produces a chemical reaction whereby the neutral molecule, say the O_2 molecule, is first polarized by a proton or by an Si^{4+} ion, and the induced dipole molecule now attracts an electron from a surface oxygen ion which changes into an O^- ion.

VIII. SUMMARY AND CONCLUSIONS

The last two decades have witnessed a rapid progress in determining the atomic structures of crystals by x-ray diffraction methods. The information thus obtained did not lead to a better understanding of the chemistry and physics of surfaces. V. M. Goldschmidt (34), who may justly be called the father of modern crystal chemistry, taught that the structure and the properties of a crystal can be explained and correlated with the fundamental properties of its ultimate building units, the ions. The ions are characterized by their electrical excess charges, by their sizes, and by their polarization properties. The polarization properties reflect the behavior of the ions in an electrical field. They are determined by the electronic configuration of the ions as well as by their sizes and charges. These three fundamental properties of the ions should be treated on a par with respect to their importance for determining the atomic structure of crystals. Our research has revealed that this is no longer true for surface properties. Whenever asymmetrical arrays of ions are involved, i.e., in surfaces, interfaces, and in defective crystals, the polarization properties assume a leading role.

Several phenomena which could not be explained previously were traced to the influence of the polarizability of ions. The hysteresis of the contact angle, the hydrophobicity of water-soluble salts ($CrCl_3$), the chemical properties of adsorbed ions, etc., can be understood only if one considers that the electron distribution probability of surface ions is highly asymmetrical. By changing their electron distribution the surface ions lower the surface energy and, with it, the free energy of the system.

It is the object of this paper to show the behavior of those substances which contain cations of low polarizability. In this case the surface structure of a crystal or of a liquid has to undergo a major geometrical rearrangement in order to bring the polarizable anions into the outer layer so that they can better screen the potential fields of the cations. The phenomenon of "fluidization of catalysts" is a result of this rearrangement. It is explained on the basis of mutual repulsion of particles having an electrical double layer.

Water represents the extreme of this group. Its cation, the proton, has zero polarizability and, consequently, it has no means of lowering its potential field when present in the outer layer of a surface film. The distortion of the water structure which takes place in order to make it unnecessary for protons to participate in the outer layer gives rise to an

electrical double layer which, in turn, produces a number of interesting phenomena.

Water droplets of small size repel one another in spite of being electrically neutral (stability of clouds and fogs).

Beyond a certain size, further subdivision of water by mechanical forces (sprays, waterfalls) leads to particles of non-stoichiometric composition and electrical excess charges (ballo-electricity). In order to have only anions in the outermost surface, droplets below a critical size must have an excess of O^{2-} ions over the stoichiometric ratio of H_2O .

Water droplets beyond a certain size fail to crystallize on cooling below $0^{\circ}C$. because crystallization would raise the surface energy of the system. In order to accommodate both the surface structure which contains only anions and the crystalline structure of ice, a droplet has to exceed a certain size because it requires a transition layer of finite distance.

The presence of a transition layer, several hundred molecules thick, having a structural gradient explains some of the puzzling properties of ice; namely, its slipperiness, the regelation phenomena, and the penetration of ice and other solids.

Faraday and Tyndall, more than a hundred years ago, advanced a theory in which they assumed that ice is coated by a film of water even below the freezing point. This concept which was violently attacked by Lord Kelvin can now be justified and reconciled with laws of thermodynamics.

The abnormal properties of water droplets and of the surface of ice originate from the tendency of the systems to avoid the participation of protons in the outer surface layer. The presence of nonpolarizable protons would raise the surface energy of a system to a very high level. The high potential field which protons produce when present in a surface is evidenced by the violent chemical reactions which take place in water when it is fractured. The cavitation of water in an ultrasonic field produces nascent surfaces which must contain protons. These nascent surfaces tear apart those oxygen and nitrogen molecules which dissolved in the water in order to produce anions which can screen the potential fields of the exposed protons.

Protons are present only in the nascent surface of water, but not in equilibrium surfaces. This concept is used for explaining the sonoluminescence of water and the oxidation reactions which accompany its cavitation in ultrasonic fields (sonochemistry). The fixation of nitrogen, i.e., the formation of ammonia and nitric acids in cavitating water at room temperature, can be explained on the same basis.

REFERENCES

1. WEYL, W. A., *Trans. N. Y. Acad. Sci. Ser. II* **12**, 245 (1950).
2. WEYL, W. A., *J. Soc. Glass Techn.* **32**, 247 (1948).

3. ROMAN, M. K., MARBOE, E. C., AND WEYL, W. A., *J. Soc. Glass Technol.* **32**, 260 (1948).
4. ENRIGHT, D. P., SONDERS, L. R., AND WEYL, W. A., *J. Applied Phys.* **20**, 1011 (1949).
5. FAJANS, K., *Chemical Forces and Optical Properties of Substances*. McGraw-Hill Book Co., New York, 1931.
6. BERNAL, J. D., AND FOWLER, R. H., *J. Chem. Phys.* **1**, 515 (1933).
7. VERWEY, E. J. W., *Rec. trav. chim.* **60**, 887 (1941).
8. VON HELMHOLTZ, H., *Ann. Physik* **7**, 337 (1879).
9. LENARD, P., *Ann. Physik* **46**, 584 (1892).
10. CHRISTIANSEN, C., *Ann. Physik* **59**, 95 (1919).
11. MALARSKI, V. T., *Acta Phys. Polon.* **3**, 43 (1934).
12. SONDERS, L. R., ENRIGHT, D. P., AND WEYL, W. A., *J. Applied Phys.* **21**, 338 (1950).
13. DORSCH, R. G., AND HACKER, P. T., Technical Note 2142. National Advisory Committee for Aeronautics, Washington, D. C., July, 1950.
14. (a) SCHAEFER, V. J., *Trans. N. Y. Acad. Sci.* **12**, [8] 260 (1950); (b) VONNEGUT, B., *Chem. Revs.* **44**, [2] 277-89 (1949).
15. HOSLER, C. L., *J. Meteorol.* **8** (5) (Oct. 1951).
16. STOCK, A., *Ber.* **72**, 1844 (1939).
17. FARADAY, M., *Proc. Roy. Inst. Gr. Brit.* (1850).
18. TYNDALL, J., *Proc. Roy. Soc. (London)* **9**, 76 (1858); *Ann. Physik* **103**, 157 (1858).
19. FARADAY, M., *Faraday's Diary*, Vol. IV, p. 79, 1839-1847. G. Bell and Sons, Ltd., London, 1933.
20. DORSEY, N. E., *Properties of Ordinary Water Substance*. Reinhold Publishing Corp., New York, 1940.
21. THOMSON, J., *Proc. Roy. Soc. (London)* **11**, 473 (1861).
22. BEILBY, G., *Aggregation and Flow of Solids*, p. 197, MacMillan and Co., London, 1921.
23. HOPKINS, W., *Phil. Mag.* **26**, 1 (1845).
24. MCHAFFIE, I. R., AND LENHER, S., *J. Chem. Soc. (London)* **127**, 1559-72 (1925).
25. (a) WEYL, W. A., *Research (London)* **3**, 230 (1950); (b) *Ind. Hyg. Foundation Trans. Am. Ser. Bull. No. 14*, 41 (1949).
26. WEYL, W. A., AND MARBOE, E. C., *Research (London)* **2**, 19 (1949).
27. LONGCHAMON, M., *Compt. rend.* **174**, 1633 (1922); *ibid.* **176**, 691 (1923).
28. WICK, F. G., *J. Optical Soc. Am.* **27**, 275 (1937).
29. HARVEY, E. N., *J. Am. Chem. Soc.* **61**, 2392 (1939).
30. SCHMITT, F. O., JOHNSON, C. H., AND OLSON, A. R., *J. Am. Chem. Soc.* **51**, 370 (1929).
31. BEUTHE, H., *Z. physik. Chem.* **A163**, 161 (1933).
32. SCHULTES, H., AND GOHR, H., *Z. angew. Chem.* **49**, 420 (1936).
33. VIRTANEN, A. I., AND ELLFOLK, N., *Acta Chem. Scand.* **4**, 93 (1950).
34. GOLDSCHMIDT, V. M., *Skrifter Norske Videnskaps-Akad. Oslo Mat. Naturw. Klasse* **1926**, No. 8, pp. 1-156.

A KINETIC BASIS FOR POLYMER PRECIPITATION AND THE SELECTION AVERAGE

D. R. Morey

*The Kodak Research Laboratories,¹ Eastman Kodak Company,
Rochester 4, New York*

Received April 16, 1951

INTRODUCTION

The last decade has seen considerable attention devoted to both the theoretical and experimental aspects of crystal nucleation and growth, with the result that, at least in the case of small molecule substances, the state of knowledge has a good foundation and framework. On the other hand, the attention given to polymer fractionation and precipitation, while considerable, has been concerned almost completely with the thermodynamic approach, based on the assumption of an equilibrium process, and leaving unexplored the actual mechanics of the process. It is important, however, to understand more about the real processes which take place, particularly if we deal with experiments which are not concerned with an equilibrium separation of two liquid layers. For an equilibrium case, the two methods should converge to agreement. Another value thus lies in checking some of the assumptions which have to be made in order to arrive at an actual solution of the formal thermodynamic framework. Not that the kinetic method is free from assumptions; quite the contrary, but they are a quite different set of assumptions. In this paper we have begun the kinetic approach, and, by directing attention toward molecular weight as the variable, have been able to put the results in the form of an average suitable for experimental test. This emphasis on molecular weight also provides an additional theoretical basis for the continuous precipitation-turbidity method for molecular weight distribution.

THEORY

In examining the origin of differential precipitation, the steps of nucleation and of further growth can be considered separately. The first step is a collision between a chain of molecular weight M_i , with some other chain M_j . A collision frequency between two types of molecules i, j in solution may be expressed by (1)

$$Z_{ij} = 4\pi(D_i + D_j)\sigma_{ij}N_iN_j1/f \quad [1]$$

¹ Communication No. 1400.

wherein D_i , D_j are the diffusion coefficients of the two species, σ_{ij} the sum of the radii, and N_i , N_j the number of molecules/ml. If the diffusion is entirely due to thermal motion, the factor f is unity. When dealing with ionic polymers, the electric forces play a part, and f is a function of the electric potential versus distance from the molecule. Since this theory is concerned with the role of molecular weights primarily, f may be considered constant if the sizes do not range to very small lengths of chain.

The collision frequency between gas molecules is given by kinetic theory as

$$Z_{ij} = \sigma_{ij}^2 N_i N_j [8\pi RT(1/M_i + 1/M_j)]^{1/2}. \quad [2]$$

Application of [2] to solutions also would require the fulfillment of a number of assumptions, and it is generally considered that these are untenable, although Moelwyn-Hughes (2) has concluded, to the contrary, that the gas collision expression can also be applied to solutions with considerable accuracy.

Now turning to the quantity σ , it is desired to establish its effective value when dealing with chains of some degree of kinking, and to relate this effective value to molecular weight. For spheres, the radius is proportional to $M^{1/3}$, and for rigid rods, it is proportional directly to M . The value for kinked chains thus lies in between. Values of this exponent have been obtained experimentally by Gralén (3) from ultracentrifuge data, as follows:

Cellulose in cuprammonium solution	0.55
Cellulose nitrate in acetone	0.68
Sodium cellulose xanthate	0.52

A reasonable assumption which is adopted for this theory is that σ is proportional to $M^{1/3}$ for the usual polymer in solution.

A parallel relationship holds for the diffusion constant. Thus, for spheres, $D = \frac{kT}{6\pi\eta r}$ and is thus proportional to $M^{-1/3}$. For the case of a long thin rod of length l and diameter d , the diffusion coefficient has been calculated by various workers as $D = \frac{kT}{3\pi\eta l} \ln\left(\frac{2l}{d}\right)$, so that in this case, D is nearly proportional to M^{-1} . For chains intermediate in kinking and shape between spheres and rods, we shall thus adopt the assumption $D \propto M^{-1/2}$.

Then, using Eq. [1], $Z \propto N^2$ and is, to the approximations used, independent of M . Using Eq. [2], $Z \propto N^2 M^{1/2}$. Nucleation requires that, after two chains are brought together by a collisional process, some minimum number of secondary links be developed between them, in order to hold them together long enough to serve as a nucleus. These

secondary links develop from active groups along the chain, and so the probability of developing a given number of them is proportional to the lengths of the chains participating; for chains not extremely different in length, we take this probability as proportional to $(M_i M_j)^{1/2}$. The nucleation rate must also contain an exponential factor, $e^{-n\Delta F/kT}$, where ΔF is the free energy for the formation of a secondary bond, and n is a minimum number of links needed to establish a recognizable nucleus. This is analogous to the concept of a critical size. The aggregation rate thus becomes, up to this point, $Z_{ij}(M_i M_j)^{1/2} e^{-n\Delta F/kT}$. Opposed to this is the rate of disappearance of formed nuclei, owing to local temperature fluctuations. This re-resolution rate will be proportional to $e^{-E_s/kT}$; E_s is defined in terms of the per cent of precipitant liquid, P ; and the molecular weight. The addition of precipitant makes the nucleus more resistant to re-resolution, since the interaction between solvent and polymer is decreased. Hence, E_s is some increasing function of P . Furthermore, while there is a critical lower limit to E_s , below which a nucleus has not sufficient lifetime to function as a center of growth, E_s may take on much larger values. A pair of chains may continue to develop more mutually shared bonds after the minimum number has been established; and the longer the chains, the greater the average value of E_s will be. Thus, E_s is also an increasing function of M .

The ratio of the rates of formation and re-resolution thus results in:

$$K = Z_{ij}(M_i M_j)^{1/2} e^{-n\Delta F/kT} e^{f(P, M)/kT} \quad [3]$$

where K lumps the constants. The role of molecular weight is made clearer by considering the case of a solution containing only a homogeneous fraction. Then

$$K = N^2 M e^{f(P, M)/kT} \quad \text{or} \quad K = N^2 M^{1/2} e^{f(P, M)/kT} \quad [4]$$

depending on the choice of [1] or [2]. If experimental systems are considered in which good mechanical stirring is used, the collision rate depends on the cross sections, but not on thermally produced movements of the molecules. The term $M^{-1/2}$ which is inherent in either [1] or [2] because of the thermal driving force, may then be omitted, and

$$K = N^2 M^2 e^{f(P, M)/kT} \quad [5]$$

indicates how molecular weight enters into the nucleation step.

Growth from Nuclei

In actual fractionations and turbidity-precipitation studies, the bulk of the precipitate consists of particles much larger than nuclei, and growth upon the formed nuclei is the important process to be examined. Growth can occur by two processes: (a) by the diffusion controlled coalescence of nuclei, and (b) by the addition of single chains to relatively

larger aggregates of precipitate. It is of interest to note that the type of fractionation to be obtained would differ for these two cases; case (a) would result in precipitates in which the weighting of the shorter chains is more pronounced than in case (b).

We shall consider the second process as the effective one in those cases of successful application of the turbidity-precipitation method (4), and shall calculate the growth rate. The effective radius σ will now take the form $aV_p^{\frac{1}{3}} + bM_i^{\frac{1}{3}}$ where M_i is the chain attaching to a particle of volume V_p . (V_p is itself a function of M , although of the chains which have already precipitated, rather than those still in solution. For reasonably shaped distributions, there is a correlation between these weights.)

The number of N_i chains available is also a factor, but we shall consider that the number of particles has been fixed in the nucleation process and is no longer a function of M in growth. The next factor, in the growth rate, is the chance of finding the necessary number, n , of potential linkage points along the chain M_i . This factor, for chains of good length, is proportional to M_i , or more exactly, to $M_i - Cn$, where C is the molecular weight of the chain portion between active groups; that is, collisions can and do occur between particles and very short chains, but they cannot affect growth. The greater the excess of M_i over the minimum value Cn , the more ways there are of assigning n points to contact the surface of the particle. We may also include the exponential term $e^{-n\Delta F/kT}$ which counts the actual activation of the bond sites over the potential barrier and into the bonded state. The manner of combining these factors again must depend upon the choice of collision mechanism. Making use of Eq. [1] leads to a growth rate proportional to

$$N_i(aV_p^{\frac{1}{3}} + bM_i^{\frac{1}{3}})M_i^{-\frac{1}{3}}(M_i - Cn)e^{-n\Delta F/kT}. \quad [6]$$

We next introduce the measure of growth which is recognized by the experiment. For example, if the experiment were one involving osmotic pressure, the particle is counted as one regardless of size, and the effect of adding a chain M_i is weighted as M_i^0 ; the effect of mass is thus unobserved. If the experiment were one of weighing the particle by gravimetric means, then M_i is weighted to the first power. The experiments which are used to supply data for the present theory involve detection of a "precipitation point" at which particles are quite small, and optical turbidity just beginning to develop strongly. Now it is known from the laws of optical scattering (5) that the radiation scattered by a particle smaller than the wavelength is proportional to the square of the volume. Hence we shall introduce the factor M_i^2 into the growth rate, remembering that for experiments dealing with larger particles or with the actual separation and weighing of a precipitate, M_i to the first power is to be used.

The ratio of the rates of aggregation and re-solution, for the case of particle growth, yields

$$G' = N_i M_i^3 (M_i - Cn) (aV_p^{\frac{1}{3}} + bM_i^{\frac{1}{3}}) e^{-n\Delta F/kT} e^{f(P,M)/kT} \quad [7]$$

or, if stirring is made the dominant factor in effecting collisions,

$$G' = N_i M_i^2 (M_i - Cn) (aV_p^{\frac{1}{3}} + bM_i^{\frac{1}{3}})^2 e^{-n\Delta F/kT} e^{f(P,M)/kT}. \quad [8]$$

In order to deal with the term $aV_p^{\frac{1}{3}}$, the reasonable assumption may be made that the larger particles have a proportionally higher average weight for the chains in such particles, so that we may substitute a term $a'M_i^{\frac{1}{3}}$. The above forms thus indicate that G' is composed of a sum of terms in M ranging from a power of 4 to one of 2. The molecular weight influence upon the precipitation process may thus be put approximately into the form

$$G = \phi_4 N_i M_i^4 e^{f(P,M)/kT} + \phi_3 N_i M_i^3 e^{f(P,M)/kT} + \phi_2 N_i M_i^2 e^{f(P,M)/kT} \quad [9]$$

where the terms involving non-integer exponents have been weighted into the nearest integer term. These weighting factors ϕ_4 , ϕ_3 , ϕ_2 will also depend upon the type of experimental conditions prevailing. When dealing with vigorous stirring and with sensitive detection of the first appearance of turbidity, the 4th-power term should predominate. When particles are allowed to grow by thermal diffusion, then the 3rd-power term should be most effective. Finally, when the particles approach a wavelength in size, the measure of turbidity increment indicated above decreases, and G is determined by the 3rd- or 2nd-power term according to the dominance of stirring or of thermal diffusion.

At this point it is helpful to clarify the meaning of the ratio of the rates, as given in Eqs. [5] and [9]. It may be pointed out that King and Garner (6) have characterized the melting points of fatty acids, in a theoretical approach, by equating the rate of the crystallization process to the rate of the melting process and solving the equation for the quantities desired. The process employed here is similar. In the actual experiment carried out to determine the beginning of particle growth, this condition is brought about by the addition of precipitant or by lowering the temperature, and the sensitivity of the turbidometric apparatus determines the actual point in terms of particle growth which is chosen. It has been found that this point is reproducible; and the experiment can be reversed and the point checked by diminishing the turbidity to the vanishing point. In other words, at whatever point the experiment requires, the process may be stopped, and the rates then become equal. In a sense, then, G resembles an equilibrium constant. If the detection method is less sensitive, a slightly higher amount of precipitant is required, and the equilibrium constant changes to fit the slightly changed

solvent, just as for simple reactions, the equilibrium constant depends on the solvent and the temperature chosen.

For the particular case of experiments dealing with turbidity increments, the first term of [9] is more important. Now dealing with this term only, we inquire as to what single average value of molecular weight would result in the same value of M as is given by the experimental range of molecular weights in solution. This average, which is here termed the "gamma average," is

$$M_\gamma = \left[\frac{\sum N_i M_i^4 e^{f(P,M)/kT}}{\sum N_i e^{f(P,M)/kT}} \right]^{\frac{1}{4}}, \quad [10]$$

the subscript gamma being employed to identify the average with the precipitation process, since the use of gamma has been well established in this connection, originally by G. V. Schulz (7).

This gamma average is not the average of the material in the precipitate phase; it represents instead the *selection* or *weighting* mechanism whereby the kinetic process scans over all the chains *in solution* and selects those which are to enter the precipitate phase. It is of interest to say a few words about the mathematical form of this average. It is not one of the family to which the weight and Z averages belong; it is more closely related to the power averages, of which the root-mean-square is the most familiar example. By considering the exponential factor as a weighting factor, the gamma average becomes a (weighted) root-mean-fourth-power average. As will be seen presently, the experimental test of the gamma average is made by finding that single fraction which gives the same precipitation point. This corresponds to the primary definition of an average: an average is that one number which, when substituted for all the different numbers being operated upon, gives the same final result. Defining an average in this manner has the advantage of being general, regardless of the functional form chosen. The geometric and harmonic means are still further examples of other functional forms.

EXPERIMENTAL

This average may be tested experimentally by the actual precipitation of mixtures of known fractions, and comparison of the molecular weight corresponding to the precipitation point, with M_γ . In order to make the necessary calculations of M_γ , $f(P,M)$ must be known. Schulz suggested that $f(P,M)$ is a linear function of both P and M . Considerable experimental data are available, making use of experiments in which P is adjusted to P_γ , and it is well established that a linear function with the precipitation point P_γ is correct. However, linearity with M is found only for a few systems; more generally, E_s is linear with $\log M$ (8). We therefore adopt the form

$$E_s = f(P,M) = \alpha P_\gamma \log M. \quad [11]$$

There remains the constant α . This has been determined in the following manner: The point of precipitation is determined by sensitive optical means, and corresponds to a very slight excess of precipitant over the saturation value. This reversible point corresponds to a definite small value of E_s . This energy must be above the prevailing kT , but not many times above, since slight increases in temperature cause re-solution. We may thus arbitrarily set $E_s = 10kT$ as defining the conditions corresponding to the first measurable sharp turbidity increase. Then for a known fraction, with a known precipitation point, we have $\alpha/kT = \frac{10}{P_\gamma \log M}$, which determines α/kT . In a sense, α/kT is an adjustable parameter, but adjustable only within rather small limits, from our knowledge of the phenomenon. This one assigned value holds for quite different polymers, as will be seen.

An actual calculation is now illustrated for the case of a mixture of two fractions of cellulose acetate butyrate, consisting of one part of molecular weight 183,000 and two parts of molecular weight 33,000. From experiments on the single fractions, it was determined that P_γ for the fraction 183,000 had the value 80.45. Then $\alpha/kT = \frac{10}{80.45 \log 183,000} = 0.0236$. In making calculations of M_γ corresponding to the mixture of fractions, the value of P_γ for the mixture should be used, so that $\frac{f(P,M)}{kT}$ becomes $0.0236(81.55) \log M$ with values of 183,000 and 33,000 inserted for M . Then:

$$M_\gamma = \left[\frac{(183,000)^3 e^{1.928(5.262)} + 2(33,000)^3 e^{1.928(4.518)}}{\frac{e^{1.928(5.262)}}{183,000} + \frac{2e^{1.928(4.518)}}{33,000}} \right]^{\frac{1}{4}} = 132,000.$$

RESULTS AND CONCLUSIONS

Table I compares the usual number, weight, and Z averages, for a number of mixtures which have been examined by the precipitation method, with the experimental average as determined from the precipitation point of the mixture. It is apparent that the number average has no connection with the actual precipitation behavior. The weight average shows some correlation, although the values are significantly too low. The Z average produces a qualitative agreement, thus indicating again, as has been known, that in normal systems the long chains are weighted heavily for precipitation. This is the basis for the assumption that chain lengths which are significantly different behave independently in their precipitation from dilute solution, and the basis for the additivity principle employed in turbidity-precipitation analysis.

Table II lists the computed gamma averages, for the cases where the energy E_s is assigned values of $10kT$ and $20kT$. The averages are also computed for the cases where the 4th-, 3rd-, and 2nd-power terms of Eq. [9] are each considered to be dominant. While no single combination of values for E_s and the exponent holds exactly for all the different polymers, this is hardly to be expected. It is to be considered that in matching the experimental value by limiting one parameter to a range of 10–20, and the other to a range of 2–4, the essential correctness of the procedure is demonstrated. Additive combinations of the power terms

TABLE I
Comparison of Averages

Fraction mixture	Source of data	$M_{\text{exp.}}$	M_n	M_w	M_z
1 { Cellulose acetate butyrate 33% of 183,000 67% of 33,000	Morey and Tamblin (4)	150,000	45,500	83,000	143,000
2 { Cellulose nitrate 33% of 143,000 67% of 41,200	A. Oth (9)	114,000	54,000	75,000	106,000
3 { GRS rubber 9.6% of 75,000 90.4% of 20,000	Gavoret and Magat (10)	30,000	21,500	25,000	36,000
4 { GRS rubber 88.4% of 220,000 11.6% of 1,000	Gavoret and Magat (10)	250,000	8,300	194,000	220,000
5 { GRS rubber 46% of 220,000 54% of 1,000	Gavoret and Magat (10)	170,000	1,800	101,000	219,000
6 { GRS rubber 13% of 220,000 87% of 1,000	Gavoret and Magat (10)	125,000	1,200	30,000	190,000
7 { Polyvinyl acetate 50% of 171,000 50% of 13,100	Gavoret and Magat (10)	161,000	Unfractionated samples		

would probably represent actual conditions better for systems wherein the simple assumptions are not obeyed. It should also be pointed out that the parameter E_s , which is seen to match experiment best by some value between 10 and $20kT$, is known from the general background of precipitation to be just such a small number. It is seen that the set of values for $E_s = 15kT$, and the 4th-power term, would give quite reasonable quantitative agreement with the experimental values. The experimental value for mixture 4 (250,000) is of course in error because the average cannot exceed the value of the highest fraction (220,000).

When the experimental method is one which achieves equilibrium, then the thermodynamic approach may also be used to compute a selection average, and this has been done by Stockmayer (12) and by Tompa (13), resulting in a qualitative agreement with experiment. The question of the identity of the critical point and the usual precipitation point has been properly raised by the latter author.

There are, of course, whole sets of mathematical averages; the weight and Z averages belong to one such set. These latter two have a direct physical connection with viscosity and ultracentrifuge phenomena, but none with precipitation. While combinations of them may be evolved, as Stockmayer has done, the combination might also be obtained using averages from some other family as building blocks. The gamma average has a valuable direct connection with the actual physical process of precipitation.

TABLE II
Computed Gamma Averages

Polymer mixture	$M_{\text{exp.}}$	$E_s = 10 \text{ kT}$			$E_s = 20 \text{ kT}$		
		$4M_\gamma$	$3M_\gamma$	$2M_\gamma$	$4M_\gamma$	$3M_\gamma$	$2M_\gamma$
1	150,000	132,000	120,000	100,000	162,000	156,000	147,000
2	114,000	106,000	97,000	85,000	123,000	118,000	110,000
3	30,000	42,000	36,000	30,000	51,000	46,000	39,000
4	250,000	204,000	199,000	189,000	220,000	220,000	220,000
5	170,000	156,000	139,000	110,000	218,000	218,000	217,000
6	125,000	111,000	88,000	56,000	213,000	211,000	206,000
7	161,000	136,000	125,000	108,000	164,000	162,000	158,000

It is of interest to point out that the nucleation and growth processes each call for a different weighting of chain lengths. Therefore, a particle of precipitate, as it grows, is not homogeneous throughout. This means that thermodynamic equilibrium between two liquid layers is not a natural or automatic consequence of precipitation, but is achieved only after coalescence of particles, and migration and diffusion to the surface of one of the layers, of those shorter chains which were weighted more heavily in the nucleation step. These shorter chains must then be re-dissolved. The matter may be stated another way: Particle formation involves a far greater ratio of surface to volume than is the case for coalesced liquid layers, and an energy term based on volumes only is not the complete description of the energy terms for particle precipitation.

SUMMARY

The kinetics of nucleation, and of further growth of a nucleus, are examined theoretically for the case of polymer chains in dilute solution. The analysis is carried out using molecular weight as the prime variable, and the results are cast into the form of an average, the gamma average,

which relates precipitation point and the role of chain length distribution. This average is tested experimentally by the precipitation of mixtures of known fractions, and substantial agreement is obtained. It has the form

$$M_{\gamma} = \left[\frac{\sum N_i M_i^4 e^{\alpha P_{\gamma} \log M_i}}{\sum N_i e^{\alpha P_{\gamma} \log M_i}} \right]^{\frac{1}{4}}$$

when dealing with the early stages of precipitation, in which the particles are smaller than a wavelength, and when mechanical stirring predominates. For later stages, the third power replaces the fourth.

REFERENCES

1. UMBERGER, J. Q., AND LA MER, V. K., *J. Am. Chem. Soc.* **67**, 1099 (1945).
2. MOELWYN-HUGHES, E. A., *Kinetics of Reactions in Solutions*, p. 17. Oxford, Clarendon Press, 1933.
3. GRALÉN, N., Dissertation, Upsala, 1944.
4. MOREY, D. R., AND TAMBLYN, J. W., *J. Applied Phys.* **16**, 419, (1945).
5. STRUTT, W., *Phil. Mag.* **12**, 81, (1881); *ibid.* **44**, 28 (1897); *ibid.* **47**, 375 (1899).
6. KING, A. M., AND GARNER, W. E., *J. Chem. Soc.* **1934**, 1449; *ibid.* **1936**, 1368.
7. SCHULZ, G. V., *Z. physik. Chem.* **A179**, 321 (1937).
8. MOREY, D. R., AND TAMBLYN, J. W., *J. Phys. & Colloid Chem.* **51**, 721, (1947).
9. OTH, A., *Bull. soc. chim. Belges* **58**, 285 (1949).
10. GAVORET, G., AND MAGAT, M., *J. Chem. Phys.* **17**, 999 (1949).
11. MOREY, D. R., TAYLOR, E. W., AND WAUGH, G. P., in press.
12. STOCKMAYER, W. H., *J. Chem. Phys.* **17**, 588 (1949).
13. TOMPA, H., *Trans. Faraday Soc.* **46**, 970 (1950).

THE INERTIAL MECHANISM IN THE MECHANICAL FILTRATION OF AEROSOLS

Eugene A. Ramskill and Wendell L. Anderson

Naval Research Laboratory, Washington 20, D. C.

Received June 8, 1951

INTRODUCTION

A theory of the mechanical filtration of aerosols was proposed by Irving Langmuir (1) during World War II. The theory was based on the limited facts available at that time and on very reasonable assumptions. The theory has been generally accepted and has been of inestimable value in interpreting certain filtration phenomena and in designing more efficient aerosol filters.

The most significant conclusion from Langmuir's theory was that there should be for a given filter a certain size of aerosol particle which would be more difficult to filter than any other size. Data which indicated that this conclusion was correct were obtained by Burton (2). Knudson and White (3) and La Mer, Gendron, and Gruen (4) were unable to verify the conclusion experimentally.

In recent years, more sensitive and accurate equipment, a wider range of filters, and improved methods of generating and measuring homogeneous aerosols have resulted in a wealth of experimental filtration data which were not previously available. It is the purpose of this paper to present some of these new data together with their current interpretation.

LANGMUIR THEORY

Limitations

In order to simplify the complex process of filtration Langmuir limited his treatment to (a) spherical aerosol particles, (b) aerosol particles of less than $1\ \mu$ diameter to avoid gravitational effects, (c) linear face velocities of less than 3.5 cm./sec., and (d) the initial effects of filtration. Any chemical or mechanical effects of the aerosol on the filter were not considered.

Assumptions

It is assumed that (a) any aerosol particle which touched a fiber of the filter was retained, (b) electrostatic effects were negligible, (c) the flow was laminar, and (d) the interfiber distances in a filter were of the same magnitude as the fiber diameters.

Mechanism

Three separate mechanisms by which aerosol particles could be captured by a filter were considered. These were as follows:

(a) *Direct Interception*. In this mechanism it is assumed that the center of each aerosol particle follows a flow line and does not deviate therefrom. Because of the initial position of certain aerosol particles and because of the compression of flow lines around a fiber, the center of some aerosol particles will come at some point along their paths within the particle radius (r) of the fiber and will be captured.

(b) *Diffusion*. In this mechanism Brownian motion causes an aerosol particle to deviate from its original flow line. If this deviation causes a particle to touch a fiber, the particle will be captured.

(c) *Inertia*. Some of the flow lines of the gaseous medium past a filter fiber must necessarily exhibit marked curvature. Some aerosol particles will deviate from their flow lines because of inertia. If this deviation causes a particle to touch a fiber, the particle will be captured.

Conclusions

Langmuir decided on the basis of calculations and meager existing data that the inertial effect should not be a significant factor for the limited case of filtration considered. Consequently, his theory includes only the two separate mechanisms: direct interception and diffusion.

It is easy to obtain a qualitative picture for the main conclusion of this theory by considering the direct interception and diffusion mechanisms. The percentage of aerosol particles retained by a given filter at a given velocity will decrease with increasing particle size because of the decreasing diffusion effect and will decrease with decreasing particle size because of the decreasing direct interception effect. Hence, some certain size of aerosol particle will be more difficult to filter than any other size; the most penetrating size would not necessarily be the same for all filters. The reader is referred to the original paper of Langmuir (1) for a mathematical analysis of filtration.

NAVAL RESEARCH LABORATORY (NRL) APPROACH

From a study of the Langmuir theory of filtration and available data it appeared that the face velocity limitation of 3.5 cm./sec. was perhaps confusing the entire picture. Consequently, the three mechanisms of filtration were reconsidered with face velocity as the primary variable. The Langmuir limitations (a), (b), and (d) are retained along with assumptions (a), (b), and (c), but not assumption (d).

A qualitative picture of each filtration mechanism is given in Fig. 1 where per cent penetration is plotted against face velocity for a given filter and a given aerosol. The relative positions indicated for the various

mechanisms were chosen arbitrarily and do not represent experimental data. The manner in which the diffusion mechanism varies with velocity is shown in sec. I of Fig. 1. The slope of this curve is dependent on the radius of the aerosol, the fiber diameter, the interfiber distance and should vary linearly with velocity. The effect of the direct interception mechanism is shown in sec. II of Fig. 1. As might be expected, this mechanism is independent of velocity, except as the flow-line pattern may be changed by velocity, and is dependent on aerosol radius, fiber diameter, and interfiber distance. The effect of inertia is shown in sec. III of Fig. 1. This mechanism is dependent on the mass of the aerosol particle, the fiber

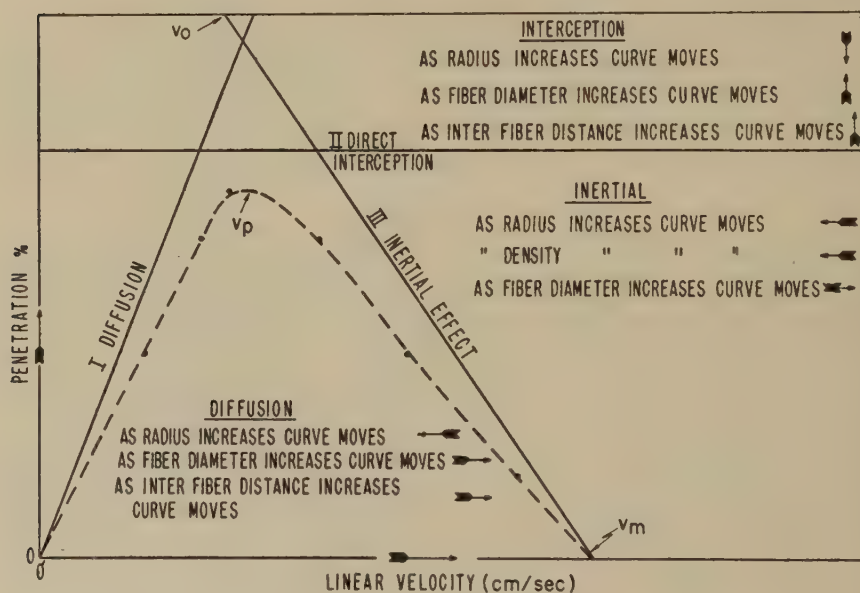


FIG. 1. Filtration mechanisms.

diameter, and the interfiber distance, and should vary linearly with velocity. It is expected that the inertial mechanism should become measurable at some velocity (v_0) and should exert no additional effect above some velocity (v_m). The horizontal portion of sec. III above velocity v_m is shown in Fig. 1 at zero per cent penetration. In the case of a very open filter, such as a single layer of wire screen, this horizontal portion above velocity v_m would be at some large value of per cent penetration. An experimentally determined penetration-velocity curve for a given aerosol and a given filter will obviously be the algebraic sum of the three separate effects; the dotted curve in Fig. 1 illustrates an expected experimental curve resulting from these mechanisms.

EXPERIMENTAL

To determine the validity of the above picture of the filtration mechanisms a series of varied filters was selected for experimental investigations. Determination of the penetration-velocity curves for various aerosols was made for each filter, and the results were compared graphically. The filters used as well as some of their characteristics are given in Table I.

Since the aerosol generator described by La Mer, Inn, and Wilson (5) was readily adaptable for the production of particles of various but uniform sizes and density, it was utilized throughout the investigation. Aerosols of dioctyl phthalate (DOP) and sulfuric acid were generated over a

TABLE I
Physical Composition of Filters

Filter	Material	Average fiber diameter	Caliper	Resistance ^a	Formation	Calender
		μ	<i>in.</i>	<i>mm. H₂O</i>		
A	Viscose	17	0.045	7	Wet	None
B	Glass	3	0.020	10	Wet	None
C	Glass	3	0.011	10	Dry	None
D	Esparto	15	0.024	67	Wet	Medium
E	Wood	15	0.006	219	Wet	Heavy
F	Viscose	12	0.060	21	Wet	None
G	Cotton	16	0.030	4	Wet	None
H	Viscose	17	0.090	14	Wet	None
I	Glass	3	0.032	14	Wet	None
J	Glass	2	0.029	40	Wet	None
K	Glass	1	0.018	100	Wet	None

^a Resistance measured at 14.2 cm./sec.

particle size range from 0.2 to 1.0 μ diameter. Penetrations were measured by the NRL E-3 Smoke Penetration Meter described by Knudson and White (3). Particle size was measured with a photoelectric particle-size meter described by Anderson and Thompson (6).

RESULTS

Resistance

Resistance measurements of some of the individual filters used are shown in Fig. 2. The wide variation in resistance among filters should be noted. The Reynolds number was calculated for each filter at the maximum velocity used. Only filter *E* gave an indication of turbulent flow.

Shape of Penetration-Velocity Curves

The shape of the penetration-velocity curves obtained experimentally varied considerably. Dependent upon the aerosol and the filter used, some combination of the three mechanism curves was obtained. Five different

curves are shown in Fig. 3. Filter *A* shows very little diffusion effect, a small but continuing direct interception, and an increasing inertial effect. Filter *B* is similar to filter *A* but with more diffusion and direct interception effects. Filter *C* illustrates how the inertial effect has moved to a lower velocity and masks the direct interception effect. Filter *D* is similar to filter *C* but with a more pronounced inertial effect. Filter *E* illustrates how the inertial effect has moved to such low velocity that both the diffusion and direct interception effects are masked.

Aerosol Size

The effect of aerosol size on the penetration-velocity curve is shown in Figs. 4 and 5. Figure 4 shows the performance of filter *F* as the aerosol

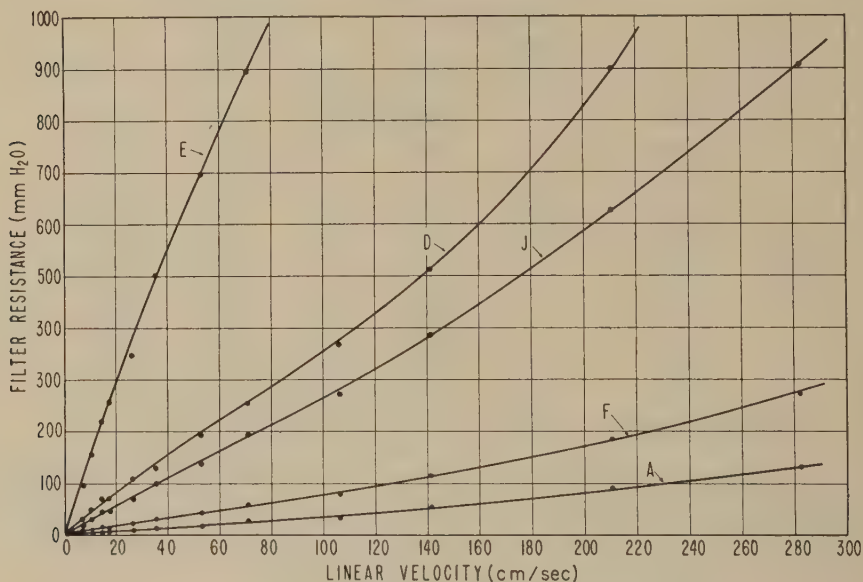


Fig. 2. Filter resistance as a function of linear velocity.

particle (H_2SO_4) size was varied from 0.3 to 1.0μ diameter. This filter is a low-resistance, loosely formed sheet requiring relatively large changes in particle size to effect major changes in penetration characteristics. An analogous situation for a higher-resistance, tighter filter, *J*, is shown in Fig. 5. In this instance, very slight changes in particle size (0.26 – 0.30μ diameter) are sufficient to cause definite alterations of the penetration characteristics.

Aerosol Density

The effect of aerosol density on the penetration-velocity curve is shown in Fig. 6. It should be noted that at low velocities the more dense aerosol

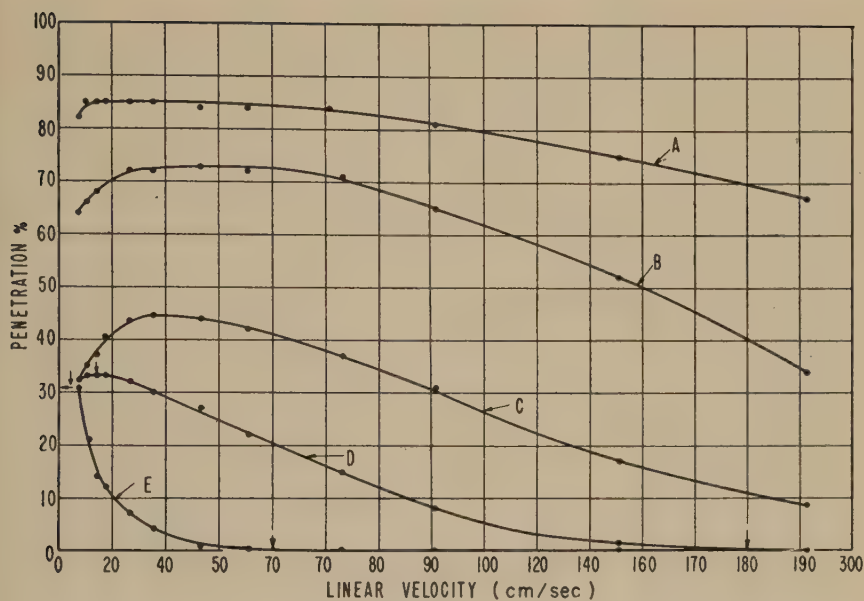


FIG. 3. Illustrative curves, penetration vs. linear velocity. Aerosol, DOP; particle diameter, 0.3μ .

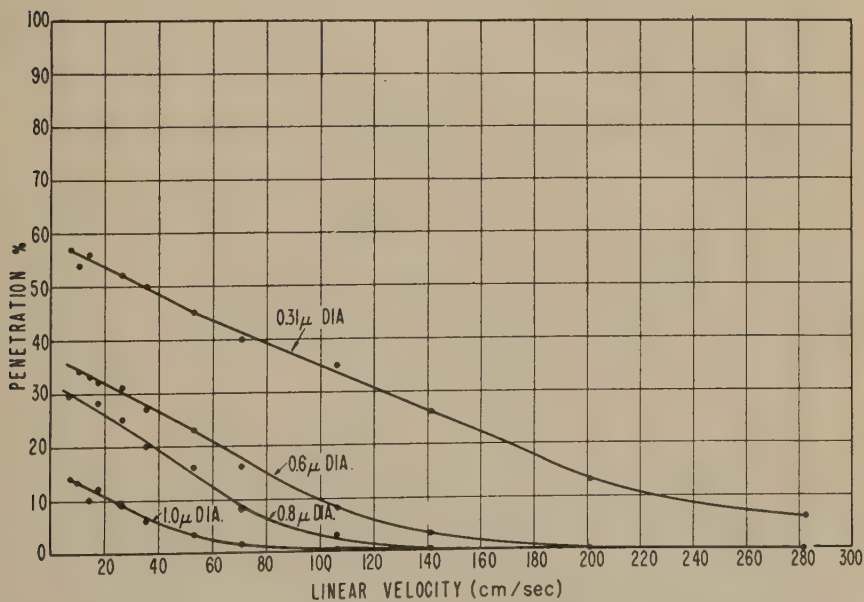


FIG. 4. Effect of aerosol size, penetration vs. linear velocity. Aerosol, H_2SO_4 ; filter, *F*.

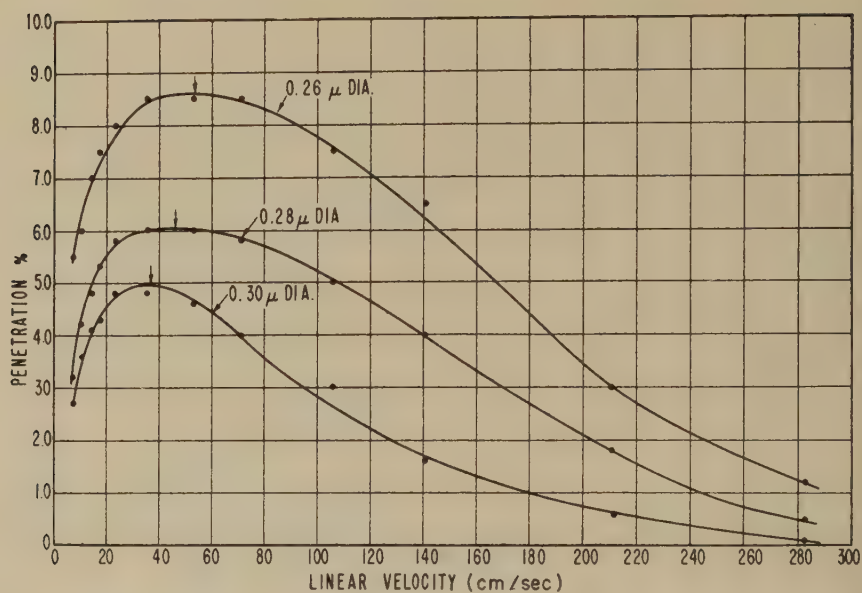


FIG. 5. Effect of aerosol size, penetration vs. linear velocity. Aerosol, DOP; filter, *J*.

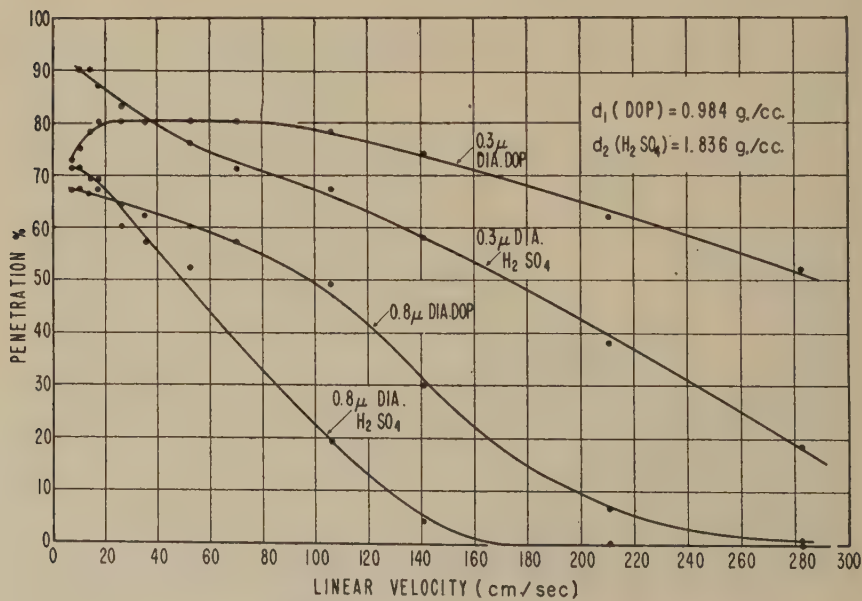


FIG. 6. Effect of aerosol density, penetration vs. linear velocity. Aerosol, DOP and H₂SO₄; filter, *H*.

particle is more difficult to filter than is the less dense particle. This phenomenon is not in accord with either the diffusion or direct interception mechanism. No explanation for this behavior is offered at this time.

Filter Fiber Size

The effect of filter fiber diameter (d_f) on the penetration-velocity curve is shown in Fig. 7. It should be noted that the inertial effect moves as expected to lower velocities as d_f decreases. The portions of the curves

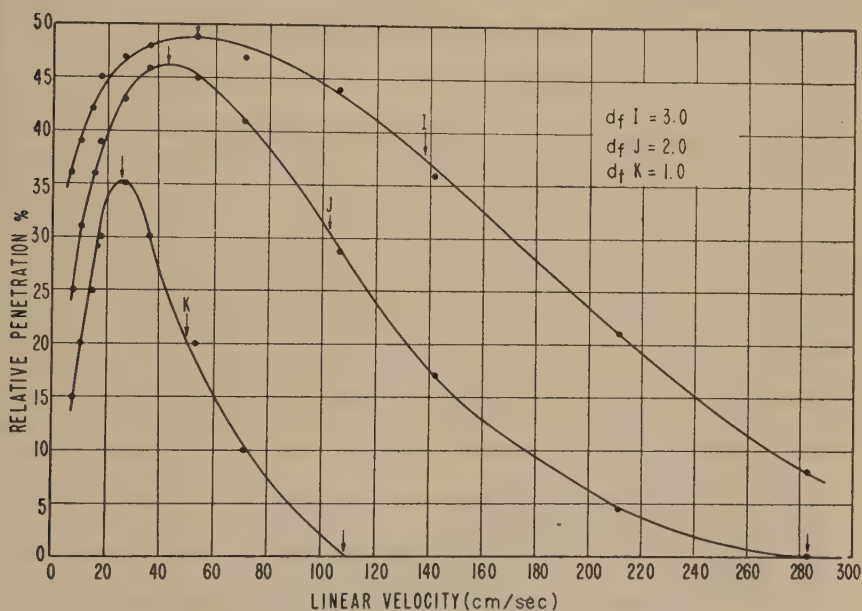


FIG. 7. Effect of filter fiber diameter, penetration vs. linear velocity. Aerosol, DOP; particle diameter, 0.3μ .

determined largely by the diffusion effects are not in the order that might be expected from Fig. 1. This is believed to be caused by the unequal filter densities as expressed by their resistances.

Interfiber Distance

If a filter is formed by the random deposition of fibers, it is reasoned that the interfiber distance (d_i) will approach a value corresponding to the fiber diameter (d_f). The value of d_i should certainly not be less than d_f , unless an external stress such as calendering is employed, but may well be greater than d_f . The relation of d_i to d_f in a filter will certainly affect the flow-line pattern and, hence, should affect the penetration-velocity curve. The penetration-velocity curves of three different filters are shown

in Fig. 8. All of these filters were made from fibers of about the same size ($d_f = 15\text{--}16\ \mu$). Filter *G* is a loose sheet made on a regular paper machine with no compression by the calender. Filter *D* received considerable calendering, while filter *E* was heavily calendered. It is noted that as the extent of calendering is increased the inertial effect becomes evident at lower velocities. The net effect of calendering is an increase in the filter density and a decrease in the interfiber distance (d_i). For filters containing essentially the same size of fibers the resistance per unit thickness is a measure of filter density and of interfiber distance. The data of Table I show an increasing resistance per unit thickness, indicating an increasing

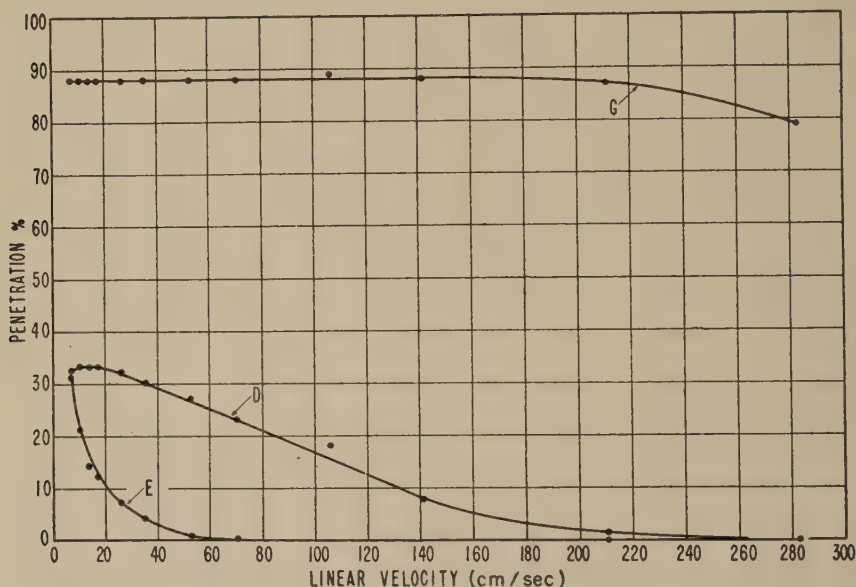


FIG. 8. Effect of filter sheet formation, penetration vs. linear velocity. Aerosol, DOP; particle diameter, $0.3\ \mu$; filter fiber diameter, $15\ \mu$.

density and a decreasing d_i , for filters *G*, *D*, and *E* as the extent of calendering is increased. It is evident then from Fig. 8 that as d_i decreases the inertial effect becomes evident at lower velocities.

INTERPRETATION

The regular manner in which the penetration-velocity curves vary with particle radius, particle density, and fiber diameter suggested that a mathematical relation should exist which would quantitatively express the inertial effect. Albrecht (7) has considered the inertial effects necessary for the deposition of hoar frost on wires exposed to wind. He derived the following equation:

$$X = 2r^2\rho v/9\eta,$$

where X is the distance a particle will move from a flow line due only to inertia, r is the particle radius, ρ is the particle density, v is the face velocity of air and particle and η is the viscosity of the gaseous medium. For air at 20°C., the equation becomes:

$$X = 1230r^2\rho v.$$

Albrecht also calculated that if the distance X was less than 0.09 times the diameter of the wire no deposition would occur. Langmuir reviewed Albrecht's calculations and arrived at a value of 0.27 for the constant. La Mer and Hochberg (8) verified Albrecht's equation experimentally when they showed that the deposition of particles on mosquitoes was a function of r^2v .

Inasmuch as Albrecht's equation was concerned with a situation analogous to that existing in a filter, it was assumed that the following applied:

$$Kd_e = 1230r^2\rho v,$$

where K is a constant (calculated by Albrecht to be 0.09 and by Langmuir to be 0.27) and d_e is the effective fiber diameter. Where the interfiber distance d_i is large compared to the fiber diameter d_f , d_e becomes equal to d_f . Where d_i is small compared to d_f , d_e should be some function of d_i and d_f which is presently not known. Accordingly, the above equation will be applied only to those filters in which d_i is believed to be at least equal to or larger than d_f .

It was indicated in Fig. 1 that the inertial effect should become measurable at some velocity v_0 and should not increase above some velocity v_m . Hence,

$$K_0d_e = 1230r^2\rho v_0,$$

$$K_md_e = 1230r^2\rho v_m.$$

The velocity v_0 is difficult to obtain from the penetration-velocity curves because it is concealed by the diffusion and direct interception effects. The best approximation to v_0 is obtained by taking the velocity v_p where the inertial effect is becoming the controlling factor, i.e., where the penetration starts to decrease with increasing velocity. Hence,

$$K_pd_e = 1230r^2\rho v_p.$$

The velocity v_m can be approximated by the velocity where per cent penetration drops to zero.

The experimental values for the constants K_p and K_m were determined using filter *C* composed of glass fibers of known fiber diameters. This filter was selected because d_i should be large compared to d_f . The aerosol consisted of very uniformly dispersed particles of known density. The values obtained for K_p and K_m are shown in Table II.

TABLE II
Experimental Values of K_p and K_m Using Filter C
 $d_f = 3 \mu$

No. of sheets	DOP radius μ	v_p cm./sec.	K_p calcd.	v_m cm./sec.	K_m calcd.
1	0.150	45	0.041	—	—
2	0.135	53	0.039	—	—
2	0.150	45	0.041	—	—
2	0.175	27	0.033	240	0.33
4	0.135	53	0.039	330	0.24
4	0.150	50	0.045	330	0.30
4	0.175	27	0.033	210	0.26
Average			0.038		0.28

The two equations then become

$$0.04 d_e = 1230r^2pv_p,$$

$$0.28 d_e = 1230r^2pv_m.$$

The above equations were applied to filters *D*, *E*, *I*, *J*, and *K* by taking values of v_p and v_m from the penetration-velocity curves and calculating d_e . The results are given in Table III.

It is noted in Table III that the calculated values of d_e for filters *I*, *J*, and *K* are in fair agreement with the actual average fiber size d_f . There is, however, a uniform indication that d_e for these filters is slightly larger than d_f . It is considered that this difference is not too serious in view of the variation which can occur in v_p due to changes in diffusion and direct interception effects.

The calculated values of d_e for filters *D* and *E* in Table III do not agree with the actual average fiber size d_f . It should be noted that K_p and K_m were determined from filter *C* in which d_i is certainly large compared to d_f because of its dry formation. Filters *I*, *J*, and *K* were made by the wet process with no calendering, and d_i might be expected to be

TABLE III
Comparison of Calculated Values of d_e with d_f

Filter	DOP radius μ	v_p cm./sec.	v_m cm./sec.	Calcd. (v_p) μ	d_e (v_m) μ	Actual average d_f μ
<i>I</i>	0.15	53	>280	3.6	>2.7	3
<i>J</i>	0.13	53	—	2.7	—	2
<i>J</i>	0.14	46	—	2.7	—	2
<i>J</i>	0.15	37	280	2.5	2.7	2
<i>K</i>	0.15	25	110	1.7	1.1	1
<i>D</i>	0.15	15	260	1.0	2.5	15
<i>E</i>	0.15	7	80	0.5	0.8	15

equal to or only slightly larger than d_f . Filters *D* and *E* were made by the wet process but with medium and heavy calendering, respectively. In this case d_i is expected to be less than d_f . Hence the calculated value of d_e for such filters is not expected to be a measure of d_f . Although there is at present no sound basis for the conclusion, it is believed that under these conditions the calculated value of d_e may actually become a measure of the interfiber distance d_i . The calculated values of d_e for filters *D* and *E* are in relative agreement with this conclusion.

As a result of the data and calculations of Table III the following tentative conclusions may be made:

- (a) When d_i is larger than or equal to d_f , d_e is a direct measure of d_f .
- (b) When d_i is less than d_f , d_e may be a direct measure of d_i .

COMPLETE FILTRATION DIAGRAM

Consider now a three-dimensional diagram with the velocity v as the x -axis, per cent penetration as the y -axis, and $r^2\rho$ as the z -axis. Since the equation $Kd_e = 1230r^2\rho v$ has been shown to apply, the projection of the v_p values for a given filter on the xz -plane will fall on the rectangular hyperbola

$$(r^2\rho) v = K_p d_e / 1230.$$

Also, the v_m values or their projections will be in the xz -plane on the rectangular hyperbola

$$(r^2\rho) v = K_m d_e / 1230.$$

Any plane parallel to the yz -plane at any value of v is a plot of per cent penetration against $r^2\rho$. Langmuir (1) predicted that essentially this plot (actually per cent penetration vs. r) should contain a maximum. So far, no maximum has been found in any of the filters studied over the size range 0.2–1.0 μ diameter. It is believed that the reason no maximum has been found in the predicted aerosol size range is that the inertial effect extends to lower values of v and r than previously suspected and actually reverses the expected diffusion effect. This reversal effect can be seen in Fig. 5 where on the so-called diffusion portion of the curves the per cent penetration is increasing with decreasing particle size instead of the reverse as expected from diffusion alone. As long as this situation persists no maximum in the per cent penetration–radius curve will be obtained. It is quite possible that by using much smaller aerosol particles a point will be reached where the diffusion effect becomes controlling and per cent penetration will decrease with decreasing particle size.

SUMMARY

It has been shown that the inertial mechanism definitely exists and plays an important role in the mechanical filtration of aerosols at lower

particle radii than calculated by Albrecht and Langmuir. The manner in which the inertial effect enters into the filtration mechanism can be expressed by the equations

$$K_p d_e = 2r\rho v_p/9\eta,$$

$$K_m d_e = 2r^2\rho v_m/9\eta,$$

where K_p and K_m are constants, d_e is the effective fiber diameter, r is the particle radius, ρ is the particle density, v_p is the velocity at which the inertial effect becomes measureable (penetration starts to decrease with increasing velocity), v_m is the velocity above which no additional inertial effect occurs, and η is the viscosity of the gaseous medium. Tentative value for the constants K_p and K_m have been determined experimentally. Calculated values of d_e for various filters are shown to be either direct measures of the actual fiber diameter (d_f), the interfiber distance (d_i), or some function of the two depending on the method of formation of the filter. The general structure of a complete three-dimensional filtration diagram for a given filter is indicated. The inertial effect is proposed as the reason that no maximum occurs in the penetration-radius curve in the predicted size range.

REFERENCES

1. LANGMUIR, I., Office Scientific Research and Development, Report 865, Sept. 4, 1942
2. BURTON, III-I-2000 C.E. 42, Univ. Toronto, Nov., 1944.
3. KNUDSON, H. W., AND WHITE, L., Naval Research Lab., Report P-2642, Sept. 14, 1945.
4. LA MER, V. K., GENDRON, AND GRUEN, *Nuclear Sci. Abstracts* **5**, No. 775 (1951).
5. LA MER, V. K., INN, E. C. Y., AND WILSON, I. B., *J. Colloid Sci.* **5**, 471 (1950).
6. ANDERSON AND THOMPSON, Naval Research Lab. Report 3808, May 28, 1951.
7. ALBRECHT, F., *Physik. Z.* **32**, 48-56 (1931).
8. LA MER, V. K., AND HOCHBERG, S., *Chem. Revs.* **44**, 341 (1949).

TITRATION AND VISCOSITY STUDIES OF TWO COPOLYMERS OF MALEIC ACID

John D. Ferry, Doyle C. Udy,¹ Feng Chi Wu, George E. Heckler
and David B. Fordyce²

Department of Chemistry, University of Wisconsin, Madison, Wisconsin

Received August 13, 1951

INTRODUCTION

Current interest in the remarkable properties of polyelectrolytes has been particularly concerned with the effects of repulsion between like charges on a flexible polymer molecule (1,2), the attraction between unlike charges on such a molecule (3) or between the polymer charges and their counter ions (4), and the repression of electrostatic effects by neutral salt (5,6). Other phenomena which have not thus far received attention can arise from the opposing effects of electrical charges and nonpolar groups on a polyelectrolyte in aqueous solution. This interplay is of particular interest in the comparison of synthetic polyelectrolytes with proteins and other biological macromolecules, whose solubilities and other interactions are markedly influenced by the presence of nonpolar groups (7). The present paper compares the behavior of a 1:1 copolymer of maleic anhydride and styrene with that of a corresponding copolymer of maleic anhydride and vinyl ethyl ether. The former exhibits some complicated phenomena, especially with respect to solubility and specific viscosity in dioxane-water mixtures, which are absent in the latter. These phenomena can be interpreted by considering the balance between the cohesive forces of phenyl groups in an aqueous medium and the repulsive forces of charged carboxyl groups. Some titration data have also been obtained to assist in interpretation of the viscosity results.

MATERIALS AND METHODS

A 1:1 copolymer of styrene and maleic anhydride (SY-MA) was obtained through the kindness of Mr. G. M. Powell, Carbide and Carbon Chemicals Division, Union Carbide and Carbon Corporation. It was dissolved in acetone and fractionated roughly by addition of benzene into four fractions representing the following percentages of the original mate-

¹ Present address: Agricultural Experiment Station, Pullman, Washington.

² Carbide and Carbon Chemicals Fellow in Physical Chemistry, 1949-50. Present address: Rohm and Haas Co., Philadelphia, Pennsylvania.

rial: *B1*, 7%; *B2*, 56%; *B3*, 18%; *B4*, discarded. Each fraction was reprecipitated from acetone by benzene and dried *in vacuo*, first at room temperature and then at 70°C. All the viscosity and most of the titration experiments were performed with fraction *B2*, whose number-average molecular weight was 190,000 as determined from osmotic pressure measurements in dioxane with a linear extrapolation ($\mu = 0.443$). Some titration experiments were made with fraction *B3*, whose molecular weight was somewhat lower; the results agreed closely with those for *B2*.

To hydrolyze the maleic anhydride residues, the dried fractionated polymer was mixed with enough water to make a 4% solution and rotated slowly at 60°C. for 2 days. The solution was then shell-frozen and dried *in vacuo* to give the polyacid in a fluffy, finely-divided form.

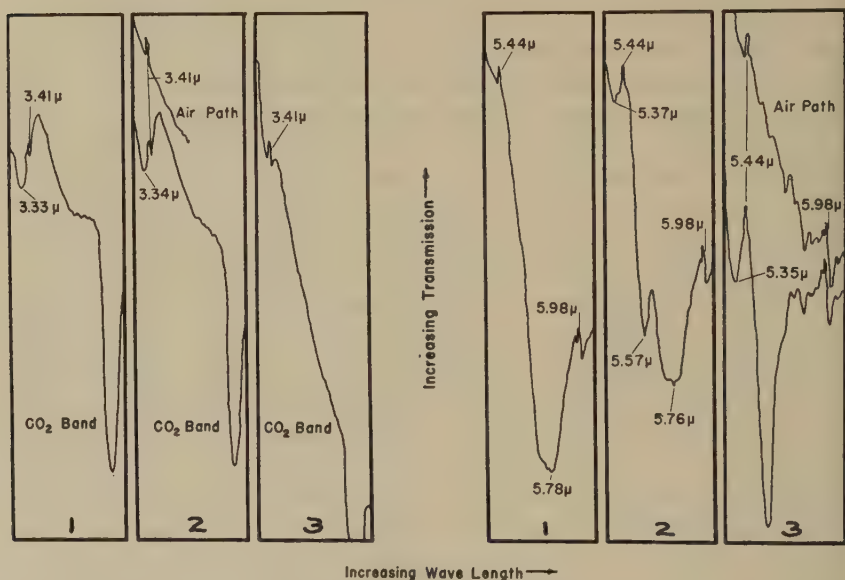


FIG. 1. Infrared absorption spectra of styrene-maleic acid copolymer at successive stages of dehydration. 1, vacuum-dried at room temperature for 24 hr.; 2, vacuum-dried at 60–65°C. for 47 hr.; 3, vacuum-dried at 110°C. for 106 hr.

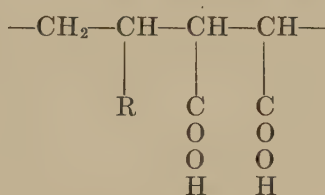
If, after having been dried at room temperature in this manner, the polyacid was heated at 110°C. *in vacuo*, it underwent a weight loss of about 8%, corresponding to the loss of one molecule of water from each maleic acid residue with reversion to the anhydride. This dehydration could be followed also by infrared absorption measurements, using a Beckman spectrophotometer,³ Model IR2. A film of polyacid was prepared

³ We are greatly indebted to Professor V. W. Meloche and Dr. K. J. McCallum for the use of this instrument and assistance in making the measurements.

by evaporation of a solution in 98% dioxane and 2% water on a rock salt crystal. The film was dried *in vacuo* first at room temperature, then at 60–65°, and finally at 110°. The absorption spectra in Fig. 1 show the progressive disappearance of the band at 3.34 μ , attributed to hydroxyl, the disappearance of the band at 5.78 μ , attributed to carboxyl carbonyl, and the appearance of a double band with minima at 5.36 μ and 5.56 μ which is characteristic of anhydride carbonyl (8).

A 1:1 copolymer of vinyl ethyl ether and maleic anhydride (VEE-MA) was also obtained from Mr. Powell. It was dissolved in methyl ethyl ketone and fractionated roughly by addition of cyclohexane into four fractions representing the following percentages of the original material: A1, 16%; A2, 28%; A3, 29%; A4, discarded. Fraction A2 was reprecipitated from methyl ethyl ketone by cyclohexane and was dried in the same manner as the SY-MA fractions. All experiments were performed with this fraction, whose number-average molecular weight was 73,000 as determined by osmotic pressure measurements in dioxane ($\mu = 0.396$). The anhydride copolymer was converted to the polyacid by hydrolysis at 60° as described above.

The structural formula of the repeating unit in both polyacids is as follows:



Dioxane was purified as described previously (9). Dioxane–water mixtures were made up on a weight basis; when hydrochloric acid or salt was present in such a mixture, its normality was expressed in terms of the volume of the final solution. Polyacid stock solutions were made up in such mixtures. In a series of viscosity measurements at different concentrations, the stock solution was diluted with a solvent which contained the same proportion of dioxane to water and the same normality of acid or salt as the stock. The reference for the relative viscosity was taken as this same solvent.

Viscosity measurements were made at 25°C. with viscometers of the Ostwald or Ubbelohde type. Kinetic energy corrections, which were estimated to be of the order of 1%, were neglected. Although at high degrees of ionization polyelectrolytes exhibit non-Newtonian effects in these conventional viscometers (4), experience indicates that such complications are absent at the very low degrees of ionization at which our viscosity measurements were made (10).

Data for titration curves were obtained by preparing series of samples containing the same concentration of polyacid and varying amounts of sodium hydroxide, and measuring the pH with a Beckman glass electrode at room temperature (25–27°C.). A lithium glass electrode was employed in the higher pH range.⁴ The degree of ionization, α , of the polyacid was estimated from the equation

$$\alpha = (c_{\text{H}^+} + c_{\text{NaOH}} - c_{\text{OH}^-})/c_P, \quad [1]$$

where c denotes concentration in equivalents per liter, except for c_P which is concentration of polymer in monomoles per liter. (One monomole consists of one residue of maleic anhydride and one of styrene or vinyl ethyl ether.) This definition, which is convenient because each polyacid carries two different classes of carboxyl groups, leads to $\alpha = 2$ at complete ionization. The concentrations of hydrogen and hydroxyl ions, which are important only at low and high pH, respectively, were calculated from the pH assuming an activity coefficient of unity.

TITRATION RESULTS

Titration curves for solutions of the two copolymers in water and in 0.1 *N* sodium chloride are given in Fig. 2. The inflection at $\alpha = 1$ for SY-MA indicates that there are two classes dissociating in quite different pH ranges. For VEE-MA the two dissociation regions are not so widely separated. Although a range of dissociation constants can be expected for each class of carboxyls (1,5), the two classes can be roughly characterized by mean dissociation constants, \bar{K} ; the values of $p\bar{K}$ are given by the pH at which $\alpha = 0.5$ and 1.5, respectively, and are listed in Table I.

The first $p\bar{K}$ is nearly the same for both polymers, indicating no great difference between the phenyl and ether groups in influencing the strength of dissociation; this conclusion agrees with experience from acids of low molecular weight in which the substituent is separated from the carboxyl group by two or more chain carbons (7). The fact that two widely separated classes exist is probably not due to differences in local molecular environment but to the regular spacing of the carboxyls; as soon as one is ionized, its companion on the adjacent chain atom is made far weaker.

The second $p\bar{K}$ is higher by about two units in SY-MA than in VEE-MA. This marked difference, again, is believed to have nothing to do with local environment, but is attributed to differences in coil configuration. When the VEE-MA is half neutralized, the coil is greatly expanded by repulsion of the negative charges (1–6). In SY-MA, the electrostatic repulsion is partly balanced by the tendency of the hydrophobic phenyl groups to cluster in aqueous solution, and the coil is more compact, as deduced from viscosity measurements reported below; the more compact

⁴ We are indebted to Professor John E. Willard for the loan of this electrode.

coil contains a more intense electrical field which enhances the work of dissociation (1). The second class of carboxyls ionizes less readily, therefore, in SY-MA than in VEE-MA.

In the presence of salt, all the $p\bar{K}$ values are diminished, as would be expected from the behavior of weak electrolytes of low molecular weight.

The breadth of distribution of dissociation constants of a weak polyelectrolyte has been characterized by Katchalsky (1) by a constant n ,

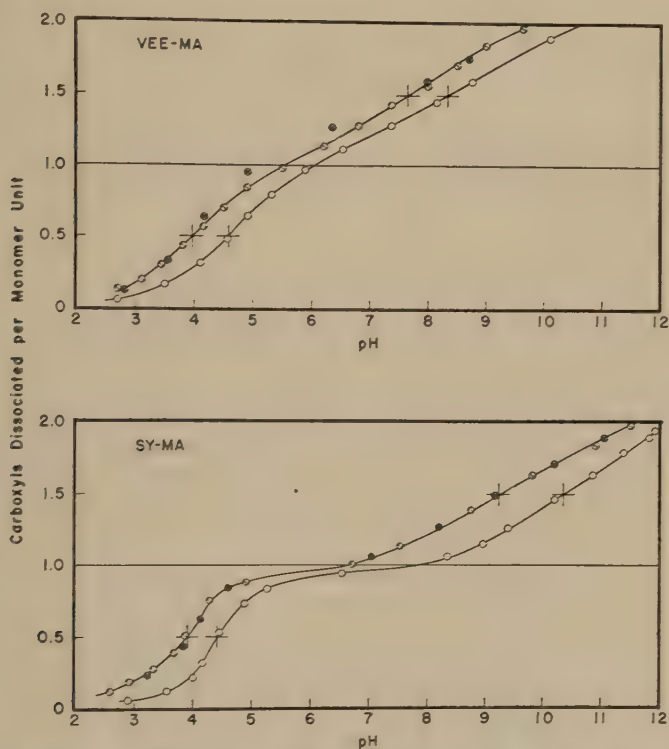


FIG. 2. Degree of dissociation plotted against pH for the two polyacids titrated with sodium hydroxide. Open circles, in water; slotted and crossed circles, two independent series in 0.1 *N* sodium chloride.

which is the negative slope of a plot of pH against $\log(1-\alpha)/\alpha$, using data near the point where $\alpha = \frac{1}{2}$. For a single dissociation constant (no distribution), $n = 1$; for several polyacids, n has been found to range from 1.2 to 2. This constant can be determined from the slope of an ordinary titration curve, $d\alpha/dpH$, where $\alpha = \frac{1}{2}$; it can easily be shown that $n = 0.58/(d\alpha/dpH)$. Values of n are also given in Table I. For the first carboxyls, n is not far from the value of 1, indicating a rather narrow distribution. This would be expected for dissociable groups spaced far apart along the

TABLE I
Constants Characterizing Titration of Polyacids

Solvent	Acid	$\frac{cp}{\text{monomoles/l.}}$	Carboxyl class	$p\bar{K}$	da/dpH	n
Water	SY-MA	0.026	1st	4.40	0.74	0.8
			2nd	10.35	0.27	2.2
Water	VEE-MA	0.032	1st	4.58	0.45	1.3
			2nd	8.34	0.23	2.5
0.1 N	SY-MA	0.023	1st	3.90	0.51	1.1
NaCl			2nd	9.22	0.23	2.5
0.1 N	VEE-MA	0.016	1st	3.97	0.40	1.4
NaCl			2nd	7.64	0.25	2.3

polymer chain (1); here the first class of carboxyls is spaced on every fourth chain atom. The high value of n (>2) found for the second carboxyls is no doubt due to the spacing of this class between groups already charged.

Titration curves such as those of Fig. 2 do not extend to degrees of ionization lower than that of the pure polyacid at the concentration investigated. To interpret the viscosity data described below, it is necessary to know the dependence of ionization on pH at lower pH values, occurring in the presence of small amounts of strong acid; this information can be obtained by suitable extrapolation. Arnold and Overbeek (11) found that the function $pH + \log (1 - \alpha)/\alpha$, which may be denoted by pK_a , was a linear function of α (at small values of α) for polymethacrylic acid. The intercept at $\alpha = 0$ is pK_0 , corresponding to the dissociation con-

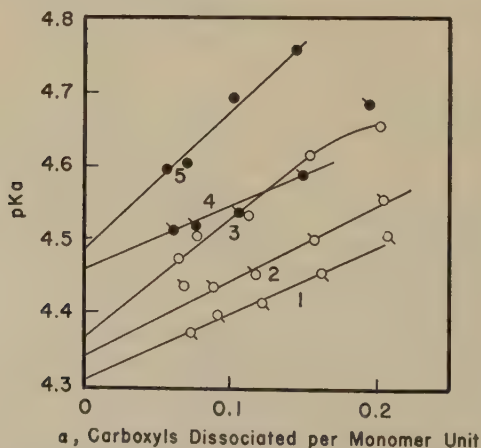


FIG. 3. Negative logarithm of apparent dissociation constant, pK_a , plotted against degree of dissociation for polyacid SY-MA. Open circles, in water; black circles, in 2.5% dioxane. Sodium chloride concentrations as follows: 1, 0.002 N; 2, 0.004 N; 3, 0.006 N; 4, 0.001 N; 5, 0.002 N.

stant of the first carboxyl. Without reference to the theoretical background of this relation, it may be used empirically for purposes of extrapolation. Titration measurements were made on dilute solutions of SY-MA in several concentrations of sodium chloride in water and 2.5% dioxane up to values of $\alpha = 0.2$. The results are plotted in Fig. 3, and the extrapolated values of pK_0 are given in Table II. They decrease slightly with increasing ionic strength, and increase with increasing dioxane concentration, as expected from the behavior of ordinary weak acids (12). The value of about 4.4 in pure water may be compared with that of 4.2 for the first carboxyl of succinic acid. From the data of Fig. 3 and Table II, values of α corresponding to given pH, ionic strength, and dioxane con-

TABLE II
First Dissociation Constants of SY-MA Extrapolated by Fig. 2

Dioxane %	NaCl <i>N</i>	<i>c_p</i>	pK_0
0	0.002	0.007	4.37
	0.004	0.007	4.34
	0.006	0.007	4.31
2.5	0.001	0.008	4.49
	0.002	0.008	4.46

centrations can be obtained by successive approximations; these are employed in the discussion below.

VISCOSITY RESULTS

Viscosities of both polyacids were measured in solvents containing various proportions of dioxane and various concentrations of hydrochloric acid and/or potassium chloride. The viscosities of the two *anhydride* copolymers (before hydrolysis) were also measured in pure dioxane.

Plots of reduced specific viscosity, η_{sp}/c , against c , the concentration in grams of polymer per deciliter, fell into two classes: those which could be extrapolated to give a finite intrinsic viscosity $[\eta]$, and those which showed an upsweep at low concentrations as often found in polyelectrolyte solutions (2,13), so that no intrinsic viscosity could be obtained unless by measurements at exceedingly low polymer concentrations. Both types are illustrated in Fig. 4.

In solutions of the polyacid VEE-MA, a finite intrinsic viscosity was obtained providing the hydrochloric acid concentration was 0.004 *N* or higher or else the dioxane concentration was 90% or higher. This polymer was soluble over the entire range of dioxane-water mixtures, and in aqueous hydrochloric acid up to a concentration of at least 0.1 *N*. The finite intrinsic viscosities obtained are given in Table III; they vary only from 0.32 to 0.47, never far from the value of 0.45 characteristic of the

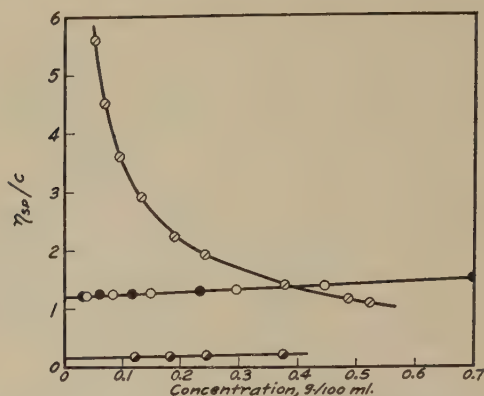


FIG. 4. Plots of η_{sp}/c against c for polyacid SY-MA. Solvents: \circ , water; \bullet , water with 0.004 N HCl; \circ , 90% dioxane; \bullet , 90% dioxane with 0.004 N HCl.

anhydride copolymer in dioxane. The latter value is normal for a polymer of this molecular weight in a good solvent, and reflects a more or less random coil configuration. The configuration is thus essentially normal under all conditions where a finite intrinsic viscosity is obtained at all.

In solutions of the polyacid SY-MA, the presence or absence of a finite intrinsic viscosity obtainable from measurements in the ordinary concentration range depended in a complicated manner on the composition of the solvent. It is represented by the map of hydrochloric acid *vs.* dioxane concentration in Fig. 5. Here the shaded area represents the conditions under which the reduced specific viscosity sweeps up with dilution, preventing calculation of a finite intrinsic viscosity. At high acid

TABLE III

Intrinsic Viscosities of Vinyl Ethyl Ether-Maleic Acid Copolymer

Dioxane %	HCl N	$[\eta]$ (g./100 cc.) ⁻¹	$d(\eta_{sp}/c)/dc$ (g./100 cc.) ⁻²
0	0.004	0.33	0.19
	0.006	0.33	0.09
	0.008	0.33	0.09
	0.010	0.32	0.09
10	0.004	0.34	0.03
25	0.004	0.34	0.03
40	0.004	0.34	0.03
50	0.004	0.42	0.06
69	0.004	0.43	0.06
85	0.004	0.47	0.08
90	0	0.45	0.09
	0.004	0.41	0.04
98	0	0.34	0.06
100 ^a	0	0.45	0.10

^a Anhydride copolymer.

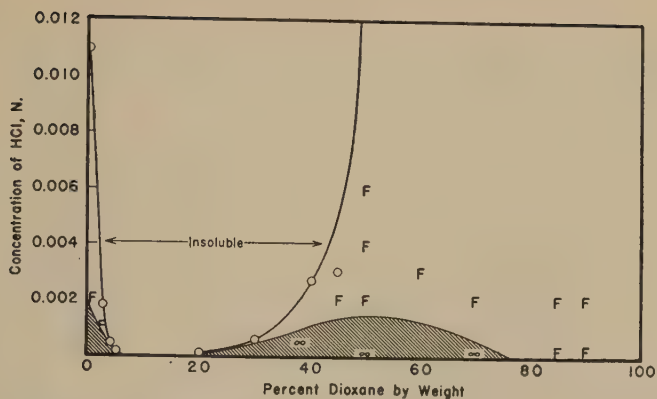


FIG. 5. Map showing solubility and viscosity behavior of polyacid SY-MA in dioxane-water-acid mixtures. Circles, solubility limits; *F*, finite intrinsic viscosity; ∞ , no finite intrinsic viscosity.

concentrations and/or intermediate dioxane concentrations, the polyacid is insoluble, as designated by the upper pair of curves, and here no measurements are possible. Only in the region between the solubility curves and the shaded area have finite intrinsic viscosities been evaluated. These are given in Table IV. Here $[\eta]$ varies from 0.09 to 1.43, being both much lower and somewhat higher than the value of 0.86 obtained for the anhy-

TABLE IV

Intrinsic Viscosities of Styrene-Maleic Acid Copolymer

Dioxane %	HCl N	KCl N	$[\eta]$ (g./100 cc.) ⁻¹	$d(\eta_{sp}/c)/dc$ (g./100 cc.) ⁻²
0	0.002	0	0.27	0.17
	0.002	0.002	0.27	-0.06
	0.002	0.004	0.23	-0.05
	0.004	0	0.17	0.04
	0.004	0.002	0.16	-0.01
	0.006	0	0.09	0.04
2.5	0.001	0	0.37	0
	0.002	0	0.16	0
45.0	0.002	0	0.32	0.17
50.0	0.002	0	0.49	0.17
	0.004	0	0.49	0.15
	0.006	0	0.49	0.13
60.0	0.003	0	0.83	0.24
70.0	0.002	0	1.17	0.29
85.0	0	0	1.43	0.50
	0.002	0	1.37	0.35
90.0	0	0	1.10	0.36
	0.004	0	1.10	0.36
100.0 ^a	0	0	0.86	0.30

^a Anhydride copolymer.

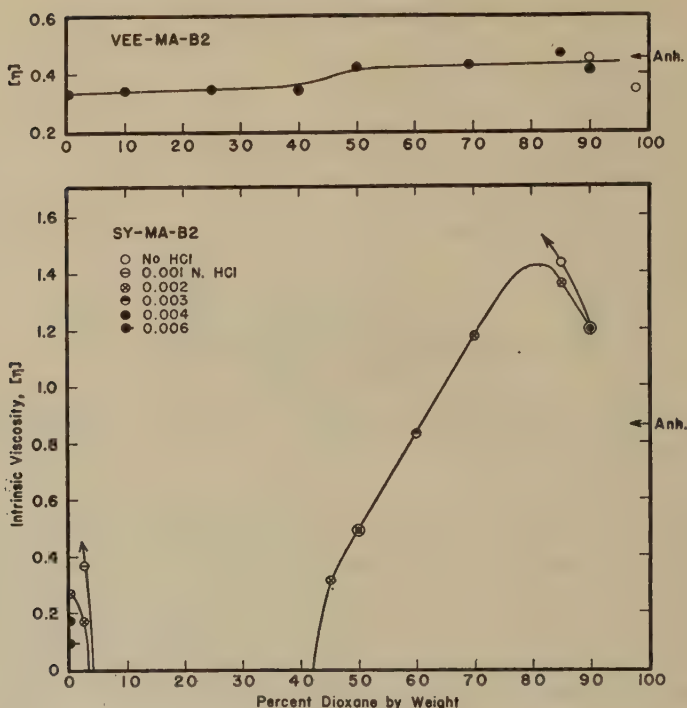


FIG. 6. Intrinsic viscosities of the two polyacids plotted against dioxane concentration, at various concentrations of HCl as shown. The intrinsic viscosities of the corresponding anhydride copolymers in pure dioxane are denoted by arrows.

dride copolymer in pure dioxane. The latter is normal for a polymer of this molecular weight; the other values correspond to configurations ranging from highly constricted to somewhat expanded coils.

The intrinsic viscosity data, exclusive of those for SY-MA in solvents containing potassium chloride, are plotted in Fig. 6. The complicated behavior of SY-MA may be described by the following general statements:

(a) At constant concentration of acid (e.g., 0.002 *N*), the intrinsic viscosity first falls with increasing dioxane concentration; then, beyond the insoluble zone, it rises and passes through a slight maximum at about 80% dioxane.

(b) On the low dioxane side of the insoluble zone, the intrinsic viscosity is abnormally small when it is finite at all, and it decreases with increasing acid concentration.

(c) On the high dioxane side of the insoluble zone, the intrinsic viscosity depends very little on the concentration of acid, as long as the latter is high enough to make $[\eta]$ finite at all (from 0.001 to 0.002 *N*, as shown by Fig. 5).

(d) Above 80% dioxane, no acid is required to make $[\eta]$ finite, and the value of $[\eta]$ is scarcely affected by the concentration of acid.

DISCUSSION

The vinyl ethyl ether copolymer, VEE-MA, gives an abnormal plot of reduced specific viscosity against concentration in pure water because its degree of dissociation increases with dilution, and the polymer coil is expanded by electrostatic forces. (Also, the electroviscous effect (6), if present, is enhanced by an increasing magnitude of charge.)

Normal viscosity behavior is exhibited in dilute hydrochloric acid because here the degree of dissociation is limited regardless of dilution. At the acid concentration which is required to suppress the upsweep in η_{sp}/c , the degree of dissociation is of the order of 0.01. Alternatively, normal behavior is obtained by increasing the dioxane concentration to 90% or more. This is undoubtedly due to a marked decrease in the dissociation constant as the dielectric constant is reduced, just as found for carboxylic acids of low molecular weight (12).

The same principles hold for the styrene copolymer, SY-MA, but here the coil configuration is influenced by the far more hydrophobic character of the phenyl group. The comparative interactions of the two copolymers with water may be gauged by the solubilities of ethyl ether and ethyl benzene in water—7.9 and 0.014 weight %, respectively, at 15°C. From the fact that SY-MA is insoluble in hydrochloric acid above a concentration of 0.01 *N* it is concluded that this molecule, unlike VEE-MA, *requires some electrical charges to put it into aqueous solution*. In pure water, SY-MA ionizes to some extent, electrostatic forces overcome the tendency of phenyl groups to cluster, and solution is possible; with dilution, the coil expands, just as with any other weak polyelectrolyte. In 0.002 *N* hydrochloric acid, the abnormal behavior with dilution is suppressed by limiting the dissociation, and the phenyl groups pull the coil into a tight configuration as evidenced by the low intrinsic viscosity. With increasing acid, the coil shrinks further until finally at about 0.01 *N* there are too few charges to oppose the cohesion of phenyl groups, and the molecule is precipitated. That the effect of hydrochloric acid is associated with ionization, and is not simply a salting-out of phenyl groups by increasing the ionic strength, is shown by the data of Table IV in which potassium chloride is substituted for acid; an increase of ionic strength at constant acid has very little influence on the intrinsic viscosity.

Addition of dioxane at constant acid decreases the intrinsic viscosity, and this is also attributed to a reduction in the number of charges per molecule, caused by depression of the dissociation constant. To test this conclusion, values of the degree of ionization were calculated from the data of Fig. 3 and Table II for solutions in water and 2.5% dioxane con-

taining different amounts of acid and salt. A plot of intrinsic viscosity against degree of ionization (Fig. 7) gives essentially a single curve for these systems from $\alpha = 0.01$ to $\alpha = 0.04$, indicating that the effects of acid and dioxane have the same source. For $\alpha > 0.04$, the intrinsic viscosity is no longer finite; for $\alpha < 0.01$, the polymer is insoluble.

At dioxane concentrations just above the insoluble zone, a different situation prevails. The ionization is very slight, and although some acid is still needed to prevent an upsweep in η_{sp}/c with dilution, there are not enough charges to aid dissolution. But now the dielectric constant is much lower and the phenyl groups are not so strongly repelled by the solvent. Thus the molecule dissolves, though with an abnormally tight coil. As the

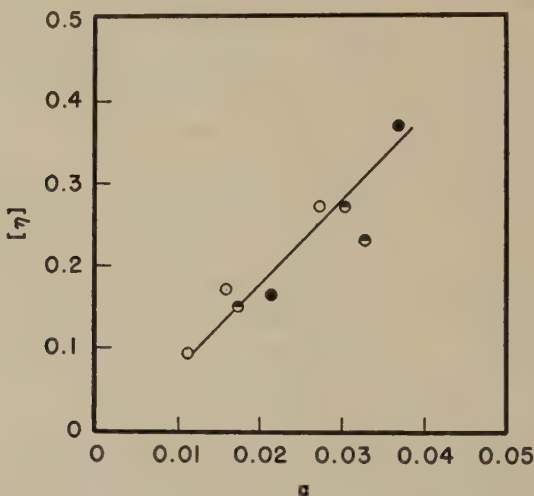


Fig. 7. Intrinsic viscosity of polyacid SY-MA plotted against degree of dissociation. Open circles, in water with HCl; half black, in water with HCl and KCl; black circles, in 2.5% dioxane with HCl.

proportion of dioxane is increased, the medium becomes more and more favorable for the phenyl groups and the coil expands, so the intrinsic viscosity increases. The values are practically independent of acid concentration because the only function of the acid is to keep the ionization negligible. Above 80% dioxane, even this function is unnecessary. The attainment of values even higher than that of the anhydride in dioxane may be due to a small difference in chain flexibility between the acid and the anhydride. The slight fall in $[\eta]$ above 80% dioxane may be due to some hydrogen bonding of carboxyl groups as the dielectric constant becomes extremely small.

These results serve to illustrate what complex behavior may arise from the interplay of electrical charges and lyophobic groups on a flexible

polymer molecule. Such effects may be important in determining the properties of flexible macromolecules of biological origin, such as myosin and nucleic acid.

ACKNOWLEDGMENTS

This work was supported in part by the Research Committee of the Graduate School of the University of Wisconsin from funds supplied by the Wisconsin Alumni Research Foundation, and in part by a grant from Research Corporation. We are also indebted to the Carbide and Carbon Chemicals Division, Union Carbide and Carbon Corporation, for support through its Fellowship in Physical Chemistry.

SUMMARY

1. Measurements of the titration with alkali and of the solution viscosities in dioxane-water mixtures containing various concentrations of acid and salt have been made for the 1:1 copolymers of maleic acid with styrene and vinyl ethyl ether, respectively.

2. In each copolymer the carboxyls dissociate in two distinct pH ranges. The first class of carboxyls has a relatively sharp distribution of dissociation constants and is about equal in strength in the two polymers. The second class has a very wide distribution of dissociation constants and is much weaker in the styrene than in the vinyl ethyl ether copolymer.

3. A minimal concentration of dioxane and/or hydrochloric acid is required to obtain a finite intrinsic viscosity extrapolation for either copolymer.

4. Above this minimal concentration, the intrinsic viscosity of the vinyl ether copolymer depends very little on the concentration of either dioxane or hydrochloric acid and is not far from the value for the corresponding anhydride (non-polyelectrolyte) copolymer in pure dioxane.

5. The intrinsic viscosity of the styrene copolymer varies in a complicated manner with dioxane and hydrochloric acid concentrations, and in certain concentration regions this polymer is insoluble.

6. The differences between the two polymers, and in particular the complicated behavior of the styrene copolymer, are explained by the hydrophobic character of the phenyl group.

REFERENCES

1. KATCHALSKY, A., AND GILLIS, J., *Rec. trav. chim.* **68**, 879 (1949).
2. FUOSS, R. M., AND STRAUSS, U. P., *J. Polymer Sci.* **3**, 246 (1948).
3. ALFREY, T., MORAWETZ, H., FITZGERALD, E. B., AND FUOSS, R. M., *J. Am. Chem. Soc.* **72**, 1864 (1950).
4. FUOSS, R. M., AND STRAUSS, U. P., *Ann. N. Y. Acad. Sci.* **51**, 836 (1949).
5. HERMANS, J. J., AND OVERBEEK, J. T. G., *Rec. trav. chim.* **67**, 761 (1948).
6. MARKOVITZ, H., AND KIMBALL, G. E., *J. Colloid Sci.* **5**, 115 (1950).
7. COHN, E. J., AND EDSALL, J. T., *Proteins, Amino Acids, and Peptides*, Chaps. 5, 9, 10, 23, and 24. Reinhold, New York, 1943.

8. BARNES, R. B., LIDDEL, U., AND WILLIAMS, V. Z., *Ind. Eng. Chem., Anal. Ed.* **15**, 659 (1943).
9. FORDYCE, D. B., AND FERRY, J. D., *J. Am. Chem. Soc.* **73**, 62 (1951).
10. STAUDINGER, H., *Die Hochmolekularen Organischen Verbindungen*. Springer, Berlin, 1932.
11. ARNOLD, R., AND OVERBEEK, J. T. G., *Rec. trav. chim.* **69**, 192 (1950).
12. HARNED, H. S., AND OWEN, B. B., *The Physical Chemistry of Electrolytic Solutions*. Reinhold, New York, 1943.
13. KERN, W., *Z. physik. Chem.* **181**, 283 (1937).

ADSORPTION OF AROMATIC HYDROCARBONS IN NONAROMATIC MEDIA ON CARBON BLACK

M. van der Waarden

Koninklijke/Shell-Laboratorium, Amsterdam, Holland

Received April 12, 1951

INTRODUCTION

Previous work (1) has shown that aromatic hydrocarbons with sufficiently long aliphatic chain(s) may stabilize carbon black dispersions in a nonaromatic medium. Aromatic nuclei were supposed to be adsorbed at the surfaces of carbon black particles, which are covered with polar carbon/oxygen groups. The adsorbed molecules may prevent the carbon black particles from approaching each other to within their van der Waals-London sphere of attraction. This repellent effect is enhanced when the molecules have longer alkyl chains.

The present paper discusses the degree of adsorption on carbon black of aromatic hydrocarbons in a nonaromatic medium and the way it is affected by the presence of alkyl chains. According to Mair and Forziati (2), low-molecular-weight aromatic compounds are very selectively adsorbed from nonaromatic media by silica gel and activated carbon.

EXPERIMENTAL

The carbon black (evacuated at 125°C.) used in the experiments and discussed previously (1) had an active surface of 325 sq.m./g., as determined by the B.E.T. method using nitrogen at -195°C. and contained 3% by weight of chemically bound oxygen; according to electron micrographs it consisted of nearly spherical elementary particles with a diameter between 100 and 300 Å.

n-Heptane or a white mineral oil (viscosity at 25°C. = 22.5 centipoises; 44% of the carbon atoms in naphthene structure, 56% in paraffin structure; average mol. wt. 320) was used as the nonaromatic medium. The following aromatic compounds were tested: benzene (redistilled), naphthalene, anthracene and phenanthrene (recrystallized), xylene (caustic treated and redistilled), alkylated naphthalenes with one C₈ alkyl chain, one C₁₆ + one C₂ alkyl chain and 2-3 (average 2.7) C₁₄ alkyl chains, respectively; these naphthalenes had been pretreated in pentane solution with 10% carbon black in order to remove any active contaminants.

The aromatic compounds were dissolved in the nonaromatic media at various concentrations. When the refractive index of the solution had

been measured, 2 g. of carbon black was added to 10 g. of the solution. After repeated mixing and standing for 1 hr. at room temperature (20–24°C.)¹ the refractive index of the clear equilibrium liquid was determined. By centrifuging the dispersions in white mineral oil for 5 min. a clear supernatant liquid was obtained. Mixing and standing for longer than 10 min. after addition of the carbon black did not change the refractive index of the clear liquid. As heptane, white mineral oil, and benzene do not remove from carbon black any components which affect the refractive indices of these liquids, the aromatic contents of the solutions before and after adsorption were calculated from the refractive indices with the aid of calibration curves of aromatic–heptane and aromatic–white mineral oil mixtures. These curves were found to be practically rectilinear over considerable concentration intervals.

We understand by adsorbed aromatics the quantities of aromatic compounds the carbon black surface contains in excess of the liquid. So the total amount of aromatic and nonaromatic hydrocarbons after adsorption can be considered as being composed of a mixture having the composition of the equilibrium liquid on the one hand and an excess of (adsorbed) aromatics on the other. The former contains the total amount of nonaromatics in the system and consists of the equilibrium liquid itself and a layer of the same composition adhering to a fraction of the carbon black surface. The quantities of adsorbed aromatics can be calculated if the aromatic contents of the liquid phase before and after adsorption are known, as the amount of nonaromatics in this phase remains constant.

E.g., 2.00 g. of carbon black is added to 10.00 g. of a mixture containing 20.00% by wt. of benzene and 80.00% by wt. of heptane. The equilibrium composition of the liquid is 19.00% by wt. of benzene and 81.00% by wt. of heptane. The amount of heptane is 8.00 g. and therefore the amount of nonadsorbed benzene after adsorption is $\frac{19.00}{81.00} \times 8.00 = 1.88$ g., and the amount adsorbed is $2.00 - 1.88 = 0.12$ g. benzene per 2 g. of carbon black.

The determination of the refractive indices was carried out at 20°C. with the aid of a Bausch & Lomb refractometer, the nearest readings differing by 0.00005.

RESULTS

Figure 1 shows the adsorption isotherms at room temperature of solutions of the above-mentioned hydrocarbons in *n*-heptane.

¹ The influence of small variations of temperature is not important, as was shown by Mair and Forziati (2). They found that the adsorption of toluene (15% by vol. in *n*-heptane) on silica gel decreased by only 0.4% (on quantity adsorbed) when the temperature was raised by 1 degree centigrade in the interval of 0–28°C.

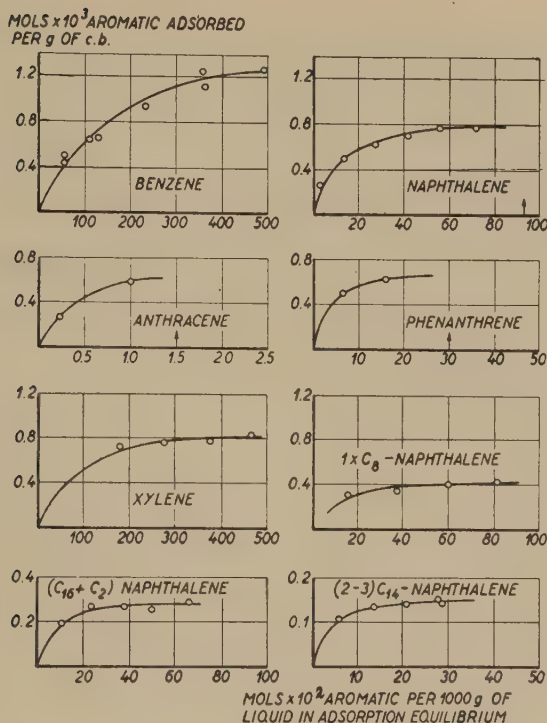


Fig. 1. Adsorption isotherms of aromatic compounds in *n*-heptane on carbon black at room temperature; \uparrow = saturation concentration in *n*-heptane.

TABLE I

Data on the Adsorption of Aromatics in n-Heptane on Carbon Black at Room Temperature

Aromatic compound	Solubility at 20°C. in <i>n</i> -heptane		Max. quantity adsorbed by carbon black	Equilibrium concentration in liquid at initial max. ads.	
	% wt.	moles/1000 g. $\times 10^2$		% wt.	moles/1000 g. $\times 10^2$
Benzene	∞	∞	ca. 1.300	ca. 30	ca. 400
Naphthalene	about 11	about 93	0.800	5	40
Anthracene	about 0.3	about 1.5	0.650	0.2	1
Phenanthrene	about 6	about 31	0.650	2	10
Xylene	∞	∞	0.850	30	300
(1 \times C ₈) naphthalene	∞	∞	0.450	5	20
(1 \times C ₁₆ + 1 \times C ₂) naphthalene	∞	∞	0.300	7	20
(2.7 \times C ₁₄) naphthalene	∞	∞	0.150	9	15

For comparison we also determined adsorption isotherms of solutions of the three alkyl naphthalenes in white mineral oil, which were found to be nearly equal to those of solutions in *n*-heptane.

The maximum number of adsorbed molecules and some other data are presented in Table I.

The maximum number of adsorbed molecules decreases with increasing number of nuclei and with increasing length and number of alkyl chains.

A steeper initial slope of the adsorption isotherms of the non-alkylated aromatics (Fig. 2) and therefore a greater adsorption energy corresponds to a decreasing solubility of these aromatics in heptane.²

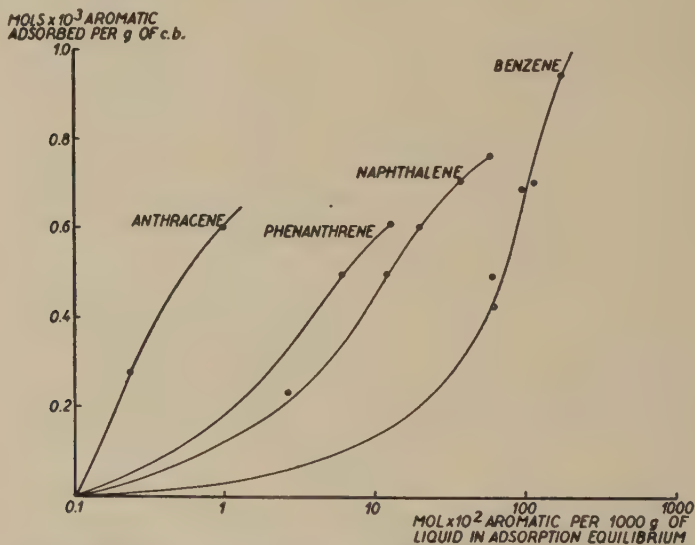


Fig. 2. Comparable adsorption isotherms of non-alkylated aromatics in *n*-heptane on carbon black at room temperature.

DISCUSSION

The hydrocarbon layer on the carbon black surface consists in general of (a) a part having the aromatic-nonaromatic composition of the liquid phase, and (b) an aromatic part which is called the surface excess (adsorbed aromatics). The latter part, which is determined in our experiments, increases with increasing aromatic content of the liquid and therefore displaces part (a) from the surface. When the amounts of adsorbed aromatics stop increasing with increasing aromatic content of the liquid the surface is saturated with adsorbed aromatics and part (a) is completely displaced, which means that the whole surface is covered with adsorbed aromatics.

² Winterstein *et al.* (3) found that in chromatographic separations the adsorption of polycyclic aromatics depends on the number and arrangement of the nuclei.

From the maximum adsorbed quantities (Table I) and the total surface area (325 sq.m./g. carbon black) the surface area covered by one adsorbed molecule can be calculated. Values of about 41, 67, 83, and 83 \AA^2 were thus found for benzene, naphthalene, anthracene, and phenanthrene, respectively.

The surface areas of the nuclei can be approximately calculated from the volume of a molecule in the liquid state (mol. wt./ (density \times Avogadro's number)) and the thickness of the rings (about 3.7 \AA .²) (4). These values are about 40, 58, and 75 \AA^2 for benzene, naphthalene, and anthracene/phenanthrene, respectively, and thus are in good agreement with those derived above. They indicate that in the case of maximum adsorption of these compounds the entire active surface of the carbon black is covered with aromatic nuclei in a flat position. Such a position may be attributed to an interaction between chemically bound oxygen on the polar carbon black surface and all partial dipoles of the aromatic rings.³

The approximate surface areas covered per adsorbed molecule of alkylated aromatics calculated from the maximum adsorbed quantity and the total active surface area are:

	\AA^2
Xylene	63
(1 \times C ₈) naphthalene	120
(1 \times C ₁₆ + 1 \times C ₂) naphthalene	180
(2.7 \times C ₁₄) naphthalene	360

The surface areas covered per benzene and naphthalene nucleus are known, so that it is possible to calculate the surface area which is blocked by the alkyl chains as a whole, and by each of their C-atoms in the case of maximum adsorption (Table II).

If the alkyl chains, like the aromatic nuclei, were adsorbed in a flat position on the carbon black surface, the area covered by each C-atom

TABLE II

Surface Areas Blocked by Alkyl Chains and per C-Atom of the Chains of Adsorbed Alkyl Aromatics

Adsorbed molecule	Number of C-atoms in alkyl chains	Total area blocked per adsorbed mol. \AA^2	Total area blocked by alkyl chains \AA^2	Area blocked per alkyl C-atom \AA^2
Benzene	0	41	0	—
Xylene	2	63	22	11
Naphthalene	0	67	0	—
(1 \times C ₈) naphthalene	8	120	53	6.6
(1 \times C ₁₆ + 1 \times C ₂) naphthalene	18	180	113	6.3
(2.7 \times C ₁₄) naphthalene	38	360	293	7.7

³ Harris and Emmett (5) as well as Smith, Pierce, and Cordes (6) obtained results which indicate that gaseous benzene molecules below their critical temperature are adsorbed in a flat position both on glass and on carbon black surfaces.

would be 12–16 Å.², the packing of the alkyl chains in the adsorbed layer being densest (4); if there is no maximum denseness of the packing this area would be larger. The area covered per alkyl C-atom of xylene (11 Å.²) is in fair agreement with the value given above. In this case the alkyl C-atom is rigidly bound to the nucleus, and will therefore probably lie on the carbon black surface, in the same plane as the aromatic ring. However, the surface areas blocked per alkyl C-atom of the long chains are considerably smaller. It is improbable that for the adsorption of alkyl aromatics a larger area is available per gram of carbon black than for the adsorption of nitrogen and that the tabulated values would therefore be too low. On the other hand, owing to the larger dimensions of the alkyl aromatic molecules certain parts of the surface may be accessible to nitrogen, but not to alkyl aromatics, so that a smaller total area is available for the latter. In that case the area blocked per alkyl C-atom would be even lower than indicated in Table II.

Based on the values calculated the conclusion may, therefore, be drawn that the alkyl chains of alkyl aromatics are not adsorbed flat on the surface.

However, although these alkyl chains are not in a flat position on the carbon black surface, and may therefore be considered to be mobile in various directions, with their points of fixation acting as a ball joint, they do block a certain surface area and seem to keep other alkyl aromatic molecules from attaching to the surface. The latter effect is stronger as the chains are longer. Previously (1), it had been concluded that chains of alkyl aromatics adsorbed to carbon black prevent a close approach of the carbon black particles; this action, too, is stronger as the alkyl chains are longer.

The alkyl chains have, therefore, a certain repelling effect both on other alkyl chains attached to the same carbon black surface and on alkyl chains attached to other carbon black particles. This model has proved to be amenable to a theoretical interpretation of the stability of dispersions in hydrocarbons. The theory will be dealt with in forthcoming publications from this laboratory.

SUMMARY

1. Isotherms have been determined at room temperature for adsorption on carbon black of alkylated and non-alkylated aromatic compounds in *n*-heptane and white mineral oil.
2. The results obtained suggest that the aromatic nuclei are adsorbed flat on the surface, and that the alkyl chains of the adsorbed aromatic compounds remain mobile in the liquid.
3. The alkyl chains of adsorbed alkyl aromatic compounds seem to have a mutually repelling effect within a certain distance.

REFERENCES

1. VAN DER WAARDEN, M., *J. Colloid Sci.* **5**, 317 (1950).
2. MAIR, B. J., AND FORZIATI, A. F., *J. Research Natl. Bur. Standards* **32**, 165 (1944).
3. WINTERSTEIN, A., *et al.*, *Z. physiol. Chem.* **230**, 146, 158, 169 (1934).
4. PAULING, L., *The Nature of the Chemical Bond*, pp. 189-92. Cornell University Press, Ithaca, 1945.
5. HARRIS, B. L., AND EMMETT, P. H., *J. Phys. & Colloid Chem.* **53**, 811 (1949).
6. SMITH, R. N., PIERCE, C., AND CORDES, H., *J. Am. Chem. Soc.* **72**, 5595 (1950).

DELAYED PLASTIC FLOWING IN CERTAIN POLYAMIDE FILMS¹

J. W. Kauffman² and Waller George²

Naval Research Laboratory, Washington, D. C.

Received August 9, 1951

ABSTRACT

Configurations of flow markings (generalized Lüders bands) are observed to form prior to the development of local necking (plastic shock waves) in polymeric films subjected to dead weight loading. Initially, the markings appear "bound" to free edges, or internal imperfections. Subsequent elapse of time under load allows further "growth" of the markings. Several typical types of development are illustrated, including "reflection" from a free edge. Repeated loading experiments suggest that the time interval during which the flow marking is "bound" is less than about 10 sec. in commercial polyamide film, at 3500 lb./in.² initial stress. When loadings for this duration are followed by sufficiently long rest periods, the effect of the initial localization disappears, and the specimen behaves on subsequent loading as a previously unloaded specimen. Time intervals under load greater than 10 sec., even when followed by reasonable "rest" periods, appear to induce irreversible localizations, which, after a sufficient number of repetitions, lead to the formation of plastic shocks. In these cases the total time under load prior to shock formation is essentially the same as the delay time for shock formations under uninterrupted dead weight loading.

The object of this paper is to demonstrate several characteristic ways in which the yield point and subsequent development and propagation of local necking in certain polymeric films may be described in terms of spatially local and delayed plastic flowing.

I. BACKGROUND

During the past hundred years, substantial evidence has accumulated in the technical literature that plastic flowing in solids is basically a spatially localized, irregular, inhomogeneous phenomenon. More recently, evidence has also been presented indicating that spatially localized plastic flowing is characterized, at least in part, by certain time intervals between application of a load to the solid and its response by plastic flowing.

In 1842, Piobert, Morin, and Didion (1) described the appearance of certain markings which are produced on the surfaces of "wrought iron"

¹ A preliminary version of this paper was presented before a meeting of the High Polymer Division, American Physical Society, held at the Brooklyn Polytechnic Institute, February, 1950.

² Staff members, Mechanics Division, Naval Research Laboratory. J. W. Kauffman is now at the University of Illinois.

armor plate during penetration by projectiles. These markings are highly symmetrical and confined by the cylindrical zone of plastically deformed plate material which is created during penetration by the attacking missile. A number of years later an analogous type of flow marking was described by Lüders (2). These markings were originally observed to appear on the polished surfaces of flat tensile specimens of wrought iron loaded above their elastic limit. The general analogy between the flow markings of Piobert and Lüders was developed during the following years by the French military. An excellent and comprehensive summary of the morphology of flow markings in metals was published by Hartmann (3), a French artillery captain. It is particularly interesting that Hartmann noted the "wave-like" propagation of distortion throughout test specimens of aluminum. A more recent summary of the same general subject may be found in the work of Nadai, who has noted the appearance of flow markings in certain waxes (4).

A particularly symmetrical set of flow markings in the form of a figure "X" appears across the plane of sheet tensile specimens. The appearance of this marking in sheet steels has been described by Gulliver (5). In these materials the X-shaped figures are observed to "collapse" into a neck or a fracture which originates in the center of the specimen at the intersection of the flow figure. The gross markings involve a reduction of thickness normal to the plane of the sheet, and contain, superimposed within them, finer deformation markings characteristic of the individual grains of the material.

While the existence of irregular plastic flowing in the ordinary tensile test may have been observed somewhat earlier, it appears that the first suggestion of plastic flowing localized in time (temporal localization) is due to Andrade (6). In connection with his well-known studies of creep in wires loaded at a constant true stress, he noted that the creep of polycrystalline copper wires proceeded in a very irregular and discontinuous manner during the latter portion of the loading epoch. He pointed to the possible analogy between the sudden elongations of the loaded copper wire and the sudden slipping of earth masses during an earthquake, and suggested that the former might be termed a "copperquake." About 20 years ago, Gough *et al.* (7) observed a definite time interval following the incremental increase of the load after which additional extension (transient creep) developed in single crystal wires of aluminum. The extent of these time intervals was not always clearly observable, but certain unambiguous observations yielded intervals as long as 3 sec., following which additional extension rapidly developed.

Jaffé and Ehrenfest (8) noted that heated single crystals of rock salt, subjected to an essentially simple shear type loading, plastically deformed in sudden, short steps at regular time intervals which were accompanied

by audible clicks. This effect has been described in greater detail by Classen-Nekudowa (9) and by Becker and Orowan (10), among others. Later, Bridgman observed what is believed to be an analogous effect in certain steels subjected to more complicated stress states (11). Recently, McReynolds has described the irregular yielding of polycrystalline aluminum specimens loaded at a low constant time rate in a "soft" testing apparatus. By means of a careful strain-gauge technique he has demonstrated that the irregularities involve the initiation and limited propagation of waves of plastic strain along the specimen (12).

The first unambiguous demonstration of the existence of a time interval between the application of load to a specimen and its response by plastic flowing was made by Clark and Wood (13) in 1948 using a damped hydraulic loading machine which applied controlled tensile loads to mild steel specimens within a few milliseconds. They have systematically studied the dependence of this delay time in mild steel on stress, temperature, and carbon content. The authors have reported that similar, but much longer delay times exist in crystalline, but unoriented polyamide and polyethylene films (14). It is by no means clear, however, that the existence of a delay time for plastic flowing is confined to crystalline solids.

II. DEMONSTRATION OF DELAYED YIELDING IN A POLYAMIDE FILM

The demonstration of a delay time for yielding in polymeric solids is easily accomplished using commercial polyamide films.³ All that is required is a simple apparatus, shown in Fig. 1, which applies a dead weight load through a spring to a suitably shaped specimen. The application of load is accomplished by lowering a weighted platform which supports the dead weight which in turn is attached to the specimen through the "soft" spring. The weighted platform is rigidly connected to a close fitting piston which slides in a closed cylinder containing a "leak" valve. To accomplish load application, the valve is opened, the piston pulled up, allowing an intake of air through the leak valve, after which the valve is closed. The specimen, spring, and dead weight to be applied are then arranged in a vertical position with no tension in the spring. The upper end of the specimen is connected to gallows through a stiff Hooke (ball and socket) joint. The motion of the dead weight is guided while the piston moves into the cylinder as the compressed air within it is released. The mechanism used allows a controlled rate of load application so that the full load appears on the specimen within less than 0.3 sec. The time delays observed in these experiments ranged from 2 to 1000 sec. There is sufficient friction between the piston and cylinder to quickly damp any oscillation which may develop during the initial load application.

The sequence of photographs reproduced in Fig. 2 shows the development of local necking in a commercial type polyamide film under dead

³ Most of the work reported here involved an experimental polyamide film, Nylon, FM 3001, procured from E. I. du Pont de Nemours, Inc.

weight load. These photographs are enlargements of a 16-mm. (color) motion picture of the phenomena. Scene (a) shows a view during load application—the spring, visible in the bottom of the frame, is not completely extended. The vertical steel columns of the gallows are visible at the edges of the frame, as is a stop watch. Scene (b) shows the incipient

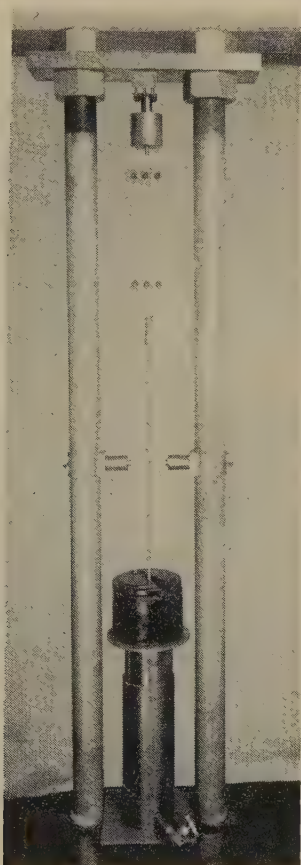


FIG. 1. Dead weight loading device. Specimen of transparent plastic film is *in situ* between heads.

necking which develops near the end of the delay time.⁴ Scene (c) shows the completed neck composed of a pair of shock fronts which are beginning to propagate up and down the specimen. Scene (d) shows the end of the propagation phase of the shock motions that have traversed the material in the original reduced section of the specimen. Slow creep is observed

⁴ The diffuse reflections are from the region which subsequently necks and which is filled with a complex series of flow figures not resolved in this photograph.

during the delay time, but the total longitudinal extension developed within the delay time is less than 1% of the extension within the necked region after the *elapse* of the delay time.

III. PHYSICAL PLAUSIBILITY OF A TIME DELAY FOR PLASTIC FLOWING

Explanation of delayed plastic flowing may be sought in various ways. We present below two arguments, one involving macroscopic parameters and another concerning processes on a molecular scale. It would appear

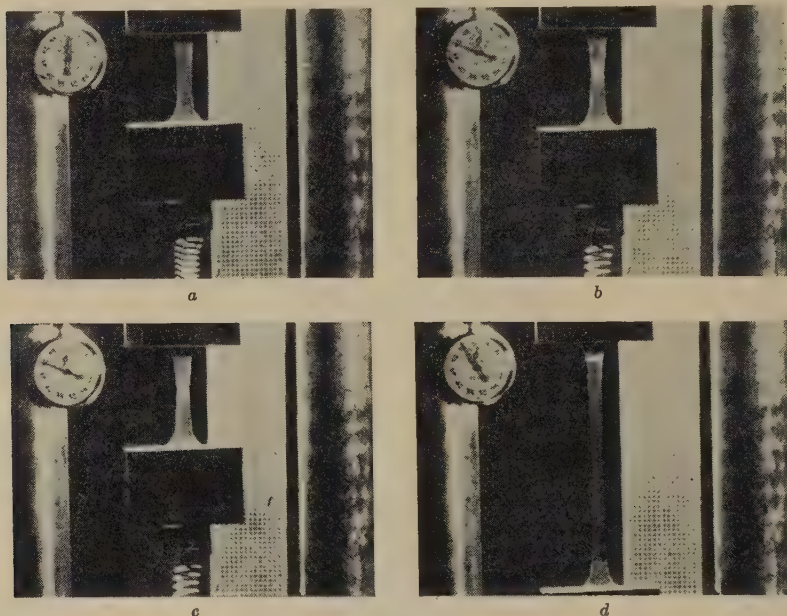


FIG. 2. Demonstration of delay time for local necking (dead weight loading).

- (a) Load application just starting (note watch and spring).
- (b) End of delay time ($\tau \approx 46$ sec.).
- (c) Flow markings within the neck (not resolved) collapse into V-shaped plastic shock waves (one moves up, the other down).
- (d) End of shock propagation (wave fronts straighten during propagation).

that a complete discussion of the physical origins of delayed, local plastic flowing will, of necessity, contain the essential portions of both arguments.

First, let us consider the general effect of the rate of application of load on the mechanical properties of solids. Usually the yield stress⁵ increases as the rate of loading is increased. An element of volume of a material, if loaded very rapidly in tension to a high stress, will behave initially elastically, provided the applied stress is slightly below the yield stress

⁵ Engineering terminology is tacitly assumed here.

corresponding to the load rate. If the stress is then maintained constant the time average rate of loading will decrease and eventually become equal to loading at a lower rate at which the yield stress is equal to the already applied stress. Therefore, we must conclude that after a time interval the material will no longer behave elastically, and plastic flow will commence. In this argument the plausibility of delayed flowing is based on a load rate effect which is found in many materials, including unoriented nylon (15).

A second plausibility argument for a delay time for the appearance of localized plastic flowing may be based on recent extensions of nucleation theory due to Turnbull (16). A discussion of the nucleation of slip bands in terms of such theory has been published by Leschen *et al.* (17). In this case the delay time is identified with a nucleation time during which the time rate of appearance of a generalized "phase" is very slow and following which the rate of "phase" transformation substantially increases until it approaches the steady state nucleation rate obtained by Becker and Volmer (18). This theory pictures the growth during the nucleation time of a subcritical embryo of a transformed phase from a parent matrix by means of a series of bimolecular reactions. At the end of such a characteristic time the embryo is pictured as possessing a "critical" size such that further growth proceeds by reduction of the free energy of the parent.

It should be noted that Leschen and co-workers attempted to demonstrate the concept of nucleation of plastic flowing by assuming that the creep rate under dead weight loading was approximately proportional to the rate at which embryos attained the critical size and became slip bands, and correspondingly attempted to relate transient creep phenomena with nucleation times. In the case of the present experiments, on the other hand, the nucleation time is to be directly identified with the delay time for a given type of localized plastic flowing. It is by no means clear that the rate of growth of localized plastic flowing is in fact a nucleation phenomenon. In particular, it would be interesting to study the temperature dependence of the growth of such and to compare it with that predicted from a nucleation theory.

IV. THE STRUCTURE AND FORM OF FLOW MARKINGS IN POLYAMIDE FILM

The morphology of flow figures which develop within the time delay for gross local necking or shock formation in polyamide films can be reduced to sets of typical component flow markings. We shall describe these below.

At any given moment, the configuration evident in any given specimen is a function of the selection and preparation of the specimen. The commercially available polyamide film, as received for study, contains two

types of obvious structure which may provide ready sources of imperfection and irregularity in the flow figures. First, the film contains grain-like domains of various sizes, typical examples of which are found in Fig. 6 described below. Secondly, the films contain "pin points" of local thickness reduction, or dimples, which are also visible in Fig. 6. These latter appear to be real imperfections; flow figures almost always tend to develop around them. Cutting, shearing, and other methods of specimen preparation affect the over-all flow figure. No particular techniques of specimen preparation as applied by the authors appeared to greatly alter the structure of the flow figures originating at the specimen edges. Therefore, a convenient punching technique of specimen preparation was insti-

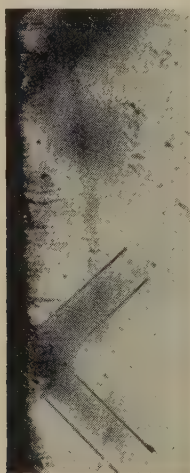


FIG. 3. Incipient flow figure in nylon film as seen under microscope, crossed Nicols, $\times 100$.

tuted. This involved punching the "gauge length" with a carefully sharpened pair of parallel spaced knives backed by a soft wood block. The fillet radii and "head" ends of the specimen were then cut with a sharp circular punch and shears, respectively.

The flow figures which develop in polyamide film under dead weight load fall into two general classes which are distinguished by their angular orientation with respect to the nominal axis of loading and their temporal development. The first class of markings is oriented at approximately 45° with respect to the axis of loading, develops during the earlier portions of the delay time for shock formation, and appears to be essentially "bound" to its origins. The second class of markings develops from the first and is characterized by a "propagation" along an orientation of approximately 60° with respect to the axis of loading.

Those flow figures of class I above, assume two characteristic geometrical patterns, an *X*-shaped figure surrounding an obvious pin point or dimple in the interior of the specimen or a *V*-shaped configuration symmetrical about the horizon and extending from the edge of the specimen

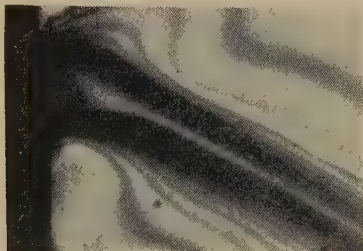


FIG. 4. Detail of flow figure propagation from stress-free edge in direction approximately 60° from the tension axis ($\times 100$, crossed Nicols).

into its interior. In our experience other configurations of class I markings were rarely observed.

A typical class I marking which originates near the free edge of the specimen is shown in Fig. 3 as viewed through analyzed polarized light in a petrographic microscope. There is some evidence that these figures require a characteristic time interval for their appearance which is appreciably



FIG. 5. Angle shock formation as seen just after the termination of the delay time ($\times 1$).

ably smaller than the delay time for plastic shock formation. This will be discussed in the section on repeated loading below.

The class I flow figure appears to become free from its origin after the elapse of further time under load and is then to be termed a class II figure. When growth is visible the orientation is changed as noted above. As the "propagation" continues the flow marking deepens, with an attendant local reduction in thickness of the specimen. Sets of characteristic

fringes develop in the stress field around it, as shown in Fig. 4. These fringe systems have not been subjected to a detailed study, but doubtless would reveal interesting information regarding the shape and changes in the surrounding field with subsequent development.



Fig. 6. Contact print of flow markings nearly collapsed into shock wave ($\times 1$).

The development of a class II (60°) flow figure can be complex if it occurs within a specimen containing an array of class I figures or concurrently developing class II markings. In these cases important interactions between the flow figures are observed of the form class II-class I or class II-class II. Occasionally a simple figure is observed which merely

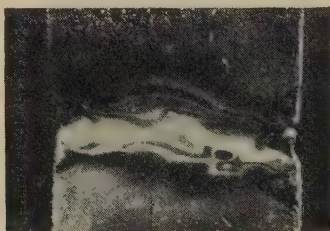


Fig. 7. Horizontal shock as viewed through crossed Polaroids ($\times 2$).

grows across the specimen and collapses into what we term an angle shock, a typical example of which is shown in Fig. 5. The specimen shown was unloaded before shock propagation had really begun to reveal the initial shock geometry.

A second typical configuration is found when essentially a number of parallel class II figures cross each other in the form of an X-shaped figure. An example of this marking is shown in Fig. 6 which represents a contact print of a specimen which received a number of alternate loading

and unloading cycles with the loading terminated just prior to the collapse of the configuration into a nearly horizontal shock front. A slightly more advanced development of this type of collapse is shown in Fig. 7 as viewed with polarized light. The initial shock front resulting from the multiple X-shaped flow marking is not always horizontal; it sometimes contains angular ends as shown in Fig. 2c. This figure is somewhat reminiscent of the typical "Mach bridge" found in flow of gases through nozzles (19). The time delay for horizontal shock formations and the modification noted specifically above is in general shorter than that for



Fig. 8. Crossed angle markings which develop the V-shaped shock front as shown in Fig. 2b.

the simple angle shock. This suggests that the former (horizontal) type of shock front involves the initially independent development and subsequent interaction of class II flow figures (derived from different class I figures). Another example of this type of flow figure is shown in Fig. 8 as visible under ordinary illumination (pin-point necking is visible in the upper portion of the specimen).

A third typical configuration of flow figures is observed which leads to a generally longer delay time than either of the two other types described above. An example is shown in Fig. 9. This involved what appears to be the reflection of a class II marking from a free edge of the specimen and its interaction with class I markings. Figure 9a shows the class II marking which originated at the lower left. It has "propagated" across about one-half the specimen width (*ca.* 0.9 cm.). In Fig. 9b the marking interacts with a class I marking associated with pin-point necking. The original marking has propagated to the specimen edge and suffered a "reflection." This reflection is not further interaction with class I edge

markings since the angles are clearly 60° with respect to the loading axis. It is possible, however, that some of these reflections resulted from the "release" of very small class I markings initially bound to the right specimen edge. Fig. 9c shows the completed development of the original class II figure, and Fig. 9d shows the shock front which developed from it. Even more complex developments may be observed to occur within a given specimen; in general they involve more complex mixtures of the

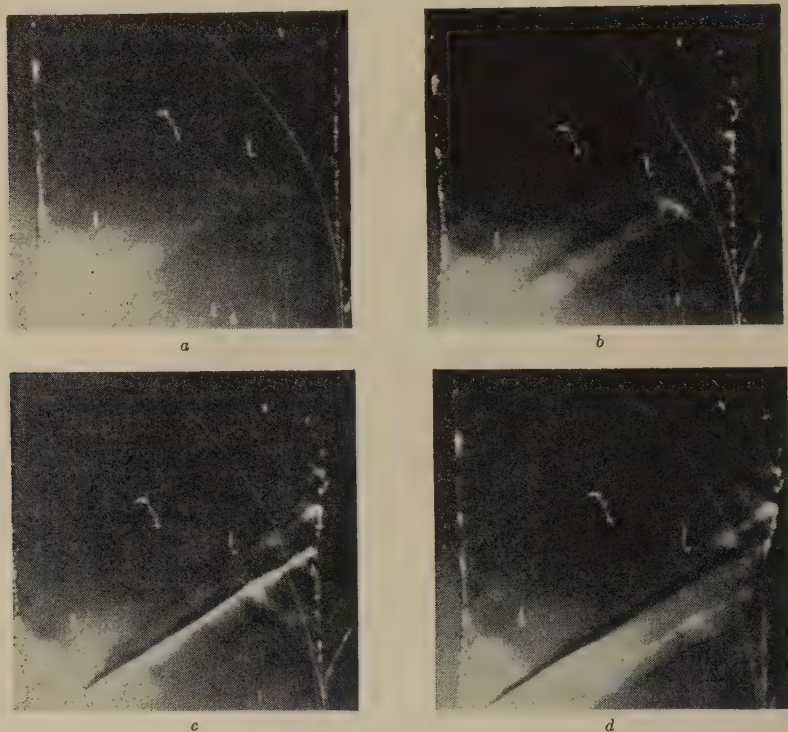


Fig. 9. Development of a "reflection" from the right edge of a nylon film (dead weight loading). For description see text, sec. IV.

interactions of the types described above. Also, in general, the time delay for shock formation increases with the complexity of the flow marking configurations.

V. QUANTITATIVE CHARACTER

In the preceding sections we have discussed qualitative features of delayed plastic flowing in polyamide films when subjected to dead weight loading. While in many respects those results are the more interesting, it is possible to obtain certain quantitative information about the phenomena.

The macroscopic tensile properties of unoriented nylon film have been discussed by Miklowitz (15). The rate of loading effect on the engineering stress-strain curve is typical of many technical materials, the curves being higher, the higher the rate of load. This engineering stress-strain relation for a polyamide film is shown schematically in Fig. 11. It is composed of an initial elastic portion followed by a rounded yield region, \overline{YA} , a nearly horizontal portion, \overline{CD} , and then a concave upward portion, \overline{DB} . It is this particular type of nonlinearity in the stress-strain relation which can be used to form the basis for a semiquantitative phenomenological description of the formation and propagation of plastic shock waves. We have already noted the rapid, almost cataclysmic collapse of the configurations of flow markings which precede the shock formation. The processes of collapse vary somewhat as to detail, but all are characterized by a rapid, local through-the-thickness reduction of the specimen and a slight lateral shift to one-half of the specimen with respect to the other (as shown in Fig. 5 and to a lesser extent in Fig. 4). The major portion of this rapid reduction in thickness, which occurs within less than 0.1 sec., results in the appearance of a relatively sharp stress "discontinuity" after a momentary unloading of this section.

A phenomenological description of shock formation can be obtained by considering the propagation of *plastic* waves in a medium characterized by a nonlinear stress-strain relation of the type shown in Fig. 10. The origins of such descriptions can be traced to the independent endeavors of G. I. Taylor, Th. v. Kármán, White and Griffiths, and Rakhmatulin (20). It is assumed that *waves* of permanent distortion are governed by a wave equation of the form

$$\frac{\partial^2 u}{\partial t^2} = c^2 \frac{\partial^2 u}{\partial x^2}, \quad [1]$$

where

$$[c(\epsilon)]^2 = 1/\rho \left. \frac{d\sigma}{d\epsilon} \right|_{\epsilon} \quad [2]$$

and $\epsilon \equiv \frac{\partial u}{\partial x}$, $u(x)$ being the displacement, and x being a Lagrange coordinate along which the disturbance is propagated. It is assumed that $\sigma = \sigma(\epsilon)$, only, describes the nonlinear medium. It is easily seen that [1] reduces immediately to the usual equation governing elastic wave propagation if $\sigma = E\epsilon$. Each plastic strain value ϵ_1 will propagate with a characteristic velocity C_1 , and for strains between $0 < \epsilon_1 < \epsilon_c$ (Fig. 11) the wave front of plastic strains will spread out along x as the time of propagation increases. If a stress $\sigma_2 > \epsilon_A$ is applied (σ_2 lying in the concave upward portion of the stress-strain curve of Fig. 12), the formula [2] for velocity

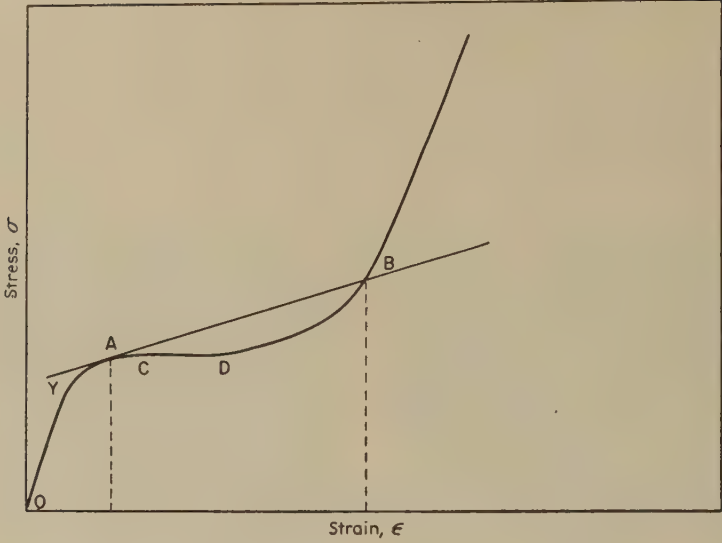


FIG. 10. Typical polymer-like stress-strain curve, exhibiting concave upward region \overline{CDB} .

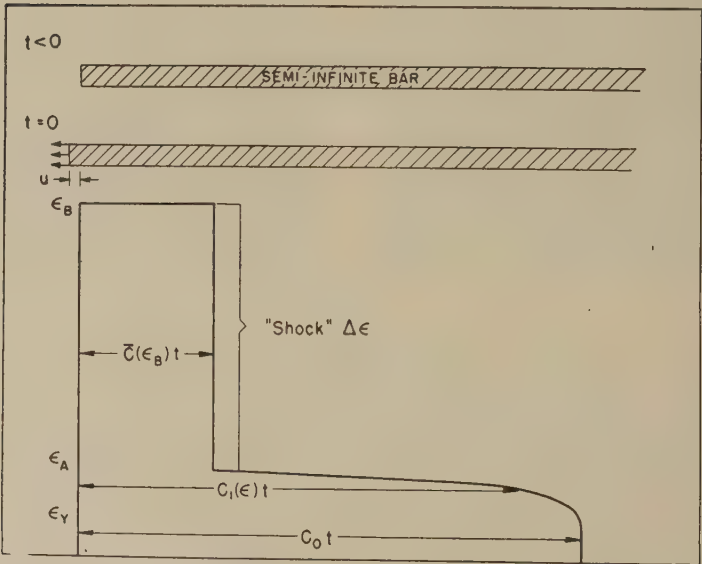


FIG. 11. Schematic plot of strain front in a semi-infinite bar at time t . The material of the bar is assumed to be described by the stress-strain relation shown in Fig. 10 and subjected to a continuing strain ϵ_B at $t = 0$.

will not be valid for the propagation velocity $c(\epsilon_2)$ since it predicts the higher strain increments will move faster than the lower increments. In the concave upward region, therefore, the strain increments pile up into a sharp wave front containing all strains from ϵ_A to ϵ_B and propagate as *shock* waves. It can be shown that the velocity of a shock characterized by a point $P: (\sigma_B, \epsilon_B)$ in the concave upward portion of the stress-strain relation is determined by the slope of the line \overline{BC} in Fig. 11. Strains less than those characterized by ϵ_c are propagated as ordinary plastic and elastic waves with velocity given by [2]. Figure 11 shows a schematic plot of the distribution of strain to be found after a time t , measured from the instant of loading of a semi-infinite bar composed of a nonlinear material described by a stress-strain relation of the type pictured in Fig. 10.

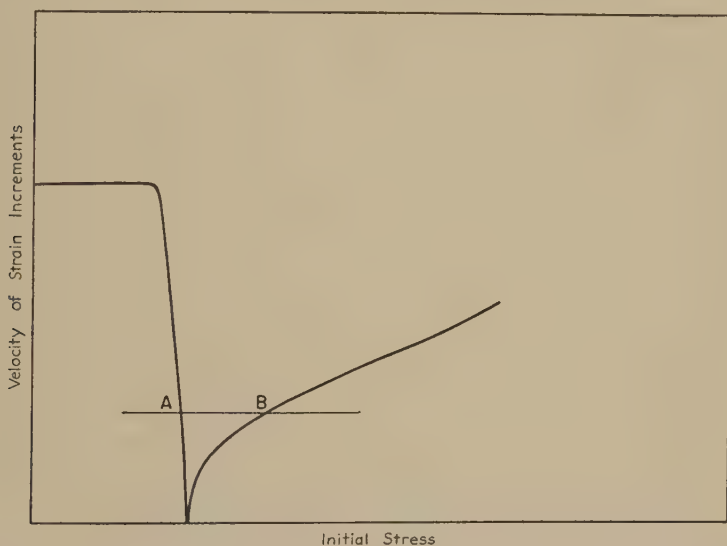


FIG. 12. Schematic plot of the velocity of strain wave increments as a function of initial stress. The left branch of the curve refers to ordinary plastic waves; the right, to shocks. The velocity $A - B$ corresponds to the shock $\epsilon_B - \epsilon_A$ shown in Fig. 11.

Strains from ϵ_c to ϵ_B are propagated as a plastic shock wave, etc. The ordinary elastic and plastic strain distribution will suffer progressive dispersion as the time under load increases. Figure 12 shows a schematic plot of the velocity of the strain wave increments as a function of initial stress. Figure 13 shows similar plots of shock wave velocity *vs.* initial stress as measured for nylon film described earlier. The initial stress (engineering) corresponding to nearly zero velocity shock waves agrees very well with the "yield" stress measured for this material in ordinary engineering tensile tests of the material (σ_c in Fig. 10). It is to be noted that

these curves are strongly dependent on the environmental water concentration. Another example of these water environmental effects is found in Fig. 14 which shows the relation between delay time for shock formation and initial stress. In spite of the appreciable scatter which is indicated in these plots, it is quite evident that specimens in "equilibrium" with different water environments yield in a given time at definitely lower stresses the higher the water concentration.⁶

Finally it should be pointed out that the magnitude of the shock velocities at stress levels appreciably greater than those of σ_c (ca. $1.3 \sigma_c$) are about three orders of magnitude lower than those to be predicted

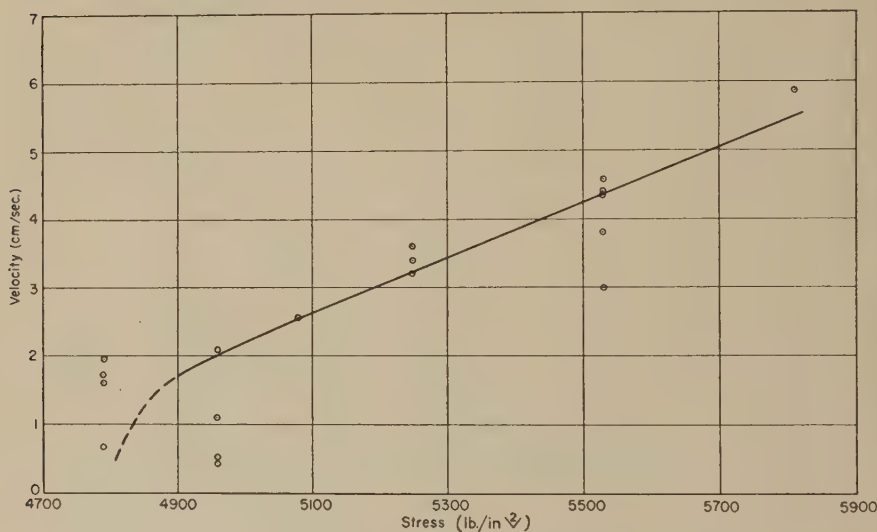


FIG. 13. Shock velocity vs. initial stress for nylon film (room temperature, 40% relative humidity).

from engineering stress-strain relations obtained from the nylon film. The data of Miklowitz (15), for example, predict at stress levels of about 4500 lb./in.² 65% relative humidity and room temperature, that the shock velocity should be about 10^3 cm./sec. where our studies indicate a velocity of the order of 1 cm./sec. for comparable conditions. This quantitative discrepancy is surely due in part to neglect of the effects of lateral motion and more probably the use of a very poor approximation to the nonlinear stress-strain relation for the material. It is hoped to discuss this discrepancy and the humidity effects in greater detail in subsequent publications.

⁶ In these experiments the equilibrium was regarded as established after maintaining the prepared specimens at the respective conditions for approximately 3 weeks.

VI. REPEATED LOADING EFFECTS

The qualitative picture of the propagation of local necking as a plastic shock wave which was sketched in V. above neglects completely the events which occur *within* the delay time. It assumes *collapse* of the flow figure at the end of that interval. In view of the quantitative discrepancy

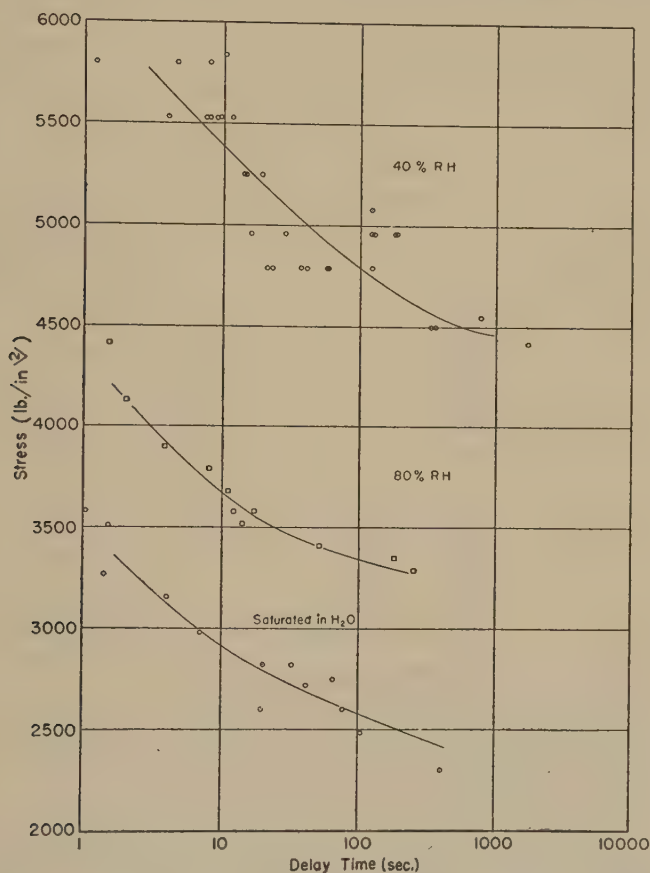


FIG. 14. Delay time for shock formation *vs.* initial stress for various humidity conditions, showing effect of absorbed water on the delay time. (All tests run at room temperature, 20°C.)

between observed shock velocities and velocities obtained from measured stress-strain relations obtained by quasi-static loading and for other reasons, it was decided to attempt some simple studies of the delay time itself.⁷ Accordingly, delay times for plastic shock wave initiation (or flow

⁷ In this connection we wish to acknowledge stimulating discussions of the possible additivity of effects occurring within the delay time with Dr. G. R. Irwin, N.R.L.;

figure collapse) were measured where the dead weight loading was alternately maintained and removed. In these cases of interrupted loading the delay time was defined as the total time under load. So long as the minimum time interval under load was greater than about 20 sec., the mean magnitude of the intermittent delay times observed at an initial (first loading) engineering stress of 4830 lb./in.² (23°C., 40% relative humidity) was experimentally indistinguishable from the simple (uninterrupted) delay time. A typical set of observations illustrating this apparent additivity of times under load is found in Table I. Here group (A)

TABLE I
Apparent Additivity of Times Under Test
Initial stress: 4830 lb./in.²

Group A Uninterrupted Delay time sec.		Group B	
		Repeated loading Time intervals under load Time intervals between loadings Delay time sec.	20 sec. 60 sec.
	318	366	
	303	282	
	289	259	
	264	256	
	246	235	
	215	167	
	190	164	
	140	160	
	128	132	
	102	119	
	219 sec.: Mean value	214 sec.: Mean value	
	64 sec.: Mean deviation	66 sec.: Mean deviation	

of 10 observations of the delay time for uninterrupted loading is arranged in decreasing order of magnitude, while group (B), similarly arranged, refers to interrupted loadings where the minimum load times and rest times were in all cases greater than or equal to 20 sec. The phenomena represented by these two groups of data are obviously indistinguishable in terms of the delay time observations. This result appears to be general for the nylon film used, and may therefore be taken to illustrate that the sequence of events which occurs after the first 20 sec. of loading is not seriously altered by load interruptions. Further experiments were performed where the minimum time interval under load was 10 and 15 sec.

The total times specimens were under load prior to shock formation in these two cases are listed in Table II. From Table II it is evident that the events which occur within the early portions of the loading epoch are essentially different from those which follow. The second entry suggests

and Dr. C. F. Tipper, Cambridge University. We are particularly indebted to the latter for a brief description of certain related unpublished studies by Mr. J. Gibson, Cambridge, England.

TABLE II
Time Under Load Prior to Shock Formation
 Stress: 4830 lb./in.²

Load time interval sec.	Minimum rest interval sec.	Time for form plastic shocks sec.
15	60	734
10	60	>1000 No shock formed

the existence of a time interval during which loads may be applied and within which no significant plastic flowing (irreversible change) occurs, *provided* sufficient periods of time are allowed for specimen "rest." Clearly these data do not definitely establish the existence of such an interval or flow-marking time delay, but the demonstration of a delay time for formation of plastic shocks provides a stimulating experimental model for an effect of this type, and the data of Table II provide a rough estimate of the upper limit of such a delay time for nonrecoverable deformation in polyamide film. This would appear to be between 1/10 and 1/100 of the time for gross necking in nylon, for stresses near the yield point. If we can draw an analogy between delayed yielding in nylon and mild steel, we would expect that similar delay times for plastic flowing in mild steels be of the order of 10^{-4} – 10^{-3} sec. [Clark and Wood (13) find time delays of about 10^{-1} sec. for gross necking in mild steel for initial stresses near the static yield stress.] Assuming such an analogy, one would expect, then, that the effects of repeated shock loading for durations in the millisecond range would exhibit an additivity roughly analogous to that found for nylon and demonstrated in Table I⁸.

VII. ACKNOWLEDGMENTS

The authors wish to express their appreciation to Dr. G. R. Irwin, N.R.L., for his interest and encouragement throughout the course of this work, and to Dr. W. H. Sanders, N.R.L., for helpful suggestions in connection with the preparation of the manuscript.

VIII. CONCLUDING DISCUSSION

We have described delayed plastic shock formations in polyamide films subjected to dead weight loading. The principal visible events which transpire within this delay time involve the relatively slow propagation of flow figures across the specimen, their "reflection" and interaction. An initially quasi-stable form of flow figure is observed oriented at nearly 45° with respect to the applied tension. Propagating flow figures proceed along paths which are oriented at about 60° with respect to the tension

⁸ Dr. W. H. Sanders has pointed out that an even more novel consequence of the analogy assumed is the possibility of recovery of localizations in mild steel formed by dynamic loading in time intervals of the order 10^{-4} – 10^{-3} sec.

field. There are characteristic patterns which, when completely formed, collapse at the termination of the delay time in an equally characteristic manner into given plastic "shock" formations. Longer delay times can be observed in which more than one characteristic flow figure develops within the specimen. Phenomenologically the propagation of the plastic shock may be qualitatively described in terms of plastic waves in nonlinear media characterized by a partially concave upward stress-strain relation.

The stress required to form a shock after a given delay time is shown to be a function of environmental water concentration at room temperatures. The higher the water concentration the lower the stress to initiate the shock under given conditions. The presence of water molecules within the polyamide film appears to accelerate the propagation of the flow figures since the delay time for shock formation is greatly lowered.

Since the complex processes mentioned above are active during the delay time it is apparent that irreversible deformations arise within this period. An intermittent loading experiment has shown that periods of time exist, a minimum time for which the specimen may be loaded in repeated intervals and still exhibit a "delay time" for shock formation. This "delay time" is now defined as the total time under load before yielding. The accumulated time under load is indistinguishable from that measured under constant, uninterrupted load.

For loads high enough to cause delayed flowing under continuing load, it has been shown, if the loading is interrupted soon enough, that the effects of the high load may be removed by allowing sufficient rest periods with the load removed. Thus we seem to find a primary delay time for permanent deformation which is a small fraction of the over-all delay time for the gross deformation characteristic of the plastic shock wave. Any deformations which may occur during this primary delay time appear to recover rapidly and, if recovery is allowed, appear to exert no measurable effects on the subsequent behavior of the specimen. This result immediately suggests a general inference.

We appear to obtain the following: It appears necessary that the events which are responsible for plastic flowing operate over a certain time interval τ_0 . After the elapse of this time under sufficient load, the plastic flowing appears to be characterized by a certain small region of the solid having a dimension l_0 and orientation α_0 with respect to the applied stress field.

It is interesting to note the complementary nature of the delay time experiment to fatigue testing. Here a threshold value of time is necessary to produce yielding under repeated loading whereas a general result in fatigue testing is a threshold value of the stress necessary to produce failure on repeated loading cycles at a given frequency.

Two different suggestions have been advanced for the existence of a delay time. These arguments, while having some theoretical basis, at present only lend plausibility to the delay time and indicate possible future theoretical approaches. An approach which appears to the present authors most promising is to attempt to use the phenomenon of delay local plastic flowing as a kind of "bridge" with which to connect microscopic statistical arguments with macroscopic descriptions of dynamic plasticity—the theory of plastic waves.

REFERENCES

1. PIOBERT, MORIN, AND DIDION, *Memorial d'Artillerie* **5**, 505 (1842).
2. LÜDERS, W., *Dinglers Polytech. J.* **155**, 18 (1860).
3. HARTMANN, L., *Distribution des Deformations dans les Metaux soumis a des Efforts*, Berger-Levrault et Cie, Paris, 1896.
4. NADAI, A., *Plasticity*. McGraw-Hill, New York, 1931.
5. GULLIVER, G. H., *Proc. Inst. Mech. Engrs. (England)* Parts **1** and **2**, 141 (1905); *ibid.*, Parts **1** and **2**, 519 (1907).
6. ANDRADE, E. N. DA C., *Proc. Roy. Soc. (London)* **A84**, 1 (1911).
7. GOUGH, H. J., HANSON, D., AND WRIGHT, S. J., *Trans. Roy. Soc.* **A226**, 1 (1928).
8. JAFFÉ, A. F., *The Physics of Crystals*, p. 51. McGraw-Hill, New York, 1938.
9. CLASSEN-NEKLUDOWA, M., *Z. Physik* **55**, 555 (1929).
10. BECKER, R., AND OROWAN, E., *Z. Physik* **79**, 566 (1932).
11. BRIDGMAN, P. W., *J. Applied Phys.* **17**, 225 (1946).
12. McREYNOLDS, A. W., *J. Metals* **1**, 32 (1949).
13. CLARK, D. S., AND WOOD, D. S., *Am. Soc. Testing Materials Proc.* **49**, 717 (1949).
14. KAUFFMAN, J., AND GEORGE, W., *Phys. Rev.* **77**, 761(A) (1950).
15. MIKLOWITZ, J., *J. Colloid Sci.* **2**, 193 (1947); *ibid.* **2**, 217 (1947).
16. TURNBULL, D., TP2365, *Metals Technol.* (June, 1948).
17. LESCHEN, J. G., CARREKER, R. P., AND HOLLOMON, J. H., *Trans. Am. Inst. Mining Met. Engrs.* **180**, 131 (1949).
18. BECKER, R., AND DORING, W., *Ann. Physik* [5] **24**, 719 (1935); VOLMER, M., AND FLOOD, H., *Z. physikal. Chem.* **A170**, 273 (1934).
19. COURANT, R., AND FRIEDRICHS, K. O., *Supersonic Flow and Shock Waves*. Interscience, N. Y., 1948.
20. TAYLOR, G. I., *J. Inst. Civil Engrs. (London)* 486 (1946); KÁRMÁN, TH. V., *N.D.R.C. Report A-29* (OSRD No. 365) (Jan., 1942); WHITE, M. P., AND GRIFFITHS, L., *J. Applied Mechanics* **14**, A-337 (1947); RAKHMATULIN, KH. A., *Prikl. Mat. i Mekh.* **9**, 1 (1945).

THE APPLICATION OF PRECIPITATION-TURBIDITY ANALYSIS TO POLYVINYL ACETATES¹

D. R. Morey, E. W. Taylor, and G. P. Waugh

Eastman Kodak Company, Research Laboratories, Rochester 4, New York

Received September 13, 1951

INTRODUCTION

It has long been a somewhat open question as to how much polyvinyl acetates made in different ways differ in their molecular-weight distribution. Since precipitation and turbidity studies provide a means of analyzing the molecular-weight distribution, this work was undertaken. When certain necessary conditions are fulfilled, the turbidity curve of a continuously precipitating polymer solution can be interpreted in terms of the molecular-weight distribution of the polymer (1, 2). A careful experimental technique is required, and the course of the precipitation should be followed by automatic recording of the transmitted light.

The use of the direct transmitted beam, and calculation of optical densities therefrom, have been found to give better correlations with distributions than measurements based on transverse scatter. However, the latter method is better suited for precise determination of the initial precipitation point, owing to the high sensitivity which can be attained.

EXPERIMENTAL TECHNIQUE

The apparatus consisted essentially of a thermostatted square glass cell in a water bath, fitted with a stirrer and an inlet beneath the surface, through which water was pumped into the polymer solution at a steady rate from a slow motor-driven piston. A beam of light passed through the cell, and a photocell was used to measure the intensity of either the direct beam of light or the light scattered at 90 degrees. An automatic recorder was used which recorded on a chart the intensity of the light as a function of time, and, therefore, of the amount of water added.

The concentration of polymer in solution must be kept low, so that even at the maximum turbidity, there is linearity between the amount of material precipitated and the optical measure. Figure 1 illustrates, on polyvinyl acetate precipitated from acetone by water, typical turbidity behavior consisting of a linear region followed by increasing deviations.

¹ Communication No. 1434 from the Kodak Research Laboratories.

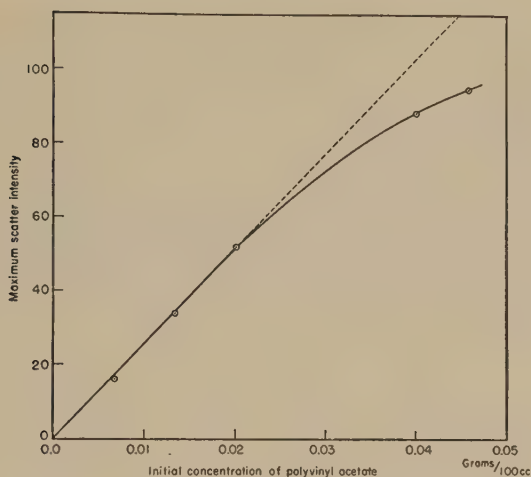


FIG. 1. Relation between maximum light scatter and initial concentration of polyvinyl acetate.

The actual value of the linear concentration range will depend on the polymer and the solvent-precipitant system, and should be found for each case.

Another necessary condition is that the solvent and precipitant chosen must be able to cause differential precipitation on a molecular-weight basis. It is known that not all combinations of solvent and precipitant are equally effective in molecular-weight separation, and indeed in some rare cases, no separation is achieved (3).

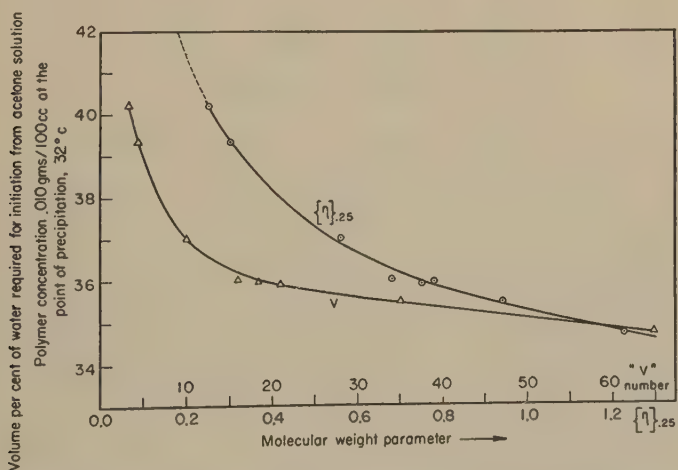


FIG. 2. P_T values of polyvinyl acetates polymerized in methyl alcohol with acetyl peroxide catalyst.

Figure 2 shows a test of acetone and water on polyvinyl acetates of different viscosities. The chain lengths of Fig. 2 are characterized by the natural log of the relative viscosity taken at 0.25 g./100 cc. of acetone solution at 25°C. The V number is the viscosity in centipoises of a benzene solution of 8.6 g./100 cc. at 25°C.

The analytical procedure which is applied to the data requires that the precipitation curve be continued to completion, so that at the end no polymer is left in solution. This is signified by the optical density, after correction for dilution, coming to a constant value as further precipitant is added. We have found polyvinyl acetate to be rather difficult to

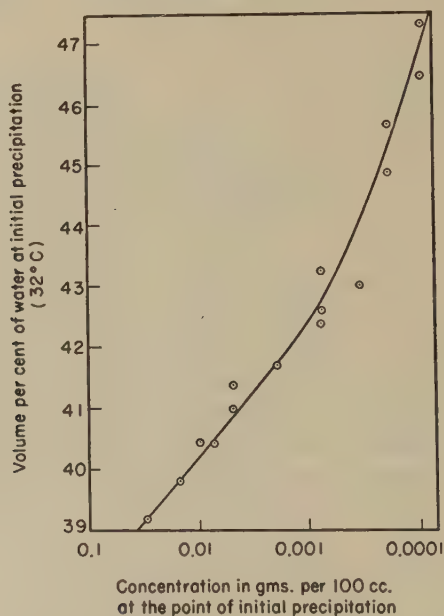


FIG. 3. Polyvinyl acetate in acetone-water V-3, 96.8% polyvinyl acetate.

precipitate completely from acetone. The water must be increased to about 98% to achieve the desired result. (It is to be recalled that these are very dilute solutions, and the gross precipitation in a commercial preparation operation is another matter.) This phenomenon is related to the upward curvatures of the graphs of water content at precipitation (P_r) vs. log critical concentration (C_r), shown in Figs. 3 and 4. In general, such types of plots in the past have been found to be linear, as was first pointed out by Schulz (4), and theoretical studies of the precipitation process also predict a linear relationship (3, 4). In Figs. 3 and 4, this is seen to be the case at the more usual concentrations. However, extending the measurements to the extreme dilution of 1 p.p.m. has resulted in a distinct upward curvature and a greater solubility than was expected.

DISTRIBUTION CURVES

It is possible, by plotting the relative amount of precipitate formed as water is added, to get a comparative idea of molecular-weight distribution. (To calibrate the water percentage in terms of molecular weights requires precipitation data on known fractions.) Proper techniques of water addition and stirring are necessary, along with good transmission measurements. In these experiments, a Leeds and Northrup Speedomax recorder was used. From these charts of transmission, the optical densities, $\log I_0/I$, are computed for intervals of water content.

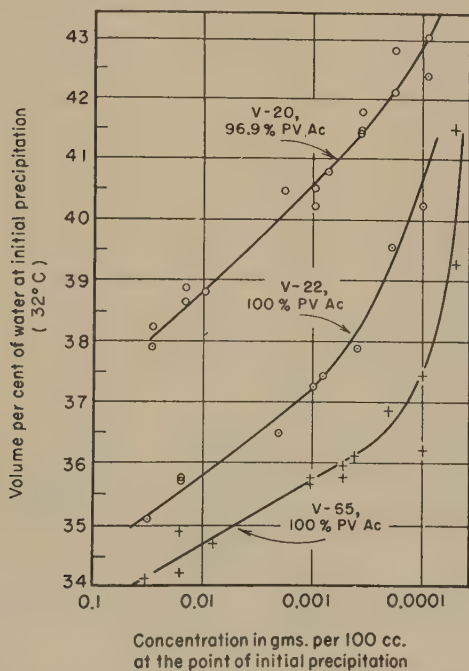


FIG. 4. Polyvinyl acetates in acetone-water.

Since the solution is being continuously diluted by the addition of water, the densities are multiplied by the ratio of the actual to the original volume to obtain a density proportional to the mass precipitated. This corrected density is then plotted against the percentage of water, to form a cumulative curve. If the concentrations have been kept in the linearity range (Fig. 1) and if the proper solvent-precipitant combination is chosen, this cumulative curve will level off to a constant value before reaching the limit in measurement or in dilution. The slope of this cumulative curve is next plotted against the percentage of precipitant, as in Fig. 5, to give a comparative, but not absolute, distribution curve. In

order to attain any sort of accuracy in the end result, it is necessary to have precise plotting of the cumulative curve and to measure its slope at many points with a tangent meter.

Figure 5 shows the comparative distribution curves for two unfractionated polyvinyl acetates, and for a fraction obtained by the usual precipitation method employing acetone and water. The fraction shows a sharp peak, as would be expected, but the wide extent of lower-molecular-weight components is surprising. The extended distributions shown in Fig. 5 are characteristic of the polyvinyl acetates studied here. A curve measured on a commercial cellulose acetate (38.5% acetyl) is included for comparison.

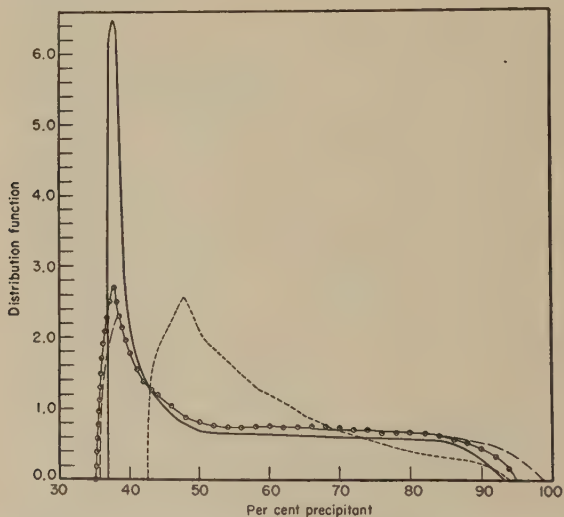


FIG. 5. Polyvinyl acetate distributions: ———, fraction from a V-22; — — —, unfractionated V-22; —○—○—, unfractionated V-35; — — — —, commercial cellulose acetate.

No significant change in shape was found between polyvinyl acetates made by dope or by bead polymerization.

It has been stated that concentrations must be kept below a limit of linear turbidities, for proper interpretations. This limit is about 0.02 g./100 cc. for polyvinyl acetates of higher molecular weights, but a lower concentration is necessary for low polyvinyl acetates. Figure 6 shows the comparative distribution curves for a V-65 material, at 0.02 and 0.01 g./100 cc. The agreement is satisfactory enough to allow the assumption that nonlinear effects are unimportant. On the other hand, Fig. 7, of a V-3 material, shows that at 0.02 g./100 cc. a stable shape of distribution curve has not been reached. The curves corresponding to measurements at 0.0133 and 0.0100 g./100 cc. do agree, however, indicating operation

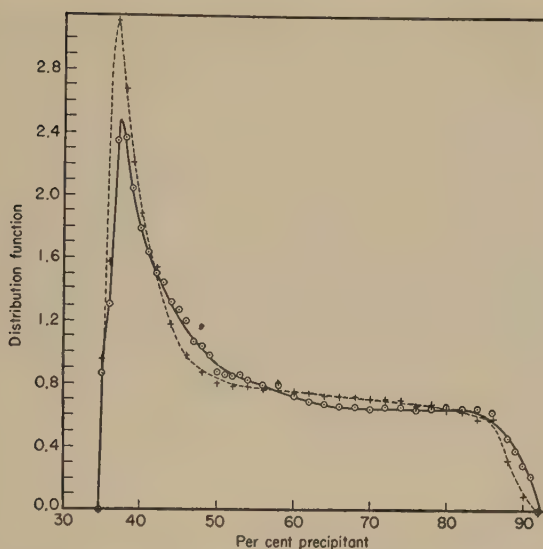


FIG. 6. V-65 polyvinyl acetate: +, precipitated from acetone solution, 0.02 g./100 cc.; O, precipitated from acetone solution, 0.01 g./100 cc.

in the linear turbidity region. The curve run at 0.04 g./100 cc. is completely spurious, and the pronounced double peak has been observed on all samples run at excessive concentrations.

On the supposition that the various molecular-weight species behave relatively independently in precipitation, it should be possible to predict, by simple addition, the result of mixing two components. Figure 8 shows

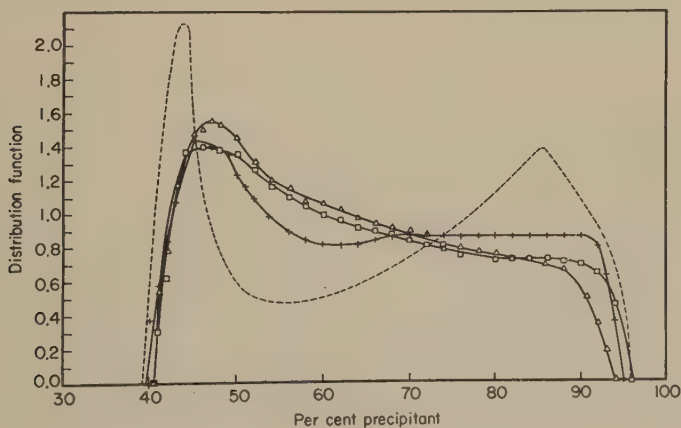


FIG. 7. V-3 polyvinyl acetate: ---, precipitated from acetone solution, 0.04 g./100 cc.; +, precipitated from acetone solution, 0.02 g./100 cc.; Δ, precipitated from acetone solution, 0.0133 g./100 cc.; □, precipitated from acetone solution, 0.010 g./100 cc.

the curve obtained on an equal-weight mixture of the materials of Figs. 6 and 7, V-65 and V-3 polyvinyl acetates. The mixture was run at a concentration of 0.02 g./100 cc. Figure 8 also shows a synthetic curve constructed by adding the ordinates of the V-65 and the V-3 curves, also at 0.02 g./100 cc. Since the V-3 precipitate was observed to have a greater scattering power than the V-65 precipitate, in the ratio 455 to 386, its apparent effect in a mixture would also be increased. Hence, rather than taking half of the V-3 and V-65 ordinates and adding, fractions of 0.54 and 0.46 were added to duplicate the curve arising from optical data. The agreement is good enough to show that chain lengths with these differences do not interact unduly under the given precipitating conditions.

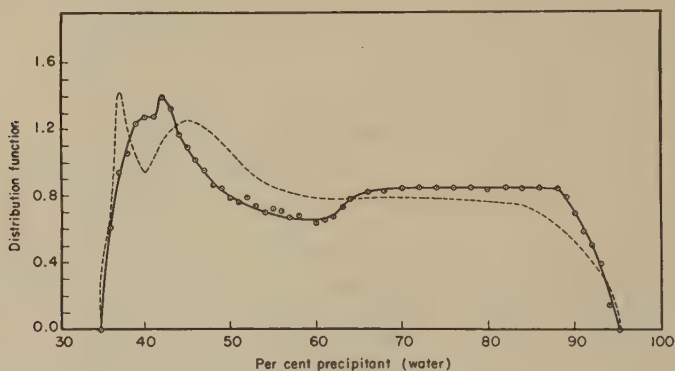


FIG. 8. $\bigcirc-\bigcirc$: Experimental curve for an equal-weight mixture of V-65 and V-3 polyvinyl acetates in acetone, 0.02 g./100 cc. ----, theoretical curve based on simple addition of V-65 and V-3 curves.

DEGREE OF HYDROLYSIS

The study has thus far considered the influence of molecular weights upon the precipitation point, and it has been tacitly assumed that the acetyl value was constant for various samples. Figure 9 shows a curve of a V-9 polyvinyl acetate prepared with potassium persulfate catalyst in the presence of water. These conditions lead to some hydrolysis. The curve of Fig. 9 has much the same shape as others, but is markedly displaced toward higher water percentages. In fact, the influence of a little free hydroxyl is much more pronounced on the value of P_γ than that of chain length. Figure 4 also shows the pronounced effect of hydroxyl, compared to molecular weight, wherein it is seen that a 3% drop in acetyl (calculated as polyvinyl acetate) has displaced the entire curve to higher values of P_γ . Increasing the chain length from a V-22 to a V-65 has only half the effect of this change of composition. The sharp increase in the

slopes of the curves of Fig. 2 at the left, representing more water needed to begin precipitation in the low-molecular-weight range, is partly due also to this effect, as the lowest members of this series (V-3 and V-4), although made by the same general method as the higher members, showed apparent hydrolysis. This lower acetyl content might possibly be due to the relatively larger proportion of inert end groups in these low polymers.

Table I shows further data on the effect of hydrolysis during preparation with the values of P_γ determined on solutions of initial concentration of 0.04 g./100 cc. Some of the materials shown in the table were made by re-acetylating the slightly hydrolyzed material with acetic anhydride in pyridine (5), precipitating, washing, and drying the polyvinyl acetate. It will be noted that after such re-acetylation the material shows the

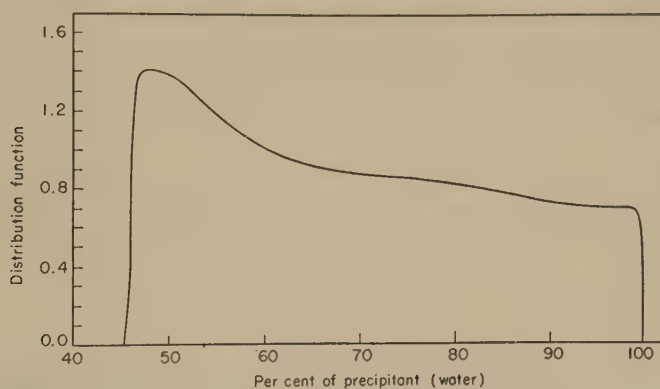


FIG. 9. Polyvinyl acetate: V-9, 91.5% polyvinyl acetate precipitated from acetone solution, 0.02 g./100 cc.

same P_γ as materials of the same viscosity made by anhydrous polymerization or bead polymerization, which suggests that there is no real difference in structure among polyvinyl acetates made by these various methods.

TABLE I

Effect of Hydrolysis on the Precipitation of Polyvinyl Acetate

Sample	Method of preparation	V number	$[\eta]$ 0.25 acetone at 25°C.	Polyvinyl acetate, %	P_γ
I	Potassium persulfate catalyst	23.5	0.72	97.4	40.6
II	I above re-acetylated with acetic anhydride	23.2	0.75	99.3	35.1
III	Potassium persulfate catalyst	9.4	0.49	91.5	44.4
IV	III above re-acetylated with acetic anhydride	9.5	0.52	98.8	36.1
V	Potassium persulfate catalyst	20	0.76	96.9	38.2
VI	Acetyl peroxide in ethyl acetate as catalyst	22	0.75	100	35.1
VII	Bead polymerization; benzoyl peroxide as catalyst	9	0.49	99.9	36.8

PREPARATION OF POLYVINYL ACETATES

Anhydrous Dope Polymerization; Acetyl Peroxide Catalyst

The polyvinyl acetates shown in Fig. 2 comprise a series made by polymerizing vinyl acetate in 0.11 to 2.0 parts of methanol, using as catalyst 0.1–0.4 wt.-% acetyl peroxide (based on the vinyl acetate) as a solution in ethyl acetate at from 4.5 to 8% concentration. Polymerization time was 1 day, at temperatures of 60, 65, or 70°C. The polyvinyl acetate was isolated and washed by kneading in warm water, and was dried at 60°C.

The viscosity was controlled principally by the amount of methanol used, more methanol giving a lower viscosity. In addition, the larger amounts of catalyst and higher temperatures were used in making the low-viscosity materials.

The acetyl peroxide was made by the reaction of equimolecular proportions of acetic anhydride and sodium perborate in several volumes of ethyl acetate (6), at room temperature, by stirring overnight. The liquid was then decanted and its peroxide content determined by titration (7).

The V-3 of Figs. 3, 7, and 8, the V-65 of Figs. 4, 6, and 8, the V-35 of Fig. 5, and the V-22 of Figs. 4 and 5 and Table I were members of this series.

The characteristics of these polyvinyl acetates are shown in Table II.

TABLE II

Properties of Polyvinyl Acetates Made Using Acetyl Peroxide as Catalyst

V	$[\eta]$	Polyvinyl acetate, %
3.3	0.25	96.8
4.3	0.30	97.4
10	0.56	100.2
16	0.68	100.0
18	0.78	99.9
22	0.75	100.1
35	0.94	100.0
65	1.23	99.6

Aqueous Dope Polymerization; Potassium Persulfate Catalyst

Samples I, III, and V of Table I were made by dissolving vinyl acetate in methanol, adding an aqueous solution of potassium persulfate, and polymerizing by heating under a reflux condenser in a bath of 60°C. Slow stirring was maintained during the first 8 hr. or so of the reaction, until the mass became very viscous. Heating was continued for a total of about 24 hr., then the mass was doped in methanol and the product was isolated in warm water, washed, and dried, as above.

For V-22, methanol, water, and potassium persulfate were used in amounts corresponding to 33.3, 15.1, and 0.3%, respectively, by weight, based on the vinyl acetate.

For V-9, the amounts used were 76.3, 20, and 0.45%, respectively.

As noted, such dopes hydrolyze a few per cent during making, presumably because of sulfuric acid formed by decomposition of the catalyst. On standing at room temperature, the hydrolysis continues, but at a much slower rate, and as a result dopes so made spontaneously gel in a period of several months.

Sample III of Table I appears in Fig. 9, and sample V appears in Fig. 4.

Bead Polymerization; Benzoyl Peroxide Catalyst

Sample VI of Table I was made by tumbling vinyl acetate containing 1.85% benzoyl peroxide with 1.3 times its weight of water containing 0.6% starch and 0.02% sodium acetate, at 50°C., for 22 hr. The polyvinyl acetate beads were washed in running water and dried at room temperature.

A similar procedure but using 1.0% benzoyl peroxide gives V-22.

The fraction from a V-22 of Fig. 5 was from such a bead polymerization, fractionated from acetone solution by precipitation with water.

SUMMARY

The continuous precipitation method of analyzing molecular-weight distribution has been applied to polyvinyl acetate, using acetone as solvent and water as precipitant. Quite low values of concentration are found necessary to achieve reliable results. All materials studied were found to have a wide range of chain lengths extending to quite small ones, difficult to precipitate from dilute solution. This difficulty of precipitation is related to deviations from the linear P_γ vs. $\log C_\gamma$ law at low values of concentration. The effect of a small amount of hydrolysis on the precipitation point, P_γ , is found to be considerable, and the degree of hydrolysis must be held closely constant in order to associate P_γ values with chain length. Widely different chain lengths behave independently in their precipitation behavior.

The percentage of water required to precipitate, from an acetone solution, polyvinyl acetate made using potassium persulfate in the presence of water has been shown to be greater than the percentage required for the precipitation of bead material or material made by anhydrous dope polymerization. This is due to the slight hydrolysis which occurs in the preparation of the former.

REFERENCES

1. OTH, A., *Bull. soc. chim. des belges* **58**, 285 (1949).
2. MOREY, D. R., AND TAMBLYN, J. W., *J. Applied Phys.* **16**, 419 (1945).
3. MOREY, D. R., AND TAMBLYN, J. W., *J. Phys. & Colloid Chem.* **51**, 721 (1947).
4. SCHULZ, G. V., *Z. physik. Chem.* **A179**, 321 (1937).
5. McDOWELL, W. H., AND KENYON, W. O., *J. Am. Chem. Soc.* **62**, 415 (1940).
6. BLAICKIE, K. G., AND BROZIER, R. N., *Ind. Eng. Chem.* **28**, 1155 (1936).
7. KOKATNUR, V. R., AND JELLING, M., *J. Am. Chem. Soc.* **63**, 1432 (1941).

A VIBRATING-PLATE VISCOMETER

J. G. Woodward

*Radio Corporation of America
RCA Laboratories Division, Princeton, New Jersey*

Received September 14, 1951

INTRODUCTION

The growing importance of viscosity measurements in research and industry through the years is well known to readers of this journal. The desire for highly precise results in some cases, and for rapid and convenient indications of viscosity in other cases has brought into existence a wide variety of techniques and instruments for the measurement of the coefficient of viscosity or of properties closely related to it. The instruments commonly used for viscosity measurement fall into three classes, namely, the rotational types, the efflux types, and the falling-sphere types. Each type has advantages and drawbacks which make it best suited for certain applications. The vibrating-plate viscometer, which is the subject of this article, depends for its operation on a principle different from those of the more common viscometers. This fact, coupled with practical considerations, gives the vibrating-plate viscometer a distinctive set of characteristics which may be listed as follows:

(a) Significant measurements in the viscosity range of 0.1 centipoise (cp.) to 100,000 cp. are possible with a single instrument.

(b) Meter indications may be given directly in terms of $\eta\rho$, η being the coefficient of viscosity and ρ the density of the liquid.

(c) Practically instantaneous indications are given.

(d) Continuous readings of $\eta\rho$ may be made or automatically recorded as the viscosity of a liquid sample changes with time.

(e) Measurements can be made in the temperature range from 100°C. to indefinitely low temperatures.

(f) The volume of liquid sample which may be used ranges from a minimum of about 0.5 ml. to indefinitely large volumes.

(g) The instrument can be quickly and easily cleaned following or preceding a test.

(h) Measurements of $\eta\rho$ accurate within $\pm 5\%$ can be made for a single liquid. Higher precision is possible when only comparisons between similar liquids are desired.

CONSTRUCTION AND OPERATION

It has long been known that a flat plate immersed in a liquid and vibrating in its own plane sets up shear waves in the liquid, and that the liquid exerts a retarding force on the motion of the plate. The magnitude of the retarding force is dependent on the value of $\eta\rho$ of the liquid. The vibrating-plate viscometer makes use of this principle by measuring the effect of the retarding force on a thin, circular plate which oscillates in its own plane in a liquid sample at a rate of approximately 800 cycles/sec. The plate, which we shall call the blade, has a thickness of 0.010 in. and a diameter of 0.200 in. It is made of silver-plated beryllium copper although many other materials would be equally suitable. The blade is mounted on the free end of a steel reed 0.010 in. thick, 0.200 in. wide and 0.875 in. long. The opposite end of the reed is firmly clamped, and the reed is set into vibration at its mechanical resonance by an electromagnetic driving system. The vibration of the reed results in the desired oscillatory motion of the blade.

With reed and blade vibrating at resonance in air, the amplitude of motion is restricted only by the internal mechanical resistance of the vibrating system and by the rather negligible damping of the surrounding air. With the blade immersed in a liquid, the amplitude of motion is further restricted by the viscous damping of the liquid in contact with the blade. Piezoelectric barium titanate blocks mounted on opposite faces of the reed generate a voltage proportional to the amplitude of motion of the reed. This readily measurable alternating voltage can be used to give a meter indication of the reed amplitude and, therefore, of the viscosity of the liquid in which the blade is immersed.

Several electrical accessories are necessary for the operation of the vibrating-plate viscometer. These include a source of direct current for magnetic polarization; a source of alternating current, variable in frequency in the neighborhood of 800 cycles/sec.; and a vacuum-tube voltmeter for measuring the voltage generated by the barium titanate blocks. The alternating current must be variable in frequency because the frequency of resonance is somewhat different for liquids of different viscosities and densities. The driving frequency must always coincide with the resonant frequency of the reed-blade-liquid system. Since a manual adjustment of the frequency for each measurement of viscosity would be time-consuming and inconvenient, the electromechanical vibrating system has been incorporated in a self-oscillating circuit which automatically drives the system at its resonance regardless of the frequency required. In addition, the driving current is automatically maintained at a constant magnitude regardless of the amplitude of motion of the reed. The circuit also provides the polarizing current and includes the vacuum-tube voltmeter.

With the exception of the vibrating system and a one-tube preamplifier, all of the circuit components and controls are housed in a cabinet 14 in. wide, 8 in. deep and $8\frac{1}{4}$ in. high. The 4-in. indicating meter is located on the sloping-front panel. The vibrating system and preamplifier are contained in a separate, cylindrical case, $1\frac{1}{2}$ in. in diameter and 6 in. long, which forms a probe unit. In use, this probe may be either held in the hand or mounted on a stand. The probe is connected to the main



FIG. 1. The vibrating-plate viscometer.



FIG. 2. The vibrating-plate viscometer probe unit with outer case removed.

cabinet by a 6-ft. flexible cable. A photograph of the complete system is shown in Fig. 1. The probe unit with its case removed is shown in Fig. 2.

In using the vibrating-plate viscometer to measure the viscosity of a liquid sample, the gain control of the vacuum-tube voltmeter circuit is adjusted to give a full-scale deflection of the meter when the reed and blade are vibrating in air. Then the blade is immersed in the liquid, and the meter reading, E_x , on the linear scale is observed. This reading can be converted into the value of $\eta\rho$ for the sample once a calibration curve has been made by using various liquids of known viscosities and densities.

This calibration can also be used to construct a meter scale giving direct indications in terms of $\eta\rho$. Such a scale is shown in Fig. 3. The scale pictured permits readings from $\eta\rho = 0.1$ to $\eta\rho = 10^5$ in three ranges corresponding to three values of meter sensitivity. The ranges are selected by a three-position switch on the meter panel. The viscosity, η , is in centipoises and the density, ρ , is in g./cc. The entire process of making the full-scale adjustment, immersing the blade, reading the meter, and raising, cleaning, and drying the blade can be completed in a matter of seconds. Liquid samples as small as 0.5 ml. are sufficient provided they are held in containers which will receive the blade with ample clearance. Obviously, the viscometer may be used with indefinitely large samples as long as they present a free surface into which the blade can be immersed.



Fig. 3. The meter scale of the vibrating-plate viscometer. Linear scale at top. Scales A, B, and C give $\eta\rho$ directly with η in centipoises and ρ in g./cc.

The fact that the meter reading, E_x , on a linear scale is a simple function of $\eta\rho$ is demonstrated by the experimental curve shown in Fig. 4. Here $\frac{1}{E_x} - 1$ as measured for a number of liquids is plotted as a function of $\eta\rho$ on a log-log chart. The dashed line has a slope of $\frac{1}{2}$ and represents an approximate theoretical equation which will be derived in the *Appendix*. All of the experimental points were obtained for glycerin-water solutions of various concentrations except the two lowest points, for which acetone and methyl alcohol were used. A number of other common liquids of known viscosity and density, including mercury, were measured and their points were found to fall properly on the calibration curve. No standard liquids were readily available to extend the calibration beyond $\eta\rho = 1200$.

When the blade is immersed in liquids of viscosity greater than about 2000 cp. the damping is too great to allow operation of the self-oscillating circuit. Consequently, for measurements of highly viscous liquids an auxiliary oscillator must be used to drive the vibrating system at the frequency of resonance. The auxiliary oscillator can be placed in the circuit simply by connecting it to two terminals provided at the rear of the cabinet.

The meter of the vibrating-plate viscometer can be read to one-fourth of the smallest division of the linear scale. This corresponds to an error of about $\pm 5\%$ in the value of $\eta\rho$ over most of the range. The probable error for a single measurement is closer to $\pm 10\%$ of the value of $\eta\rho$

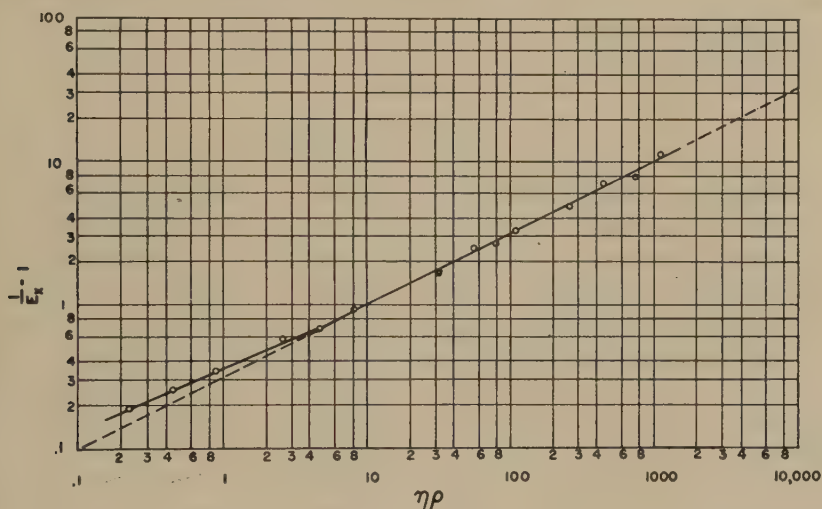


Fig. 4. Experimental values of $\frac{1}{E_x} - 1$ as a function of $\eta\rho$ for various liquids. Experimental points are for glycerin-water solutions except for the two lowest points, which are for acetone and methyl alcohol. The broken line represents an approximate theoretical relation.

because of normal variations in making the full-scale adjustment and in adjusting the depth of immersion of the blade. To counteract the errors due to these last-mentioned variations, several independent measurements should be made and the results averaged.

Higher precision is possible when only comparative measurements of similar liquids are desired. To take advantage of this possibility, the full-scale adjustment is made with the blade immersed in the liquid having the smallest value of $\eta\rho$ in the group under test. Then deflections less than full scale will be observed for the other liquids. A calibration curve can be made for the range under study if desired.

An upper limit in the range of temperatures within which the vibrating-plate viscometer may be used is set by the barium titanate. The electrical and physical properties of polycrystalline barium titanate have been discussed in detail elsewhere (1). It is sufficient for present purposes to say that the piezoelectric activity falls off rapidly above 100°C. and is lost completely at 120°C. where the crystal structure of the material undergoes an abrupt change. Consequently the upper limit of usefulness of the viscometer is about 100°C. The barium titanate blocks retain their activity to indefinitely low temperatures and constitute no serious hindrance to low-temperature measurements of viscosity. The activity of barium titanate does vary somewhat with temperature, however, so that the full-scale adjustment must be made with the vibrating system at the same temperature it will have when the blade is immersed for a viscosity measurement.

APPLICATIONS AND RESULTS

The results of three experiments will be described to illustrate some of the types of measurement possible with the vibrating-plate viscometer.

The first experiment involves Newtonian liquids and is the simple one of measuring $\eta\rho$ for several mixtures of turpentine and linseed oil having concentrations ranging from 100% by volume of turpentine to 100% by volume of linseed oil. The results are given in Fig. 5. The value of $\eta\rho$ as a function of per cent turpentine is plotted in the lower graph. In the upper graph the values of E_z , as read on the linear scale of the meter, are plotted as a function of per cent turpentine. For curve *A* the full-scale adjustment was made with the blade in air. For curve *B* the full-scale adjustment was made with the blade in turpentine. The greater slope of curve *B* as compared with curve *A* reflects an increased precision for the former.

Viscosity measurements of non-Newtonian liquids are difficult to analyze irrespective of the type of instrument used in making the measurements, and the vibrating-plate viscometer is no exception in this regard. The effective shearing force and rate of shear fall off rapidly from relatively high values in the liquid layer immediately adjacent to the blade to negligibly low values at a short distance from the blade. Moreover, the shearing force varies with time, passing from zero to a maximum and back to zero twice during each cycle of vibration of the blade. At best, only an effective or root-mean-square (r.m.s.) value of the shearing force at the surface of the blade can be specified. Notwithstanding these complexities, interesting and useful results of an empirical nature have been obtained for non-Newtonian liquids.

Tests were performed on thixotropic ferrite suspensions such as are used in the slip casting of "powdered iron," radio-frequency transformer

cores. The slips were allowed to stand at room temperature until the thixotropic setting was complete. Then the viscometer blade was immersed in the slip. The viscosity of the slip adjacent to the blade decreased as a result of the stirring action of the blade, falling rapidly at first and then more slowly, and eventually reaching an equilibrium value dependent on the amplitude of vibration of the blade. The value of η as a function of the time following immersion of the blade is plotted in Fig. 6 for two slips differing only in pH.

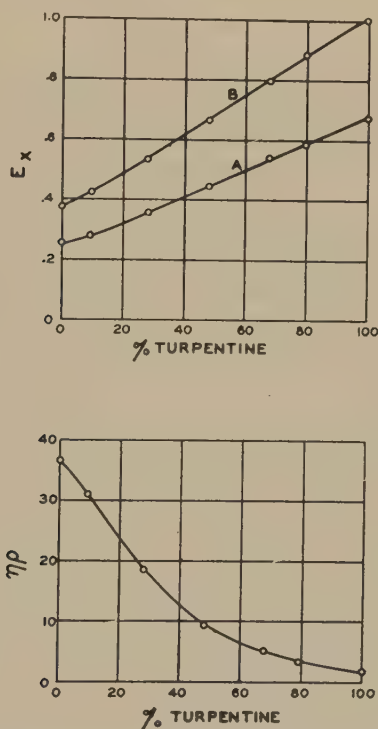


FIG. 5. Lower: Measured values of η/p for turpentine-linseed oil mixtures as a function of per cent by volume of turpentine. Upper: E_x as read on linear scale as a function of per cent by volume of turpentine. Full-scale adjustment made with blade in air and in turpentine for curves A and B, respectively.

Tests of the type just described were unsuccessful with thixotropic clay suspensions of the type used in the manufacture of china and sanitary ware because of the high yield value of the clay slips. An alternative experiment was attempted in which the viscometer blade was immersed in a freshly stirred slip and the change in viscosity was noted as the thixotropic setting proceeded. This process usually required a length of time inconveniently long, and the reproducibility in duplicate

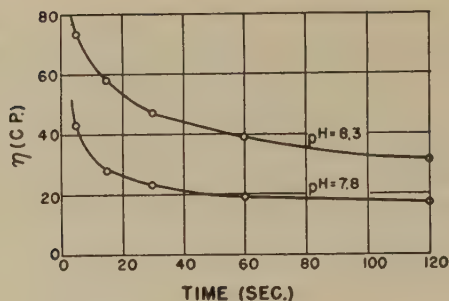


FIG. 6. Viscosity as a function of time following immersion of blade in thixotropic ferrite suspensions.

tests was poor. A more useful technique was developed in which the change in viscosity of a slip was noted as it was cast in a mold. For this purpose a number of identical, small, rectangular plaster of Paris molds were prepared. The viscometer blade was set in a mold at a predetermined distance from the mold wall. The freshly stirred slip was then poured into the mold, and the change in the viscometer meter indication was observed as the slip changed from a fluid to a semisolid state with the passage of liquid from the slip into the plaster of Paris. Typical curves obtained in this way are shown in Fig. 7. The curves shown are copied from originals which were drawn by automatic curve-tracing equipment used in conjunction with the vibrating-plate viscometer. The scale at the left is in arbitrary units corresponding to the recorder indication. The right-hand scale permits one to judge the order of magnitude of $\eta\rho$, η being in centipoises and ρ in g./cc.

The three curves shown in Fig. 7 illustrate the effect of the addition

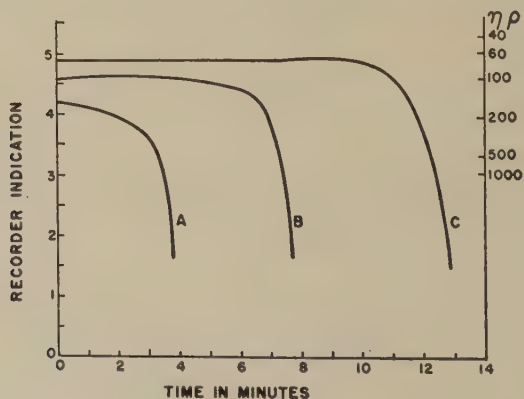


FIG. 7. Viscosity of clay slips as a function of time in mold. Arbitrary scale at left. Order of magnitude of $\eta\rho$ indicated by right-hand scale with η in centipoises and ρ in g./cc.

to the slip of small amounts of deflocculant, in this case a sodium silicate solution. All three curves represent an under-deflocculated condition, with C having the greatest and A the least amount of electrolyte addition.

The casting time of dilatant as well as thixotropic slips can be measured by this method. Duplicate tests are reproducible within $\pm 10\%$. Empirical though they may be, results obtained by means of this technique have already yielded fundamental knowledge of the slip-casting process. Further elaboration lies beyond the scope of this presentation.

CONCLUSIONS

The features which characterize the operation of the vibrating-plate viscometer were listed in the *Introduction* and need not be repeated here. Where high temperatures, the presence of highly corrosive liquids, or requirements of extremely high precision do not preclude its use, the vibrating-plate viscometer can give indications of viscosity quickly, conveniently, and over a wide range. For Newtonian liquids the measurement is a straightforward matter. For non-Newtonian materials special techniques will usually be required. Those techniques outlined above have proved useful but the possibilities are far from being exhausted. It is expected that other special procedures will be developed for dealing with various types of non-Newtonian materials in various situations, and that the vibrating-plate viscometer used in these ways will furnish information not readily obtainable with other types of instrumentation.

APPENDIX

A complete theoretical knowledge of the operation of the vibrating-plate viscometer is not necessary for an understanding of the basic principles involved. However, for the benefit of those whose interests and technical requirements make a theoretical discussion desirable, the mathematical analysis of the vibrating system will be outlined here. A completely rigorous analysis is neither practical nor profitable, and the derivation to be presented is only approximate. The various necessary assumptions will be mentioned as the derivation proceeds.

Consider a flat plate of infinite extent immersed in a viscous liquid. Let the plate be the $y - z$ plane and let it execute sinusoidal vibrations in the y direction, given by $V = V_0 \cos \omega t$, where V is the instantaneous velocity and V_0 is the peak velocity of vibration. Then the velocity of transverse motion in the liquid at a distance x from the plate is

$$v = V_0 \cos \left(\omega t - \sqrt{\frac{\omega \rho}{2\eta}} x \right) \exp \left[- \sqrt{\frac{\omega \rho}{2\eta}} x \right], \quad [1]$$

where $\omega = 2\pi f$, f being the frequency of vibration, and η is the coefficient of viscosity and ρ is the density of the liquid. Equation [1] is derived in various treatises on hydrodynamics (2). The coefficient of viscosity is defined by

$$F_\eta = - \eta \left(\frac{\partial v}{\partial x} \right)_{x=0}, \quad [2]$$

where F_η is the tangential force per unit area acting on one side of the vibrating plate. Taking the derivative of [1] and substituting in [2] gives

$$F_\eta = \sqrt{\frac{1}{2}\omega\eta\rho} \left(V - \frac{1}{\omega} \frac{dV}{dt} \right) \quad [3]$$

or, since for sinusoidal vibrations $\frac{dV}{dt} = -i\omega V$, where $i = \sqrt{-1}$,

$$F_\eta = V\sqrt{\frac{1}{2}\omega\eta\rho} (1 + i). \quad [4]$$

The retarding force, F_η , is seen to comprise two equal parts of magnitude $V\sqrt{\frac{1}{2}\omega\eta\rho}$, one real, the other imaginary, and both dependent on the frequency. The real part is a dissipative force corresponding to a mechanical resistance. The imaginary part is an equivalent addition to the mass per unit area of the plate.

Equation [1], and hence [4] also, was based on the following assumptions: (a) A constant value of η , i.e., a Newtonian liquid; (b) a sufficiently small amplitude of motion to avoid turbulence in the liquid; (c) an infinite plate in an infinite liquid. Condition (a) requires no comment. Condition (b) appears to have been met in the case of the viscometer since no evidences of turbulence appear for the greatest amplitudes of which the device is capable. Condition (c) obviously cannot be completely fulfilled. It may be fulfilled approximately over a wide range, however, since the wavelength of the transverse vibrations in ordinary liquids is short, and the amplitude of vibration drops off very rapidly with distance from the blade. Keeping this possible limitation in mind we proceed to see how the approximate force given by [4] affects the motion of the vibrating system.

The oscillatory motion of the viscometer blade for a driving force, F_x , varying sinusoidally with time is described by

$$F_x = AF_\eta + Z_0V_x, \quad [5]$$

where A is the effective area of the blade, Z_0 is the mechanical impedance of the vibrating system referred to the blade, and V_x is the velocity of vibration of the blade. The mechanical impedance is, in general, made up of a real and an imaginary component.

$$Z_0 = R_0 + jX_0. \quad [6]$$

Substituting [4] and [6] in [5] and specifying that the system shall always be operated at resonance, which means that the imaginary part of the equation is zero, we get

$$F_x = V_x A \sqrt{\frac{\omega\eta\rho}{2}} + V_x R_0. \quad [7]$$

When the reed and blade vibrate freely in air the first term on the right is zero and we have

$$F_0 = V_0 R_0. \quad [8]$$

The ratio of [7] to [8] gives

$$\frac{F_x}{F_0} = \frac{V_x}{V_0} \left(\frac{A \sqrt{\frac{\omega_x\eta\rho}{2}} + R_0}{R_0} \right).$$

If the amplitudes of blade vibration in liquid and in air are u_x and u_0 , respectively,

$$V_x = -i\omega_x u_x, \quad V_0 = -i\omega_0 u_0$$

and

$$\frac{F_x}{F_0} = \frac{\omega_x u_x}{\omega_0 u_0} \left(\frac{A \sqrt{\frac{\omega_x\eta\rho}{2}} + R_0}{R_0} \right). \quad [9]$$

We next specify that the driving force shall remain constant regardless of the load on the blade, i.e., $F_x = F_0$, a condition met in practice by maintaining a constant driving current in the coil. Now [9] can be reduced to

$$\eta\rho = K \frac{f_0}{f_x} \left(\frac{f_0 u_0}{f_x u_x} - 1 \right)^2, \quad [10]$$

where $K = \frac{2R_0^2}{A^2\omega_0}$ is an instrumental constant, $f_0 = \frac{\omega_0}{2\pi}$ and $f_x = \frac{\omega_x}{2\pi}$.

The voltage developed by the barium titanate blocks is proportional to the amplitude of motion, u , of the blade. This voltage is indicated by a reading, E , on the linear scale of the meter. Equation [10] may be rewritten in terms of the meter reading as

$$\eta\rho = K \frac{f_0}{f_x} \left(\frac{f_0 E_0}{f_x E_x} - 1 \right)^2. \quad [11]$$

Except for liquids having very high values of $\eta\rho$, the resonant frequency, f_x , for the blade in the liquid is not more than 1 or 2% different from f_0 , the resonant frequency for the blade in air. Only a small error results from assuming $f_0 = f_x$, which simplifies [11] to

$$\eta\rho = K \left(\frac{1}{E_x} - 1 \right)^2 \quad [12]$$

after setting $E_0 = 1$ for full-scale deflection. According to Eq. [12], a log-log plot of $\frac{1}{E_x} - 1$ vs. $\eta\rho$ should give a straight line of slope = $\frac{1}{2}$. This prediction is put to the test in Fig. 4 where the dashed line corresponds to the relationship given by [12]. The agreement between experiment and the theory is satisfactory in view of the approximate nature of the theory. The lack of an adequate exact theory and the unavailability of suitable standard liquids of high viscosity make it impossible to estimate with complete certainty the applicability of [12] for values of $\eta\rho$ much greater than 1000.

REFERENCES

1. Cf. VON HIPPEL, A., *Revs. Modern Phys.* **22**, 221-37 (1950).
2. Cf. RAYLEIGH, J. W. S., *Theory of Sound*, Vol. II. p. 317. Macmillan and Co., London, 1929.

A THEORETICAL APPROACH OF THE COLLOID-CHEMICAL STABILITY OF DISPERSIONS IN HYDROCARBONS

The stability of hydrophobic colloids is now satisfactorily accounted for by the double-layer theory (1) and the long-range attractive forces of the Van der Waals-London type (2).

No satisfactory quantitative explanation, however, has yet been given of the stability of colloidal dispersions in hydrocarbons. Experimental evidence collected by Van der Waarden (3) shows that aromatic molecules substituted with long aliphatic chains which are adsorbed on the surface of carbon black particles dispersed in medicinal oil have a profound stabilizing effect, which is increased by increasing the chain length.

It has been assumed (3) that the aliphatic chains fixed to the surface by the aromatic nucleus, but otherwise free, exert a repulsive force when two particles approach each other and thereby prevent agglomeration. Elaborating this assumption we will show that the repulsion is due to the decrease of the number of possible configurations of the adsorbed hydrocarbon chains when two particles approach one another. The following discussion is based on a model consisting of two interacting parallel plates of surface area ω a distance d apart, on which the substituted aromatic nuclei are adsorbed.

Although in general the possibility of the occurrence of an electrical double layer in hydrocarbon media cannot be ruled out, electrical repulsion is assumed to be unimportant in these experiments.

The free enthalpy¹ of the repulsion ΔG_R per unit area of one plate (due to the carbon chains) is given by:

$$\Delta G_R = G_s^d - G_s^\infty. \quad [1]$$

G_s^d and G_s^∞ are the free enthalpies of the surface per unit area of one plate (G_s is numerically equal to the surface tension) when the plates are at a distance d , and d equals infinity.

G_s is derived from the integrated form of Gibbs's adsorption formula in which G_s is related to the surface excess Γ and the change in the thermodynamic potential μ of the aromatic molecules as

$$G_s = - \int_{-\infty}^{\mu} \Gamma d\mu + G_s^{(0)}. \quad [2]$$

¹ The Gibbs function.

$G_s^{(0)}$, the free enthalpy of the surface in the pure solvent, can be omitted in the following equations, as only changes in G_s are important.

In order to solve Eq. [2], which is the key to the whole problem, a model has to be introduced from which the adsorption isotherm of the substituted aromatic molecule can be derived as a function of the plate distance d .

We have analyzed several models which are all based on the assumption that the aliphatic chain can be represented by a rod, either rigid or consisting of a number of segments, fixed at one end to the surface by the aromatic part of the molecule. One can introduce into these models either a lattice model of the liquid, as is usually done in the statistical thermodynamics of polymer molecules, or a homogeneous medium in which all directions of the rod with respect to the surface have equal probability.

The second model will be used here, as it leads to simple analytical expressions from which the consequences can be readily deduced. This model, however, is only amenable to small surface coverage Θ , sufficiently small to neglect the mutual interaction of the chains. The lattice model, although limited in other respects, can be used for the treatment of high values of Θ .

Assuming an ideal localized monolayer, the adsorption isotherm can be found for the adsorbed molecule where the aromatic part attaches the aliphatic chain to the surface, allowing it a number W of orientations with equal probability. Thus there are two contributions to the entropy of the adsorbed molecule; one term is given by the number of permutations of the molecules on the surface, and another term is given by the number of possible configurations W of the aliphatic chain, which is W_d and W_∞ for distances between the plates of d and ∞ , respectively.

Using this adsorption isotherm, Eq. [2] can be solved, and using [1] the following expression for ΔG_R is found:

$$\Delta G_R = N_s k T \Theta_\infty (W_\infty - W_d) / W_\infty, \quad [3]$$

Θ being the surface fraction of the plate covered when $d_\infty = \infty$. For the calculation of $(W_\infty - W_d) / W_\infty$ as a function of d , a simple model is

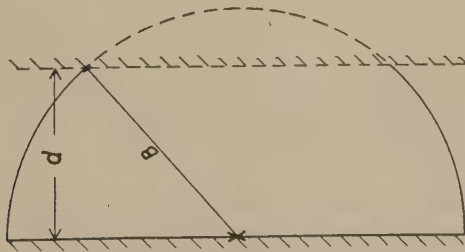


FIG. 1. Model used for calculations.

introduced, consisting of a rod of length B connected to the surface by a ball joint (Fig. 1). The number of configurations of the rod is proportional to the surface area of the hemisphere described by the rod, as given by $W_\infty \sim 2\pi B^2$, whereas if d is less than B a certain number of configurations are no longer available, which number is proportional to the area cut off by the second plate, being $2\pi B^2(1 - d/B)$ and so

$$(W_\infty - W_d)/W_\infty = 1 - d/B. \quad [4]$$

The free enthalpy of the repulsion ΔG_R which is therefore given by

$$\Delta G_R = N_s k T \Theta_\infty (1 - d/B) \quad [5]$$

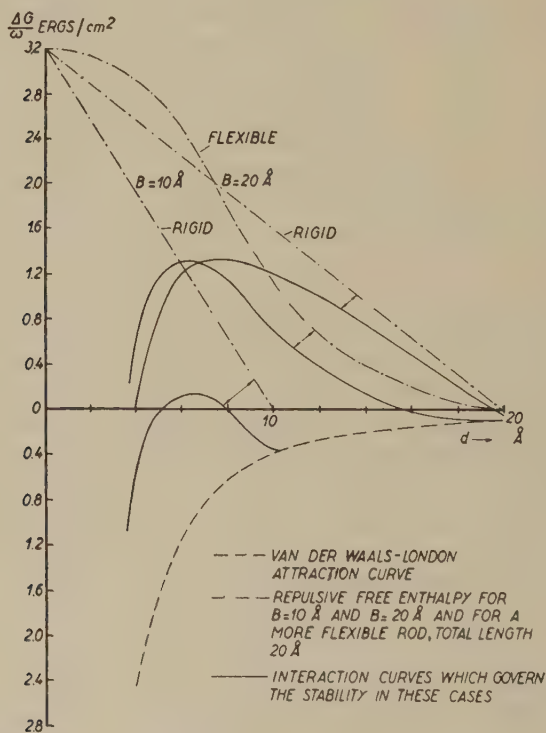


FIG. 2. The interaction curves for two parallel plates.

is a linear function of d in this model. The repulsion is of the right order of magnitude if one puts $N_s = 2 \times 10^{14} \text{ cm.}^{-2}$, $\Theta_\infty = 0.2$, and $kT = 4 \times 10^{-14} \text{ ergs}$, in order to explain the stabilization. Putting $d/B = \frac{1}{2}$, ΔG_R is about 1 erg/cm.^2 or $10^{-12} \text{ ergs per } 100 \text{ Å.}^2$. Thus for two interacting colloidal particles ΔG_R is several times kT .

ΔG_R is plotted in Fig. 2, putting B equal to 10 and 20 Å., respectively, together with the Van der Waals-London free enthalpy of attraction,

given by $\Delta G_A = - (A/24\pi)d^{-2}$, putting $A = 1.5 \times 10^{-13}$ ergs. So the change in the free enthalpy of the system per unit area $\Delta G/\omega$ can be found (4).

In this example a rod of 20 Å. stabilizes the colloid to a large extent, whereas with a rod of 10 Å. rapid flocculation will occur.

Figure 2 also shows the influence of greater flexibility of the rod. The alkyl chain is represented by two rigid rods of equal lengths connected by a ball joint. It will be seen that the free enthalpy of the repulsion in this case is an S-shaped function of d . The maximum value of $\Delta G/\omega$, which chiefly governs the stability, is equal in both models. The total length of the rod is 20 Å. in both cases.

Detailed theoretical studies of this model and also of the lattice type, model will be published shortly.

ACKNOWLEDGMENTS

The writer is indebted to the management of the Koninklijke/Shell-Laboratorium Amsterdam, for being given the opportunity to publish this letter and to Dr M. van der Waarden and Dr J. H. van der Waals for their suggestions.

REFERENCES

1. VERWEY, E. J. W., AND OVERBEEK, J. TH. G., *Theory of the Stability of Lyophobic Colloids*. Elsevier, Amsterdam, 1948.
2. DE BOER, J. H., *Trans. Faraday Soc.* **32**, 21 (1936); HAMAKER, H. C., *Physica* **4**, 1058 (1937).
3. VAN DER WAARDEN, M., *J. Colloid Sci.* **5**, 317 (1950); *ibid.* **6**, 443 (1951).
4. MACKOR, E. L., Thesis, Utrecht, 1951; to be published in *Rec. trav. chim.* **70**, (1951).

Koninklijke/Shell-Laboratorium,
Amsterdam, Holland

E. L. MACKOR

Received August 30, 1951

A NEW CONTINUOUSLY SENSITIVE DIFFUSION CLOUD CHAMBER *

Langsdorf (2) as well as Cowan (1), Needles and Nielson (3) have developed continuously sensitive cloud chambers which use alcohol and alcohol-water mixtures to indicate ion tracks. Recently, Schaeffer (4) has employed a similar apparatus using water vapor as the flux material, to study the number and properties of small particles in samples of air. By adding sublimation and freezing nuclei to the chamber, he has observed the condensation of water vapor on the particles, the temperature of solidification of the resulting droplets and their subsequent growth as ice crystals.

* The research reported in this paper has been sponsored by the Geophysics Research Division of the Air Force Cambridge Research Center under Contract AF19(122)380.

The continuous cloud chamber in operation in our laboratory also uses water vapor but has been modified to enable the classification of various nuclei according to the supersaturation that they will tolerate. As is usual, the air is saturated with water at a high temperature and, as it diffuses to an area at a lower temperature, it becomes supersaturated. However, in contrast to the other chambers, the temperature gradient along the walls of this chamber can be controlled. This is effected by winding a heating element around the outside and enclosing the chamber in a glass water jacket. Water, flowing at a constant rate over the wire, gradually heats the walls, preventing any condensation there. Therefore, the degree of supersaturation increases uniformly down the column until critical supersaturation is reached as shown by the appearance of a self-nucleated cloud. When a steady state is obtained in the chamber, air is present in all possible stages of supersaturation; the degree can be calculated from the temperatures at various heights. When nuclei are inserted at the top, and fall gradually, they form a cloud at a height, or supersaturation, characteristic for that substance.

So far several inorganic nuclei, including sodium, calcium and manganese chloride and calcium and copper sulfate, have been used and gave clouds at different distinct levels. It is expected that, after a more complete investigation, a correlation between the supersaturation tolerance of the nuclei and their physical properties will be established.

REFERENCES

1. COWAN, E. W., *Rev. Sci. Instruments* **21**, 991 (1950).
2. LANGSDORF, A., JR., *Rev. Sci. Instruments* **10**, 91 (1939).
3. NEEDLES, T. S., AND NIELSON, C. E., *Rev. Sci. Instruments* **21**, 976 (1950).
4. SCHAEFFER, V. J., Paper presented to the International Congress of Pure and Applied Chemistry, Sept. 11, 1951.

*Department of Chemistry,
University of Montreal,
Montreal, Canada*

Received October 3, 1951

DAPHNE SCHIFF
PIERRE R. GENDRON

SOLUBILIZATION OF DYES IN MINERAL OIL AND ITS APPLICATION TO A MODEL BIOLOGICAL CELL MEMBRANE

Sydney Ross

Department of Chemistry, Rensselaer Polytechnic Institute, Troy, New York

Received October 19, 1951

INTRODUCTION

Substances that are normally insoluble may be brought into solution in water in the presence of small concentrations of soaps or colloidal electrolytes. The same effect also takes place in nonaqueous solvents, where dilute solutions of oil-soluble surface-active agents can solubilize substances normally insoluble in oil. The term solubilization was introduced by McBain to distinguish this effect from the related but different processes of hydrotopy, formation of ordinary colloidal sols, colloidal suspension, emulsification, blending, and cosolvency. Solubilization depends on the spontaneous formation by association of a colloidal micelle in or upon which the molecules of the solubilized material are incorporated. Many studies have been made of solubilization, and a comprehensive review was published recently by Klevens (2), in which 258 separate references are cited. Of this work only a small fraction treats of solubilization in nonaqueous solvents. The topic has, however, an interesting application in biology that has not previously been realized, namely, in the permeability of cells.

The lipoid theory of cell permeability postulates an organic solvent whose dissolving power, compared to that of water, parallels the permeating power of the solute. No single, generally appropriate, pure solvent could be found, however, whose dissolving properties were such that for a large number of organic nonelectrolytes there would be a correspondence between their solubility in the solvent and their ability to permeate cell membranes. The best solution so far discovered comes from an exhaustive series of experiments done by Nirenstein (3), who correlated the vital staining of *Paramecium* by dyes with the solubility of the dyes in a mixture of olive oil, oleic acid, and diamylamine. This model cell solution simulates the cell membrane rather than the complete cell, and therefore only substances taken up by the model cell have a chance to go into the inner part of the real biological cell. Any such mixture, referred to as a "model biological cell," would have to meet the conditions that on extraction with aqueous dye solutions, the oil system would take up the same type and amount of dye as the living system would, and it would reject those dyes

that are rejected by the living system. Nirenstein's "model biological cell" consists of 18 parts olive oil, 6 parts oleic acid, and 1 part diamylamine. The dyes that are extracted from aqueous solutions by this oil mixture correspond remarkably to those that are able to stain *Paramecium*.

As well as going far toward elucidating the mechanism of cell permeability, Nirenstein's results provide the possibility of a system *in vitro* that would come close to duplicating some of the behavior of a living organism. It still suffers from the disadvantages of uncertain composition, as olive oil is by no means a standard material, and even oleic acid is difficult to obtain pure. It therefore seems important to set on foot experiments that might lead to the discovery of another model biological cell that would be free of these defects.

It is immediately apparent that oleic acid and diamylamine are able to combine, and that one of the constituents of Nirenstein's model cell is the amine salt of oleic acid. This substance belongs to the general class of surface-active agents, and the close relation of Nirenstein's results to the study of solubilization in oils becomes clear. This paper presents a series of qualitative and quantitative experiments that might be the basis for a desired continuation of Nirenstein's work.

EXPERIMENTAL

I

To eliminate the uncertainty of the composition of olive oil, these experiments have all been done on a highly refined white mineral oil, *Drakeol No. 10*, of the Pennsylvania Refining Co. The replacement of the olive oil denies us the presence of other substances, present in the oil, that are also effective solubilizing agents. It was found immediately that olive oil by itself was already a better solubilizing solvent than white mineral oil. A series of experiments were done with 35 different dyes, taken from Nirenstein's list, which were examined both for solubility in mineral oil alone and in mineral oil containing 1% di-*n*-butylamine oleate. Sixteen dyes were found to be solubilized by the addition of the amine oleate. A second series of tests was made using Nirenstein's technique, namely, dissolving the dye in water and then extracting it with a 1% solution of the amine oleate in mineral oil. The results did not correspond exactly with those of the previous test: a smaller number showing signs of solubilization. The presence of water, of course, complicates the system, as water may itself be solubilized in the oil, as well as the dye. These experiments showed, however, that the presence of even a small quantity of an amine oleate is enough to cause solubilization of many dyes, normally insoluble in oil, and that therefore the results obtained by Nirenstein can be grouped as examples of the phenomenon that is described by the title of this paper.

II

McBain, Merrill, and Vinograd (5) have reported over 200 qualitative observations on the solubilization of dyes in nonaqueous solvents. Only a few of these were made with mineral oil as the solvent, and accordingly several similar experiments were made, using mineral oil, to find systems that would be suitable for further study. As a result of this search eight commercial surface-active agents were selected (Table I), for comparison

TABLE I
List of Agents used for Dye Solubilization in Oil

No.	Trade name	Major chemical constituent
1	Span 20	Sorbitan monolaurate
2	Span 85	Sorbitan trioleate
3	Glyceryl oleate	
4	G-954	Mannitan monooleate
5	G-2000	Mannitan monopalmitate
6	Tween 81	Polyoxyethylene sorbitan monooleate
7	Arlacel B	Mannitan monooleate
8	Amine soap	Di- <i>n</i> -butylamine oleate

of their action on a series of water-soluble dyes. The dyes chosen are those federally certified for use in foods, drugs, and cosmetics, manufactured by the National Aniline Co. and supplied through its generosity. These dyes are described in the Merck Index, 5th edition, p. 593 (1940). As solubilizing agents, the chemicals found to have the best effect are those generally used as oil-soluble emulsifying agents, more particularly the nonionic substances, as exemplified by the fatty esters of the sugar alcohols. Materials of this sort are made and sold under the trade names *Span* and *Arlacel* by Atlas Powder Co., and are essentially partial esters of the common fatty acids (lauric, palmitic, stearic, and oleic) and hexitol anhydrides (hexitans and hexides), derived from sorbitol and mannitol. The agents known by the trade name *Tween* are derived from the sorbitan esters by adding polyoxyethylene chains to the non-esterified hydroxyls, thus changing the hydrophile-lipophile balance toward a more water-soluble product. The hydrophilic character of these surface-active agents is supplied by free hydroxyl and oxyethylene groups, and the lipophilic portion comes from the hydrocarbon chain of the fatty acid used. All of them are actually complex mixtures of several compounds. Neither these materials nor the dyes were purified beyond the stage supplied by the manufacturer, as the present problem is more concerned with the existence and relative magnitude of the effect, than with an investigation of the effect of variations in the molecular structure of the agent. Nevertheless, because of the variation in hydrophile-lipophile balance in these materials, some information on this point was obtained.

The amine soap was made by adding exactly equivalent amounts of

di-*n*-butylamine (Eastman Organic Chemicals, P1260) to oleic acid, whose equivalent weight had been obtained by titration.

Each of these agents is soluble in mineral oil at room temperature. Solutions of each, 1.00% by weight, were made in white mineral oil that had been dried by the addition of metallic sodium. To small portions of each of these solutions a pinch of each solid crystalline dye was added, and the mixture was stored in a constant temperature cabinet at 25°C. for 2 months, with occasional shaking during the first week or two. At the end of 2 months a deep color was present in each sample and the excess solid dye had settled to the bottom of the tube.

TABLE II

Solubilization F. D. and C. Dyes by 1% Solutions of Various Agents in Refined Mineral Oil
Values are in micromoles of dye/liter of solution

F. D. and C. Dye	Solubilizing agents of Table I								
	λ^a	1	2	3	4	5	6	7	8
Blue No. 1	640	21.3	1.3	118	35.8	0.9	0.3	9.7	3.2
Blue No. 2	610	13.3	3.2	2.6	8.4	0	0.4	0.4	1.1
Green No. 1	620	23.8	3.5	53.4	277	2.0	0.1	143	2.9
Green No. 2	630	94.5	0	274	234	0.9	0.5	60.1	1.5
Green No. 3	625	223	0.7	3.3	128	2.2	0.2	0.2	3.0
Orange No. 1	475	135	1.1	11.9	160	2.3	0	17.5	0
Red No. 1	500	24.5	3.5	0	24.5	2.4	1.6	3.5	7.1
Red No. 2	515	60.9	1.5	2.5	55.5	0	0	0	0
Red No. 3	525	57.8	10.6	0.4	304	0.3	0.1	0	0
Red No. 4	505	44.8	6.3	7.7	61.5	7.1	1.6	2.1	20.8
Yellow No. 1	430	56.7	2.7	4.2	57.0	0.8	1.7	0.3	0
Yellow No. 5	425	131	0	5.5	78.8	2.9	1.0	0	0
Yellow No. 6	480	33.5	0.4	0.1	19.7	0	0.6	0	0

^a Lambda (λ) = wavelength in millimicrons of minimum transmission.

The frequencies of minimum transmission were determined by measuring, with a Beckman model B spectrophotometer, the transmission of an aqueous solution containing about 10^{-4} mole/l. of each dye to be tested. These wavelengths are reported in col. 2, Table II; they were later used in the standardization and analysis of each dye. Many dyes are known to have a "spectral shift," i.e. a change in the wavelength of minimum transmission, with changes of concentration or on solubilization with certain agents. In none of these solubilized dye systems, however, does a spectral shift occur.

The standardization curve for each dye was obtained from measurements of a series of aqueous solutions of known concentration. The use of aqueous solutions gets around practical difficulties that might have

occurred had solubilized dye-in-oil solutions been used, but invites the serious criticism that the transmission of a solubilized system may not correspond to that of an equal concentration of dye in water, even after a correction is made for the difference in the transmission of the solvents. The complete (visible range) transmission spectrum for F. D. and C. Blue No 1 dissolved in water was measured and compared to that of the same dye solubilized in oil with Span 20 and again with G954. No difference could be observed. For the other dyes the absence of any spectral shift, either in aqueous solution or in the solubilized system, was taken as an indication of the same congruity, and the congruity itself interpreted as a justification for the use of aqueous standards for the analysis of solubilized dyes in oils.

In Table II are reported the final results, corrected where necessary for the slight solubility of the dye in oil when no agent is present, so as to give solely the solubilizing effect of the added agent.

Some interesting conclusions can be drawn from these results. The dyes have, between themselves, greater variance in molecular structure than have the first seven of the eight solubilizing agents between themselves. Nevertheless, greater differences are to be observed by reading the columns of Table II horizontally than by reading vertically; the agents are less selective in their behavior than are the dyes; speaking generally and loosely, a good agent will solubilize each and every dye, disregarding (within rather wide limits) the details of its molecular structure; but change the structure of the agent (within rather narrow limits) and its solubilizing ability is greatly lessened, again for all dyes. Whatever may be its cause, this effect is encouraging in the search for a model biological cell, where a single solution must be capable of solubilizing many different compounds. There is a parallel between this behavior and the behavior of biological systems.

Although the data are not sufficiently extensive to give more than an indication, the hydrophile-lipophile balance of the agents appears to be important. The more hydrophilic Tween 81 (agent 6) and the amine soap (agent 8) are notably less effective solubilizers. At the other extreme the lipophilic Span 85 (agent 2) is also less effective.¹ The importance of this balance is no more than has been found to be generally true in most applications of surface-active agents, and it is a useful guide in selecting the suitable agent for a given application. A numerical index of the hydrophile-lipophile balance has been proposed in the publications of the Atlas Powder Company (1), but the method by which it is determined has not been published.

Another well-known characteristic of surface-active agents is indicated

¹ Span 85 is believed to be more lipophilic than the other agents on the authority of the manufacturer (1).

in these results, and by a comparison of the effect of the amine soap with the mixture composed by Nirenstein, namely, the synergetic effect: the enhancement of an effect, beyond the ability of any single component, when a mixture is used. All the agents used here, with the exception of the amine soap, are mixtures; agents 4 and 7 are mixtures with the same principal constituent, yet differing in their effects. This too must be taken into account in devising any other model biological cell.

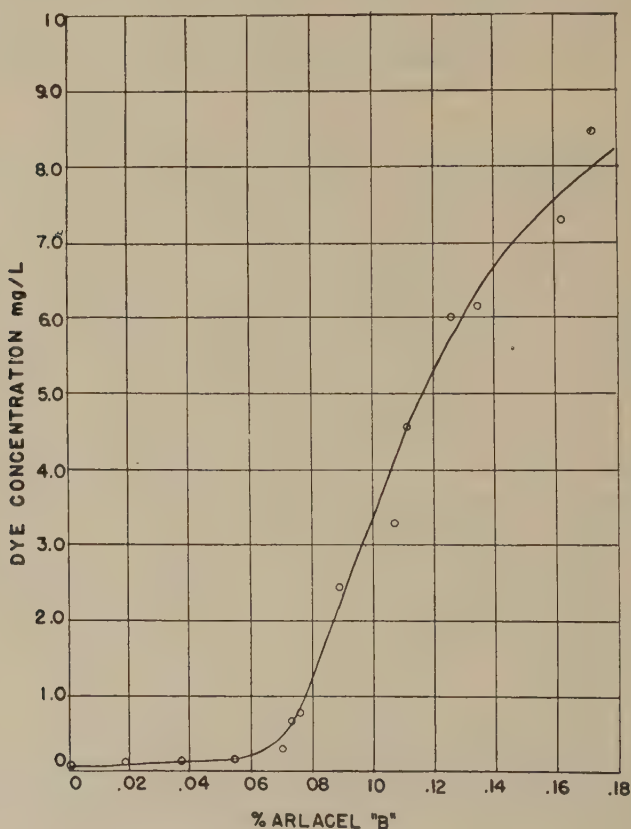


Fig. 1. Solubilization of methylene blue in mineral oil by Arlcel B. Equilibrium concentration of dye solubilized in mg./l. vs. concentration of Arlcel B in solution.

III

It now seemed of interest to select one of the agents and study the effect of varying its concentration. Agent No. 7 (Arlcel B) was selected, and its effect on three dyes, methylene blue (Merck Co. product, recrystallized from absolute alcohol), F. D. and C. Green No. 1 (Guinea Green), and F. D. and C. Orange No 1, was evaluated.

It was found that reproducible results could not be obtained unless care was taken to remove moisture from the system. Each solution of the agent in oil was treated with Drierite (CaSO_4) for 24 hr. in a rotating sample holder at 30°C . The Drierite was removed by centrifugation and a portion of the oil solution was retained as a blank for comparison with the solubilized dye system.

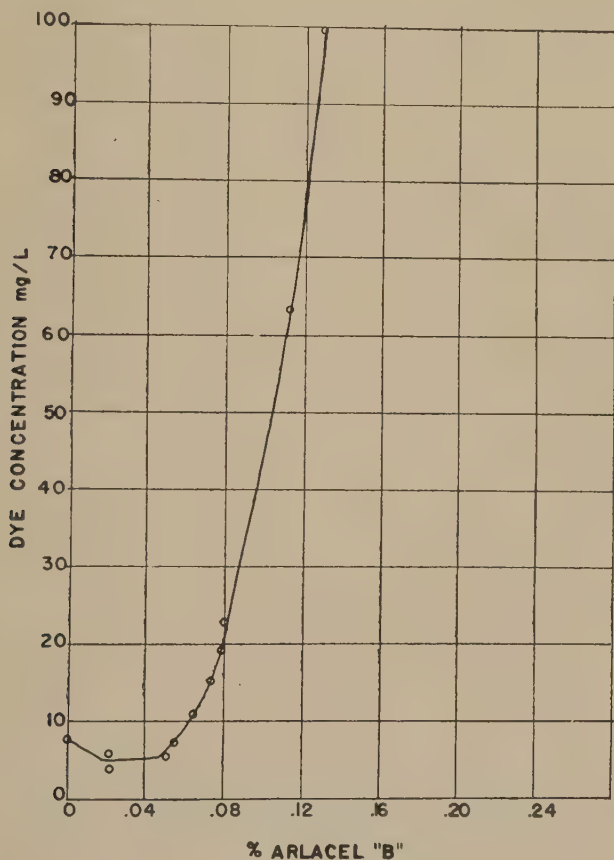


FIG. 2. Solubilization of Guinea Green (F. D. and C. Green No. 1 Dye) in mineral oil by Arlachel B. Equilibrium concentration of dye solubilized in mg./l. vs. concentration of Arlachel B in solution.

The dyes were solubilized in screw-cap test-tubes by adding excess solid dye to the dried oil solution of the agent, and placing the tubes in a rotating sample holder inside an air bath at 30°C . for a week. Excess solid was removed by centrifugation, and the color intensity of the system was measured with a Lumetron colorimeter, equipped with appropriate filters and a line-voltage stabilizer. The standardization curve was ob-

tained from aqueous solutions, as before. Methylene blue is known to have a spectral shift as the concentration is increased (7), but it does not become significant even for the most concentrated of the solutions measured in this work (3×10^{-5} mole/l). The transmission for the visible range of the spectrum is the same for the dye dissolved in water as it is for the solubilized dye; this holds for the three dyes.

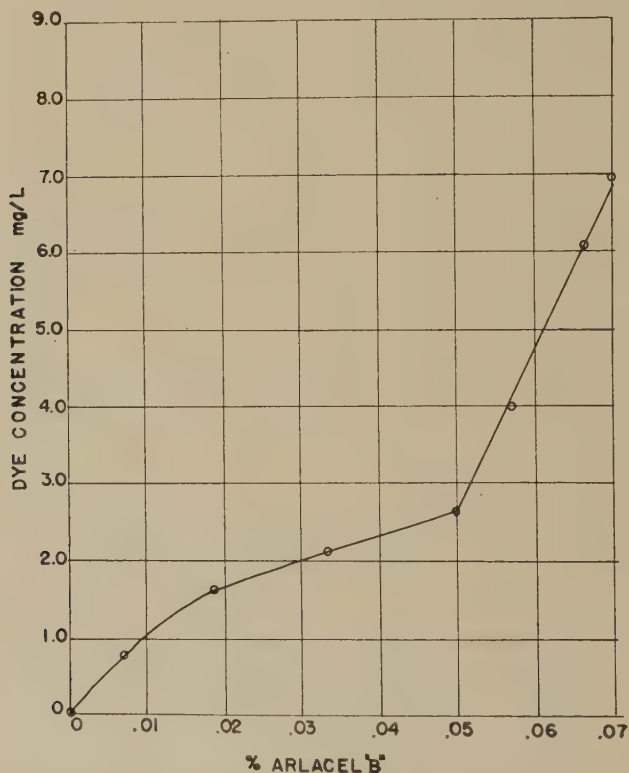


FIG. 3. Solubilization of F. D. and C. Orange No. 1 Dye in mineral oil by Arlacel B. Equilibrium concentration of dye solubilized in mg./l. vs. concentration of Arlacel B. in solution.

The results of this portion of the work are reported in Figs. 1, 2, and 3 showing the amount of dye put into solution in a liter of oil at different concentrations of agent. Each figure shows the same general pattern: slight solubilization at low concentrations and then at a critical concentration the beginning of a rapid rise in the amount of dye solubilized. For aqueous solutions of surface-active agents, the critical concentration at which solubilization begins to increase is interpreted as the stage at which significant amounts of the solute are spontaneously associating to form

large aggregates or colloidal micelles. The existence of a so clearly defined, or critical, concentration for micelle formation (sometimes referred to as CMC—critical micelle concentration) is demonstrated in aqueous solutions of dodecyl sulfonic acid by the change of other physicochemical properties with concentration: such properties as equivalent conductivity

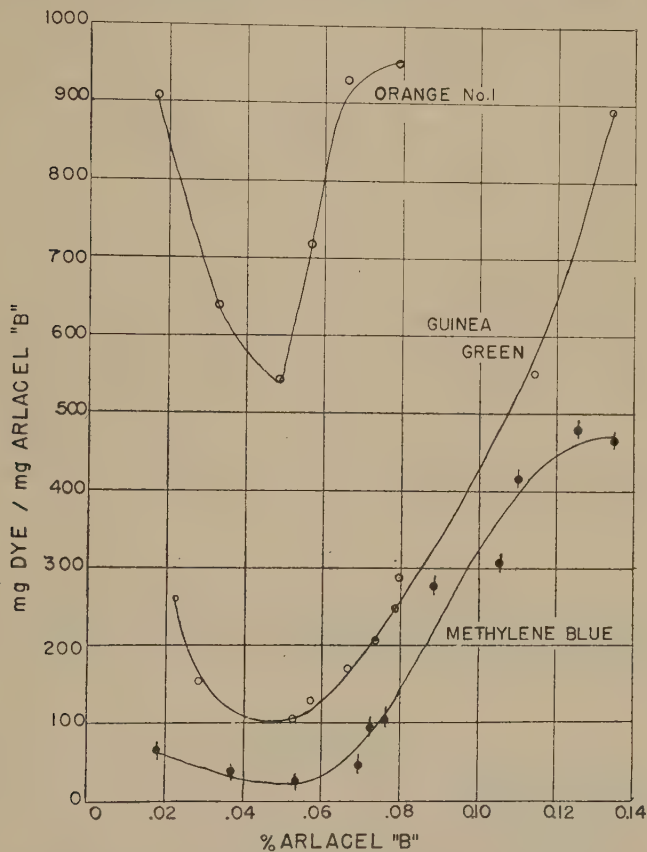


FIG. 4. An alternative method of plotting the solubilization data of the previous figures, to show the similarity of the effect of the solubilizing agent on each dye. The equilibrium amount of dye solubilized per mg. of agent *vs.* concentration of the agent in solution.

ties, transport numbers, and diffusion coefficients (6). Association colloids occur in nonaqueous media almost as much as in water, and it is therefore not surprising to find a critical micelle concentration in these oil solutions, just as in aqueous solutions of soaps and other association colloids. That the critical micelle concentration is a function of the agent and is independent of the dye being solubilized is demonstrated in Fig. 4, where the data

are plotted in the form mg. dye/mg. Arlacel B *vs.* per cent Arlacel B. The curves for the three different dyes have the same form, and all have a minimum at the same concentration of agent (about 0.05% by weight), which may be taken as the CMC of Arlacel B in mineral oil.

By an application of the mass law to the equilibrium $nA \rightleftharpoons A_n$, where A represents the formula of the solubilizing agent, and by assuming that the concentration of solubilized dye is a direct measure of the concentration of the micelle, A_n , it can be shown that the function illustrated by Fig. 4 cannot have either maxima or minima. Only if two or more micelles are simultaneously present can minima and maxima appear in this function. In the equilibrium $nA \rightleftharpoons A_n$ there must therefore be at least two different values of n present. The energy differences between different micellar forms is so small that it is probable that a series of micellar sizes exists. It is certainly correct to conclude that, in coincidence with the findings of McBain and Huff (4) for aqueous solutions of some colloidal electrolytes, it may also be said of these oil solutions that no one formulation of a micelle is valid over the whole range of concentration. Vold (8) has recently demonstrated the possibility of there being a distribution of micellar sizes in aqueous solutions of all colloidal electrolytes, even for those where the data have previously been sufficiently described by a monodisperse micellar system. The present results would encourage a similar interpretation for nonaqueous solutions of association colloids.

ACKNOWLEDGMENTS

The author acknowledges the students who have helped with the experimental portions of this work: with Part I, R. Minnich and G. Forbes; with Part II, D. S. Beard, T. Donnelly, and R. Lacoste; with Part III, B. A. Becker, F. A. Phillips, Jr., and R. L. Zimmerman.

SUMMARY

1. The model biological cell of Nirenstein is shown to operate by solubilization of dyes in oil.
2. The solubilization in oil of the oil-insoluble F. D. and C. dyes is measured for different solubilizing agents at 1% concentration.
3. The solubilizing ability of each agent depends on its physicochemical behavior in solution and, within wide limits, does not depend on the structure of the dye.
4. The effect was observed of a single agent, at different concentrations, on the solubilization of three different dyes.
5. The change of solubilizing power with change in concentration is of the same general form for one agent with different dyes.
6. In these oil solutions of association colloids, there is an equilibrium between different kinds of micelles present in the same solution, changing with concentration and other factors.

REFERENCES

1. INDUSTRIAL CHEMICALS DEPARTMENT, ATLAS POWDER Co., Atlas Surface Active Agents. Wilmington, Del., 1948.
2. KLEVENS, H. B., *Chem. Revs.* **47**, 1-74 (1950).
3. NIRENSTEIN, E., *Arch. ges. Physiol. (Pflügers)* **179**, 233 (1920).
4. MCBAIN, J. W., AND HUFF, H. M., *J. Colloid Sci.* **4**, 383 (1949).
5. MCBAIN, J. W., MERRILL, R. C., JR., AND VINOGRAD, J. R., *J. Am. Chem. Soc.* **62**, 2880 (1940).
6. MCBAIN, M. E. L., *J. Phys. Chem.* **47**, 196 (1943).
7. MICHAELIS, L., AND GRANICK, S., *J. Am. Chem. Soc.* **67**, 1212 (1945); VICKERSTAFF, T., AND LEMIN, D. R., *Nature* **157**, 373 (1946).
8. VOLD, M. J., *J. Colloid Sci.* **5**, 506 (1950).

DYNAMO-OPTICAL PROPERTIES OF DETERGENT MICELLES ¹

John K. Backus and Harold A. Scheraga

Department of Chemistry, Cornell University, Ithaca, New York

Received October 23, 1951

INTRODUCTION

It has been shown that aqueous salt solutions of *n*-hexadecyltrimethylammonium bromide exhibit streaming birefringence (1). Extinction angle measurements support the conclusion of Debye and Anacker (2), based on light-scattering and viscosity data, that the micelles formed from this detergent are elongated, rodlike structures whose length increases with salt concentration. It has been postulated (2) that the hydrocarbon tails project radially from the axis of the cylindrical micelle ending in the polar heads which make up the surface of the particle. The present report gives further streaming birefringence results for the effect of hydrocarbon chain length and solvent composition on the size and optical properties of the micelle.

EXPERIMENTAL

The preparation of the *n*-alkyltrimethylammonium bromides and the apparatus used for the flow birefringence measurements have already been described (1). A differential refractometer was used for refractive increment measurements. For experiments carried out in aqueous media the solvent temperatures and viscosities were:

Detergent	Temp. °C.	Viscosity, η poise
C ₁₄	34.0	0.0074
C ₁₆	34.0	0.0074
C ₁₈	44.0	0.0061

In the experiments involving variation of solvent composition, Baker and Adamson reagent-grade glycerol was used. Density determinations indicated that the composition of this reagent was 95.15 wt. % glycerol; the remainder was assumed to be water. Solutions of the *n*-octadecyltrimethylammonium bromide in glycerol-water mixtures were prepared in 50.0-ml. volumetric flasks, the percentage of glycerol being determined by weight. All measurements in glycerol solutions were carried out at 44.0°C.

The detergent concentration, *c*, has been expressed as g./l. in all calculations.

¹ This work was carried out in connection with ONR project N6-onr 26414.

RESULTS AND DISCUSSION

Extinction Angle Measurements; Extrapolation Procedure

Flow birefringence measurements give values of the extinction angle, χ , and the birefringence, Δn , as a function of the applied velocity gradient, G . These measurements may be interpreted using the orientation theory of Peterlin and Stuart (3), based on a rigid, prolate, ellipsoidal model. Recently computed numerical solutions (4) make possible the calculation of the rotary diffusion constants, Θ , and, thereby the lengths and refractive indices of the micelles from measurements over a wide range of velocity gradients.

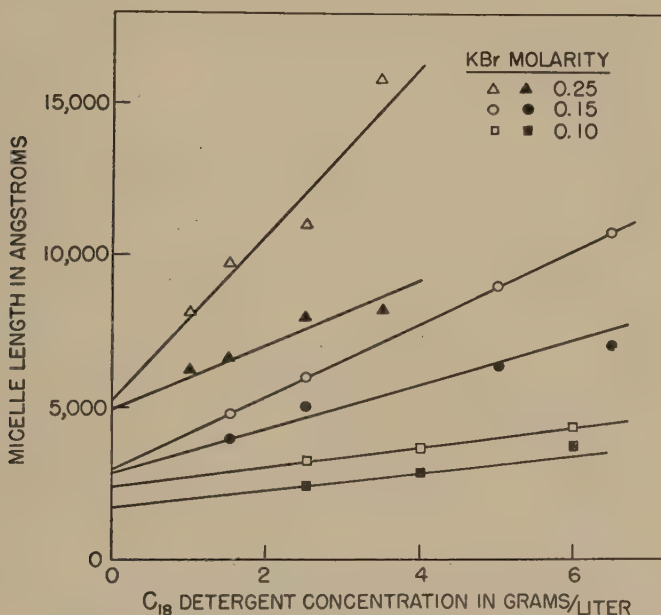


FIG. 1. Dependence of apparent micelle length on detergent concentration for various salt concentrations. Open symbols represent data obtained at lowest velocity gradient ("maximum" length); solid symbols represent data obtained at highest gradient ("minimum" length).

The experimental behavior of χ and Δn is similar to that reported previously for the C₁₆ detergent (1). It should be emphasized that the Peterlin-Stuart theory is valid only for particles at infinite dilution where there is no solute-solute interaction. It is, therefore, necessary to make measurements at extremely low concentrations where such interactions become negligible, or else use some satisfactory extrapolation procedure to obtain values at zero concentration. A moderate micelle concentration was required for precise measurements; since there is no suitable theory for

performing the extrapolation an empirical one was used. It was found that the apparent micelle length is a linear function of detergent concentration at any gradient. This is shown in Fig. 1. for the C_{18} detergent. The linearity of L with c may be compared with the linearity of $1/\theta$ with c found by Rich (6) for the desoxypentose nucleic acid of squid testis. For very elongated particles $1/\theta$ is essentially proportional to L^3 .

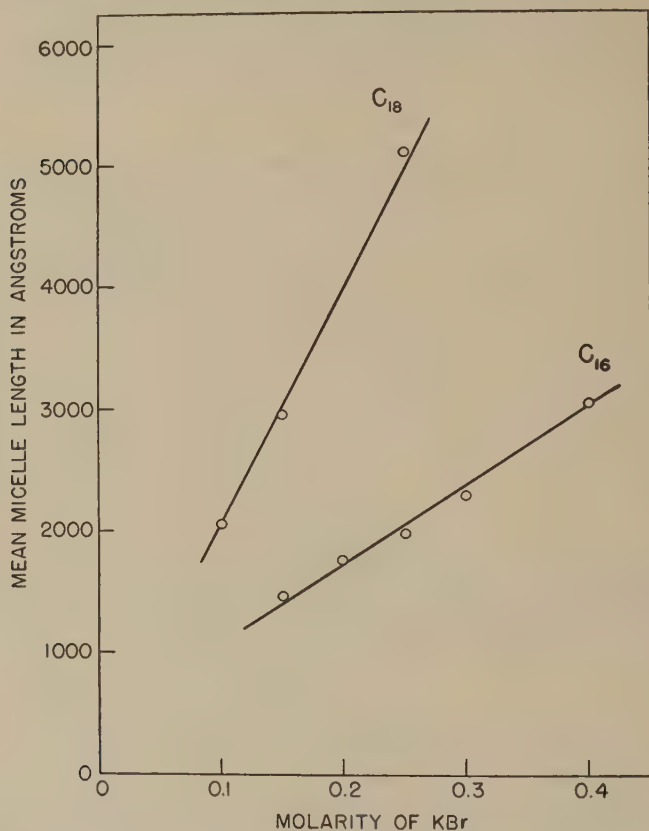


FIG. 2. Effect of salt concentration on mean micelle length. No birefringence was observed with the C_{14} detergent.

Since the system is polydispersed, as found previously (1), the apparent length depends on the gradient. Therefore, the extrapolation has to be carried out at each gradient. For each KBr concentration the data are plotted only for the minimum and maximum velocity gradients employed in the measurements. It can be seen that the extrapolated values at zero micelle concentration indicate a somewhat lower degree of polydispersity than was indicated for the C_{16} detergent (1) where the data were not precise enough to warrant carrying out this extrapolation. Nevertheless,

the data indicate that there is a distribution of particle sizes, for each salt concentration, given approximately by the intercepts at zero detergent concentration. It does not appear worth-while to try to analyze this polydispersity to any greater extent because the data are not precise enough to determine a unique set of parameters required to characterize the distribution (7). It can also be seen in Fig. 1 that the extrapolated lengths increase with increasing KBr concentration. The effect of salt on

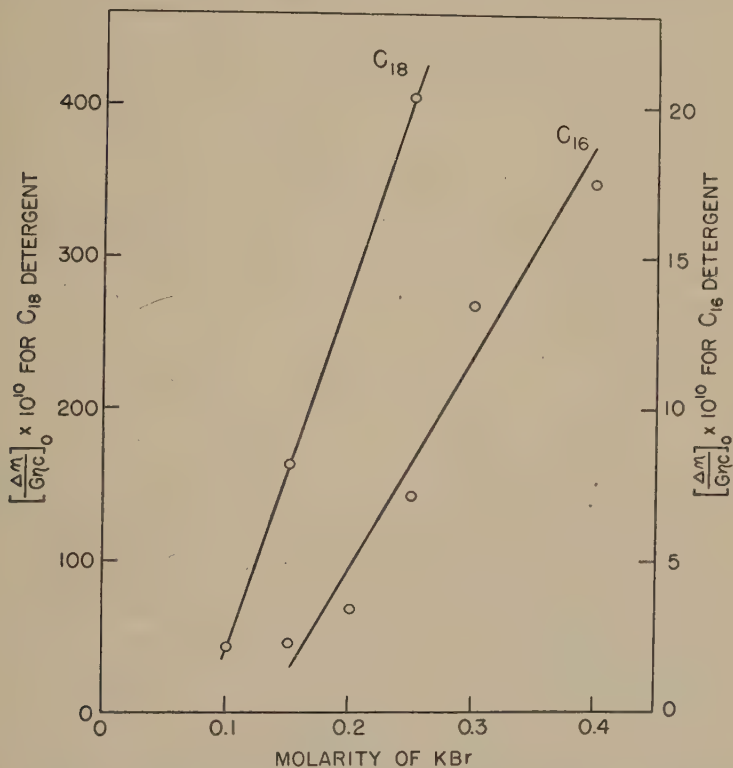


FIG. 3. Effect of salt concentration on the initial birefringence. No birefringence was observed with the C_{14} detergent. Because of the relatively small magnitude of the birefringence for the C_{16} detergent the data in this case are not as precise as for the C_{18} detergent.

the micelle size for detergent molecules of different hydrocarbon chain lengths is shown in Fig. 2. No birefringence was observable for the C_{14} detergent indicating that its length² is smaller than about 300 Å. A similar upper size limit for this detergent was given by Debye and

² In calculating this maximum size limit it was assumed that the intrinsic anisotropy of the C_{14} detergent is the same as that of the C_{16} and C_{18} and that the minimum observable Δn value is 10^{-8} . See footnote 4.

Anacker (2) on the basis of the absence of any significant angular dissymmetry of scattered light. As already pointed out (5), an increase in the number of carbon atoms in the hydrocarbon tail leads to increased micelle size.

Optical Properties of Micelles in Water

The effect of KBr concentration on the birefringence, $\left(\frac{\Delta n}{G\eta c}\right)_0$, is shown in Fig. 3. The zero subscript indicates that this quantity is calculated from the initial slope of the Δn versus G curve. The much greater magnitude of the birefringence for the C_{18} micelle arises primarily from its greater length and, therefore, its greater ease of orientation in the streaming liquid.

To obtain information about the optical properties of the micelles it should be noted that χ is a function only of the degree of orientation, which in turn depends on the size and shape of the solute particles, whereas Δn , on the other hand, depends not only on the degree of orientation but also on an optical factor determined by the internal structure of the particle.

$$\chi = \chi(\alpha, a/b) \quad [1]$$

and

$$\Delta n = \frac{2\pi\phi}{n} (g_1 - g_2) \times f(\alpha, a/b), \quad [2]$$

where $\alpha = G/\Theta$, a/b is the axial ratio of the particle, ϕ the volume fraction of the solute, f the orientation factor, $(g_1 - g_2)$ the optical factor, and n the index of refraction of the solvent. Values of χ and f as a function of α and a/b have been tabulated (4) so that a knowledge of $\chi(\alpha, a/b)$ gives $f(\alpha, a/b)$. Thus, simultaneous measurements of χ and Δn enable one to determine $(g_1 - g_2)$.

The quantities g_1 and g_2 are also related (3) to the refractive increment $\delta n/\phi$.

$$\delta n = \frac{2\pi\phi}{n} \frac{(g_1 + 2g_2)}{3}, \quad [3]$$

where δn is the increase in refractive index of the solution over that of the pure solvent.³ Thus g_1 and g_2 can be determined from flow birefringence and refractive increment measurements (8) using Eqs. [1], [2], and [3].

Individual values of g_1 and g_2 are given by the relations (9)

$$g_i = \frac{3n^2 n_i^2 - n^2}{4\pi D_i}, \quad [4]$$

³ If concentrations, c , are expressed in g./l. then ϕ in Eqs. [2] and [3] must be replaced by $\frac{c\bar{v}}{1000}$, where \bar{v} is the partial specific volume of the solute in cc./g.

where

$$D_i = (n_i^2 + 2n^2) + \frac{2}{i} (-1)^i e(n_i^2 - n^2) \quad [5]$$

for $i = 1$ or 2 . The form factor e depends only on the axial ratio of the particle (9). For a prolate ellipsoid e increases from zero when $a = b$ to a limiting value of 0.5 for $a/b > 10$; n_1, n_2, n_3 are the principal axes of the index of refraction ellipsoid of the particle. For ellipsoids of revolution, two of the indices are identical. It is assumed that the principal axes of the index of refraction ellipsoid coincide with the principal axes of the geometrical ellipsoid of the particle. Thus, for a prolate ellipsoid of revolution, n_1 would lie in the direction of the major axis and $n_2 = n_3$ in the direction of the minor axes.

From Eqs. [4] and [5] the expression for the optical factor becomes

$$g_1 - g_2 = \frac{9n^4}{4\pi D_1 D_2} \left[(n_1^2 - n_2^2) + \frac{e}{n^2} (n_1^2 - n_2^2) (n_2^2 - n^2) \right] \\ = \frac{9n^4}{4\pi D_1 D_2} (A_I + A_F). \quad [6]$$

A_I is a term arising from the *intrinsic* anisotropy of the particle and A_F from the *form* anisotropy. A_F is always positive while A_I is positive or negative according to whether n_1 is greater or less than n_2 . A particle intrinsically isotropic ($A_I = 0$) can still exhibit flow birefringence (i.e., a non-zero value of $g_1 - g_2$) if it is asymmetric and if its mean index of refraction is different from that of the solvent. An asymmetric, isotropic particle will not give double refraction of flow if immersed in a solvent of the same index of refraction as the particle. On the other hand an anisotropic sphere would have a zero value for A_F and a non-zero value for A_I . However, the index of refraction ellipsoid of a rigid, spherical particle could not be oriented by shearing forces and so the system would not exhibit double refraction of flow. $g_1 - g_2$ can be zero if the negative intrinsic anisotropy compensates the form anisotropy (i.e., $A_I = -A_F$) and can change sign when the index of refraction of the solvent is suitably varied. For a prolate ellipsoid a change of sign can occur only if $n_2 > n_1$; if, in addition, $e = 0.5$, then the curve $g_1 - g_2$ vs. n will have a minimum at a value of n equal to the mean index of refraction of the particle. The Δn value at this point is a measure of the intrinsic anisotropy of the particle. These points and others are summarized in detail by Peterlin and Stuart (9) in graphs giving essentially the dependence of $g_1 - g_2$ on the index of refraction of the solvent for particles of various axial ratios and intrinsic anisotropy.

On this basis we can examine the implications of the observed Δn values for detergent micelles. It should be pointed out that only semi-quantitative use will be made of these relations because of certain approxi-

mations which will have to be made. However, these approximations will not alter the essential features of the situation.

From the flow birefringence data, the optical factors, $g_1 - g_2$, have been calculated in the manner indicated by Edsall and Foster (10) who made similar calculations for several proteins. Debye and Anacker (2) obtained estimates of the density of detergent micelles from intrinsic viscosity studies assuming spherical shapes. As these authors point out,

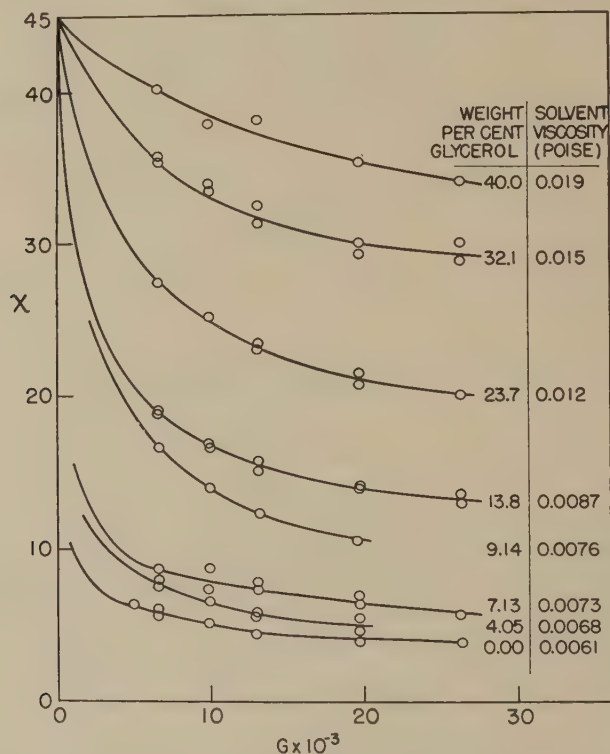


FIG. 4. Behavior of the extinction angle as a function of velocity gradient in 0.5% solutions of the C_{18} detergent in 0.15 M KBr to which varying amounts of glycerol were added.

while the shapes are certainly not spherical, the calculated density is at least of the right order of magnitude (i.e., approximately unity) and different from the case of a randomly coiled polymer whose density is much lower. Unit density has thus been assumed in calculating volume fractions.

Using data for the refractive increment of the detergent solutions, g_1 and g_2 were calculated from Eqs. [1], [2], and [3], and n_1 and n_2 from Eqs. [4] and [5]. For all of the salt concentrations shown in Fig. 3, for

both the C_{16} and C_{18} micelles the principal indices of refraction are $n_1 = 1.48$ and $n_2 = 1.49$ indicating that the micelles have a negative intrinsic anisotropy which is *independent* of the micelle size or monomer chain length.⁴ Thus, the observed positive birefringence, which is a function of salt concentration (and, therefore, of micelle size) arises primarily from the orientation factor and the form anisotropy of the micelle since it is long and highly asymmetric ($e = 0.5$) and has a mean index of refraction (1.49) different from that of the solvent (1.33).

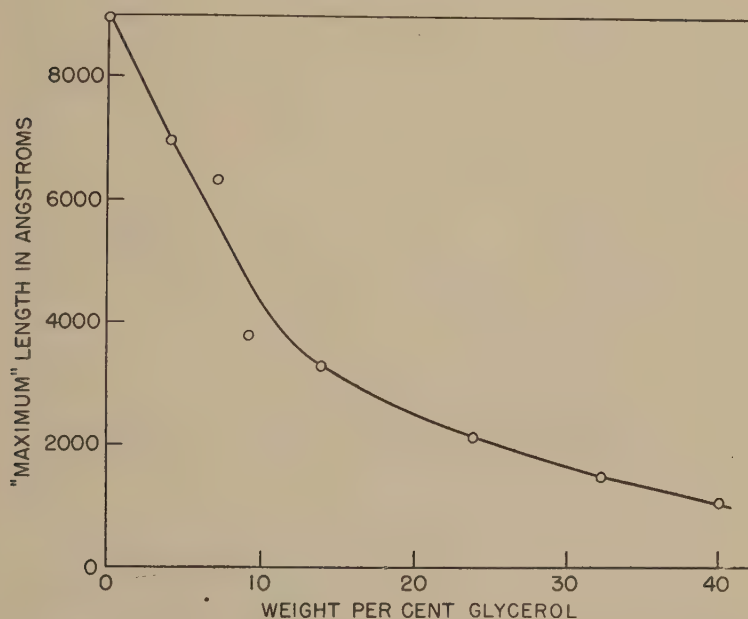


FIG. 5. Effect of glycerol on the "maximum" length of C_{18} micelles obtained from the data of Fig. 4. It should be pointed out that the magnitude of the birefringence is smallest at 7.13% and 9.14% glycerol (see Fig. 6). The corresponding extinction angle data for these solutions are, therefore, not as precise as at other glycerol concentrations.

The negative intrinsic anisotropy means that the micelle has a greater polarizability perpendicular to the rod axis than it has along this axis. This appears reasonable if the micelle is assumed to have hydrocarbon chains extending radially from the axis of the rod, since the polarizability of a hydrocarbon is greater along the chain than perpendicular to it as can be seen from Kerr effect data (11,12). The assumption of a spherical micelle is incompatible with these observations.

⁴ The assumption that these values hold for the C_{14} micelles, as indicated in footnote 2, therefore seems justified.

Optical Properties of Micelles in Glycerol-Water Mixtures

The dynamo-optical properties of the micelle should be greatly affected by variation of the solvent composition, i.e., by changes in the index of refraction and dielectric constant of the solvent. Since glycerol had been shown to affect the micelle size (13), the effect of this substance on the C_{18} detergent was investigated by the flow birefringence method.

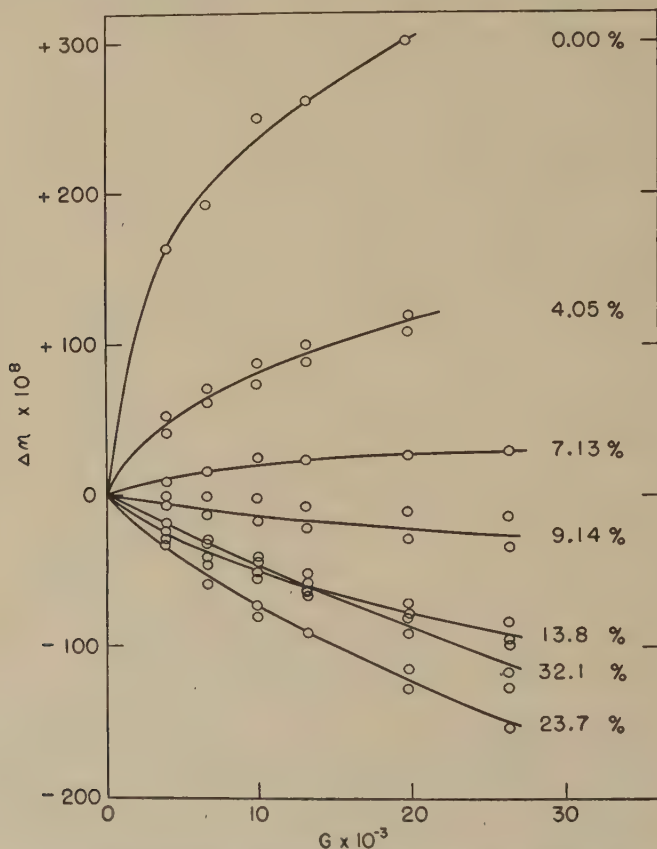


FIG. 6. Birefringence curves corresponding to extinction angle data of Fig. 4 for the glycerol concentrations indicated.

The effect of glycerol on the extinction angle is evident in Fig. 4 where χ is plotted against G for various glycerol concentrations. The corresponding micelle lengths are shown in Fig. 5 as a function of glycerol content. The decrease in micelle size with increasing glycerol concentration is similar to that indicated by light scattering (13).

The effect of glycerol on the birefringence is shown in Fig. 6 where Δn is plotted against G . The curves exhibit the characteristic saturation

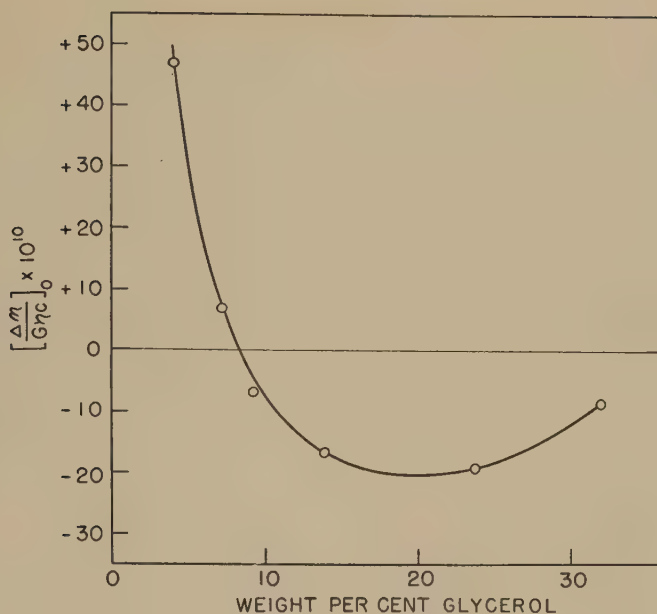


FIG. 7. Effect of glycerol on the initial birefringence for data of Fig. 6.

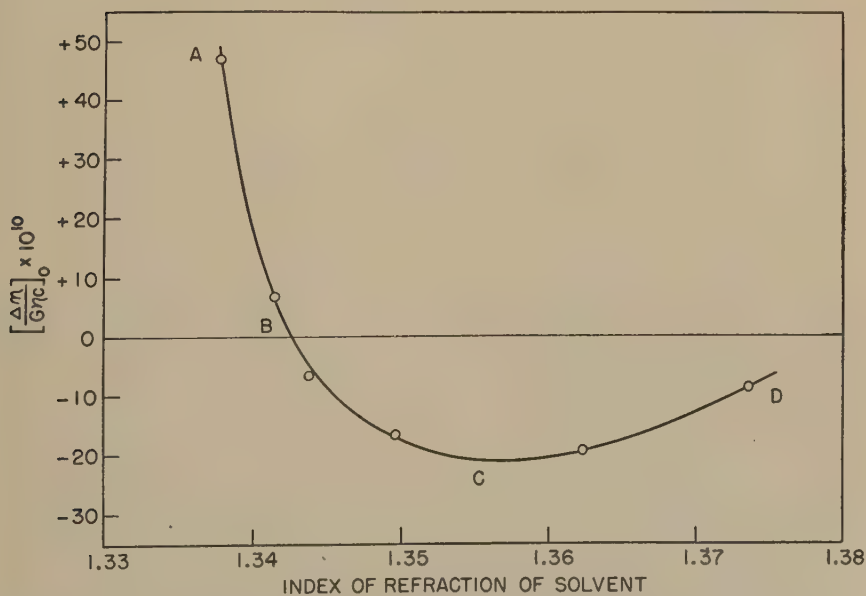


FIG. 8. Relation between solvent index of refraction and the initial birefringence for data of Fig. 6.

effect due to the orientation of rigid particles. In addition, it should be noted that the birefringence is positive in the absence of glycerol and decreases to zero upon addition of small quantities of glycerol. Upon further addition the birefringence increases again but with a negative sign. Still further increases of the glycerol concentration produce a reduction in the negative birefringence. These results are summarized in Figs. 7 and 8, where $\left(\frac{\Delta n}{G\eta c}\right)_0$ is plotted against the glycerol concentration and index of refraction of the solvent, respectively.

If the glycerol did not affect the micelle size but contributed only to a variation in the solvent index of refraction, then the behavior illustrated

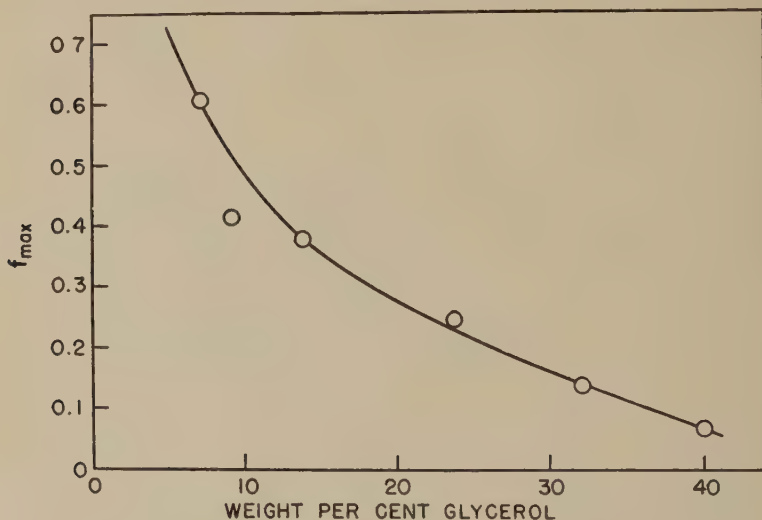


FIG. 9. Effect of glycerol on the orientation factor, f , for data of Fig. 6.

in Fig. 8 would be interpreted in terms of a variation of form anisotropy with n , i.e., A_F would be zero at a value of n of approximately 1.36. This would mean that the mean micelle refractive index would also have to be 1.36. However, from birefringence and refractive increment measurements in glycerol-water mixtures it has been found that the mean micelle refractive index is essentially the same as in the absence of glycerol, approximately 1.50. The explanation, of course, lies in the effect of reduced micelle size superimposed on this other effect. As has been shown in Fig. 5, the micelle size decreases with increasing glycerol concentration. Figure 9 shows how the orientation factor, f , decreases simultaneously. Thus, referring to Fig. 8 and Eq. [2], the decrease in Δn may be attributed primarily to the decrease in f . There is a simultaneous change in the

magnitude of the form anisotropy in the various regions of Fig. 8. Thus

$$\begin{aligned} \left| \frac{A_F}{A_I} \right| &> 1 \text{ from } A \text{ to } B, \\ \left| \frac{A_F}{A_I} \right| &= 1 \text{ at } B, \\ \left| \frac{A_F}{A_I} \right| &< 1 \text{ along } BCD. \end{aligned} \quad [7]$$

Because of the behavior indicated by Eq. [7] and the negative value of A_I , the birefringence changes sign at B . The simultaneous rapid decrease in f means that the negative birefringence must approach zero at high glycerol concentrations since the micelle becomes too small to be oriented by the streaming liquid. If f did not decrease, then, since the mean micelle index of refraction is about 1.50, the minimum of the curve would occur at $n = 1.50$. Figure 10 illustrates how the minimum is shifted

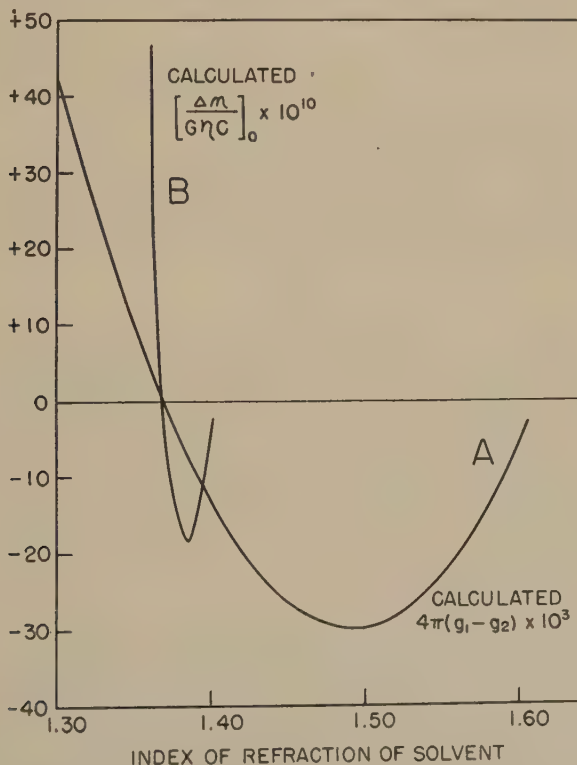


FIG. 10. Variation of birefringence with solvent index of refraction for A, the case where the particle size remains constant, and B, the case where there is a simultaneous decrease in particle size given in terms of the variation in the orientation factor of Fig. 9. In case B, the minimum is shifted toward lower n values even though the mean refractive index of the particle remains constant at 1.5.

toward a lower value of n . Curve *A* is a theoretical one for constant f showing only the variation of $g_1 - g_2$ with n . Curve *B* is a calculated one showing the variation of $\left(\frac{\Delta n}{G\eta c}\right)_0$ with n arising primarily from the simultaneous variation of f with glycerol content from Fig. 9. In these calculations it was assumed that the micelle has a negative intrinsic anisotropy of $n_1 - n_2 = -0.01$ with a mean index of refraction of 1.5, the value determined from the birefringence and refractive increment measurements. Thus the effect illustrated in Fig. 8 is not the commonly observed one of decreasing form anisotropy of particles of constant size as n is varied but one of simultaneous decrease in form anisotropy and particle length as the solvent composition is varied. Excellent agreement is obtained between the calculated and observed positions of the minimum in the curve.

	n_{min}	$\left(\frac{\Delta n}{G\eta c}\right)_0 \times 10^{10}$
Observed (Fig. 8)	1.36	-21
Calculated (Fig. 10)	1.38	-19

The addition of glycerol appears to decrease the micelle length without changing its structure or optical parameters.

All the observations reported here are thus compatible with the assumed structure of the micelle and the applicability of the Peterlin-Stuart theory to account for the dynamo-optical behavior of the micelles in water and in glycerol-water solutions.

SUMMARY

Rodlike micelles formed in aqueous salt solutions of several n -alkyl-trimethylammonium bromides have a size which increases with the KBr concentration and length of the hydrocarbon tail. The C_{14} micelles are too small to be oriented in the streaming liquid while the larger C_{16} and C_{18} micelles are readily oriented. The large birefringence arises primarily from the form anisotropy and high degree of orientation of the particles, the intrinsic anisotropy being negative and independent of salt concentration or chain length.

The addition of glycerol to the detergent solutions decreases the micelle size and resulting birefringence but does not affect the intrinsic anisotropy of the micelle. It appears that this decrease in size is not accompanied by any other changes in the structure of the micelle. The observations are in accord with the Peterlin-Stuart orientation theory which accounts for the size, shape, and optical properties of the solute particles.

REFERENCES

1. SCHERAGA, H. A., AND BACKUS, J. K., *J. Am. Chem. Soc.* **73**, 5108 (1951).
2. DEBYE, P., AND ANACKER, E. W., *J. Phys. & Colloid Chem.* **55**, 644 (1951).

3. PETERLIN, A., AND STUART, H. A., *Hand- u. Jahrb. Chem. Physik*, Bd. 8, Abt. IB (1943).
4. SCHERAGA, H. A., EDSALL, J. T., AND GADD, JR., J. O., *J. Chem. Phys.* **19**, 1101 (1951).
5. DEBYE, P., *J. Phys. & Colloid Chem.* **53**, 1 (1949); *Ann. N. Y. Acad. Sci.* **51**, 575 (1949).
6. EDSALL, J. T., SCHERAGA, H. A., AND RICH, A., Abstracts of 119th meeting of the American Chemical Society, p. 5 J, April, 1951.
7. SCHERAGA, H. A., *J. Chem. Phys.* **19**, 983 (1951).
8. CERF, R., *Compt. rend.* **226**, 405 (1948).
9. PETERLIN, A., AND STUART, H. A., *Z. Physik* **112**, 1 (1939).
10. EDSALL, J. T., AND FOSTER, J. F., *J. Am. Chem. Soc.* **70**, 1860 (1948).
11. STUART, H. A., *Hand- u. Jahrb. Chem. Physik*, Bd. 10, 27, (1939).
12. DENBIGH, K. G., *Trans. Faraday Soc.* **36**, 936 (1940).
13. HAGEN, R. M., Ph.D. thesis, Cornell University, 1949.

THE EFFECT OF pH ON THE RATE OF SURFACE TENSION LOWERING¹

Emil J. Burcik and Carlos R. Vaughn

School of Petroleum Engineering, University of Oklahoma, Norman, Oklahoma

Received August 20, 1951

INTRODUCTION

The sodium salts of the fatty acids hydrolyze in water solution, and the free acid formed associates with fatty acid ions to form acid soap (4). The extent of hydrolysis is partially controlled by the pH of the solution in that the formation of acid soap is repressed by the addition of free base and enhanced by the addition of free acid. It has been shown that a finite time is necessary for a newly formed surface to reach surface equilibrium by diffusion of the surface-active components contained in the bulk solution to the interface (1,2). If acid soap is surface active, it is probable that the rate of surface tension lowering is a function of pH since the rate of diffusion of acid soap would be different from that of single ions. On the other hand, surface-active agents which do not hydrolyze should have rates of surface tension lowering which are independent of pH if the electrolyte effect (2) of the added acid or base can be neglected. In this research the effect of pH on the rate of surface tension lowering of pure sodium myristate, dodecylamine hydrochloride, and sodium dodecyl sulfate was determined. These compounds exhibit a hydrolysis alkalinity, a hydrolysis acidity, and no hydrolysis, respectively.

EXPERIMENTAL

Methods

The technique employed to measure the rate of surface tension lowering has been described previously (2). The method is based on the fact that a liquid jet issuing from a noncircular orifice will produce a series of standing waves along the jet whose wavelength is a function of the surface tension of the liquid. When a solution containing a surface-active agent is allowed to flow through the orifice, the wavelength of successive waves increases due to the decreasing surface tension of the liquid. If the rate of flow and the dimensions of the jet are known, the surface tension as a function of time can be determined.

¹ This investigation is a joint undertaking of the Research Institute of the University of Oklahoma and the Office of Naval Research.

In these experiments two rates of flow were employed: 91.3 cc./min. and 100.0 cc./min. The results reported are the averages of two or more separate determinations. All experiments were conducted at 20°C.

To alter the pH of sodium myristate, either carbonate-free sodium hydroxide or free myristic acid was added. Free dodecylamine or hydrochloric acid was added to dodecylamine hydrochloride. The pH of the sodium dodecyl sulfate was controlled with either sodium hydroxide or hydrochloric acid.

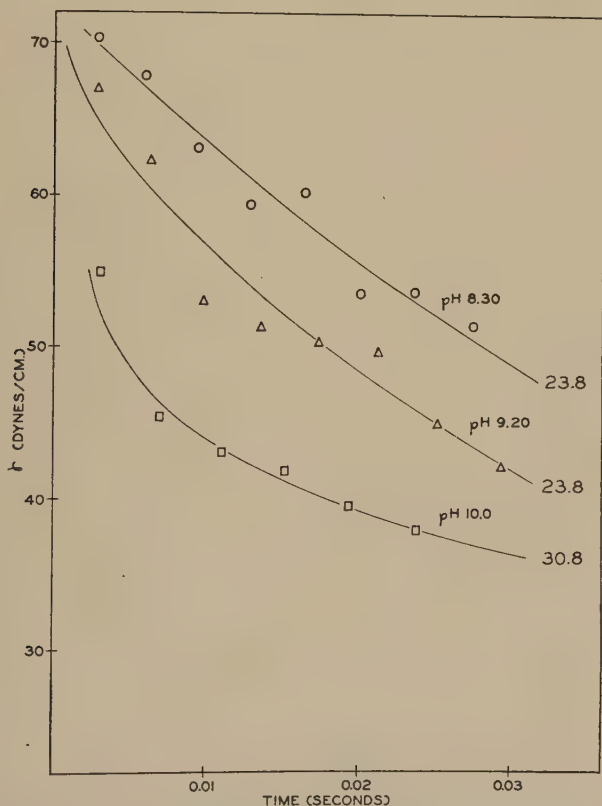


FIG. 1. Effect of pH on the rate of surface tension lowering of 0.005 *N* sodium myristate.

Equilibrium surface tensions were measured with a du Noüy Interfacial Tensiometer. The corrections suggested by Zuidema and Waters (7) were applied.

Measurements of pH were made using a Beckman model M pH meter.

Materials

The preparation and properties of sodium dodecyl sulfate have been previously described (2).

Sodium Myristate. Myristic acid was redistilled in vacuum. The fraction employed in the preparation of the soap had an equivalent weight of 230.9 (theory 228.4). The sodium soap was prepared in the same manner as previously described (2).

Dodecylamine Hydrochloride. A commercial sample consisting of about 90% dodecylamine was redistilled in vacuum. The fraction employed to prepare the hydrochloride had an equivalent weight of 184.9 (theory

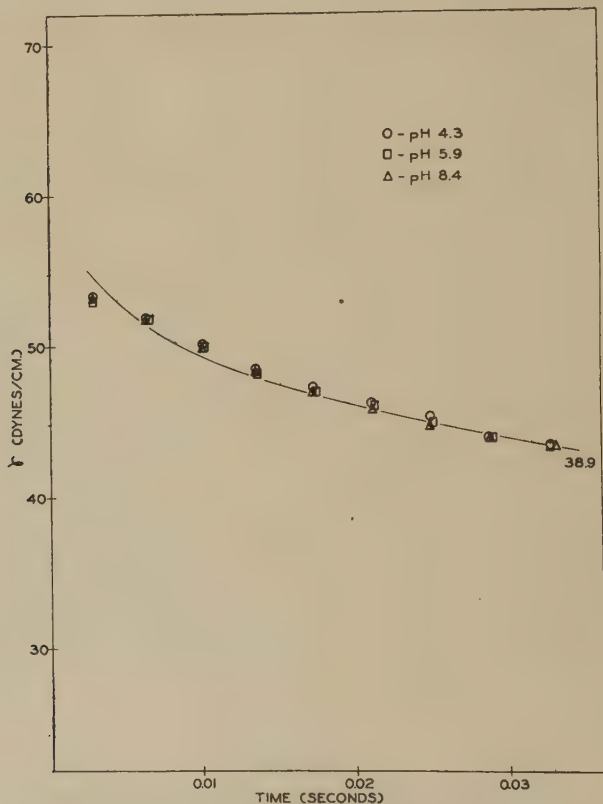


Fig. 2. Effect of pH on the rate of surface tension lowering of 0.005 *N* sodium dodecyl sulfate.

185.3). Twenty grams of the purified amine was added to 15 cc. of concentrated hydrochloric acid in 100 cc. of alcohol. The water and excess hydrochloric acid were distilled off and the product was recrystallized three times from an alcohol-ether mixture.

RESULTS

The effect of pH on the rate of surface tension lowering of 0.005 *N* sodium myristate at 20°C. is shown in Fig. 1. Here the surface tension in

dynes/cm. is plotted as a function of time. Results for solutions at three different pH values are presented: pH = 8.3 by addition of myristic acid, pH = 9.2 with no additive, and pH = 10.0 by addition of sodium hydroxide. An examination of Fig. 1 will show that an increase in pH results in an increase in the rate of surface tension lowering. The static, equilibrium surface tensions as determined by the du Noüy ring method are recorded at the end of each curve. The addition of sodium hydroxide caused an

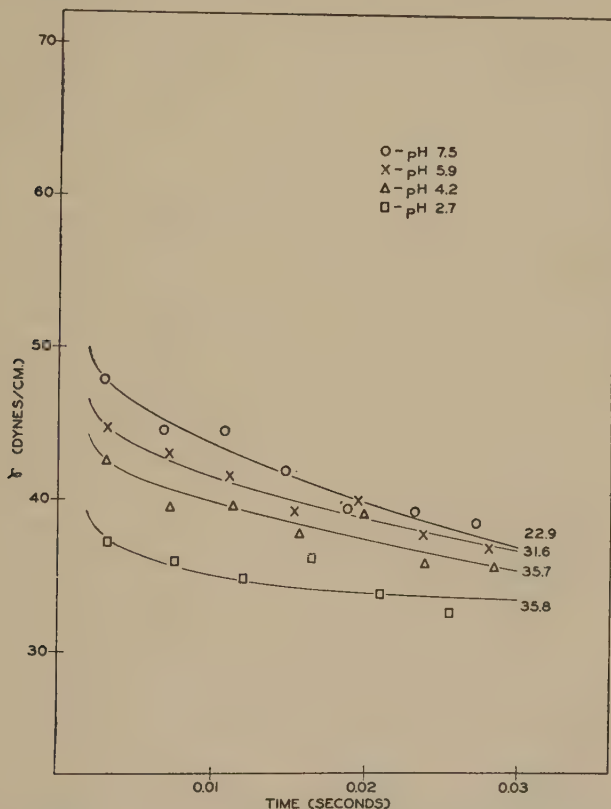


Fig. 3. Effect of pH on the rate of surface tension lowering of 0.01 *N* dodecylamine hydrochloride.

increase in the equilibrium tension (5) indicating that acid soap is a surface-active component of the solution.

The effect of pH on the rate of surface tension lowering of 0.005 *N* sodium dodecyl sulfate, which is not readily susceptible to hydrolysis, is shown in Fig. 2. No pH effect is evident.

For 0.01 *N* dodecylamine hydrochloride, a cationic surface-active agent which exhibits acid hydrolysis, an increase in pH by the addition of

dodecylamine results in a decrease in the rate of lowering. Addition of hydrochloric acid increases the rate, as is shown in Fig. 3. In this case an increase in pH resulted in a decrease in equilibrium surface tension.

DISCUSSION

These experimental results can be explained if one allows that, in the case of sodium myristate, acid soap is a surface-active component. The addition of free fatty acid will result in the formation of additional acid soap so that the more mobile ions are partially replaced by less soluble, more slowly diffusing acid soap. Furthermore, the addition of free acid promotes micelle formation which also results in a decrease in ion concentration. Sodium hydroxide will have the opposite effect since the hydrolysis will be suppressed and the acid soap decomposed. In addition, if appreciable amounts of free base are introduced there will be an increase in rate due to the electrolyte effect (2) since the potential barrier at the interface will be reduced by the presence of electrolyte (3). The combined effect of an increase in pH will be an increase in the rate of surface tension lowering.

In the case of cationic surfactants which are subject to hydrolysis, it is necessary to assume that a surface-active complex forms between the ions and the free base. An increase in pH by addition of free base would result in the formation of the more slowly diffusing complex and a decrease in rate. Addition of hydrochloric acid will reduce the concentration of the complex with an increase in rate. Here again, the electrolyte effect of the added acid may be an important factor. The large increase in rate for the dodecylamine hydrochloride at pH 2.7 is probably due, to a large extent, to the electrolyte effect since in this case the concentration of the added acid is comparable to that of the surface-active agent.

The rate of surface tension lowering of sodium dodecyl sulfate which does not hydrolyze is unaffected by addition of acid or base provided it is not added in sufficient amount to cause an increase in rate by virtue of the electrolyte effect.

The magnitude of the pH effect would be determined by the degree of hydrolysis of the particular surface-active agent in question. Consequently one would expect this effect to be very pronounced in the higher-molecular-weight soaps because of their more pronounced hydrolysis (6).

SUMMARY

1. The rate of surface tension lowering of 0.005 *N* sodium myristate, a hydrolyzable anionic surface-active agent, increases with increasing pH.
2. The rate of surface tension lowering of 0.01 *N* dodecylamine hydrochloride, a hydrolyzable cationic surface-active agent, decreases with increasing pH.

3. The rate of surface tension lowering for 0.005 *N* sodium dodecyl sulfate, a surfactant which does not hydrolyze, is independent of pH.

REFERENCES

1. ADDISON, C. C., *J. Chem. Soc.* **1943**, 535; *ibid.* **1944**, 252, 477; *ibid.* **1945**, 98, 354.
2. BURCIK, E. J., *J. Colloid Sci.* **5**, 421 (1950).
3. DOSS, K. S. G., *Kolloid-Z.* **86**, 205 (1939).
4. EKWALL, P., *Kolloid-Z.* **92**, 141 (1940).
5. POWNEY, J., *Trans. Faraday Soc.* **31**, 1510 (1935).
6. POWNEY, J., AND JORDAN, D. O., *Trans. Faraday Soc.* **34**, 363 (1938).
7. ZUIDEMA, H. H., AND WATERS, G. W., *Ind. Eng. Chem., Anal. Ed.* **13**, 312 (1941).

RHEOLOGY OF SYNTHETIC LATEX. I. TEST OF SOME FLOW EQUATIONS¹

Irvin M. Krieger and Samuel H. Maron

*Physical Chemistry Laboratory, Department of Chemistry and Chemical Engineering,
Case Institute of Technology, Cleveland, Ohio*

Received August 27, 1951

INTRODUCTION

The viscosity behavior of synthetic rubber latex is a problem of considerable theoretical interest. Whereas most systems exhibiting non-Newtonian behavior are suspensions of anisotropic particles, the particles in synthetic latices are semirigid spheres.

Earlier viscosity studies of natural and synthetic latices treated these systems as Newtonian fluids. When cognizance was taken of their non-Newtonian character, it was arbitrarily assumed in most instances (1) that they exhibited "plastic" flow, as defined by Bingham (2). Thus Jordan, Brass, and Roe (3) developed a capillary viscometer which measured the rate of flow of latex under two different pressure heads, and used the data so obtained to calculate the two constants of Bingham's flow equation. A different treatment was used by Winding, Kranich, and Baumann (4). Assuming a Newtonian velocity distribution, they obtained approximations to rate of shear-shearing stress curves for latex. These curves were almost linear when plotted logarithmically.

The objects of the present investigation were the definition of the flow behavior of latex in fundamental terms and the interpretation of the results obtained. This paper is confined to the former aspect of the problem, while subsequent papers in this series will be concerned with the question of interpretation.

THEORY OF MEASUREMENT

The functional relationship between shearing stress, F , and the velocity gradient (or rate of shear), G , is known as the equation of flow. For ordinary fluids F is proportional to G , the proportionality constant being the viscosity coefficient η . For many colloidal systems, however, the ratio of F to G varies with the rate of shear. The former fluids are called Newtonian, the latter non-Newtonian.

¹ Presented at the Annual Meeting of the Society of Rheology, New York, N. Y., November 4, 1949.

Newton's simple flow law is written

$$G = \frac{1}{\eta} F. \quad [1]$$

To modify this equation, Bingham postulated a substance which deforms but does not flow until a critical shearing stress F_0 , called the "yield point," is exceeded. Beyond this point the "Bingham body" behaves like a Newtonian fluid with "limiting viscosity" η . The equation for such flow (5) is

$$G = \begin{cases} 0 & \text{for } F < F_0 \\ \frac{1}{\eta} (F - F_0) & \text{for } F \geq F_0 \end{cases} \quad [2]$$

Again, Porter and Rao (6) and Farrow, Lowe, and Neale (7), in their investigations of the flow of starch pastes, used an exponential equation of the form

$$F^N = \eta' G. \quad [3]$$

N is an index of non-Newtonian behavior ($N = 1$ in the Newtonian limit) and η' is the viscosity at unit shearing stress.

Viscometers commonly employed in the study of non-Newtonian fluids are of two types: capillary and concentric cylinder instruments. In capillary viscometers the rate of flow Q of fluid through a tube is measured as a function of the pressure drop P across the tube; in concentric cylinder viscometers, one of the cylinders is rotated with an angular velocity Ω , the required torque M being determined. The relationships between P and Q in the first case and between Ω and M in the second are integrals of the velocity gradient containing instrumental parameters. In the derivations which follow, laminar flow and no slippage are assumed.

For a capillary viscometer of radius R and length L , the shearing stress at a distance r from the capillary axis is

$$F = \frac{rP}{2L} \quad [4]$$

while the velocity gradient is

$$G = -\frac{dv}{dr} \quad [5]$$

v being the fluid velocity at r . The rate of flow is then

$$Q = \int_{v=0}^{v_{\max}} \pi r^2 dv = - \int_{r=R}^0 \pi r^2 \frac{dv}{dr} dr. \quad [6]$$

Integration of Eq. [6] for the three flow equations under consideration yields the values for Q given below. Expressions for G at the capillary

wall, where in all instances

$$F = \frac{RP}{2L} \quad [7]$$

are also given.

Newtonian:

$$Q = \frac{\pi R^4 P}{8L\eta} \quad [8]$$

$$G = \frac{4Q}{\pi R^3} \quad [9]$$

Bingham Body (5):

$$Q = \begin{cases} 0 & \text{for } P < \frac{2LF_0}{R} \\ \frac{\pi R^4 P}{8L\eta} - \frac{\pi R^3 F_0}{3\eta} + \frac{2\pi L^3 F_0^4}{3\eta P^3} & \text{for } P \geq \frac{2LF_0}{R} \end{cases} \quad [10]$$

$$G = \begin{cases} 0 & \text{for } P < \frac{2LF_0}{R} \\ \frac{1}{\eta} \left[\frac{RP}{2L} - F_0 \right] & \text{for } P \geq \frac{2LF_0}{R} \end{cases} \quad [11]$$

Exponential (7):

$$Q = \frac{\pi R^3}{\eta'(N+3)} \left(\frac{RP}{2L} \right)^N \quad [12]$$

$$G = \frac{(N+3)Q}{\pi R^3} \quad [13]$$

For a concentric cylinder instrument of length L , rotating bob of radius R_1 , and stationary cup of radius R_2 , we have the following. At a radius r from the axis, where the fluid rotates with angular velocity ω ,

$$F = \frac{M}{2\pi r^2 L} \quad [14]$$

$$G = -r \frac{d\omega}{dr} \quad [15]$$

The angular velocity of the bob is thus

$$\Omega = - \int_{R_1}^{R_2} G \frac{dr}{r} \quad [16]$$

Integration of Eq. [16] using the various flow equations, together with G at the bob wall, are given below. At the bob wall

$$F = \frac{M}{2\pi R_1^2 L} \quad [17]$$

regardless of the flow equation.

Newtonian:

$$\Omega = \frac{M}{4\pi\eta L} \frac{(R_2^2 - R_1^2)}{R_1^2 R_2^2} \quad [18]$$

$$G = \frac{2R_2^2\Omega}{R_2^2 - R_1^2} \quad [19]$$

Bingham Body (8):

$$\Omega = \begin{cases} 0 & \text{for } \frac{M}{2\pi R_1^2 L} \leq F_0 \\ \frac{1}{2\eta} \left[\frac{M}{2\pi R_1^2 L} - F_0 - F_0 \ln \frac{M}{2\pi R_1^2 L F_0} \right] & \text{for } \frac{M}{2\pi R_2^2 L} < F_0 \leq \frac{M}{2\pi R_1^2 L} \\ \frac{M(R_2^2 - R_1^2)}{4\pi R_1^2 R_2^2 L \eta} - \frac{F_0}{\eta} \ln \frac{R_2}{R_1} & \text{for } \frac{M}{2\pi R_2^2 L} \geq F_0 \end{cases} \quad [20]$$

$$G = \begin{cases} 0 & \text{for } \frac{M}{2\pi R_1^2 L} < F_0 \\ 2\Omega + \frac{F_0}{\eta} \ln \frac{M}{2\pi R_1^2 L F_0} & \text{for } \frac{M}{2\pi R_2^2 L} < F_0 \leq \frac{M}{2\pi R_1^2 L} \\ \frac{2R_2^2\Omega}{R_2^2 - R_1^2} + \frac{F_0}{\eta} \left[\frac{2R_2^2}{R_2^2 - R_1^2} \ln \frac{R_2}{R_1} - 1 \right] & \text{for } \frac{M}{2\pi R_2^2 L} \geq F_0 \end{cases} \quad [21]$$

Exponential (7):

$$\Omega = \frac{1}{2N\eta'} \left(\frac{M}{2\pi R_1^2 L} \right)^N \frac{R_2^{2N} - R_1^{2N}}{R_2^{2N}} \quad [22]$$

$$G = \frac{2N\Omega R_2^{2N}}{R_2^{2N} - R_1^{2N}} \quad [23]$$

EXPERIMENTAL

The latices studied were commercial type III products. These are aqueous dispersions of a 50:50 butadiene-styrene ratio polymer emulsified with rosin soap. The normal *ca.* 40% solids product was concentrated by evaporation, and all dilutions were made from this concentrate by the addition of distilled water. Solids contents of the latices were determined by drying weighed samples of the latices at 100°C. to constant weight.

The capillary viscometer used initially consisted of a jacketed 50-ml. buret fitted at the lower end with a ground joint to which various capillaries could be attached. Subsequently this instrument was modified to the

one shown in Fig. 1. For operation the viscometer was filled with filtered latex, brought to temperature, and the latex allowed to drain under its own head. The times required for the meniscus to sweep through successive 5-ml. volumes were recorded; the effective pressure heads were taken as the vertical distances between the midpoints of the 5-ml. volumes and the capillary end. Capillary lengths were measured with a cathetometer, radii by filling with mercury and weighing.

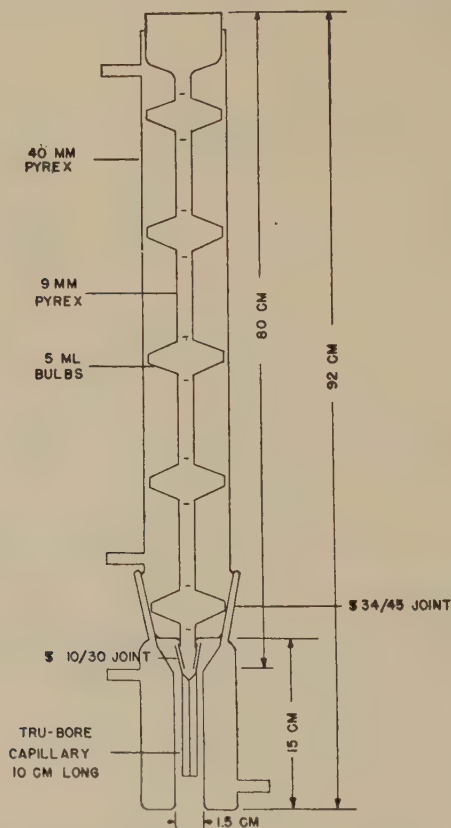


FIG. 1. Modified capillary viscometer.

The concentric cylinder viscometer employed was identical with that described by Mooney and Ewart (9). To make a measurement the space between the cylinders was filled with fluid, equal weights were placed on the pans, and the weights were raised by turning the rotor, thus wrapping the strings around the spindle. The rotor was then released, allowed to turn freely under the torque supplied by the falling weights, and its angular velocity measured after it had reached a constant value.

All measurements were made at 25°C.

RESULTS

None of the latices studied in this investigation exhibited any evidence of thixotropic behavior.

Typical experimental data for a high solids latex are plotted for the capillary viscometer in Fig. 2, and for the concentric cylinder apparatus in Fig. 3. The curvature of these plots is proof of non-Newtonian behavior since Eqs. [8] and [18] require linear P - Q and M - Ω variations, respectively. Bingham body behavior is also ruled out by these data. Eqs. [10] and [20] require positive intercepts on the horizontal axes and linear asymptotes at high shearing rates, neither of which is observed. The ab-

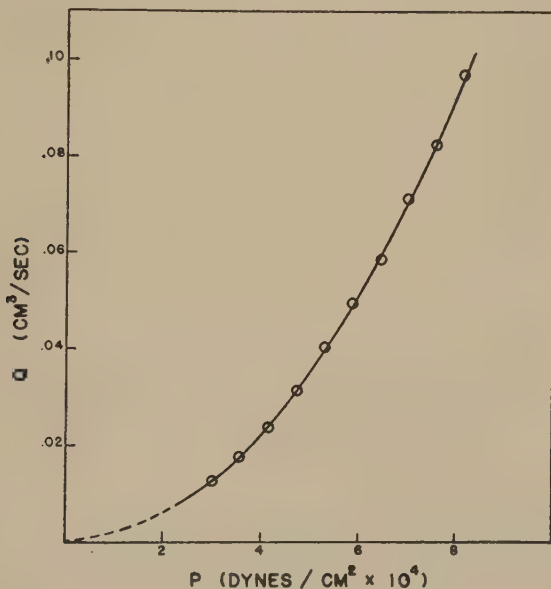


FIG. 2. Flow curve for 63% solids latex in capillary viscometer.

sence of a yield point is strikingly demonstrated in Fig. 3, where appreciable angular velocity is observed even at very low torques.

If the exponential flow equation is obeyed by the latex, logarithmic plots of the experimental data will be linear. From Eqs. [12] and [22] it follows that

$$\log Q = \log \left[\frac{\pi R^{N+3}}{\eta'(N+3)2^N L^N} \right] + N \log P \quad [24]$$

$$\log \Omega = \log \left[\frac{R_2^{2N} - R_1^{2N}}{2^{N+1} \pi^N \eta' N R_1^{2N} R_2^{2N} L^N} \right] + N \log M. \quad [25]$$

The constants N and η' can be recovered from the slopes and intercepts of the logarithmic plots. Figure 4 shows such a plot for five different capil-

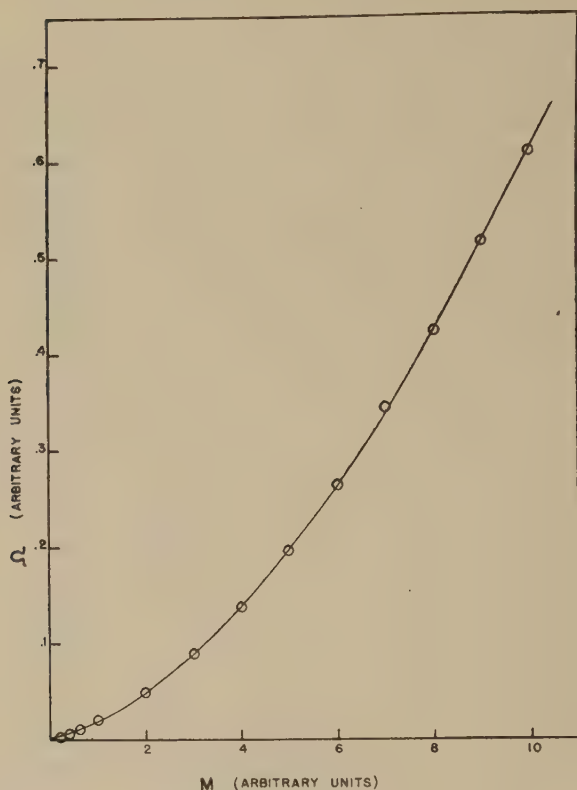


Fig. 3. Flow curve for 59% solids latex in concentric cylinder viscometer.

laries; these plots are all linear and of the same slope, as is required by Eq. [24]. Figures 5 and 6 are logarithmic plots for low- and high-solids latices in the concentric cylinder viscometer. The less concentrated material exhibits excellent linearity over the entire range, whereas the higher solids latex gives two apparently linear portions. This latter phenomenon is similar to the behavior of starch pastes (5).

Table I compares π values of N and η' obtained for several latices using capillary and concentric cylinder viscometers. The agreement is good, particularly when it is realized that $\log \eta'$ rather than η' itself is the

TABLE I
*Comparison of Capillary and Mooney-Ewart Results Obtained on
Evaporated Type III Latex*

Latex	$N(\text{cap})$	$N(M-E)$	$\eta'(\text{cap})$	$\eta'(M-E)$
Latex 304, 48.3% solids	1.15	1.11	0.28	0.25
Latex 304, 53.0% solids	1.28	1.25	1.28	1.00
Latex 304, 59.4% solids	1.56	1.62	24.0	30.5
Latex 360, 56.1% solids	1.82	1.82	264	239

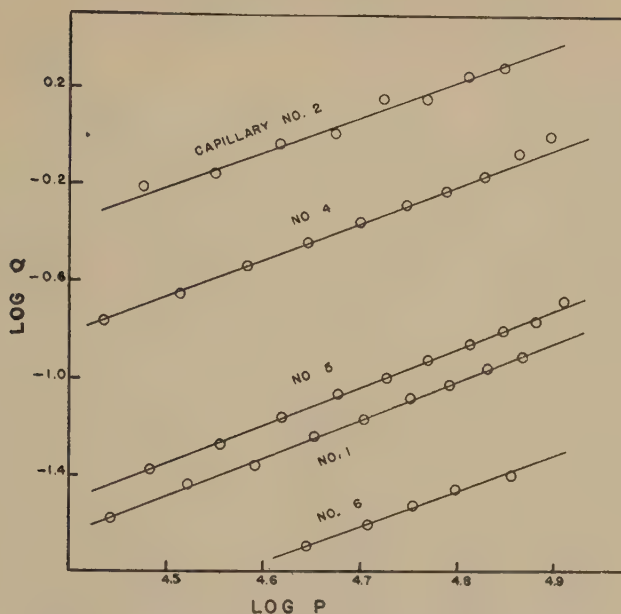


FIG. 4. Logarithmic plot of flow data for 59% solids latex in five capillaries.

directly determined quantity. Variation of N and η' as a function of concentration from 0 to 60% solids is shown in Figs. 7 and 8. It is significant that N starts to deviate from unity at about 25% solids, indicating that

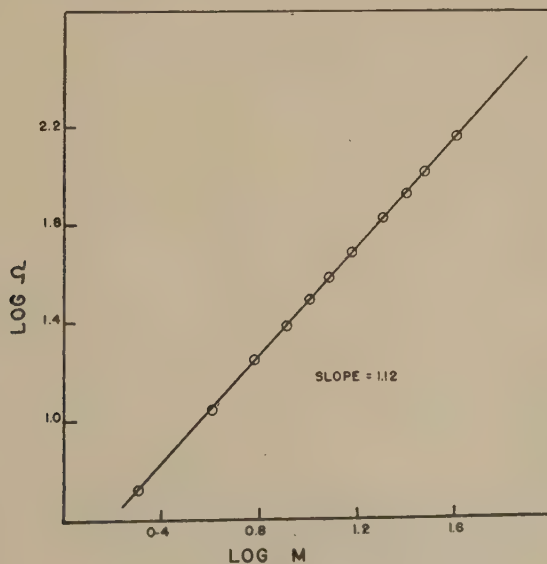


FIG. 5. Logarithmic plot of flow data for 46% solids latex in concentric cylinder viscometer.

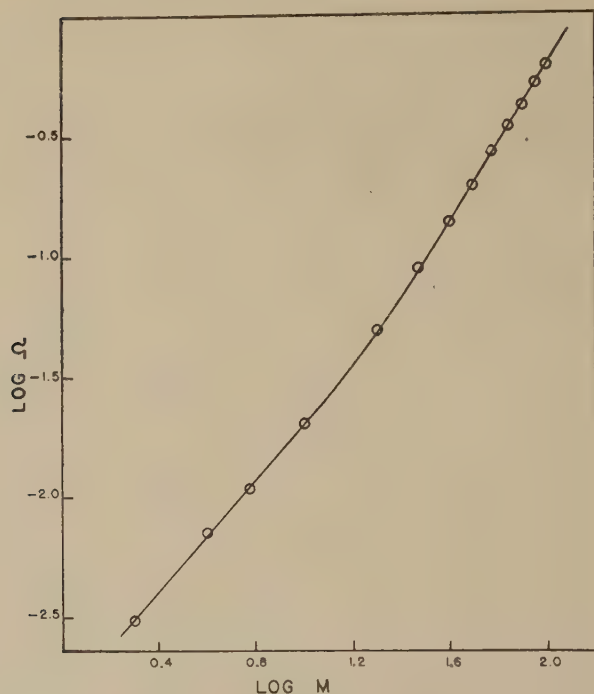


FIG. 6. Logarithmic plot of flow data for 59% solids latex in concentric cylinder viscometer.

the latex is Newtonian below this concentration over the range of shearing rates investigated. Above about 45% solids, where two linear portions on the logarithmic plot were observed, the constants shown are for the upper portion.

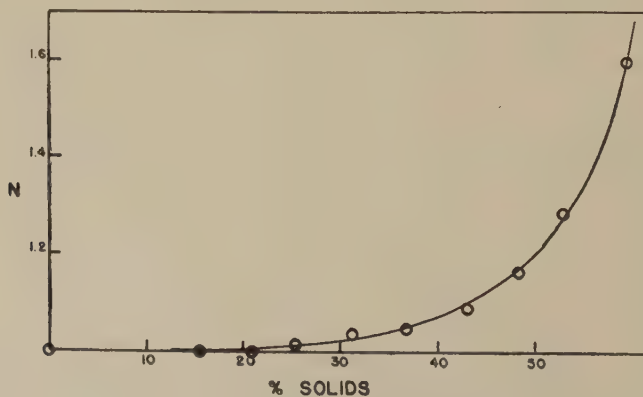


FIG. 7. Variation of N with solids content for type III latex.

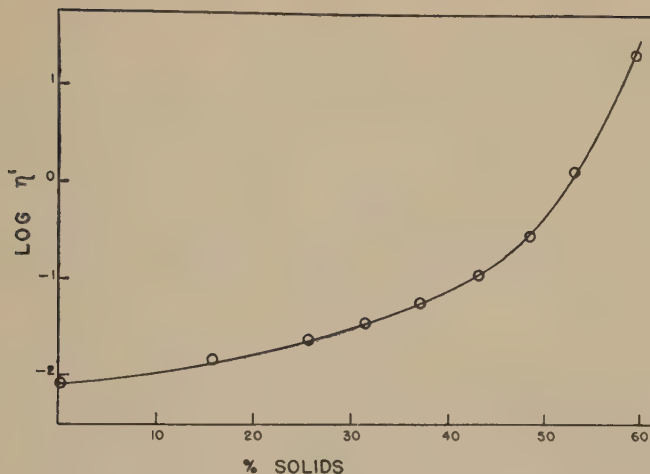


FIG. 8. Variation of η' with solids content for type III latex.

Once N and η' have been determined, the P - Q data for the capillary viscometer can be converted to rate of shear-shearing stress values by means of Eqs. [7] and [13], and the M - Ω data for the concentric cylinder viscometer by means of Eqs. [17] and [23]. Figure 9 shows a composite rate of shear-shearing stress curve as determined with three different capillaries and the concentric cylinder viscometer. The fact that all four sets of points fall along a single curve demonstrates the usefulness of the

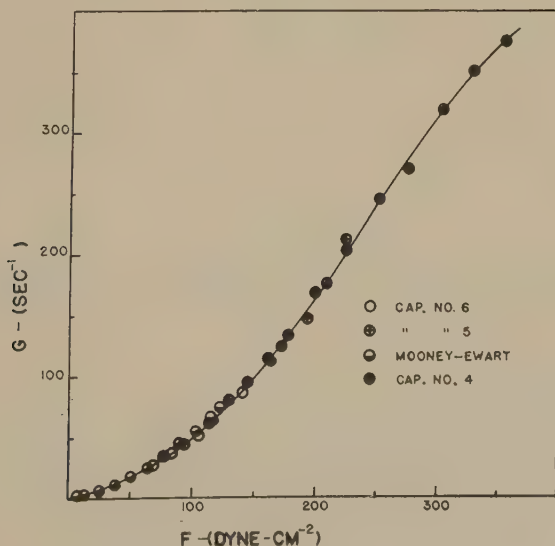


FIG. 9. Composite flow curve for 59% solids latex.

exponential equation in the determination of the flow behavior of type III synthetic latex.

Results similar to those reported here for type III latex have been observed in this laboratory with other types of latex, both synthetic and natural.

ACKNOWLEDGMENT

This research was sponsored by the Office of Rubber Reserve, Reconstruction Finance Corporation, as part of the Government Synthetic Rubber Program, and was first reported in October, 1947.

SUMMARY

Measurements made with both concentric cylinder and capillary viscometers show that type III synthetic latex is Newtonian at concentrations below *ca.* 25% solids, and non-Newtonian above. Analysis of the data demonstrates the absence of either a yield point at low shearing stresses or a limiting viscosity at high, ruling out Bingham body behavior. The linearity of logarithmic plots of the data indicates the applicability of the exponential flow equation of Farrow, Lowe, and Neale for the conversion of experimental observables to rate of shear-shearing stress values. However, above *ca.* 45% solids, separate exponential flow equations must be used at high and low shearing stresses.

A composite rate of shear-shearing stress plot, including values obtained from three capillaries and the concentric cylinder viscometer, yields a single smooth curve, confirming the validity of the conversion procedure. Comparison of values of the two constants of the exponential equation, as determined independently using the capillary and concentric cylinder instruments, shows agreement between the two types of viscometer.

Similar results have been observed for other latices, both synthetic and natural.

REFERENCES

1. LIVINGSTON, H. K., *Ind. Eng. Chem.* **39**, 550 (1947).
2. BINGHAM, E. C., *Fluidity and Plasticity*, McGraw-Hill, New York, 1920.
3. JORDAN, H., BRASS, P., AND ROE, C., *Ind. Eng. Chem.* **9**, 182 (1937); *ibid.* **11**, 377 (1939).
4. WINDING, C. C., KRANICH, W. L., AND BAUMANN, G. P., *Chem. Eng. Progress* **43**, 527, 613 (1947).
5. BUCKINGHAM, E., *Am. Soc. Testing Materials, Proc.* **21**, 1154 (1921).
6. PORTER, A. W., AND RAO, P. A. M., *Trans. Faraday Soc.* **23**, 311 (1927).
7. FARROW, F., LOWE, G., AND NEALE, S., *J. Textile Inst.* **19**, T18 (1928).
8. REINER, M., AND RIWLIN, R., *Kolloid-Z.* **43**, 1 (1927).
9. MOONEY, M., AND EWART, R. H., *J. Applied Phys.* **5**, 350 (1934).

STUDIES IN POLYELECTROLYTES. II. GUM ARABATE

Sadhan Basu, Pares Ch. Dasgupta and Anil K. Sircar

Indian Association for Cultivation of Science, Lady Willingdon Road, Calcutta 32, India

Received May 17, 1951

INTRODUCTION

Natural arabic gum is a mixture of potassium, magnesium, and calcium salts of a high-polymeric acid, which may be liberated by treatment with mineral acids. Gum arabic purified by repeated precipitation from water with alcohol has an equivalent weight of 1000–1200 and a molecular weight of about 240,000 (1). On hydrolysis it yields a mixture of galactose, arabinose, rhamnose, and as high as 28% of an aldobionic acid which has been proved to be L-galacturonic acid 6-galactose (2,3). Very little is known as to the nature of the chemical union between these groups in the molecule of arabic gum. A ring formula suggested by Norman (4) has been rejected on the basis of various physicochemical considerations. Strain double refraction of a thread of arabic gum showed that the molecules are elongated and most probably linear; but the x-ray examination of the thread revealed no fiber diagram. A reconciliation between these two structures has been proposed and it has been suggested that the constituent units in a gum arabic molecule are arranged in a chain, but the chains are not very regular and therefore cannot fit into a well-ordered lattice owing to side-branching (5).

An indirect way of deciding the chain-like character or otherwise of the gum arabic molecule, is to study the folding-unfolding phenomenon of such a molecule in solution. The folding-unfolding phenomenon in a high-molecular-weight compound may be strikingly demonstrated by simple physicochemical measurements if the compound can be converted into a soluble, ionizable compound; that is to say, into a polyelectrolyte, as suggested by Fuoss (6).

THEORETICAL

By the term polyelectrolyte is meant a high-molecular-weight compound which contains a number of ionizable groups distributed along the polymer chain. Polyelectrolytes, unlike their analogs the simple electrolytes, on the one hand, and neutral polymers on the other, show some characteristic behavior in solution, e.g., viscosity, conductivity, osmotic pressure, etc. These peculiar behaviors of the polyelectrolytes arise, according to

Fuoss, due to the presence of high charge densities on the polymer chain in dilute solution and flexibility of the polymer chain. If the degree of ionization of the polyelectrolyte chain is decreased by any factor, say by an increase of concentration or by adding a suitable electrolyte, the average distance between the charge centers in the polymer chain increases; consequently the coulombic repulsion between the charge centers decreases and the polymer chain coils up. Fuoss (6) studied a number of synthetic polyelectrolytes and interpreted their peculiar behaviors by his folding-chain theory. Katchalsky (7), by mathematical analysis, also interpreted the polyelectrolytic behavior in the same light. It has emerged from these investigations that the folding-chain theory of Fuoss (6) is almost the only explanation for the peculiar viscometric and other behavior of polyelectrolytes, and neither in neutral polymers nor in colloidal electrolytes could such peculiarities be detected.

It has been shown that arabic gum disperses to molecular units in solution and the colloidal character of the solution is associated with the colloidal dimension of the molecule itself (8). If in the gum arabic molecule the constituent units are arranged in a chain with the carboxyl group of the uronic acid distributed along the chain, the sodium salt of the acid in dilute solution will behave as a polyelectrolyte. With this end in view, the present investigation was undertaken, the results of which are summarized in the present paper.

EXPERIMENTAL

Preparation of the Gum Arabic Acid

The arabic gum supplied by Messrs. Bengal Chemical & Pharmaceutical Works, Calcutta, was dissolved in water, filtered, and precipitated with alcohol. The process was repeated three times. The purified gum was then dissolved in water and brought to pH 2.5 by adding the requisite quantities of hydrochloric acid, kept at that pH for 24 hr., and then dialyzed till the dialyzate had an ash content of only about 0.05%. The acid was titrated electrometrically using a glass electrode in conjunction with a model G Beckman pH-meter. The equivalent weight was found to be 1208, a result, in good agreement with the recorded data in the literature, which is in the range of 1000–1200 (1).

Preparation of Sodium Salt of Arabic Acid

A solution of arabic acid was neutralized with sodium hydroxide solution, the sodium salt precipitated out of the solution with alcohol, redissolved in water, and dialyzed for 4 hr. against distilled water in order to remove any adhering alkali. The concentration of the solution was determined by evaporating and vacuum drying a portion of the solution. Ash estimation of the gum arabate corresponded to sodium calculated

from the equivalent weight of the acid. The solution had a pH of 6.8, and was used as such, or with dilution wherever necessary, in all subsequent measurements. The solution remained unchanged, i.e., without any hydrolysis, for more than 15 days.

Measurement of Viscosity

The viscosity measurements were done with two Ostwald viscometers having flow times of 230.7 sec. and 324.7 sec., respectively, with water at a temperature of $35 \pm 0.1^\circ\text{C}$. The specific and relative viscosities were calculated from the following equations:

$$\begin{aligned}\text{relative viscosity} &= \frac{\eta}{\eta_0} = \frac{\rho_1 t_1}{\rho t} \\ \text{specific viscosity} &= \eta_{sp} = \eta/\eta_0 - 1\end{aligned}$$

where η and η_0 are the viscosities, ρ_1 and ρ the densities and t_1 , and t the time of efflux (in seconds) for the solution and solvent, respectively. In the range of dilute solutions used, the difference in densities of the solution and water was insignificant and no density measurements were taken.

RESULTS

The results of reduced viscosity (η_{sp}/c , where c is the concentration in g./100 cc.) measurements at different concentrations of gum arabate are summarized in Table I and the corresponding η_{sp}/c versus c curves are given in Fig. 1.

TABLE I

Change in Reduced Viscosity with Concentration of Gum Arabate

Concentration g./100 cc. water	η_{sp}/c
1.3140	1.1640
0.8760	1.1760
0.5840	1.2630
0.3893	1.3640
0.2595	1.4810
0.1730	1.6160
0.1153	1.7870
0.0577	1.9670

It is evident from Table I and Fig. 1 that η_{sp}/c rises as the concentration of gum arabate is reduced.

The measurements of reduced viscosity of gum arabate solutions were done at various constant sodium chloride concentrations, the results of which are given in Table II and the corresponding η_{sp}/c versus c curves are drawn in Fig. 1.

It becomes evident from Table II that the viscosity of gum arabate solution is lowered by the addition of NaCl, the lowering increasing with

increasing concentration of NaCl. The curves at three NaCl concentrations, viz., 11.518×10^{-5} , 17.277×10^{-5} , and 28.795×10^{-5} g.-equiv./l., show well-defined maxima at nearly equivalent concentrations of gum arabates, i.e., 12.62×10^{-5} , 18.32×10^{-5} , and 29.403×10^{-5} equiv./l., respectively. At higher NaCl concentrations, e.g., 17.852×10^{-4} and 46.647×10^{-4} , the η_{sp}/c versus c curves are similar to those of neutral polymers.

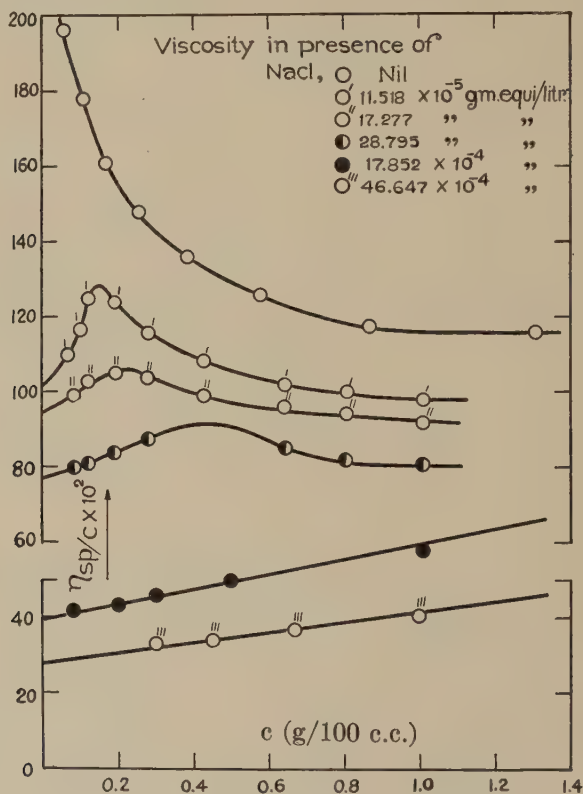


Fig. 1. Reduced viscosity versus concentration.

Viscosity measurements were extended to different solutions of gum arabate neutralized to different extents. The results are summarized in Table III, and the corresponding η_{sp}/c versus α (extent of neutralization) curves are given in Fig. 2.

Calculation of the extents of neutralization were done in the following way: when to a 10 cc. solution of arabic acid (2.628%) 2.65 cc. of 0.0819 N NaOH was added, the acid was completely neutralized, as obtained from a potentiometric titration curve. The resulting solution was then taken as 100% neutralized. Therefore, when to 10 cc. each of the same

TABLE II

Viscosity-Concentration Effect in Presence of NaCl

Concentration of gum arabate g./100 cc.	Concentration of NaCl g. equiv./l.	η_{sp}/c
1.0146	11.518×10^{-5}	0.9802
0.8117		1.0040
0.6494		1.0260
0.4329		1.0890
0.2886		1.1640
0.1924		1.2310
0.1283		1.2530
0.1015		1.1760
0.0676		1.1040
1.0146	17.277×10^{-5}	0.9270
0.8117		0.9452
0.6494		0.9614
0.4329		0.9933
0.2886		1.0390
0.1924		1.0520
0.1283		1.0360
0.0885		0.9891
1.0146	28.795×10^{-5}	0.8143
0.8117		0.8268
0.6494		0.8506
0.2886		0.8722
0.1924		0.8476
0.1283		0.8130
0.0855		0.8096
1.0146	17.852×10^{-4}	0.5805
0.4504		0.5012
0.3006		0.4668
0.2004		0.4321
0.0891		0.4238
1.0146	46.647×10^{-4}	0.4058
0.6764		0.3734
0.4509		0.3474
0.3006		0.3303

arabic acid solution, 0.4, 0.8, and 2.2 cc., etc., of 0.0819 *N* NaOH were added the solutions were neutralized to the extent of 15.10, 30.19, and 83.03% etc., respectively.

Finally the relative viscosity of a solution was measured at constant concentration of gum arabate with increasing pH, the pH increment being obtained by the addition of a few drops of alkali to a large volume of the gum arabate solution such that practically no variation in the concentration appeared. At first the viscosity fall with pH was small while above about 9 pH the fall was much more rapid. When again the pH of this

final solution was reversed and gradually brought back to the initial pH value by the addition of acid (viz., 6.8), there was no rise in viscosity, which remained practically constant from 11 to 6.8 pH. When this final solution was dialyzed, the viscosity gradually increased with time, till at last nearly the original value was regained. All these points are well illustrated in Fig. 3.

TABLE III
Viscosity Variation with the Extent of Neutralization

Concentration of gum acid %	Per cent neutralized	η_{sp}/c
1.3140	100.00	1.164
	93.09	1.223
	83.03	1.141
	72.97	1.094
	50.31	0.908
	30.19	0.748
	15.10	0.615
	0.00	0.518
0.6570	100.00	1.229
	93.09	1.342
	83.03	1.295
	72.97	1.249
	50.31	1.049
	30.19	0.871
	15.10	0.719
	0.00	0.613
0.3285	100.00	1.406
	93.09	1.483
	83.03	1.588
	72.97	1.444
	50.31	1.246
	30.19	1.053
	15.10	0.864
	0.00	0.735

DISCUSSION

It has been found that the η_{sp}/c versus c plot (Fig. 1) of sodium arabate solution increased sharply with dilution, which evidently indicates some increase in the hydrodynamic volume unit. This phenomenon may reasonably be explained from the consideration of the folding-unfolding properties of the high-polymeric chain compounds. At a finite concentration of the gum arabate in solution some of the sodium ions dissociated from one molecule, and are drawn back by another molecule, so that on a time average, a polyion always has some amount of oppositely charged ions closely associated with it. As the solution is diluted, i.e., as the concentration of

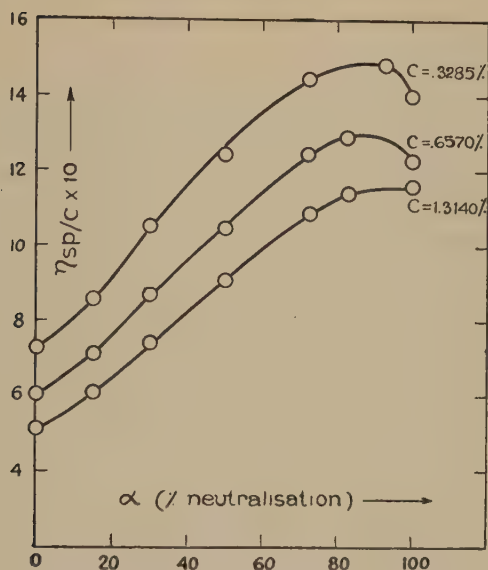


FIG. 2. Reduced viscosity versus per cent neutralization.

the gum arabate is reduced, the probability of a polyion finding an oppositely charged ion near its vicinity diminishes, and as a result the effective charge on the polyion increases with dilution. Repulsion between similarly charged centers on the gum arabate chain causes the molecule to extend which evidently increases with an increase in the dissociation of the gum arabate molecule, i.e., the extension of the chain increases with dilution.

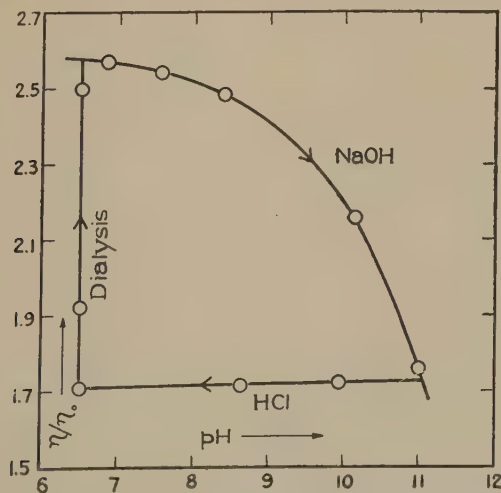


FIG. 3. Relative viscosity versus pH.

This explains the rapid rise in viscosity of a gum arabate solution at lower concentrations.

Various η_{sp}/c versus c curves for gum arabate solution in the presence of different amount of NaCl are also given in Fig. 1. It has been found that by the addition of 11.518×10^{-5} g. equiv. NaCl/l. the sharp rise in the η_{sp}/c versus c curve vanishes, the curve showing a well-defined maximum which appears when the stoichiometric concentration of the Na ion from the polymer becomes nearly equal to that from the added NaCl. With increasing NaCl concentration, the maximum shifts toward higher values of sodium arabate concentration till at last it vanishes completely and the curves resemble those of the neutral polymer. This type of peculiar viscosity behavior has been noticed in the case of a large number of polyelectrolytes, e.g., polyacrylic acid (11), pneumococcus polysaccharides (9), sodium pectinates (10), and a number of polyvinyl pyridonium derivatives (6), and fits with the general behavior of polyelectrolytes.

There is another important characteristic of a solution of gum arabic acid which can also be explained by the folding-chain theory. As the acid is neutralized, the reduced viscosity of the solution increases. This is evident from the curves in Fig. 2. As the acid is neutralized with sodium hydroxide, more and more sodium salt of the acid dissociates, the effective charge on the polymer goes up, and, hence, the reduced viscosity increases. Nearabout the point of complete neutralization, the η_{sp}/c value decreases although slowly. This fall in η_{sp}/c value has been explained by Katchalsky and Kuhn (7) as due to a high charge density on the polymer chain and an increased concentration of oppositely charged sodium ions. This viscosity behavior is exactly the opposite of what happens to, and is expected of, a weakly acidic colloidal electrolyte.

The viscosity of the gum arabate solution (even of a dilute solution) changes markedly with pH. It will be evident from Fig. 3 that at pH 9.5, obtained by adding few drops of alkali to the gum arabate solution, the viscosity of the 1.05% solution of sodium gum arabate falls sharply. When the pH is reversed from 11 to 6.8 by neutralizing the alkali with acid, the curve is not retraced and the viscosity remains nearly constant, showing a slight fall with diminishing pH. If, after bringing the pH back to the original value with acid, the solution be dialyzed, the viscosity gradually rises with time and the original viscosity is nearly recovered after about 8–10 hr.

If this effect be due simply to pH, then there is no reason why the viscosity behavior should depend on the mode of pH variation. Further this pH effect cannot be due to breakdown of micellar units since in dilute solution gum arabate is dispersed to molecular units. It has been shown by Tendeloo (12) and also by us (Table II and Fig. 1) that a similar fall in viscosity takes place when, instead of sodium hydroxide, an increasing

amount of sodium chloride solution is added step by step to the gum arabate solution. Thus if the fall in viscosity in the presence of NaOH be attributed to the presence of sodium ion, then the explanation of the above phenomenon will follow simply from the folding-chain theory of polyelectrolytes. When the pH is reversed from 11 to 6.8 by the addition of successive quantities of HCl, the NaOH present is simply neutralized to NaCl. There is no change in Na ion concentration and hence the viscosity of the solution remains unaltered because the coiling of the chain remains constant. But when this solution is dialyzed, the sodium salt present in the system passes out, and as a result the viscosity increases owing to an increased extension of the polymer chain.

It is evident, therefore, that all the peculiar viscometric characteristics of the gum arabate solution may satisfactorily be explained by the folding-chain theory of polyelectrolytes which presupposes the existence of flexible chain molecules in solution. As the chain is irregular due to side branching, the coiling up of the molecules cannot proceed to a great extent, and consequently the relative rise in viscosity on dilution is much less in the case of gum arabic as compared to other polyelectrolytes recorded in the literature (6,10).

ACKNOWLEDGMENT

Thanks are due to Prof. S. R. Palit, Indian Association for the Cultivation of Science, for his keen interest, helpful suggestions, and constant encouragement during the course of these investigations.

SUMMARY

Measurements of viscosity with varying concentration of solute, added sodium chloride, and the extent of neutralization of the solutions of gum arabate and arabic acid have been reported. A connected explanation for all the different observations has been formulated by the assumption of the existence of flexible chain molecules in solutions of gum arabate. From the same considerations the effect of pH variation with alkali on the relative viscosity of gum arabate solution has been attributed to the effect of sodium ion from alkali rather than the particular pH value.

REFERENCES

1. OAKLEY, H. B., *Trans. Faraday Soc.* **31**, 136 (1935).
2. HEIDELBERGER, M., AND KENDALL, F. E., *J. Biol. Chem.* **84**, 639 (1929).
3. CHALLINOR, S. W., HAWORTH, W. N., AND HISST, E. A., *J. Chem. Soc.* **1931**, 258.
4. NORMAN, A. G., *The Biochemistry of Cellulose, the Polyuronides, Lignin, etc.*, p. 125. Oxford Press, London, 1937.
5. MEYER, K. H., *Natural and Synthetic High Polymers*, Vol. IV, p. 375. Interscience Publishers Inc., New York.
6. FUOSS, R. M., *Science* **108**, 545 (1948); *J. Polymer. Sci.* **3**, 246, 602 (1948); *ibid.* **4**, 97 (1949).

7. KATCHALSKY, A., KUHN, W., AND KUNZLE, O. *Helv. Chem. Acta*, **31**, 1994 (1948).
8. HARTLEY, G. S., *Quarterly Rev. Chem. Soc.* **2**, 152 (1948).
9. HEIDELBERGER, M., AND KENDALL, F. E., *J. Biol. Chem.* **95**, 127 (1932).
10. PALS, D. T. F., AND HERMANS, J. J., *J. Polymer Sci.* **3**, 897 (1948).
11. STAUDINGER, H., *Die hochmolekularen Organischen Verbindungen*, Part II D. Springer, Berlin, 1932.
12. TENDELOO, H. J. C., *Rec. trav. chim.* **48**, 23 (1929).

THE EFFECT OF SURFACE CONDITIONS ON THE ELECTROPHORESIS OF SOLID PARTICLES

F. Booth

*Department of Theoretical Physics, Wheatstone Laboratory,
King's College, Strand, W.C. 2, London, England*

Received May 11, 1951

1. INTRODUCTION

In this paper we shall examine theoretically how the existing theory of the electrophoresis of solid spherical particles is modified if adequate account is taken of the electrical boundary conditions at the solid-liquid interface. The basic theory of the electrophoresis of solids is due to Henry (1). In this analysis it was assumed that the surface charge density on the solid boundary (apart from the small change which arises from the difference in conductivity of solid and electrolyte) retained during electrophoresis its value when the particle was stationary. Later work has extended the Henry theory in various ways, for example by taking into account relaxation effects in the surrounding electrolyte (2), or the "inertia terms" in the equations of motion of the solution (3). In all these treatments however, assumptions similar to those made in Ref. (1) are made about the surface charge. In fact, of course, it is unlikely that the surface charge density does remain strictly unaltered, since it is not a fixed intrinsic property of the surface, but must be regarded as due to some form of chemical equilibrium between the surface layer of the solid and the electrolyte in which the particle is immersed. Thus it is well known that the total charge carried by colloidal particles is conditioned by the ionic composition of the solution in which they are immersed, and in many cases even the sign of the charge may be reversed by suitable manipulation of the ionic concentrations. Hence the charge density at any point on the surface must be a function of the composition of electrolyte in its neighborhood. Now there is no reason for supposing that in electrophoresis the ionic concentrations at various positions near the surface are not modified by the applied field and the fluid motion. Hence it is not strictly legitimate to assume that there is, of necessity, no variation in the total charge or the local surface charge density in the electrophoretic process, even though the ordinary ionic composition at points far from the particle remains unchanged. Under these conditions it does not follow, without further examination, that the usual theory is still valid.

In the next section it will be shown that, provided the electrophoretic velocity is proportional to the applied field, the results of Henry's theory are still valid *whatever the electrical boundary conditions at the surface*, if the particle is nonconducting. The third section of the paper deals briefly with the case of *conducting* particles; it is shown in this case that the same general conclusion cannot be drawn, but no detailed quantitative theory is put forward. The results of the more general theories (2), in which terms of the order of the square and higher powers of the zeta potential are included, may on the other hand be affected by the surface conditions even for nonconducting particles. Unfortunately the analysis of these terms is extremely complicated, but it is hoped to carry out an investigation in a later paper.

2. ELECTROPHORESIS OF NONCONDUCTING PARTICLES

We shall use spherical polar coordinates (r, θ, α) , fixed with respect to the center of the spherical particle, which is taken to be of radius a . The θ axis is taken along the direction of the applied field, E . When there is no external field and no fluid motion, the conditions are those of statistical equilibrium and the potential, ψ_1 , in the neighborhood of the particle will have spherical symmetry. Application of the external field will modify both the pressure and potential distributions even when the particle has settled down to steady motion. Let p and ϕ denote the changes in the pressure and potential brought about by the field when the steady velocity of translation is U . If the electrophoretic velocity U is proportional to the strength of the applied field, then we may take p , ϕ , and \mathbf{v} , the fluid velocity, to be proportional to the field strength. This follows since the equations determining the motion are linear in these quantities; any other terms of order E^2 must have a negligible effect. The assumption that U is proportional to E is almost universally true in the usual experimental arrangements, and it simplifies the analysis enormously.

The equations to determine p and \mathbf{v} in terms of ϕ are

$$\eta \operatorname{curl}^2 \mathbf{v} + \operatorname{grad} p = \frac{\epsilon}{4\pi} \left[\frac{d\psi_1}{dr} \nabla^2 \phi + \nabla^2 \psi_1 \operatorname{grad} \phi \right], \quad [2.1]$$

and

$$\operatorname{div} \mathbf{v} = 0. \quad [2.2]$$

Equation [2.1] follows easily from the equation of motion of the electrolyte. η and ϵ are the coefficient of viscosity and the dielectric constant, respectively, of the solvent; they are both assumed to be uniform throughout the liquid. Equation [2.2] follows from the equation of continuity since the liquid may be regarded as incompressible. The solution of Eqs. [2.1] and [2.2] can be obtained by expanding ϕ and p in a series

of spherical harmonics, $P_n(\mu)$ where μ equals $\cos \theta$.

$$\phi = E \sum_{n=0}^{\infty} \phi_n(r) P_n(\mu), \quad [2.3]$$

$$p = E \sum_{n=0}^{\infty} p_n(r) P_n(\mu), \quad [2.4]$$

where ϕ_n and p_n are functions of r only. Provided the ϕ_n are known, both p and \mathbf{v} are easily calculated by the following method. First, taking the divergence of Eq. [2.1] eliminates \mathbf{v} , giving an equation for p ; for p_n we find

$$\Delta_n p_n = \frac{\epsilon}{4\pi} \left[\frac{d\psi_1}{dr} \frac{d(\Delta_n \phi_n)}{dr} + \frac{d(\Delta_0 \psi_1)}{dr} \frac{d\phi_n}{dr} + 2\Delta_0 \psi_1 \Delta_n \phi_n \right], \quad [2.5]$$

where

$$\Delta_n = \frac{d^2}{dr^2} + \frac{2}{r} \frac{d}{dr} - \frac{n(n+1)}{r^2}. \quad [2.6]$$

The solution of this equation is

$$p_n = A_n r^n + B_n r^{-n-1} + I_n(r), \quad [2.7]$$

where I_n denotes the particular integral of the equation, and A_n and B_n are constants of integration. Next, the curl of Eq. [2.1] eliminates p and leaves an equation for curl \mathbf{v} . The solution is obtained by taking an expansion for the α component of curl \mathbf{v} in the form

$$\text{curl}_\alpha \mathbf{v} = E \sin \theta \sum_{n=1}^{\infty} w_n(r) P_n'(\mu), \quad [2.8]$$

where $P_n'(\mu)$ equals $dP_n(\mu)/d\mu$, and assuming that the other two components vanish. Finally, if we take solutions for the components of \mathbf{v} of the form

$$\left. \begin{aligned} v_r &= E \sum_{n=1}^{\infty} v_{r,n}(r) P_n(\mu), \\ v_\theta &= E \sin \theta \sum_{n=1}^{\infty} v_{\theta,n}(r) P_n'(\mu), \\ v_\alpha &= 0, \end{aligned} \right\} \quad [2.9]$$

where the $v_{r,n}$ and $v_{\theta,n}$ are functions of r only, equations [2.2] and [2.8] give the following equations for the $v_{r,n}$ and $v_{\theta,n}$ functions;

$$\left. \begin{aligned} \Delta_n(r v_{r,n}) &= n(n+1) w_n, \\ \Delta_n(r v_{\theta,n}) &= \frac{1}{r^2} \frac{d(r^3 w_n)}{dr}. \end{aligned} \right\} \quad [2.10]$$

These are both of the same type as Eq. [2.5] and have similar solutions. The various arbitrary constants which occur in the expressions for p , v_r and v_θ are fixed by the boundary condition that \mathbf{v} must be zero at the surface of the particle and also that p and \mathbf{v} must remain finite at infinity.

The detailed solution is quite straightforward, but we have only sketched the method since we shall eventually require only the functions p_1 , $v_{r,1}$ and $v_{\theta,1}$. It is necessary however to demonstrate, as we have just done, that the relevant quantities, namely, p_n , $v_{r,n}$ and $v_{\theta,n}$, have the particular analytical form indicated by Eqs. [2.4] and [2.9]. For the case of n equal to 1, we find

$$\left. \begin{aligned} v_{r,1} &= \frac{U}{E} \left[-1 + \frac{3a}{2r} - \frac{a^3}{2r^3} \right] + \frac{\epsilon}{12\pi\eta} \left[\left(\frac{3a}{r} - \frac{a^3}{r^3} \right) \right. \\ &\quad \times \left. \int_a^\infty \xi(r) dr - 2 \int_r^\infty \xi(r) dr - \frac{2}{r^3} \int_a^r r^3 \xi(r) dr \right], \\ v_{\theta,1} &= \frac{U}{E} \left[1 - \frac{3a}{4r} - \frac{a^3}{4r^3} \right] - \frac{\epsilon}{12\pi\eta} \left[\left(\frac{3a}{2r} + \frac{a^3}{2r^3} \right) \right. \\ &\quad \times \left. \int_a^\infty \xi(r) dr - 2 \int_r^\infty \xi(r) dr + \frac{1}{r^3} \int_a^r r^3 \xi(r) dr \right], \end{aligned} \right\} \quad [2.11]$$

$$\left. \begin{aligned} p_1 &= \frac{3\eta a U}{2r^2 E} + \frac{\epsilon}{12\pi} \left[\frac{3}{r^2} \int_a^\infty \xi(r) dr + \int_r^\infty \left(2\Delta_1 \phi_1(z) \cdot \Delta_1 \psi_1(z) \right. \right. \\ &\quad \left. \left. + \frac{d\psi_1(z)}{dz} \frac{d(\Delta_1 \phi_1(z))}{dz} + \frac{d\phi_1(z)}{dz} \frac{d(\Delta_0 \psi_1(z))}{dz} \right) \left(\frac{z^3}{r^2} - r \right) dz \right], \end{aligned} \right\} \quad [2.12]$$

where

$$\xi(r) = \frac{1}{3} \int_r^\infty \left[\frac{d\psi_1(z)}{dz} \cdot \Delta_1 \phi_1(z) - \phi_1(z) \frac{d(\Delta_0 \psi_1(z))}{dz} \right] \left(\frac{z^2}{r^2} - \frac{r}{z} \right) dz. \quad [2.13]$$

Further details of the derivation of Eqs. [2.11] and [2.12] may be obtained by reference to an earlier paper by the writer [Ref. (2b), sec. 6], where a very similar problem is discussed.

To find the electrophoretic velocity it is now necessary to evaluate the forces on the sphere due to the electrical stresses and viscous fluid stresses over the surface. The purely electrical force is determined entirely by ϕ , but the fluid stresses depend on the value chosen for U in Eq. [2.11]; the electrophoretic velocity is simply the value which just causes the two forces to counterbalance. The total force due to the fluid stresses over the surface is

$$F_s = 2\pi a^2 \int_0^\pi \left[\left(-p_a + 2\eta \frac{\partial v_r}{\partial r} \Big|_a \right) \cos \theta \sin \theta - \eta \frac{\partial v_\theta}{\partial r} \Big|_a \sin^2 \theta \right] d\theta. \quad [2.14]$$

Substituting expressions [2.4] and [2.9] for p and the components of \mathbf{v} ,

we find

$$F_s = \frac{4\pi a^2 E}{3} \left[2\eta \left(\frac{dv_{r,1}}{dr} \Big|_a - \frac{dv_{\theta,1}}{dr} \Big|_a \right) - p_1(a) \right]. \quad [2.15]$$

All the contributions from the p_n , $v_{r,n}$, and $v_{\theta,n}$, apart from the functions with n equal to 1, vanish by virtue of the integral properties of the Legendre polynomials.

The total electrical force on the sphere F_e is easily calculated from the potential ϕ by means of the Maxwell stress tensor.

$$F_e = \frac{\epsilon a^2}{4} \int_0^\pi \left[\left(\frac{\partial(\psi_1 + \phi)}{\partial r} \Big|_a \right)^2 - \frac{1}{a^2} \left(\frac{\partial\phi}{\partial\theta} \Big|_a \right)^2 \right] \cos\theta \\ - \frac{2}{a} \frac{\partial\phi}{\partial\theta} \Big|_a \frac{\partial(\psi_1 + \phi)}{\partial r} \Big|_a \sin\theta \Big] \sin\theta d\theta. \quad [2.16]$$

Carrying through the integrations over the θ coordinate, we finally get

$$F_e = \frac{E\epsilon a^2}{3} \frac{d\psi_1}{dr} \Big|_a \left[\phi_1'(a) + \frac{2}{a} \phi_1(a) \right]. \quad [2.17]$$

The condition that the sum of F_s and F_e must vanish gives for U

$$U = - \frac{\epsilon E}{6\pi\eta} \int_a^\infty \xi(r) dr. \quad [2.18]$$

This formula shows that to determine the electrophoretic velocity we now only require the potentials ψ_1 and ϕ_1 .

The calculation of ψ_1 has been made in previous papers [for example, Ref. (2b), sec. 3], and so we shall merely quote the results. The potential may be expanded in a power series of the charge on the sphere or of the potential at the surface ζ . To the degree of approximation we will require, only the *first* term of either series is needed; hence we may write

$$\psi_1 = \frac{a\zeta}{r} \exp - \kappa(r - a), \quad [2.19]$$

where

$$\kappa^2 = \frac{4\pi e^2 \sum_{i=1}^s n_i z_i^2}{\epsilon k T}, \quad [2.20]$$

n_i is the concentration of ions of type i at infinity and z_i their valency.

Now consider the function ϕ_1 ; this must be deduced from the equations of continuity and of motion of the ions. If s_i denotes the difference between the ionic concentration of the i ions at any point fixed with respect to the sphere, when the external field is applied and when it is not, two equations connecting the s_i and ϕ are obtained. We shall not give here the details of the calculation or the results since these have already been set out in an earlier paper [Ref. (4), Eqs. (5.3) and (5.4)].

To eliminate the s_i between the two equations we expand them in the form

$$s_i = E \sum_{\nu=0}^{\infty} \sum_{n=0}^{\infty} e^{2\nu-1}(\epsilon a)^{-\nu}(\mathbf{k}T)^{1-\nu} Q^{\nu} \gamma_{i,\nu,n}(r) P_n(\mu), \quad [2.21]$$

where Qe is the charge on the particle; also it is convenient to expand $\phi_1(r)$ in powers of Q .

$$\phi_1(r) = \sum_{\nu=0}^{\infty} e^{2\nu-1}(\epsilon a)^{-\nu}(\mathbf{k}T)^{1-\nu} Q^{\nu} \phi_{1,\nu}(r). \quad [2.22]$$

Substituting [2.21] and [2.22] in Eqs. (5.3) and (5.4) of Ref. (4) and equating coefficients of like powers of Q , we get a series of equations for the successive functions $\phi_{1,0}$, $\phi_{1,1}$, and so on. However, we require U correct to the *first* power only of ζ or Q and so it will only be necessary to examine the first terms of the series [2.21] and [2.22]. The equations connecting the $\gamma_{i,0,1}$ and $\phi_{1,0}$ are

$$\Delta_1(\mathbf{k}T\gamma_{i,0,1} + n_i e z_i \phi_{1,0}) = 0 \quad i = 1, \dots, s, \quad [2.23]$$

$$\Delta_1 \phi_{1,0} = - \frac{4\pi e}{\epsilon} \sum_{i=1}^s z_i \gamma_{i,0,1}. \quad [2.24]$$

Integrating Eq. [2.23],

$$\mathbf{k}T\gamma_{i,0,1} + n_i e z_i \phi_{1,0} = \alpha_i r + \beta_i r^{-2}, \quad [2.25]$$

where α_i and β_i are constants. At infinity we have

$$\phi_{1,0} = -r, \quad \gamma_{i,0,1} = 0. \quad [2.26]$$

Also since the particle is nonconducting, the normal component of the mean velocity of each ion must vanish at the interface.

$$\mathbf{k}T \frac{d\gamma_{i,0,1}}{dr} \Big|_a + n_i e z_i \frac{d\phi_{1,0}}{dr} \Big|_a = 0 \quad [2.27]$$

Hence

$$\alpha_i = -n_i e z_i, \quad \beta_i = -n_i e z_i a^3/2. \quad [2.28]$$

Combining Eqs. [2.25], [2.24], and [2.28], we find

$$(\Delta_1 - \kappa^2)\phi_{1,0} = \kappa^2 \left(r + \frac{a^3}{2r^2} \right). \quad [2.29]$$

Substituting Eq. [2.29] in Eq. [2.18], and using Eq. [2.19] we finally obtain

$$U = \frac{E\epsilon\zeta}{6\pi\eta} \left[1 + \frac{1}{16} b^2 - \frac{5}{48} b^3 - \frac{1}{96} b^4 + \frac{1}{96} b^5 \right. \\ \left. + \frac{1}{8} b^4 E_i(b) \left(1 - \frac{1}{12} b^2 \right) \right], \quad [2.30]$$

where b equals κa . Thus it is seen that Henry's theory is still valid for nonconducting particles at any rate, although no special assumptions are made about the surface charge.¹

3. ELECTROPHORESIS OF CONDUCTING PARTICLES

In this case it is clear that formula [2.30] will, in general, no longer be valid. This follows since the boundary condition embodied in Eq. [2.27] is no longer necessarily true, and hence the right-hand side of Eq. [2.29] will be modified. The only cases of conducting particles of practical interest are those of metallic particles. Since for these the current in the metal is carried by electrons, whereas in the electrolyte it is conveyed by ions, it follows that some form of charge transfer involving neutralization of ions must occur at the solid-liquid interface. Evidently, the boundary condition which must replace Eq. [2.27] must depend very closely on the nature of the chemical changes accompanying the transfer of charge from electrolyte to metal and vice versa. In view of this, any simple extension of the analysis of the preceding paragraph to cover the case of conducting particles seems out of the question unless various further a priori assumptions are made; we shall therefore not develop any detailed quantitative theory.

Even for metallic particles, however, it is likely that the analysis of sec. 2 will apply in many cases. This follows since metals often seem to behave effectively as nonconductors in electrophoresis. Thus the mobilities of colloidal metal particles are usually of the same order of magnitude as those of nonconducting particles. If Henry's theory applied strictly, the mobilities would be extremely small since the conductivity of metals is high compared with that of electrolytes. The absence of conduction may be due to a thin layer of nonconducting material between the metal and the electrolyte, or, as various writers have pointed out (1, 5, 6), a consequence of polarization effects at the metal-solution interface. For cases in which transfer of charge involves evolution of gas, the metal will behave as an insulator, unless the overvoltage for the particular transfer reaction in question happens to be extremely small. This follows since the maximum difference in potential between metal and electrolyte must be of the order Ea ; for the usual experimental arrangements, this will be a very small potential. If the field is sufficiently strong and the overvoltage sufficiently small to cause appreciable charge transfer, the evolution of gas will of course completely upset the fluid motion round the sphere, and the method we have used breaks down completely.

The only case for which the theory we have outlined does not apply

¹ In formula [2.30] we have corrected a mistake in the second equation on p. 124 of Henry's paper.

would seem to be that of a metallic particle immersed in an electrolyte containing a salt of the metal. Owing to the absence of the overvoltage effect, easy transfer of charge could occur by deposition of metal on one side of the particle and its removal from the other. Owing to the high conductivity of the metal, it is to be expected that Henry's theory for the case of conducting particles would be quite adequate. Some confirmation of this is furnished by the observation due to Henry (1) that fine silver fibers immersed in a solution of silver nitrate give a very small electrophoretic effect.

SUMMARY

A generalized form of Henry's theory of the electrophoresis of spherical particles is developed. It is shown that, provided the electrophoretic velocity U is proportional to the strength of the applied field, a simple perfectly general formula for U in terms of the potential in the neighborhood of the particle, can be given.

Using this formula, it is shown that for *nonconducting* particles, the same result as that due to Henry is obtained, without the need of any special assumptions as to how the charge on the surface is affected in electrophoresis. It is pointed out that the special assumption made by Henry will not in general be true. Hence the present analysis shows that a possibly serious defect of the usual theory is in fact of no importance.

For conducting particles no corresponding result can be given, and the problem is discussed qualitatively. In the case of metallic particles, unless the overvoltage effect at the metal-liquid interface is very small or nonexistent, the particles will behave as if they were nonconducting.

REFERENCES

1. HENRY, D. C., *Proc. Roy. Soc. (London)* **A133**, 106 (1931).
2. (a) OVERBEEK, J. TH. G., *Kolloid-Beihfte* **54**, 287 (1943). (b) BOOTH, F., *Proc. Roy. Soc. (London)* **A203**, 514 (1950).
3. BOOTH, F., *J. Chem. Phys.* **18**, 1361 (1950).
4. BOOTH, F., *Proc. Roy. Soc. (London)* **A203**, 534 (1950).
5. BULL, H. B., AND SÖLLNER, K., *Kolloid-Z.* **60**, 263 (1932).
6. FRUMKIN, J., *J. Colloid Sci.* **1**, 277 (1946).

THE ELECTROCHEMISTRY OF PERMSELECTIVE MEMBRANES.
III. THE ELECTRICAL RESISTANCE OF PERMSELECTIVE
COLLODION MEMBRANES IN SOLUTIONS
OF VARIOUS ELECTROLYTES¹

Karl Sollner² and Harry P. Gregor³

*Department of Physiology, University of Minnesota, Minneapolis, Minnesota; and the
Laboratory of Physical Biology, National Institute of Arthritis and Metabolic
Diseases, National Institutes of Health, Public Health Service,
Federal Security Agency, Bethesda, Maryland*

Received September 24, 1951

Two preceding papers dealt with the rates of establishment of final, stable concentration potentials across several types of permselective collodion membranes (1), and with these potentials themselves (2). The present communication furnishes an analogous general survey of the electrical resistance of the same types of permselective collodion membranes.

A. THE TIME REQUIRED FOR THE ESTABLISHMENT OF THE FINAL, STABLE
ELECTRICAL RESISTANCE OF PERMSELECTIVE
COLLODION MEMBRANES

I

This section presents experimental data on the time required for the establishment of the final, stable electrical resistance across several types of permselective collodion membranes in solutions of various electrolytes at three different concentration levels. These rate studies can be expected to give some information of pertinence in the elucidation of the geometrical and electrical structure of the membranes. More important, they are a necessary basis of the meaningful physicochemical investigation of these membranes and of their use as physicochemical tools, as membrane electrodes (3-6), for the study of Donnan equilibria (4,6-9), and as parts of membrane model systems (6,10).

The studies on the rates of the establishment of final, stable resistances can be carried out under two experimental conditions (1). First, a mem-

¹ Based on a portion of a thesis submitted by Harry P. Gregor to the Graduate School of the University of Minnesota, 1945, in partial fulfillment of the requirements for the Ph.D. degree.

² Present address: Laboratory of Physical Biology, National Institute of Arthritis and Metabolic Diseases, National Institutes of Health, Bethesda 14, Maryland.

³ Present address: Polytechnic Institute of Brooklyn, Brooklyn, New York.

brane having its fixed ionizable groups compensated for electrically with critical ions of one type, e.g., hydrogen ions, is brought in contact with a solution having some other critical ion. Or the membrane is immersed in a solution which has the same species of cations as are carried by the dissociable groups of the membrane. The former case was investigated experimentally; the results obtained there also give information relative to the other problem. As the initial standard condition of the membranes, the acidic state was chosen, hydrogen ions being the counter ions of the fixed surface groups (1).

II

The membranes were prepared according to the previously described method (11). Under carefully controlled conditions of temperature, speed, etc., highly porous three-layer collodion membranes are cast on the outside of rotating test tubes and oxidized in 1 *M* sodium hydroxide for specified periods (8–14 min.). The membranes are dried in air of controlled relative humidity while they are still on the tubes; after removal from the latter, they are mounted on glass rings. These membranes, which are about 30 μ thick, are now ready for use. In certain instances they may be subjected to slight swelling by immersion in alcohol (11). The designation of the various types of permselective collodion membranes used here follows the previously established usage (11), e.g., a membrane designated Ox 10 Hum 43 Alc 65 is oxidized for 10 min., dried at 43% relative humidity, and swelled in 65% alcohol.

As in the case of the rate studies on the concentration potential, membrane Ox 8 Hum 43 was selected as an example of a membrane which shows maximum characteristic concentration potential, high bi-ionic potential (B.I.P.), and relatively high resistance; membrane Ox 12 Hum 43 was taken because it combines maximum characteristic concentration potential with medium B.I.P. and low resistance, thus being for many purposes the most useful type of membrane. As an example of alcohol-swollen membranes the type Ox 10 Hum 43 Alc 65 was used, having a high, although not maximum, characteristic concentration potential, a low B.I.P., and very low resistance. The latter type of membrane is of considerable interest and usefulness when dealing with electrolytes having bi- or polyvalent anions.

In order to assure that relatively small differences in the behavior of different electrolytes may not be overshadowed by minor differences between different membrane specimens of the same type, all experiments on the time effect reported for one type of membrane were performed with the same membrane specimen. The membranes were aged by about 3 days' immersion in 0.1 *N* potassium chloride solutions (1).

The membranes were brought to the acidic state by prolonged washing with repeatedly changed double-distilled water or by acid treatment and

washing (1). This reconversion of the membranes to the standard acidic state was repeated prior to each transfer to a new solution.

The apparatus and techniques used for the resistance measurements were the same as those described in a preceding communication. The electrode system consisted of two test tube-shaped platinum electrodes between which the bag-shaped membranes having effective areas of about 50 cm.² were mounted. The data presented in this section are expressed in ohms/100 cm.², as was done previously (11). Resistances of 10 ohms (Ω) and greater are accurate within ± 3 to $\pm 5\%$; values below 10 Ω have a probable error of $\pm 0.5 \Omega$.

Table I summarizes the resistances as a function of time for three types of permselective membranes with three concentrations of potassium chloride, lithium chloride, and potassium sulfate.

III

In view of the limited accuracy of the measurements presented in Table I it is not possible to ascertain accurately when equilibrium between the membrane and the surrounding solution is established. The data, however, show that the periods of time in which the final, stable electrical resistances are established vary from about 15 min. to many hours. There is some indication that equilibration is reached somewhat faster with membranes of relatively high porosity. A large noncritical ion does not seem to retard the establishment of the equilibrium to a significant extent. A large critical ion, however, seems to slow down equilibration. The concentration of the solution in contact with the membrane seems to be of small significance.

The differences found between different electrolytes with the same membrane, and between the various membranes with the same electrolyte are less pronounced than those observed in the case of the establishment of final, stable concentration potentials (1).

These results in themselves seem to be of indifferent interest only; nevertheless, they may assume considerable significance in a future attempt to clarify in detail the geometrical and electrical structure of permselective membranes.

One fact, however, is of considerable and immediate importance. The periods of time required to establish the equilibrium resistances are considerably greater than those previously reported for the establishment of stable, well-defined concentration potentials across the same types of membranes in the same electrolytes (1). Final, stable concentration potentials apparently are attained before the slow leak of "nonexchange electrolyte" into the pores of the membrane structure has brought about a stable, stationary state. The potential-determining mechanism is virtually established long before the whole pore system of the membrane, which is

TABLE I

The Time Required for the Establishment of the Final, Stable Electrical Resistance of Various Permselective Collodion Membranes in Solutions of Different Electrolytes at Several Concentration Levels
($t = 25.0 \pm 0.1^\circ\text{C.}$)

Membrane Conc. of solution, equiv./l. Time	Ox 8 Hum 43			Ox 12 Hum 43			Ox 10 Hum 43 Alc 65		
	0.001	0.01	0.1	0.001	0.01	0.1	0.001	0.01	0.1
KCl									
$\Omega/100 \text{ cm.}^2$									
min.									
5	40.8	—	17.4	23.5	7.1	2.9	18.5	3.7	1.5
15	40.3	15.5	15.0	22.5	5.5	2.7	18.5	3.4	1.0
30	38.3	14.0	11.2	23.5	5.3	2.4	18.3	3.3	0.7
60	38.3	13.9	9.6	23.3	5.0	2.2	18.8	3.2	0.5
120	38.0	13.9	9.3	23.0	5.1	2.2	18.8	3.2	0.6
180	38.0	14.0	9.4	23.3	5.0	2.2	18.8	3.2	0.6
240	38.5	14.1	9.3	23.3	5.0	2.2	18.8	3.2	0.5
360	38.0	14.0	9.4	23.5	5.0	2.1	18.5	3.1	0.5
LiCl									
$\Omega/100 \text{ cm.}^2$									
min.									
5	72.1	64.3	37.8	35.5	20.3	7.8	25.8	9.7	3.0
15	71.8	67.7	32.4	36.3	28.0	6.3	24.5	9.1	2.5
30	71.3	68.0	32.3	35.3	21.5	6.0	24.0	8.8	2.4
60	71.5	65.8	31.1	33.0	18.8	5.9	24.5	10.1	2.4
120	71.5	64.3	29.2	33.5	17.9	5.6	24.8	9.5	2.4
180	71.3	67.5	28.0	35.3	18.6	5.4	24.8	8.6	2.5
240	71.8	65.8	27.3	35.3	18.0	5.3	24.5	9.0	2.3
360	71.8	65.8	27.0	35.0	18.3	5.4	24.5	8.9	2.4
1260	—	—	25.9	—	—	5.3	—	—	2.3
K ₂ SO ₄									
$\Omega/100 \text{ cm.}^2$									
min.									
5	43.0	32.4	14.3	29.2	7.9	3.0	24.2	4.6	1.1
15	40.8	28.2	13.2	28.8	6.9	2.6	24.2	3.7	1.0
30	40.8	25.9	12.5	27.3	5.9	2.5	23.7	3.1	1.0
60	40.0	25.3	11.2	26.9	6.0	2.6	23.3	3.3	1.0
120	40.1	25.2	11.1	27.1	5.8	2.5	23.3	3.3	1.0
180	40.3	25.1	11.2	27.3	6.1	2.5	23.4	3.2	1.0
240	40.3	23.3	11.3	27.3	6.0	2.5	23.5	3.2	1.0
360	40.5	25.3	11.3	27.3	6.0	2.5	23.3	3.2	1.0

different from the *functional* membrane (8), is equilibrated with the adjacent solutions. True equilibration between membrane and solution is obviously much slower than seemed to be indicated by the prior studies on the rate of the establishment of the concentration potential. Therefore, when these membranes are used for physicochemical purposes it is

necessary to allow for the longer adaptation periods which are indicated by resistance measurements.

With regard to the question of the rates of the establishment of the equilibrium resistances in the case of membranes which previously have undergone ion exchange with the critical species of ions under consideration, the following conclusion can be drawn from the data of Table I. Since the resistances of the membranes vary greatly with the concentration of the outside solutions, a prior saturation of the dissociable wall groups with the critical ions cannot be expected to accelerate significantly the rates of the establishment of the final, stable membrane resistance. This situation is opposite to that found in the case of the concentration potential, where prior saturation with the critical ion greatly accelerates the establishment of final, stable potentials; adaptation periods of more than 2 or 3 min. in this latter case are rare (1). From the practical, experimental point of view this means that in order to establish final, stable membrane resistances it is always necessary to equilibrate the membranes for considerable periods of time with the solution or solutions under investigation.

B. THE EQUILIBRIUM RESISTANCE OF PERMSELECTIVE COLLODION MEMBRANES IN SOLUTIONS OF VARIOUS ELECTROLYTES

I

This section deals with the final, stable electrical resistances of permselective collodion membranes equilibrated with solutions of various electrolytes at three different concentration levels.

The literature contains only scanty data on the resistance of membranes of high ionic selectivity. The most important paper is a study by Green, Weech, and Michaelis on "dried" collodion membranes of very high resistance (12). Further, one might mention experiments with potassium chloride only, by Manegold and Solf (13) and by Meyer and Bernfeld (14), some data by Gregor on various electrolytes (4,6), and a preliminary paper by Schmid in which an attempt is made to deduce rational formulas for the membrane resistance from considerations based on the Teorell, Meyer-Sievers fixed-charge theory of electrochemical membrane behavior (15). Mention also should be made of the investigations on the conductance of ion-exchange resins, particularly a paper by Heymann and O'Donnell which, though undertaken from an entirely different point of view, is of considerable interest here (16). This work will be referred to in the subsequent paper (17). It must suffice to mention only the very interesting impedance studies on synthetic membranes by Goldman and by Albrink and Fuoss, since their central objective is considerably different from ours (18,19).

In a systematic study of the electrochemistry of membranes the question arises as to the terms in which membrane resistances are expressed

most appropriately. From a formal, purely abstract point of view one might be inclined to choose the specific conductance (conductivity) or its reciprocal, the specific resistance (resistivity). There are, however, some objections to this. The first is that the primary experimental data are obtained in terms of resistances per unit area of membrane. The conversion of these data into specific resistances could be truly meaningful only if the inherently highly improbable assumption could be justified that the electrochemical and geometrical structure of the membranes is homogeneous throughout their thickness (20). Moreover, the thickness of many natural and of many thin artificial membranes can be determined only with a very limited degree of accuracy; any error in the thickness of a membrane would make for a correspondingly large error in its calculated specific resistance. Formally, of course, the (hypothetical) specific resistance, ρ , is related to the empirical resistance per unit area, $^*\rho$, by the equation:

$$\rho = \frac{^*\rho}{d} \quad [1]$$

where d is the thickness in centimeters of the membrane (which is of the order of 0.003 cm. in the case of three-layer permselective collodion membranes).

The second objection to the use of the specific resistance in the description of membranes lies in the fact that this unit which refers to the "centimeter cube" is not appropriate in the consideration of the *functional* electrochemistry of membranes, that is, in the study of the *electrochemistry of membranes as membranes* [see, however, (29)]. That property of membranes which determines the rate at which ionic processes occur across them is their resistance or conductance per unit area.⁴ In this case membranes of different thickness become directly comparable with respect to one of their fundamental electrical properties, namely, the rates at which ionic processes (with a given critical ion) occur across them.

The experimental data reported here were obtained as ohms per membrane of about 50 cm.² effective area (measured accurately in each instance), from which the resistances/cm.² can be readily computed. Since there is no particular advantage in presenting the resistance data in the form of their reciprocals, namely as conductances per unit area, they will be reported here as resistances in ohms/cm.², $^*\rho$.⁵

⁴ The permeability through membranes of electrolytes and nonelectrolytes alike is conventionally measured per unit area of membrane.

⁵ The symbol for the unit area resistance, $^*\rho$, was not used in connection with the data on the time required to establish final, stable resistances, which are presented in Table I, because $^*\rho$ is meant to refer only to final, stable unit area resistances under well-defined, stable conditions. These conditions may be either a true equilibrium if a membrane is immersed in a single solution, or a stationary state with the membrane separating two solutions of different but constant concentration from each other.

II

Data on the equilibrium resistances, $\ast\rho$, of four types of permselective membranes in solutions of six electrolytes are given in Table II. The experiments on one type of membrane were performed with a single membrane specimen in order to ensure a strict comparability of the data. The accuracy of the data in Table II can be estimated to be about $\pm 3\%$ with

TABLE II

The Unit Area Resistances, $\ast\rho$, of Various Permselective Collodion Membranes in Equilibrium with Solutions of Several Electrolytes
($t = 25.0 \pm 0.1^\circ\text{C}.$)

1	2	3	4	5	6	7	8	9
Solution			Unit area resistance					
Electro- lyte, x	Concen- tration, c	Specific resist- ance, ρ_s	$\frac{\rho_s}{t_+}$	$\ast\rho_{cx}$ Ox 8 Hum 43	$\ast\rho_{cx}$ Ox 12 Hum 43	$\ast\rho_{cx}$ Ox 14 Hum 43	$\ast\rho_{cx}$ Ox 14 Hum 43 Ale 50	$\ast\rho_{cx}$ Ox 8 Hum 43 Ox 14 Hum 43 Ale 50 $\ast\rho_{cx}$
	equiv./l.	Ω	Ω	$\Omega/\text{cm.}^2$ ratio	$\Omega/\text{cm.}^2$ ratio	$\Omega/\text{cm.}^2$ ratio	$\Omega/\text{cm.}^2$ ratio	
KCl	0.001	6780	13850	3850 (2.3)	1760(?)	2060	1160	3.3
	0.01	693	1410	1680 (1.6)	480	360	300	5.6
	0.1	78	159	1080	230	90	80	18
K ₂ SO ₄	0.001	6820	14200	6130 (2.3)	3260	2270	1250	4.9
	0.01	746	1550	2680 (2.0)	610	390	320	8.4
	0.1	91	186	1310	240	80	70	19
K ₃ Citr.	0.001	7300		8950 (2.6)	3980	2380	1380	6.5
	0.01	844		3460 (2.1)	490	450	330	10
	0.1	107		1670	200	170	110	15
LiCl	0.001	8760	22000	12630 (2.1)	5130	2890	2090	6.0
	0.01	935	2830	6030 (1.6)	1100	530	400	15
	0.1	105	332	3680	630	240	150	25
MgCl ₂	0.001	7870	20200	44880 (1.5)	21610	4730	4380	10
	0.01	862	2240	30270 (1.3)	14840	2690	1940	16
	0.1	99	280	22460	9610	1950	1020	22
HCl	0.001	2380	2880	6820 (2.6)	2120	1070	870	7.8
	0.01	243	296	2670 (2.1)	510	410	180	15
	0.1	25	31	1300	250	120	50	26

membranes of a unit area resistance of 1000 ohms and higher; values below 1000 ohms have a probable error of not more than ± 30 ohms.

In Table II, col. 1 names the electrolytes with which the membranes are equilibrated; col. 2 gives the concentration of the various solutions; col. 3 shows the specific resistance, ρ_s , of the latter; col. 4 gives the specific resistance of the solutions, ρ_s , divided by the transference number of its cation, t_+ , in other words the reciprocal of that part of the specific conductivity of the solution which is due to the cation; cols. 5 to 8 present the unit area resistance, $\ast\rho$, in ohms/cm.² of membrane, the ratios of each

two adjacent figures pertaining to different concentrations of the same electrolyte being added in parentheses. Column 9 gives the ratio of the unit area resistances of two different membranes equilibrated with solutions of the same electrolytes at the same concentrations.

III

The data of Table II, although limited in scope, show what range of resistances can be expected with permselective collodion membranes, prepared according to the previously described methods (11).

There was a time interval of about 8 months between the preparation of the membranes used for the equilibrium resistance measurements of Table II and of those used in the rate studies of Table I. It will be noted that the resistance values for equilibrium conditions which are given in Table II deviate considerably in several instances from the corresponding values of Table I. These differences can be taken as an indication of the differences which exist between membranes prepared under the same nominal conditions but at different times and from different batches of the same commercial brand of collodion. Membranes which are cast simultaneously from the same collodion solution show a very much better agreement in their resistance, though significant differences even in this case cannot be avoided completely.

There is, of course, not much difficulty in the preparation of membranes of higher resistance—all our past efforts having been made in the direction of low-resistance membranes. There is but little doubt that membranes might be prepared by essentially the same methods which would combine still lower resistances with a very high degree of ionic selectivity, at least in the lower range of electrolyte concentrations.

The experimental data of Table II can be considered from several specific angles according to the various variables.

The first of the *three simplest approaches* to the evaluation of the data consists of a comparison of the resistances of the *different* types of *membranes* equilibrated with solutions of the *same electrolytes* at the *same concentrations*. It shows that with all the 18 solutions used (6 electrolytes at 3 concentrations) the resistance of the different membranes decreases (with one doubtful exception) in the sequence: Ox 8 Hum 43, Ox 12 Hum 43, Ox 14 Hum 58, and Ox 14 Hum 43 Alc 50. The differences between the resistances of the various membranes are the greater, the higher the concentration of the solutions with which they are equilibrated. This is shown in a quantitative manner in col. 9 which, as an example, gives the ratios of the unit area resistances of the two extremes in porosity of the 4 types of membranes, $\frac{* \rho_{cz} \text{ Ox 8 Hum 43}}{* \rho_{cz} \text{ Ox 14 Hum 43 Alc 50}}$. Table II thus confirms on a broader scale the conclusion drawn previously (2) from limited data—on 0.1 *N*

KCl only—concerning the relative permeabilities of the various types of permselective collodion membranes, which also had to be anticipated from the differences in their methods of preparation.

Another simple approach to the evaluation of the data of Table II consists of a comparison of the resistance of the *same membranes* equilibrated with solutions of *different concentrations* of the *same electrolytes*. It shows that in the case of all four types of membranes the resistance is the greater the more dilute are the solutions of the six investigated electrolytes. The variation in the unit area resistance of the membranes with varying concentrations of the solutions is not nearly as great as the variation in the specific resistance of the latter, ρ_s , as can be seen from a comparison of col. 3 of Table II with the $\ast\rho$ values of cols. 5 to 8 or with the corresponding ratio figures in parentheses. The comparison of the resistance of the membranes with the specific resistance of the outside solution divided by the transference number (in free solution) of the critical species of ions, $\frac{\rho_s}{t_+}$ (col. 4), might actually be slightly more pertinent since the conductance of the membranes is due to a large extent to the critical ions, the cations in the case at hand.

The third of the straightforward approaches to the evaluation of the data of Table II consists of a comparison of the resistance of the *same membranes* in equilibrium with solutions of the *same concentration* (normality) of *different electrolytes*; it shows the following:

With the two more porous membranes, Ox 14 Hum 58 and Ox 14 Hum 43 Alc 50, the resistances, $\ast\rho$, of the membranes in contact with solutions of the same normality of the potassium chloride, sulfate, and citrate are approximately the same, independent of the nature of the anion. With the two more dense membranes, Ox 8 Hum 43 and Ox 12 Hum 43, there exists a considerable difference—the smaller the anion (and the lower its valence) the lower the resistance; with these latter two membranes the nature of the noncritical ions is of considerable influence.

With lithium chloride the resistances, $\ast\rho$, are with all membranes and at all concentrations appreciably higher than with potassium chloride. With the two more porous membranes the ratio of the resistances of the membranes equilibrated with potassium chloride and with lithium chloride solutions is nearly the same as the ratio of the reciprocal of the ionic diffusion coefficients of K^+ and Li^+

$$\frac{1}{D_{K^+}} : \frac{1}{D_{Li^+}} \approx 1:2.$$

In other words, the ratio of the membrane resistances is nearly the same as that of the corresponding values ρ_s/t_+ of col. 4. With the two less porous membranes the resistance with lithium chloride is considerably larger than corresponds to this ratio.

With MgCl_2 solutions the membranes show a resistance several fold that observed with the univalent cations, the difference being greatest with the densest membranes.

The resistance of the membranes in contact with HCl is somewhat higher than with KCl in the case of the dense membranes, while in the case of the less dense membranes it is somewhat lower. These observations are distinctly different from those of Green, Weech, and Michaelis who found that the resistances of their "dried" collodion membranes when equilibrated with hydrochloric acid were lower by one order of magnitude and more than the resistances of the same membranes when saturated with alkali chlorides (12). This difference in behavior between the Michaelis type of membranes and the permselective collodion membranes is undoubtedly due to the much lower porosity of the former. All the available experimental evidence indicates that these membranes are so dense that a very large percentage of pathways across their thickness which are accessible to the hydrogen ions are inaccessible to the alkali ions; steric hindrance of the noncritical ion, in this case, is a predominant factor in the mechanism of membrane selectivity.⁶ In view of the change in electrochemical structure which oxidized collodion membranes undergo in strongly acid solution, a detailed discussion of the hydrochloric acid-equilibrated membranes might advantageously be suspended for the present.

Of the more complex relations which might be considered on the basis of the data presented in Table II we shall briefly mention only two.

The first is a comparison of the *concentration functions of the resistance of the same membranes equilibrated with solutions of different electrolytes*. It is based on a comparison of the ratios of the unit area resistances of the same membranes at different concentrations of the same electrolyte. These ratios are given in parentheses in cols. 5 to 8 of Table II. For the purpose on hand the four vertical rows of figures are considered. Their evaluation, in spite of their limited accuracy, shows with all four membranes a fair degree of uniformity of the concentration function with all electrolytes having a univalent critical ion. With magnesium chloride, there is much

⁶ That steric hindrance of the noncritical ion is a predominant factor in the mechanism of the ion selectivity of the Michaelis type of "dried" collodion membranes in contact with hydrochloric acid solutions, is evident from the following. Michaelis, Ellsworth, and Weech (21) have found that the concentration potential with hydrochloric acid is higher than with potassium or lithium chloride, a situation which is the reverse of that observed with the much less dense permselective collodion membranes (2). It is interesting to note that the "dried" collodion membranes of the Michaelis type at concentrations of hydrochloric acid greater than 0.02 *N* give concentration potentials which are higher than those across the permselective membranes (2,21). (In comparing the data of Michaelis *et al.* and of Sollner and Gregor, the reader should keep in mind that the former data are not corrected for the asymmetry of the liquid junction potential.)

less change in $*\rho$ with a change in the concentration of the outside solution than in the former cases; an exceptional position of the bivalent critical ion in this respect, too, becomes apparent.

The quantitative comparison of the *concentration functions of the resistance of different membranes equilibrated with solutions of the same electrolytes* is based on a comparison of the ratios of the unit area resistances of the same membranes at different concentrations of the same electrolytes. From an inspection of the experimental data and more precisely from a comparison (of the horizontal rows) of the ratio figures in parentheses, it is evident that the relative changes in membrane resistance with changes in the concentration of the adjacent solutions are the greater the more porous the membranes—the lower their resistance. With a hundred fold increase in the outside concentration, $*\rho$ decreases in the case of potassium chloride and membrane Ox 14 Hum 43 Alc 50 by a factor of nearly 20, whereas the same increase in solution concentration with magnesium chloride and membrane Ox 8 Hum 43 is accompanied only by a reduction in membrane resistance by a factor of 2. This observation might be also stated in a more general manner in the following way: The higher the porosity of the membranes the more the concentration function of $*\rho$ resembles that of the specific conductance, ρ_s , of the adjacent solutions. The smaller the porosity of a membrane (in terms of mean, effective pore diameter) the more will it approach the behavior of a solid electrolyte phase, the resistance of which is independent of the outside concentration. In this connection the membranes equilibrated with magnesium chloride solutions are particularly interesting; in this case the *effective* mean pore diameter can be assumed to be not much larger than corresponds to the size of the hydrated magnesium ion, numerous small pores which are accessible to alkali ions being inaccessible to it.

A discussion of the equilibrium unit area resistances, $*\rho$, from the point of view of the fixed charge theory is omitted here. It is postponed to the subsequent companion paper on the resistances of the electropositive permselective protamine collodion membranes where it will find its proper place after the presentation of the experimental data obtained with the protamine membranes (17).

IV

Originally, in 1946, it had been our plan to add to the papers on the concentration potential (1,2) and to the present paper on the ohmic resistance, a short paper on the bi-ionic potential (4). In view of the fact that considerable theoretical work on the bi-ionic potential was carried out in the meantime (22) and that a fairly comprehensive experimental study of this phenomenon is currently being carried out, it seems appropriate to conclude the present experimental study of the permselective

collodion membranes with a few critical remarks concerning certain shortcomings of these membranes and their possible improvement (6).⁷

The preparation of the permselective collodion membranes requires more skill, patience, and experience than seems desirable if they are to be widely used; also, their mechanical strength, while adequate, should be improved if possible. A more fundamental shortcoming of these membranes, however, lies in their inherent weak acid character. Their fixed dissociable groups are the carboxyl groups of "nitrocellulosic acid" which has hardly a greater acid strength than salicylic acid (25). This is bound to make the collodion membranes rather sensitive to changes of pH on the acid side of the neutral point where they lose a good part of their characteristic electrochemical properties. Membranes with acid groups of much greater acid strength, such as those of the sulfonic acids, would constitute a great improvement. Still more important would be an increase in the number per unit area of the potentially dissociable groups on the pore walls of the membrane structure. This would automatically result in membranes of a higher degree of ionic selectivity at higher concentration levels than is obtainable with the heretofore described permselective oxidized collodion membranes.

As these points became apparent in the course of the work in our laboratory, a search was made for materials other than collodion which might be suitable for our purpose. The obvious choice seemed to be the preparation of membranes from commercial ion exchangers provided the porosity of the material could be adequately adjusted. It was well known that ion exchangers in many instances carry potentially dissociable groups on their pore walls nearly as closely packed as is geometrically possible. However, the ion exchangers which were available commercially before and during the war did not lend themselves to the preparation of membranes. Several early attempts to secure suitable ion-exchange material from manufacturers failed.

Anyone attempting to produce new types of permselective membranes

⁷ The authors would like to point out that the data on concentration potentials in potassium chloride concentration chains in previous papers were presented in the conventional manner as measured with calomel electrodes and saturated potassium chloride agar bridges, without a correction for the asymmetry of the liquid junction potentials (which was properly taken into account in the case of all other electrolytes) (2,6,11,23,24, etc.). Thus the potential values given previously for the potassium chloride chains with a 2:1 concentration ratio should properly be reduced by 0.3 mv. in the case of the collodion membranes, and increased by 0.3 mv. in the case of the protamine collodion membranes. Likewise, the values of the "characteristic concentration potential" in the chains KCl 0.1 *N*/membranes/KCl 0.01 *N* are too high by 1.2 mv. with the negative collodion, and too low with the positive protamine collodion membranes. Accordingly, the deviation from ideality of the permselective collodion membranes is somewhat greater than previously assumed, that of the protamine membranes somewhat less.

from materials other than collodion will consider the experimental suggestions which are contained in the papers of Meyer and collaborators (14,26), but much development work might be necessary before membranes with the desired combination of properties can be produced.

During the last year several independent groups of investigators have announced the seemingly successful preparation of membranes of fairly low resistance and high ionic selectivity which in one way or another are based on the use of the conventional type of ion-exchange substances. An appraisal of these methods, however, will become possible only after experimental details are available (27-31).⁸ With the art of making "tailor-made" ion exchangers developing rapidly, there seems to be little doubt that membranes of highly desirable properties prepared from strong acid types of ion exchangers will be readily available in the near future. Such membranes might be destined ultimately to supersede, at least for many purposes, the weak acid type of permselective collodion membranes.

SUMMARY

1. A study was made of the time required in which final, stable electrical resistances are established with three electrolytes—potassium chloride, lithium chloride, potassium sulfate—across three types of permselective oxidized collodion membranes, being originally in the acidic state. These periods vary from 15 min. to many hours.

Equilibration is reached somewhat faster with membranes of higher porosity. A large noncritical ion does not seem to retard the establishment of the equilibrium to a significant extent. A large critical ion, however, seems to slow down equilibration. The concentration of the solution in contact with the membrane seems to be of little significance.

The establishment of final, stable resistances requires much longer periods than those necessary for reaching final, stable concentration potentials under comparable conditions.

2. The final, stable resistances of four types of permselective collodion membranes equilibrated with solutions of six electrolytes at three concentrations, 0.1, 0.01, and 0.001 *N*, were measured and tabulated. The data are evaluated as to the differences of the various types of membranes, the influence of the concentration on membrane resistance, and the influence of the nature of the electrolyte. A comparison is also made of the concentration function of the resistance of the same membranes equilibrated with solutions of different electrolytes; and of the concentration function of the resistance of different membranes with solutions of the same electrolytes.

3. Certain shortcomings of the permselective oxidized collodion mem-

⁸ The unit area resistances of these membranes seem to be of the same order of magnitude as those of the permselective oxidized collodion membranes described in this paper.

branes, their deficiency in mechanical strength, and mainly their weak acid character are discussed, and possible ways of improving them are indicated.

REFERENCES

1. SOLLNER, K., AND GREGOR, H. P., *J. Phys. Chem.* **50**, 470 (1946).
2. SOLLNER, K., AND GREGOR, H. P., *J. Phys. Chem.* **51**, 299 (1947).
3. SOLLNER, K., *J. Am. Chem. Soc.* **65**, 2260 (1943).
4. GREGOR, H. P., Ph.D. Thesis, University of Minnesota, 1945.
5. GREGOR, H. P., AND SOLLNER, K., in preparation.
6. SOLLNER, K., *J. Electrochem. Soc.* **97**, 139C (1950).
7. SOLLNER, K., AND GREGOR, H. P., *J. Am. Chem. Soc.* **67**, 346 (1945).
8. SOLLNER, K., *J. Phys. Chem.* **49**, 265 (1945).
9. SOLLNER, K., *J. Am. Chem. Soc.* **68**, 156 (1946).
10. NEIHOF, R., AND SOLLNER, K., *J. Phys. & Colloid Chem.* **54**, 157 (1950).
11. GREGOR, H. P., AND SOLLNER, K., *J. Phys. Chem.* **50**, 53 (1946).
12. GREEN, A. A., WEECH, A. A., AND MICHAELIS, L., *J. Gen. Physiol.* **12**, 473 (1929).
13. MANEGOLD, E., AND SOLF, K., *Kolloid-Z.* **55**, 273 (1931).
14. MEYER, K. H., AND BERNFELD, P., *Helv. Chim. Acta* **28**, 972 (1945).
15. SCHMID, G., *Z. Elektrochem.* **54**, 424 (1950).
16. HEYMAN, E., AND O'DONNELL, I. J., *J. Colloid Sci.*, **4**, 405 (1949).
17. SOLLNER, K., AND GREGOR, H. P., *J. Colloid Sci.* in press.
18. GOLDMAN, D. E., *J. Gen. Physiol.* **27**, 37 (1943).
19. ALBRINK, W. S., AND FUOSS, R. M., *J. Gen. Physiol.* **32**, 453 (1949).
20. SOLLNER, K., AND CARR, C. W., *J. Gen. Physiol.* **26**, 309 (1943).
21. MICHAELIS, L., ELLSWORTH, R. McL., AND WEECH, A. A., *J. Gen. Physiol.* **10**, 671 (1927).
22. SOLLNER, K., *J. Phys. & Colloid Chem.* **53**, 1211, 1226 (1949).
23. GREGOR, H. P., AND SOLLNER, K., *J. Phys. Chem.* **50**, 88 (1946).
24. SOLLNER, K., AND GREGOR, H. P., *J. Phys. & Colloid Chem.* **54**, 330 (1950).
25. SOLLNER, K., AND ANDERMAN, J., *J. Gen. Physiol.* **27**, 433 (1944).
26. MEYER, K. H., AND SIEVERS, J.-F., *Helv. Chim. Acta* **19**, 665 (1936).
27. WYLLIE, M. R. J., AND PATNODE, H. W., *J. Phys. & Colloid Chem.* **54**, 204 (1950).
28. NEIHOF, R., Ph.D., Thesis, University of Minnesota, 1950.
29. JUDA, W., AND McRAE, W. A., *J. Am. Chem. Soc.* **72**, 1044 (1950).
30. KRESSMAN, T. R. E., *Nature* **165**, 568 (1950).
31. SOLLNER, K., AND NEIHOF, R., *Arch. Biochem. Biophys.* **33**, 166 (1951).

HYDROPHOBIC FILMS ON SOLID SURFACES

George J. Kahan

Research Laboratory, Sprague Electric Company, North Adams, Massachusetts

Received March 12, 1951; revised October 26, 1951

INTRODUCTION

Interest in hydrophobic films and monolayers on solid surfaces has been shown in a number of publications (1-5). Metal finishers have known for a long time a type of film formation that is obtained by a technique somewhat different from those described in the literature. Metal that is dipped into a soap solution appears to be hydrophobic, i.e., it will shed water when the soap solution is rinsed off, while a clean metal surface will be perfectly wetted by water. This method of film formation has been used for many years in industry to expedite the drying of metal parts, and to give metal parts a temporary protective coating against corrosion.

EXPERIMENTAL TECHNIQUE AND MATERIALS

Essentially the dipper technique of Bigelow, Pickett, and Zisman (4) was used. The platinum dipper was made by attaching a piece of platinum wire to a platinum foil. Before each experiment it was fused with potassium pyrosulfate, rinsed in deionized water, and heated to red heat to insure a clean metal surface. Glass dippers were made by blowing small glass bulbs of Pyrex glass which were allowed to cool in a dust-free atmosphere.

The dippers were immersed in solutions of specified composition, and rinsed in a rinse tank with running deionized water. The conductivity of the deionized water was 10^{-5} ohm $^{-1}$ cm. $^{-1}$. The solutions were 0.1% in the active ingredients. The surface of the rinse tank was maintained clean by means of an overflow dam. The pH values of the solutions were adjusted by addition of 6 *N* KOH or 6 *N* HCl. The water, acid, and base were tested for purity by immersing the clean platinum dipper and rinsing it in deionized water. A perfectly wetted dipper was accepted as proof that the water, acid, and base were of adequate purity. Observation of nonwetting, i.e., of a definite contact angle of water on the dippers after immersion in solutions of specified composition and rinsing, was accepted as proof of film formation.

The potassium stearate used was prepared by neutralization of Mallinckrodt's stearic acid, U. S. P. XIII with reagent-grade potassium

hydroxide. The trisodium salt of ethylenediaminetetraacetic acid was obtained from Alrose Chemical Company. Cetyldiethylmethylammonium chloride, benzyldimethyloctadecylammonium bromide, and dimethylethyloctadecenylammonium bromide were obtained from Rhodes Chemical Company. Technical alkyl sulfate was obtained as Orvus from Procter and Gamble Co. Sodium alkyl aryl sulfonate was obtained as Nacconol NR from National Aniline Co.

All experiments were carried out at room temperature, with the exception of those with potassium stearate. In these experiments the temperature was raised to 40°C.

EXPERIMENTAL RESULTS

The clean platinum dipper was immersed in a 0.1% potassium stearate solution ($\text{pH} = 9.5$), withdrawn, and rinsed in running deionized water. Both water and stearate solution were kept at 40°C. The slightly elevated temperature was favored because potassium stearate was more soluble at this temperature. After being withdrawn from the rinse tank, the metal was not wetted by the water.

The foregoing experiment was repeated with a potassium stearate solution to which enough of the trisodium salt of ethylenediaminetetraacetic acid had been added to complex all the calcium that may have been present as a contaminant. The metal again showed film formation.

Similar experiments were carried out with cationic wetting agents. With cetyldiethylmethylammonium chloride ($\text{pH} = 6.5$) the platinum dipper was not wetted on rinsing, indicating film formation of the cationic wetting agent on the metal. Film formation on metals was also obtained with benzyldimethyloctadecylammonium bromide and dimethylethyloctadecenylammonium bromide.

The experiment with cetyldiethylmethylammonium chloride was extended over a wider pH range. The pH was varied from 1.5 to 11. Over the entire range, film formation was obtained on rinsing.

Another series of experiments was carried out with glass dippers and a potassium stearate solution ($\text{pH} = 9.5$). The glass was perfectly wetted, and showed no indication of film formation as in the case of a metal surface.

The foregoing experiment was extended over a wider pH range. The pH of the potassium stearate solution was varied from 7.5 to 10.0. Over the entire pH range the glass was perfectly wetted when withdrawn from the potassium stearate solution, and it remained perfectly wetted on rinsing, regardless of the pH of the potassium stearate solution.

A similar experiment with glass dippers and cetyldiethylmethylammonium chloride solutions ($\text{pH} = 6.5$), showed that the glass was not

wetted by the water on rinsing, showing definite film formation of the cationic wetting agent on the glass.

The foregoing experiment was extended over a wider pH range. The pH of the solution of this quaternary ammonium compound was varied from 1.5 to 11.0. Film formation on rinsing was observed over the whole range.

Film formation on glass could also be obtained with other cationic surface-active compounds, such as benzyldimethyloctadecylammonium bromide and dimethylethyloctadecylammonium bromide.

A similar test with Orvus (a technical sodium alkyl sulfate) and a platinum dipper gave a perfectly wetted platinum surface after rinsing in deionized water.

Nacconol NR, a technical sodium alkyl aryl sulfonate had the same effect on a platinum surface.

The metal dipper was immersed in a solution of stannous chloride which was slightly acidified, slightly oxidized, and colloidal in nature, rinsed in tap water (conductivity 3×10^{-4} ohm $^{-1}$ cm. $^{-1}$), immersed in a 0.1% potassium stearate solution, and rinsed again in tap water. The water wetted the metal surface perfectly.

The preceding experiment was repeated, using cetyldiethylmethylammonium chloride instead of potassium stearate solution. Again film formation was inhibited.

The same procedure was carried out using sodium metasilicate instead of stannous chloride; and again no film formation was obtained.

If a solution of barium chloride was substituted for the stannous chloride solution, film formation was observed. If the dipper was rinsed in deionized water instead of tap water after immersion in the colloidal solution, film formation was observed.

DISCUSSION

Under the experimental conditions of this investigation, film formation was obtained on metals with both cationic and anionic surface-active compounds; whereas on glass, film formation was obtained only with cationic wetting agents. This is understandable if one recalls that the glass surface offers mainly a surface of negatively charged oxygen atoms, the positively charged silicon atoms being located in the small spaces between oxygen atoms. Therefore only the positively charged cationic wetting agents can form films on this surface. The great mobility of the electron cloud in the metal allows the polar group of the organic molecules to attract or repel these electrons, and to set up image charges in the metal which will hold the film to the metal; this effect is independent of the sign of the charge. Bigelow, Pickett, and Zisman (4) observed film formation from solutions of *n*-eicosyl alcohol, primary *n*-octadecylamine,

and *n*-nonadecanoic acid in hexadecane on both Pyrex and platinum. No significant ionization can be expected in this nonpolar solvent; the polarity effects observed in our experiments with polar solvents were not found.

Blodgett's (1) films were obtained by lifting an insoluble film of metal stearates from a water through. Our experiment with a complexing agent added to the potassium stearate solution shows that under present experimental conditions the film formation was not due to an insoluble film of calcium stearate being lifted from the surface of the potassium stearate solution. In Blodgett's (1) and in Shafrin and Zisman's (5) experiments the slide emerged unwetted from the trough. In our experiments conditions were somewhat more complicated. The dipper is perfectly wetted when being withdrawn from the potassium stearate solution. Only after rinsing off the potassium stearate solution does the hydrophobic film become apparent.

It has generally been accepted that in alkaline solutions soap is micellar, the large micelles consisting of duplex lamellae of soap molecules, with the methyl groups of one layer directed toward the methyl groups of the second layer, and the polar groups extending toward the outside, i.e., toward the solution. The perfect wetting of the metal by the alkaline soap solution suggests that the adsorbed film in this medium is of the same duplex structure as suggested for the micelles. On rinsing, the second layer is removed whereupon the slide appears hydrophobic.

Several wetting agents have been used successfully for the cleaning of metals, and have found considerable use in industry for the preparation of metals for plating and painting. Foremost among them are alcohol sulfates and alkylaryl sulfonates. Like stearic acid, these compounds consist of a polar group and a long hydrocarbon chain. Their behavior, however, as shown by the experiments, is strikingly different. It is this property of leaving a metal surface perfectly wettable by water that makes these compounds valuable for technological applications.

It is a known fact that colloids will be adsorbed on clean metal surfaces. It has now been shown that certain adsorbed colloids prevent the formation of a film on a metal surface. It has also been shown that colloidal particles rather than ions are responsible for this inhibition effect. Significant is the fact that a certain electrolyte concentration in the rinse water was necessary to retain the colloid adsorbed on the metal surface. Rinsing in tap water left the colloid adsorbed on the metal surface. Rinsing in deionized water caused desorption of the colloid.

TECHNOLOGICAL APPLICATION

The inhibition of film formation after immersion in a potassium stearate solution and rinsing may be used as a test for the presence of certain adsorbed colloids on metal surfaces.

Such a test is of considerable interest and value to the metal-finishing and plating industry where the preparation of metal surfaces is of critical importance for the adhesion of metal deposits or paints. In metal-finishing operations the cleanliness of a surface and the efficiency of a cleaning cycle is usually judged by the appearance—the degree of wetting—of a surface. If a surface is without water breaks, it is usually considered clean. An adsorbed colloid, however, cannot be detected by water breaks. Considerable argument has taken place about the effect of adsorbed colloids on the adhesion of electroplated deposits. Since most metal cleaners contain sodium metasilicate, and since sodium metasilicate forms colloidal solutions, this question is of more than academic interest. The debate whether the presence of colloids in a metal cleaner is harmful or not, has not been settled because of the lack of a testing method for the presence of colloids on a metal surface. The aforementioned inhibition of film formation offers such a test, and the experiments also disclose a method to desorb colloids from a metal surface. While rinsing with tap water was inefficient, deionized water accomplished this desorption readily.

It must be pointed out that the effect discussed here is caused only by certain true colloids, and is not necessarily the same as the conditions described by George Hogaboom (6), where a silicate film is formed on the metal by acidification of incompletely rinsed-off silicate solution. The test described by Hogaboom (6) (application of an immersion copper deposit) is applicable to steel only, and covers a different, though industrially important, condition.

SUMMARY

Hydrophobic films are obtained from solution of wetting agents in aqueous solutions. Hydrophobic films are formed on metals regardless of the sign of the charge of the polar group, while only cationic wetting agents form films on glass.

The difference in the behavior of potassium stearate and sulfated or sulfonated wetting agents is shown with the dipper technique.

The inhibition of film formation by certain colloids is shown.

REFERENCES

1. BLODGETT, K. B., *J. Am. Chem. Soc.* **56**, 495 (1934).
2. BLODGETT, K. B., *J. Am. Chem. Soc.* **57**, 1007 (1935).
3. CLARK, G. L., STERRET, R. R., AND LEPLA, P. W., *J. Am. Chem. Soc.* **57**, 330 (1935).
4. BIGELOW, W. C., PICKETT, D. L., AND ZISMAN, W. A., *J. Colloid Sci.* **1**, 513 (1946).
5. SHAPRIN, E. G., AND ZISMAN, W. A., *J. Colloid Sci.* **4**, 571 (1949).
6. HOGABOOM, G. B., *Proc. Am. Electroplaters' Soc.* **35**, 215 (1948).

EFFECT OF MICELLE FORMATION ON THE ABSORPTION SPECTRA OF DECYL AND DODECYL PYRIDINIUM IODIDES¹

William D. Harkins,² Helen Krizek and M. L. Corrin³

From the Department of Chemistry, University of Chicago, Chicago, Illinois

Received August 2, 1951

INTRODUCTION

It has been shown (1,2) on the basis of transport number and conductance determinations that a large fraction of ions of opposite charge are so closely associated with the micelle of long-chain electrolytes that they move with it in an electric field. The color of aqueous solutions of cetyl pyridinium iodide has been cited (3) as additional evidence of such an association. It was pointed out that neither pyridinium ion nor iodide ion absorbs in the visible, while on the other hand solutions of the salt in a nonionizing solvent such as benzene are intensely yellow. The pale yellow color of the aqueous solutions therefore indicates that at least some of the iodine must be present in some other form than free ions. Hartley suggested (4) that a quantitative study of the light absorption in this case might provide an independent method of determining the extent of the association. Estimates from electrical properties are, in the present state of the theory of these electrolytes, highly uncertain.

We have, therefore, made a preliminary study of the absorption spectra of solutions of decyl and dodecyl pyridinium iodides. Our results show that the spectra are affected by the presence of micelles, as Hartley surmised, and can in fact be used to determine the critical micelle concentration of these salts. However, we find it impossible at this time to treat the effect quantitatively.

In the course of the work, the critical micelle concentrations in water for the same preparations of the two soaps were determined by the spectrophotometric method of Corrin, Kleven, and Harkins (5) and by dye solubilization. The results of these methods were in agreement with those based on the absorption spectra of these salts.

¹ This investigation was carried out under the sponsorship of the Reconstruction Finance Corporation, Office of Rubber Reserve, in connection with the Government's synthetic rubber program.

² Professor Harkins died March 7, 1951.

³ Present address: General Electric Research Laboratories, Schenectady, N. Y.

EXPERIMENTAL

A Beckman quartz spectrophotometer and 10-mm. quartz cells were used. The use of light paths of 0.47 and 0.99 mm., obtained by means of quartz inserts into the cells, extended the range of concentration which could be studied. Where duplicate determinations of regions of the spectrum above 2700 Å. were made by using two different light paths, the light absorption indicated with the shorter light path was almost invariably larger. Somewhat better agreement with Lambert's law was obtained, especially at low optical densities, by the use of filters; between about 2720 and 3050 Å. the purple Corex filter furnished with the instrument was used; above 3050 Å. a clear Corex filter was used. In all cases the values used were those for the longer light path. The discrepancy at concentrations where the 10-mm. light path could no longer be used was probably not more than 10%, based on the 10-mm. light path. The temperature was kept at an estimated $25 \pm 2^\circ\text{C}$.

The decyl and the dodecyl pyridinium iodides were prepared from the alkyl iodide (Halogen Chemicals and Columbia Organic Chemicals products, respectively) and pyridine. The salts were crystallized 5 to 6 times from a mixture of approximately 1 vol. of absolute ethanol to 6 vol. of absolute ether, and were dried *in vacuo* over potassium hydroxide. The resulting pale greenish-yellow solids were not appreciably hygroscopic.

The solvents used were of a high grade and were used without further purification. The benzene and absolute alcohol, therefore, probably contained traces of water; the chloroform contained 0.7% ethanol as a preservative. Further purification was not considered necessary to establish the character of the results.

The critical micelle concentration was determined by the spectrophotometric dye method with the use of Sky Blue FF (5,6). Dye solubilization experiments were done with Orange OT recrystallized from ethanol-water solution. The critical micelle concentration was determined from these by essentially the method of Kolthoff and Stricks (7).

RESULTS

In Fig. 1 are given absorption spectra of dodecyl pyridinium iodide at various concentrations in water. These are characterized by a maximum at 2580 Å., and, for the most dilute solutions, essentially zero absorption above 2800 Å. As concentration of the soap increases, a broad band appears in the region between 2800 and 4000 Å. as a step-out on the main absorption peak. This step-out remains apparently unchanged in 0.001 *M* thiosulfate, as can be seen from the curve for the 0.0229 *M* solution, and cannot therefore be ascribed to iodine as an impurity. The extension of this broad shoulder into the visible gives the most concentrated solutions of the soap a pale yellow color. No significant changes

were noted in the extinction at 2580 Å. up to a concentration of 0.0093 *M*. This concentration is near the upper limit where this maximum could be studied with our instrument.

In ethanol the soap shows a similar band in the 2800–4000-Å. region, but, as indicated by the two curves of Fig. 1, the effect of concentration is not nearly so pronounced as in the case of some of the water solutions. In chloroform the character of the spectrum changes, as indicated in

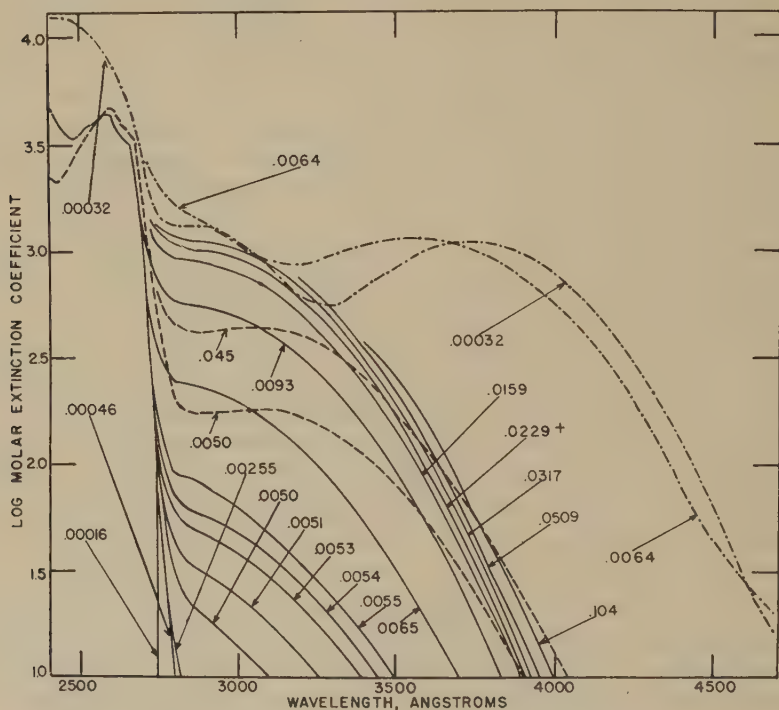


FIG. 1. Effect of concentration on the absorption spectra of dodecyl pyridinium iodide. solutions. ————— Water solutions. - - - - - Ethanol solutions. - · - · - Chloroform solutions.

+ Solution 0.001 *M* in sodium thiosulfate.

Fig. 1. There is a slight shift for the band at 2580 Å. toward lower wavelengths and a great intensification. A band appears in the region of 3600 Å. for the 0.00032 *M* solution. This shifts to lower wavelengths as concentration increases. A similar maximum in the 3600-Å. region was noted for benzene and acetone. In general the spectra for the ethanol and chloroform solutions and for the most dilute aqueous solutions agree with those given by Hantzsch (8,9) for methyl and ethyl pyridinium iodides. It may be noted, however, that for chloroform solutions the maximum observed

by us in the region of about 2900 Å. is not nearly as pronounced as that reported by him; and the effect of concentration in chloroform does not agree with the findings of Hantzsch.

The results for decyl pyridinium iodide are similar and are given in Fig. 2.

If for the aqueous solutions values of the molar extinction coefficient $\log I_0/I$, at 2900 Å. are plotted against molarity, as in Fig. 3, a sharp break occurs at 0.0050 *M* for the dodecyl pyridinium iodide, and at

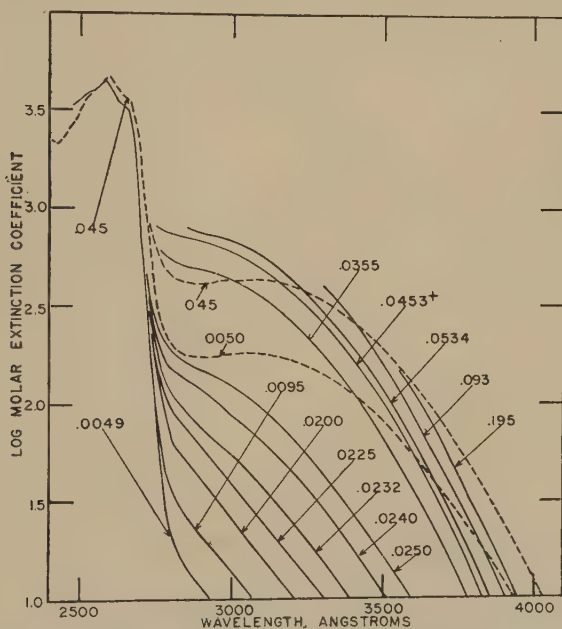


FIG. 2. Effect of concentration on the absorption spectra of decyl pyridinium iodide solutions. — Water solutions. - - - - - Ethanol solutions.

+ Solution 0.001 *M* in sodium thiosulfate.

0.0225 *M* for the decyl salt. The critical micelle concentration as determined with Sky Blue FF was 0.0050–0.0055 *M* for the dodecyl and 0.0220–0.0225 *M* for the decyl compound. By dye solubilization, the values were, for an estimated temperature of $23 \pm 4^\circ\text{C}$., 0.0056 and 0.024 *M*, respectively.

DISCUSSION

Application of the principle of mass action (10,11) has shown that an abrupt change of properties is to be expected when a number of long-chain ions aggregate to form micelles. Davies and Bury (12) found an abrupt change in partial specific volume of potassium octoate at a concentration

where freezing-point measurements indicated a change in the state of aggregation of the salt. The abrupt change in equivalent conductivity which is typical of colloidal electrolytes (13) has been interpreted (2,14) likewise on the basis of a change in aggregation (2,14,15,16). The abrupt change in the molecular extinction coefficient observed for the long-chain pyridinium iodides can be interpreted similarly.

The breaks in the curves of Fig. 1 at 0.0050 *M* for the dodecyl compound and 0.0225 *M* for the decyl compound may therefore be taken as the critical concentrations for the formation of micelles of these salts. Because of the type of plot used, the critical concentration appears as a

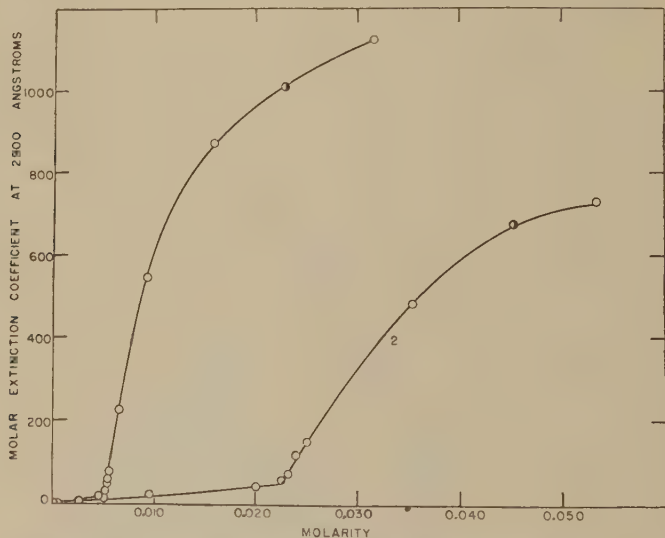


FIG. 3. Effect of concentration on the molar extinction coefficient at 2900 Å. for aqueous solutions of two long-chain alkyl pyridinium iodides. 1. Dodecyl pyridinium iodide. 2. Decyl pyridinium iodide. ● Solution 0.001 *M* in sodium thiosulfate.

unique point rather than as a more or less narrow range of concentrations. If, instead of $\frac{\log I_0/I}{\text{cm.} \times \text{molarity}}$, one plots $\frac{\log I_0/I}{\text{cm.}}$ there does appear a range where the slope of the curve does change rapidly. Our data are not sufficiently precise for an attempt to define this range.

Values for the critical micelle concentration as determined, respectively, by the spectral method, the spectrophotometric dye method, and by dye solubilization are 0.0050, 0.0050–0.0055, and 0.0056 *M* for dodecyl pyridinium iodide; for the decyl compound they are 0.0225, 0.0220–0.0225, and 0.024 *M*. The satisfactory agreement indicates that all these methods are determining substantially the same phenomenon.

The absorption spectrum, therefore, provides a new and independent method of determining the critical micelle concentration. It provides also an independent method for determining the effect of temperature and additives such as salts, alcohols, and hydrocarbons on the critical micelle concentration. The method has the advantage over methods using dyes in that it is self-indicating, and thus obviates addition of materials which may affect the critical micelle concentration.

It seems reasonable to ascribe the light absorption of these compounds in the region around 2900–3000 Å., in ethanol solutions and in aqueous

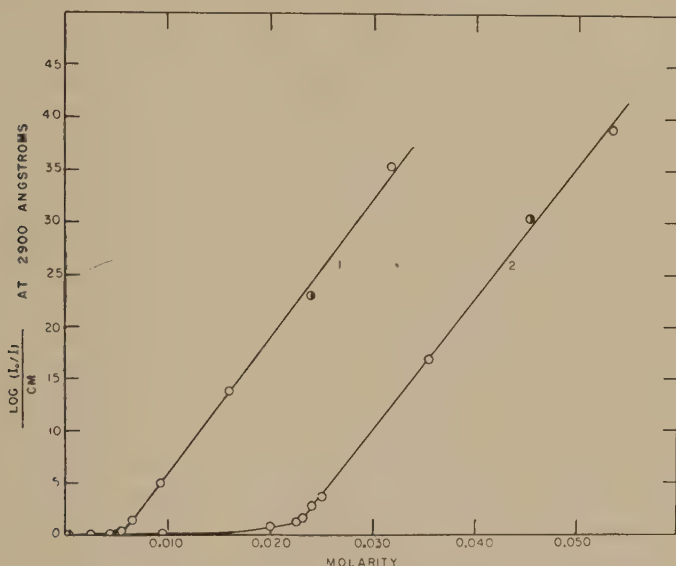


FIG. 4. Effect of concentration on the extinction coefficient $\frac{\log I_0/I}{\text{cm.}}$ at 2900 Å. for aqueous solutions of two long-chain alkyl pyridinium iodides. 1. Dodecyl pyridinium iodide. 2. Decyl pyridinium iodide. ● Solution 0.001 *M* in sodium thiosulfate.

solutions below the critical micelle concentration, to association of the alkyl pyridinium and the iodide ion. Evidence for this view is given by (a) the similarity of the spectra in the two solvents, (b) the relatively greater absorption in the case of ethanol solutions, and (c) the increase of absorption with increasing concentration in both solvents. Above the critical micelle concentration the increased absorption can be interpreted similarly in terms of a greater fraction of iodide ions associated with alkyl pyridinium ions, since there seems to be no significant change in character of the spectrum, other than an intensification of the band.

On this basis the curves of Figs. 1 and 2 must be composites of two kinds of absorption spectra: that of the ionized pyridinium iodide, having

a single maximum at 2580 Å.; and that of the undissociated material, showing absorption in the 2900-Å. region in addition to the 2580-Å. band.

For calculation of the fraction of iodide ions associated with the micelle the molar extinction coefficient of the undissociated material is necessary. Various attempts to determine this quantity failed. At the highest concentration in alcohols we were able to study, dodecyl pyridinium iodide appeared to be too highly dissociated. The material was not appreciably soluble in the nonpolar solvent hexane. The absorption spectra for the chloroform solutions are of little help, as is obvious from Fig. 1.

It is interesting to note that when the extinction coefficient, $\frac{\log I_0/I}{\text{cm.}}$, is plotted against concentration (Fig. 4), the slope of the upper branch of the curve is constant within experimental error for each salt. Whatever may be the actual fraction of iodide ions associated with the micelle, this fraction thus appears to be constant for each salt in the ranges of concentrations studied. This may be taken to indicate, if we assume a spherical micelle, either (a) that the micelle size is constant in these ranges, or (b) that the fraction of gegen-ions associated with the micelle is not much influenced by the micelle size. A second interesting feature of Fig. 4 is that the slopes appear to be equal for the two salts. The data do not warrant more than speculation regarding this, especially since deviation from Lambert's law was somewhat different for each compound. An equality of slope, however, would not be inconsistent, if one assumed alternative (b) above, with the finding of Debye (17) that the micelle size of the long-chain trimethylammonium bromides increases with chain length.

The range of concentrations was in general too low to enable any conclusion regarding "retrograde dissociation," which Hartley and his co-workers (2) were forced to conclude occurs at high concentrations, to explain the increase in equivalent conductivity there observed.

SUMMARY

1. Absorption spectra are presented for solutions of dodecyl pyridinium iodide in water, ethanol, and chloroform (containing 0.7% ethanol), and for decyl pyridinium iodide in water and in ethanol.
2. The change of absorption spectrum with concentration in water can be related to the critical micelle concentration of these salts.
3. The changes of absorption spectrum above the critical micelle concentration have been discussed in terms of the structure of the micelle.

REFERENCES

1. MOILLIET, J. L., COLLIE, B., ROBINSON, C., AND HARTLEY, G. S., *Trans. Faraday Soc.* **31**, 120 (1935).
2. COLLIE, B., SAMIS, G. S., AND HARTLEY, G. S., *Trans. Faraday Soc.* **32**, 795 (1936).
3. HARTLEY, G. S., *Kolloid-Z.* **88**, 22 (1939).

4. HARTLEY, G. S., *Quart. Revs.* (London) **2**, 152 (1948).
5. CORRIN, M. L., KLEVENS, H. B., AND HARKINS, W. D., *J. Chem. Phys.* **14**, 480 (1946).
6. CORRIN, M. L., AND HARKINS, W. D., *J. Am. Chem. Soc.* **69**, 679 (1947).
7. KOLTHOFF, I. M., AND STRICKS, W., *J. Phys. & Colloid Chem.* **52**, 915 (1948).
8. HANTZSCH, A., *Ber.* **44**, 1783 (1911).
9. HANTZSCH, A., *Ber.* **52**, 1544 (1919).
10. JONES, E. R., AND BURY, C. R., *Phil. Mag.* **4**, 481 (1927).
11. GRINDLEY, J., AND BURY, C. R., *J. Chem. Soc.* **1929**, 679.
12. DAVIES, D. G., AND BURY, C. R., *J. Chem. Soc.* **1930**, 2263.
13. HARTLEY, G. S., Aqueous Solutions of Paraffin-Chain Salts. Hermann et Cie, Paris, 1936.
14. LOTTERMOSER, A., AND PÜSCHEL, F., *Kolloid-Z.* **63**, 175 (1933).
15. MCBAIN, J. W., *Trans. Faraday Soc.* **9**, 99 (1913).
16. MCBAIN, J. W., AND SALMON, C. S., *J. Am. Chem. Soc.* **42**, 426 (1920).
17. DEBYE, P., *Ann. N. Y. Acad. Sci.* **51**, 575 (1949).

RHEOLOGY OF SYNTHETIC LATEX.¹ II. CONCENTRATION DEPENDENCE OF FLOW IN TYPE V GR-S LATEX

S. H. Maron, B. P. Madow and I. M. Krieger

*Physical Chemistry Laboratory, Department of Chemistry and Chemical Engineering,
Case Institute of Technology, Cleveland, Ohio*

Received October 29, 1951

INTRODUCTION

The first paper in this series (1) showed that GR-S latex is a Newtonian fluid up to a concentration of *ca.* 25% solids and non-Newtonian thereafter, that it is not thixotropic, that no yield value is exhibited, and that an exponential flow equation (2,3) can be used to convert the experimental data into rate of shear-shearing stress curves. The purpose of the present paper is to present more detailed data on the concentration dependence of the flow behavior of type V GR-S latex, and to discuss the significance of the results obtained.

EXPERIMENTAL

The type V latex investigated was a standard commercial product consisting of an aqueous dispersion of 80:20 butadiene-styrene copolymer emulsified with a mixture of Dresinate 731 and potassium oleate. The original concentration of the latex was 59.96% solids and 57.86% rubber by weight. This latex was concentrated by evaporation to 62.3% solids; the concentrate was diluted with distilled water to obtain the lower concentrations.

The concentric cylinder and capillary viscometers, as well as the procedures employed, have been described before (1). To obtain rubber contents, weighed samples of the latex were added to 99% isopropanol, and the mixtures were refluxed with two changes of alcohol and with two of distilled water. The rubber was then removed, dried in a vacuum oven at 50°C., and weighed. To convert rubber content to volume fraction a density of 0.930 for the polymer was used.

All viscosity measurements were made at $30.00 \pm 0.01^\circ\text{C}$.

RESULTS AND DISCUSSION

Figures 1 and 2 show logarithmic plots of the flow curves for type V GR-S latex at moderate and high solids contents, respectively. As with the

¹ The contents of this paper were presented at the Annual Meeting of the Society of Rheology, New York, N. Y., November 4, 1949.

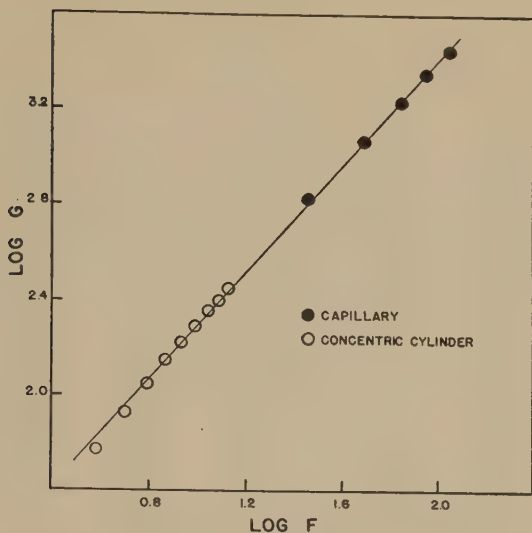


FIG. 1. Flow curve for type V GR-S latex at 40% solids content.

type III latices previously studied, the plot for the moderate concentration is linear over the entire experimental range, whereas the high concentration plot yields two linear portions. However, the slope at high shearing stress exceeds that at low stress, whereas the reverse was observed with type III latex. We believe that these "breaks" merely reflect the inadequacy of a single exponential equation to express the behavior of a complex system like latex over a wide range of shearing stresses. Further evidence for this point of view will be presented in subsequent papers.

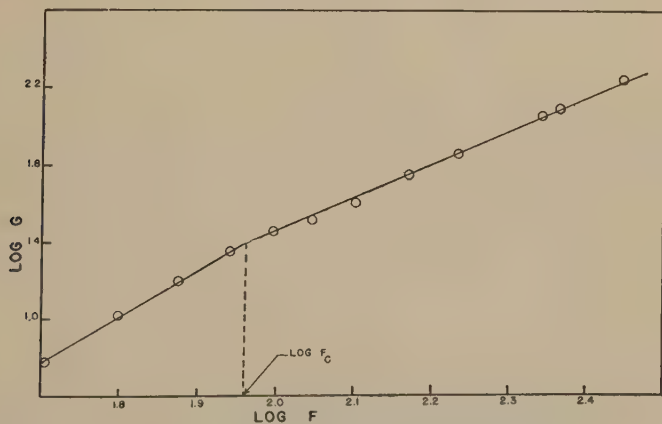


FIG. 2. Flow curve for type V GR-S latex at 62% solids content.

TABLE I

Flow Constants for Type V GR-S Latex

Rubber content (wt.-%)	ϕ	N_1	$\log(\eta'_1/\eta_0)$	N_2	$\log(\eta'_2/\eta_0)$	F_c (dynes/cm ² .)
0	0	1.00	0	—	—	—
12.03	0.1282	0.99	0.1565	—	—	—
22.68	0.2397	1.00	0.347	—	—	—
27.73	0.2920	1.01	0.462	—	—	—
33.55	0.3516	1.04	0.657	—	—	—
38.59	0.4028	1.08	0.889	1.19	1.014	11.1
43.32	0.4483	1.13	1.143	1.30	1.353	14.5
48.30	0.5005	1.32	1.690	1.51	1.901	20.8
53.04	0.5475	1.49	2.369	1.76	2.757	35.6
57.83	0.5948	1.73	3.559	2.21	4.414	65.8
59.03	0.6065	1.84	4.138	2.40	5.212	90.9
59.74	0.6135	1.81	4.323	2.24	5.195	114.4
60.06	0.6166	1.75	4.328	2.05	5.022	213.1

Separate exponential flow equations of the form

$$F^N = \eta' G, \quad [1]$$

where F is the shearing stress, G the velocity gradient, and N and η' constants of the fluid, have been fitted to the experimental data. Table I summarizes the values obtained for the constants of Eq. [1] at various solids contents. Here the subscripts 1 refer to the high shearing stress range, i.e., above a "critical" shearing stress F_c as shown in Fig. 2, and the subscripts 2 refer to shearing stresses below F_c . Phi (ϕ) is the volume fraction of rubber.

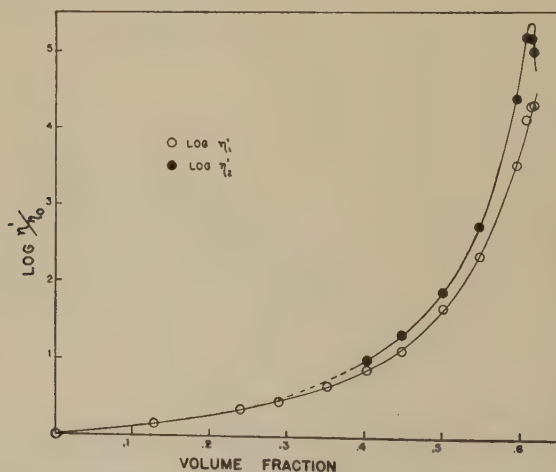


FIG. 3. Variation of η' with volume fraction of rubber.

The data of Table I are plotted in Figs. 3 and 4. Several interesting observations may be drawn from these graphs. From Fig. 3 it is apparent that type V latex is Newtonian below about 25% rubber, and that the degree of non-Newtonian behavior, measured by N , increases up to 59% rubber and drops thereafter. η' , which is numerically equal to the viscosity coefficient at unit shearing stress, climbs very steeply with concentration, covering a 100,000-fold range as rubber content varies from 0 to 60%. η_1' , the high shearing stress coefficient, goes through a maximum at 59% rubber, while η_2' increases monotonically.

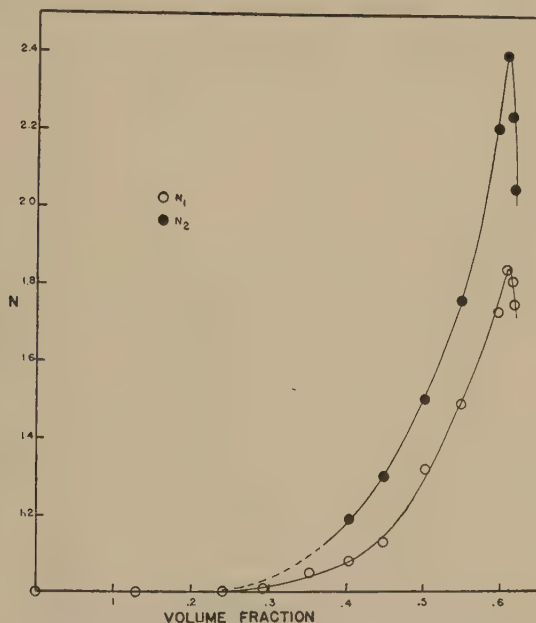


FIG. 4. Variation of N with volume fraction of rubber.

To fit the curves of Fig. 3 by an analytic expression is a difficult task because of the tremendous range covered by η' . It was recognized by Rhoades *et al.* (4) in their study of natural latex that the concentration variable should be one which climbs rapidly with rubber content. They employed the "rubber to serum ratio" q , defined by

$$q = \frac{\phi}{1 - \phi}; \quad [2]$$

q becomes infinite as ϕ approaches 1, hence, q parallels more closely the rise in viscosity with ϕ . η' , however, becomes essentially infinite when the suspended particles are closely packed, which occurs long before ϕ reaches

unity. We shall define therefore an "apparent volume fraction"

$$\phi' = \alpha\phi, \quad [3]$$

where α is a constant, and a new concentration variable

$$Z = \frac{\phi'}{1 - \phi'} = \frac{\alpha\phi}{1 - \alpha\phi}. \quad [4]$$

Z thus becomes infinite when $\phi = 1/\alpha$.

We have found that with a suitable choice of α it is possible to obtain linear plots of $\log (\eta'/\eta_0)$ vs. Z which pass through the origin, and which

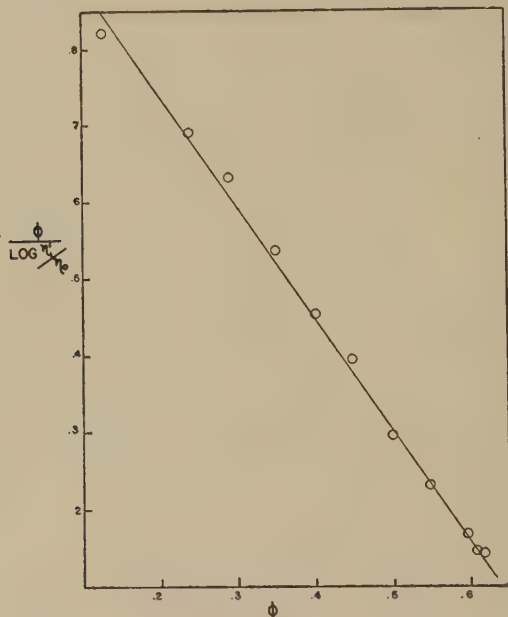


FIG. 5. Graphical determination of α and b .

cover both the Newtonian and non-Newtonian ranges up to a concentration of *ca.* 60% rubber. η_0 is the viscosity of water at 30°C. Since the equation for such lines is

$$\log \frac{\eta'}{\eta_0} = bZ, \quad [5]$$

rearrangement and use of Eq. [4] yields

$$\frac{\phi}{\log \eta' / \eta_0} = \frac{1}{\alpha b} - \frac{\phi}{b}. \quad [6]$$

Thus a graph of $\frac{\phi}{\log \eta' / \eta_0}$ vs. ϕ should be linear with slope $-1/b$ and intercept $1/\alpha b$, permitting evaluation of both α and b .

Such a plot is presented in Fig. 5; from this plot $b = 0.677$ and

$\alpha = 1.412$. Using this value of α , a plot of $\log \eta_1'/\eta_0$ vs. Z , shown in Fig. 6, may be seen to be linear up to a volume fraction of 0.61 rubber, where a pronounced break is observed. The position of this break corresponds closely to the position of the maximum in Fig. 2. It is possible that a degree of order sets in at this concentration, reducing the Brownian movement of the particles to a vibrational motion, and permitting flow to occur along more or less definite slip planes. Such an explanation, advanced here on a tentative basis, might account for the fact that as concentration increases above $\phi = 0.61$ rubber, the latex becomes less viscous and more nearly Newtonian.

Using Eq. [5] as an extrapolation formula, the viscosity should become infinite at $\phi = 1/\alpha = 0.708$. Close packing of rigid spheres is

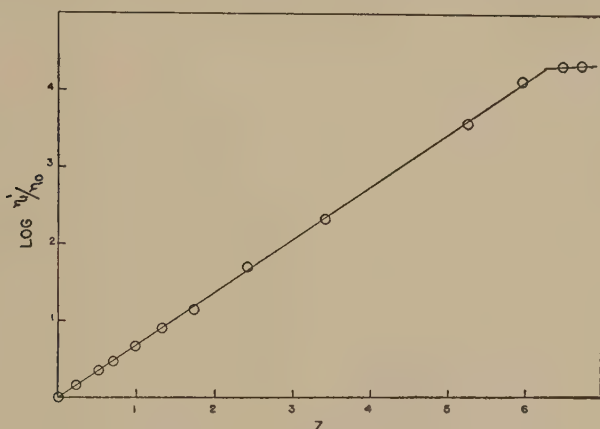


FIG. 6. Plot of $\log \eta_1'/\eta_0$ vs. Z for type V latex.

achieved at a volume fraction of 0.74–0.78, depending on the uniformity of the particle diameter. The difference can be attributed to the monolayer of soap surrounding the rubber particle, as the following calculation shows. Suppose that, in unit volume of the latex, there are n_i particles of diameter D_i , each surrounded by a soap monolayer of thickness Δ . The volume of rubber is $\phi = \frac{\pi}{6} \sum_i n_i D_i^3$, while ϕ_t , the volume of rubber plus soap layer, is

$$\phi_t = \frac{\pi}{6} \sum_i n_i (D_i + 2\Delta)^3 = \frac{\pi}{6} \sum_i n_i D_i^3 \left(1 + \frac{2\Delta}{D_i} \right)^3. \quad [7]$$

Since $D_i \gg \Delta$, the binomial may be expanded neglecting higher terms to give

$$\phi_t = \frac{\pi}{6} \sum_i n_i D_i^3 \left(1 + \frac{6\Delta}{D_i} + \dots \right). \quad [8]$$

The ratio ϕ_t/ϕ is given by

$$\frac{\phi_t}{\phi} = 1 + 6\Delta \frac{\sum n_i D_i^2}{\sum n_i D_i^3}, \quad [9]$$

but the quantity $\frac{\sum n_i D_i^2}{\sum n_i D_i^3}$ is the reciprocal of the volume-to-surface average particle diameter D_{av} . Hence

$$\frac{\phi_t}{\phi} = 1 + \frac{6\Delta}{D_{av}}. \quad [10]$$

For the type V latex studied here, D_{av} was found to be 1920 Å. by the soap titration method,² which yields this type of average. The thickness of the monolayer should be roughly equivalent to the length of the fully extended oleate ion, 27.5 Å., since the oleate ion is longer than the rosin soap ion. Using these values for D_{av} and Δ ,

$$\phi_t = 1.086 \phi.$$

Thus the actual volume fraction of the suspended phase corresponding to $\phi = 0.709$ is 0.768, a value within the range to be expected for close packing of nonuniform spheres.

Investigation of the low concentration limit also yields information of interest. Equation [5] may be converted to natural logarithms and expanded to give

$$\frac{\eta'}{\eta_0} - 1 + \dots = 2.303b (\alpha\phi + \dots)$$

or, for small values of ϕ ,

$$\eta' = \eta_0 (1 + 2.303 \alpha b \phi). \quad [11]$$

The factor $2.303 \alpha b$ is equal to 2.20, a value not far from the 2.5 of Einstein's theoretical expression (5) for the viscosity of a dilute suspension of rigid spheres. Thus Eq. [5] is in effect an empirical extension of the Einstein equation to high concentrations. The constants of Eqs. [4] and [5] were evaluated also for the low shearing stress range, and the graph of $\log \frac{\eta_2'}{\eta_0}$ vs. Z presented as Fig. 6. Here $\alpha = 1.441$, $b = 0.730$, and $2.303 \alpha b = 2.44$. The total volume fraction of rubber plus soap corresponding to close packing is 0.753.

Mooney (6) has recently derived theoretically a viscosity-concentration relation similar to Eq. [5] for a monodisperse suspension of rigid spheres, namely,

$$\ln \frac{\eta}{\eta_0} = \frac{2.5\phi}{1 - k\phi}. \quad [12]$$

² To be published.

This relation is a special case of Eq. [5] with $\alpha = k$, and $b = \frac{2.5}{2.303k}$, and applies only in the Newtonian range. Since, for type V latex, $2.303 \alpha b < 2.5$, Mooney's relation is not as satisfactory as Eq. [5] for the non-Newtonian viscosities and high concentrations studied here.

ACKNOWLEDGMENT

This research was sponsored by the Office of Rubber Reserve, Reconstruction Finance Corporation, as part of the Government Synthetic Rubber Program, and was first reported in March, 1949.

SUMMARY

Type V GR-S latex is non-Newtonian at all concentrations above about 0.25 rubber by volume, Newtonian below. The exponential flow equation may be used to convert experimental observations in capillary and concentric cylinder viscometers to rate of shear and shearing stress values. For volume fractions above about 0.40, however, separate exponential equations must be used for the high and low shearing stress ranges, due to the inadequacy of a single two-parameter equation to express the wide variation observed. The constants N and η' of the exponential equation increase in a regular manner with concentration for both shearing stress ranges up to a volume fraction of about 0.60, and either decrease or "level off" from 0.60 to 0.62, the highest concentration studied. This unusual behavior, equivalent to a decrease in viscosity with increasing volume fraction, is tentatively attributed to the setting in of a degree of order, which would restrict Brownian motion of the particles, and permit flow to occur along more or less definite planes.

An empirical extension of the Einstein equation of the form $\log \frac{\eta'}{\eta_0} = bZ$, where $Z = \frac{\alpha\phi}{1 - \alpha\phi}$, holds well all the way from 0 to 0.60 volume fraction of rubber. The limiting form of this equation at low volume fraction is identical with that of the Einstein equation, with a factor not far from Einstein value of 2.5. Extrapolation of the formula predicts infinite viscosity at a total volume fraction of rubber plus an adsorbed soap monolayer of about 0.75–0.77, a value which corresponds closely to the maximum obtainable by tight packing of spheres.

REFERENCES

1. KRIEGER, I. M., AND MARON, S. H., *J. Colloid Sci.* **6**, 528 (1951).
2. PORTER, A. W., AND RAO, P. A. M., *Trans. Faraday Soc.* **23**, 311 (1927).
3. FARROW, F., LOWE, G., AND NEALE, S., *J. Textile Inst.* **19**, T18 (1928).
4. RHOADES, E., SMITH, H., SEKAR, K., AND WAHAB, C., *India-Rubber J.* **97**, 21 (1939).
5. EINSTEIN, A., *Ann. Physik* **19**, 289 (1906).
6. MOONEY, M., *J. Colloid Sci.* **6**, 162 (1951).

BOOK REVIEWS

The Surface Chemistry of Solids. By S. J. GREGG, Ph.D., F.R.I.C., Reader in Surface Chemistry, University College of the South-West of England, Exeter. Reinhold Publ. Corp., New York, Sept. 27, 1951. 291 pp., 105 figs. Price \$8.50.

The author states, "My aim has been to give a brief survey of the various branches of this rapidly growing subject, adopting as far as practicable a consistent viewpoint. It is a subject which at first sight seems largely composed of a bewildering mass of unrelated and empirical observations, and it appeared to me more useful to lay the emphasis on general principles—where ascertainable—rather than on detailed descriptions of individual observations. Throughout stress has been laid on the consequences which result from the presence of a field of force at the surface of the solid; adsorption, adhesion, spreading phenomena, catalysis, and related effects can all be viewed from this angle, as can the great effect of the adsorbed film on adhesion, which is so important in friction and in lubrication."

The author has been successful in his objective and since it is well organized, clearly written, lucidly illustrated and documented, the book should find a welcome place on the shelf not only of beginners, but of moderately advanced students interested in these fields.

V. K. LA MER, New York, New York

Statistical Methods for Chemists. By W. J. YUDEN, National Bureau of Standards, Washington, D. C. John Wiley and Sons, Inc., New York, Sept. 21, 1951. 126 pp. Price \$3.00.

The author of this book holds a Ph.D. degree in analytical chemistry and is a close student of the important advantages which modern statistical methods offer all scientists in interpreting their own results or judging the work of others. He is consequently justified in saying, "This book is written for those who make measurements and interpret experiments. The book is characterized by an absence of statistical theory and proofs. I am convinced, from observation, that young men who have been given a fine mathematical grounding in statistics often have an inadequate grasp of the ways in which measurements behave. Observation has equally shown that most experimental workers have a very real understanding of the meaning of their experiments. They are, unfortunately, inarticulate. The purpose of this book is to make available to the scientist the modern statistical system of units for expressing scientific conclusions."

The book is written in a style which attracts and holds the attention of one who is not mathematically minded. Most important of all, it focuses attention upon the problem of how an experimentalist can improve his plan of experiments. Anyone who makes measurements will be helped by reading this little book.

V. K. LA MER, New York, New York

Quantitative Organic Microanalysis. By AL STEYERMARK, Head, Microchemical Department, Hoffmann-La Roche Inc., Nutley, New Jersey. The Blakiston Company, Philadelphia, Pa., Oct. 10, 1951. 389 pp., 155 illustrations. Price \$7.00.

Microchemistry during the past 30 years has been developing at an ever-increasing rate, yet many chemists using microchemical methods have had little or no formal training in microchemistry.

This is a practical, usable book by one who has had much experience in the field. Because of its simplicity of style and attention to minute manipulative details, it should prove helpful for the beginning microanalyst to whom it is addressed.

V. K. LA MER, New York, New York

AUTHOR INDEX

A

ATKINS, DON C., JR. See Doscher, 223

B

BACKUS, JOHN K., AND SCHERAGA, HAROLD A. Dynamo-optical properties of detergent micelles, 508

BALDWIN, DAVID E. See Gregor, 20

BASU, SADHAN, DASGUPTA, PARES CH., AND SIRCAR, ANIL K. Studies in Polyelectrolytes. II. Gum arabate, 539

BOOTH, F. The effect of surface conditions on the electrophoresis of solid particles, 549

BREGMAN, J. I. See Gregor, 20, 245, 323

BROADLEY, ROBERT D. See Gregor, 20

BROWNING, GEORGE V. See Ferry, 377

BURCH, ROBERT J., CALDWELL, MARY L., AND CARROLL, BENJAMIN. Diffusion through paper membranes, 374

BURCIK, EMIL J., AND VAUGHN, CARLOS R. The effect of pH on the rate of surface tension lowering, 522

C

CALDWELL, MARY L. See Burch, 372

CARROLL, BENJAMIN. See Burch, 374

CASHIN, W. M. Light scattering of polyvinylpyridine-nitromethane solutions, 271

CERF, ROGER. Contribution to the discussion on the shape of the polystyrene molecule in dilute solutions by means of flow birefringence measurements, 293

CHRISTIANSEN, E. B. See Salt, 146

CHRISTIANSEN, J. A. The mechanism of bimolecular reactions in solutions, 213

COLLINS, F. C. See Gregor, 304

CORRIN, M. L. See Harkins, 576

D

DASGUPTA, PARES CH. See Basu, 539

DEAN, ROBERT B. Waterproof adhesives for cellulose, 348

DE WAELE, A. See Mardles, 42

DOSCHER, TODD M. MYERS, GEORGE E., AND ATKINS, DON. C., JR. The behaviour of nonionic surface active agents in salt solutions, 223

DURRUM, E. L. Two-dimensional electrophoresis and ionophoresis, 274

F

FAIR, W. F. JR. Acceptance of the Bingham medal, 93

FERRY, JOHN D., FOSTER, EDWARD L., BROWNING, GEORGE V., AND SAWYER, W. M. Viscosities of concentrated polyvinyl acetate solutions in various solvents, 377

FOSTER, EDWARD L. See Ferry, 377

G

GENDRON, PIERRE R. See Schiff, 495

GILMORE, G. D. See Spencer, 118

GREGOR, HARRY P., BREGMAN, J. I., GUTOFF, FRADELLE, BROADLEY, ROBERT D., BALDWIN, DAVID E., AND OVERBERGER, C. G. Studies on Ion-Exchange Resins. Capacity of sulfonic acid cation-exchange resins, 20

GUTOFF, FRADELLE, AND BREGMAN, J. I. Studies on ion-exchange resins. II. Volumes of various cation-exchange resin particles, 245

COLLINS, F. C., AND POPE, MARTIN. Studies on ion-exchange resins. III. Diffusion of neutral molecules in a sulfonic acid cation-exchange resin, 304

AND BREGMAN, J. I. Studies on ion exchange resins. IV. Selectivity coefficients of various cation exchangers towards univalent cations, 323

See Sollner, 557

GUTOFF, FRADELLE, See Gregor, 20, 245

H

HARKINS, WILLIAM D., KRIZEK, HELEN, AND CORRIN, M. L. Effect of micelle

- formation on the absorption spectra of
deeryl and dodecyl pyridinium iodides,
576
- HELLER, WILFRIED, AND THOMPSON,
ARTHUR C. The volume requirements
of Polymer molecules. I. The apparent
specific volume of polystyrene in solu-
tions, 57
- I**
- INN, EDWARD C. Y. Measurement of
particle size and concentration of homo-
geneous aerosols, 368
- INOUE, KATSUYA. A modern theory on
the structure and caking properties of
coal from the rheological viewpoint,
190
- K**
- KAHAN, GEORGE J. Hydrophobic films on
solid surfaces, 571
- KRIEGER, IRVIN M., AND MARON, SAMUEL
H. Rheology of synthetic latex. I. Test
of some flow equations, 528
See Maron, 584
- KRIZEK, HELEN. See Harkins, 576
- L**
- LEVINE, S. The interaction of colloidal
particles. VI. Application of the Stern
theory of the double layer, 1
- LINDQUIST, CARL G., AND SIERICH, WIL-
LIAM C. The measurement of the flow
properties of a pseudoplastic with a
concentric cylinder viscometer, 33
- LOEB, ARTHUR L. An interionic attraction
theory applied to diffuse layer around
colloid particles, 75
- M**
- MACKOR, E. L. A. theoretical approach of
for determination of cation-exchange
capacity of clay, 219
- MACKOR, E. L. A. theoretical approach of
the colloid-chemical stability of disper-
sions in hydrocarbons, 492
- MADOW, B. P. See Maron, 584
- MARDLES, E. W. J., AND DE WAELE, A.
Some aspects of the rheology and the
stability of emulsions and suspensions,
42
- MARON, SAMUEL H. See Krieger, 528
- MADOW, B. P. AND KRIEGER, I. M.
Rheology of synthetic latex. II. Con-
centration dependence of flow in type
V GR-S latex, 584
- MASON, S. G. See Trevelyan, 354
- MCDONALD, HUGH J., URBIN, MATTHEW
C., AND WILLIAMSON, MARTIN B. Ion-
ography: Some aspects of ion migra-
tion on paper in an electric field, 236
- MOREY, D. R. A kinetic basis for polymer
precipitation and the selection average,
406
- MYERS, GEORGE E. See Doscher, 223
- MOONEY, M. Secondary stresses in visco-
elastic flow, 96
The viscosity of a concentrated suspen-
sion of spherical particles, 162
- O**
- OVERBERGER, C. G. See Gregor, 20
- P**
- POPE, MARTIN. See Gregor, 304
- R**
- ROSS, SYDNEY. Solubilization of dyes in
mineral oil and its application to a
model biological cell membrane, 497
- RYAN, N. W. See Salt, 146
- S**
- SALT, D. L., RYAN, N. W., AND CHRISTIAN-
SEN, E. B. The rheology of carboxy-
methylcellulose dispersions in water,
146
- SAWYER, W. M. See Ferry, 377
- SCHERAGA, HAROLD A. See Backus, 508
- SCHIFF, DAPHNE, AND GENDRON, PIERRE
R. A new continuously sensitive dif-
fusion cloud chamber, 495
- SIERICH, WILLIAM C. See Lindquist, 33
- SINGLETERRY, C. R., AND STONE, E. E.
Rheological properties of a lubricating
grease, 171
- SIRCAR, ANIL K. See Basu, 539
- SOLLNER, KARL, AND GREGOR, HARRY P.
The electrochemistry of permselective
membranes. III. The electrical resist-
ance of permselective collodion mem-
branes in solutions of various electro-
lytes, 557

- SPENCER, R. S., AND GILMORE, G. D. Some
flow phenomena in the injection mold-
ing of polystyrene, 118
AND WILEY, R. M. The mixing of very
viscous liquids, 133
STONE, E. E. See Singleterry, 171
SURIANI, LOUIS R. See Voet, 155

T

- TAYLOR, E. W. See Morey, 470
THOMPSON, ARTHUR C. See Heller, 57
TREVELYAN, B. J., AND MASON, S. G.
Particle motions in sheared suspensions.
I. Rotations, 354

U

- URBIN, MATTHEW C. See McDonald, 236

V

- VAUGHN, CARLOS R. See Burcik, 522
VOET, ANDRIES, AND SURIANI, LOUIS R.
Dielectrics and rheology of dispersed
magnetized particles, 155

W

- WAUGH, G. P. See Morey, 470
WEYL, W. A. Surface structure of water
and some of its physical and chemical
manifestations, 389
WILEY, R. M. See Spencer, 133
WILLIAMSON, MARTIN B. See McDonald, 236
WOODWARD, J. G. A vibrating-plate
viscometer, 481

SUBJECT INDEX

A

- Absorption spectra, effect of micelle formation on, of decyl and dodecyl pyridinium iodides, HARKINS, KRIZEK AND CORRIN, 576
- Adhesives, water proof, for cellulose, DEAN, 348
- Adsorption, of aromatic hydrocarbons in nonaromatic media on carbon black, VAN DER WAARDEN, 443
- Aerosols, inertial mechanism in the mechanical filtration of, RAMSKILL AND ANDERSON, 416; —, measurement of particle size and concentration of homogeneous, INN, 368

C

- Carbon black, adsorption of aromatic hydrocarbons in nonaromatic media on, VAN DER WAARDEN, 443
- Carboxymethylcellulose, rheology of dispersions of, in water, SALT, RYAN AND CHRISTIANSEN, 146
- Cations, univalent, selectivity coefficients of various cation exchangers towards, GREGOR AND BREGMAN, 323
- Cellulose, waterproof adhesives for, DEAN, 348
- Clay, a micromethod for determination of cation-exchange capacity of, MACKENZIE, 219
- Cloud chamber, continuously sensitive diffusion, SCHIFF AND GENDRON, 495
- Coal, a modern theory on the structure and caking properties of, INOUE, 190

D

- Detergent micelles, dynamo-optical properties of, BACKUS AND SCHERAGA, 508
- Dielectrics, of dispersed magnetized particles, VOET AND SURIANI, 155
- Dispersions, in hydrocarbons, colloid-chemical stability of, MACKOR, 492

- Dyes, solubilization in mineral oil and its application to a model biological cell membrane, ROSS, 497

E

- Electric field, aspects of ion migration on paper in an, McDONALD, URBIN AND WILLIAMSON, 236
- Electrochemistry, of permselective membranes III. SOLLNER AND GREGOR, 557
- Electrophoresis, effect on surface conditions on the, of solid particles, BOOTH, 549; —, two-dimensional, DURRUM, 274
- Emulsions, some aspects of the rheology and stability of, MARDLES AND DE WAELE, 42

F

- Films, hydrophobic, on solid surfaces, KAHAN, 571
- Flow, viscoelastic, secondary stresses in, MOONEY, 96
- Flow properties, measurement of, of a pseudoplastic system, LINDQUIST AND SIERICHS, 33

G

- Gum arabate. BASU, DASGUPTA AND SIRCAR, 539

H

- Hydrocarbons, aromatic, adsorption in nonaromatic media on carbon black, VAN DER WAARDEN, 443

I

- Interionic attraction theory, applied to the diffuse layer around colloid particles, LOEB, 75
- Ionography, McDONALD, URBIN AND WILLIAMSON, 236
- Ionophoresis, two-dimensional, DURRUM, 274

L

- Latex, synthetic, rheology of, KRIEGER AND MARON, 528; MARON, MADOW AND KRIEGER, 584, —, —, sintering of particles of, DILLON, MATHESON AND BRADFORD, 108
- Light scattering, of polyvinylpyridine-nitromethane solutions, CASHIN, 271
- Liquids, mixing of very viscous, SPENCER AND WILEY, 133
- Lubricating grease, rheological properties of a, SINGLETERRY AND STONE, 171

M

- Maleic acid, copolymers of, titration and viscosity studies, FERRY ET AL., 429
- Membranes, permselective, electrochemistry of III. Electrical resistance of permselective collodion membranes in solutions of various electrolytes, SOLLNER AND GREGOR, 557
- Molecules, polymer, volume requirements of, HELLER AND THOMPSON, 57

P

- Paper, aspects of ion migration on, in an electric field, McDONALD, URBIN AND WILLIAMSON, 236
- Paper membranes, diffusion through, BURCH, CALDWELL AND CARROLL, 372
- Particles, colloidal, interaction of, LEVINE, 1; — — interionic attraction theory applied to the diffuse layer around, LOEB, 75; —, magnetized, dielectrics and rheology of dispersed, VOET AND SURIANI, 155; —, solid, effect of surface conditions on the electrophoresis of, BOOTH, 549; —, spherical, viscosity of a concentrated suspension of, MOONEY, 162
- Polyamide films, delayed plastic flowing in, KAUFFMAN AND GEORGE, 450
- Polyelectrolytes, studies in. II. Gum arabate, BASU, DASGUPTA AND SIRCAR, 539
- Polymers, kinetic basis for precipitation of, MOREY, 406; —, volume requirements of molecules of, I., HELLER AND THOMPSON, 57
- Polystyrene, apparent specific volume of, in solution, HELLER AND THOMPSON, 57; —, flow birefringence measurements of molecules of, in dilute solutions, CERF, 293; —, flow phenomena in the injection molding of, SPENCER AND GILMORE, 118

- Polyvinyl acetate, application of precipitation-turbidity analysis to, MOREY, TAYLOR AND WAUGH, 470; viscosities of concentrated solutions of, in various solvents, FERRY, FOSTER, BROWNING AND SAWYER, 377
- Polyvinylpyridine-nitromethane solutions, light scattering of, CASHIN, 271
- Pseudoplastics, measurement of flow properties of, LINDQUIST AND SIERICHS, 33
- Pyridinium iodide, effect of micelle formation on the absorption spectra of decyl and dodecyl, HARKINS, KRIZEK AND CORBIN, 576

R

- Reactions, bimolecular, mechanism of, in solutions, CHRISTIANSEN, 213
- Resins, ion-exchange, GREGOR ET AL., 20, 245, 304, 323; —, volumes of particles of various cation-exchange, GREGOR ET AL., 245
- Rheology, of carboxymethylcellulose dispersions in water, SALT, RYAN AND CHRISTIANSEN, 146; —, of dispersed magnetized particles, VOET AND SURIANI, 155; —, of emulsions, MARDLES AND DE WAELE, 42; of a lubricating grease, SINGLETERRY AND STONE, 171; of synthetic latex, I., KRIEGER AND MARON, 528; II., MARON, MADOW AND KRIEGER, 584

S

- Salt solutions, behavior of nonionic surface active agents in, DOSCHER, MEYERS AND ATKINS, JR., 223
- Sintering, of synthetic latex particles, DILLON, MATHESON AND BRADFORD, 108
- Solutions, mechanism of bimolecular reactions in, CHRISTIANSEN, 213
- Stresses, secondary, in viscoelastic flow, MOONEY, 96

- Sulfonic acid cation-exchange resins, capacity of, GREGOR ET AL., 20; — —, diffusion of neutral molecules in, GREGOR ET AL., 304
- Surface active agents, behavior of non-ionic, in salt solutions, DOSCHER, MYERS AND ATKINS, JR., 223
- Surface tension, effect of pH on lowering of, BURCIK AND VAUGHN, 522
- Surfaces, solid, hydrophobic films on, KAHAN, 571
- Suspensions, some aspects of the rheology and stability of, MARDLES AND DE WAELE, 42; —, particle motions in sheared particle, TREVELYAN AND MASON, 354
- ### V
- Viscometer, vibrating-plate, WOODWARD, 481
- Viscosity, of concentrated suspensions of spherical particles, MOONEY, 162
- ### W
- Water, rheology of carboxymethylcellulose dispersions in, SALT, RYAN AND CHRISTIANSEN, 146; —, surface structure of, WEYL, 389

INDEX OF BOOK REVIEWS

- GREGG, S. J., The Surface Chemistry of Solids (LA MER, V. K.), 592
- McBAIN, J. W., Colloid Science (MARK, H.), 291
- SIMONS, J. H. (ed.) Fluorine Chemistry. Vol. I. (HILDEBRAND, J. H.), 291
- STEYERMARK, AL., Quantitative Organic Microanalysis (LA MER, V. K.), 592
- VICKERSTAFF, T., The Physical Chemistry of Dyeing (NEALE, S. M.), 374
- YODEN, W. J., Statistical Methods for Chemists (LA MER, V. K.), 592

JOURNAL OF COLLOID SCIENCE

Editor-in-Chief

VICTOR K. LA MER, Columbia University, New York

Advisory Board

C. O. BECKMANN	J. TH. G. OVERBEEK
KATHARINE B. BLODGETT	R. RUYSSSEN
K. F. BONHOEFFER	E. K. RIDEAL
M. L. CORRIN	WILLIAM SEIFRIZ
P. J. W. DEBYE	LEO SHEDLOVSKY
JOHN T. EDSALL	THEODORE SHEDLOVSKY
I. FANKUCHEN	ROBERT SIMHA
JOHN D. FERRY	JACINTO STEINHARDT
A. R. GORDON	THE SVEDBERG
WILFRIED HELLER	HUGH S. TAYLOR
ERIC HUTCHINSON	ARNE TISELIUS
GEORGE JURA	ROBERT D. VOLD
JOHN G. KIRKWOOD	BERNARD VONNEGUT
E. C. LINGAFELTER	RALPH W. G. WYCKOFF
L. G. LONGSWORTH	BRUNO H. ZIMM
J. W. MCBAIN	

VOLUME 6

1951

ACADEMIC PRESS INC., PUBLISHERS
NEW YORK, N. Y.

Copyright 1951, by Academic Press Inc.
Made in United States of America

CONTENTS OF VOLUME 6

NUMBER 1, FEBRUARY, 1951

S. LEVINE. The Interaction of Colloidal Particles. VI. Application of the Stern Theory of the Double Layer	1
HARRY P. GREGOR, J. I. BREGMAN, FRADELLE GUTOFF, ROBERT D. BROADLEY, DAVID E. BALDWIN AND C. G. OVERBERGER. Studies on Ion-Exchange Resins. Capacity of Sulfonic Acid Cation-Exchange Resins	20
CARL G. LINDQUIST AND WILLIAM C. SIERICHS. The Measurement of the Flow Properties of a Pseudoplastic with a Concentric Cylinder Viscometer	33
E. W. J. MARDLES AND A. DE WAELE. Some Aspects of the Rheology and the Stability of Emulsions and Suspensions	42
WILFRIED HELLER AND ARTHUR C. THOMPSON. The Volume Requirements of Polymer Molecules. I. The Apparent Specific Volume of Polystyrene in Solutions	57
ARTHUR L. LOEB. An Interionic Attraction Theory Applied to Diffuse Layer Around Colloid Particles	75

NUMBER 2, APRIL, 1951

BINGHAM AWARD to W. F. FAIR, JR.	93
W. F. FAIR, JR. Acceptance of the Bingham Medal	93
M. MOONEY. Secondary Stresses in Viscoelastic Flow	96
R. E. DILLON, L. A. MATHESON AND E. B. BRADFORD. Sintering of Synthetic Latex Particles	108
R. S. SPENCER AND G. D. GILMORE. Some Flow Phenomena in the Injection Molding of Polystyrene	118
R. S. SPENCER AND R. M. WILEY. The Mixing of Very Viscous Liquids ...	133
D. L. SALT, N. W. RYAN AND E. B. CHRISTIANSEN. The Rheology of Carboxymethylcellulose Dispersions in Water	146
ANDRIES VOET AND LOUIS R. SURIANI. Dielectrics and Rheology of Dispersed Magnetized Particles	155
M. MOONEY. The Viscosity of a Concentrated Suspension of Spherical Particles	162
C. R. SINGLETERRY AND E. E. STONE. Rheological Properties of a Lubricating Grease	171
KATSUYA INOUE. A Modern Theory on the Structure and Caking Properties of Coal from the Rheological Viewpoint	190

NUMBER 3, JUNE, 1951

J. A. CHRISTIANSEN. The Mechanism of Bimolecular Reactions in Solutions	213
ROBERT C. MACKENZIE. A Micromethod for Determination of Cation-Exchange Capacity of Clay	219
TODD M. DOSCHER, GEORGE E. MEYERS AND DON C. ATKINS, JR. The Behavior of Nonionic Surface Active Agents in Salt Solutions	223
HUGH J. McDONALD, MATTHEW C. URBIN AND MARTIN B. WILLIAMSON. Ionography: Some Aspects of Ion Migration on Paper in an Electric Field	236

